Topics in Current Chemistry Collections

Barbara Kirchner · Eva Perlt *Editors*

Ionic Liquids II

Springer

Topics in Current Chemistry Collections

Aims and Scope

The series *Topics in Current Chemistry Collections* presents critical reviews from the journal *Topics in Current Chemistry* organized in topical volumes. The scope of coverage is all areas of chemical science including the interfaces with related disciplines such as biology, medicine and materials science.

The goal of each thematic volume is to give the non-specialist reader, whether in academia or industry, a comprehensive insight into an area where new research is emerging which is of interest to a larger scientific audience.

Each review within the volume critically surveys one aspect of that topic and places it within the context of the volume as a whole. The most significant developments of the last 5 to 10 years are presented using selected examples to illustrate the principles discussed. The coverage is not intended to be an exhaustive summary of the field or include large quantities of data, but should rather be conceptual, concentrating on the methodological thinking that will allow the non-specialist reader to understand the information presented.

Contributions also offer an outlook on potential future developments in the field.

More information about this series at http://www.springer.com/series/14181

Barbara Kirchner • Eva Perlt
Editors

Ionic Liquids II

With contributions from

Giovanni Battista Appetecchi • Andrea Balducci • Natalia Borisenko
Leslie Brown • Lucy C. Brown • Fabrizio Lo Celso • Cinzia Chiappe
Martyn J. Earle • Frank Endres • Manuela A. Gîlea • James M. Hogg
Patricia A. Hunt • Charl J. Jafta • Christoph Janiak • Abhishek Lahiri
Natalia V. Plechkova • Christian Silvio Pomelli • Olga Russina
Mathieu Salanne • Christian Schröder • Kenneth R. Seddon
Małgorzata Swadźba-Kwaśny • Alessandro Triolo • Susann Wegner

Springer

Editors
Barbara Kirchner
Mulliken Center for Theoretical Chemistry
University of Bonn
Bonn, Germany

Eva Perlt
Department of Chemistry
University of California, Irvine
Irvine, CA, USA

Partly previously published in Top Curr Chem (Z) Volume 375 (2017); Top Curr Chem (Z) Volume 376 (2018).

ISSN 2367-4067
Topics in Current Chemistry Collections
ISBN 978-3-319-89793-6

Library of Congress Control Number: 2009940397

© Springer International Publishing AG, part of Springer Nature 2018
The chapters “Ionic Liquid–Liquid Chromatography: A New General Purpose Separation Methodology”, “Proteins in Ionic Liquids: Current Status of Experiments and Simulations”, “Lewis Acidic Ionic Liquids” and “Quantum Chemical Modeling of Hydrogen Bonding in Ionic Liquids” are licensed under the terms of the Creative Commons Attribution 4.0 International License (http://creativecommons.org/licenses/by/4.0/). For further details see license information in the chapters.
This work is subject to copyright. All rights are reserved by the Publisher, whether the whole or part of the material is concerned, specifically the rights of translation, reprinting, reuse of illustrations, recitation, broadcasting, reproduction on microfilms or in any other physical way, and transmission or information storage and retrieval, electronic adaptation, computer software, or by similar or dissimilar methodology now known or hereafter developed.
The use of general descriptive names, registered names, trademarks, service marks, etc. in this publication does not imply, even in the absence of a specific statement, that such names are exempt from the relevant protective laws and regulations and therefore free for general use.
The publisher, the authors and the editors are safe to assume that the advice and information in this book are believed to be true and accurate at the date of publication. Neither the publisher nor the authors or the editors give a warranty, express or implied, with respect to the material contained herein or for any errors or omissions that may have been made. The publisher remains neutral with regard to jurisdictional claims in published maps and institutional affiliations.

This Springer imprint is published by the registered company Springer Nature Switzerland AG
The registered company address is: Gewerbestrasse 11, 6330 Cham, Switzerland

Dedication

This volume is dedicated to Professor Kenneth R. Seddon OBE, the Founder and Director of the Queen's University Ionic Liquids Laboratories. Ken has had a great influence to many people. Although it was often remarked that he made lasting impressions "on everyone he met... be it admiration - or fear", personally we admired him for his protective and supportive nature toward younger and less experienced researchers. He was always trying to keep the idea of science pure and reminded us to work properly and be honest. To this book, he has not only contributed with his chapter, but also with the lasting impressions and the changes he has caused in our minds.

Contents

Foreword

Eight years on from doing the same for the 2010 ‘Ionic Liquids’ Topics in Current Chemistry (290), I find myself writing this Foreword and reflecting on what has changed in that time and what remains the same. The greatest constant is the popularity of ionic liquids as a field of study. It seemed impossible that this could be maintained at the pace that it showed in 2009, with 2,207 papers published with ionic liquid(s) in the title (Web of Science), yet in 2017 there have been over 3,600. Web of Science has also noted 44 of the papers from 2009 as ‘highly cited’. All of this attests to the great good health of our field.

I also find myself thinking another snapshot in time. My first foray into the world of molten salts, as it was then called, was a wonderful meeting more than 30 years ago - *The NATO Advanced Study Institute on Molten Salt Chemistry*, Camerino, Italy, August 3-15, 1986. As I look through the lists of talks and speakers it is possible to see the roots of much of what we still study. The conference opened with John Enderby (now Sir John) talking about structures of molten salts. I particularly remember a discussion with him in one of the breaks in which he said that it would help me to think of ionic liquids not as simple liquids, but more like ‘runny solids’. This was prescient of current discussions of the mesoscopic organization in ionic liquids (see contribution 9, also discussed in the previous volume in Chapter 5). Our host, Roberto Marassi, told us about molten salt batteries, which is still one of the hottest of topics for potential applications of ionic liquids (see contributions 1 and 3). Many of the talks concentrated on electrochemical properties and applications of molten salts, including one by Doug Inman on electrodeposition (see contribution 3), while Bernard Tremillon told us about acid-base effects in molten salts (see contribution 7). *Plus ça change, plus c’est la même chose.*

What we would find surprising today is that in the entire meeting there were only two talks that concentrated on room temperature liquids, one from Bob Osteryoung on the chemistry of organic chloroaluminates and the other from Ken Seddon on using these as solvents for UV-VIS spectroscopy, although they did also get a mention in a talk from John Wilkes on Friedel-Crafts reactions in chloroaluminate molten salts. While these proponents of these room temperature systems extolled the virtues of not having to work at elevated temperatures, of course these systems were highly sensitive to moisture and required specialist equipment and techniques that generated a barrier to entry to working with chloroaluminate ionic liquids. The older, more easily handled systems of Walden were yet to be rediscovered.

Today's collection contains subjects that could not have been imagined 30 years ago. Most of these have been made possible by the revolution in ionic liquid chemistry that arose from the advent of room temperature ionic liquids composed of ions that produce a relatively gentle environment for delicate species, such as proteins (see contribution 5). It is remarkable that ionic liquids have been found that can even enhance the stabilities of some proteins. This is now a significant field of research. The high temperatures associated with molten salts made it impossible to study gaseous species in these, let alone think that ionic liquids might be used to capture noxious gases such as H_2S (see contribution 10). The modern ionic liquids can also be used with molecular solvents without the need for the extreme forms of drying that were required if they were to be used with the chloroaluminate ionic liquids. This has enabled the application of ionic liquids in ionic liquid-liquid chromatography (see contribution 4). The huge range of ionic liquids that has come about this century has enabled sophisticated approaches to the synthesis of nanoparticles (see contribution 6), for which ionic liquids have proven to be very useful. Given the excellent properties of ionic liquids for electrochemical applications, it is perhaps surprising that the exploration of their potential for supercapacitors is such a recent topic (see contribution 2). However, in a relatively short time a great deal of progress has been made. Finally, one must recognise another revolution that has occurred over the same period – the astonishing increase in the power of computers. Combined with a number of advances in the handling of the theories of bonding and intermolecular interactions this has transformed our ability to study complex systems such as ionic liquids using theory (see contribution 8 and Chapter 7 of the previous volume).

While Barbara has brought together this collection to focus on some key issues of today, there have also been considerable advances in many of the areas discussed in the previous volume, which remains a useful reference. The synthesis of ionic liquids (Chapter 1 of the previous volume) remains an important topic, particularly in regards of bringing the price of ionic liquids down for commercial application on the on hand and to make new task specific ionic liquids (Chapter 3). Understanding the thermal stability of ionic liquids (Chapter 6) has also shown to be important for their commercial application. Much work has also appeared on manipulating the effects of ionic liquids on organic reactions (Chapter 2) and particularly biomass processing (Chapter 10).

Bringing this all together, we can see that the study and use of ionic liquids is a field that is in great good health, with a combination of on-going themes and the introduction of new ideas. I am very happy to say that I see no evidence for this not to continue for a long time to come.

Professor Tom Welton
Imperial College London

This topical collection entitled 'Ionics Liquids II' is edited by Barbara Kirchner and Eva Perlt.

Top Curr Chem (Z) (2017) 375:20
DOI 10.1007/s41061-017-0109-8

REVIEW

Ionic Liquids in Lithium-Ion Batteries

Andrea Balducci[1,2]

Received: 21 November 2016 / Accepted: 18 January 2017 / Published online: 2 February 2017

Abstract Lithium-ion batteries are among the most widespread energy storage devices in our society. In order to introduce these devices in new key applications such as transportation, however, their safety and their operative temperature range need to be significantly improved. These improvements can be obtained only by developing new electrolytes. Ionic liquids are presently considered among the most attractive electrolytes for the development of advanced and safer lithium-ion batteries. In this manuscript, the use of various types of ionic liquids, e.g. aprotic and protic, in lithium-ion batteries is considered. The advantages and the limits associated to the use of these innovative electrolytes are critically analysed.

Keywords Lithium-ion batteries · Ionic liquids · Electrolytes · Cathodes · Anodes

1 Lithium-Ion Batteries

Lithium-ion batteries (LIBs) are nowadays some of the most popular energy storage devices [1–5]. LIBs display high energy densities (up to 250 Wh/kg or up to 800 Wh/L), relatively high power, and a good cycle life, and they can be realized in many different shapes and sizes. Because of these characteristics, LIBs dominate the 4C (camera, computer, cellular phone, cordless tools) market, and they are presently

---

Chapter 1 was originally published as Balducci, A. Top Curr Chem (Z) (2017) 375: 20. DOI 10.1007/s41061-017-0109-8.

✉ Andrea Balducci
andrea.balducci@uni-jena.de

[1] Institute for Technical Chemistry and Environmental Chemistry, Friedrich-Schiller-University Jena, Philosophenweg 7a, 07743 Jena, Germany

[2] Center for Energy and Environmental Chemistry Jena (CEEC Jena), Friedrich-Schiller-University Jena, Philosophenweg 7a, 07743 Jena, Germany

indicted as the most promising storage technology for the realization of hybrid and electric vehicles (HV, EV). Furthermore, they are also seen as the most suitable storage technology to realize high performance delocalized energy storage units (Fig. 1). Obviously, the introduction of LIBs in these new applications will further strengthen the central role of these systems in the field of energy storage [1–5]. Nevertheless, in order to be successfully introduced in these large markets, the energy, as well as the safety of LIBs need to be significantly improved.

In the state-of-the-art LIBs, the cathode is typically based on metal oxides, whereas graphite is the most used anodic active material [2, 6] (Fig. 1). In the last years, in order to increase the energy of these devices, enormous efforts have been made toward the development of high voltage cathode (>4 V) and high capacity anodes [2, 6]. The electrolytes used in the state-of-the-art LIBs are containing mixture of organic carbonates (e.g. ethylene carbonate, EC; diethyl carbonate, DEC; ethyl methyl carbonate, EMC) and a lithium salt. Although these electrolytes display several favourable features, e.g. good ionic conductivities, they are flammable and volatile, and their use poses a serious safety risk and strongly reduces the battery operative temperature range [1–6]. For these reasons, alternative electrolytes for LIBs, with improved safety and able to work in a broader operative temperature range, are today urgently needed. Recently, a large number of alternative components/classes of electrolytes have been proposed. Among them, ionic liquids (ILs) appear as some of the most promising. This manuscript is dedicated to this class of electrolytes and the its aim is to give a critical overview about the main advantages and limitations related to their use in LIBs.

2 Electrolyte in Lithium-Ion Batteries: Requirements and State-of-the-Art

In LIBs the electrolyte acts as the medium for the transport of lithium ions between the electrodes during the charge–discharge processes. For that, this component is essential for the operation of these devices.

The electrolyte of LIBs needs to display several features, which are all important for the functioning of these devices [7–11]:

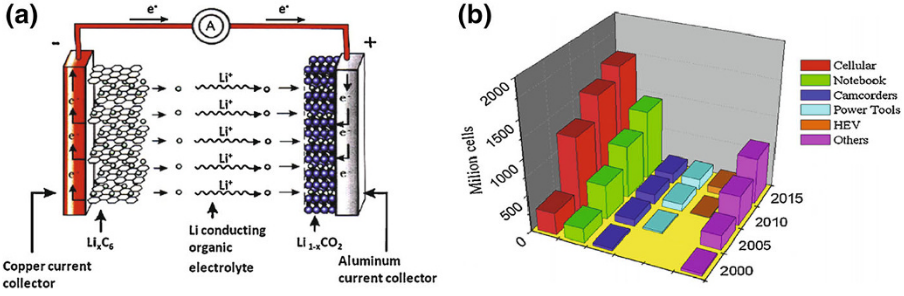

Fig. 1 **a** Scheme of a lithium-ion battery and **b** evolution of the lithium ion battery sale in the consumer electronic and HEV market. Taken with permission from Scrosati and Garche [2]

1. *Favorable transport properties,* which are necessary to guarantee a fast transport of lithium ions between the two electrodes during the charge–discharge process.
2. *Chemical and electrochemical stability*, which are indispensable to preserve the electrolyte (and the electrodes) during the charge–discharge process.
3. *Low melting and high boiling points*, which are required to allow a large operative temperature range of use.
4. *Low vapor pressure*, which is necessary to reduce the risk of dangerous events.

As mentioned above, graphite is the most used anodic material in LIBs technology. In order to insert/extract lithium ions between the graphite layers, the presence of a passive layer, called solid electrolyte interphase (SEI), is required [12]. As a matter of fact, if no SEI is present at the surface of the graphite, exfoliation processes occur, leading to a deterioration of the material itself and consequently of the battery [7–14]. For this reason, the use of graphite as anode material requires an additional property of electrolytes for LIBs: the *film forming ability.* It is important to remark that such ability is also required for the use of other types of anodic materials, e.g. silicon.

In the past, several types of electrolyte systems, *liquid*, *solid*, and *composite,* have been developed [7]. This work will consider only liquid electrolytes, which are the system of choice in most of the commercial LIBs.

Since the use of only one component does not allow the fulfilment of all the properties mentioned above, the use of multi-component electrolytes is presently the most used and effective strategy for the realization of electrolyte for LIBs [7–15]. For this reason, when talking about electrolytes for LIBs, it would be more appropriate to use the term “electrolyte systems”. In these systems each component fulfils one (or more) of the properties requested for the electrolyte. These components can be divided into three main categories: lithium salt, solvents, and additives (Fig. 2).

The lithium salt is responsible for the transfer of the lithium ions through the electrolyte system between the two electrodes during the charge–discharge processes [6–8, 12]. Lithium hexafluorophosphate ($LiPF_6$) is the salt in state-of-the-art LIBs. This salt is rather thermally and chemically unstable and, in the presence of traces of water, decomposes, generating hydrofluoric acid (HF). In spite of this, the use of $LiPF_6$ in combination with many (organic) solvents allows the realization of electrolytes with high conductivity. Furthermore, $LiPF_6$ displays the ability to form a passive layer on the aluminum current collectors used in the cathode. This layer prevents the occurrence of Al dissolution and, thus, the degradation of the cathode. In the past, several alternative lithium salts have been proposed as a substitute for $LiPF_6$ [6, 7]. Nevertheless, $LiPF_6$ is still the most used salt in LIBs.

In order to realize electrolytic solutions with high conductivity and high salt concentration, mixtures of two or more solvents, typically cyclic and acyclic carbonates, are used [6, 7]. Cyclic carbonates, e.g. EC and propylene carbonate (PC), display high dielectric constant and they are able to dissolve high amount of Li salt. Nevertheless, these solvents are usually quite viscous and, for this reason,

Fig. 2 Electrolytes for lithium-ion batteries: state-of-the-art components and advantages and disadvantages of these systems

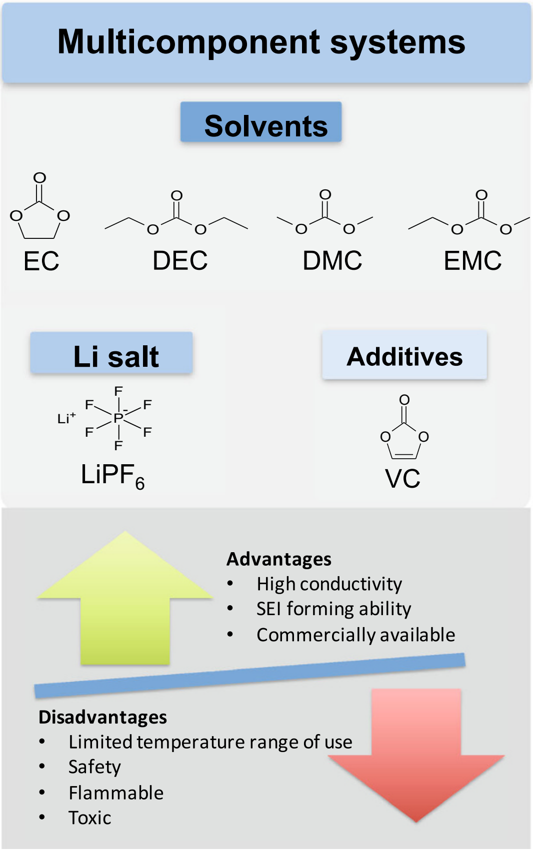

they are used in combination with low viscous acyclic carbonates, e.g. DEC, dimethyl carbonate (DMC), ethyl-methyl carbonate (EMC). However, these acyclic carbonates have the drawback of displaying low flash points (∼15–35 °C) and high vapour pressures.

In order to improve the film-forming ability and the safety of the electrolytes, also additional components are typically added to the lithium salt and the solvents [7]. These components are added in trace amounts (<5%) and for that they are indicated as additives. A widely used additive is the vinylene carbonate (VC), which is used to optimize the SEI formation. VC is consumed within the first cycles and its addition, as those of large part of the additives, does not have a strong impact on the bulk properties of the electrolytes [7, 16].

The state-of-the-art electrolytes display high ionic conductivities and satisfactory film forming ability [6, 7]. However, the properties of the solvents and lithium salts are limiting the safety, as well as the operative temperature range of LIBs [6, 7, 16] (Fig. 2). These drawbacks represent a serious problem for the introduction of these devices in new application, especially in automotive application. Therefore, alternative electrolyte systems with improved safety and the ability to work in a broader operative temperature range are urgently needed [7, 16]. In order to be really effective, however, the introduction of these advanced electrolyte systems should not reduce the battery performance.

3 Ionic Liquids

Ionic liquids (ILs) are molten salts with a melting point below 100 °C [17–19]. They are generally composed of a bulky, asymmetric organic cation and a weakly coordinating inorganic/organic anion. ILs are typically non-flammable, have negligible vapor pressure, and display high chemical and thermal stabilities [17–19]. Moreover, they can also display high ionic conductivity and wide electrochemical stability window (ESW) [17–19]. Because of these properties, ILs are presently considered one of the most interesting class of alternative electrolytes for LIBs and supercapacitors [20, 21].

On the basis of their chemical structure, ILs can be divided in different classes. Among them, two of the most important are the aprotic ionic liquids (AILs) and the protic ionic liquids (PILs) [22]. AILs and PILs share all the above mentioned properties of ILs and the main difference between these two classes of ILs resides on the presence of an "available" (or free) proton on the cation of the PILs (Fig. 3).

In this work the use of both these classes of ILs as electrolytes for LIBs will be considered. Furthermore, also the properties of mixtures of ILs and organic solvents will be analysed. Finally, the interaction between IL-based electrolytes and non-active components will be discussed.

3.1 Aprotic Ionic Liquids As Electrolytes for LIB

The large ESW, the high thermal stability and low vapor pressure of ILs make these class of chemicals very attractive for the realization of electrolytes for LIBs. For more than 10 years, a large number of studies have been dedicated to the use of ILs in LIBs and several types of cations and anions have been used to realize AILs. So far, imidazolium, pyridinium, pyrrolidinium, and piperidinium have been the most investigated cations [23–49]. On the other hand, tetrafluoroborate (BF_4^-), PF_6^- and

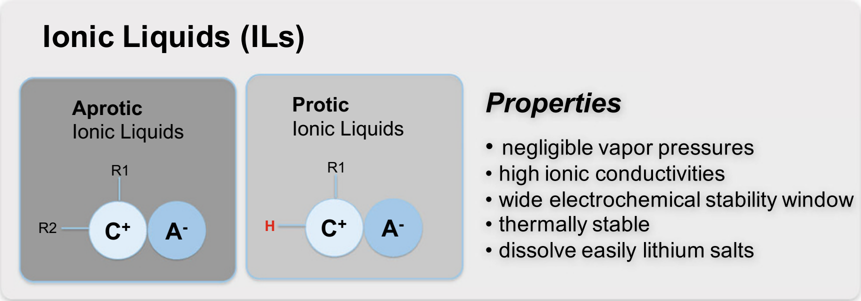

Fig. 3 Classes and properties of ionic liquids

perfluoroalkyl-based anions, such as bis(trifluoromethansulfonyl)imide ($TFSI^-$) and bis(fluorosulfonyl)imide (FSI^-), have been the most used anions (Fig. 4). The combination of these ions leads, in most cases, to the realization of AILs, which are liquids at room temperature (often indicated with the acronym RTILs). In order to realize electrolytes suitable for LIBs these AILs are used in combination with a

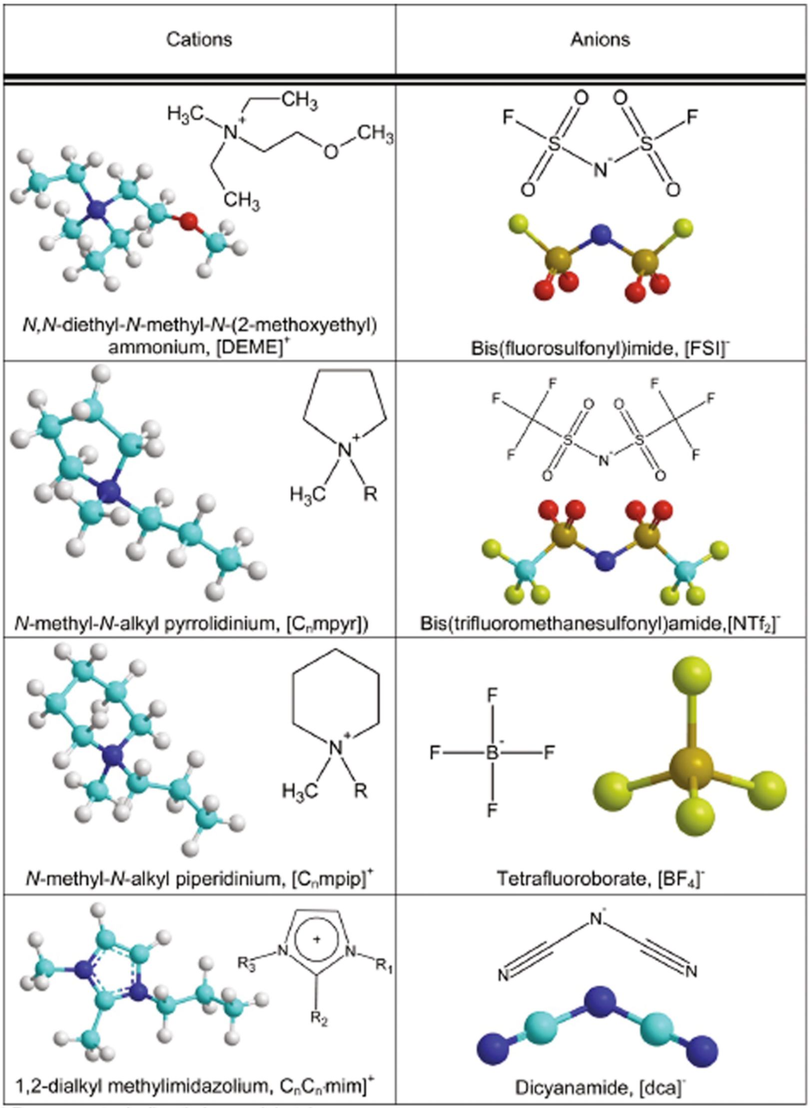

* R groups – typically ethyl, propyl, butyl.

\# this compound (along with many other nitrogen centred anions) is described as an "amide" in the inorganic literature, but incorrectly as an "imide" in the materials and electrochemical literature. FSI should also be described as an amide (ie FSA) but that is so uncommon in this field that we have retained FSI in this article.

Fig. 4 Common ionic liquids ion families utilized in lithium-ion batteries. Taken with permission from MacFarlane et al. [25]

lithium salt. To reduce the complexity of the electrolytic solution, the lithium salt typically contains the same anion of the used AILs. Since no solvent(s) is needed to realize these liquid electrolytic solutions, they are often addressed as “solvent-free” electrolytes [50]. Neverheless, it has to be noticed that many groups criticize this definition and they rather prefer to specify that ILs act both as salt and solvent.

The cation–anion combination has a tremendous impact on the properties of ILs. For example, the use of the imidazolium cations allows the realization of ILs with higher conductivity with respect to the pyrrolidinium and piperidinium cations [16, 46]. On the other hand, the use of these latter cations allows the realization of ILs with large ESW compared to imidazolium [46]. The thermal stability of ILs containing PF_6^- are typically lower than those containing $TFSI^-$ [50]. AILs containing the FSI^- display lower viscosity with respect to the TFSI-based one [36, 50]. Taking into account the features associated to the use of each of these ions, it is evident that one of the great advantages related to the use of IL-based electrolyte is the possibility to design the properties of the electrolyte by changing the cation–anion combination.

An AIL, which has been largely used in the past, is *N*-butyl-*N*-methylpyrrolidinium bis(trifluoromethanesulfonyl)imide ($PYR_{14}TFSI$) [50, 51]. $PYR_{14}TFSI$ is an air-stable, hydrophobic AILs, which displays very good thermal stability (up to 300 °C). At 20 °C it displays conductivity and viscosity of 1.85 $mScm^{-1}$ and 95 mPas, respectively [50, 51]. The overall ESW of this AIL is more than 5.5 V [50, 51]. Passerini and co-workers [27, 28], as well as several other groups [29–31], investigated the use of $PYR_{14}TFSI$ in combination with a variety of cathodic and anodic materials, showing that it is possible to realize IL-based LIBs with high cycling stability. Encouraging results have been obtained also with other AILs, e.g. containing different types of imidazolium cations and $TFSI^-$ anion [46]. In recent years, the use of FSI^- became quite popular as it enables the realization of electrolytes with higher ionic conductivities than those based on $TFSI^-$ and even of PF_6^-. For example, $PYR_{14}FSI$ displays at 20 °C a conductivity on ca. 4 $mScm^{-1}$, which is double of that showed by $PYR_{14}TFSI$ at the same temperature. Nevertheless, the thermal stability of FSI-based ILs appears to be lower than that of TFSI-based ILs [50].

As mentioned in the introduction, a good film-forming ability is required for LIBs electrolytes. For this reason, the film-forming ability of ILs has been considered by several groups, investigating the influence of the cation and the anion on the SEI formation [3–38, 46, 50–52]. It has been shown that while the use of the FSI^- anion makes possible the realization of an effective SEI, $TFSI^-$ does not have this ability (Fig. 5) [37, 38, 52]. The use of the pyrrolidium cations seems to be less favourable compared to the use of the imidazolium cations [46]. Ishikawa and co-workers showed that the use of 1-ethyl-3-methylimidazolium bis(fluorosulfonyl)imide (EMIFSI) can provide a stable, reversible capacity for a graphitized negative electrode without any additives or solvents at ambient temperature [38]. However, for most of the IL-based electrolytes considered in the literature, the use of additives, e.g. VC, appears to be beneficial for the realization of a stable and effective SEI [46, 50–52]. In addition to graphite, IL-based electrolytes have been tested also in combination with other anodic materials, e.g. lithium titanate (LTO),

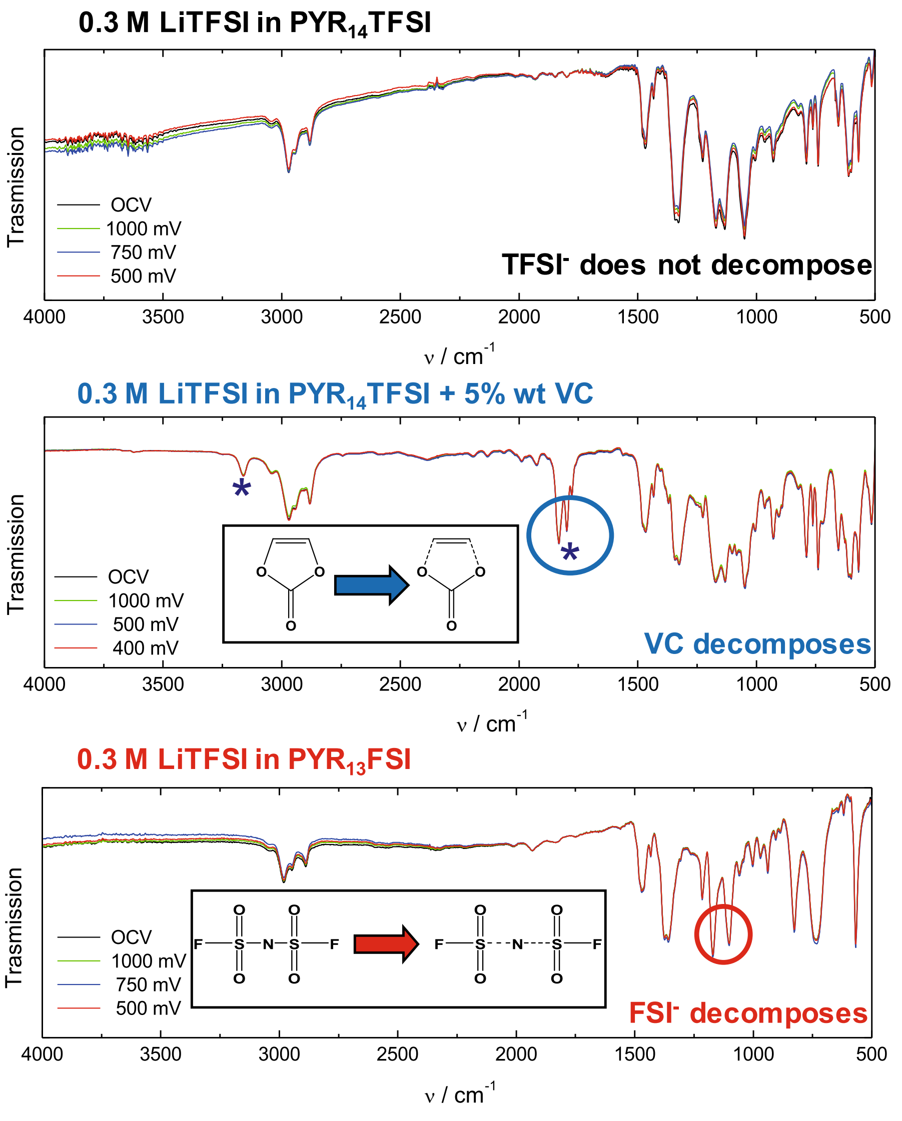

Fig. 5 Comparison of in situ FTIR spectra of pyrrolidinium-based ionic liquids commonly utilized in lithium-ion batteries, namely $PYR_{14}TFSI$ and $PYR_{13}FSI$. As shown, at 500 mv vs. Li/Li^+ the $TFSI^-$ does not decompose, while the FSI^- does. As a consequence, the use of $PYR_{14}TFSI$ in combination with a graphite anode requires the use of an additive, e.g. VC. To the contrary, $PYR_{13}FSI$ can be used without any additive (as it displays film-forming ability)

silicon-based anodes, and conversion electrodes [50–52]. When used in combination with IL-based electrolytes, all these materials display high cycling stability and good performance at low-medium C-rate [46, 50–52].

In recent years also a large number of cathodic materials have been tested in combination with IL-based electrolytes [46, 53, 54]. It has been shown that lithium iron phosphate (LFP), which is one of the most used cathodes in commercial LIBs, display very good affinity for different types of ILs [46, 50, 51]. For example, the specific capacity of LFP-based cathode in $PYR_{14}TFSI$ at low-medium C-rate was found to be comparable with that of conventional electrolytes [50]. The large ESW of AILs make them promising candidates also for the realization of high voltage LIBs. Consequently, several studies focused on the use of high voltage cathodes in combination with these electrolytes [46, 54]. It has been reported that the *N*-methyl-*N*-propylpyrrolidinium bis(trifluoromethylsulfonyl) imide (PMPyrTFSI)/LiTFSI electrolyte has the ability to form a passivation layer on the surface of $LiNi_{0.5}Mn_{1.5}O_4$ electrodes and that its use improves the performance of this material at elevated temperatures (Fig. 6) [54].

One of the main advantages associated with the use of ILs is the high thermal stability of these electrolytes, which has been extensively reported by many authors [46, 50]. Nevertheless, it is important to remark that only a rather limited number of studies investigated the thermal stability of IL-based electrolytes in the presence of charged electrode materials [16]. In a recent review, Kalhoff et al. outlined the influence of the ion composition/selection on this important aspect [16]. The use of pyrrolidinium and piperidinium cation, as well as the use of $TFSI^-$, appears to have a positive influence on the thermal stability of the electrolyte and, thus, on the safety of LIBs. On the other hand, EMI^+ and FSI^-, do not provide this advantage. It has been shown that in the presence of charged electrode materials the stability of electrolytes containing these ions is even lower than that of conventional electrolytes [16].

The performance of IL-based LIBs has been studied by several authors, and in most cases small laboratory cells have been used to carry out these investigations [50]. Nevertheless, also studies dedicated to the performance of LIB prototypes are

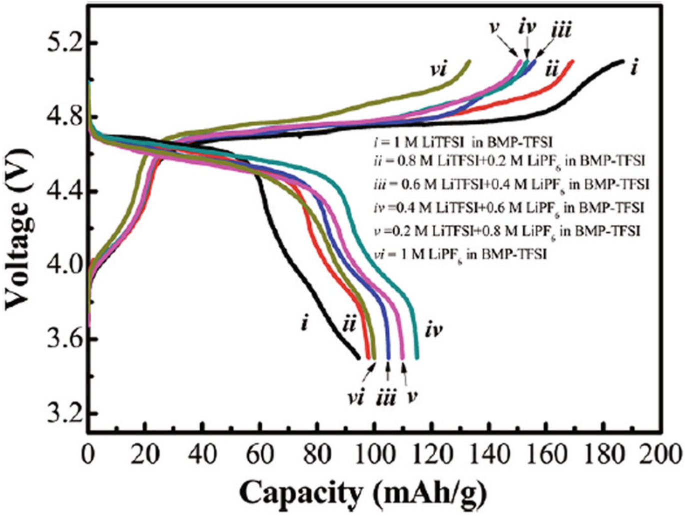

Fig. 6 Voltages profiles of $LiNi_{0.5}Mn_{1.5}O_4$ cathodes in ionic liquid-based electrolytes. The test have been carried out at 0.1 C and at 50 °C. Taken with permission from Wongittharom et al. [54]

available [50–55]. Appetecchi et al. reported on a LIB prototype (0.7 Ah) containing LFP and LTO as anodic and cathodic materials, respectively, and an electrolyte consisting of mixtures of $PYR_{14}FSI$ and LiTFSI. At C/20 the prototype displayed an energy of 80 W h kg^{-1} and 105 W h dm^{-3}, and it was able to retain more than 80% of its initial capacity after 800 cycles [55]. These results indicated that the used cell chemistries are suitable for the realization of batteries with performance approaching that obtained with conventional organic electrolytes (Fig. 7).

Overall, the results obtained with AIL-based electrolytes indicate that this class of electrolytes is a promising alternative to the state-of-the art [46, 50, 55]. The safety and thermal stability of ILs are higher than those of liquids electrolytes containing organic solvents. Their use appears compatible with all cathodic and anodic materials used in LIBs. At low C-rate the performance of IL-based LIBs is

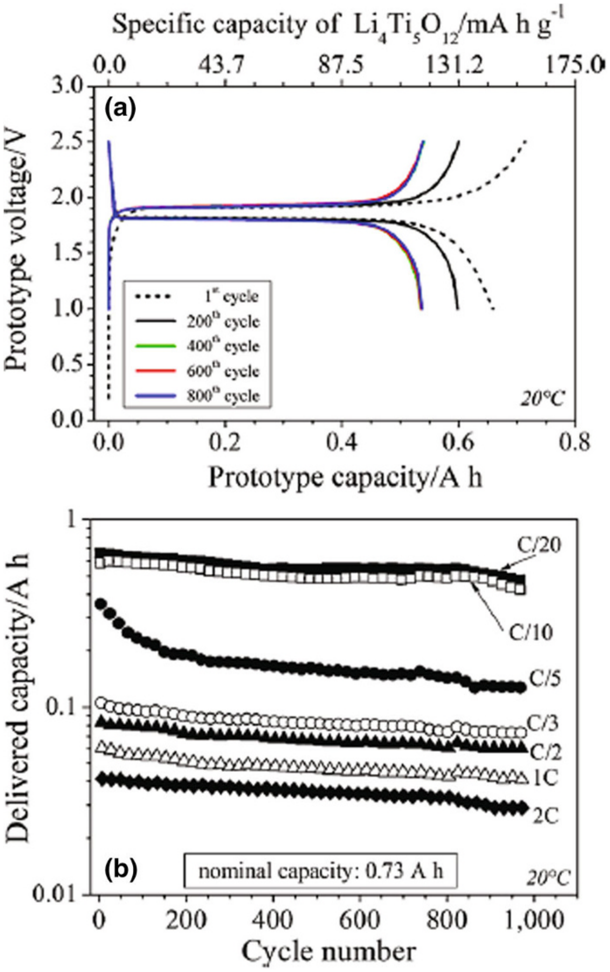

Fig. 7 Electrochemical performance of an ionic liquid-based LTO/LFP LIB prototype at 20 °C. Taken with permission from Kim et al. [55]

comparable with that of conventional electrolytes. However, due to the higher viscosity and reduced lithium diffusivity of ILs compared to organic solvents [16, 50], at high C-rate the performance of IL-based LIBs results lower than that of devices containing the state-of-the-art electrolytes. This latter aspect appears is one of the most serious drawbacks hindering the implementation of ILs in commercial devices. Another aspect that affects the commercialization of IL-based LIB is the cost of these electrolytes, which is higher than that of conventional electrolytes. This higher cost is mainly related to the purification processed needed to reach the purity required for a use in LIBs.

3.2 Protic Ionic Liquids As Electrolytes for LIBs

Protic ionic liquids (PILs) are a subset of ILs, and they are typically synthesized by neutralization reactions of a Brønsted acid (proton donor) and a Brønsted base (proton acceptor) [20, 56]. PILs display all the favorable properties of ILs, but they have the advantage of being easier to synthesize and cheaper compared to AILs. Clearly, these properties make them interesting candidates for use as electrolyte components for electrochemical devices. In the past, PILs have been proposed as electrolytes for fuel cells and supercapacitors [20, 56–62]. In the case of fuel cells, PIL-based electrolytes are considered interesting candidates for non-humidifying intermediate-temperature fuel cells operating at a relatively high temperature [56, 58]. In the case of supercapacitors, it has been shown that the use of PILs allows the realization of devices with stable performance at different temperatures [62]. Nevertheless, PIL-based devices display lower operating voltage compared to that of conventional systems [62].

It is interesting to notice that for very long time the use of PILs as electrolyte components for LIBs was not considered [5, 7, 21]. The availability of an acidic proton and its strong reactivity towards lithium were seen as an obstacle for the introduction of PILs into these devices, and consequently all efforts were focused on AILs. In 2013, Bockenfeld, et al. showed that in dry PILs (with water content lower that 20 ppm) the labile proton of the cation is not "free" and that this cation is not subject to reversible protonation–deprotonation [63]. In this study it was shown that LFP–based electrode can be used in combination with electrolytes containing dry PILs without being subject to structural changes [63]. The performance of an LFP-based cathode in PIL-based electrolytes was promising in terms of both capacity and cycling stability. After this study, Menne et al. reported the first example of PIL-based LIBs [64], demonstrating that also this class of ILs can be successfully introduced in LIBs. The PILs used in this investigation was the triethylammonium bis(tetrafluoromethylsulfonyl) amide ($Et_3NHTFSI$). LFP was used as cathodic active material, while LTO was used as anode. The investigated LIBs was able to deliver capacities comparable with those possible with AIL-based electrolytes and a stable cycling behaviour (Fig. 8).

After these initial studies, the same group investigated in more detail the chemical–physical properties of a series of electrolytes containing pyrrolidinium-based PILs [65]. Specifically, pyrrolidinium bis(trifluoromethanesulfonyl)-imide ($PYR_{HH}TFSI$) and *N*-butylpyrrolidinium bis(trifluoromethanesulfonyl)imide

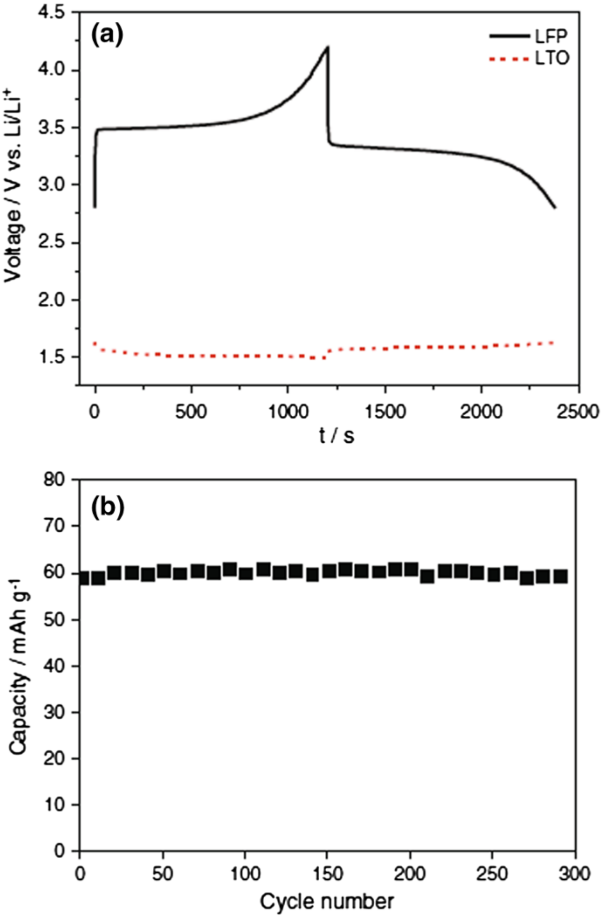

Fig. 8 Voltages profiles (**a**) and cycling stability (**b**) of a LIB containing the protic ionic liquid $Et_3NHTFSI$. Taken with permission from Menne et al. [64]

($PYR_{H4}TFSI$) were used in combination with LiTFSI to realize LIB electrolytes. The viscosity, conductivity, and thermal stability of these two PIL-based electrolytes were investigated and compared to that of the “conventional” $PYR_{14}TFSI$. Furthermore, also the lithium mobility of these PIL-based electrolytes was investigated for the first time. The results of this study showed that the conductivity, viscosity, and lithium-ion self-diffusion coefficient of PIL-based electrolytes are comparable to those of pyrrolidinium-based AILs [65]. Nevertheless, using Raman spectroscopy, the lithium coordination number in PIL-based electrolytes was found to be significantly lower than that of AIL-based electrolytes [66]. This difference was attributed to the different ion–ion interactions occurring in these two types of ILs. In AILs, due to sterical shielding of the ILs cations, the interactions between the cation and the $TFSI^{-}$ anions are very weak [65, 66]. In PILs, on the other hand, the ions of the ILs are interacting due to the less shielded (positive) charge of the cation. When a lithium salt (LiTFSI in the case of this study) is added into an AILs, the $TFSI^-$ ions preferentially coordinate with the lithium ions. When the same salt is added in a PILs, due to the presence of interactions between the cation of the PIL and the anion, the $TFSI^-$ ions are coordinated by both the lithium ions and the cation of the ILs, which are "competing" for the coordination of the $TFSI^-$. It was shown that as a consequence of this ''competition'' between the cation and lithium ions, in the case of equal lithium ion concentration, the coordination number of lithium in PIL-based electrolytes is always lower than that of AIL-based electrolytes [65, 66] (Fig. 9). This lower coordination makes lithium ions more ''free'' to move in PIL-based electrolytes than in AIL-based electrolytes, and has the beneficial effect of reducing the charge transfer resistance associated to the charge–discharge process in the former compared to the latter electrolytes [66]. The reduced charge-transfer resistance at the electrode–electrolyte interface in PIL-based electrolytes allows the realization of

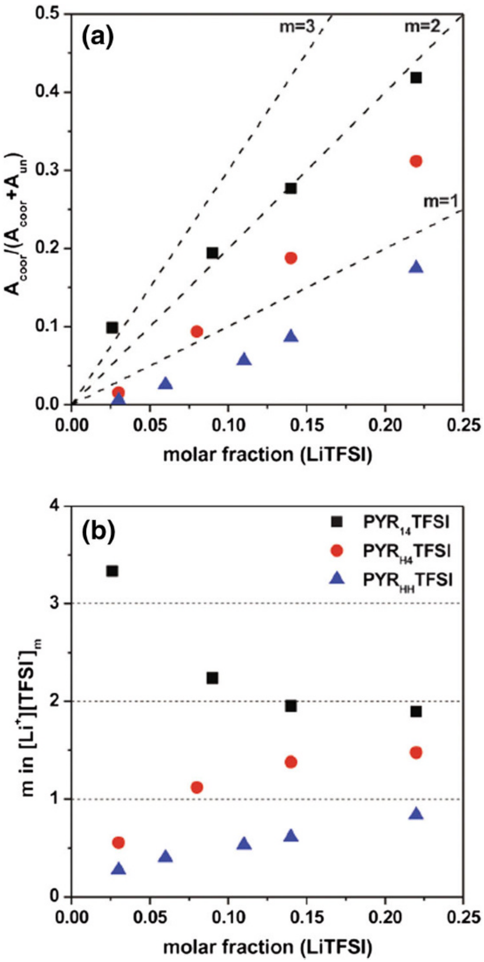

Fig. 9 Comparison of the lithium-ion coordination (by $TFSI^-$) in aprotic and protic ionic liquids electrolytes for lithium-ion batteries. Reproduced from Menne et al. [66] with permission from the PCCP Owner Societies

systems able to display higher performance compared to the classic AILs, especially in term of capacity and capacity retention at high C-rates. Very recently, also the influence of the cation chemistry on the chemical-physical properties of TFSI-based PILs have been investigated [67]. It has been shown that the viscosities, ionic conductivities, and lithium average coordination number of PILs are strongly affected by the characteristics of the cation, e.g. ring size and the alkyl chain length [67]. The results of this study indicated that the design of PILs displaying a right balance in terms of (low) viscosity and (low) average lithium coordination number should be the goal for the realization of advanced PIL-based electrolytes for LIBs [67].

As mentioned in the part dedicated to the AILs, the use of the FSI^- anion appears of great interest as it makes possible the realization of ILs with low viscosity and high conductivity. Menne et al., investigated the use of $PYR_{H4}FSI$ as electrolyte for LIBs [68]. It was shown that this electrolyte displays high conductivity and low viscosity at room and higher temperatures. Interestingly, using this PILs is possible to realize LIBs with performance significantly higher than those containing classical aprotic ionic liquids, e.g. $PYR_{14}FSI$, and close to that of conventional organic electrolytes at room temperature [68] (Fig. 10).

Graphite is the state-of-the-art anode in LIBs and, consequently, also the use of PIL-based electrolytes in combination with this material has been considered [69]. Menne et al. showed that even if the lithium intercalation and de-intercalation process of graphite occurs outside the electrochemical stability window of neat PILs, the addition of film-forming additive makes possible the formation of a stable SEI and, consequently, the use of PIL-based electrolytes in combination with this material. The performance of graphite electrode in PIL-based electrolytes is comparable, and even slightly higher, than that observed in AIL-based electrolytes (Fig. 11).

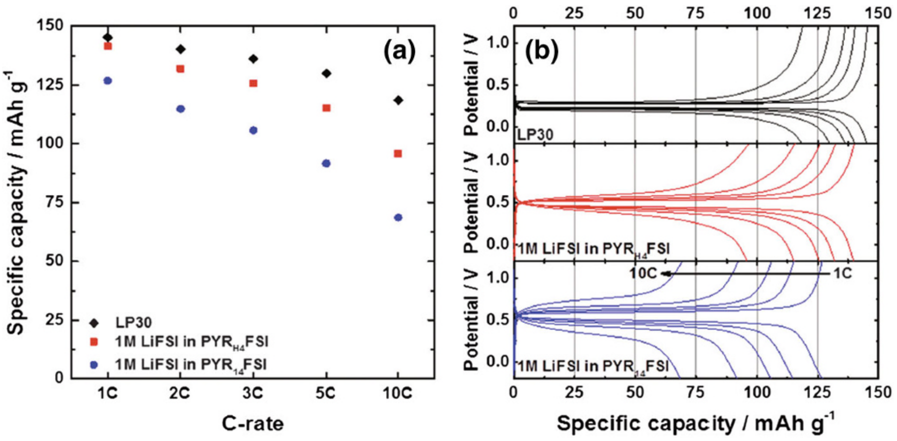

Fig. 10 Specific capacity vs. C-rate (**a**) and corresponding voltage profiles (**b**) of a LIB containing $PYR_{H4}FSI$ as electrolyte. Reproduced from Menne et al. [68] with permission from the Royal Society of Chemistry

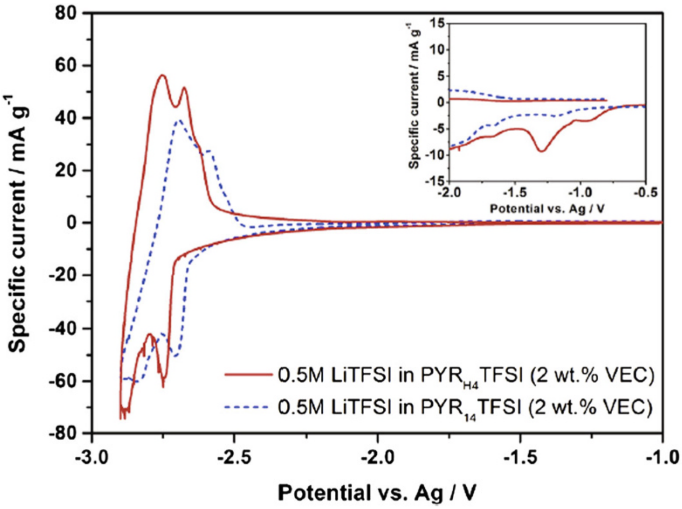

Fig. 11 Comparison of cyclic voltammetry of graphite electrode in aprotic and protic ionic liquids electrolytes. Taken with permission from Menne et al. [69]

Considering the results obtained so far, PILs can be considered a new and interesting class of electrolytes for LIBs. The main advantage related to the use of these electrolytes is the possibility to realize LIBs displaying high performance at high C-rate. Nevertheless, several aspects need to be further investigated in order to better assess the advantages and the limits associated to the use of these ILs. Among them, the safety of these electrolytes as well as the behavior at high/low temperature appear particularly important.

3.3 Mixtures of Ionic Liquids and Organic Solvents As Electrolytes for Lithium-Ion Batteries

As shown in the previous sections, the use of solvent-free electrolytes containing ILs represents a very promising strategy for the realization of safe LIBs. Nevertheless, the overall performance of IL-based LIBs appears still lower than that of systems containing conventional electrolytes. A convenient strategy to overcome this problem is the use of electrolytes based on mixtures of ILs and organic electrolytes [7, 13, 16]. As a matter of fact, a careful selection of the type of ILs, solvent(s) and lithium salt, as well as the ratio between these components, makes possible the realization of electrolytes with tailorable properties. For this reason, the use of these mixtures has become a popular strategy recently.

Guerfi et al. were among the first to investigate the use of this type of mixtures in LIBs [70]. In their work they considered mixtures containing EC, DEC, and EMITFSI. $LiPF_6$ was used as lithium salt. LFP and LTO were used as cathodic and anodic materials, respectively. An optimum range of conductivity and viscosity was observed for electrolytes containing 30–40% of ILs in the organic solvents. The performance of the LIB containing these mixtures was comparable to that of conventional systems, but with the big advantage of displaying an improved safety. In the following years other groups considered the use of EMITFSI in combination with other solvents and lithium salts. For example, Wang et al. investigated the properties of mixtures containing imidazolium-based ILs and PC, showing that also these types of mixtures display appealing features for a use in LIBs [71]. More recently, Wilken et al. reported a detailed study about the chemical-physical properties of mixtures containing EMITFSI, EC, and DEC and the lithium salts LiTFSI and $LiPF_6$ [72]. In this latter study, the influence of the amount of ILs on the viscosity, conductivity, flammability has been considered in detail. Furthermore, the authors supply information also about the Li solvation occurring in these mixtures, showing the influence of the ILs on this key process [72] (Fig. 12).

In recent years, also mixtures containing organic solvents and pyrrolidinium-based ILs have been intensively investigated. Kühnel et al. investigated the chemical-physical properties of electrolytes containing PC, $PYR_{14}TFSI$, and LiTFSI [73]. It was shown that these mixtures might display high conductivities, low viscosities, and overall stability windows of more than 5 V. The flammability of these mixtures could be tuned by changing the amount of ILs present in the electrolyte. For example, a mixture containing 80 wt% ILs (which displays flash point of 153 °C) was non-flammable. Interestingly, it was also found that the presence of ILs reduce the kinetic of PC evaporation as well as the anodic dissolution of Al [73]. The same group investigated also the transport properties and the Li^+ ion solvation in these type of mixtures, showing that the substitution of $PYR_{14}TFSI$ by PC has a strong influence on the mobility, as well as on the lithium coordination [74]. Using an electrolyte containing 0.3 M LiTFSI in PC–$PYR_{14}TFSI$

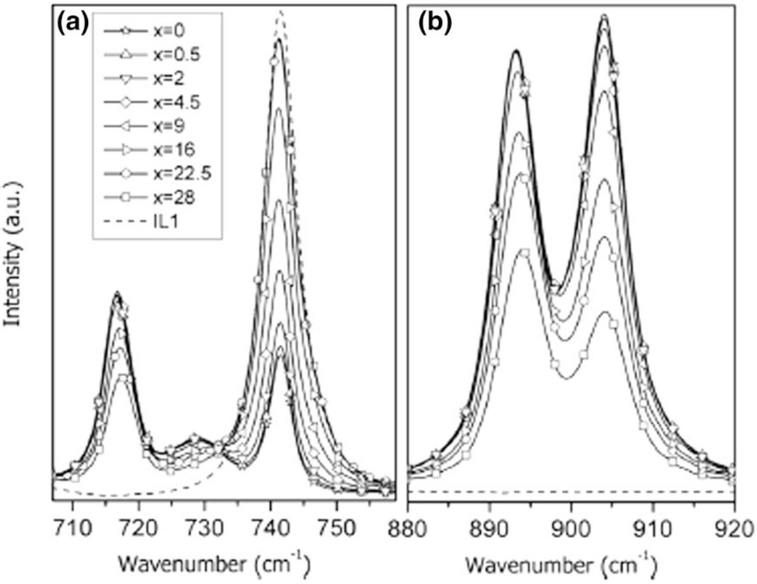

Fig. 12 Comparison of FT-Raman spectra of mixtures of ionic liquid and organic electrolytes. Taken with permission from Wilken et al. [72]

(50:50 wt%), Menne et al. realized a LIBs containing LFP and LTO as the active materials, which was able to display high capacity over 25,000 cycles (Fig. 13). At 60 °C, this IL-based LIBs displayed higher stability with respect to LIBs containing organic solvents and the conventional $LiPF_6$ [75].

As mentioned in the previous section, PILs are emerging as a new and interesting category of electrolytes for LIB. In 2014 Vogl et al. investigated, for the first time, the chemical-physical properties of mixtures containing PC and PILs [76]. This investigation showed that these mixtures might display conductivity and viscosity comparable to those of conventional electrolytes. It was found that, due to the unique ion–ion interaction of PILs, the coordination of lithium ions by $TFSI^-$ in these mixtures is different compared to the one observed for mixtures of PC and AILs [76]. Furthermore, the results of these studies indicate that by using these mixtures it is possible to realize high performance devices containing a limited amount of organic solvent (lower than that needed for solutions containing AILs).

Safety is one of the most crucial aspects that needs to be considered while developing advanced electrolytes for LIBs [1–5]. Since organic solvents are

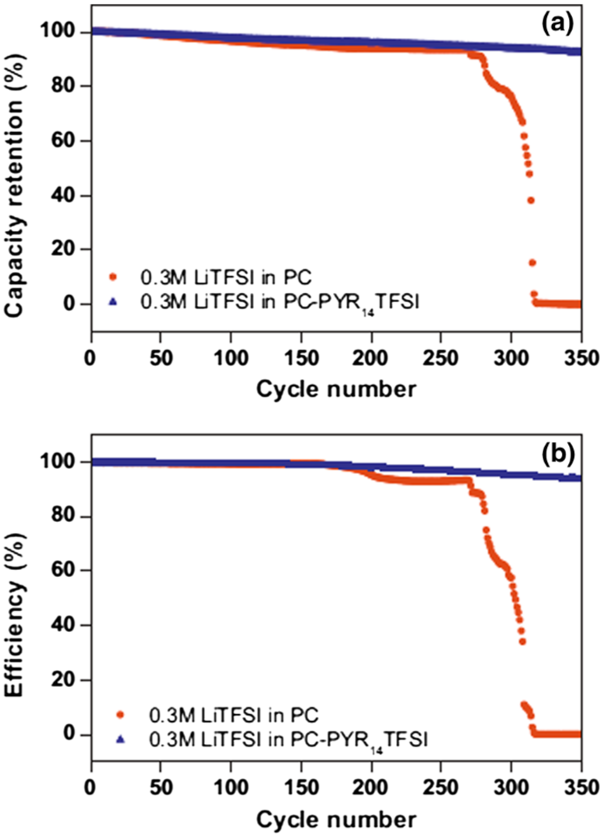

Fig. 13 Comparison of the cycling stability of LIB containing conventional electrolytes and mixture of ionic liquid and organic solvents. Taken with permission from Menne et al. [75]

flammable, the investigation of the flammability of mixtures of ILs and organic solvents appears to be of importance to understand the advantages and limits related to the use of these electrolytes. Arbizzani et al. investigated the flammability of mixtures containing EC, DMC, $LiPF_6$, and $PYR_{14}TFSI$ [77]. It was found that the flammability of these electrolytes was strongly dependent on the amount of ILs: The higher the IL content, the lower was the flammability, and the solution containing 50% of ILs displayed very low tendency to ignite [77]. Interestingly, it was also found that the ILs acted as retardant rather than a flame-inhibitor (Fig. 14). Analogous observations have been reported by Montanino et al. for mixtures consisting of EC, DEC, LiTFSI, and $PYR_{13}TFSI$ [78]. Also, in this case, it was found that electrolytes containing organic solvents up to a mole fraction of 0.3 were not flammable even in intimate contact with ignition sources [78].

The use of mixtures of ILs and organic solvents in combination with graphite based electrodes has been investigated by Gao et al. [79]. In this study a

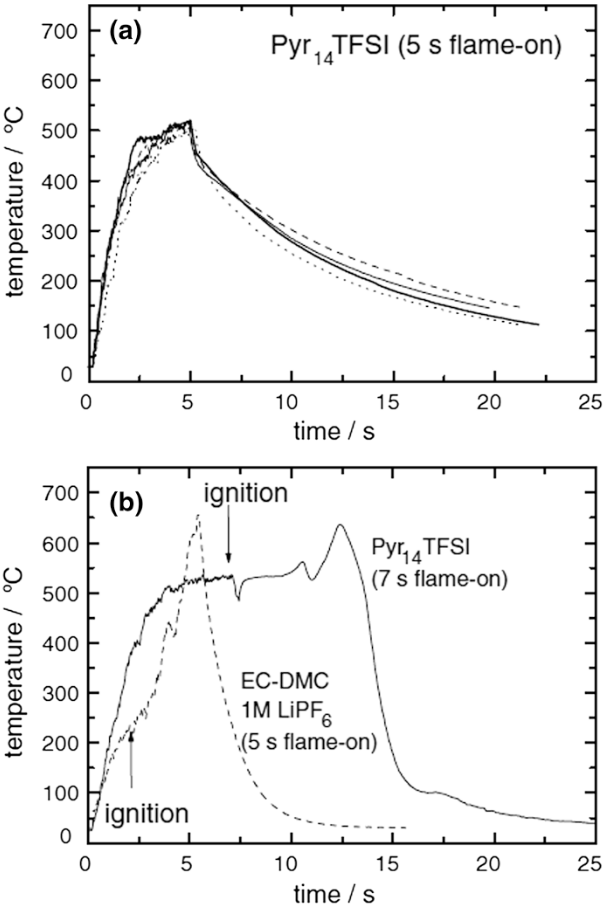

Fig. 14 Comparison of flammability and ignition time of neat ionic liquids and conventional electrolytes for lithium-ion batteries. Taken with permission from Arbizzani et al. [77]

pipiridinium-based IL ($PP_{13}TFSI$) was used in combination with EC and DEC. Because of the occurrence of co-intercalation of the ILs cation into the graphite layers, the use of neat ILs was not possible. However, the addition of the organic solvents made possible the formation of a stable SEI, allowing the achievement of good performance in terms of both capacity and cycling stability [79].

In 2013, the group of Rochefort proposed the use of mixtures of redox ILs (1-ferrocenyl(methyl)-3-methylimidazolium TFSI) in combination with carbonate solvents for the realization of innovative redox shuttle for LIBs [80]. The use of redox shuttle is considered a good strategy to minimize the risk of overcharge in LIBs [2, 6]. Because of the high miscibility of the redox moieties components on these mixtures, it was possible to realize an electrolyte with a high content of these moieties. This high content in turn made possible the shuttling of a higher number of electrons through the overcharge condition than in the case of conventional electrolytes [80]. Thus, the use of redox ILs could be used to improve overcharge protection, especially at high rates of charge (Fig. 15).

The possibility to realize and use mixtures containing very high content of ILs was explored by Armand and coworkers [81], who indicated these mixtures as “Solvent-in-Salt’ electrolytes. The electrolytes investigated in this work contained ultrahigh salt concentration and displayed high lithium ion transference number (0.73) thanks to the contribution of the salt to the lithium ion transport [81]. The interest on these electrolytes in now significantly growing and, very likely, many publications will be dedicated to this subject in the near future.

As shown above, the main advantages related to the use of mixtures of organic solvents and ILs is the possibility to realize electrolytes with tailored properties. It is important to underline that the optimum ratio organic solvent(s)/ILs depends on the

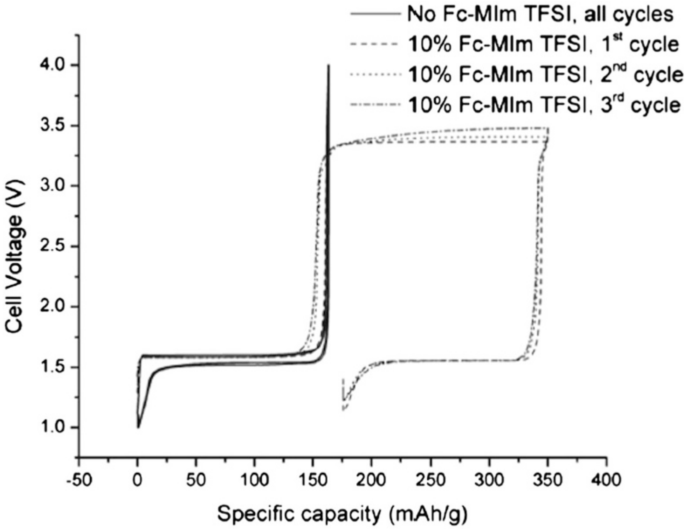

Fig. 15 Example of redox shuttle electrolytes for LIB containing redox active ionic liquids. Taken with permission from Forgie et al. [80]

targeted application. In general, the use of these mixtures appears extremely convenient as it makes possible the realization of an electrolytic solutions with properties close to that of conventional electrolytes, but with improved safety. However, a deeper understanding of the chemical-physical properties of these mixtures appears of importance. The lithium coordination, the interaction between ILs and solvents/salt are some of the aspects, which need to be better understood, since they would make possible a more rational design of these promising electrolytes.

3.4 Ionic Liquids-Based Electrolytes and Inactive Components: the Case of Anodic Dissolution of Aluminum

In addition to the lithium ions insertion-extraction into/from the electrodes, there are a number of processes that might affect the performance of LIBs [2, 6]. Among them, the anodic dissolution of the Al current collector used for the cathode of LIBs might become one of the most detrimental for the life of these devices.

In order to use Al current collector in LIBs, the formation a protective (passive) layer on the surface of this metal in needed [2, 6, 7]. As a matter of fact, without the presence of this layer the current collector would dissolve, making the LIBs unusable. As mentioned in the section dedicated to the state-of-the-art electrolytes, although $LiPF_6$ display a number of drawbacks, its use in combination with organic solvent makes possible the realization of high conductive electrolyte. Furthermore, this salt displays the ability to form an effective SEI and to prevent the anodic dissolution of Al and has positive influence on the stability of some cathodic materials. For these reasons $LiPF_6$ is still the state-of-the art lithium salt [2, 6, 7].

The salt LiTFSI, which has been used in many of the electrolytes considered in previous sections, displays a number of promising properties, e.g. high chemical and thermal stability. Nevertheless, the use of LiTFSI in combination with organic solvents does not allow the formation of an effective protective layer on the Al surface, causing anodic dissolution of this metal [2, 6, 7, 9]. This drawback hinders the introduction of LiTFSI in commercial devices.

For several years, the anion $TFSI^-$ is one of the most used for the realization of AIL and PILs. Consequently, the investigation of the anodic dissolution in ILs containing this anion appears to be of great importance in view of their introduction in LIBs. Garcia et al. [82] were the first to report about this process. Interestingly, they observed that in IL-based electrolytes containing LiTFSI the anodic dissolution of Al was suppressed. In the following years, similar observations have been made by several groups [16, 72, 73].

Wang et al. proposed a mechanism of Al dissolution in LiTFSI-based electrolytes involving the formation of Al-TFSI complexes on the Al foil surface [83]. In this model the protection of the Al surface strongly depends on the solubility of these Al-TFSI complexes. In the case where they are easily soluble in the electrolyte solution, these complexes will move away from the Al surface and, consequently, they will not be able to protect this metal from the occurrence of anodic dissolution. To the contrary, if the Al-TFSI complexes are hardly soluble in the electrolyte, they stay on the Al surface, suppressing the anodic dissolution of Al.

In order to confirm this model and to understand the behavior of TFSI-based electrolytes, Kühnel et al. investigated the solubility of the complexes $Al(TFSI)_3$ in PC, in $PYR_{14}TFSI$ and in mixtures containing PC and $PYR_{14}TFSI$. In all these electrolytes, LiTFSI was used as salt [84]. Indeed, the results of this investigation confirmed that solubility of $Al(TFSI)_3$ on the electrolyte plays a key role on the anodic dissolution and that this complex is hardly soluble in this IL. This study also showed that mixtures of ILs and organic solvents might also display the ability to prevent the anodic dissolution of Al [84] (Fig. 16).

After these initial works, other groups investigated in detail the Al anodic dissolution occurring in IL-based electrolytes [85–88]. Hofmann et al. considered the conducting salt lithium bis(trifluoromethanesulfonyl)azanide (LiTFSA) in combination with PC, sulfolane, and the ionic liquid *N*,*N*-diethyl-*N*-methyl-*N*-(2-methoxyethyl)ammonium bis(trifluoromethanesulfonyl)azanide (DMMATFSA) [85]. This systematic investigation showed that the concentration of the salt, as well as the composition of the solvent mixture, are strongly influencing the Al anodic dissolution process. From this study it appears the Al dissolution might be repressed using highly concentrated LiTFSA solutions and also by adding the ionic liquid to the organic solvents. In another work, the same group considered mixtures of PC and DMMATFSA and investigated the influence of different types of lithium salts on the Al anodic dissolution, showing the great impact of this component on such a process [86]. In recent years, several works have been dedicated to this topic, and many types of ILs and organic solvents have been considered [87–91]. Overall, these results indicate that ILs have a strong influence on the anodic dissolution of Al and that their presence in an electrolytic solution might suppress such a process.

These studies outline the importance of a rational design of advanced electrolyte for LIBs. The use of ILs might be advantageous not only because it might improve the safety of the electrolytes, but also because it might suppress unwanted process, e.g. Al anodic dissolution, which occur in this system and, consequently, improve the overall LIBs performance. In this sense, these investigations represent an important contribution toward the introduction of ILs in commercial devices.

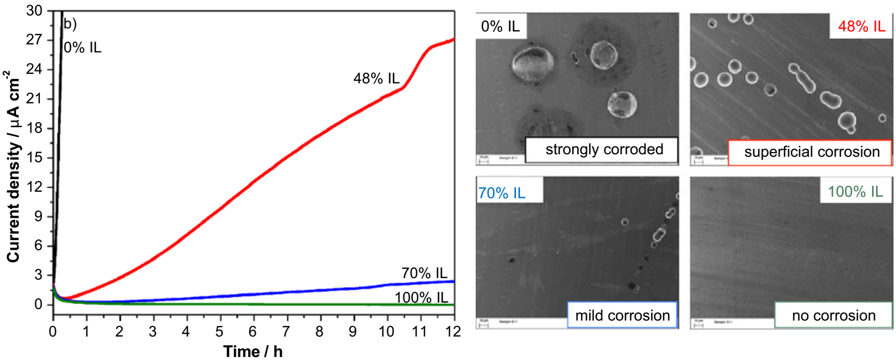

Fig. 16 Influence of ionic liquids on the Al anodic dissolution process

4 Conclusions

ILs are promising electrolytes for LIBs. The large ESW, high thermal stability, and low flammability of ILs positively affect the properties of LIBs electrolytes. It has been shown that these electrolytes can be conveniently used with all active materials suitable for LIBs and that at low C-rate the performance of IL-based LIBs is comparable with that of conventional devices. Nevertheless, due to the high viscosity and relative low lithium mobility displayed by most of the IL-based electrolytes [7, 72, 73, 92], the performance of IL-based LIBs at high C-rate appears still not fully comparable with that of devices containing conventional electrolytes. Additionally, the cost of ILs should be reduced as it too high with respect to the conventional electrolytes.

In this scenario, the design of new IL-based electrolytes appears as the most convenient strategy to overcome these drawbacks. In the future new anions and cations should be considered for the realization of AILs with tailored properties. While at the beginning of the studies dedicated to IL-based electrolytes many ions have been proposed, in recent years the number of new ions decreased considerably. Nevertheless, taking into account the enormous number of possible ILs, there is still the possibility to introduce new ion chemistries in this field. For that, the search of new ions should be “relaunched”. An appealing and effective strategy to carry out this search appears to be the use of computational screening [93–97]. As for other field, e.g. pharmaceutical chemistry, the use of this strategy could contribute to minimize and rationalize the time of this important search.

The results obtained with PIL-based electrolytes are very encouraging. Nevertheless, several aspects related to the use of these innovative electrolytes need to be further investigated. So far, the behaviour at high/low temperature of PIL-based LIBs has not been investigated. Since to extend the operative temperature range of LIBs is one of the priority for this technology, it is evident that this is a very important point that needs to be addressed. The influence of the protonated cation of the SEI formation, as well as on the stability of carbonaceous anodes is another aspect, which should be addressed. So far, there are indications that PILs can be used in combination with graphite, but the influence of these ILs on the lithium insertion/extraction process is not known. Finally, it has been shown that PILs display thermal stability comparable to that of AILs. Nevertheless, no studies about the stability of charged electrodes in contact with PILs are available. These studies are needed to assess the impact of these electrolytes on the safety of LIBs.

The use of ILs in combination with organic electrolytes is certainly an interesting strategy in view of the design of advanced electrolytes. In the past, several studies focused on the impact of these electrolytes on the performance and on the safety, especially in term of flammability, of LIBs. A significantly lower number of studies addressed the IL-solvent interactions. Nevertheless, the understanding of these interactions could give valuable input for a rational design of these electrolytes. For that, this latter investigation appears of great importance. In recent years a growing number of studies showed that ILs can be advantageously used to prevent undesired reactions, e.g. Al anodic dissolution, or to improve the properties of additives, e.g.

redox shuttle. The use of ILs as an additive in conventional LIBs electrolytes appears, therefore, very interesting, and further investigations about this use of ILs should be made in the near future.

Acknowledgements The authors wish to thank the Deutsche Forschungsgemeinschaft (DFG) within the project "Protic ionic liquids as electrolytes for lithium-ion batteries" and the Friedrich-Schiller University Jena for the financial support. The author wish also to thank Dr. Ruben-Simon Kühnel, Dr. Sebastian Menne, Dr. Thomas Vogl for the work carried out in the last years on IL-based electrolytes.

References

1. Armand M, Tarascon JM (2008) Building better batteries. Nature 451(7179):652–657
2. Scrosati B, Garche J (2010) Lithium batteries: status, prospects and future. J Power Sources 195(9):2419–2430
3. Scrosati B, Hassoun J, Sun Y-K (2011) Lithium-ion batteries. A look into the future. Energy Environ Sci 4(9):3287–3295
4. Dunn B, Kamath H, Tarascon J-M (2011) Electrical energy storage for the grid: A battery of choices. Science 334(6058):928–935
5. Thackeray MM, Wolverton C, Isaacs ED (2012) Electrical energy storage for transportation—approaching the limits of, and going beyond, lithium-ion batteries. Energy Environ Sci 5(7):7854–7863
6. Scrosati B, Abraham K, van Schalkwijk WA, Hassoun J (2013) Lithium batteries: Advanced technologies and applications, vol 58. Wiley, New Jersey
7. Lex-Balducci A, Henderson W, Passerini S, Yuan X, Liu H, Zhang J (2011) Lithium-ion batteries: Advanced materials and technologies. CRC Press, Boca Raton, pp 147–197
8. Winter M, Besenhard JO, Spahr ME, Novák P (1998) Insertion electrode materials for rechargeable lithium batteries. Adv Mater 10(10):725–763
9. Xu K (2004) Nonaqueous liquid electrolytes for lithium-based rechargeable batteries. Chem Rev 104(10):4303–4418
10. Nishi Y (2001) The development of lithium ion secondary batteries. Chem Rec 1(5):406–413
11. Nishi Y (2001) Lithium ion secondary batteries; past 10 years and the future. J Power Sources 100(1):101–106
12. Peled E (1979) The electrochemical behavior of alkali and alkaline earth metals in nonaqueous battery systems—the solid electrolyte interphase model. J Electrochem Soc 126(12):2047–2051
13. Bresser D, Paillard E, Passerini S, Menictas C, Skyllas-Kazacos M, Lim TM (2014) Advances in batteries for medium and large-scale energy storage: Types and applications. Elsevier, Amsterdam
14. Agubra VA, Fergus JW (2014) The formation and stability of the solid electrolyte interface on the graphite anode. J Power Sources 268:153–162
15. Hammami A, Raymond N, Armand M (2003) Lithium-ion batteries: Runaway risk of forming toxic compounds. Nature 424(6949):635–636
16. Kalhoff J, Eshetu GG, Bresser D, Passerini S (2015) Safer electrolytes for lithium-ion batteries: State of the art and perspectives. ChemSusChem 8(13):2154–2175
17. Johnson KE (2007) What's an ionic liquid? Interface Electrochem Soc 16(1):38–41
18. Wasserscheid P, Welton T (2008) Ionic liquids in synthesis, vol 1. Wiley, New Jersey
19. Kirchner B, di Dio PJ, Hutter J (2011) Real-world predictions from ab initio molecular dynamics simulations. Multiscale molecular methods in applied chemistry. Springer, New York, pp 109–153
20. Angell CA, Byrne N, Belieres JP (2007) Parallel developments in aprotic and protic ionic liquids: Physical chemistry and applications. Acc Chem Res 40(11):1228–1236
21. Armand M, Endres F, MacFarlane DR, Ohno H, Scrosati B (2009) Ionic-liquid materials for the electrochemical challenges of the future. Nat Mater 8(8):621–629
22. Eshetu GG, Grugeon S, Laruelle S, Boyanov S, Lecocq A, Bertrand J-P, Marlair G (2013) In-depth safety-focused analysis of solvents used in electrolytes for large scale lithium ion batteries. Phys Chem Chem Phys 15(23):9145–9155
23. Kubota K, Nohira T, Hagiwara R, Matsumoto H (2010) Thermal properties of alkali (fluorosulfonyl)(trifluoromethylsulfonyl) amides. Chem Lett 39(12):1303–1304

24. Weingärtner H (2008) Understanding ionic liquids at the molecular level: facts, problems, and controversies. Angew Chem Int Ed 47(4):654–670
25. MacFarlane DR, Tachikawa N, Forsyth M, Pringle JM, Howlett PC, Elliott GD, Davis JH, Watanabe M, Simon P, Angell CA (2014) Energy applications of ionic liquids. Energy Environ Sci 7(1):232–250
26. Navarra MA (2013) Ionic liquids as safe electrolyte components for Li-metal and Li-ion batteries. MRS Bull 38(07):548–553
27. Shin J-H, Henderson WA, Passerini S (2003) Ionic liquids to the rescue? Overcoming the ionic conductivity limitations of polymer electrolytes. Electrochem Commun 5(12):1016–1020
28. Shin J-H, Henderson WA, Passerini S (2005) An elegant fix for polymer electrolytes. Electrochem Solid State Lett 8(2):A125–A127
29. Sun J, Forsyth M, MacFarlane D (1998) Room-temperature molten salts based on the quaternary ammonium ion. J Phys Chem B 102(44):8858–8864
30. Howlett PC, MacFarlane DR, Hollenkamp AF (2004) High lithium metal cycling efficiency in a room-temperature ionic liquid. Electrochem Solid State Lett 7(5):A97–A101
31. Zhou ZB, Matsumoto H, Tatsumi K (2006) Cyclic quaternary ammonium ionic liquids with perfluoroalkyltrifluoroborates: synthesis, characterization, and properties. Chem A Eur J 12(8):2196–2212
32. Egashira M, Tanaka-Nakagawa M, Watanabe I, Okada S, J-i Yamaki (2006) Charge–discharge and high temperature reaction of LiCoO 2 in ionic liquid electrolytes based on cyano-substituted quaternary ammonium cation. J Power Sources 160(2):1387–1390
33. Balakrishnan P, Ramesh R, Kumar TP (2006) Safety mechanisms in lithium-ion batteries. J Power Sources 155(2):401–414
34. Sakaebe H, Matsumoto H, Tatsumi K (2007) Application of room temperature ionic liquids to Li batteries. Electrochim Acta 53(3):1048–1054
35. Wang Y, Zaghib K, Guerfi A, Bazito FF, Torresi RM, Dahn J (2007) Accelerating rate calorimetry studies of the reactions between ionic liquids and charged lithium ion battery electrode materials. Electrochim Acta 52(22):6346–6352
36. Ishikawa M, Sugimoto T, Kikuta M, Ishiko E, Kono M (2006) Pure ionic liquid electrolytes compatible with a graphitized carbon negative electrode in rechargeable lithium-ion batteries. J Power Sources 162(1):658–662
37. Appetecchi GB, Montanino M, Balducci A, Lux SF, Winterb M, Passerini S (2009) Lithium insertion in graphite from ternary ionic liquid-lithium salt electrolytes: I. Electrochemical characterization of the electrolytes. J Power Sources 192(2):599–605
38. Lux SF, Schmuck M, Appetecchi GB, Passerini S, Winter M, Balducci A (2009) Lithium insertion in graphite from ternary ionic liquid–lithium salt electrolytes: II. Evaluation of specific capacity and cycling efficiency and stability at room temperature. J Power Sources 192(2):606–611
39. Montanino M, Moreno M, Alessandrini F, Appetecchi G, Passerini S, Zhou Q, Henderson W (2012) Physical and electrochemical properties of binary ionic liquid mixtures: (1 − x) PYR 14 TFSI–(x) PYR 14 IM 14. Electrochim Acta 60:163–169
40. Kunze M, Jeong S, Appetecchi GB, Schönhoff M, Winter M, Passerini S (2012) Mixtures of ionic liquids for low temperature electrolytes. Electrochim Acta 82:69–74
41. Holzapfel M, Jost C, Novák P (2004) Stable cycling of graphite in an ionic liquid based electrolyte. Chem Commun 18:2098–2099
42. Holzapfel M, Jost C, Prodi-Schwab A, Krumeich F, Würsig A, Buqa H, Novak P (2005) Stabilisation of lithiated graphite in an electrolyte based on ionic liquids: an electrochemical and scanning electron microscopy study. Carbon 43(7):1488–1498
43. Zheng H, Jiang K, Abe T, Ogumi Z (2006) Electrochemical intercalation of lithium into a natural graphite anode in quaternary ammonium-based ionic liquid electrolytes. Carbon 44(2):203–210
44. Lewandowski A, Świderska-Mocek A (2007) Properties of the graphite-lithium anode in N-methyl-N-propylpiperidinium bis (trifluoromethanesulfonyl) imide as an electrolyte. J Power Sources 171(2):938–943
45. Bayley PM, Lane GH, Rocher NM, Clare BR, Best AS, MacFarlane DR, Forsyth M (2009) Transport properties of ionic liquid electrolytes with organic diluents. Phys Chem Chem Phys 11(33):7202–7208
46. Lewandowski A, Świderska-Mocek A (2009) Ionic liquids as electrolytes for Li-ion batteries—an overview of electrochemical studies. J Power Sources 194(2):601–609

47. Han H-B, Liu K, Zhou S-S, Feng S-W, Nie J, Li H, Huang X-J, Armand M, Zhou Z (2010). ECS Meeting Abstracts 2010 MA2010-02
48. Liu K, Zhou Y-X, Han H-B, Zhou S-S, Feng W-F, Nie J, Li H, Huang X-J, Armand M, Zhou Z-B (2010) Ionic liquids based on (fluorosulfonyl)(pentafluoroethanesulfonyl) imide with various oniums. Electrochim Acta 55(23):7145–7151
49. Reiter J, Jeremias S, Paillard E, Winter M, Passerini S (2013) Fluorosulfonyl-(trifluoromethanesulfonyl) imide ionic liquids with enhanced asymmetry. Phys Chem Chem Phys 15(7):2565–2571
50. Balducci A, Jeong S, Kim G, Passerini S, Winter M, Schmuck M, Appetecchi G, Marcilla R, Mecerreyes D, Barsukov V (2011) Development of safe, green and high performance ionic liquids-based batteries (ILLIBATT project). J Power Sources 196(22):9719–9730
51. Lux SF, Schmuck M, Jeong S, Passerini S, Winter M, Balducci A (2010) Li-ion anodes in air-stable and hydrophobic ionic liquid-based electrolyte for safer and greener batteries. Int J Energy Res 34(2):97–106
52. Balducci A, Schmuck M, Kern W, Rupp B, Passerini S, Winter M (2008) Ionic liquids as electrolyte in lithium batteries: In situ FTIRS studies on the use of electrolyte additives. ECS Trans 11(29):109–114
53. Srour H, Chancelier L, Bolimowska E, Gutel T, Mailley S, Rouault H, Santini CC (2016) Ionic liquid-based electrolytes for lithium-ion batteries: review of performances of various electrode systems. J Appl Electrochem 46(2):149–155
54. Wongittharom N, Lee T-C, Hung I-M, Lee S-W, Wang Y-C, Chang J-K (2014) Ionic liquid electrolytes for high-voltage rechargeable Li/LiNi 0.5 Mn 1.5 O 4 cells. J Mater Chem A 2(10):3613–3620
55. Kim G-T, Jeong S, Xue M-Z, Balducci A, Winter M, Passerini S, Alessandrini F, Appetecchi G (2012) Development of ionic liquid-based lithium battery prototypes. J Power Sources 199:239–246
56. Angell CA, Ansari Y, Zhao Z (2012) Ionic liquids: past, present and future. Faraday Discuss 154:9–27
57. Anouti M, Caillon-Caravanier M, Dridi Y, Galiano H, Lemordant D (2008) Synthesis and characterization of new pyrrolidinium based protic ionic liquids. Good and superionic liquids. J Phys Chem B 112(42):13335–13343
58. Matsuoka H, Nakamoto H, Susan MABH, Watanabe M (2005) Brønsted acid–base and–polybase complexes as electrolytes for fuel cells under non-humidifying conditions. Electrochim Acta 50(19):4015–4021
59. Mayrand-Provencher L, Lin S, Lazzerini D, Rochefort D (2010) Pyridinium-based protic ionic liquids as electrolytes for RuO 2 electrochemical capacitors. J Power Sources 195(15):5114–5121
60. Timperman L, Skowron P, Boisset A, Galiano H, Lemordant D, Frackowiak E, Béguin F, Anouti M (2012) Triethylammonium bis (tetrafluoromethylsulfonyl) amide protic ionic liquid as an electrolyte for electrical double-layer capacitors. Phys Chem Chem Phys 14(22):8199–8207
61. Timperman L, Galiano H, Lemordant D, Anouti M (2011) Phosphonium-based protic ionic liquid as electrolyte for carbon-based supercapacitors. Electrochem Commun 13(10):1112–1115
62. Brandt A, Pires J, Anouti M, Balducci A (2013) An investigation about the cycling stability of supercapacitors containing protic ionic liquids as electrolyte components. Electrochimica Acta 108:226–231
63. Böckenfeld N, Willeke M, Pires J, Anouti M, Balducci A (2013) On the use of lithium iron phosphate in combination with protic ionic liquid-based electrolytes. J Electrochem Soc 160(4):A559–A563
64. Menne S, Pires J, Anouti M, Balducci A (2013) Protic ionic liquids as electrolytes for lithium-ion batteries. Electrochem Commun 31:39–41
65. Vogl T, Menne S, Kühnel R-S, Balducci A (2014) The beneficial effect of protic ionic liquids on the lithium environment in electrolytes for battery applications. J Mater Chem A 2(22):8258–8265
66. Menne S, Vogl T, Balducci A (2014) Lithium coordination in protic ionic liquids. Phys Chem Chem Phys 16(12):5485–5489
67. Vogl T, Goodrich P, Jacquemin J, Passerini S, Balducci A (2016) The influence of cation structure on the chemical-physical properties of protic ionic liquids. J Phys Chem C 120(16):8525–8533
68. Menne S, Vogl T, Balducci A (2015) The synthesis and electrochemical characterization of bis (fluorosulfonyl) imide-based protic ionic liquids. Chem Commun 51(17):3656–3659
69. Menne S, Schroeder M, Vogl T, Balducci A (2014) Carbonaceous anodes for lithium-ion batteries in combination with protic ionic liquids-based electrolytes. J Power Sources 266:208–212

70. Guerfi A, Dontigny M, Charest P, Petitclerc M, Lagacé M, Vijh A, Zaghib K (2010) Improved electrolytes for Li-ion batteries: Mixtures of ionic liquid and organic electrolyte with enhanced safety and electrochemical performance. J Power Sources 195(3):845–852
71. Wang M, Shan Z, Tian J, Yang K, Liu X, Liu H, Zhu K (2013) Mixtures of unsaturated imidazolium based ionic liquid and organic carbonate as electrolyte for Li-ion batteries. Electrochim Acta 95:301–307
72. Wilken S, Xiong S, Scheers J, Jacobsson P, Johansson P (2015) Erratum to" Ionic liquids in lithium battery electrolytes: Composition versus safety and physical properties" [J Power Sources 275 (2015) 935–942]. J Power Sources 283:531
73. Kühnel R-S, Böckenfeld N, Passerini S, Winter M, Balducci A (2011) Mixtures of ionic liquid and organic carbonate as electrolyte with improved safety and performance for rechargeable lithium batteries. Electrochim Acta 56(11):4092–4099
74. Kühnel R-S, Balducci A (2014) Lithium ion transport and solvation in *N*-butyl-*N*-methylpyrrolidinium bis (trifluoromethanesulfonyl) imide–propylene carbonate mixtures. J Phys Chem C 118(11):5742–5748
75. Menne S, Kühnel R-S, Balducci A (2013) The influence of the electrochemical and thermal stability of mixtures of ionic liquid and organic carbonate on the performance of high power lithium-ion batteries. Electrochim Acta 90:641–648
76. Vogl T, Menne S, Balducci A (2014) Mixtures of protic ionic liquids and propylene carbonate as advanced electrolytes for lithium-ion batteries. Phys Chem Chem Phys 16(45):25014–25023
77. Arbizzani C, Gabrielli G, Mastragostino M (2011) Thermal stability and flammability of electrolytes for lithium-ion batteries. J Power Sources 196(10):4801–4805
78. Montanino M, Moreno M, Carewska M, Maresca G, Simonetti E, Presti RL, Alessandrini F, Appetecchi G (2014) Mixed organic compound-ionic liquid electrolytes for lithium battery electrolyte systems. J Power Sources 269:608–615
79. Gao K, Song X-H, Shi Y, Li S-D (2013) Electrochemical performances and interfacial properties of graphite electrodes with ionic liquid and alkyl-carbonate hybrid electrolytes. Electrochim Acta 114:736–744
80. Forgie JC, El Khakani S, MacNeil DD, Rochefort D (2013) Electrochemical characterisation of a lithium-ion battery electrolyte based on mixtures of carbonates with a ferrocene-functionalised imidazolium electroactive ionic liquid. Phys Chem Chem Phys 15(20):7713–7721
81. Suo L, Hu Y-S, Li H, Armand M, Chen L (2013) A new class of solvent-in-salt electrolyte for high-energy rechargeable metallic lithium batteries. Nat Commun 4:1481
82. Garcia B, Armand M (2004) Aluminium corrosion in room temperature molten salt. J Power Sources 132(1):206–208
83. Wang X, Yasukawa E, Mori S (2000) Inhibition of anodic corrosion of aluminum cathode current collector on recharging in lithium imide electrolytes. Electrochim Acta 45(17):2677–2684
84. Kühnel R-S, Lübke M, Winter M, Passerini S, Balducci A (2012) Suppression of aluminum current collector corrosion in ionic liquid containing electrolytes. J Power Sources 214:178–184. doi:10.1016/j.jpowsour.2012.04.054
85. Hofmann A, Schulz M, Winkler V, Hanemann T (2014) Anodic aluminum dissolution in conducting salt containing electrolytes for lithium-ion batteries. J Electrochem Soc 161(3):A431–A438
86. Hofmann A, Merklein L, Schulz M, Hanemann T (2014) Anodic aluminum dissolution of LiTFSA containing electrolytes for Li-ion-batteries. Electrochim Acta 116:388–395
87. Kühnel R-S, Reiter J, Jeong S, Passerini S, Balducci A (2014) Anodic stability of aluminum current collectors in an ionic liquid based on the (fluorosulfonyl)(trifluoromethanesulfonyl) imide anion and its implication on high voltage supercapacitors. Electrochem Commun 38:117–119
88. Mun J, Yim T, Choi CY, Ryu JH, Kim YG, Oh SM (2010) Linear-sweep thermammetry study on corrosion behavior of Al current collector in ionic liquid solvent. Electrochem Solid State Lett 13(8):A109–A111
89. Peng C, Yang L, Zhang Z, Tachibana K, Yang Y, Zhao S (2008) Investigation of the anodic behavior of Al current collector in room temperature ionic liquid electrolytes. Electrochim Acta 53(14):4764–4772
90. Cho E, Mun J, Chae OB, Kwon OM, Kim H-T, Ryu JH, Kim YG, Oh SM (2012) Corrosion/passivation of aluminum current collector in bis (fluorosulfonyl) imide-based ionic liquid for lithium-ion batteries. Electrochem Commun 22:1–3
91. Dilasari B, Jung Y, Kwon K (2016) Comparative study of corrosion behavior of metals in protic and aprotic ionic liquids. Electrochem Commun 73:20–23

92. Indris S, Heinzmann R, Schulz M, Hofmann A (2014) Ionic liquid based electrolytes: Correlating Li diffusion coefficients and battery performance. J Electrochem Soc 161(14):A2036–A2041
93. Husch T, Yilmazer ND, Balducci A, Korth M (2015) Large-scale virtual high-throughput screening for the identification of new battery electrolyte solvents: computing infrastructure and collective properties. Phys Chem Chem Phys 17(5):3394–3401
94. Dohm S, Spohr E, Korth M (2017) Developing adaptive QM/MM computer simulations for electrochemistry. J Comput Chem 38(1):51–58. doi:10.1002/jcc.24513
95. Schütter C, Husch T, Korth M, Balducci A (2015) Toward New Solvents for EDLCs: From Computational Screening to Electrochemical Validation. J Phys Chem Part C 119:13413–13424
96. Schütter C, Husch T, Viswanathan V, Passerini S, Balducci A, Korth M (2016) Rational design of new electrolyte materials for electrochemical double layer capacitor. J Power Sources 326:541–548
97. Husch T, Korth M (2015) Charting the known chemical space for non-aqueous lithium–air battery electrolyte solvents. Phys Chem Chem Phys 17:22596–22603

Top Curr Chem (Z) (2017) 375:63
DOI 10.1007/s41061-017-0150-7

REVIEW

Ionic Liquids for Supercapacitor Applications

Mathieu Salanne[1,2]

Received: 9 March 2017 / Accepted: 16 May 2017 / Published online: 30 May 2017

Abstract Supercapacitors are electrochemical energy storage devices in which the charge is accumulated through the adsorption of ions from an electrolyte on the surface of the electrode. Because of their large ionic concentrations, ionic liquids have widely been investigated for such applications. The main properties that have to be optimized are the electrochemical window, the electrical conductivity, and the interfacial capacitances. Ionic liquids allow a significant improvement of the former, but they suffer from their high viscosity. In this review, I will discuss the advantages and the inconvenience of using ionic liquids in supercapacitors. Some innovative approaches using mixtures of ionic liquids or redox-active ions will also be critically addressed.

Keywords Energy storage · Electrolytes · Electrochemistry

1 Introduction

Supercapacitors are electrochemical energy storage devices that are characterized by high power densities (with charge/discharge times ranging from milliseconds to a few seconds) and a very good stability upon cycling (i.e. more than 1,000,000 cycles). Their main drawback is the energy density, which is rather low with respect

---

Chapter 2 was originally published as Salanne, M. Top Curr Chem (Z) (2017) 375: 63. DOI 10.1007/s41061-017-0150-7.

✉ Mathieu Salanne
mathieu.salanne@upmc.fr

[1] Sorbonne Universités, UPMC Univ Paris 06, CNRS, Laboratoire PHENIX, 75005 Paris, France

[2] Maison de la Simulation, CEA, CNRS, Université Paris-Sud, UVSQ, Université Paris Saclay, 91191 Gif-sur-Yvette, France

to the one of other types of energy storage devices such as Li-ion batteries. They are, therefore, involved in applications where high power delivery or uptake is needed for short times. For example, they are used to store and release the braking energy in individual and collective vehicles or in industrial equipment, which allows substantial savings in their fuel consumption (between 10 and 40 %) [1].

From the materials point of view, supercapacitors can be classified into two groups: electrochemical double-layer capacitors (EDLCs) that employ porous carbon electrodes [3, 4], and pseudocapacitors for which metallic oxide materials (such as MnO_2, RuO_2 or Nb_2O_5) are used [5]. The charging mechanisms of EDLCs and pseudocapacitors strongly differ [6]. Although in EDLCs the carbon surface is progressively charged upon the application of voltage through the adsorption of ions (as shown on Fig. 1), pseudocapacitors are characterized by Faradaic reactions involving the metal ions at their surface. Currently most of the commercial devices employ EDLCs, mostly because they are much more stable upon cycling.

In this review I will only discuss the case of EDLCs since pseudocapacitive mechanisms are generally not active when ionic liquids (ILs) electrolytes are employed. The energy density and the power of EDLCs are respectively given by

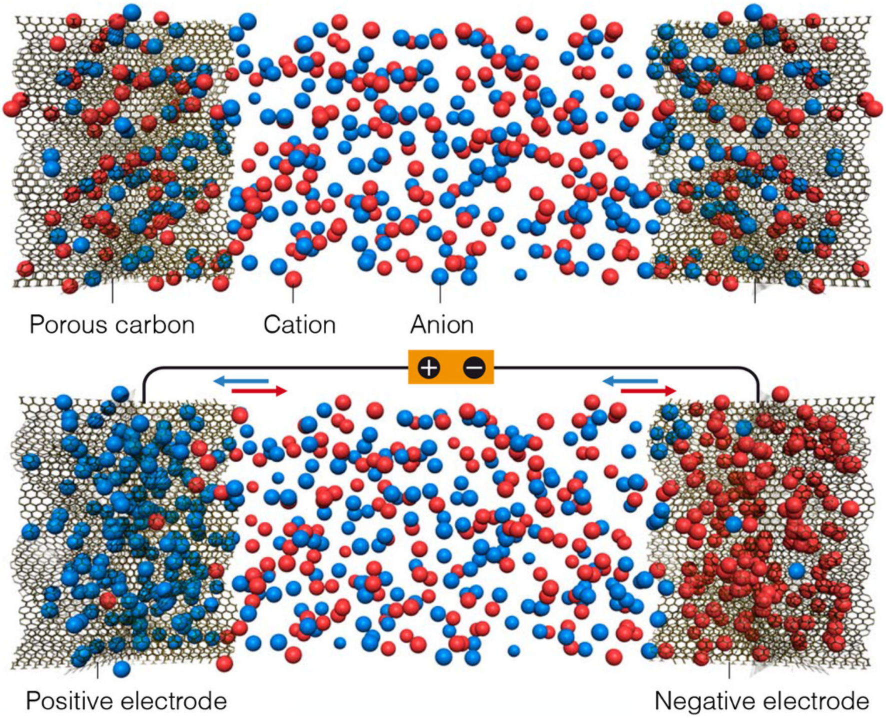

Fig. 1 Molecular scale representation of an electrochemical double-layer capacitors. At the open circuit voltage (*top panel*), the ions from the electrolytes lie either within the porous carbon electrodes or between them. Upon application of a voltage (*bottom panel*), the cations (resp. anions) accumulate at the negative (resp. positive) electrode. The electrolyte is either a pure ionic liquid or it consists of a concentrated solution of ions (no solvent molecules are shown here). Adapted with permission from Ref. [2]

$$E_{\mathrm{m}} = \frac{1}{2} C V^2 \tag{1}$$

$$P = \frac{4V^2}{R} \tag{2}$$

where C is the specific capacitance (measured in F/g), V is the applied voltage (in V), and R the equivalent series resistance (in Ω) of the whole device. Typical values for current commercial devices are 5 Wh kg^{-1} for the energy density and 10,000 W kg^{-1} for the power density. The corresponding characteristic time for charge/discharge is thus $\tau = 1.8$ s. In order to expand the range of applications of EDLCs, it is necessary to increase their energy density. To this end, one can either enhance the operating voltage or the specific capacitance. However, this should not be done by sacrificing the power density, so R should be kept as low as possible. As we shall see, room-temperature ionic liquids (RTILs) may impact the three relevant quantities, thus they have attracted a lot of attention from the EDLC community in the past. Since they are liquid salts that do not contain neutral solvent molecules, they are also used in many fundamental simulations and spectroscopy studies in order to understand the complex mechanisms of ion adsorption inside electrified nanopores [6, 7].

It is almost 20 years ago that McEwen et al. noticed that ILs were relevant electrolytes for EDLCs [8]. They measured the electrochemical properties of a series of imidazolium-based salts and anticipated that they may be used either as neat solvents or dissolved in organic solvents such as propylene carbonate and acetonitrile. Since then, many groups have proposed to use pure ILs inside supercapacitors [9–12]. This research has been hindered by the lack of fundamental knowledge on the structure of the double-layer formed by pure ionic liquids, which differs markedly from the one of conventional dilute electrolytes [13]. Although many issues remain to be understood, we have a much better knowledge of the IL/electrode interface now [14] and many experimental results have been rationalized from the combination of theory, simulation, and spectroscopy [15]. The synthesis of new ionic liquids for electrochemical applications remains a very active research field; for example, new families of ether-functionalized sulfonium [16]or pyrrolidinium [17] ionic liquids have recently been proposed for EDLCs. Another strategy consisting in mixing two ionic liquids [18, 19] together or one ionic liquid with a solvent [20, 21] is also widely investigated, with the objective of enhancing the bulk and/or the interfacial properties with respect to the single-component liquid.

In this article I will discuss the advantages and inconvenience of ionic liquids from the device point of view, in light of the current knowledge of their microscopic structure. In particular, their stability under extreme temperatures and at high voltage will be addressed. I will then analyze the main physical properties that determine EDLCs performances, i.e. the transport properties (ionic conductivity, the ionic diffusion coefficients, and the viscosity) of the bulk liquid, and the capacitance of the carbon/ionic liquid interface. For the latter, it is the interaction between the ions and the carbon surface that plays a major role. It is, therefore, much more delicate to understand and rationalize. Finally, I will discuss new storage concepts such as biredox ionic liquids that have recently been proposed to enhance the performances of supercapacitors [22].

2 Bulk Properties

2.1 Thermal Stability

Under operating conditions, for conventional applications such as in electric vehicles, a supercapacitor may be exposed to temperatures roughly ranging from −50 to 80 °C. The carbon materials are stable over the whole range (and much beyond), so that the electrolyte will be the main responsible for temperature-related failures. Even with added salt, aqueous electrolytes are not able to reach the lowest temperatures due to the freezing of water. In the case of organic solvents, lower temperatures may be reached, but they often have boiling points which are slightly too low (for example, $T_b = 82\,^{\circ}\mathrm{C}$ for acetonitrile) to ensure a good safety at high temperatures. This is due to the cohesive forces at play in such solvents, which are mostly related to relatively weak interactions such as van der Waals ones.

In the case of ionic materials, the Coulombic attraction between ions of opposite charges is much stronger. The liquid state of ILs is, therefore, stable up to much higher temperatures than conventional solvents. In fact, it is very hard to obtain a gas phase, and for years it was thought that ionic liquids could not be distilled. This was proven wrong by Earle et al., who were able to distill ionic liquids at temperatures of 200–300 °C and low pressure [23]. However, the stability at high temperatures is limited by decomposition reactions that break the molecular species [24]. It is not possible to determine decomposition temperatures as precisely as boiling points because it is not a phase transition; however, methods such as thermogravimetric analysis are able to detect the temperature at which the degradation process may start [25, 26]. These temperatures are generally well above 200 °C, which shows that high temperatures are not problematic for the use of ILs in supercapacitors.

ILs are much more limited as electrolytes at low temperatures (even without considering the dynamic properties). In general they have melting points around room temperature, which prevents their use in devices aiming at low temperatures uses such as electric vehicles for example. However, Lin et al. have recently overcome this difficulty by mixing two ionic liquids sharing a similar anion but having different cations [27]. As can be seen from the differential scanning calorimetry profiles reproduced on Fig. 2a, the pure *N*-methyl-*N*-propylpiperidinium bis(fluorosulfonyl)imide ($\mathrm{PIP_{13}FSI}$) and *N*-butyl-*N*-methylpyrrolidinium bis(fluorosulfonyl)imide ($\mathrm{PYR_{14}FSI}$) respectively show melting points of 6 and −18 °C. For their eutectic mixture, however, no peak is observed down to −80 °C, which excludes the presence of first- or second-order phase transition. This work remarkably shows that it is possible to operate IL-based supercapacitors at very low temperatures—albeit with degraded performances as we shall see below.

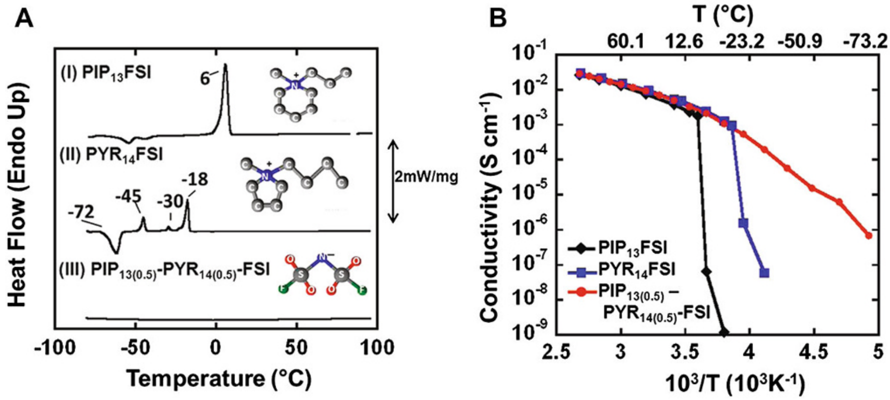

Fig. 2 Characteristics of ionic liquids mixtures. **a** Differential scanning calorimetry profiles of (*I*) PIP$_{13}$FSI, (*II*) PYR$_{14}$FSI and (*III*) (PIP$_{13}$FSI)$_{0.5}$(PIP$_{13}$FSI)$_{0.5}$ mixture, and their chemical structures. **b** Variation of the ionic conductivity versus the inverse temperature for the three electrolytes. Reprinted with permission from Ref. [27]. Copyright 2011 American Chemical Society

2.2 Operating Voltage

The main advantage of ionic liquids with respect to solvent-based electrolytes consists in their wide electrochemical window. From this point of view, aqueous solutions are very limited, due to the thermodynamics of the oxidation/reduction reactions, which result in the formation of oxygen and hydrogen at the anode and the cathode, respectively. The addition of salts and/or the use of basic conditions allows to operate at larger voltages than in pure water (for example using a sodium acetate salt allows to reach 1.5 V [28]), but this remains rather low compared to other electrolytes. An interesting concept consisting in two separated electrolytes with different pH values was recently proposed [29], which extends the capacitor voltage up to 2.1 V.

A comparison of the operating voltages in various organic electrolytes and ionic liquids is shown in Fig. 3. Commercial devices generally use acetonitrile or propylene carbonate solvents, with a corresponding voltage of 2.8 V. Alternative solvents have also been proposed, which allow going beyond 3 V, such as sulfone-based [30], alkylated cyclic carbonates [31], adiponitrile [32], or cyano ester [33] solvents. However, ionic liquids generally outclass them; in particular, the pyrrolidinium or the ether-functionalized sulfonium [16] families exhibit very wide electrochemical windows, leading to operating voltages over 3.5 V. Balducci et al. have investigated the possibility of mixing such ionic liquids with organic solvents, in order to determine whether such electrolytes would exhibit the same electrochemical window as the latter taken alone [21]. They showed that it is not the case, which means that the composition can be fine-tuned in order to find the best compromise between operating voltage and the other properties.

In order to find new electrolytes that maximize the voltage of the device, an emerging strategy consists in using high-throughput computational screening. Such

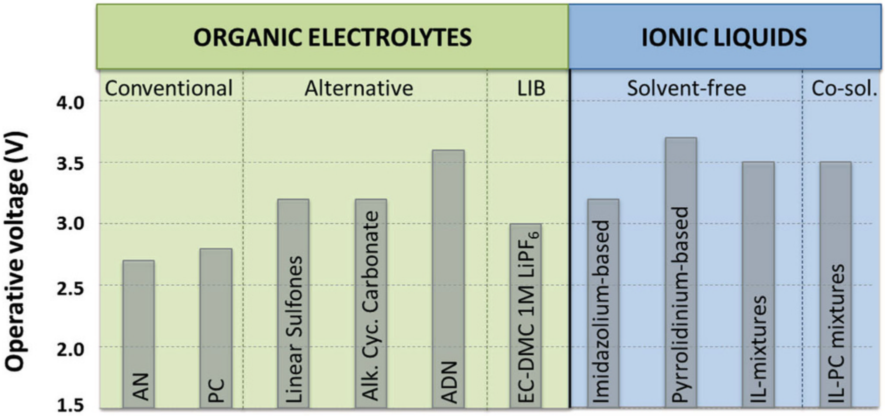

Fig. 3 Comparison of the EDLCs operating voltage achievable with organic electrolyte and ionic liquids based electrolytes. *AN* acetonitrile, *PC* propylene carbonate, *ADN* adiponitrile, *Alkylat. Cyc. Carb.* alkylated cyclic carbonate, *EC* ethylene carbonate, *DMC* dimethyl carbonate, *LiPF* $_6$ lithium hexafluorophosphate, *IL* ionic liquids. Reproduced with permission from Ref. [4]

approaches were recently applied successfully to the cases of organic solvents for EDLCs [34] and nonaqueous redox flow battery electrolytes [35] (in the framework of the materials genome initiative [36]), but the various families of ionic liquids have not been investigated using such techniques so far. A key difficulty is that performing the required ab initio calculations to determine the electronic properties is computationally involving due to the need to include a sufficiently large number of ion pairs in the simulation setup to have a bulk liquid [37, 38]. In addition the organic species that are used generally have many valence electrons that have to be included explicitly in the calculation. This may be overcome through the introduction of an implicit solvation model in order to mimic the environmental effect while reducing a lot the computational costs, an approach which was successfully applied for designing ionic liquids for CO_2 absorption [39].

2.3 Ionic Conductivity

The equivalent series resistance that was introduced for the power of supercapacitors in Eq. 2 is a combination of several contributions arising from the resistance to charge transport inside the porous electrodes, the bulk electrolyte, and the various interfaces [40]. Among these contributions, bulk is the only one that can easily be measured and tuned; fortunately, it plays the main overall role. Ionic liquids are dense ionic solutions without any neutral solvent species, thus they are in principle expected to exhibit an excellent ionic conductivity. However, this property is not solely determined by the concentration of charge carriers. In ionic liquids, the self-diffusion coefficient of the ions is too low (and correspondingly the viscosity is too high). Typical values are 0.495×10^{-10} and 0.309×10^{-10} m^2 s^{-1} for the cation and anion, respectively, in the 1-ethyl-3-methylimidazolium (EMIM) bis(trifluoromethane)sulfonimide (TFSI) ionic liquid at room temperature [41]. Such values are two orders of magnitude lower than the one of pure water (2.3×10^{-9} m^2 s^{-1} at the same temperature [42]).

In addition, the strong correlations occurring between the displacements of the ions in RTILs lead to large deviations from the Nernst–Einstein equation [43]. Indeed, the latter predicts that the ionic conductivity is directly proportional to the self-diffusion coefficient by neglecting all ionic correlations, which is only true for the case of highly diluted salts in aqueous or organic solvents. This behavior, which is reminiscent to the case of high temperature molten salts [44, 45], leads to even poorer ionic conduction in ionic liquids compared to conventional liquid electrolytes. As a consequence, typical electrical conductivities are of the order of a few mS cm^{-1} in ionic liquids at room temperature. The best performing ones are based on the EMIM cation, for example when it is combined with perfluoroalkyl-trifluoroborate anions, the resulting liquids have conductivities, which may reach up to 13 mS cm^{-1} at 298 K [46]. As discussed above, however, a major target is to find electrolytes that operate well at low temperatures. Figure 2 shows the temperature dependence of the ionic conductivity of the equimolar PIP$_{13}$FS-PYR$_{14}$FSI mixture mentioned above. It follows an approximate Arrhenius law, and so it quickly decreases by several orders of magnitude, reaching values below 1 mS cm^{-1} for temperatures inferior to −20 °C. The main consequence is that the charging time of the devices will accordingly be increased substantially—reducing a lot their efficiency. In this specific case, the conductivity of the mixture was similar to the one of the pure ionic liquids, but Every et al. reported positive deviations from ideal behavior when mixing EMIM-TFSI with EMIM-trifluoromethanesulfonate [47], which reinforces the idea that mixtures of ionic liquids are more efficient for supercapacitor applications.

It is worth noting the existence of ionogels, which are hybrid materials in which an RTIL is immobilized in an inorganic solid material (e.g. mesoporous silica) [48]. Such systems exhibit improved operating temperature range while keeping the ionic conductivity of the ionic liquid, and are, therefore, extensively investigated for Li-ion batteries, as well as supercapacitors [49]. However, the main difficulty is to ensure a good contact between the two solid phases (electrode and electrolyte), which will require future developments.

3 Interfacial Properties

3.1 The Double-Layer in ILs

3.1.1 Planar Interfaces

Ten years ago, Kornyshev opened the question of the necessity of a paradigm change for describing the double-layer in ionic liquids [13]. He showed that using the conventional Gouy–Chapman–Stern (GCS) model was not accurate since many of the underlying assumption are not fulfilled. In particular, GCS model neglects the correlation between ions, which are central to the physical properties of ionic liquids. It also treats the ions as a point charge. He proposed a new mean-field theory accounting for the finite-size of the ions [13] and their mutual interactions [51], which predicted a very different structure of the double-layer. At the same period, several groups were able to provide a first insight of ionic liquid interfaces using various experimental techniques. The first intriguing behavior, which was observed by atomic force microscopy (AFM), is a strong layering effect at the interface [52–54]. This was later confirmed by surface force apparatus (SFA) [55–58] or by high-energy X-ray reflectivity [50, 59]. An illustration of the result obtained by the latter approach for the PYR_{14}-tris(pentafluoroethyl)-trifluorophosphate (FAP) ionic liquid is provided in Fig. 4. Each layer is highly dense in ions, which should imply a rapid screening of the charged electrode surface. Although the layering is present for all the ionic liquids, Perkin et al. have shown that dramatic differences may be observed for the characteristic length corresponding to the distance between the successive layers of adsorbed ions. This denotes some kind of "self-assembling" properties, and indeed the characteristic length can be related to the ions dimension, suggesting the formation of patterns such as alternating cation-anion monolayers or tail-to-tail cation bilayers. The latter are formed when the hydrocarbon chain of the cation is longer, due to the propensity of these non-polar domains to aggregate [60]. This effect is reminiscent to the case of bulk ionic liquids in which nanoscale domains have been observed, whose size mostly depends on the length of the alkyl chain of the ions [61]. Many simulation studies have also reported the existence of multiple layers of ionic liquids [14, 62–66], in agreement with the AFM and SFA works. They also provide quantitative values for the concentration of each ionic species in the various adsorbed layers. The use of vibrational sum frequency generation (SFG) spectroscopy at various liquid/vapor or solid/liquid interfaces of ionic liquids did not lead to similar conclusions [67–69]; however, it is difficult to assess exactly the length of the liquid layer which is probed with this technique. It is likely that the main signal arises from the top layer only [70], which would explain why layering could not be observed using this setup.

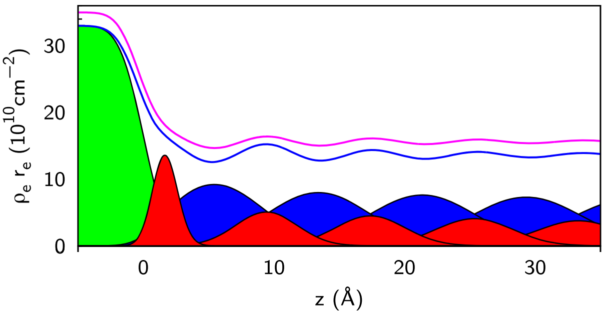

Fig. 4 Partial interfacial electron density profile for the pure PYR_{14}-FAP ionic liquid. The total electron density (*blue line*) is the sum of contributions from the sapphire substrate (*green*), PYR_{14} cations (*red*) and FAP anions (*blue*). Profiles obtained by the generic layering model (*purple line*, vertically shifted for clarity) are provided for comparison. Adapted from [50] with the permission of AIP Publishing

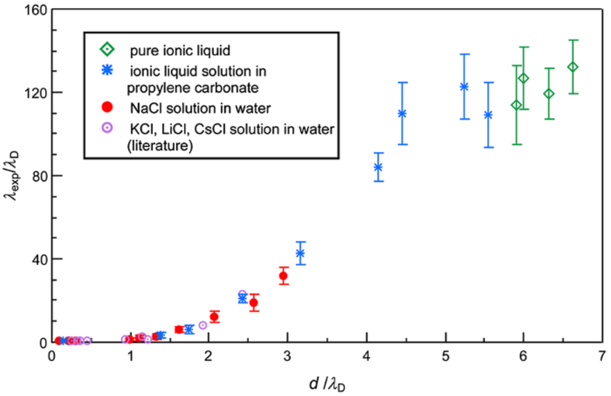

Fig. 5 Deviation of the experimental long-range decay length, obtained using surface force balance, from the Debye length, $\lambda_{\mathrm{exp}}/\lambda_D$, plotted versus d/λ_D (where d is the mean ion diameter in the electrolyte) for pure ionic liquids (*open diamonds*), aqueous NaCl solutions (*filled circles*), and solutions of an ionic liquid, PYR_{14}-TFSI, mixed with propylene carbonate (*asterisk symbols*). Literature values are also included for aqueous LiCl, KCl, and CsCl solutions (*open circles*) [71, 72]. Adapted with permission from Ref. [73]. Copyright 2016 American Chemical Society

Despite this intense activity, some structural aspects of the electric double-layer in ionic liquids remain to be understood, in particular about the width of the layer of liquid, which is affected by the polarized electrode. In particular, intriguing long-range interaction effects were observed by Gebbie et al. in a study employing SFA [74, 75]. Although this was firstly interpreted by the authors as ionic liquids behaving as dilute electrolytes, there are many arguments that contradict this picture [15, 76]. Further SFA studies on a series of electrolytes ranging from dilute ionic solutions to pure ionic liquids showed that beyond an ionic concentration threshold the screening length increases with increasing concentration [73] (Fig. 5). The origin of these long-range interactions remains to be fully established, with many open questions [77].

The structure inside the adsorbed layers also shows interesting features. In particular, many studies have recently shown that interfacial transitions may occur in the first adsorbed layer of ionic liquid on a planar electrode [81] (see Fig. 6 for examples of simulation results). In a seminal study, Freyland et al. [82] have shown by using in situ scanning tunneling microscopy (STM) that an adsorbed layer of 1-butyl-3-methylimidazolium (BMIM) PF_6^- on the (111) face of gold formed Moiré-like patterns at potentials greater than −0.2 V with respect to a platinum reference electrode, which were attributed to the formation of an ordered adlayer of PF_6^-. At negative potentials, the STM images were consistent with the formation a layer of anions with the $(\sqrt{3} \times \sqrt{3})$ structure, indicating a two-dimensional ordering transition at this interface. Further STM studies also reported the formation of ordered structures for various ionic liquids on gold electrodes [83, 84]. The main advantage of this metal is that single crystals are rather easily made; however, the observations may be rendered difficult by potential surface reconstructions. Recently, Elbourne et al. also reported the existence of ordered structures of BMIM-TFSI at the surface of highly oriented pyrolytic graphite [85], thus showing

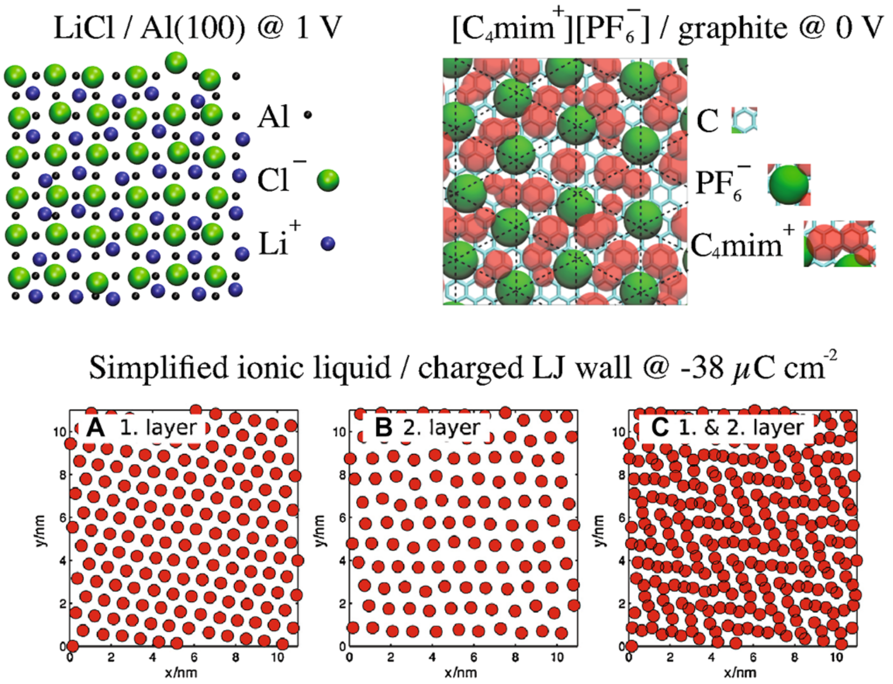

Fig. 6 Snapshots of typical ordered structures observed in computer simulations. *Top left* first adsorbed layer of a LiCl molten salt electrolyte on the (100) surface of an aluminum electrode at a negative potential. Adapted with permission from Ref. [78]. Copyright 2010 American Chemical Society. *Top right* first adsorbed layer of a [C$_4$mim$^+$][PF$_6^-$] RTIL on a graphite electrode at a neutral potential. Adapted with permission from Ref. [79]. Copyright 2014 American Chemical Society. *Bottom* first two adsorbed layers of a simplified RTIL on a charged Lennard–Jones wall with a large negative surface charge density. Reproduced from Ref. [80], with permission from Elsevier

that such effects occur under a large variety of conditions. Beyond the field of supercapacitors, these structures may impact many ionic liquid interfacial properties since they can induce slow dynamics [86], varying reactivity [87], voltage-dependent friction properties [88], etc.

Here also, MD simulations have recently provided an interesting molecular-scale picture of the mechanisms at play (Fig. 6). A first example of voltage-driven ordering transition was observed for the interface formed between a high temperature molten salt (LiCl) and an aluminum electrode [78, 90]. At low voltages (i.e. below the point of zero charge of the electrode), the molten salt adopted a disordered structure at the interface, while for larger potentials an ordered structure was obtained. In another study, the formations of Moiré-like and herring-bone structures at different electrode surface charges were reported for a primitive model of an ionic liquid [80]. The herring-bone structure even involved the two first layers of adsorbed fluid. The BMIM-PF$_6$ ionic liquid (simulated using a coarse-grained model [91]) also formed an ordered structure which could be monitored by computing the in-plane structure factor in the first layer of the adsorbed liquid. This structure factor was liquid-like on a wide range of potentials, but it showed some

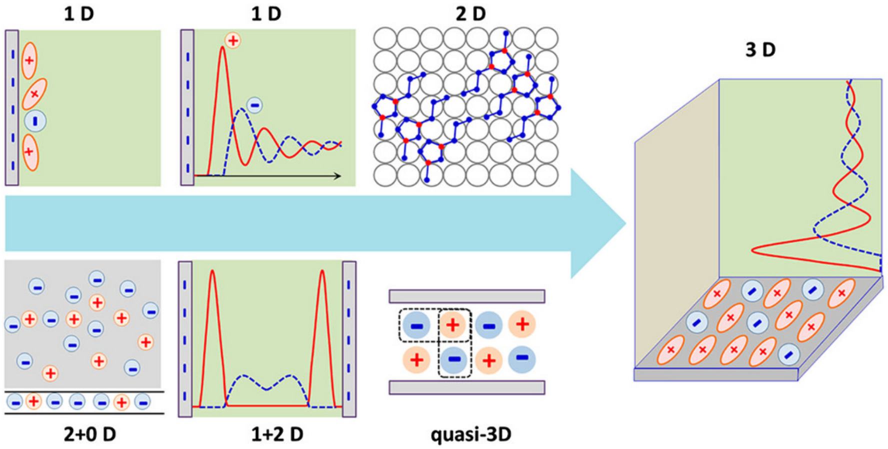

Fig. 7 Double layers in ionic liquids as 3D entities. The double layers near open electrodes (*left top panels*) were first perceived as 1D Helmholtz layers homogeneous in the lateral plane. This "1D" picture of the double layer was later refined as alternating layers of counterions and co-ions in the direction normal to the electrode surface. The discovery that ions adsorbed on the electrode surface form a well-defined pattern in a certain voltage window indicates that double layers can have distinct structures in the lateral plane, at least in the first layer adjacent to the electrode—call it "2D features". The double layers in nanopores (*left bottom panels*) are 2D entities in nanopores accommodating only one layer of ions, but exhibit 1 + 2D and quasi-3D features in wider pores. From these diverse pictures of the double layers and the latest reports of structural ordering inside an adsorbed layer emerges a new paradigm that the 3D nature of double layers in RTILs should be taken seriously. Reproduced with permission from Ref. [89]. Copyright 2014 American Chemical Society

strong Bragg-like peaks suggesting a two-dimensional lattice-like organization for both the anions and cations at low voltages [79]. These results were summarized in an editorial by Kornyshev and Qiao, who insisted on the fact that the double-layer formed by ionic liquids at electrode surface should now be viewed as a three-dimensional entity [89]. Their schematized view of the current knowledge about the structure formed at the interface is shown on Fig. 7. A very recent report of a capillary freezing of an ionic liquid, which occurs over typical lengthscales ranging from 60 to 160 nanometers on electrified graphite, gold, and platinum [92], may further change this view in the future, showing that many structural aspects of the double-layer remain to be elucidated.

3.1.2 Confinement Effects

Confinement may have a very strong impact on the structure of fluids, and consequently on their physical properties. In water, for example, the breaking of the hydrogen bond network inside carbon nanotubes may lead to very quick diffusion [94]. Similar effects have been reported for a viscous ionic liquid [95]. However, compared to the planar surfaces, it is much more difficult to probe experimentally the structure of the liquid inside the pores when a potential is applied. In the case of ionic liquids, the first question is if the ions will either locate preferentially at the surface or try to keep a bulk-like local structure. Small-angle neutron scattering experiments performed on a system consisting of a hierarchical porous carbon filled with a BMIM-TFSI electrolyte at various loadings showed that the RTIL wetted all the pore surfaces uniformly, rather than leaving some pores unsaturated [96]. Spontaneous wetting was also observed by nuclear magnetic resonance spectroscopy of adsorbed EMIM-TFSI [93]. The corresponding spectra are shown on Fig. 8, for both ions they are characterized by two peaks, a thin, intense one corresponding to the bulk liquid and a broader one due to the adsorbed ions [97, 98]. In this study, it was possible to monitor the variation of the spectra when changing the applied potential in the electrode. A shift on the position and a variation on the intensity of the second peak is observed, which allows understanding the charging mechanism. In this specific case, the authors concluded on an ionic exchange mechanism: Starting from a neutral adsorbed electrolyte at

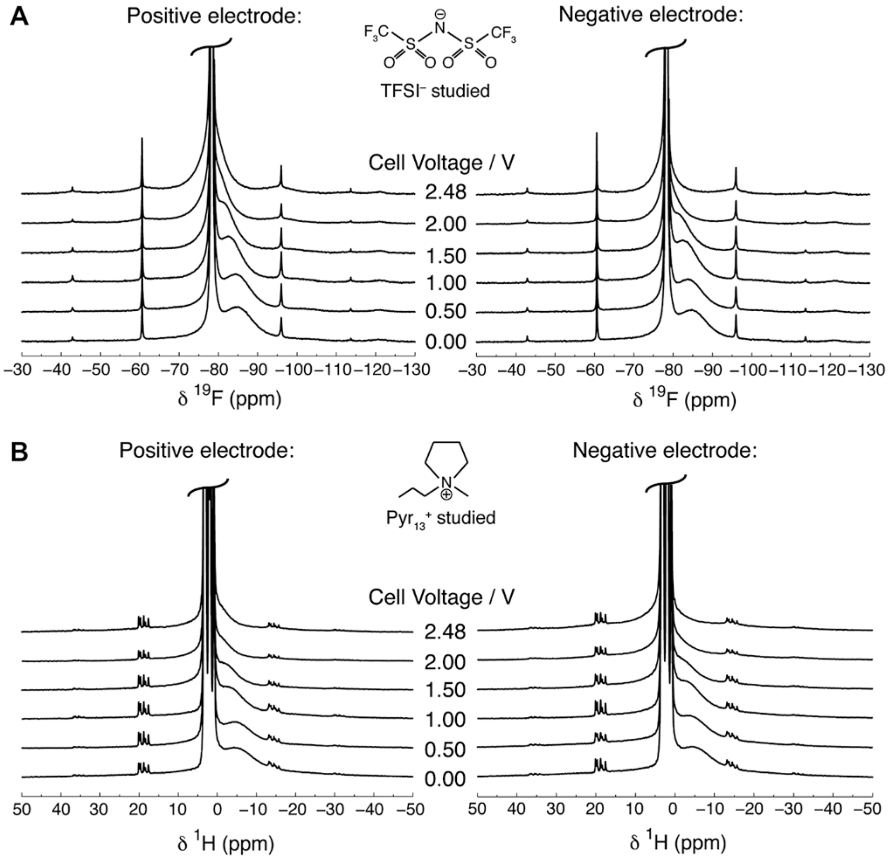

Fig. 8 **a** ^{19}F and **b** ^{1}H MAS NMR (7.1 T) spectra of electrodes extracted from disassembled supercapacitors (YP50F carbon and PYR$_{13}$-TFSI ionic liquid) charged to a range of different cell voltages. In-pore resonances show noticeable increases in chemical shift as the voltage is increased. Reproduced from Ref. [93] with permission. Copyright 2015 American Chemical Society

0 V, when applying a potential, anions are replaced by cations in the negative electrode and vice-versa.

These results are in agreement with molecular simulations, which have been performed on a wide series of materials ranging from idealized structure to realistic nanoporous carbons. For example, Shim and Kim have studied the EMIM-BF_4 adsorbed inside carbon nanotubes of various dimensions [99]. They showed that the size of the tube impacts strongly on the structure of the liquid, with the smaller tubes showing the formation of a single file of counterions under polarization, while the larger ones contain both cations and anions as shown on Fig. 9a, b. Similar results arose from simulations of slit-shaped pores, which were performed with a large variety of ionic liquids either using molecular dynamics [102–105] or classical density functional theory [106, 107] approaches. The case of disordered nanoporous carbon materials is more difficult to simulate. Indeed, it is necessary to use an atomic structural model accounting for the various pore size distributions and the presence of many defects. Realistic structures of carbide-derived carbons, which are typical nanoporous materials that have been investigated experimentally by the groups of Gogotsi and Simon [108, 109], were obtained from quenched molecular dynamics [110] or by hybrid reverse Monte Carlo simulations [111]. Using such carbons, we showed that the ionic liquid did not conserve its layered structure inside the nanopores [100]. The presence of well-defined structures is more complex to track than in simple nanotubes or slit-shaped pores as shown in Fig. 9c and d. In

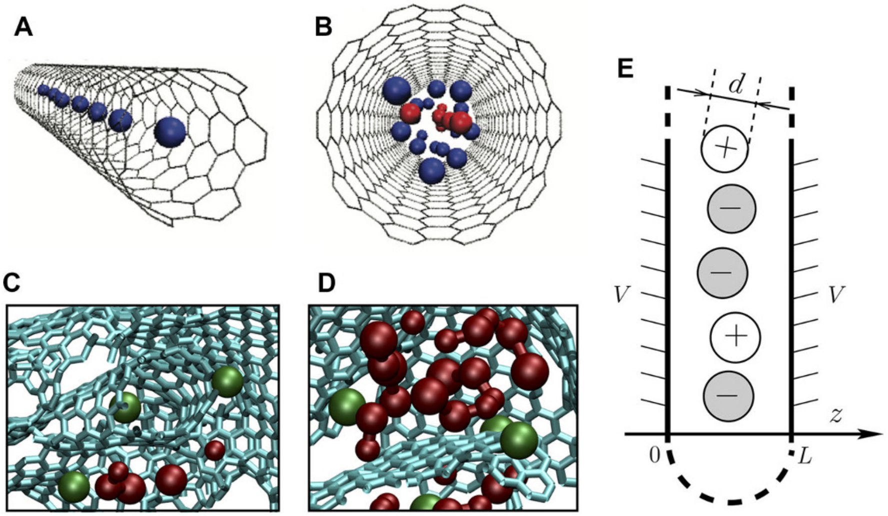

Fig. 9 Typical structures adopted by ionic liquids in nanopores. **a**, **b** Snapshots of the EMIM-BF_4 adsorbed inside (6,6) and (10,10) nanotubes, respectively (*red* and *blue spheres* represent the center-of-mass positions of EMIM and BF_4^- ions). Adapted with permission from Ref. [99]. Copyright 2010 American Chemical Society. **c**, **d** Typical structure of the BMIM-PF_6 inside electrified nanopores of a carbide-derived carbon material (*blue* C–C bonds, *red* BMIM, and *green* PF_6^-). Adapted with permission from Ref. [100]. **e** Schematic view of the cross-section of a single, laterally infinite, slit-like narrow pore as a part of a porous electrode. The pore width is *L*, *V* is the voltage with respect to the reference electrode (in the "bulk" outside the pore), and *d* is the diameter of ions [101]

order to analyze more deeply the coordination of the ions, we introduced a new quantity, the degree of confinement [112]. It is defined as the percentage of the solid angle around the ion, which is occupied by the carbon atoms [113], normalized by the maximal value taken by this quantity (which would correspond to the hypothetical case of an ion entrapped in a carbon sphere). We showed that the ions experience various environments, which were labeled as edge, planar, hollow, and pocket sites upon increase of the coordination of the molecular species by the carbon atoms (Fig. 9c, d correspond to a pocket and a planar site, respectively). As a consequence, the decoordination of the ions (and alternatively, their desolvation in mixtures with acetonitrile) systematically increases with the degree of confinement. These results were further confirmed in various simulation studies [114], but also in a recent experimental work dedicated to aqueous electrolyte [115].

The formation of ionic arrangements where ions of the same sign are packed together is intriguing at first sight. Indeed, ionic liquids are room-temperature molten salts, and their bulk short-range structure is mainly characterized by the formation of a first coordination shell of ions of opposite charge around a central ion [116]. Additional medium-range effects arising from the presence of polar/non-polar domains also play an important role on the physical properties [61, 117, 118], but they do not break the Coulombic ordering effects. This means that the intermolecular forces are deeply modified inside the nanopores. This effect was explained by Kondrat and Kornyshev by the formation of image forces that exponentially screen the electrostatic interactions inside the pores. They introduced this effect into a mean-field theory [101] and into Monte Carlo simulations [119], which lead them to the conclusion that the ionic liquid formed a “superionic state” when ions of the same sign are packed together inside electrified nanoporous carbons, as illustrated on Fig. 9e. The model was further extended to include finite electric field penetration into the pore walls to account for the fact that carbon materials are generally not perfect metallic conductors, but the results remained qualitatively similar [120].

3.2 Performances of ILs in Supercapacitors

3.2.1 Methodological Aspects

The physical property quantifying the performance of an electrode/electrolyte couple for EDLC applications is the capacitance. However, one can define several quantities:

– the single-electrodes differential capacitances,

$$C^{\pm}_{\mathrm{diff}} = \frac{\partial\sigma^{\pm}}{\partial\Delta\Psi^{\pm}_{\mathrm{interface}}}, \tag{3}$$

where $\sigma^{\pm}$ is the average surface charge of the electrode; the symbol ± is used for quantities which can be measured or calculated for both the positive and negative electrodes (for the specific case of the surface charge we have

$\sigma^+ = -\sigma^-$) and $\Delta\Psi^{\pm}_{\text{interface}} = \Psi^{\pm} - \Psi^{\text{bulk}}$ is the potential drop at the electrode/electrolyte interface. In electrochemistry, the latter cannot be measured since Ψ^{bulk} is not known. However the use of a three electrode setup, where the third electrode plays the role of the reference, overcomes this difficulty since it allows measuring $\Delta\Psi^{\pm}_{\text{interface}}$ up to a constant. In computer simulations, $\Delta\Psi^{\pm}_{\text{interface}}$ is easily determined in some specific case, e.g. when the two electrodes are planar, then allowing to compute an electrostatic potential in the direction perpendicular to the electrode using the Poisson equation [121].

- the full electrochemical cell differential capacitance,

$$C^{\text{cell}}_{\text{diff}} = \frac{\partial\sigma^+}{\partial\Delta\Psi}, \tag{4}$$

  where $\Delta\Psi$ is the applied (measured) potential between the electrodes $\Delta\Psi = \Psi^+ - \Psi^-$.
- it is also possible to define an "integral" capacitance, given for the full electrochemical cell by

$$C_{\text{int}} = \frac{\sigma^+}{\Delta\Psi}. \tag{5}$$

The latter is more often used in applied studies since it is the one that will ultimately quantify the energy density of the EDLC, but the differential capacitances give much more information on the physico-chemical processes at play.

Although these quantities have a thermodynamic character and should therefore take a single value for a given system, there are several methods for measuring the capacitance, which may give different results [40]. Firstly, cyclic voltammetry (CV) yields the electric current with respect to the applied potential; it is mostly used to analyze the differential capacitances. Secondly, galvanostatic cycling (GC), which consists in measuring the potential response to a fixed applied current, provides an accurate measure of the cell integral capacitance. Finally, electrochemical impedance spectroscopy (EIS) may provide a more detailed picture [123]. The impedance is measured by applying low-amplitude alternative voltages of varying frequencies to a steady-state potential, and measuring the output current. However, in all these approaches, the measure is dynamical through the use of a potential scan rate (in CV), of a fixed current (in GC) and of the frequency-dependence of the applied alternative voltage (in EIS). The complex capacitance plane for a typical ionic liquid at various steady-state potentials is shown on the left panel of Fig. 10. For each method, the measured capacitances, therefore, vary with the experimental conditions. This may lead to important effects, for example, when slow processes are at play as was observed by Roling et al. in some RTILs [122, 124–126].

In molecular simulations, similar difficulties may arise. The typical timescale for supercapacitor charging differs markedly from its experimental counterpart due to the microscopic scale, which is used (in a typical simulation cell the two electrodes are separated by a layer of liquid of width ≈10 nm). Therefore, it is expected that the formation of the double-layer structure is fast enough to ensure that the

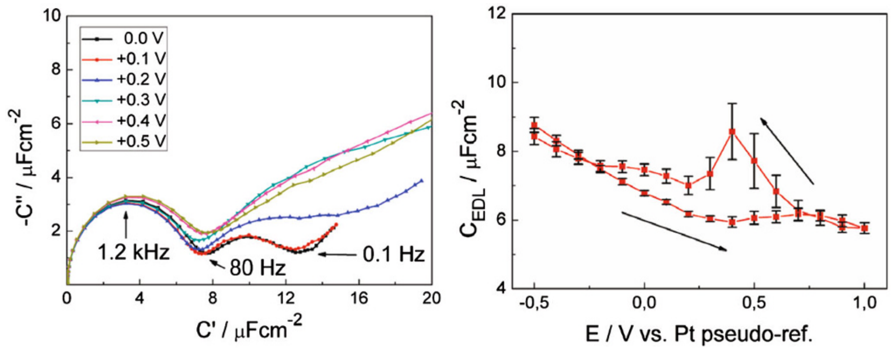

Fig. 10 *Left* complex capacitive plane plots for the interface between EMIM-FAP and a Au(111) electrode in the potential range between 0.0 and 0.5 V versus a Pt reference electrode. *Right* potential dependence of the differential capacitance, showing an hysteresis effect. Adapted with permission from Ref. [122]. Copyright 2011 American Chemical Society

capacitance is calculated unambiguously by simulating the system over a few nanoseconds, but the high viscosity of ionic liquids leads to an increase of the needed simulation time. In addition, some cases where collective processes are at play may be very difficult to sample. For example, when an order/disorder transition is observed it is necessary to involve enhanced sampling methods to evaluate the capacitance correctly [79]. Inside carbide-derived carbon nanoporous carbon electrodes, the diffusion of the ions may be slowed down by one order of magnitude [127], making the equilibration of the system an issue from the computational cost point of view. A final difficulty resides in the choice of the simulation technique. Indeed, constant applied potential algorithms have been proposed for molecular dynamics [128–131] and Monte Carlo [132–134] in order to model realistic experimental conditions. However, such approaches are implemented in a few codes only [135], and many simulations are performed at constant charge instead, which does not correspond to electrochemical setups. Although a few comparisons of the approaches were proposed [136], the extent of the error which is made in simplified approaches is hard to appreciate. As a consequence in the following simulations results from both constant potential and constant charge setups will be discussed indifferently.

Finally, it is worth noting that the capacitances are generally normalized in order to have comparable numbers, i.e. with the accessible surface of the electrode, its mass or its volume. The former approach may be problematic since it is very difficult to measure accurately the accessible surface in the range of pore sizes of interest (typically average pore sizes below 2 nm), contrarily to mesopores, which are much more easily characterized through gas adsorption experiments [137]. Surfacic capacitances should, therefore, be reported for planar electrodes only, keeping the specific and volumetric capacitances for comparing the performances of nanoporous carbon-based supercapacitors [6, 138]. In addition, the two latter normalizations are more adapted to the benchmark of the materials since the mass and the volume are very important parameters that need to be minimized in the final devices.

3.2.2 Interfacial Capacitances

Many experimental results have reported the existence of non-trivial shapes for the differential capacitance versus potential drop (*C*–*V*) curves [139–142]. However, Lockett et al. showed that many hysteresis effects occurred in these experiments [143], an observation that was later confirmed by Drüschler et al. [124] (see the right panel of Fig. 10). An important parameter is the structure of the electrode surface, which is often far from the perfect flat surface assumed in the theory since most of the experiments involve either polycrystalline metal surfaces or glassy carbon electrodes [144]. An alternative is to use a liquid electrode, e.g. mercury. This idea was extensively investigated by Costa et al. [145]. By systematically changing the length of the alkyl chain of imidazolium cations, they concluded that the longer chains displayed a preferential adsorption on the mercury surface [146]. Finally, they observed that mixing two ionic liquids (with the same cations), but different anions lead to *C*–*V* plots, which were well-represented by a weighted average of the results for the two pure liquids, indicating the absence of specific effects [147]. Several studies also showed the existence of large peaks in the capacitance, which would hardly be attributed to simple adsorption effects. They were generally attributed to the ordering transitions mentioned above [83, 148]. In conclusion, the huge variety of experimental results show that it is probably impossible to cast all the experimental results using a few simple mechanisms since many specific effects due to the ionic liquid/electrode interactions that are at play.

Here again, theoretical studies have, however, brought an important contribution to the field. In particular, it is worth noting that most of these experimental works were published after the seminal article of Kornyshev, who questioned the use of the Gouy–Chapman–Stern model for ionic liquids [13]. In this work he first predicted the existence of “bell-shapes” for the variation of the differential capacitance with the applied voltage. These results were soon confirmed from molecular simulations in which the ionic liquid was represented using a simplified generic model [149, 150]. In a further extension of the model, Fedorov et al. also showed that the particular structure of ionic liquids cations (i.e. charged heads and neutral counterparts) lead to the formation of a “camel-shaped” *C*–*V* plot [151]. These studies highlighted the existence of several regimes for the capacitance of planar electrodes. Firstly, at low potentials, the layered structure adopted by the ionic liquid for planar interfaces leads to an effect, which is called overscreening [51, 150, 152]. This effect arises from ionic correlations: the polarization of the first layer is coupled to that of the next layers. The first adsorbed layer carries a charge, which is more important than the electrode one and is therefore counterbalanced in the subsequent layer. This phenomenon extends in the following layers, until the bulk structure is recovered (i.e. up to several nm). This overscreening effect is maximum for low voltage electrodes, and it disappears when high charging regime are reached [149, 150]. As a result, only a fraction of the adsorbed ions are *effectively* used in the electricity storage process. At large applied potentials, a totally different effect arises. Because of the finite-size of the ions, the first adsorbed layer cannot accommodate enough counterions to balance the electrode charge. This was, therefore, called the crowding regime [15, 51]. Finally, even if the experimental results are often more complex, these theoretical works have allowed for a deep understanding of the impact of the double-layer on the capacitance in ionic liquids.

Although studies involving planar electrodes provide many insight from the fundamental point of view, the commercial EDLCs employ nanoporous carbons in order to maximize the specific surface area. Following the IUPAC, nanopores designate pores ranging from micropores (size <2 nm) to mesopores (from 2 to 50 nm). Until 10 years ago, micropores were believed to contribute only marginally to the electricity storage because they did not allow (solvated) ions to adsorb for steric reasons. However, Chmiola et al. showed that in organic solvent-based electrolytes, on the contrary, there was an increase of the capacitance when using microporous carbons with a very narrow pore size distribution [108], and in the absence of mesopores. These results were quickly confirmed for aqueous salts [153], leading to the conclusion that ions could desolvate in order to enter into narrow pores. It is worth noting that the increase in the performance is observed whatever the normalization used for the capacitance (i.e. surface, mass, or volume) [138], which means that the storage mechanism strongly differs from the case of mesoporous carbons. However, the applicability of this conclusion to the case of RTILs was not straightforward, since the first coordination sphere of an ion does not consist in neutral molecules, but rather of ions of opposite sign. Largeot et al., therefore, studied the case of EMIM-TFSI inside microporous carbons of various pore size distributions, and concluded that here again the capacitance was maximal when the pore size is very close to the ion dimension [109], as illustrated

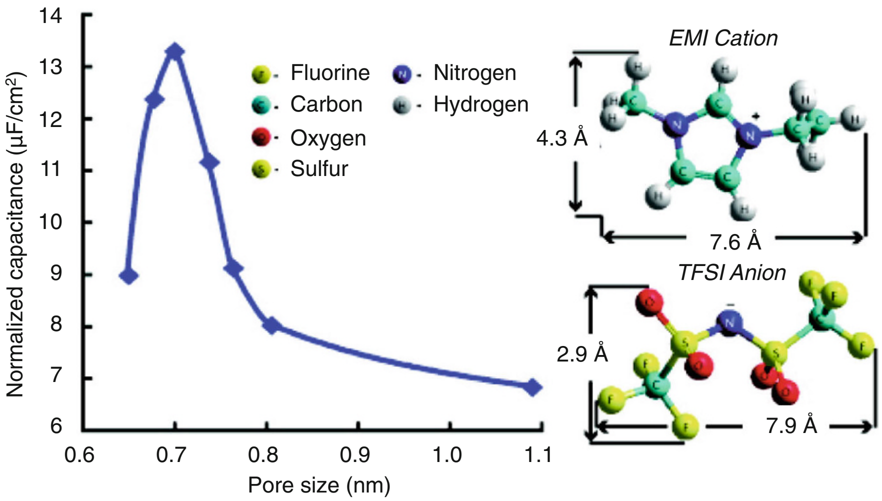

Fig. 11 "Anomalous" increase of the capacitance in nanoporous carbons with a EMIM-TFSI ionic liquid electrolyte. Reproduced with permission from Ref. [109]. Copyright 2008 American Chemical Society

on Fig. 11. The corresponding normalized integral capacitance was 13 μF cm^{-2} for an average pore size of 0.7 nm, compared to a much lower value of 7 μF cm^{-2} for a size of 1.1 nm. This increase in the capacitance is now well understood based on the knowledge of the structure adopted by the liquid inside the pores, as discussed above. The main features are: (1) the formation of a superionic state due to the metallic screening of the electrostatic interaction [101] and (2) the absence of layered structure due to the confinement of the liquid [100]. More specifically, the latter observation leads to the absence of overscreening effects at low applied potentials. A lot of efforts were also devoted to the study of the dependence of the capacitance with the pore size, generally assuming a slit-like or a nanotube geometry for the latter. These studies agreed with the presence of a maximum in the capacitance for pore sizes corresponding to a monolayer of adsorbed ions [99], but they also predicted the existence of further oscillations in the variations, with several secondary maxima of the capacitance [102, 103, 106]. These maxima occur when an optimal number of adsorbed layers are formed. The effect of electrode curvature and/or roughness were also investigated (both for porous and non-porous electrodes) [154, 155]. In general, the presence of such structural patterns in the electrode, that lead to a breaking of the layered structure of the liquid, result in marked increases of the interfacial capacitance [156, 157].

An important question is whether the use of ionic liquids lead to enhanced capacitances compared to organic solvents. Although there are not many comparative studies, a short answer is that it does not since the capacitance values are generally of the same magnitude. In an attempt to solve this issue, we recently performed a combined electrochemical/simulation study in which the electrolyte was switched from a pure ionic liquid to its mixture with acetonitrile [127]. It showed that the capacitance exhibited almost no variation, a result that we attributed to an increase in the difficulty of separating ions of opposite charges when they are more concentrated, i.e. in the absence of a solvent which screens the Coulombic interactions.

3.2.3 Redox-Active ILs

Although conventional RTILs do not show enhanced capacitances with respect to organic solvents, it is also possible to take profit from their wide tunability to propose new concepts. First steps were taken in that direction by Li et al., who studied dicationic RTILs [158, 159] by electrochemistry experiments and molecular simulations. In their electrolytes, the cations have a charge of +2 e, with the aim to accumulate more charge on the surface of the electrodes. However, this approach was not very successful, since no significant increase of the capacitance was observed. This is because the cations roughly occupy a volume that is double of the single-charged ones, so that the charge density is not enhanced. In addition, the corresponding liquids are very viscous, so that the temperature needs to be increased (or some organic solvents has to be added [160]) to obtain correct performances in supercapacitor applications.

Another option consists in including redox-active species inside the RTIL [161]. This idea has already been explored in aqueous electrolytes-based EDLC, in which using the iodide/iodine redox couple lead to significant enhancement of the

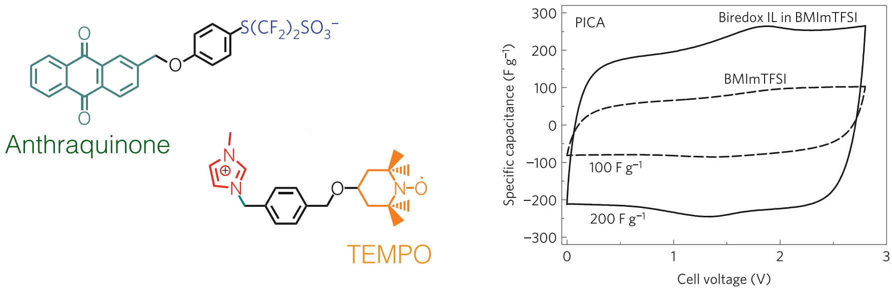

Fig. 12 **a** Structure of a biredox ionic liquid made by functionalizing perfluorosulfonate anion (PFS$^-$) and imidazolium cation respectively with anthraquinone (AQ) and 2,2,6,6-tetramethylpiperidinyl-1-oxyl (TEMPO) moieties. **b** Cyclic voltammetry at 5 mV s^{-1} with 0.5 mol L^{-1} biredox IL dissolved in BMIM-TFSI (*solid line*) and pure BMIM-TFSI (*dashed line*), respectively, and electrodes made with an activated carbon. Adapted with permission from Ref. [22]

performance of the device [162, 163]. The same couple was tested in a RTIL by Tooming et al. by adding EMIM-I into EMIM-BF$_4$, at a concentration of 5 wt%. Although the physical properties were not drastically modified (i.e. the conductivity dropped from 13.6 to 12.8 mS cm^{-1}, while the melting point increased from 17 to 19.5 °C), a noticeable increase in specific capacitance was obtained [164]. In the cyclic voltammetry, a clear Faradaic contribution appears on top of the conventional capacitive current, resulting in a higher stored charge by approximately 50 % (specific energy of 36.7 Wh kg^{-1} for the device).

Even better performances are obtained when the ionic liquids are specifically designed. The most recent example is the use of biredox ionic liquids, which were proposed by Mourad et al. [165]. They consist of perfluorosulfonate anion (PFS$^-$) and imidazolium cation that are respectively functionalized with anthraquinone (AQ) and 2,2,6,6-tetramethylpiperidinyl-1-oxyl (TEMPO) moieties. When the supercapacitor is charged with this liquid, the AQ-PFS$^-$ is adsorbed at the negative electrode and is reduced as AQ$^-$-PFS$^-$, or further to AQ^{2-}-PFS$^-$. Concurrently, MIM$^+$-TEMPO is adsorbed at the positive electrode and oxidized as MIM$^+$-TEMPO$^+$ [22]. As shown on Fig. 12, the use of this redox-active electrolyte leads to a doubling of the capacitance compared to pure BMIM-TFSI [22], which clearly opens new perspective for capacitive energy storage. The interplay between the adsorption of the ions inside the porous carbons and the kinetics of electron transfer remains to be fully understood, so that applying the same simulation and in situ spectroscopy methodology [6] as for conventional RTIL would be very useful for elucidating the charging mechanism in biredox ionic liquids.

4 Conclusions and Perspectives

Ionic liquids have widely been investigated as potential electrolytes for supercapacitors. Despite this intense activity, it is still not clear whether they will be able to replace conventional organic electrolytes such as acetonitrile or propylene carbonate in commercial devices. This is mainly due to their bulk properties. On the one hand, they show enhanced stability at high temperature, with very high boiling point, which ensures a better safety. They also have a very wide electrochemical window, which is very important since the energy density is proportional to the square of the operating voltage (and the power density is proportional to it as well). On the other hand, they have relatively high melting point, which prevents their use at extremely low temperature conditions (but this problem may be overcome by using mixtures of ionic liquids). Finally, and most importantly, their electrical conductivity and the individual diffusion coefficients of the ions are lower than in organic electrolytes by at least one order of magnitude (correspondingly, the viscosity is much higher). This is highly detrimental for the power density of the devices, since it may cancel one of the advantages of supercapacitors over batteries.

Concerning the interfacial properties, we now have a much better knowledge of the structure of ionic liquids adsorbed on metallic electrodes than 10 years ago [13]. The combination of many experimental, theoretical, and simulation techniques showed that RTILs adopt a layered structure at planar surfaces. Inside these layers, ordered or disordered structures have been observed, which may impact some properties such as the differential capacitance. Surface defects, such as the presence of curvature or roughness, may partially break this layering, resulting in a more efficient charging of the double-layer upon application of a voltage. But the best performances are obtained when using nanoporous carbons. Because of the strong screening of the electrostatic interactions by the electrically conducting walls, a “superionic” state forms in which it is possible to pack together ions of the same sign. However, the largest concentration of ions inside RTILs compared to conventional electrolytes does not lead to noticeable increase in the capacitance because the ions are more difficult to separate.

As a consequence, the most promising perspectives for ionic liquids to be used in supercapacitors are (1) mixing them with organic solvents in order to obtain the best compromise for all the bulk and interfacial properties and (2) taking profit from their structural versatility to functionalize them in order to introduce specific interactions with the surface or redox properties. In this light, the recent synthesis of biredox ionic liquids appears as a very promising lead to improve the energy density of electric-double layer capacitors.

References

1. Miller JR, Simon P (2008) Science 321:651
2. Salanne M, Rotenberg B, Simon P (2014) La Recherche 491:52
3. Simon P, Gogotsi Y (2008) Nat Mater 7:845
4. Béguin F, Presser V, Balducci A, Frackowiak E (2014) Adv Mater 26:2219
5. Brousse T, Belanger D, Long JW (2015) J Electrochem Soc 162:A5185
6. Salanne M, Rotenberg B, Naoi K, Kaneko K, Taberna PL, Grey CP, Dunn B, Simon P (2016) Nat Energy 1:16070
7. Forse AC, Merlet C, Griffin JM, Grey CP (2016) J Am Chem Soc 138:5731
8. McEwen AB, Ngo HL, LeCompte K, Goldman JL (1999) J Electrochem Soc 146:1687
9. Sato T, Masuda G, Takagi K (2004) Electrochim Acta 49:3603

10. Lewandowski A, Galínski M (2004) J Phys Chem Solids 65:281
11. Balducci A, Bardi U, Caporali S, Mastragostino M, Soavi F (2004) Electrochem Commun 6:566
12. Tee E, Tallo I, Thomberg T, Jänes A, Lust E (2016) J Electrochem Soc 163:A1317
13. Kornyshev AA (2007) J Phys Chem B 111:5545
14. Merlet C, Rotenberg B, Madden PA, Salanne M (2013) Phys Chem Chem Phys 15:15781
15. Fedorov MV, Kornyshev AA (2014) Chem Rev 114:2978
16. Coadou E, Goodrich P, Neale AR, Timperman L, Hardacre C, Jacquemin J, Anouti M (2016) ChemPhysChem 17:3992
17. Lee JH, Ryu JB, Lee AS, Na W, Yoon HS, Kim WJ, Koo CM (2016) Electrochim Acta 222:1847
18. Niedermeyer H, Hallett JP, Villar-Garcia IJ, Hunt PA, Welton T (2012) Chem Soc Rev 41:7780
19. Clough MT, Crick CR, Gräsvik J, Hunt PA, Niedermeyer H, Welton T, Whitaker OP (2015) Chem Sci 6:1101
20. Krause A, Balducci A (2011) Electrochem Commun 13:814
21. Pohlmann S, Olyschlager T, Goodrich P, Vicente JA, Jacquemin J, Balducci A (2015) Electrochim Acta 153:426
22. Mourad E, Coustan L, Lannelongue P, Zigah D, Mehdi A, Vioux A, Freunberger SA, Favier F, Fontaine O (2016) Nat Mater. doi:10.1038/nmat4808
23. Earle MJ, Esperança JMSS, Gilea MA, Canongia Lopes JN, Rebelo LPN, Magee JW, Seddon KR, Widegren JA (2006) Nature 439:831
24. Clough MT, Geyer K, Hunt PA, Mertes J, Welton T (2013) Phys Chem Chem Phys 15:20480
25. Maton C, De Vos N, Stevens CV (2013) Chem Soc Rev 42:5963
26. Villanueva M, Coronas A, Garcá J, Salgado J (2013) Ind Eng Chem Res 52:15718
27. Lin RY, Taberna PL, Fantini S, Presser V, Perez CR, Malbosc F, Rupesinghe NL, Teo KBK, Gogotsi Y, Simon P (2011) J Phys Chem Lett 2:2396
28. Piwek J, Platek A, Fic K, Frackowiak E (2016) Electrochim Acta 215:179
29. Fic K, Meller M, Menzel J, Frackowiak E (2016) Electrochim Acta 206:496
30. Chiba K, Ueda T, Yamagushi Y, Oki Y, Shimodate F, Naoi K (2011) J Electrochem Soc 158:A872
31. Chiba K, Ueda T, Yamaguchi Y, Oki Y, Saiki F, Naoi K (2011) J Electrochem Soc 158:A1320
32. Brandt A, Isken P, Lex-Balducci A, Balducci A (2012) J Power Sources 204:213
33. Schütter C, Passerini S, Korth M, Balducci A (2017) Electrochim Acta 224:278
34. Schütter C, Husch T, Korth M, Balducci A (2015) J Phys Chem C 119:13413
35. Cheng L, Assary RS, Qu X, Jain A, Ong SP, Rajput NN, Persson K, Curtiss LA (2015) J Phys Chem Lett 6:283
36. Jain A, Persson KA, Ceder G (2016) APL Mater 4:053102
37. Izgorodina EI (2010) Phys Chem Chem Phys 13:4189
38. Izgorodina EI, Seeger ZL, Scarborough DLA, Tan SYS (2017) Chem Rev. doi:10.1021/acs.chemrev.6b00528
39. Firaha DS, Hollóczki O, Kirchner B (2015) Angew Chem Int Ed 54:7805
40. Conway BE (1999) Electrochemical supercapacitors: scientific fundamentals and technological applications. Kluwer, Dordrecht
41. Tokuda H, Hayamizu K, Ishii K, Susan MABH, Watanabe M (2004) J Phys Chem B 108:16593
42. Krynicki K, Green CD, Sawyer DW (1978) Faraday Discuss 66:199
43. Kashyap HK, Annapuredy HVR, Raineri FO, Margulis CJ (2011) J Phys Chem B 115:13212
44. Salanne M, Simon C, Groult H, Lantelme F, Goto T, Barhoun A (2009) J Fluorine Chem 130:61
45. Levesque M, Sarou-Kanian V, Salanne M, Gobet M, Groult H, Bessada C, Rollet AL (2013) J Chem Phys 138:184503
46. Zhou ZB, Takeda M, Ue M (2004) J Fluorine Chem 125:471
47. Every H, Bishop AG, Forsyth M, MacFarlane DR (2000) Electrochim Acta 45:1279
48. Le Bideau J, Viau L, Vioux A (2011) Chem Soc Rev 40:907
49. Brachet M, Brousse T, Le Bideau J (2014) ECS Electrochem Lett 3:A112
50. Mezger M, Roth R, Schröder H, Reichert P, Pontoni D, Reichert H (2015) J Chem Phys 124:164707
51. Bazant MZ, Storey BD, Kornyshev AA (2011) Phys Rev Lett 106:046102
52. Atkin R, Warr GG (2007) J Phys Chem C 111:5162
53. Hayes E, Warr GG, Atkin R (2010) Phys Chem Chem Phys 12:1709
54. Atkin R, Borisenko N, Drüschler M, Zein El Abedin S, Endres F, Hayes R, Huber B, Roling B (2011) Phys Chem Chem Phys 13:6849
55. Perkin S, Albrecht T, Klein J (2010) Phys Chem Chem Phys 12(6):1243

56. Perkin S, Crowhurst L, Niedermeyer H, Welton T, Smith AM, Gosvami NN (2011) Chem Commun 47:6572
57. Perkin S (2012) Phys Chem Chem Phys 14:5052
58. Smith AM, Lovelock KRJ, Gosvami NN, Licence P, Dolan A, Welton T, Perkin S (2013) J Phys Chem Lett 4:378
59. Mezger M, Schröder H, Reichert H, Schramm S, Okasinski JS, Schröder S, Honkimäki V, Deutsch M, Ocko BM, Ralston J, Rohwerder M, Stratmann M, Dosch H (2008) Science 322:424
60. Duarte D, Salanne M, Rotenberg B, Bizeto MA, Siqueira LJA (2014) J Phys Condens Matter 26:284107
61. Canongia Lopes JNA, Pádua AAH (2006) J Phys Chem B 110:3330
62. Hu Z, Vatamanu J, Borodin O, Bedrov D (2013) Phys Chem Chem Phys 15:14234
63. Hu Z, Vatamanu J, Borodin O, Bedrov D (2014) Electrochim Acta 145:40
64. Méndez-Morales T, Carrete J, Pérez-Rodríguez M, Cabeza O, Gallego LJ, Lynden-Bell RM, Varela LM (2014) Phys Chem Chem Phys 16:13271
65. Ivanistsev V, Fedorov MV, Lynden-Bell RM (2014) J Phys Chem C 118:5841
66. Ivanistsev V, Méndez-Morales T, Lynden-Bell RM, Cabeza O, Gallego LJ, Varela LM, Fedorov MV (2016) Phys Chem Chem Phys 18:1302
67. Baldelli S (2005) J Phys Chem B 109:13049
68. Baldelli S (2008) Acc Chem Res 41:421
69. Baldelli S (2013) J Phys Chem Lett 4:244
70. Sulpizi M, Salanne M, Sprik M, Gaigeot MP (2013) J Phys Chem Lett 4:83
71. Pashley RM, Israelachvili JN (1984) J Colloid Interface Sci 101:511
72. Baimpos T, Shrestha BR, Raman S, Valtiner M (2014) Langmuir 30:4322
73. Smith AM, Lee AA, Perkin S (2016) J Phys Chem Lett 7:2157
74. Gebbie MA, Valtiner M, Banquy X, Fox ET, Henderson WA, Israelachvili JN (2013) Proc Natl Acad Sci USA 110:9674
75. Gebbie MA, Dobbs HA, Valtiner M, Israelachvili JN (2015) Proc Natl Acad Sci USA 112:7432
76. Perkin S, Salanne M, Madden P, Lynden-Bell R (2013) Proc Natl Acad Sci USA 110:E4121
77. Gebbie MA, Smith AM, Dobbs HA, Lee AA, Warr GG, Banquy X, Valtiner M, Rutland MW, Israelachvili JN, Perkin S, Atkin R (2017) Chem Commun 53:1214
78. Tazi S, Salanne M, Simon C, Turq P, Pounds M, Madden PA (2010) J Phys Chem B 114:8453
79. Merlet C, Limmer DT, Salanne M, van Roij R, Madden PA, Chandler D, Rotenberg B (2014) J Phys Chem C 118:18291
80. Kirchner K, Kirchner T, Ivanistsev V, Fedorov MV (2013) Electrochim Acta 110:762
81. Rotenberg B, Salanne M (2015) J Phys Chem Lett 6:4978
82. Freyland W (2008) Phys Chem Chem Phys 10:923
83. Su YZ, Fu YC, Yan JW, Chen ZB, Mao BW (2009) Angew Chem Int Ed 48:5148
84. Wen R, Rahn B, Magnussen OM (2015) Angew Chem Int Ed 54:6062
85. Elbourne A, McDonald S, Voitchovsky K, Endres F, Warr GG, Atkin R (2015) ACS Nano 9:7608
86. Uysal A, Zhou H, Feng G, Lee SS, Li S, Fenter P, Cummings PT, Fulvio PF, Dai S, McDonough JK, Gogotsi Y (2014) J Phys Chem C 118:569
87. Garcia Rey N, Dlott DD (2015) J Phys Chem C 119:20892
88. Sweeney J, Hausen F, Hayes R, Webber GB, Endres F, Rutland MW, Bennewitz R, Atkin R (2012) Phys Rev Lett 109:155502
89. Kornyshev AA, Qiao R (2014) J Phys Chem C 118:18285
90. Pounds M, Tazi S, Salanne M, Madden PA (2009) J Phys Condens Matter 21:424109
91. Roy D, Maroncelli M (2010) J Phys Chem B 114:12629
92. Comtet J, Niguès A, Kaiser V, Bocquet L, Siria A, arXiv:1611.08448 (2017)
93. Forse AC, Griffin JM, Merlet C, Bayley PM, Wang H, Simon P, Grey CP (2015) J Am Chem Soc 137:7231
94. Hummer G, Rasaiah JC, Noworyta JP (2001) Nature 414:188
95. Chaban VV, Prezhdo OV (2014) ACS Nano 8:8190
96. Nuelos JLB, Feng G, Fulvio PF, Li S, Rother G, Dai S, Cummings PT, Wesolowski DJ (2014) Chem Mater 26:1144
97. Wang H, Koster TKJ, Trease NM, Segalini J, Taberna PL, Simon P, Gogotsi Y, Grey CP (2011) J Am Chem Soc 133:19270
98. Deschamps M, Gilbert E, Azais P, Raymundo-Piñero E, Ammar MR, Simon P, Massiot D, Béguin F (2013) Nat Mater 12:351

99. Shim Y, Kim HJ (2010) ACS Nano 4:2345
100. Merlet C, Rotenberg B, Madden PA, Taberna PL, Simon P, Gogotsi Y, Salanne M (2012) Nat Mater 11:306
101. Kondrat S, Kornyshev AA (2011) J Phys Condens Matter 23:022201
102. Wu P, Huang JS, Meunier V, Sumpter BG, Qiao R (2011) ACS Nano 5:9044
103. Feng G, Cummings PT (2011) J Phys Chem Lett 2:2859
104. Wu P, Huang J, Meunier V, Sumpter BG, Qiao R (2012) J Phys Chem Lett 3:1732
105. Rajput NN, Monk JD, Singh R, Hung FR (2012) J Phys Chem C 116:5170
106. Jiang DE, Jin Z, Wu J (2011) Nano Lett 11:5373
107. Pizio O, Sokolowski S, Sokolowska Z (2012) J Chem Phys 137:234705
108. Chmiola J, Yushin G, Gogotsi Y, Portet C, Simon P, Taberna PL (2006) Science 313:1760
109. Largeot C, Portet C, Chmiola J, Taberna PL, Gogotsi Y, Simon P (2008) J Am Chem Soc 130:2730
110. Palmer JC, Llobet A, Yeon SH, Fisher JE, Shi Y, Gogotsi Y, Gubbins KE (2010) Carbon 48:1116
111. Farmahini AH, Opletal G, Bhatia SK (2013) J Phys Chem C 117:14081
112. Merlet C, Péan C, Rotenberg B, Madden PA, Daffos B, Taberna PL, Simon P, Salanne M (2013) Nat Commun 4:2701
113. van Meel JA, Filion L, Valeriani C, Frenkel D (2012) J Chem Phys 136:234107
114. Varanasi SR, Farmahini AH, Bhatia SK (2015) J Phys Chem C 119:28809
115. Prehal C, Koczwara C, Jäckel N, Schreiber A, Burian M, Amenitsch H, Hartmann MA, Presser V, Paris O (2017) Nat Energy 2:16215
116. Salanne M, Madden PA (2011) Mol Phys 109:2299
117. Urahata SM, Ribeiro MCC (2004) J Chem Phys 120:1855
118. Kashyap HK, Hettige JJ, Annapuredy HVR, Margulis CJ (2012) Chem Commun 48:5103
119. Kondrat S, Georgi N, Fedorov MV, Kornyshev AA (2011) Phys Chem Chem Phys 13:11359
120. Rochester CC, Lee AA, Pruessner G, Kornyshev AA (2013) ChemPhysChem 14:4121
121. Pean C, Daffos B, Merlet C, Rotenberg B, Taberna PL, Simon P, Salanne M (2015) J Electrochem Soc 162:A5091
122. Drüschler M, Huber B, Roling B (2011) J Phys Chem C 115:6802
123. Taberna PL, Simon P, Fauvarque JF (2003) J Electrochem Soc 150:A292
124. Drüschler M, Huber B, Passerini S, Roling B (2010) J Phys Chem C 114:3614
125. Druschler M, Borisenko N, Wallauer J, Winter C, Huber B, Endres F, Roling B (2012) Phys Chem Chem Phys 14:5090
126. Roling B, Drüschler M, Huber B (2012) Faraday Discuss 154:303
127. Burt R, Breitsprecher K, Daffos B, Taberna PL, Simon P, Birkett G, Zhao XS, Holm C, Salanne M (2016) J Phys Chem Lett 7:4015
128. Siepmann JI, Sprik M (1995) J Chem Phys 102:511
129. Reed SK, Lanning OJ, Madden PA (2007) J Chem Phys 126:084704
130. Limmer DT, Merlet C, Salanne M, Chandler D, Madden PA, van Roij R, Rotenberg B (2013) Phys Rev Lett 111:106102
131. Breitsprecher K, Szuttor K, Holm C (2015) J Phys Chem C 119:22445
132. Kiyohara K, Asaka K (2007) J Phys Chem 111:15903
133. Kiyohara K, Sugino T, Asaka K (2010) J Chem Phys 132:144705
134. Kiyohara K, Yamagata M, Ishikawa M (2016) J Chem Phys 144:134701
135. Wang Z, Yang Y, Olmsted DL, Asta M, Laird BB (2014) J Chem Phys 141:184102
136. Merlet C, Péan C, Rotenberg B, Madden PA, Simon P, Salanne M (2013) J Phys Chem Lett 4:264
137. Thommes M, Kaneko K, Neimark AV, Olivier JP, Rodriguez-Reinoso F, Rouquerol J, Sing KSW (2015) Pure Appl Chem 87:1051
138. Jäckel N, Simon P, Gogotsi Y, Presser V (2016) ACS Energy Lett 1:1262
139. Alam MT, Islam MM, Okajima T, Ohsaka T (2007) Electrochem Commun 9:2370
140. Islam M, Alam M, Ohsaka T (2008) J Phys Chem C 112:16568
141. Islam M, Alam M, Okajima T, Ohsaka T (2009) J Phys Chem C 113:3386
142. Alam MT, Islam MM, Okajima T, Ohsaka T (2009) J Phys Chem C 113:6596
143. Lockett V, Sedev R, Ralston J, Horne M, Rodopoulos T (2008) J Phys Chem C 112:7486
144. Lockett V, Horne M, Sedev R, Rodopoulos T, Ralston J (2010) Phys Chem Chem Phys 12:12499
145. Silva F, Gomes C, Figueiredo M, Costa R, Martins A, Pereira CM (2008) J Electroanal Chem 622:153
146. Costa R, Pereira CM, Silva F (2013) RSC Adv 3:11697
147. Costa R, Pereira CM, Silva AF (2016) Electrochim Acta 195:150

148. Costa R, Pereira CM, Silva AF (2015) Electrochem Commun 57:10
149. Fedorov MV, Kornyshev AA (2008) J Phys Chem B 112:11868
150. Fedorov MV, Kornyshev AA (2008) Electrochim Acta 53:6835
151. Fedorov MV, Georgi N, Kornyshev AA (2010) Electrochem Commun 12:296
152. Feng G, Huang J, Sumpter BG, Meunier V, Qiao R (2011) Phys Chem Chem Phys 13:14723
153. Raymundo-Piñero E, Kierzek K, Machnikowski J, Béguin F (2006) Carbon 44:2498
154. Feng G, Jiang D, Cummings PT (2012) J Chem Theory Comput 8:1058
155. Paek E, Pak AJ, Hwang GS (2013) J Phys Chem C 117:23539
156. Vatamanu J, Vatamanu M, Bedrov D (2015) ACS Nano 9:5999
157. Vatamanu J, Bedrov D (2015) J Phys Chem Lett 6:3594
158. Li S, van Aken KL, McDonough JK, Feng G, Gogotsi Y, Cummings PT (2014) J Phys Chem C 118:3901
159. Li S, Feng G, Cummings PT (2014) J Phys Condens Matter 26:284106
160. Li S, Zhang P, Fulvio PF, Hillesheim PC, Feng G, Dai S, Cummings PT (2014) J Phys Condens Matter 26:284105
161. Akinwolemiwa B, Peng C, Chen GZ (2015) J Electrochem Soc 162:A5054
162. Frackowiak E, Meller M, Menzel J, Gastol D, Fic K (2014) Faraday Discuss 172:179
163. Fic K, Meller M, Frackowiak E (2015) J Electrochem Soc 162:A5140
164. Tooming T, Thomberg T, Siinor L, Tõnurist K, Jänes A, Lust E (2014) J Electrochem Soc 161:A222
165. Mourad E, Coustan L, Freunberger SA, Mehdi A, Vioux A, Favier F, Fontaine O (2016) Electrochim Acta 206:513

Top Curr Chem (Z) (2018) 376:9
https://doi.org/10.1007/s41061-018-0186-3

REVIEW

Electrochemical Synthesis of Battery Electrode Materials from Ionic Liquids

Abhishek Lahiri[1] · Natalia Borisenko[1] · Frank Endres[1]

Received: 31 August 2017 / Accepted: 9 January 2018

Abstract Electrode materials as well as the electrolytes play a decisive role in batteries determining their performance, safety, and lifetime. In the last two decades, different types of batteries have evolved. A lot of work has been done on lithium ion batteries due to their technical importance in consumer electronics, however, the development of post-lithium systems has become a focus in recent years. This chapter gives an overview of various battery materials, primarily focusing on development of electrode materials in ionic liquids via electrochemical route and using ionic liquids as battery electrolyte components.

Keywords Ionic liquids · Battery · Electrode materials · Electrodeposition

1 Introduction

Portable devices, such as laptops, mobile phones, mp3 players etc., as well as electric vehicles need batteries as an energy source. Due to recent developments, the demand for energy has increased and therefore batteries with higher energy and power density are needed. Therefore, in the last two decades, a lot of research has been done on the development of a new generation of batteries, especially with high energy storage and fast charging capability.

Chapter 3 was originally published as Lahiri, A., Borisenko, N. & Endres, F. Top Curr Chem (Z) (2018) 376: 9. https://doi.org/10.1007/s41061-018-0186-3.

✉ Natalia Borisenko
natalia.borissenko@tu-clausthal.de

[1] Institute of Electrochemistry, Clausthal University of Technology, Arnold-Sommerfeld-Straße 6, 38678 Clausthal-Zellerfeld, Germany

Over the years, different types of batteries have been developed with the first commercialization of a portable rechargeable battery in 1991 by Sony [1]. A commercial lithium ion battery (LIB) usually consists of a graphite anode, a Li_xCoO_2 cathode, and an organic electrolyte. Lithium intercalation and deintercalation processes take place during charging and discharging of the battery according to Eqs. (1) and (2).

$$x\mathrm{LiC}_6 = x\mathrm{Li}^+ + xe^- + x\mathrm{C}_6 \tag{1}$$

$$\mathrm{Li}_{1-x}\mathrm{CoO}_2 + x\mathrm{Li}^+ + xe^- = \mathrm{LiCoO}_2 \tag{2}$$

During charging of the battery, Li intercalates into graphite, forming LiC_6, and deintercalates during the discharge process. The opposite reaction takes place at the other electrode, wherein Li deintercalates during the charging, forming a sub-stoichiometric $Li_{1-x}CoO_2$, whereas during discharging of the battery it forms $LiCoO_2$. The total storage capacity for a graphite anode was found to be 372 mAh g^{-1}. In order to improve the storage capacity and cell voltage, different cathode and anode materials have been developed. Recently, silicon has been identified as a promising material with a theoretical capacity of 4200 mAh g^{-1}. However, issues related to silicon volume changes, low conductivity, and material disintegration hamper battery performance [2–4]. Spinel-based cathodes, such as $Li(M_2)O_4$, have also been developed and modified in order to improve the storage capacity and the solid-state diffusion of Li^+ ions [5]. Finally, the electrolyte itself plays a pivotal role for the battery performance. In present commercial batteries, organic electrolytes are used. The main disadvantage of these electrolytes is their high flammability that compromises the safety of the battery. Therefore, non-inflammable ionic liquids (IL) have attracted a great research interest as promising battery electrolytes [6–8]. Intercalation/deintercalation or alloying/dealloying processes have been used for developing of various metal-ion (Na-ion, K-ion, and Ca-ion) batteries [9–12]. Na is more abundant than lithium, therefore currently a lot of research is focused on the development of Na-ion batteries, which might significantly reduce the battery costs. However, finding a suitable anode and cathode materials for Na-ion batteries is still at its infancy.

Metal–air batteries exhibit higher energy densities in comparison to metal–ion batteries [13]. In a metal–air battery, a metal electrode (e.g., Li, Zn or Al) serves as the anode, while the cathode is a porous electrode where the oxygen reduction reaction (ORR) takes place. Both aqueous and non-aqueous electrolytes have been used for metal–air batteries. However, various drawbacks in metal–air battery chemistry need to be overcome prior to commercialization. Therefore, a lot of fundamental research has been started to improve the battery performance and to evaluate the electrode–electrolyte interface. For example, one of the major issues in Li–air and Zn–air batteries is the formation of dendritic metal during battery cycling that leads to battery damage [14]. Strategies into developing a dendrite-free metal deposition at high current densities are ongoing. Similarly, at the cathode, for the ORR reaction to be efficient, a formation of a triple phase boundary is important. Furthermore, novel catalysts without the need of noble metals have to be developed in order to reduce the overall battery costs. Other major issues are electrolytes. As aqueous electrolytes can dry out, non-volatile electrolytes are of interest. Therefore, ionic liquids and ionic liquid–water mixtures have become quite interesting as promising electrolytes for metal–air batteries [15]. However, metal–air batteries are still far away from widespread commercialization.

From the above brief introduction, it is evident that current battery technology still needs a lot of improvement to match the current high energy demand. Therefore, the synthesis of new electrode materials with high storage capacity and appropriate safe electrolytes becomes essential for the development of future batteries with high energy storage capacity and fast charging capability.

In this chapter, we will give an overview on electrode materials that have been synthesized electrochemically from ionic liquids and that have been applied as battery electrodes with ionic liquid-based electrolytes. An overview of various battery systems of Li-ion, Na-ion, Li–air, Zn-based and Al-based batteries will be discussed. The importance of the electrode–electrolyte interface with respect to battery performance will also be briefly mentioned.

2 Electrode Materials for Li-Ion Batteries

Lithium-ion batteries (LIB) are practically used in every portable devices. The major impediments for using lithium-ion batteries for large-scale storage systems are the low storage capacity, relatively low long-term stability, and safety. Therefore, it becomes essential to find new materials or to modify existing materials in order to increase the storage capacity and to improve the long-term stability. Also, the development of a safe electrolyte is a primary issue to avoid a thermal runaway of such batteries. In this sub-section, we will give insight into the latest developments in battery materials that have been electrochemically synthesized in ionic liquids for Li-ion battery; furthermore, we will address safety issues.

Currently, carbonaceous materials are used as lithium-ion battery anodes [16]. Silicon, germanium, tin, aluminum, etc., have shown to be good alternative anode materials with a higher storage capacity compared to carbonaceous materials [17–20]. For example, the alloying of silicon and tin with Li leads to the formation of $Li_{22}Si_5$ and $Li_{22}Sn_5$, which gives a theoretical capacity of 4200 and 990 mAh g^{-1}, respectively. This is considerably better than graphite electrodes that can store only 372 mAh g^{-1}. However, silicon electrodes undergo about 300% volume expansion during lithiation/delithiation processes leading to capacity fading during cycling that limits their practical use. One approach to limit capacity fading is to reduce the particle size of electrode materials to the nanometer scale, which has shown to improve battery performance [21, 22]. However, the existence of side reactions and difficulties in maintaining interparticle contact reduce the battery performance [23]. Other approaches, such as encapsulating the nanoparticles in different carbon matrices or developing core–shell structures, have shown to improve the battery significantly [24–27]. Ma et al. [28] found that silicon nanoparticles encapsulated with ionic liquid-based carbon precursors lead to a stable battery performance. They showed that the choice of the ionic liquid is important as the carbon source, which leads to a tight integration of silicon and carbon, thereby cushioning the volume change during lithiation/delithiation processes. Galvanostatic charge–discharge cycling shows a good reversible capacity retention of 1380 mAh g^{-1} at a charge rate of 200 mA g^{-1}. Nevertheless, comparatively little has been studied with electrodeposited silicon as battery anodes for LIB. In 2004, the possibility of the electrodeposition of silicon in ionic liquids was reported [29]. Silicon was electrodeposited at room temperature on highly oriented pyrolytic graphite (HOPG) from 1-butyl-1-methlylpyrrolidinium bis(trifluoromethylsulfonyl)amide ($[Py_{1,4}]$TFSA) containing 1 M $SiCl_4$ [29]. In 2010, Schmuck et al. [30] showed that Si electrodeposited from $[Py_{1,4}]$TFSA containing $SiCl_4$ can be used as an anode material for LIB with both organic electrolyte and an ionic liquid-based electrolytes containing a lithium salt. Although the battery performance was not very good due to an inhomogeneous and thin Si deposit, the possibility of using electrodeposited silicon as battery electrode material was demonstrated. Recently, Vlaic et al. [31] showed that a thick layer of silicon can be deposited electrochemically on copper from 1 M $SiCl_4$ in $[Py_{1,4}]$TFSA and then used for LIB. The authors compared the LIB performance of the electrodeposited Si with two different electrolytes of 1 M $LiPF_6$ in ethylene carbonate/dimethyl carbonate and 1 M lithium bis(trifluoromethylsulfonyl)amide (LiTFSA) in $[Py_{1,4}]$TFSA. In the organic electrolyte, a specific capacity of 1200 mAh g^{-1} could be achieved at 0.1 C (400 mA g^{-1}), which decreased to 1000 mAh g^{-1} at 0.2 C (800 mA g^{-1}). However, comparatively lower values of 630 and 460 mAh g^{-1} were reached with the ionic liquid electrolyte at 0.1 C and 0.2 C, respectively, which the authors claimed was due to some hindrance during the lithiation process [31].

Similar to silicon, germanium undergoes a large volume change during lithiation/delithiation processes. Germanium has a theoretical capacity of 1600 mAh g^{-1} for the formation of $Li_{22}Ge_5$. Moreover, the diffusivity of lithium at room temperature in Ge is 400 times faster compared to silicon [32], which makes Ge an attractive anode material. Recently, the development of nanotubes and three-dimensional ordered macroporous (3DOM) structures by electrodeposition from ionic liquids has shown to be a simple process for developing electrode materials [33, 34]. Both of these structures have shown to be beneficial due to their bicontinous network, easier transportation of electrolyte inside of the porous structure, and short diffusion lengths that results in improved battery performance and cycling behavior. The electrodeposited macroporous Ge was tested as an anode material for LIB with an organic electrolyte of 1.1 M $LiPF_6$ in ethylene carbonate-diethyl carbonate. Compared to electrodeposited Ge film, the 3DOM structure retained a capacity of 844 mAh g^{-1} for 50 cycles at a rate of 0.2 C [35]. On increasing the C-rate, it was shown that the reversible capacity for the 3DOM structure was about 30% greater than electrodeposited thin film of Ge. Furthermore, the authors showed that after 50 charge–discharge cycles, cracks developed for the electrodeposited Ge film. In comparison, although significant changes in the 3DOM structure were observed, no crack formation was seen [35]. The same group showed the use of template-assisted electrodeposited Ge nanotubes as anode for LIB [36]. Compared to 3DOM structure, Ge nanotubes showed a capacity of more than 1025 mAh g^{-1} for 50 cycles at 0.2 C. Furthermore, Ge nanotubes were shown to be very stable between 50th and 250th cycle with a capacity loss of only 0.01%. The electrodeposited Ge nanotubes synthesized using ionic liquids showed much better performance compared to Ge nanotubes developed using Kirkendall effect, which is a high-temperature process [36]. Furthermore, it was shown that Ge nanotubes retain a higher capacity at relatively high charge rates of 2 C compared to Ge nanowires grown using vapor–liquid–solid (VLS) technique. At 2 C rate, a capacity of 844 mAh g^{-1} could be achieved for the electrodeposited Ge nanotubes, whereas only 600 mAh g^{-1} was achieved for Ge nanowires. This could be due to better electrode–electrolyte contact and higher surface area of the Ge nanotubes. In 2015, Hao et al. [37] electrodeposited Ge nanotubes on carbon nanotubes from 1-ethyl-3-methylimidazolium bis(trifluoromethylsulfonyl)amide ([EMIm]TFSA) to form a Ge nanotube-carbon composite. It was shown that at over 100 cycles, a capacity of 810 mAh g^{-1} at 0.2 C is achieved for Ge nanotube-carbon composite, which is less than the capacity obtained for electrodeposited 3DOM and Ge nanotube structures. The reversible capacity was also shown to fade with increase in cycle number. This indicates that the electrodeposited Ge nanotube on carbon nanotube did not form a stable composite, which might have led to a capacity loss.

Recently, ionic liquids have attracted great interest as possible electrolytes instead of organic solvents for LIB. Compared to organic solvents, ionic liquids are much safer electrolytes due to their low vapor pressure and non-inflammability. Furthermore, ionic liquids possess wide electrochemical windows and relatively high thermal stability, which make them promising solvent media for LIB. Atomic force microscopy (AFM) has been used to study the interface of electrodeposited Ge during the lithiation/delithiation process in an ionic liquid-based electrolyte [38]. First, a thin layer of Ge was electrodeposited at a constant potential of − 1.9 V for 30 min on Cu from $[Py_{1,4}]$TFSA containing 0.25 M $GeCl_4$. After the electrodeposition, the remaining ionic liquid in the cell was removed and the electrodeposited Ge was cleaned with the pure IL inside of the glove box. Subsequently, Li deposition and stripping cycles were performed in 0.5 M LiTFSA-$[Py_{1,4}]$TFSA on the deposited Ge. It was found that during the lithiation process, a layer known as solid electrolyte interphase (SEI) forms on the electrodeposited Ge [38]. The morphology and the composition of this SEI layer was studied in detail using AFM, scanning electron microscopy (SEM) and X-ray photoelectron spectroscopy (XPS) at various cut-off potentials during Li intercalation/deintercalation cycles. Figure 1 shows 3D AFM images and force–distance curves of the electrodeposited Ge before and after cycling in 0.5 M LiTFSA-$[Py_{1,4}]$TFSA. The 3D morphology of the electrodeposited Ge reveals the formation of Ge clusters (Fig. 1a). Force–distance measurements show a direct contact as expected when the cantilever touches the surface of the electrodeposited Ge. However, after one charge–discharge cycle, the morphology of the surface changes significantly, as an SEI layer forms on the surface of the electrodeposited Ge (Fig. 1b). As the AFM tip moves towards the surface, a broad layer is obtained at 149 nm and a force of 381 nN is needed to rupture this layer. Furthermore, from the force–distance measurements, the formation of the SEI layer with a multi-layered structure is evident, as seen by a linear increase followed by a plateau region in Fig. 1b. Thus, after the first lithiation/delithiation cycle, the SEI layer has a porous structure, which suggests that the SEI layer was not stable in the first cycle. After ten lithiation/delithiation cycles, a relatively stable SEI layer is obtained (Fig. 1c). The thickness of the layer does not change significantly during subsequent scanning. After ten cycles, an SEI layer of about 151 nm in thickness is obtained,

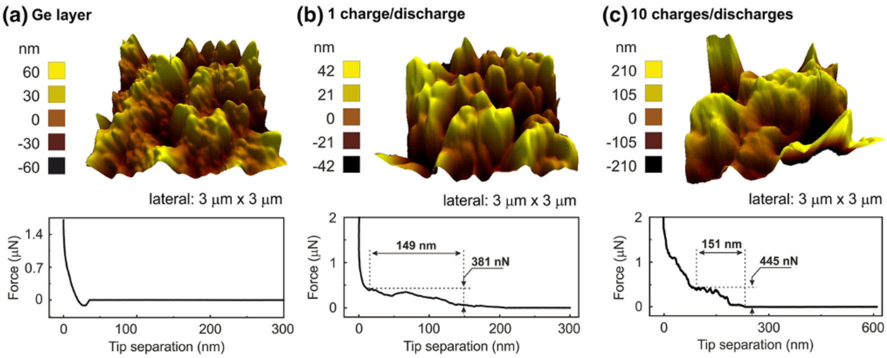

Fig. 1 3D AFM images of the electrodeposited Ge and force–distance curves **a** before cycling, **b** after one charge–discharge cycle, and **c** after ten charge–discharge cycles in 0.5 M LiTFSA-[$Py_{1,4}$]TFSA. Reproduced from Lahiri et al., *Phys. Chem. Chem. Phys.,* 2016 [38] with permission from the PCCP Owner Societies

however the force required to rupture the layer increases to 445 nN, as some change in the composition of the SEI layer might take place during charge–discharge cycles leading to the formation of a stable SEI layer [38]. XPS measurements indicate that during lithiation, Ge_xLi is formed, whereas during delithiation, a dealloying takes place. Besides, the formation of Li_2CO_3, LiOH, Li_2O_2, Li_2S is observed, which are products of the SEI layer. Infrared spectroscopy has shown changes in the lithium coordination in the ionic liquid during the lithiation and delithiation processes, which was related to the decomposition of the ionic liquid for the formation of a stable SEI layer [38].

Various ionic liquid-based electrolytes, such as mixtures of ionic liquids and ionic liquid-organic solvent mixtures, were evaluated as potential LIB electrolytes [39, 40]. It was found that 1-butyl-1-methylpyrrolidinium bis(fluorosulfonyl)amide ([$Py_{1,4}$]FSA) containing 1 M LiTFSA is a better solvent media for LIB compared to 1 M LiTFSA-[$Py_{1,4}$]TFSA with electrodeposited Ge as anode host material, as an almost two times higher charge–discharge capacity was found when LiTFSA-[$Py_{1,4}$] FSA was used [39]. This is due to a lower viscosity of [$Py_{1,4}$]FSA, which might have improved the diffusion of Li^+ ions. Moreover, Raman spectroscopy revealed that the Li ion coordination is different in [$Py_{1,4}$]TFSA and [$Py_{1,4}$]FSA. After charge–discharge cycles, it was observed that there is a decomposition in LiTFSA-[$Py_{1,4}$]TFSA, whereas LiTFSA-[$Py_{1,4}$]FSA was found to be more stable due to the formation of a stable SEI layer [39]. Kerner et al. [41] reported that ionic liquid electrolytes containing two anions are promising for high-temperature LIB up to 100 °C. However, from spectroscopic investigation, the authors concluded that the lithium coordination in the mixture of ionic liquids is quite complicated. These studies show that the mixture of ionic liquids containing two anions are more promising electrolytes for LIB compared to ionic liquids containing a single anion.

As ionic liquids containing lithium salts are viscous and have lower conductivities compared to lithium salts in organic solvents, mixtures of ionic liquid-organic solvents might be beneficial for improving the battery performance as well as for battery safety. Studies using such mixtures have been performed on various electrodes, but contradictory results have been obtained for battery performance [8, 42–44]. The influence of the addition of polar organic solvents to 1 M LiFSA-[$Py_{1,4}$]FSA was recently investigated on electrodeposited Ge [40]. It was found that using high polar organic solvents (acetonitrile) with ionic liquids resulted in better battery performance at low C-rates. Also, the conductivity of the electrolyte was found to be high due to the change in the cation–anion interaction of the ionic liquid [40]. On using less polar organic solvents (dimethyl carbonate), the battery performance decreased significantly. However, at higher C-rates, the ionic liquid containing lithium salt outperformed the ionic liquid-organic solvent mixtures. AFM and XPS studies revealed that the change in the battery performance is related to the difference in the structure of the SEI layer formed on the electrodeposited Ge in the presence and absence of organic solvents. Furthermore, XPS showed that on using mixtures of ionic liquid-organic solvent, after 50 charge–discharge cycles, some lithium was still alloyed with Ge, leading to a lower capacity with increase in cycle number [40].

Sn and SnO_2 have also been reported as promising candidates for the LIB anode [45]. During lithiation of SnO_2 anode, first a reduction step occurs forming Sn and Li_2O, followed by alloying of Li with Sn forming Li_xSn. However, alloying of Li with Sn also leads to a volume increase, which results in a decrease in capacity with charge–discharge cycles. To overcome volume changes, Sn/SnO_2-carbon-based composites have been developed using various techniques [45]. Ionic liquids have also been applied as a source for developing such composites. SnO_2-graphene composites were formed by ultrasonication in choline chloride/ethylene glycol ionic liquid-like electrolytes [46]. Using this composite, a stable battery performance was achieved giving a specific capacity of 535 mAh g^{-1} at 100 mA g^{-1} for 50 cycles, which was much higher compared to bare SnO_2. The role of graphene was to buffer the volume expansion during the lithiation process thereby improving capacity and stability of the electrode.

Sn and Sn nanowires and composites were electrodeposited from ionic liquids as potential electrode materials for LIB. It was observed that the tin morphology changed significantly on changing the anion of the ionic liquid. On using 1-butyl-1-methlylpyrrolidinium trifluoromethylsulfonate ([$Py_{1,4}$]TfO), agglomerated Sn deposits were obtained, whereas on using 1-butyl-1-methlylpyrrolidinium dicyanamide ([$Py_{1,4}$]DCA), dendritic Sn was obtained [47]. As dendritic growth is disadvantageous for any battery electrode, it is important to choose a suitable ionic liquid for metal deposition. Template-assisted electrodeposition of Sn nanowires was achieved using [$Py_{1,4}$]DCA ionic liquid [48]. Hsu et al. [49] compared the electrodeposited Sn from ionic liquids and aqueous solution as electrodes for LIB. The authors reported that electrodeposition from ionic liquids led to an increased deposition current efficiency and suppressed the corrosion of the Cu current collector. Also, the Sn deposit morphology could be altered simply by changing the deposition potential. On battery testing, it was found that Sn deposited from ionic liquids led to a much better performance compared to Sn deposited from aqueous solutions. The electrodeposited Sn nanospheres gave a reversible capacity of 980 mAh g^{-1}

at 100 mA g^{-1}. Furthermore, a capacity of 588 mAh g^{-1} could be achieved at quite a high current density of 15 A g^{-1}.

Other potential anodes for LIB are Sn-based composites nanostructures, which can be electrochemically synthesized from ionic liquids. Recently Ge_xSn_{1-x} was electrodeposited at room temperature in both $[Py_{1,4}]$TFSA and $[Py_{1,4}]$TfO containing $GeCl_4$ and $SnCl_2$ as precursors [50]. It was found that the anion of the ionic liquid influences the morphology of the electrodeposits. In the case of $[Py_{1,4}]$TFSA, Ge_xSn_{1-x} deposits consist of nanoparticles with a size of less than 100 nm, whereas clustered deposits were obtained in $[Py_{1,4}]$TfO. Furthermore, in $[Py_{1,4}]$TFSA the solubility of $SnCl_2$ was quite low, which led to the formation of a Ge-rich Ge_xSn_{1-x}. In $[Py_{1,4}]$TfO the composition of Ge_xSn_{1-x} could be varied by changing the concentration of $SnCl_2$ in the electrolyte [50]. Zn–Sn alloys was also electrodeposited in $[Py_{1,4}]$TfO containing 0.05 M zinc trifluoromethylsulfonate ($Zn(TfO)_2$) and 0.05 M tin trifluoromethylsulfonate ($Sn(TfO)_2$) as precursors [51]. It was found that the composition and the morphology of the deposits are strongly dependent on the deposition potential, and by changing the deposition potential, alloys with different ratios of Zn and Sn was achieved. Furthermore, Zn–Sn nanowires with different diameters was synthesized electrochemically in $[Py_{1,4}]$TfO containing $Zn(TfO)_2$ and $Sn(TfO)_2$ using a template-assisted electrodeposition technique [51].

Aluminum is an attractive anode material for LIB with a theoretical capacity of 2234 mAh g^{-1} for the formation of Al_4Li_9 and 790 mAh g^{-1} for the formation of LiAl [45]. However, like for other materials, volume expansion during lithiation is inevitable. Recently, Al nanostructures have shown to be perspective anodic materials for LIB, which can be synthesized electrochemically in ionic liquids using template-assisted electrodeposition technique. In 2011, macroporous Al electrodes were made by template-assisted electrodeposition from 1-ethyl-3-methylimidazolium chloride ([EMIm]Cl) containing $AlCl_3$ (40:60 mol%) [52]. Polystyrene (PS) spheres, self-assembled on copper sheets, were used as a template for the electrodeposition. After Al deposition, the remaining [EMIm]Cl-$AlCl_3$ was removed by subsequent washing in $[Py_{1,4}]$TFSA. An Al macroporous structure was obtained by chemical dissolution of the PS template in tetrahydrofuran (THF) (Fig. 2a). The macroporous Al was cycled in 0.5 M LiTFSA-$[Py_{1,4}]$TFSA, from which alloying and dealloying processes were observed. It was found that the macroporous structure remains intact after one cyclic voltammetric (CV) cycle (Fig. 2b). However, after ten CV cycles,

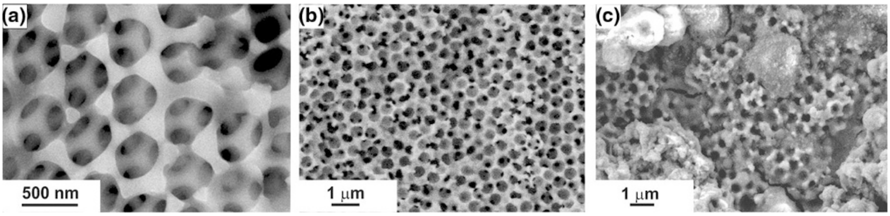

Fig. 2 SEM images of the macroporous Al **a** before cycling, **b** after 1 voltammetric cycle, and **c** after ten voltammetric cycles in 0.5 M LiTFSA-$[Py_{1,4}]$TFSA. Reproduced from Gasparotto et al., *J. Power Sources,* 2011 [52] with permission from Elsevier

the macroporous structure does not retain its pores and some agglomeration takes place (Fig. 2c).

In 2012, it was reported that free-standing Al nanowires can be synthesized from EMImCl/$AlCl_3$ (40:60 mol%) through a template-assisted deposition technique [53]. For this purpose, track-etched nanoporous polycarbonate membranes were used as templates for the electrodeposition. In order to develop free-standing nanowires, Al was electrodeposited on the Au sputtered side of the porous polymer template, wherein initially nanowires were formed, after which a thick supporting Al layer was formed. Then the membrane was dissolved in dichloromethane to obtain free-standing nanowires. It was found that the deposition time of Al is crucial in order to form a stable supporting layer, which keeps the Al nanowires free-standing. A deposition time of 40 min was found to be optimum to synthesize nanowires of 15 μm in length. It was shown that different mechanically stable nanowire architectures, such as free-standing nanowires, vertically aligned tree-shaped arrays, and bunched nanowire films, could be made using template-assisted electrodeposition technique by controlling the deposition parameters [53]. Electrodeposited free-standing Al nanowires were used as anode for LIB. On cycling the Al nanowires in 0.5 M LiTFSA-[$Py_{1,4}$]TFSA, clear alloying and dealloying peaks were observed in the CV cycles [54]. After ten and 50 deposition/stripping cycles, the microstructure of the nanowires were intact, which indicates that the electrodeposited nanowires are very stable (Fig. 3). A charge capacity of 791 mAh g^{-1} was achieved at 1 C rate for the first cycle, which then decreased to 677 mAh g^{-1} after the 4th cycle. These results clearly show the possible use of electrochemically synthesized Al nanowires as LIB anode.

3 Electrode Materials for Na-Ion Batteries

Na is more abundant compared to lithium and therefore the overall cost of Na-ion batteries (NIB) might be cheaper than commercial Li-ion batteries. It has been estimated that, compared to commercial LIB, Na-ion batteries are about 10% less expensive [55]. However, Na ions do not intercalate well in graphite, which is used as the anode for LIB. Unlike graphite, hard carbon was found to be a useful anode for NIB. Other potential high-capacity anodes include different elements, such as

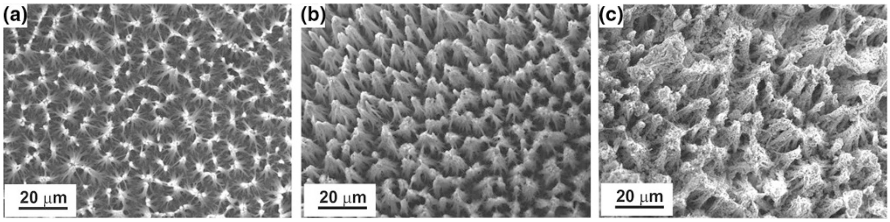

Fig. 3 SEM images of Al nanowires **a** before cycling, **b** after ten voltammetric cycle, and **c** after 50 voltammetric cycles in 0.5 M LiTFSA-[$Py_{1,4}$]TFSA. Reproduced from Zein El Abedin et al., *Aust. J. Chem.*, 2012 [54] with permission from CSIRO Publishing

Ge, Sn, Sb, In, P, etc., and their compounds [55–58]. Currently, many of these elements and compounds have been synthesized using various techniques including the electrodeposition in ionic liquids. However, most of these electrodeposited materials have not yet been tested as NIB electrodes.

Germanium has a theoretical capacity of 369 mAh g^{-1} for the formation of NaGe. At present, electrodeposition of Ge with different nanostructures (thin films, nanowires, nanotubes, and 3DOM structure) has been shown from four different ionic liquids, namely 1-butyl-3-methylimidazolium hexafluorophosphate ([BMIm] PF_6), 1-butyl-1-methylpyrrolidinium dicyanamide ($[Py_{1,4}]$DCA), $[Py_{1,4}]$TFSA and [EMIm]TFSA [59]. For NIB, Ge thin films synthesized by magnetron sputtering and by electron beam heating techniques showed a capacity drop to zero after 30 cycles at very low C-rates of 0.1 C [60, 61]. In comparison, Ge electrodeposited from $[Py_{1,4}]$TFSA on Cu showed a stable capacity of 140 mAh g^{-1} at 1.5 C after 50 cycles [62]. This indicates that materials synthesized by electrodeposition might have much better properties compared to materials synthesized using other techniques.

Sb and Sn possess a higher capacity for Na storage with theoretical values of 660 and 847 mAh g^{-1} for the formation of Na_3Sb and $Na_{15}Sn_4$, respectively [55]. Electrodeposition of Sn and Sn-based composites has been shown in ionic liquids [57–61]. Sb has mainly been synthesized using vacuum techniques [55]. However, aqueous solutions were employed as electrolytes for the electrodeposition of Sb and Sb-based composites [63, 64]. Nam et al. [63] reported that electrodeposited three-dimensional porous Sb/Cu_2Sb structures exhibit outstanding cycling stability and excellent rate capability. Sb/Cu_2Sb electrodes show a capacity of 485 mAh g^{-1} at 0.1 C rate for 120 cycles in propylene carbonate (PC) containing 1 M $NaClO_4$ and 0.5 vol% of fluoroethylene carbonate (FEC). Sb nanorod array anodes were synthesized from aqueous electrolytes via a template-assisted electrodeposition technique [64]. On cycling at a current density of 0.2 A g^{-1} in a mixture of ethylene carbonate (EC) and PC (1:1 vol%) containing 1 M $NaClO_4$ and 5 vol% FEC, capacities of 612.7 and 521 mAh g^{-1} were found after 100 cycles and 250 cycles, respectively, which the authors explained was superior to other Sb nanostructures and Sb/C-based composites. Zn_4Sb_3 electrodeposited from aqueous electrolyte shows a capacity of 450 mAh g^{-1} in the first cycle and retains about 90% of the capacity after 250 cycles at 0.2 C rate in PC containing 1 M $NaClO_4$ and 5 vol% FEC [65].

In comparison to electrodeposition from aqueous solutions, Ge modified by electroless deposition of Sb from $[Py_{1,4}]$TFSA containing 0.1 M $SbCl_3$ could be cycled at 2 C rate in $[Py_{1,4}]$FSA containing 1 M sodium bis(fluorosulfonyl)amide (NaFSA) [62]. A capacity of 290 mAh g^{-1} was observed initially, which dropped to 225 mAh g^{-1} after 50 cycles. Interestingly, SEM, XPS and Auger electron spectroscopy (AES) reveal the formation of a twin SEI layer: a thick organic outer SEI layer with a cauliflower-like structure (Fig. 4a), and a comparatively thin inorganic SEI layer consisting of NaF, sodium sulphide and sulphate (Fig. 4b) [62].

Ionic liquid electrolytes have been used in NIB with Na anode and various cathodes. Recently, NIB of $Na/Na_{0.44}MnO_2$ cells with $[Py_{1,4}]$TFSA containing different sodium salts (1 M $NaClO_4$, 1 M $NaBF_4$, 1 M NaTFSA, 1 M $NaPF_6$) was tested [66]. Among the different solutes, $NaClO_4$ was found to exhibit a much better charge/discharge performance due to the formation of SEI layer with a low charge transfer

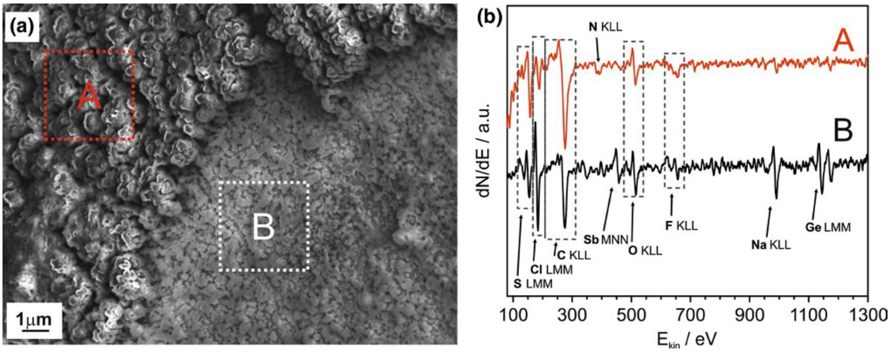

Fig. 4 **a** SEM image of Sb modified Ge after the first sodiation process recorded at a beam energy of 5 kV. **b** AES spectra of the regions marked in the SEM image. Reproduced from Lahiri et al., *Phys. Chem. Chem. Phys.*, 2016 [62] with permission from the PCCP Owner Societies

resistance on both Na and $Na_{0.44}MnO_2$ electrodes. The capacity at 25 and 50 °C was found to be between 100 and 115 mAh g^{-1} (at 0.05 C) for all the electrolytes. At 50 °C, a capacity retention of 80% was found at 0.3 C rate after 100 cycles for 1 M $NaClO_4$-$[Py_{1,4}]$TFSA, which was the highest among all tested electrolytes. Rechargeable Na/$NaFePO_4$ cells were tested with NaTFSA-$[Py_{1,4}]$TFSA containing various concentrations of NaTFSA [67]. It was showed that the NaTFSA concentration greatly affects the electrochemical performance of the $NaFePO_4$ electrode. On increasing NaTFSA concentration, the cycling stability improves, however the cell capacity decreases. A concentration of 0.5 M NaTFSA was found to be an optimum for the Na/$NaFePO_4$ cell; a capacity of 56 mAh g^{-1} was achieved on using 0.5 M NaTFSA in the IL, which decreased on increasing the concentration of Na ions. The decrease in capacity was attributed to the reduced electrolyte conductivity. At 50 °C, the storage capacity doubled to 125 mAh g^{-1} using 0.5 M NaTFSA in the IL [67].

The stability of Na was tested in 1-butyl-3-methylimidazolium bis(trifluoromethylsulfonyl)amide ([BMIm]TFSA) and 1-butyl-3-methylimidazolium bis(fluorosulfonyl)amide ([BMIm]FSA) over time to evaluate its reactions and formation of a SEI layer [68]. It was obtained that Na metal reacts with [BMIm]TFSA and a visible change is observed after 4 weeks. However, no changes were found on using [BMIm]FSA. Electrochemical impedance spectra (EIS) indicated the formation of a resistive film for [BMIm]TFSA, whereas a protective layer was obtained over the Na metal in the case of [BMIm]FSA. However, the EIS spectra did not show much change in the presence of Na ions in the ILs, due to immediate formation of a Na^+ containing surface film. XPS measurements revealed that the chemical composition of the surface film formed in TFSA and FSA ILs was not very different. However, the authors claimed that the stability of the film formed with FSA IL was much better compared to TFSA IL.

4 Li–Air and Zn–Air Batteries with Ionic Liquid Electrolyte

Metal–air batteries are, in principle, attractive due to a high capacity in the several kWh kg^{-1} regime. In the metal–air battery system, the metal is oxidized at the anode releasing electrons, which then drives the reduction of oxygen at the cathode. Although a high energy density can be achieved, there are number of fundamental issues, which need to be overcome if these battery systems shall ever be commercialized. For example, in the case of the anode, dendritic metal deposits occur during cycling. Also, during the oxidation of the metal, Li_2O_2 and Li_2O are formed at the porous cathode in the case of Li blocking the pores and impeding the oxygen reduction reaction (ORR). Furthermore, the stability of the metal in the electrolyte is also an issue for long-term operating of the battery. In this section, we will present the latest developments in the Li–air and Zn–air batteries with ionic liquids as solvent media.

4.1 Li–Air Batteries

Metallic lithium along has a theoretical capacity of 3860 mAh g^{-1}. During the discharge process, lithium is oxidized to Li_2O_2 according to reactions shown below [69]. However, lithium superoxide (LiO_2) can also form, which undergoes a disproportionation reaction to form Li_2O_2.

$$\mathrm{Li^+ + O_2 + \mathit{e}^- \rightarrow LiO_2}$$

$$\mathrm{2LiO_2 \rightarrow Li_2O_2 + O_2}$$

$$\mathrm{LiO_2 + Li^+ + \mathit{e}^- = Li_2O_2}$$

$$\mathrm{Li_2O_2 + 2Li^+ + 2\mathit{e}^- = 2Li_2O}$$

Kuboki et al. [70] showed for the first time the use of ionic liquids in a lithium–air cell in 2005. Four different hydrophobic ionic liquids, namely 1-ethyl-3-methylimidazolium bis(pentafluoroethyl)amide ([EMIm]BETA), [EMIm]TFSA, 1-methyl-3-octylimidazolium bis(trifluoromethylsulfonyl)amide ([OMIm]TFSA) and $[BMIm]PF_6$, were tested as electrolytes and compared with organic electrolytes like EC/PC. Porous carbon electrodes were used as cathodes. Using the organic electrolyte, at a discharge rate of 0.1 mA cm^{-2} in air, a capacity of 2430 mAh g^{-1} was achieved. It was found that at lower discharge rates, there is the evaporation of the PC electrolyte and formation of LiOH at the anode that leads to a lower capacity. The stability of lithium was tested in various ionic liquids. It was found that lithium is most stable in $[BMIm]PF_6$ and the stability of lithium decreases in the order [EMIm]TFSA < [EMIm]BETA < [OMIm]TFSA. The Li–air cell showed a discharge capacity of 640 mAh g^{-1} at a discharge rate of 0.01 mA cm^{-2} with [OMIm]TFSA and considerably improved to 1790 and 5360 mAh g^{-1} on using [EMIm]BETA and [EMIm]TFSA electrolytes, respectively. Furthermore, the authors showed that the batteries ran 56 days in air and the humidity and long discharge time did not significantly affect the discharge behavior [70].

Mizuno et al. [71] used *N*-methyl-*N*-propylpiperidinium bis(trifluoromethylsulfonyl)amide ($[PP_{13}]TFSA$) as an electrolyte for Li-O_2 battery. It was found that the employed electrolyte is stable in the presence of lithium metal as well as against O_2 radicals. However, a reversible capacity of less than 150 mAh g^{-1} was achieved with a carbon electrode containing MnO_2 as catalyst. Moreover, only 60% of the initial capacity could be retained after 40 cycles at 60 °C. In a later study, Nakamoto et al. [72] compared four different ionic liquids, namely $[PP_{13}]TFSA$, *N*-methoxyethyl-*N*-methylpiperidinium bis(trifluoromethylsulfonyl) amide ($[PP_{1201}]TFSA$), *N*,*N*-diethyl-*N*-methyl-*N*-(2-methoxyethyl)ammonium bis(trifluoromethylsulfonyl)amide ([DEME]TFSA) and $[Py_{1,4}]TFSA$, with the same anion and different cations for O_2 radical stability. Among the ionic liquids, $[PP_{1201}]$ TFSA showed the lowest stability, whereas other ILs showed a high oxygen radical stability. From NMR studies the authors claimed that the rate limiting step was the generation of LiO_x compounds. Furthermore, the battery performance improved using [DEME]TFSA electrolyte as the rate of formation of LiO_x compounds was the highest.

In 2013, Soavi et al. [73] studied the performance of a lithium-oxygen battery with a catalyst-free porous carbon cathode in LiTFSA-[BMP]TFSA (1:9 molar ratio). Interestingly, the authors observed a reduced recharge potential of 3.4 V vs. Li/Li^+, which might be useful in avoiding secondary reactions. Furthermore, a capacity of 2500 mAh g^{-1} was achieved at 60 °C and on continuous cycling to a discharge limit of 200 mAh g^{-1} led to a stable cycling with an efficiency of about 80%. In comparison, Garsuch et al. [74] observed very poor cell performance with a MnO_2-based carbon cathode and 10% LiTFSA-$[Py_{1,4}]TFSA$ electrolyte. A capacity of only 60 mAh g^{-1} was found with 58% efficiency. LiTFSA-$[Py_{1,4}]TFSA$ was tested for a Li–air battery system with a catalyst-free carbonaceous electrode [75]. It was observed that the discharge and charge voltages corresponding to the formation and dissolution of Li_2O_2 differed only by 0.6 V. From SEM and TEM, it was found that Li_2O_2 nanoparticles of about 200 nm in size were formed after fully discharging, returning back to the initial state upon charging that might have led to a low cell polarization. A capacity of 4500 mAh g^{-1} was achieved with respect to carbon loading. However, XPS results showed the presence of some remaining Li_2O_2 even after charging suggesting that some side reactions occurred during the charge–discharge processes.

Recently, Das et al. [76] re-evaluated various ionic liquids by changing the anion and cation of the ILs for use as electrolytes in a Li-O_2 battery. Differential electrochemical mass spectrometry (DEMS) was used to measure the gas output during the discharge and charge processes. They showed that the TFSA anion was much more stable than the FSA anion. Furthermore, $[Py_{1,4}]TFSA$ and $[Py_{1,3}]TFSA$ showed a better rechargeability below 4.2 V than $[Py_{1,4}]FSA$ and $[PP_{13}]TFSA$. Moreover, ILs with imidazolium and quaternary ammonium cations were less stable for battery applications. From XRD, it was found that the discharge products (Li_2O_2 and LiF) were formed in all the IL-based electrolytes except for those with the FSA ion. Furthermore, it was observed that on charging/discharging of the cell, the amount of the electrochemical degradation reactions increases. Finally, the authors concluded that although $[Py_{1,4}]TFSA$ is the best candidate among the seven ionic liquids tested for $Li\text{-}O_2$ battery, a suitable electrolyte is far from reality and more fundamental work in developing new types of ILs is necessary [76].

Another important aspect of a Li–air battery is the formation of dendrite-free lithium and a stable SEI layer during the charging/discharging processes. It has been suggested that during lithium deposition, cracks are formed when the deposition process is not uniform. As the lithium ion diffusion through these cracks is easy, it results in the growth of dendritic lithium [61]. Aurbach et al. [77] indicated that lithium metal is thermodynamically unstable in organic solvents. Various strategies have been developed to overcome the formation of dendritic lithium and to form a stable SEI layer. In 2004, Howlett et al. [78] reported that lithium deposition at current densities of 1.75 mA cm^{-2} in $[Py_{1,4}]TFSA$ does not lead to the formation of dendrites. Also, an average cycling efficiency of $> 99\%$ could be achieved at a current density of 1.0 mA cm^{-2}. In a later study, the SEI layer formed during the lithium deposition was characterized [79]. IR and Raman spectroscopy revealed that the bulk of the electrolyte remains unchanged, whereas the surface species of the lithium changes significantly. Furthermore, a clear indication of TFSA decomposition on lithium was obtained. XPS showed that the decomposed products (such as Li_2CO_3, LiOH and Li_2O_2) can be found on the lithium surface.

From a fundamental point of view, the electrodeposition of lithium was studied on Au(111) using cyclic voltammetry (CV) and in situ scanning tunneling microscopy (STM) from $[Py_{1,4}]TFSA$ containing 0.5 M LiTFSA [80]. In situ STM revealed that the underpotential deposition (UPD) of lithium begins at electrode potentials of more than 1 V positive to the potential for the bulk deposition and follows a layer-by-layer growth mechanism with the formation of at least two monolayers. The sequence of the in situ STM images of the lithium UPD process on Au(111) in $[Py_{1,4}]TFSA$ containing 0.5 M LiTFSA is presented in Fig. 5. At OCP (− 0.2 V vs. Pt) a defect rich surface pattern typical for the Au(111) structure in the pure $[Py_{1,4}]TFSA$ is obtained (Fig. 5a). The defects are one monolayer deep and the step heights between the terraces is 250 ± 30 pm. At − 0.8 V vs. Pt the holes on the Au(111) surface start to disappear and a monolayer growth of lithium is observed (Fig. 5b). If the electrode potential is decreased to − 0.9 V, the gold surface is completely covered by the first lithium monolayer and a growth of a second layer (islands indicated by arrows) occurs (Fig. 5c). With time the islands grow and merge laterally until an almost complete second monolayer of lithium is formed (Fig. 5d). After about 20 min, the complete second monolayer is clearly seen on the surface (Fig. 5e). These results suggest that UPD processes of lithium in ionic liquids are different compared to organic electrolytes.

In 2011, Stark et al. [81] reported that dendritic-free lithium can be electrodeposited from two ionic liquids, $[EMIm]Cl\text{-}AlCl_3$ and trimethylbutylammonium bis(trifluoromethylsulfonyl)amide ($[N_{1114}]TFSA$), containing both LiTFSA and NaTFSA. It was found that Na ions in the electrolyte were essential to form a dendrite-free lithium, which also improved the coulombic efficiency. Vinylene carbonate (VC) was added to $[N_{1114}]TFSA$ to form a stable SEI layer. Sano et al. [82] applied [EMIm]FSA and $[PP_{13}]TFSA$ with and without VC to study the lithium

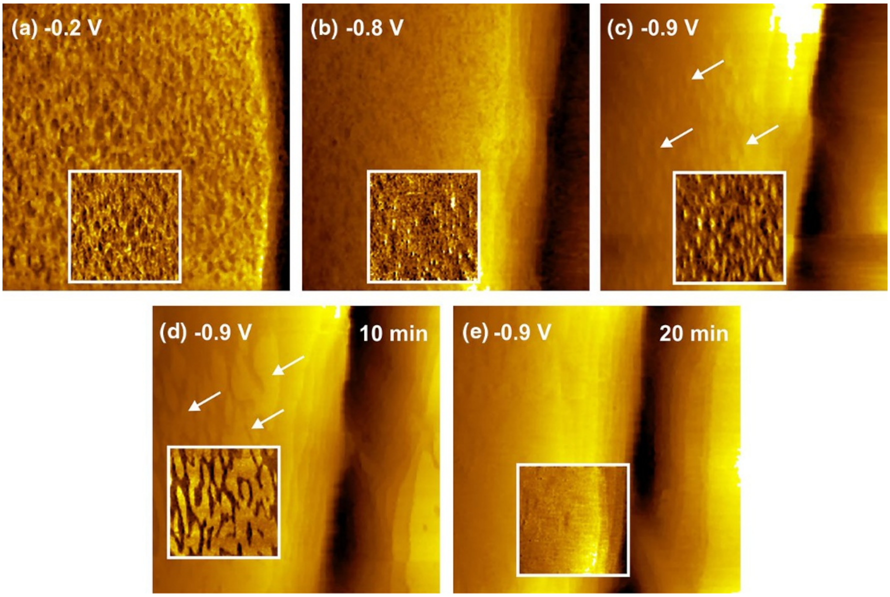

Fig. 5 In situ STM images of the Au(111) surface in 0.5 M LiTFSA-[$Py_{1,4}$]TFSA at **a** − 0.2 V, **b** − 0.8 V and **c**, **d** − 0.9 V vs. Pt. Resolution of the images is 300 nm × 300 nm. *Insets* show zoom in (150 nm × 150 nm) area of the corresponding images. Adapted from Gasparotto et al., *Phys. Chem. Chem. Phys.,* 2009 [80] with permission from the PCCP Owner Societies

deposition/stripping processes on nickel electrodes using in situ optical microscopy. It was found that a non-uniform dendritic deposit of lithium forms in [EMIm]FSA both with and without VC. However, in the case of [PP_{13}]TFSA, dendritic particles were obtained in [PP_{13}]TFSA without VC, whereas a uniform dendrite-free lithium deposit was found in [PP_{13}]TFSA containing VC. It was suggested that a uniform film consisting of decomposed VC is formed on the surface in the case of [PP_{13}] TFSA, which suppresses the dendritic growth of lithium. In a different study with [$Py_{1,4}$]FSA containing LiFSA, Bhatt et al. [83] did not find the formation of dendritic lithium after cycling. The lithium electrode was cycled in the FSA containing IL for 800 cycles with various current densities of 0.1, 10, and 100 mA cm^{-2}. From EIS measurements, the authors found that at low current densities there is a pitting corrosion, which is filled up during subsequent cycling. However, at higher current densities, the pits are not filled. In spite of this pitting corrosion, after cycling, SEM did not show any evidence for the formation of dendrites.

Lithium containing solvate ionic liquids of [$Li(L)_n$][X] with ligands L = 1,2-dimethoxyethane (G1, monoglyme) or 1-methoxy-2-(2-methoxyethyl)ether (G2, diglyme) and different anions (X = Br, I or TFSA) have been tested as electrolytes for lithium electrodeposition [84]. The formation of an SEI during electrodeposition of lithium was studied by electrochemical quartz crystal microbalance (EQCM) and Auger electron spectroscopy. It was found that a solvate ionic liquid with the TFSA anion is a well suited electrolyte for Li–air batteries. In comparison to the TFSA anion, halide anions resulted in a lower coulombic efficiency for lithium deposition/stripping due to the formation of an unstable SEI layer as well as a dendritic lithium deposit. Furthermore, copper, platinum, and titanium working electrodes were tested for the lithium deposition/stripping. It was found that copper and platinum give the best efficiencies.

Grande et al. [85] studied lithium deposition/stripping from $[Py_{1,4}]$TFSA and $[Py_{1,4}]$FSA and their mixtures containing LiTFSA on both lithium and nickel substrates. In comparison to many other reports, it was observed that dendritic lithium was formed on nickel during deposition in $[Py_{1,4}]$TFSA, whereas on using $[Py_{1,4}]$FSA, no dendrites were obtained, which indicated that SEI layer formation is crucial and different on various substrates. By measuring the interfacial resistance at different temperatures of 20, 40, and 60 °C, it was found that the mixtures of ionic liquid with a higher FSA content (7:3 molar ratios of FSA:TFSA) gave a quicker and more stable interfacial resistance at 20 and 40 °C. Finally, with the mixed ionic liquid no dendrites were formed on the nickel substrate after deposition at 0.1 mA cm^{-2} for 10 h. However, the lithium deposits on nickel were not uniform. Therefore, an alternative efficiency estimation method was applied. A symmetrical cell was made of two 50-µm-thick Li electrodes (~ 10.32 mAh cm^{-2} each) and, prior to cycling, 90% of the Li was stripped from one or two electrodes, so that only 1 mAh cm^{-2} remained on the nickel current collector [85]. The modified nickel electrode was then cycled in the mixture of FSA/TFSA electrolyte. On deposition/stripping on this modified electrode, interestingly, fiber-like lithium deposits were achieved. Furthermore, no dendrites were seen, which, as the authors claimed, was due to the formation of a stable SEI layer.

4.2 Zn–Air Batteries

Like Li–air batteries, Zn is also a potential and safe anode for use in metal–air batteries. Compared to Li, the energy density of Zn is about ten times lower, giving a value of 1300 Wh kg^{-1}. However, as Zn is easier to handle and it is more or less abundant, it has a lot of potential as an energy storage device. Aqueous electrolytes such as KOH have been predominantly used for Zn–air batteries. The anodic and cathodic reactions in aqueous electrolyte are shown below [86].

Anode: $Zn + 4OH^- \rightarrow Zn(OH)_4^{2-} + 2e^-$

$Zn(OH)_4^{2-} \rightarrow ZnO + H_2O + 2OH^-$.

Cathode: $O_2 + 2H_2O + 4e^- \rightarrow 4OH^-$.

Overall: $2Zn + O_2 = 2ZnO$.

However, there are certain critical issues using aqueous electrolytes, such as electrode corrosion, electrolyte drying out, formation of dendritic zinc, and air cathode flooding. Therefore, a lot of interest is being generated for using non-aqueous electrolytes, especially ionic liquids.

In 2012, Simons et al. [87] studied the zinc electrodeposition/dissolution process in 1-ethyl-3-methylimidazolium dicyanamide ([EMIm]DCA) ionic liquid with different Zn salts ($Zn(DCA)_2$, $Zn(SO_4)$, $ZnCl_2$ and zinc acetate) in the presence and absence of water in the IL. It was observed that the deposition potential of Zn varies considerably depending on the Zn salt and the lowest reduction potential was found on using $Zn(DCA)_2$, whereas a reduction potential of − 2.4 V vs. Fc/Fc^+ was needed to reduce Zn from Zn acetate. Furthermore, with a higher concentration of water (3 wt%), a uniform Zn deposition was achieved with $Zn(DCA)_2$, whereas with lower water concentration, a porous structure was observed.

Xu et al. [88] studied the Zn/Zn(II) redox reactions in four ionic liquids having different cation and anion species ([EMIm]TFSA, $[Py_{1,4}]$TFSA, 1-butyl-1-methylpyrrolidinium dicyanamide ($[Py_{1,4}]$DCA) and 1-methyl-1-pentylpyrrolidinium bis(trifluoromethylsulfonyl)amide ($[Py_{1,5}]$TFSA)). It was found that the kinetic behavior of the Zn species is controlled by the anion of the IL. Among the various ILs tested, a small overpotential for the Zn redox process was obtained on using [EMIm]DCA. It was proposed that in ILs with TFSA, a single-step two-electron transfer process occurs according to the equation below.

$$Zn^{2+} + 2e^- = Zn$$

However, in the case of ILs with DCA, it was suggested that the reaction takes place in two steps with one-electron transfer in each step as shown below [88].

$$Zn(DCA)_x^{(x-2)-} + e^- = Zn(DCA)_x^{(x-1)-}$$

$$Zn(DCA)_x^{(x-1)-} + e^- = Zn + x(DCA)^-$$

Electrodeposition of zinc was also investigated from zinc triflate ($Zn(TfO)_2$) in $[Py_{1,4}]$TfO and [EMIm]TfO and from ILs-water mixtures at various temperatures [89]. The morphology of the obtained Zn deposits was different in the two ionic liquids. Dense, uniform, and well-adhering silvery zinc was electrodeposited from [EMIm]TfO, whereas on using $[Py_{1,4}]$TfO, less adhering and dark grey zinc deposits were obtained on gold. Furthermore, both temperature and water have a significant effect on the deposition process and the morphology of Zn electrodeposits. XRD reveals that in the pure ILs both Zn and Zn–Au alloys were observed, while in the presence of water only Zn was formed. In situ STM was applied to a detail study of Zn electrodeposition on Au(111) at room temperature from [EMIm]TfO containing 0.2 M $Zn(TfO)_2$ [90]. It was found that the structure of the Au(111)/[EMIm]TfO interface is very complex and the addition of $Zn(TfO)_2$ changes the interfacial structure significantly. Thus, at the OCP (+ 0.8 V vs. Zn), the Au(111) surface was very rough in the pure [EMIm]TfO, while in the presence of $Zn(TfO)_2$, a typical terraces-like Au(111) surface was probed. In situ STM images in Fig. 6 represent an underpotential deposition of Zn on Au(111) in [EMIm]TfO containing 0.2 M $Zn(TfO)_2$. The first monoatomically high Zn islands appears on Au(111) at + 0.3 V vs. Zn (Fig. 6a). These islands then slowly grow until a thin UPD layer is obtained at 0.0 V (Fig. 6b, c). Upon further reducing the electrode potential, a bulk deposition of Zn occurs. Furthermore, in situ STM revealed that the deposition of Zn is accompanied by the formation of Zn–Au alloys [90].

As the zinc speciation governs the deposition/stripping processes, the solvation of zinc ions in $[Py_{1,4}]$TfO and [EMIm]TfO in the presence and absence of water and the interaction of [EMIm]TfO with water were evaluated using infrared and Raman spectroscopy [91]. It was found that in the presence of water the bulk interaction networks between [EMIm] cations and TfO anions are interrupted by association with

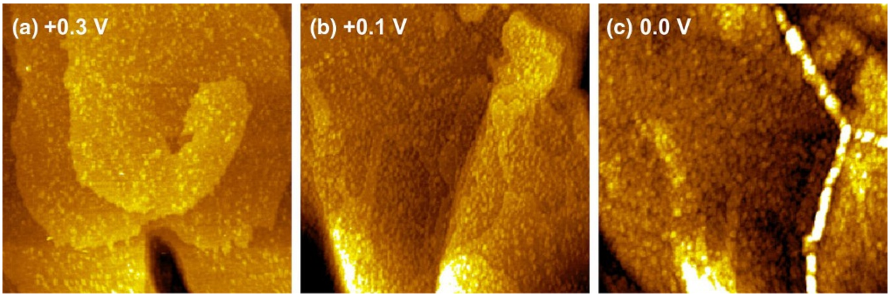

Fig. 6 In situ STM images of the Au(111) surface in 0.2 M $Zn(TfO)_2$-[EMIm]TfO at **a** + 0.3 V, **b** + 0.1 V and **c** 0.0 V vs. Zn. Resolution of the images is 400 nm × 400 nm. Reproduced from Liu et al., *J. Solid State Electrochem.,* 2014 [90] with permission from Springer Nature

water molecules and the structure is changed from ionic-liquid-like to water-like solutions by increasing the water content. Raman spectroscopy showed that in pure [EMIm]TfO, Zn coordinates with TfO anions with an average coordination number of 3.8, indicating the formation of $[Zn(TfO)_4]^{2-}$ and $[Zn(TfO)_3]^{-}$ complexes. However, on addition of water, the coordination number changes, as water interacts preferentially with the zinc ions leading to the formation of aqueous zinc species. In the case of $[Py_{1,4}]$TfO, the average coordination number was 4.5 indicating the presence of a mixture of $[Zn(TfO)_4]^{2-}$ and $[Zn(TfO)_5]^{3-}$ complexes.

In 2015, the Zn deposition/stripping processes were investigated in $[Py_{1,4}]$TfO containing 0.2 M $Zn(TfO)_2$ on a modified zinc/polystyrene composite electrode [92]. A brass substrate covered by polystyrene (PS) spheres was used to produce a zinc composite electrode. First, the PS spheres (600 nm) were self-assembled to form a hexagonal closed-packed structure on the brass substrate. Zn was then electrochemically deposited on PS/brass to get a macroporous zinc structure. The obtained structure was further used as a working electrode to study the Zn deposition/stripping processes in $[Py_{1,4}]$TfO containing 0.2 M $Zn(TfO)_2$. The reversibility of the zinc macroporous electrode was investigated by galvanostatic deposition/stripping and potentiostatic deposition/stripping cycles. For this purpose, after cycling, the working electrode was rinsed in isopropanol and THF to remove the electrolyte and the PS spheres, respectively. The morphology of the resulted 3DOM Zn deposit was subsequently analyzed by SEM. It was observed that the 3DOM structure retains its integrity after ten deposition/stripping cycles over 6 h between − 1.6 and + 0.4 V vs. Zn. The coulombic efficiency was found to be between 60 and 80%. A slightly modified 3DOM structure was obtained on cycling for over 50 h at a current of ± 100 μA. However, at certain sites, the 3DOM structure changed into less ordered zinc nanoparticles [92]. Figure 7 shows SEM images of the macroporous zinc structure before cycling and after 100 potentiostatic zinc deposition/stripping cycles in $[Py_{1,4}]$TfO containing 0.2 M $Zn(TfO)_2$ at room temperature. The deposition/stripping cycles were performed by applying a constant reduction potential of − 1.6 V vs. Zn for 15 min, immediately followed by an oxidation potential of + 0.4 V for 15 min. As can be seen in Fig. 7b, after 100 cycles, a dendritic growth

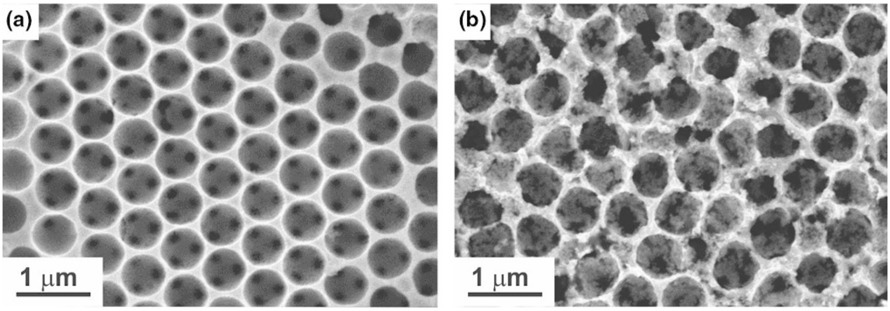

Fig. 7 SEM images of the macroporous Zn **a** before cycling and **b** after 100 deposition/stripping cycles at constant potentials of − 1.6 V/ + 0.4 V vs. Zn in $[Py_{1,4}]TfO$ containing 0.2 M $Zn(TfO)_2$ at room temperature

of Zn does not occur and the macroporous structure prevails. These results suggest that macroporous zinc can be used as an anode material in rechargeable zinc-based batteries.

In situ AFM has also been used to study the electrodeposition of Zn on Pt in [BMIm]TfO containing $Zn(TfO)_2$ [93]. The measurements revealed that initially hexagonal Zn islands appear on the surface. With time, these islands grow and merge forming Zn domains with co-aligned platelets, which by further growing lead to the formation of a dense thick zinc film.

The electrodeposition of Zn was investigated on gold in 1-ethyl-3-methylimidazolium acetate ([EMIm]OAc) containing various concentrations of Zn acetate ($Zn(OAc)_2$) at 100 °C [94]. It was found that a minimum concentration of 4 M is required to obtain bulk zinc deposition, probably due to the presence of reducible species in solution. Raman spectroscopy revealed that the speciation of Zn changes with concentration. At lower concentration of 0.2–2 M, $[Zn(OAc)_6]^{4-}$ and $[Zn(OAc)_5]^{3-}$ complexes are present in the solution. On increasing the concentration to 4 M, a mixture of both $Zn(OAc)_2$ and $Zn(OAc)^+$ complexes are formed. XRD patterns indicate the formation of Zn and Zn–Au alloys.

Quaternary alkoxy-ammonium bis(trifluoromethylsulfonyl)amide ionic liquids were used as electrolytes for zinc cycling [95]. It was shown that these ionic liquids are well suited for Zn deposition/stripping. Furthermore, it was found that the addition of water reduces the activation barrier required to deposit Zn and assists in stable charge/discharge cycling. With an optimum water concentration of 2.5 wt%, the authors showed a stable cycling of Zn for 750 cycles at a current density of 0.1 mA cm^{-2}.

Similar to the Li–air battery, the formation of dendrite-free zinc is another important aspect of Zn–air batteries. Although the formation of dendritic zinc is usually limited in ionic liquids, needle-shaped and dendrite structures of zinc have been observed [93]. Liu et al. [96, 97] demonstrated two different approaches to avoid the formation of dendritic zinc and to obtain a stable Zn cycling. In the first approach, nickel triflate ($Ni(TfO)_2$) was used as an additive in [EMIm]TfO containing 0.1 M $Zn(TfO)_2$. A thin film of a Zn–Ni alloy formed on the surface together with the formation of a stable SEI layer, which affect the zinc nucleation and growth. It was shown using in situ AFM that the addition of 0.015 M $Ni(TfO)_2$ alters the interfacial structure significantly leading to the formation of a dendrite-free Zn deposit with a nanocrystalline structure [96]. In the second approach, two Zn precursors (ZnO and $Zn(TfO)_2$) were dissolved in a protic ionic liquid 1-ethylimidazolium trifluoromethylsulfonate ([EIm]TfO) [97]. From Raman and NMR spectroscopy, a deprotonation reaction was shown and the formation of cationic ($[Zn(EIm)_2]^{2+}$) and anionic ($[Zn(TfO)_4]^{2-}$) species was demonstrated when both ZnO and $Zn(TfO)_2$ were added to the IL. It was suggested that a synergetic effect of both cationic and anionic complexes prevents the dendritic growth of Zn. Compact, homogeneous and dendrite-free Zn deposits were obtained in [EIm]TfO containing both precursors, while dendritic Zn deposits were formed in [EIm]TfO containing either ZnO or $Zn(TfO)_2$.

Besides the Zn anode, the air cathode is another important issue in Zn–air battery, where a four-electron transfer process takes place. The three-phase boundary between the liquid electrolyte, air and the solid catalyst needs to ensure an efficient reduction process. In non-aqueous electrolytes, the oxygen reduction reaction (ORR) and oxygen evolution reaction (OER) are complicated. In 2014, Kar et al. [69] summarized the various experimental results for ORR/OER processes in ionic liquids. In ILs, the first step for the ORR process is the formation of superoxide ($O_2^{\cdot-}$) according to the following equation:

$$O_2 + e^- \rightarrow O_2^{\cdot-}.$$

In the case of protic ILs, the superoxide then reacts with the protons via a protonation reaction to form perhydroxyl radicals ($HO_2^{\cdot}$), which is then reduced to peroxidate ($HO_2{}^-$), finally forming hydrogen peroxide as shown by the equations below.

$$O_2^{\cdot-} + H^+ = HO_2^{\cdot}$$

$$HO_2^{\cdot} + e^- = HO_2^-$$

$$HO_2^- + e^- = H_2O_2$$

The formation of peroxide to water is dependent on the metal catalyst used. Pt has been shown to be the best catalyst for the reduction process of H_2O_2 to water according to the equation below.

$$H_2O_2 + 2H^+ + 2e^- = 2H_2O$$

However, in the case of aprotic ionic liquids, things become more complicated. Switzer et al. [98] showed the possibility of a four-electron transfer process using an aprotic ionic liquid (1-butyl-2,3-dimethylimidazolium trifluoromethanesulfonate) mixed with protic species. Pozo-Gonzalo et al. [99] found that ionic liquids with phosphonium ions mixed with protic species act as good electrolytes for ORR reactions. Using such ionic liquids with different anions, the authors showed that the superoxide is stable and does not undergo a disproportionation reaction, thereby promoting further reduction steps to take place. However, in the case of the air cathode, studies with IL electrolytes are still at its infancy especially for aprotic ILs. The kinetics of the ORR and OER reactions are slow compared to aqueous systems and radical modifications in the ILs might be required for commercial applications.

5 Al–Air, Al–Ion and Al–S Batteries

Aluminum is the third most abundant element in the earth's crust. Among other metals, it has the highest volumetric capacity of 8040 mAh cm^{-3} [100]. A recent overview by Elia et al. [100] summarizes the various Al batteries and discusses the use of various electrolytes.

5.1 Al-Ion Battery

Over the last three decades, various ionic liquids have been developed for Al electrodeposition at room temperature. Among them, the most common is $AlCl_3$ in [EMIm]Cl and $[Py_{1,4}]Cl$ (chloroaluminate ILs). Depending on the IL:$AlCl_3$ ratio, the electrolyte is either basic or acidic. When the ratio of $AlCl_3$:[EMIm]Cl is less than 1, there is a coexistence of $AlCl_4^-$ and Cl^-, making the electrolyte basic. On increasing the ratio above 1, there is a formation of $Al_2Cl_7^-$ and larger complexes making the electrolyte acidic [101]. It was shown that the deposition of Al from $[Py_{1,4}]Cl$ leads to the formation of nanocrystalline Al and the Al morphology and grain size can be altered by using a mixture of $[Py_{1,4}]Cl$ and [EMIm]Cl with $AlCl_3$ [102]. It was observed that below 70:30 vol% of $[Py_{1,4}]Cl$:[EMIm]Cl, a microcrystalline Al is obtained and above this ratio, a nanocrystalline Al is deposited indicating that the cation plays an important role on Al crystal size.

In 2011, Jayaprakash et al. [103] used the [EMIm]Cl:$AlCl_3$ mixture as electrolyte for an Al–ion battery with a V_2O_5 nanowires cathode and an Al metal anode. The open circuit voltage of the battery was found to be 1.8 V. On cycling in the potential window between 0.02 and 2.5 V, the authors found cathodic and anodic processes, which were attributed to the insertion and deinsertion of Al^{3+} ions. On passing a constant current of 125 mA g^{-1}, a capacity of 305 mAh g^{-1} was achieved, which decreased to 273 mAh g^{-1} after 20 cycles. Although, this is much lower than the theoretical capacity for V_2O_5, which was found to be 442 mAh g^{-1}, the cell showed a promising first step for the development of Al-ion batteries. In 2013, Reed and Menke [104] studied an electrochemical cell based on [EMIm]Cl:$AlCl_3$, V_2O_5 cathode and Al anode. The electrochemical behavior of the cells was found to be independent of the V_2O_5 and dependent entirely on the stainless-steel current collector. It was shown that the charge/discharge of the cell was from the stainless-steel collector leading to the formation of $FeCl_2$ and $CrCl_2$. Wang et al. [105] analyzed the V_2O_5 nanowire cathode system with the same ionic liquid electrolyte on a nickel foam current collector. It was found that the charge/discharge process is due to the Al^{3+} insertion and deinsertion process with an initial discharge capacity of 239 mAh g^{-1}. The possibility of using VO_2 as cathode with an Al anode was shown in [106]. During the discharge process, the following reactions occur at the anode and cathode.

Anode: $x\mathrm{Al} = x\mathrm{Al}^{3+} + 3xe^-$.

Cathode: $\mathrm{VO_2} + x\mathrm{Al}^{3+} + 3xe^- = \mathrm{Al}_x\mathrm{VO_2}$.

Using [EMIm]Cl:$AlCl_3$ as electrolyte, an initial capacity of 165 mAh g^{-1} was achieved, which decreased to 116 mAh g^{-1} after 100 cycles, thus showing good progress in development of Al–ion batteries. In 2015, Lin et al. [107] showed an Al–ion battery using an Al anode and a three-dimensional graphite foam cathode with [EMIm]Cl:$AlCl_3$. The setup was based on the first Al-ion battery system shown by Gifford and Palmisano in 1988 [108] using $AlCl_3$: 1,2-dimethyl-3-propylimidazolium chloride. With the ionic liquid electrolyte, Lin et al. [107] found that the Al/graphite cell shows a good stability with a high coulombic efficiency of > 98% at high current densities of 66 mA g^{-1}. A capacity of 70 mAh g^{-1} could be achieved. The battery was also tested at quite high current densities of 4–5 A g^{-1} for 7500 charge/discharge cycles, which gave a discharge capacity of 60 mAh g^{-1}. This meant that the 3D graphite cathode was a suitable electrode for withstanding such high current densities and could accommodate the insertion and deinsertion of Al^{3+}. These results show that chloroaluminate ionic liquids are in principle suitable electrolytes for Al-ion batteries. However, the main disadvantages of these electrolytes are their low electrochemical window and corrosive nature. Therefore, the development of a new generation of Al containing electrolytes might be beneficial for industrial applications.

In 2006, it was reported that Al can be electrodeposited in $[Py_{1,4}]$TFSA, [EMIm]TFSA and trihexyl-tetradecyl-phosphonium bis(trifluoromethylsulfonyl)amide ($[Py_{14,6,6,6}]$TFSA) containing $AlCl_3$ [109]. Depending on the ratio of $AlCl_3$:IL, a biphasic liquid was formed and Al was electrodeposited only from the upper phase. Interestingly, it was found that the cation of the IL significantly influences the deposit morphology. Microcrystalline Al could be deposited from [EMIm]TFSA, whereas nanocrystalline Al was formed from $[Py_{1,4}]$TFSA. Compared to chloride and other halide ILs, the TFSA ionic liquids showed a large electrochemical window, which is advantageous for an Al battery system.

Wang et al. [110] used $AlCl_3$:[BMIm]TfO as electrolyte for an Al-ion battery and tested it with a V_2O_5 nanowire cathode. It was shown that the concentration of $AlCl_3$ in [BMIm]TfO influences the cyclability and storage capacity and the best discharge capacity is obtained with 0.5 M $AlCl_3$ in the IL. Compared to the chloride ILs, the capacity was found to be low and an initial capacity of 87 mAh g^{-1} was recorded, which decreased to 40 mAh g^{-1} after 20 cycles. Besides the use of vanadium pentaoxide cathodes, other cathodes such as fluorinated graphite [111], Mo_6S_8 [112] and Ni_2S_2/graphene composite [113] have also been considered with ionic liquid as electrolytes. Fluorinated graphite was cycled in $AlCl_3$:[BMIm]Br, which gave a capacity of 250 mAh g^{-1}. However, the low coulombic efficiency of 75% limits its practical application [111]. In the case of Mo_6S_8, the first discharge capacity obtained in $AlCl_3$:[BMIm]Cl at 50 °C was 148 mAh g^{-1} [112]. Ex situ XRD showed that during discharge, $Al_2Mo_6S_8$ is formed, which gives a theoretical capacity of 193 mAh g^{-1}. However, during charging, a capacity of 85 mAh g^{-1} was obtained, which indicates that some Al^{3+} ions remain trapped in the sulfide electrode. Cycling over 50 cycles gave a reversible capacity of about 80 mAh g^{-1}. In comparison, the Ni_2S_2/graphene composite gave a first discharge capacity of 350 mAh g^{-1} at a current density of

100 mA g^{-1} using $AlCl_3$:[EMIm]Cl as electrolyte. However, the discharge capacity dropped to 60 mAh g^{-1} after 20 cycles and then remained stable for 100 cycles. This shows that metalsulfide cathodes are well suited for an Al-ion battery but need to be modified in order to improve the insertion/deinsertion process of Al^{3+} ions.

5.2 Al–Air Battery

Very little work has been done on using Al–air batteries in ionic liquid systems. In 2014, Gelman et al. [114] first showed the possibility of an Al–air battery with a 1-ethyl-3-methylimidazolium oligo-fluoro-hydrogenate (EMIm(HF)2.3F) ionic liquid electrolyte. At a discharge current density of 1.5 mA cm^{-2}, a discharge capacity of 140 mAh g^{-1} was observed. It was shown that Al_2O_3 forms at the air cathode. However, the reversibility of an Al–air battery was not tested. In another study, Revel et al. [115] used the standard $AlCl_3$:[EMIm]Cl mixture as electrolyte for an Al–air battery. On discharging at different current densities from 100 to 600 µA cm^{-2}, a capacity between 50 and 125 mAh g^{-1} was obtained.

5.3 Al–S Battery

Aluminum–sulfur batteries with an Al anode, a composite sulfur cathode and an ionic liquid electrolyte $AlCl_3$:[EMIm]Cl was demonstrated by Cohn et al. [116]. The best discharge capacity of 1400 mAh g^{-1} at a current density of 30 mA g^{-1} for the first discharge cycle was achieved with [EMIm]Cl:$AlCl_3$ molar ratios of 1:1.3 and 1:1.15. Unfortunately, the capacity dropped to almost zero with consecutive charge/discharge cycles. Gao et al. [117] showed a stable cycling capability of an Al–S battery with an activated carbon cloth/sulfur cathode and an Al anode. The electrolyte was [EMIm]Cl:$AlCl_3$ in the ratio of 1:1.3. On cycling, a maximum capacity of 1320 mAh g^{-1} was achieved at a current density of 50 mA g^{-1}. A reversible capacity of 1000 mAh g^{-1} was obtained for 20 cycles. Furthermore, it was shown that high loading of sulfur (> 1 mg cm^{-2}) lead to lower sulfur utilization and higher capacity loss. The discharged product analyzed using XPS showed that not all sulfur was converted to Al_2S_3. The presence of some partially reduced sulfur was also observed.

6 Conclusions

In the last two decades, a lot of research was done on different types of metal–ion and metal–air batteries. The development of safer batteries has directed the focus more towards using ionic liquids as safe and stable electrolytes and the use of ionic liquids as perspective electrolytes for the electrochemical synthesis of various electrode materials for battery applications. Although the electrochemical synthesis of battery electrodes from ionic liquids for Li-ion and Na-ion batteries remains elusive for commercial application at present, potential exists for high-energy metal–air batteries. The major impediment for the metal–air battery system remains in the air cathode with an appropriate IL electrolyte. From a prospective, one can envisage ionic liquids being used as safe electrolytes for Li-ion and Na-ion batteries for energy storage. Furthermore, the electrochemical synthesis of battery electrodes in ionic liquids with novel architecture such as 3DOM structure, nanowires/nanotubes might be a simple and viable technique. The current results show that the use of ILs both as safe electrolyte components in batteries and as solvent media for the electrochemical synthesis of electrode materials opens great promises for large scale commercial usage of such batteries.

References

1. Flandrois S, Simon B (1999) Carbon materials for lithium-ion rechargeable batteries. Carbon 37(2):165–180. https://doi.org/10.1016/S0008-6223(98)00290-5
2. Szczech JR, Jin S (2011) Nanostructured silicon for high-capacity lithium battery anodes. Energy Environ Sci 4(1):56–72. https://doi.org/10.1039/c0ee00281j
3. Su X, Wu Q, Li J, Xiao X, Lott A, Lu W, Sheldon BW, Wu J (2014) Silicon-based nanomaterials for lithium-ion batteries: a review. Adv Energy Mater 4(1):1300882. https://doi.org/10.1002/aenm.201300882
4. Ge M, Fang X, Rong J, Zhou C (2013) Review of porous silicon preparation and its application for lithium-ion battery anodes. Nanotechnology 24(42):422001
5. Whittingham MS (2004) Lithium batteries and cathode materials. Chem Rev 104(10):4271–4302. https://doi.org/10.1021/cr020731c
6. Lewandowski A, Åšwiderska-Mocek A (2009) Ionic liquids as electrolytes for Li-ion batteries—an overview of electrochemical studies. J Power Sources 194(2):601–609. https://doi.org/10.1016/j.jpowsour.2009.06.089
7. Ponrouch A, Monti D, Boschin A, Steen B, Johansson P, Palacin MR (2015) Non-aqueous electrolytes for sodium-ion batteries. J Mater Chem A 3(1):22–42. https://doi.org/10.1039/c4ta04428b
8. Kalhoff J, Eshetu GG, Bresser D, Passerini S (2015) Safer electrolytes for lithium-ion batteries: state of the art and perspectives. Chemsuschem 8(13):2154–2175. https://doi.org/10.1002/cssc.201500284
9. Palomares V, Serras P, Villaluenga I, Hueso KB, Carretero-Gonzalez J, Rojo T (2012) Na-ion batteries, recent advances and present challenges to become low cost energy storage systems. Energy Environ Sci 5(3):5884–5901. https://doi.org/10.1039/c2ee02781j
10. Ellis BL, Nazar LF (2012) Sodium and sodium-ion energy storage batteries. Curr Opin Solid State Mater Sci. 16(4):168–177. https://doi.org/10.1016/j.cossms.2012.04.002
11. Eftekhari A, Jian Z, Ji X (2017) Potassium secondary batteries. ACS Appl Mater Interfaces 9(5):4404–4419. https://doi.org/10.1021/acsami.6b07989
12. Ponrouch A, Frontera C, Barde F, Palacin MR (2016) Towards a calcium-based rechargeable battery. Nat Mater 15(2):169–172
13. Rahman MA, Wang X, Wen C (2013) High energy density metal–air batteries: a review. J Electrochem Soc 160(10):A1759–A1771
14. Lee J-S, Tai Kim S, Cao R, Choi N-S, Liu M, Lee KT, Cho J (2011) Metal–air batteries with high energy density: Li–air versus Zn–air. Adv Energy Mater 1(1):34–50. https://doi.org/10.1002/aenm.201000010
15. Kraytsberg A, Ein-Eli Y (2011) Review on Li–air batteries—opportunities, limitations and perspective. J Power Sources 196(3):886–893. https://doi.org/10.1016/j.jpowsour.2010.09.031
16. Wu YP, Rahm E, Holze R (2003) Carbon anode materials for lithium ion batteries. J Power Sources 114(2):228–236. https://doi.org/10.1016/S0378-7753(02)00596-7
17. Liang B, Liu Y, Xu Y (2014) Silicon-based materials as high capacity anodes for next-generation lithium ion batteries. J Power Sources 267:469–490. https://doi.org/10.1016/j.jpowsour.2014.05.096
18. Idota Y, Kubota T, Matsufuji A, Maekawa Y, Miyasaka T (1997) Tin-based amorphous oxide: a high-capacity lithium-ion-storage. Mater Sci 276(5317):1395–1397. https://doi.org/10.1126/science.276.5317.1395

19. Wu S, Han C, Iocozzia J, Lu M, Ge R, Xu R, Lin Z (2016) Germanium-based nanomaterials for rechargeable batteries. Angew Chem Int Ed 55(28):7898–7922. https://doi.org/10.1002/anie.201509651
20. Hamon Y, Brousse T, Jousse F, Topart P, Buvat P, Schleich DM (2001) Aluminum negative electrode in lithium ion batteries. J Power Sources 97–98:185–187. https://doi.org/10.1016/S0378-7753(01)00616-4
21. Chan CK, Patel RN, O'Connell MJ, Korgel BA, Cui Y (2010) Solution-grown silicon nanowires for lithium-ion battery anodes. ACS Nano 4(3):1443–1450. https://doi.org/10.1021/nn901409q
22. Kennedy T, Mullane E, Geaney H, Osiak M, O'Dwyer C, Ryan KM (2014) High-performance germanium nanowire-based lithium-ion battery anodes extending over 1000 cycles through in situ formation of a continuous porous network. Nano Lett 14(2):716–723. https://doi.org/10.1021/nl403979s
23. Eshetu GG, Armand M, Scrosati B, Passerini S (2014) Energy storage materials synthesized from ionic liquids. Angew Chem Int Ed 53(49):13342–13359. https://doi.org/10.1002/anie.201405910
24. Cui L-F, Yang Y, Hsu C-M, Cui Y (2009) Carbon-silicon core–shell nanowires as high capacity electrode for lithium ion batteries. Nano Lett 9(9):3370–3374. https://doi.org/10.1021/nl901670t
25. Yang LY, Li HZ, Liu J, Sun ZQ, Tang SS, Lei M (2015) Dual yolk-shell structure of carbon and silica-coated silicon for high-performance lithium-ion batteries. Sci Rep 5:10908
26. X-y Zhou, J-j Tang, Yang J, Xie J, L-l Ma (2013) Silicon–carbon hollow core–shell heterostructures novel anode materials for lithium ion batteries. Electrochim Acta 87:663–668. https://doi.org/10.1016/j.electacta.2012.10.008
27. Zhang T, Fu L, Gao J, Yang L, Wu Y, Wu H (2006) Core–shell Si/C nanocomposite as anode material for lithium ion batteries. Pure Appl Chem 78(10):1889–1896. https://doi.org/10.1351/pac200678101889
28. Ma Y, Ji G, Ding B, Lee JY (2013) N-doped carbon encapsulation of ultrafine silicon nanocrystallites for high-performance lithium ion storage. J Mater Chem A 1(43):13625–13631. https://doi.org/10.1039/c3ta13268d
29. Zein El Abedin S, Borissenko N, Endres F (2004) Electrodeposition of nanoscale silicon in a room temperature ionic liquid. Electrochem Commun 6(5):510–514. https://doi.org/10.1016/j.elecom.2004.03.013
30. Schmuck M, Balducci A, Rupp B, Kern W, Passerini S, Winter M (2010) Alloying of electrodeposited silicon with lithium—a principal study of applicability as anode material for lithium ion batteries. J Solid State Electrochem 14(12):2203–2207. https://doi.org/10.1007/s10008-008-0763-4
31. Vlaic CA, Ivanov S, Peipmann R, Eisenhardt A, Himmerlich M, Krischok S, Bund A (2015) Electrochemical lithiation of thin silicon-based layers potentiostatically deposited from ionic liquid. Electrochim Acta 168:403–413. https://doi.org/10.1016/j.electacta.2015.03.216
32. Park M-H, Cho Y, Kim K, Kim J, Liu M, Cho J (2011) Germanium nanotubes prepared by using the Kirkendall effect as anodes for high-rate lithium batteries. Angew Chem Int Ed 50(41):9647–9650. https://doi.org/10.1002/anie.201103062
33. Lahiri A, Willert A, Abedin SZE, Endres F (2014) A simple and fast technique to grow free-standing germanium nanotubes and core–shell structures from room temperature ionic liquids. Electrochim Acta 121:154–158. https://doi.org/10.1016/j.electacta.2013.12.084
34. Meng X, Al-Salman R, Zhao J, Borissenko N, Li Y, Endres F (2009) Electrodeposition of 3D ordered macroporous germanium from ionic liquids: a feasible method to make photonic crystals with a high dielectric constant. Angew Chem Int Ed 48(15):2703–2707. https://doi.org/10.1002/anie.200805252
35. Liu X, Zhao J, Hao J, Su B-L, Li Y (2013) 3D ordered macroporous germanium fabricated by electrodeposition from an ionic liquid and its lithium storage properties. J Mater Chem A 1(47):15076–15081. https://doi.org/10.1039/c3ta12923c
36. Liu X, Hao J, Liu X, Chi C, Li N, Endres F, Zhang Y, Li Y, Zhao J (2015) Preparation of Ge nanotube arrays from an ionic liquid for lithium ion battery anodes with improved cycling stability. Chem Commun 51(11):2064–2067. https://doi.org/10.1039/c4cc08722d
37. Hao J, Li N, Ma X, Liu X, Liu X, Li Y, Xu H, Zhao J (2015) Ionic liquid electrodeposition of germanium/carbon nanotube composite anode material for lithium ion batteries. Mater Lett 144:50–53. https://doi.org/10.1016/j.matlet.2015.01.022
38. Lahiri A, Borisenko N, Borodin A, Olschewski M, Endres F (2016) Characterisation of the solid electrolyte interface during lithiation/delithiation of germanium in an ionic liquid. Phys Chem Chem Phys 18(7):5630–5637. https://doi.org/10.1039/c5cp06184a

39. Lahiri A, Schubert TJS, Iliev B, Endres F (2015) LiTFSI in 1-butyl-1-methylpyrrolidinium bis(fluorosulfonyl)amide: a possible electrolyte for ionic liquid-based lithium ion batteries. Phys Chem Chem Phys 17(17):11161–11164. https://doi.org/10.1039/c5cp01337b
40. Lahiri A, Li G, Olschewski M, Endres F (2016) influence of polar organic solvents in an ionic liquid containing lithium bis(fluorosulfonyl)amide: effect on the cation-anion interaction, lithium ion battery performance, and solid electrolyte interphase. ACS Appl Mater Interfaces 8(49):34143–34150. https://doi.org/10.1021/acsami.6b12751
41. Kerner M, Plylahan N, Scheers J, Johansson P (2015) Ionic liquid-based lithium battery electrolytes: fundamental benefits of utilising both TFSI and FSI anions? Phys Chem Chem Phys 17(29):19569–19581. https://doi.org/10.1039/c5cp01891a
42. Xu K (2014) Electrolytes and interphases in li-ion batteries and beyond. Chem Rev 114(23):11503–11618. https://doi.org/10.1021/cr500003w
43. Kühnel RS, Böckenfeld N, Passerini S, Winter M, Balducci A (2011) Mixtures of ionic liquid and organic carbonate as electrolyte with improved safety and performance for rechargeable lithium batteries. Electrochim Acta 56(11):4092–4099. https://doi.org/10.1016/j.electacta.2011.01.116
44. Lombardo L, Brutti S, Navarra MA, Panero S, Reale P (2013) Mixtures of ionic liquid—alkylcarbonates as electrolytes for safe lithium-ion batteries. J Power Sources 227:8–14. https://doi.org/10.1016/j.jpowsour.2012.11.017
45. Kamali AR, Fray DJ (2011) Tin-based materials as advanced anode materials for lithium ion batteries: a review. Rev Adv Mater Sci 27:14–24
46. Gu C, Zhang H, Wang X, Tu J (2013) One-pot synthesis of SnO_2/reduced graphene oxide nanocomposite in ionic liquid-based solution and its application for lithium ion batteries. Mater Res Bull 48(10):4112–4117. https://doi.org/10.1016/j.materresbull.2013.06.041
47. Giridhar P, Elbasiony AM, Zein El Abedin S, Endres F (2014) A comparative study on the electrodeposition of tin from two different ionic liquids: influence of the anion on the morphology of the tin deposits. ChemElectroChem 1(9):1549–1556. https://doi.org/10.1002/celc.201402155
48. Elbasiony AMR, Zein El Abedin S, Endres F (2014) Electrochemical synthesis of freestanding tin nanowires from ionic liquids. J Solid State Electrochem 18(4):951–957. https://doi.org/10.1007/s10008-013-2340-8
49. Hsu C-H, Yang C-H, Wang Y-C, Chang J-K (2014) Nanostructured tin electrodeposited in ionic liquid for use as an anode for Li-ion batteries. J Mater Chem A 2(39):16547–16553. https://doi.org/10.1039/c4ta03709j
50. Lahiri A, Pulletikurthi G, Zein El Abedin S, Endres F (2015) Electrodeposition of Ge, Sn and $GexSn_{1-x}$ from two different room temperature ionic liquids. J Solid State Electrochem 19(3):785–793. https://doi.org/10.1007/s10008-014-2675-9
51. Liu Z, Elbasiony AM, Zein El Abedin S, Endres F (2015) Electrodeposition of zinc-copper and zinc-tin films and free-standing nanowire arrays from ionic liquids. ChemElectroChem 2(3):389–395. https://doi.org/10.1002/celc.201402350
52. Gasparotto LHS, Prowald A, Borisenko N, El Abedin SZ, Garsuch A, Endres F (2011) Electrochemical synthesis of macroporous aluminium films and their behavior towards lithium deposition/stripping. J Power Sources 196(5):2879–2883. https://doi.org/10.1016/j.jpowsour.2010.10.104
53. Zein El Abedin S, Endres F (2012) Free-standing aluminium nanowire architectures made in an ionic liquid. ChemPhysChem 13(1):250–255. https://doi.org/10.1002/cphc.201100639
54. Zein El Abedin S, Garsuch A, Endres F (2012) Aluminium nanowire electrodes for lithium-ion batteries. Aust J Chem 65(11):1529–1533. https://doi.org/10.1071/CH12330
55. Kim Y, Ha K-H, Oh SM, Lee KT (2014) High-capacity anode materials for sodium-ion batteries. Chem Eur J 20(38):11980–11992. https://doi.org/10.1002/chem.201402511
56. Li Z, Ding J, Mitlin D (2015) Tin and tin compounds for sodium ion battery anodes: phase transformations and performance. Acc Chem Res 48(6):1657–1665. https://doi.org/10.1021/acs.accounts.5b00114
57. Kubota K, Komaba S (2015) Review-practical issues and future perspective for Na-ion batteries. J Electrochem Soc 162(14):A2538–A2550. https://doi.org/10.1149/2.0151514jes
58. Kundu D, Talaie E, Duffort V, Nazar LF (2015) The emerging chemistry of sodium ion batteries for electrochemical energy storage. Angew Chem Int Ed 54(11):3431–3448. https://doi.org/10.1002/anie.201410376
59. Borisenko N, Lahiri A, Endres F (2017) Electrodeposition of semiconductors from ionic liquids, second edition. In: Endres F, Abbott A, MacFarlane D (eds) Electrodeposition from ionic liquids. Wiley-VCH Verlag GmbH & Co. KGaA, pp 187–210. https://doi.org/10.1002/9783527682706.ch6

60. Abel PR, Lin Y-M, de Souza T, Chou C-Y, Gupta A, Goodenough JB, Hwang GS, Heller A, Mullins CB (2013) Nanocolumnar germanium thin films as a high-rate sodium-ion battery anode material. J Phys Chem C 117(37):18885–18890. https://doi.org/10.1021/jp407322k
61. Baggetto L, Keum JK, Browning JF, Veith GM (2013) Germanium as negative electrode material for sodium-ion batteries. Electrochem Commun 34:41–44. https://doi.org/10.1016/j.elecom.2013.05.025
62. Lahiri A, Olschewski M, Gustus R, Borisenko N, Endres F (2016) Surface modification of battery electrodes via electroless deposition with improved performance for Na-ion batteries. Phys Chem Chem Phys 18(22):14782–14786. https://doi.org/10.1039/c6cp02364a
63. Nam D-H, Hong K-S, Lim S-J, Kwon H-S (2014) Electrochemical synthesis of a three-dimensional porous Sb/Cu_2Sb anode for Na-ion batteries. J Power Sources 247:423–427. https://doi.org/10.1016/j.jpowsour.2013.08.095
64. Liang L, Xu Y, Wang C, Wen L, Fang Y, Mi Y, Zhou M, Zhao H, Lei Y (2015) Large-scale highly ordered Sb nanorod array anodes with high capacity and rate capability for sodium-ion batteries. Energy Environ Sci 8(10):2954–2962. https://doi.org/10.1039/c5ee00878f
65. Jackson ED, Green S, Prieto AL (2015) Electrochemical performance of electrodeposited Zn_4Sb_3 films for sodium-ion secondary battery anodes. ACS Appl Mater Interfaces 7(14):7447–7450. https://doi.org/10.1021/am507436u
66. Wang C-H, Yeh Y-W, Wongittharom N, Wang Y-C, Tseng C-J, Lee S-W, Chang W-S, Chang J-K (2015) Rechargeable Na/$Na_{0.44}MnO_2$ cells with ionic liquid electrolytes containing various sodium solutes. J Power Sources 274:1016–1023. https://doi.org/10.1016/j.jpowsour.2014.10.143
67. Wongittharom N, Lee T-C, Wang C-H, Wang Y-C, Chang J-K (2014) Electrochemical performance of Na/$NaFePO_4$ sodium-ion batteries with ionic liquid electrolytes. J Mater Chem A 2(16):5655–5661. https://doi.org/10.1039/c3ta15273a
68. Hosokawa T, Matsumoto K, Nohira T, Hagiwara R, Fukunaga A, Sakai S, Nitta K (2016) Stability of ionic liquids against sodium metal: a comparative study of 1-ethyl-3-methylimidazolium ionic liquids with bis(fluorosulfonyl)amide and bis(trifluoromethylsulfonyl)amide. J Phys Chem C 120(18):9628–9636. https://doi.org/10.1021/acs.jpcc.6b02061
69. Kar M, Simons TJ, Forsyth M, MacFarlane DR (2014) Ionic liquid electrolytes as a platform for rechargeable metal–air batteries: a perspective. Phys Chem Chem Phys 16(35):18658–18674. https://doi.org/10.1039/c4cp02533d
70. Kuboki T, Okuyama T, Ohsaki T, Takami N (2005) Lithium–air batteries using hydrophobic room temperature ionic liquid electrolyte. J Power Sources 146(1–2):766–769. https://doi.org/10.1016/j.jpowsour.2005.03.082
71. Mizuno F, Nakanishi S, Shirasawa A, Takechi K, Shiga T, Nishikoori H, Iba H (2011) Design of non-aqueous liquid electrolytes for rechargeable Li-O_2 batteries. Electrochemistry 79(11):876–881. https://doi.org/10.5796/electrochemistry.79.876
72. Nakamoto H, Suzuki Y, Shiotsuki T, Mizuno F, Higashi S, Takechi K, Asaoka T, Nishikoori H, Iba H (2013) Ether-functionalized ionic liquid electrolytes for lithium–air batteries. J Power Sources 243:19–23. https://doi.org/10.1016/j.jpowsour.2013.05.147
73. Soavi F, Monaco S, Mastragostino M (2013) Catalyst-free porous carbon cathode and ionic liquid for high-efficiency, rechargeable Li/O_2 battery. J Power Sources 224:115–119. https://doi.org/10.1016/j.jpowsour.2012.09.095
74. Garsuch A, Badine DM, Leitner K, Gasparotto Luiz HS, Borisenko N, Endres F, Vracar M, Janek J, Oesten R (2012) Investigation of various ionic liquids and catalyst materials for lithium-oxygen batteries. Z Phys Chem 226:107–120. https://doi.org/10.1524/zpch.2011.0136
75. Elia GA, Hassoun J, Kwak WJ, Sun YK, Scrosati B, Mueller F, Bresser D, Passerini S, Oberhumer P, Tsiouvaras N, Reiter J (2014) An advanced lithium–air battery exploiting an ionic liquid-based electrolyte. Nano Lett 14(11):6572–6577. https://doi.org/10.1021/nl5031985
76. Das S, Højberg J, Knudsen KB, Younesi R, Johansson P, Norby P, Vegge T (2015) Instability of ionic liquid-based electrolytes in Li-O_2 batteries. J Phys Chem C 119(32):18084–18090. https://doi.org/10.1021/acs.jpcc.5b04950
77. Aurbach D, Zinigrad E, Cohen Y, Teller H (2002) A short review of failure mechanisms of lithium metal and lithiated graphite anodes in liquid electrolyte solutions. Solid State Ionics 148(3):405–416. https://doi.org/10.1016/S0167-2738(02)00080-2
78. Howlett PC, MacFarlane DR, Hollenkamp AF (2004) High lithium metal cycling efficiency in a room-temperature ionic liquid. Electrochem Solid State Lett 7(5):A97–A101

79. Howlett PC, Brack N, Hollenkamp AF, Forsyth M, MacFarlane DR (2006) Characterization of the lithium surface in *N*-methyl-*N*-alkylpyrrolidinium bis(trifluoromethanesulfonyl)amide room-temperature ionic liquid electrolytes. J Electrochem Soc 153(3):A595–A606. https://doi.org/10.1149/1.2164726
80. Gasparotto LHS, Borisenko N, Bocchi N, Zein El Abedin S, Endres F (2009) In situ STM investigation of the lithium underpotential deposition on Au(111) in the air- and water-stable ionic liquid 1-butyl-1-methylpyrrolidinium bis(trifluoromethylsulfonyl)amide. Phys Chem Chem Phys 11(47):11140–11145. https://doi.org/10.1039/b916809e
81. Stark JK, Ding Y, Kohl PA (2011) Dendrite-free electrodeposition and reoxidation of lithium-sodium alloy for metal-anode battery. J Electrochem Soc 158(10):A1100–A1105. https://doi.org/10.1149/1.3622348
82. Sano H, Sakaebe H, Matsumoto H (2011) Observation of electrodeposited lithium by optical microscope in room temperature ionic liquid-based electrolyte. J Power Sources 196(16):6663–6669. https://doi.org/10.1016/j.jpowsour.2010.12.023
83. Bhatt AI, Kao P, Best AS, Hollenkamp AF (2013) Understanding the morphological changes of lithium surfaces during cycling in electrolyte solutions of lithium salts in an ionic liquid. J Electrochem Soc 160(8):A1171–A1180. https://doi.org/10.1149/2.056308jes
84. Vanhoutte G, Brooks NR, Schaltin S, Opperdoes B, Van Meervelt L, Locquet J-P, Vereecken PM, Fransaer J, Binnemans K (2014) Electrodeposition of lithium from lithium-containing solvate ionic liquids. J Phys Chem C 118(35):20152–20162. https://doi.org/10.1021/jp505479x
85. Grande L, von Zamory J, Koch SL, Kalhoff J, Paillard E, Passerini S (2015) Homogeneous lithium electrodeposition with pyrrolidinium-based ionic liquid electrolytes. ACS Appl Mater Interfaces 7(10):5950–5958. https://doi.org/10.1021/acsami.5b00209
86. Xu M, Ivey DG, Xie Z, Qu W (2015) Rechargeable Zn–air batteries: progress in electrolyte development and cell configuration advancement. J Power Sources 283:358–371. https://doi.org/10.1016/j.jpowsour.2015.02.114
87. Simons TJ, Torriero AAJ, Howlett PC, MacFarlane DR, Forsyth M (2012) High current density, efficient cycling of Zn^{2+} in 1-ethyl-3-methylimidazolium dicyanamide ionic liquid: the effect of Zn^{2+} salt and water concentration. Electrochem Commun 18:119–122. https://doi.org/10.1016/j.elecom.2012.02.034
88. Xu M, Ivey DG, Xie Z, Qu W (2013) Electrochemical behavior of Zn/Zn(II) couples in aprotic ionic liquids based on pyrrolidinium and imidazolium cations and bis(trifluoromethanesulfonyl) imide and dicyanamide anions. Electrochim Acta 89:756–762. https://doi.org/10.1016/j.electacta.2012.11.023
89. Liu Z, Abedin SZE, Endres F (2013) Electrodeposition of zinc films from ionic liquids and ionic liquid/water mixtures. Electrochim Acta 89:635–643. https://doi.org/10.1016/j.electacta.2012.11.077
90. Liu Z, Borisenko N, Zein El Abedin S, Endres F (2014) In situ STM study of zinc electrodeposition on Au(111) from the ionic liquid 1-ethyl-3-methylimidazolium trifluoromethylsulfonate. J Solid State Electrochem 18(9):2581–2587. https://doi.org/10.1007/s10008-014-2516-x
91. Liu Z, El Abedin SZ, Endres F (2015) Raman and FTIR spectroscopic studies of 1-ethyl-3-methylimidazolium trifluoromethylsulfonate, its mixtures with water and the solvation of zinc ions. ChemPhysChem 16(5):970–977. https://doi.org/10.1002/cphc.201402831
92. Ghazvini MS, Pulletikurthi G, Liu Z, Prowald A, Zein El Abedin S, Endres F (2015) Electrodeposition and stripping behavior of a zinc/polystyrene composite electrode in an ionic liquid. J Solid State Electrochem 19(5):1453–1461. https://doi.org/10.1007/s10008-015-2757-3
93. Keist JS, Orme CA, Wright PK, Evans JW (2015) An in situ AFM study of the evolution of surface roughness for zinc electrodeposition within an imidazolium-based ionic liquid electrolyte. Electrochim Acta 152:161–171. https://doi.org/10.1016/j.electacta.2014.11.091
94. Ghazvini MS, Pulletikurthi G, Lahiri A, Endres F (2016) Electrochemical and spectroscopic studies of zinc acetate in 1-ethyl-3-methylimidazolium acetate for zinc electrodeposition. ChemElectroChem 3(4):598–604. https://doi.org/10.1002/celc.201500444
95. Kar M, Winther-Jensen B, Armand M, Simons TJ, Winther-Jensen O, Forsyth M, MacFarlane DR (2016) Stable zinc cycling in novel alkoxy-ammonium-based ionic liquid electrolytes. Electrochim Acta 188:461–471. https://doi.org/10.1016/j.electacta.2015.12.050
96. Liu Z, Cui T, Pulletikurthi G, Lahiri A, Carstens T, Olschewski M, Endres F (2016) Dendrite-free nanocrystalline zinc electrodeposition from an ionic liquid containing nickel triflate for

rechargeable Zn-based batteries. Angew Chem Int Ed 55(8):2889–2893. https://doi.org/10.1002/anie.201509364

97. Liu Z, Pulletikurthi G, Lahiri A, Cui T, Endres F (2016) Suppressing the dendritic growth of zinc in an ionic liquid containing cationic and anionic zinc complexes for battery applications. Dalton Trans 45(19):8089–8098. https://doi.org/10.1039/c6dt00969g
98. Switzer EE, Zeller R, Chen Q, Sieradzki K, Buttry DA, Friesen C (2013) Oxygen reduction reaction in ionic liquids: the addition of protic species. J Phys Chem C 117(17):8683–8690. https://doi.org/10.1021/jp400845u
99. Pozo-Gonzalo C, Howlett PC, Hodgson JL, Madsen LA, MacFarlane DR, Forsyth M (2014) Insights into the reversible oxygen reduction reaction in a series of phosphonium-based ionic liquids. Phys Chem Chem Phys 16(45):25062–25070. https://doi.org/10.1039/c4cp04101a
100. Elia GA, Marquardt K, Hoeppner K, Fantini S, Lin R, Knipping E, Peters W, Drillet J-F, Passerini S, Hahn R (2016) An overview and future perspectives of aluminum batteries. Adv Mater 28(35):7564–7579. https://doi.org/10.1002/adma.201601357
101. Lai PK, Skyllas-Kazacos M (1988) Electrodeposition of aluminium in aluminium chloride/1-methyl-3-ethylimidazolium chloride. J Electroanal Chem 248(2):431–440. https://doi.org/10.1016/0022-0728(88)85103-9
102. Giridhar P, Zein El Abedin S, Endres F (2012) Electrodeposition of aluminium from 1-butyl-1-methylpyrrolidinium chloride/$AlCl_3$ and mixtures with 1-ethyl-3-methylimidazolium chloride/$AlCl_3$. Electrochim Acta 70:210–214. https://doi.org/10.1016/j.electacta.2012.03.056
103. Jayaprakash N, Das SK, Archer LA (2011) The rechargeable aluminum-ion battery. Chem Commun 47(47):12610–12612. https://doi.org/10.1039/c1cc15779e
104. Reed LD, Menke E (2013) The roles of V_2O_5 and stainless steel in rechargeable Al-ion batteries. J Electrochem Soc 160(6):A915–A917. https://doi.org/10.1149/2.114306jes
105. Wang H, Bai Y, Chen S, Luo X, Wu C, Wu F, Lu J, Amine K (2015) Binder-free V_2O_5 cathode for greener rechargeable aluminum battery. ACS Appl Mater Interfaces 7(1):80–84. https://doi.org/10.1021/am508001h
106. Wang W, Jiang B, Xiong W, Sun H, Lin Z, Hu L, Tu J, Hou J, Zhu H, Jiao S (2013) A new cathode material for super-valent battery based on aluminium ion intercalation and deintercalation. Sci Rep 3:3383. https://doi.org/10.1038/srep03383
107. Lin M-C, Gong M, Lu B, Wu Y, Wang D-Y, Guan M, Angell M, Chen C, Yang J, Hwang B-J, Dai H (2015) An ultrafast rechargeable aluminium-ion battery. Nature 520(7547):324–328
108. Gifford PR, Palmisano JB (1988) An aluminum/chlorine rechargeable cell employing a room temperature molten salt electrolyte. J Electrochem Soc 135(3):650–654. https://doi.org/10.1149/1.2095685
109. Zein El Abedin S, Moustafa EM, Hempelmann R, Natter H, Endres F (2006) Electrodeposition of nano- and microcrystalline aluminium in three different air and water stable ionic liquids. ChemPhysChem 7(7):1535–1543. https://doi.org/10.1002/cphc.200600095
110. Wang H, Gu S, Bai Y, Chen S, Wu F, Wu C (2016) High-voltage and noncorrosive ionic liquid electrolyte used in rechargeable aluminum battery. ACS Appl Mater Interfaces 8(41):27444–27448. https://doi.org/10.1021/acsami.6b10579
111. Rani JV, Kanakaiah V, Dadmal T, Rao MS, Bhavanarushi S (2013) Fluorinated natural graphite cathode for rechargeable ionic liquid-based aluminum-ion battery. J Electrochem Soc 160(10):A1781–A1784. https://doi.org/10.1149/2.072310jes
112. Geng L, Lv G, Xing X, Guo J (2015) Reversible electrochemical intercalation of aluminum in Mo_6S_8. Chem Mater 27(14):4926–4929. https://doi.org/10.1021/acs.chemmater.5b01918
113. Wang S, Yu Z, Tu J, Wang J, Tian D, Liu Y, Jiao SC (2016) A novel aluminum-ion battery: Al/$AlCl_3$-[EMIm]Cl/Ni_3S_2@graphene. Adv Energy Mater 6(13):1600137. https://doi.org/10.1002/aenm.201600137
114. Gelman D, Shvartsev B, Ein-Eli Y (2014) Aluminum–air battery based on an ionic liquid electrolyte. J Mater Chem A 2(47):20237–20242. https://doi.org/10.1039/c4ta04721d
115. Revel R, Audichon T, Gonzalez S (2014) Non-aqueous aluminium–air battery based on ionic liquid electrolyte. J Power Sources 272:415–421. https://doi.org/10.1016/j.jpowsour.2014.08.056
116. Cohn G, Ma L, Archer LA (2015) A novel non-aqueous aluminum sulfur battery. J Power Sources 283:416–422. https://doi.org/10.1016/j.jpowsour.2015.02.131
117. Gao T, Li X, Wang X, Hu J, Han F, Fan X, Suo L, Pearse AJ, Lee SB, Rubloff GW, Gaskell KJ, Noked M, Wang C (2016) A rechargeable Al/S battery with an ionic-liquid electrolyte. Angew Chem Int Ed 55(34):9898–9901. https://doi.org/10.1002/anie.201603531

Top Curr Chem (Z) (2017) 375:74
DOI 10.1007/s41061-017-0159-y

REVIEW

Ionic Liquid–Liquid Chromatography: A New General Purpose Separation Methodology

Leslie Brown[1] · **Martyn J. Earle**[2] · **Manuela A. Gîlea**[2] · **Natalia V. Plechkova**[2] · **Kenneth R. Seddon**[2]

Received: 2 May 2017 / Accepted: 1 July 2017 / Published online: 10 August 2017

Abstract Ionic liquids can form biphasic solvent systems with many organic solvents and water, and these solvent systems can be used in liquid–liquid separations and countercurrent chromatography. The wide range of ionic liquids that can by synthesised, with specifically tailored properties, represents a new philosophy for the separation of organic, inorganic and bio-based materials. A customised countercurrent chromatograph has been designed and constructed specifically to allow the more viscous character of ionic liquid-based solvent systems to be used in a wide variety of separations (including transition metal salts, arenes, alkenes, alkanes, bio-oils and sugars).

Keywords Ionic liquids · Countercurrent chromatography · Ionic liquid–liquid chromatography · Separations · Solvent engineering

Abbreviations

ABS	Aqueous biphasic solvents
CCC	Countercurrent chromatography
CPC	Centrifugal partition chromatography
[$C_n$mim]	1-Alkyl-3-methylimidazolium, where n = alkyl chain length
[$C_n$py]	1-Alkylpyridinium, where n = alkyl chain length
$[N_{111}(C_2OH)]^+$	Cholinium or 2-(hydroxyethyl)trimethylammonium

---

Chapter 4 was originally published as Brown, L., Earle, M. J., Gîlea, M. A., Plechkova, N. V. & Seddon, K. R. Top Curr Chem (Z) (2017) 375: 74. DOI 10.1007/s41061-017-0159-y.

✉ Martyn J. Earle
quill@qub.ac.uk

[1] AECS-QuikPrep Ltd, 55 Gower Street, London WC1 6HQ, UK

[2] The QUILL Research Centre, School of Chemistry, The Queen's University of Belfast, Stranmillis Road, Belfast, Northern Ireland BT9 5AG, UK

DR_X	Distribution ratio (of component X)
DMSO	Dimethyl sulfoxide
DPS	Dense phase stationary (in biphasic solvent systems)
GC	Gas chromatography
HEMWat	Hexane, Ethyl ethanoate, Methanol, Water
HPCCC	High-performance countercurrent chromatography
HPLC	High performance liquid chromatography
HPLLC	High performance liquid–liquid chromatography
HSCCC	High-speed countercurrent chromatography
IL	Ionic liquid
ILLC	Ionic liquid–liquid chromatography
LLC	Liquid–liquid chromatography
LPS	Light phase stationary (in biphasic solvent systems)
MP	Mobile phase
NTf_2	Bis{(trifluoromethyl)sulfonyl}amide or $[N(SO_2CF_3)_2]^-$
OTf	Trifluoromethanesulfonate or $[SO_3CF_3]^-$
PEG	Polyethylene glycol
SP	Stationary phase
S_f	Stationary phase retention factor
$[P_{6\,6\,6\,14}]^+$	Trihexyltetradecylphosphonium cation
VOCs	Volatile organic compounds

1 Introduction

Over the last two decades, there have been considerable advances in the science of liquid–liquid chromatography (LLC) [1, 2] and its variant, countercurrent chromatography (CCC), with the latter considered to be a continuous, automated form of liquid–liquid separation [3]. These techniques are based on the ability of solutes to distribute themselves between two mutually immiscible phases: a mobile liquid phase (MP) and a stationary liquid phase (SP) [4]. LLC sits at the interface of three areas of research: chemical engineering [5], solvent engineering [6, 7] and chromatographic science [1]. In this chapter, we use the term solvent engineering in the sense of design, production and use of a solvent (or solvent system) to give enhanced control, performance, yield and/or selectivity in physical, chemical or biochemical reactions, processes and separations. The evolution of CCC instrumentation, in large part carried out by Ito [8], has allowed higher stationary phase retention, which in turn generates better resolution, faster separations and continuous processes with industrial applicability [9].

The use of large amounts of mixed organic solvents in LLC is usually associated with difficulties in the recycling of solvents [10] and the release of volatile organic compounds (VOCs) [11]. The option of solvent recycling [12] allows the reuse of the column effluent, but the full separation of effluents into single solvent components is a cumbersome and expensive process due to the similarity in boiling points of individual components (with potential azeotrope formation in some cases) [13, 14]. However, in spite of these limitations, industrial processes based on LLC have been described [9, 15, 16]. In order to expand the range of stationary and mobile phases available in CCC and related technologies and to make use of the unique and greater dissolution capabilities of ionic liquids [17], ionic liquids have been examined as new and alternative solvents in CCC.

Ionic liquids have been described as “designer solvents”, as they can be engineered to solve specific problems, such as the dissolution of a large range of materials, replace toxic and volatile solvents, produce multiphasic solvent systems to enhance separation efficiency or allow simplified separations [19]. Their use in chromatographic separations has greatly increased since their first use in 1999 [20], and the growth in the number of publications is shown in Fig. 1.

In this chapter, we demonstrate that a combination of solvent engineering and chromatographic and analytical techniques can be used to enable a diverse range of separations, including inorganic, organic, biochemical and petrochemical applications [21].

2 Introduction to Countercurrent Chromatography

Since 1970 [22], several variants of CCC have been developed [1]. These include high-performance countercurrent chromatography (HPCCC) [23], high-speed countercurrent chromatography (HSCCC), and centrifugal partition chromatography (CPC). Among the different types of CCC centrifuge systems developed [24, 25], Ito’s J-type centrifuge (Fig. 2) [26] has gained a prominent position due to its suitability for scale-up [27]. In the J-type centrifuge, the coils are connected to the chassis by means of non-rotating flying leads. This is achieved through planetary motion of a coiled pipe, as shown in Fig. 2 [8, 25]. The result is that the head and tail connections of the flying leads flex, but do not exhibit any overall rotation. In the related technique of CPC, a series of linked chambers is rotated around a sun-type axis, and the fluids are pumped through the system of chambers through a pair

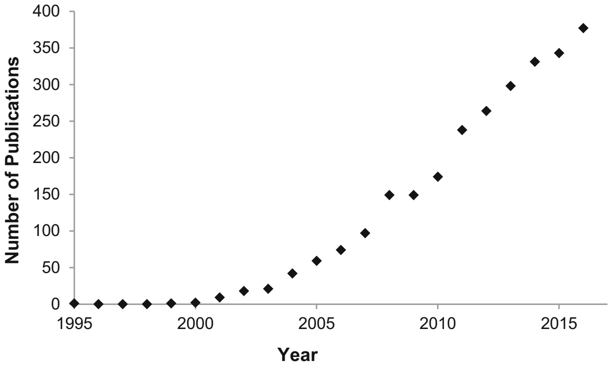

Fig. 1 The number of journal articles based on a Web of Science [18] search of the terms “ionic liquid” and “chromatography” for the time period 1995–2016

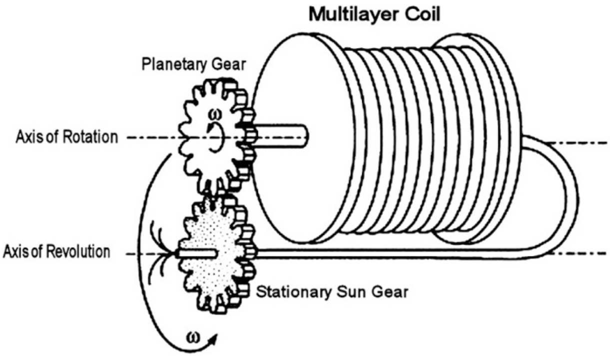

Fig. 2 Schematic of the J-type synchronous planetary motion centrifuge used in countercurrent chromatography [8]. Granted with the permission from Wiley

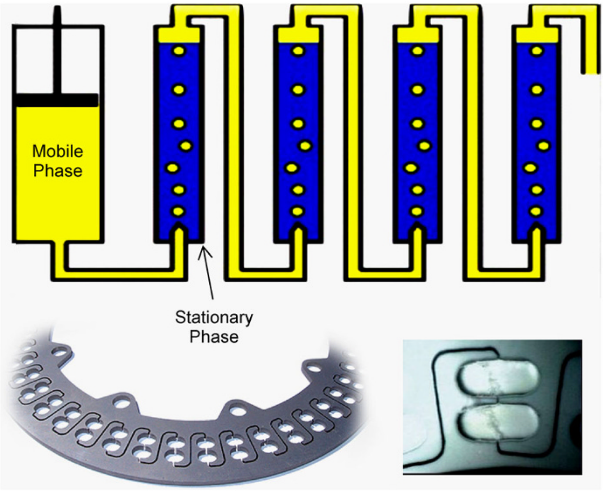

Fig. 3 A schematic of a centrifugal partition chromatography (CPC) rotor (*top*) containing a mobile phase (*yellow*) and stationary phase (*blue*) in ascending mode, showing the flow of the light phase (ascending) through the dense phase; a section of a CPC rotor plate showing the chambers (*lower left*) and the chambers in a CPC rotor during operation with a biphasic solvent system (*lower right*)

of rotating seals, as shown in Fig. 3. In general, CPC systems are preferred for larger scale separations (>100 g), and the J-type centrifuge HPCCC systems are used for smaller scale separations (<100 g), although it must be noted that both instrument designs are capable of successfully operating outside these regions.

In HPCCC, also known as hydrodynamic CCC, the stationary phase is retained within a helical coil wound around a drum, while the mobile phase is pumped into one end of the coil. A combination of hydrostatic and hydrodynamic forces is produced as the drum rotates in both planetary and solar motion around a central shaft (Fig. 2). The phases are forced towards opposite ends of the coil [28]; the mobile phase is pumped into the end of the coil, whereas the stationary phase accumulates. The design of the J-type centrifuge [29] produces zones of ballistic mixing and zones of settling as the mobile phase passes through the stationary phase. Compounds carried in the mobile phase elute in order of their distribution ratio (DR) of the compound between the mobile phase and stationary phase. The DR of a compound can be defined as:

$$\mathrm{DR} = [\mathrm{SP}]/[\mathrm{MP}] \tag{1}$$

where [MP] and [SP] are the concentrations of the solute in the MP and SP, respectively [1].

The volumes of the stationary phases used in CCC (and related technologies) enable separations on a much larger scale than is feasible in gas chromatography (GC) or high-performance liquid chromatography (HPLC). Also, in CCC, less solvent is required for a given separation than is required for a similar scale preparative HPLC separation. The performance of the separations in CCC is therefore determined largely by the difference in the partition coefficients of the solutes dissolved in the two liquid phases. It is by careful design of the solvent system that the desired distribution ratios of the solutes can be achieved (see Section 3).

The conventional biphasic solvent systems used in CCC are based on molecular solvents. The most commonly used solvents are mixtures of water, methanol, ethyl ethanoate and hexane [4], and combinations of these are sometimes referred to as the Arizona liquid system [30], or more recently as the “HEMWat” system [31]. Other solvents include butanol, butanenitrile, *N*,*N*-dimethylformamide, dimethyl sulfoxide (DMSO), dichloromethane, ethanenitrile, toluene and trichloromethane, which are known to be both toxic and volatile [32–35]. In addition, it can be difficult to completely remove dipolar aprotic solvents from the isolated product of a CCC separation. The process of solvent selection involves testing the DRs of the solutes being separated, between a large number of solvent systems, and selecting the best overall solvent system. This process can be greatly simplified by the use of automation [6].

3 Ionic Liquids in Chromatography

Some of the conventional problems encountered with specialised chromatographic techniques, such as CCC and CPC, originate as a result of the restricted set of solvents which can be utilised as mobile phases. The recent developments in the field of ionic liquids offer opportunities to vastly expand the range of available solvents and provide the ability to tune the solvent properties [21]. In this section, we consider specifically the implications that arise when the application of ionic liquids to chromatography is taken into account.

3.1 Introduction to Ionic Liquids

Ionic liquids were originally defined as salts that are liquid at or below 100 °C [19], composed entirely of ions. More recently, a simpler and more fundamental definition is being used, “an ionic liquid is a liquid containing only ions, derived from a solid which melts before its decomposition temperature". This removes the artificial imposition of a melting point upon the definition [36].

Ionic liquids have unique properties that can help overcome some of the problems associated with the use of conventional organic solvents (see Section 2). For example, many ionic liquids have no measurable vapour pressure at ambient temperatures and pressures [37], resulting in their non-flammability. In addition, they are usually thermally and chemically stable, which can make them inherently safe and environmentally friendly [19]. By simply varying the anion and cation combination, $>10^6$ possible simple ionic liquids, $>10^{12}$ binary mixtures and $>10^{18}$ ternary mixtures can be produced [38, 39]. Ionic liquids can be excellent solvents, being capable of dissolving many inorganic, organic, biochemical and petrochemical materials, sometimes with a remarkably high capacity, thus opening new potential routes for the separation and purification of such compounds, which are difficult to separate by classical methodologies.

The properties of ionic liquids can be adjusted by the choice of the appropriate anion and cation, allowing them to be optimised for specific applications. For example, ionic liquids can be contacted with a second immiscible phase, which could be a molecular solvent, or an aqueous salt solution, or even a second ionic liquid [40]. This gives rise to a huge number of potential biphasic solvent systems that can be optimised for any given separation, generating a wide range of distribution ratios of solutes; the latter in turn can improve separation performance [41, 42]. We term here the use of ionic liquid-based solvent systems, and their use in CCC, as ionic liquid–liquid chromatography (ILLC).

3.2 The Use of Ionic Liquids in Chromatography

The use ionic liquids in chromatography has been growing steadily since 1999, with a total of 2647 publications by the end of 2016, based on a Web of Science search of the terms "ionic liquid" and "chromatography" [18]. As can be seen in Fig. 1, ionic liquids have been found to provide new avenues of investigation in chromatographic science.

In 1999, Anderson and co-workers reported the first use of ionic liquids in GC, utilising their negligible vapour pressure at ambient pressures [37]. These authors used $[C_4mim][PF_6]$ or $[C_4mim]Cl$ as stationary phases coated on the surface of fused silica capillaries. This design allowed the separation of a wide range of organic molecules (alkanes, chloroalkanes, alcohols, amines, aromatics and carboxylic acids) according to their polarity and proton-donor or -acceptor characteristics [20]. Only 7 years later, a full review of applications of ionic liquids in analytical chemistry was published [43].

In 2002, the first use of ionic liquids in capillary electrophoresis was reported to separate Sildenafil and its metabolite UK-103,320 [44]. In the same year, using a stacked disk CPC instrument, a number of salts (referred to as chiral selectors, but could also be described as chiral ionic liquids) were utilised for the enantiomeric separation of *N*-substituted amino acids [45]. More general information on chiral separations using CCC, including those involving ionic chiral selectors, has been reviewed by Ito et al. [46]. It is interesting to note that many of the chiral separations using CCC were carried out on model compounds, which are usually racemic dinitrobenzyl derivatives of amino acids. Very little research exists on the chiral separation of other racemates using ionic liquid-containing solvent systems [47].

In the field of liquid chromatography, the determination of ionic liquid cations by reversed-phase HPLC [48] was reported in 2003, and the first use of ionic liquids as additives to the mobile phase in HPLC was reported in 2004 [49]. The use of ionic liquids as stationary phases in LLC or CCC was detailed by Berthod et al. [16] who measured the partitioning of 38 aromatic compounds in the biphasic ionic liquid solvent system: [C_4mim][PF_6]/water. These authors found that “the viscosity of pure RTILs [room-temperature ionic liquids] is too high for direct use as a liquid phase in countercurrent chromatography (CCC)”. A measure of progress in the use of ionic liquids in chromatography is that, for example, Supelco now sells a wide range of capillary GC columns which employ ionic liquids as the stationary phase [50].

Recently, over 40 reviews have been published describing the use of ionic liquids in analytical and chromatographic science, as summarised in Table 1.

3.3 The Use of Ionic Liquids in Countercurrent Chromatography

The aim of the research into ILLC is to develop a technology that is capable of separating mixtures of most soluble organic compounds [97], with a similar goal for inorganic compounds [98], using the methodologies based on the principles of CCC [21]. Due to the very large number of ionic liquids that can be used as stationary phases and mobile phases [99], a wide range of separations should be achievable. With more than one million possible ionic liquids [19, 38], the number of possible phases that can be generated is immense. In conventional LLC or CCC, only about a dozen different molecular solvents are commonly used, and these are usually based on mixtures of three to five (or more) solvents in order to generate useable biphasic solvent systems [100].

Berthod et al. carried out the initial testing of diluted ionic liquids in CCC instruments between 2003 and 2009 [16, 24, 101, 102]. This research group noted and reported that the use of ionic liquids in CCC had a number of drawbacks, such as “UV absorbance limiting the use of the convenient UV detector”, “non-volatility precluding the use of the evaporative light-scattering detector for continuous detection” and “high viscosity producing pressure build-up” [101]. Berthod et al. went on to conclude that CCC was unsuitable at that time, as the instrumentation available “was not able to cope with the high back-pressures generated by the large viscosities of many ionic liquids” [101].

The UV–Vis absorbance of ionic liquids can be problematic and interfere with detection of the analyte. The absorbance depends on the structure of the ionic liquid being used, and the absorbance of both the anion and cation must be separately taken into account. For example, imidazolium cation ionic liquids absorb light strongly at wavelengths below 260 nm. However, ammonium and phosphonium cation ionic liquids can be used over the whole 200- to 800-nm range of modern UV–Vis spectrophotometers. Anions (such as chloride) can also be used over the

Table 1 A list of selected reviews published on use of ionic liquids in analytical and chromatographic science

Chromatographic area of research	Year	References
General reviews on the use of ionic liquids in chromatography	2005	[51]
	2005	[52]
	2006	[53]
	2007	[54]
	2007	[55]
	2007	[56]
	2008	[24]
	2008	[57]
	2009	[58]
	2010	[59]
	2011	[60]
	2012	[61]
	2014	[62]
	2016	[63]
The use of ionic liquids in capillary electrophoresis and related technology	2004	[64]
	2006	[65]
	2008	[66]
	2009	[67]
	2013	[68]
	2014	[69]
	2016	[63]
The use of chiral ionic liquids in chromatography	2005	[70]
	2008	[71]
	2008	[72]
	2012	[73]
	2014	[74]
The use of ionic liquids in CCC	2008	[24]
	2013	[75]
The use of ionic liquids in GC	2009	[76]
	2009	[77]
	2011	[78]
	2014	[79]
	2014	[80]
	2016	[81]
	2016	[82]
The use of ionic liquids in HPLC	2006	[83]
	2009	[84]
	2011	[85]
	2012	[86]
	2012	[87]
	2015	[88]

Table 1 continued

Chromatographic area of research	Year	References
Chromatographic measurement of ionic liquid properties	2004	[89]
The use of ionic liquids in liquid chromatography	2007	[90]
	2014	[91]
	2015	[92]
	2015	[93]
The use of ionic liquids in micellar chromatography	2012	[94]
The use of ionic liquids in supercritical fluid chromatography	2009	[95]
The use of ionic liquids in hydrophilic interaction chromatography	2016	[96]

full 200- to 800-nm range, but anions such as triflate or bis{(trifluoromethyl)sulfonyl}amide absorb light at wavelengths below 250 nm. Coloured impurities in the ionic liquid can also affect the performance of the UV–Vis detector, but these can be removed by filtering the ionic liquid through charcoal [103]. A second problem with UV–Vis detectors is that small bubbles of stationary phase can be present in the mobile phase as it elutes from the coil, and these bubbles produce spikes in the chromatogram. Careful orientation or design of the UV–Vis flow cell can help minimise this problem.

The non-volatility of ionic liquids can be problematic for the use of evaporative light scattering detectors (ELSDs) [101]. Provided that the mobile phase contains very low concentrations of ionic liquids, as is the case with many solvent systems, this detector may be used, but factors such as unintended bleeding of the stationary phase into the mobile phase eluting from the coil make the use of ESLDs unviable. Alternatively, two types of detectors that could be used are refractive index and conductivity detectors, although none has been tested at the time of writing.

To overcome the greater viscosity of ionic liquid solvent systems, the CCC instrumentation requires careful design and construction of the fluid flow paths to prevent excessive pressure build-up, particularly at high flow rates. For ILLC, the machine, based on a J-type centrifuge, must withstand high working pressures (at least 50 bar) for extended periods of time. This requires that the coils be made from either stainless steel or, in the case of highly corrosive materials, titanium. The centrifuge must also be capable of running at elevated temperatures (up to 50 °C), which, through a reduction of viscosity, can dramatically improve the ILLC separation performance [21, 97, 98, 104]. Based on these requirements, AECS-QuikPrep Ltd. (London, UK) produce CCC instruments suitable for use with ionic liquid solvent systems [104].

It is not usually possible to use a neat ionic liquid in CCC because the addition of a second immiscible solvent often dilutes the ionic liquid as a result of mutual solubility effects described in Section 3.4 [105]. Berthod et al. [101] explicitly state: “Mutual solubility with other solvents is a critical issue, because the viscosity of [room-temperature ionic liquids] is too high to be of practical use in CCC”. For example, the ionic liquid $[C_4mim][PF_6]$ has a viscosity of 312 cP [16, 106] when pure, which is far too high to be reliably pumped by an HPLC pump. Berthod et al.

found that the phase [C_4mim][PF_6]/water (1.8% v/v water) had a viscosity of approximately 30–40 cP at 20 °C, but this was "too viscous, for easy CCC use" [16, 106]. The addition of ethanenitrile (20–40% w/w) to the [C_4mim][PF_6]/water solvent system was required to obtain successful operation of the CCC instrument [101]. Unfortunately, also in 2003, Rogers and coworkers [107] found that the ionic liquid [C_4mim][PF_6] can undergo hydrolysis. Thus, the $[PF_6]^-$ anion can hydrolyse to give a mixture of aqueous phosphate (or phosphoric acid) and hydrofluoric acid, which is highly toxic and corrosive [107]. This problem is solved by using the bis{(trifluoromethyl)sulfonyl}amide $[NTf_2]^-$ anion as a direct replacement for the $[PF_6]^-$ anion. Not only is the $[NTf_2]^-$ anion hydrolytically stable, but ionic liquids derived from it tend to have low viscosities [108].

For the separation of polar and/or strongly hydrogen bonding molecules, such as saccharides or proteins, aqueous biphasic solvents (ABS) [109] have been successfully used in CCC [110, 111]. These are usually based on concentrated aqueous inorganic salt solutions, combined with a second aqueous phase, saturated with an organic solvent [such as ethanol or polyethylene glycol (PEG)] [112, 113], which employ the mismatch between kosmotropic and chaotropic interactions (increasing or decreasing, respectively, the structuring of water) to produce biphasic solvent systems [114, 115]. For example, they have been used in the CPC separation of saccharides using the ethanol/DMSO/aqueous ammonium sulfate (300 g l^{-1}) (0.8:0.1:1.8, v/v/v) solvent system [116]. Berthod et al. found that chaotropic chloride ionic liquids (such as [C_4mim]Cl) are immiscible with many kosmotropic concentrated salt solutions and that these solvent systems can be used in a CCC machine [117]. The ABS system [C_4mim]Cl/aqueous 2.5 M $K_2[HPO_4]$, first described by Berthod et al., has been used for the purification of the anti-cancer drug lentinan [42]. Here, the ionic liquid-based ABS solvent system [C_4mim]Cl/aqueous 2.5 M $K_2[HPO_4]$ has a much greater solute capacity (approx. tenfold greater) than the previously used PEG-based ABS solvent system (PEG 1000/$K_2[HPO_4]$/$K[H_2PO_4]$/water (0.5:1.25:1.25:7.0, mol/mol/mol)) [113]. The ionic liquid ABS solvent system allows for much larger amount of lentinan to be separated by boosting the space–time yield of the chromatographic apparatus. Finally, a related approach for separating polar compounds in CCC involves the use of deep eutectic solvent systems (such as mixtures of choline chloride/glucose) [118].

Since the initial work of Berthod et al. in ILLC, there have been a number of papers describing the use of ionic liquids in CCC. These include the analysis of mycotoxins [119] and chlorophenols in red wines [120], the potential use of aqueous biphasic solvent systems containing ionic liquids in the separation of caffeine from xanthine and nicotine [121] and in the separation of neomangiferin and mangiferin from *Rhizoma anemarrhenae*, all using the hydrolytically unstable [C_4mim][PF_6] [107] as an additive to aqueous ethyl ethanoate [122].

3.4 Phase Behaviour of Ionic Liquids

Two immiscible liquids are present when there is a visible barrier between two phases. However, immiscibility is not the same as insolubility, as shown in Fig. 4. For the purpose of CCC separations, the phases chosen (either ionic liquid–organic

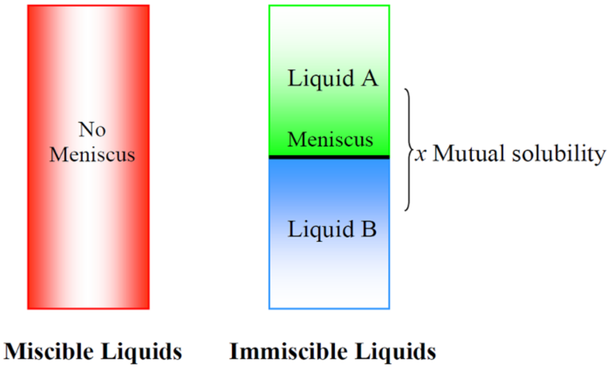

Fig. 4 The effect of mixing two immiscible liquids. Each liquid phase is partially soluble in the opposite immiscible liquid phase

solvent, ionic liquid–water, or mixtures of ionic liquids) should be immiscible, but they will possess a degree of solubility in each other.

Ionic liquid-molecular solvent biphasic systems are very useful in chromatography, as they allow for easy analyte isolation and solvent recovery. There is usually very little ionic liquid contained in the molecular solvent phase, and so the molecular solvent usually is employed as the mobile phase. Solvent recovery usually involves distillation of the volatile solvent from the ionic liquid phase and the analyte-containing mobile phase, which can then be directly reused [123]. Also, ionic liquid solvent systems usually contain just two or three components rather that four or five, as is the case with molecular solvents. This makes solvent recovery much more straightforward [6] due to the lower number of volatile components that need separating. Solutes that remain dissolved in an ionic liquid phase after the volatile solvent recovery step can be removed by a number of techniques, such as solvent extraction, precipitation with an antisolvent or filtration of a solution of the ionic liquid through silica or charcoal, or a combination of these methods [103].

3.4.1 Ionic Liquid-Organic Solvent

The miscibility of ionic liquid–organic solvent mixtures is an important property in chromatography and influences the analyte distribution ratios. Many solvents can form biphasic mixtures with ionic liquids, where the solvent is soluble in the ionic liquid phase, whereas the ionic liquid is poorly soluble in the solvent phase. Eight examples of the mutual solubilities of ionic liquids with an organic solvent (hexane) are shown in Table 2. The eight ionic liquids tested were [cholinium][NTf_2], [$C_n$py][NTf_2] ($n = 2$, py = pyridinium), [$C_n$mim][NTf_2] ($n = 2$, 4, 6, 10, or 12) and [$P_{6\ 6\ 6\ 14}$][NTf_2]. The ionic liquid phases contain significant amounts of hexane, but the organic phase (hexane) does not contain the ionic liquid [124, 125].

The effect of dissolving a molecular solvent in an ionic liquid dramatically reduces the ionic phase's viscosity [105, 126] to the point that it can effectively be pumped with an HPLC pump. This has enabled viscous hydrophobic ionic liquids,

Table 2 Composition of the biphasic ionic liquid/hexane solvent systems, showing the solubility of hexane in the ionic phase [124, 125] at 25 °C

Ionic liquid[a]	Ionic phase composition (mol%)		Organic phase composition/mol%
	Ionic liquid	Hexane	Hexane
[cholinium][NTf_2]	98.5	1.5	>99.9
[$C_n$py][NTf_2]	95	5	>99.9
[C_2mim][NTf_2]	96	4	>99.9
[C_4mim][NTf_2]	91	9	>99.9
[C_8mim][NTf_2]	70	30	>99.9
[C_{10}mim][NTf_2]	58	42	>99.9
[C_{12}mim][NTf_2]	44 (79, 87)[b]	56 (21, 13)[b]	>99.9
[$P_{6\ 6\ 6\ 14}$][NTf_2]	9 (30, 37)[b]	91 (70, 63)[b]	>99.0

[a] See Abbreviation List for details

[b] Ionic phase composition is given in mol%, followed in parenthesis by vol% and wt%, respectively

such as [$P_{6\ 6\ 6\ 14}$]Cl (viscosity = 2729.1 cP at 25 °C), to be used in separations of metal salts, as discussed later in this chapter [127].

An important factor to be considered in the selection of ionic liquids used in CCC is the rate of exchange of solutes between the two liquid phases, which depends in part on the viscosity of the phases used in CCC. This experimental observation is valid irrespective of the nature of the two phases employed. The higher viscosities of ionic liquid phases can reduce the equilibration rate of the solutes between the two liquid phases and can result in the problem of band-spreading [128]. This can be partially offset by running the separation at higher temperatures or by diluting the ionic liquid phase. However, the viscosities of ionic liquids are highly dependent on the nature of both the anion and the cation. One approach to reducing the viscosity of the ionic phase is to use fluorinated anions, such as $[OTf]^-$ (trifluoromethanesulfonate) or [SO_3CF_3] or $[NTf_2]^-$. Also, using cations containing asymmetrical, delocalised charge centres can lower the viscosity.

The chemical structure and spatial charge distribution of ionic liquids can be varied in order to alter their phase behaviour in biphasic solvent systems. An example is the solubility and distribution ratio of benzene in the hexane-[$C_n$mim][NTf_2] ($n = 2$, 4, 6, 10 or 12) biphasic solvent systems [124] (Fig. 5). The solubility of benzene increases from 23 mol% in the [C_2mim][NTf_2] phase to complete miscibility with [C_{12}mim][NTf_2]. The three-phase diagrams clearly show the dramatic effect of how changes in the cation give rise to very large variations in the phase behaviour. Also, the ionic liquids used are not measurably soluble in the hexane phase. This property can be used to completely separate benzene from hexane, using a hexane mobile phase in liquid–liquid extractions [124, 125].

The type of the cation used in four $[NTf_2]^-$ anion ionic liquids has also been shown to affect the distribution ratio of benzene [125] and, more generally, aromatic compounds [129]. In Fig. 6, the biphasic hexane/[cation][NTf_2] solvent systems (where cation = $[C_2mim]^+$, $[C_2py]^+$, (2-hydroxyethyl)trimethylammonium, or $[P_{6\ 6\ 6\ 14}]^+$) show a remarkable difference in their phase behaviour, with the

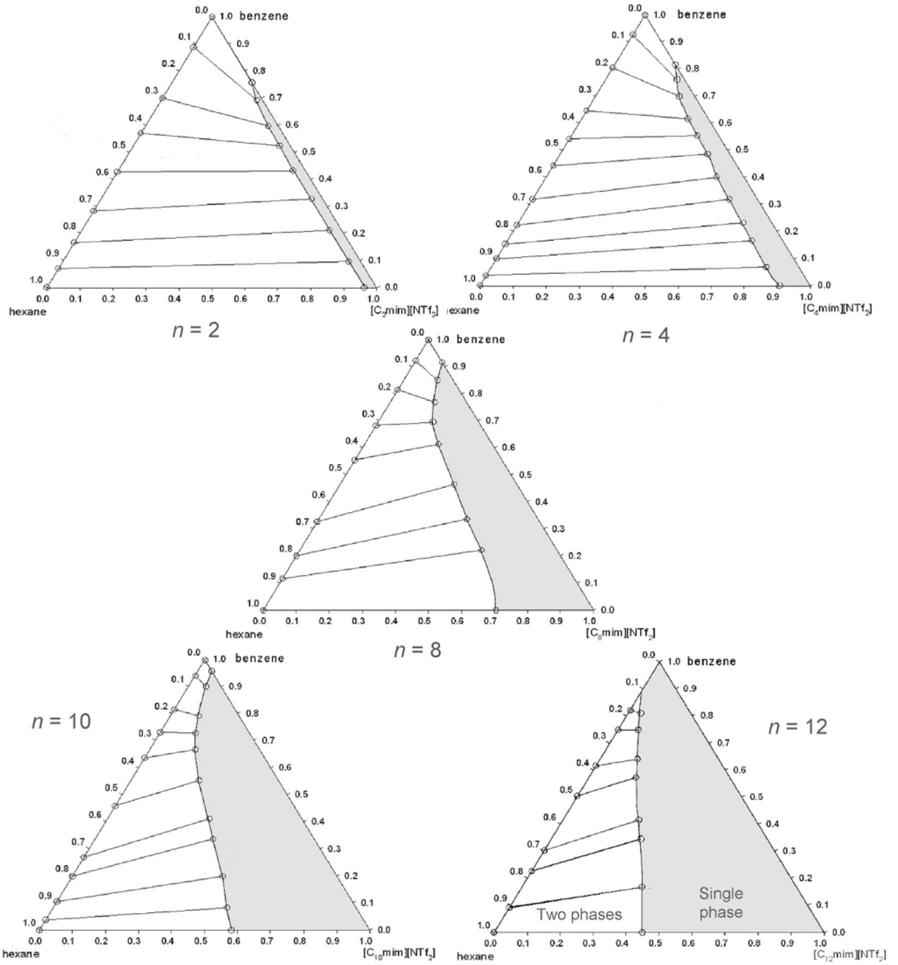

Fig. 5 The effect of the variation in the length of the alkyl chain of 1-alkyl-3-methylimidazolium bis{(trifluoromethyl)sulfonyl}amide $[C_n mim][NTf_2]$, where $n = 2$, 4, 8, 10 or 12, on the phase equilibria of benzene dissolved in a hexane/$[C_n\text{mim}][\text{NTf}_2]$ ionic liquid solvent system [124]

solute distribution ratios of benzene in the solvent systems at 40 °C being 1.20, 1.24, 0.69, and 0.94, respectively [125]. This information is useful in ionic liquid–liquid chromatography and demonstrates how the design of an ionic liquid affects the distribution ratios of solutes. A number of reviews [115, 130–133] and further information on the liquid–liquid equilibria of ionic liquids have been published elsewhere.

3.4.2 Ionic Liquid–Water Systems

Mixtures composed of an organic polymer, such as PEG, and an inorganic salt, such as sodium or potassium hydrogen phosphate ($K_2[HPO_4]$), are able to separate into

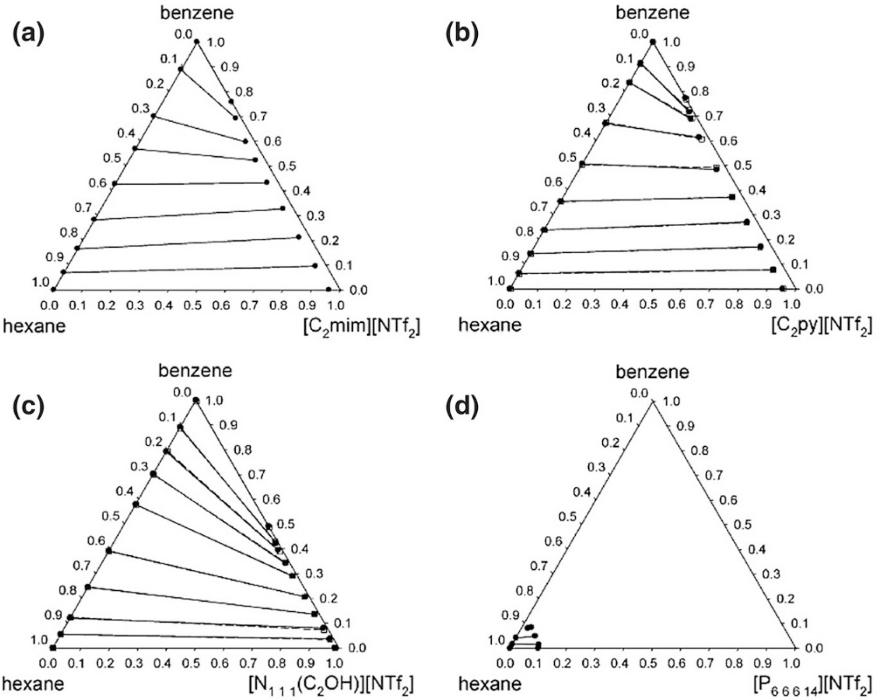

Fig. 6 The effect of the cation on the phase equilibria of benzene dissolved in a hexane/[cation][NTf$_2$] ionic liquid solvent system [125]. Cation: **a** 1-ethyl-3-methylimidazolium ([C$_2$mim]$^+$), **b** 1-ethylpyridinium ([C$_2$py]$^+$), **c** (2-hydroxyethyl)trimethylammonium, **d** trihexyltetradecylphosphonium

two layers, as first described by Albertson [134]. Such mixtures are known as aqueous biphasic systems, as both layers are aqueous solutions of different compositions: the upper layer contains most of the PEG, whereas the lower layer contains most of the inorganic salt. Aqueous biphasic systems have proven to be useful in CCC for the purification of biological materials [121, 135–137].

Using ternary mass or molar phase diagrams, Berthod and coworkers studied the putative formation of ionic liquid-based aqueous biphasic systems by mixing [C$_4$mim]Cl with aqueous solutions of inorganic salts (K$_2$[HPO$_4$], K$_3$[PO$_4$], Na$_2$[HPO$_4$], Na[H$_2$PO$_4$], Na$_2$[CO$_3$] or bases (NaOH and KOH) [21, 22, 24]. In addition, these researchers found out that the [C$_4$mim]Cl/K$_2$[HPO$_4$]/water system was much easier to retain in the CCC columns than the similar aqueous biphasic system containing PEG 1000. However, the significant polarity difference between PEG 1000 and [C$_4$mim]Cl aqueous biphasic systems is responsible for the different behaviour of the two selected systems towards protein separation using CCC variants.

There have been a number of other studies on the phase behavior of ionic liquids in aqueous biphasic solvent systems. These include the study on [C$_4$py]Br/H$_2$O/Na$_2$SO$_4$ at various temperatures by Li and coworkers [138] and that on choline-amino acid ionic liquids/K$_2$CO$_3$/H$_2$O by Li and coworkers [139], as well as the analysis on an extensive range of these ionic liquid-based aqueous biphasic solvent systems by Sen and Chakraborty [140].

As hydrophobic ionic liquids can easily form biphasic systems with water, they are possible alternatives in CCC to the existing [C_4mim]Cl/inorganic salt aqueous biphasic systems. Most hydrophobic ionic liquids are very poorly soluble in water phases, but water has appreciable solubility in the ionic liquid phase. Thus, if the mobile phase in CCC is water, then product isolation is simply a matter of evaporating the water phase [40, 124, 125, 129, 141–144].

3.4.3 Ionic Liquid–Ionic Liquid

The first examples of ionic liquids which were shown to be mutually immiscible with each other were published in 2006 [40]. Similarly, tetraphasic solvent systems can be constructed, as shown in Fig. 7 [40]. Mutually immiscible ionic liquid systems can be produced by mixing very hydrophilic ionic liquids with very hydrophobic ones, such as with [$P_{6\,6\,6\,14}$]Cl and [C_2mim]Cl (Fig. 7 right image).

The mutual miscibility of two ionic liquids, namely [C_2mim][NTf_2] and [$P_{6\,6\,6\,14}$][NTf_2], at different temperatures is shown in Fig. 8 [40]. This biphasic solvent system becomes completely miscible as the temperature rises. In contrast, in the cases of [$C_n$mim]Cl ($n = 1$ or 2)/[$P_{6\,6\,6\,14}$]Cl, the mutual solubility decreases with increasing temperature (see Fig. 9) [40]. It is also possible to construct a ternary phase diagram for three ionic liquids, as shown in Fig. 10.

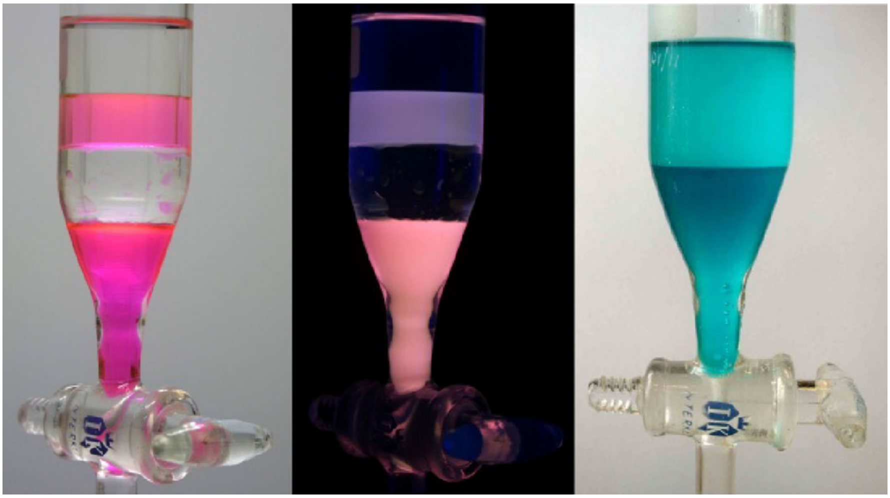

Fig. 7 A picture of a four-phase solvent system (*left* and *centre*) composed of (*top* to *bottom*) hexane, trihexyltetradecylphosphonium bis{(trifluoromethyl)sulfonyl}amide ([$P_{6\,6\,6\,14}$][NTf_2]), water and 1-ethyl-3-methylimidazium bis{(trifluoromethyl)sulfonyl}amide ([C_2mim][NTf_2]), using eosin Y as a luminescent dye which is soluble in the two ionic liquid-containing phases. The central photograph is of a system illuminated with 254-nm UV light. Also shown is a two-phase solvent system (*right*) of [$P_{6\,6\,6\,14}$]Cl (*upper* phase) and [C_2mim] Cl (*lower* phase) with cobalt(II) Cl as the blue chromophore. In the two blue phases, the complex is tetracobaltate(II) [40]

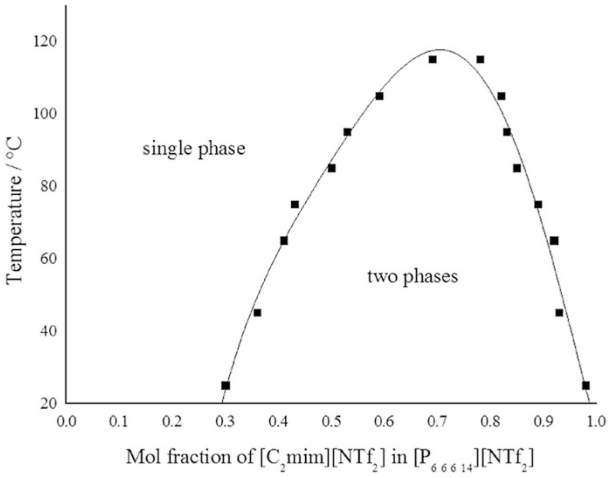

Fig. 8 The phase diagram of two ionic liquids at varying temperatures [40, 141]

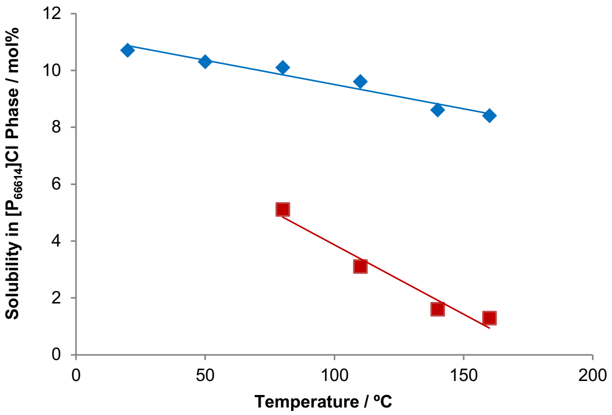

Fig. 9 The solubility of [C_1mim]Cl (*red line*) and [C_2mim]Cl (*blue line*) in the immiscible [$P_{6\ 6\ 6\ 14}$]Cl phase at various temperatures [40]

3.5 Solvent Engineering and Ionic Liquid–Liquid Chromatography

The inherent tunability of ionic liquids imparts control over their physicochemical properties, such as viscosity, hydrophobicity, hydrophilicity, density, surface and interfacial tensions and corrosivity. Moreover, and of vital importance, the distribution ratios of a solute between an ionic liquid phase and a second phase (which may be either water, an organic solvent or another ionic liquid) can be controlled by the design of the ionic liquid. For example, if a solute in a biphasic hexane–ionic liquid solvent system is not soluble enough in the ionic liquid phase, then the solvent engineering approach is to redesign the ionic liquid cation to have longer alkyl chains. Alternatively, the anion can be redesigned and replaced with a

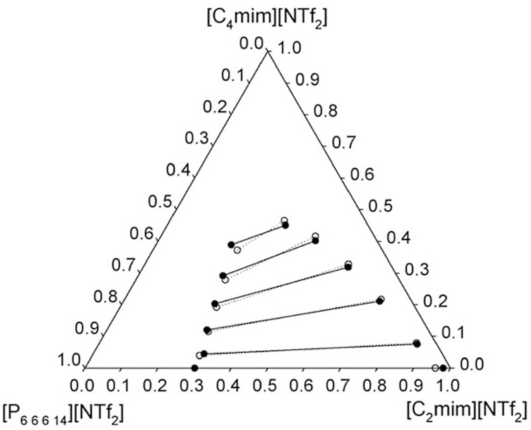

Fig. 10 The ternary phase diagram of a mixture of three ionic liquids: [C$_2$mim][NTf$_2$], [C$_4$mim][NTf$_2$], and [P$_{6\ 6\ 6\ 14}$][NTf$_2$] at 25 °C (*solid circle*) and 40 °C (*open circle*) [141]

larger (usually with longer alkyl chains) and/or the use of a more charge delocalised anion. As will be demonstrated later, this versatility allows a general purpose methodology for a very large number of separations to be developed, including separations that were previously thought to be too difficult to implement.

4 Ionic Liquid Solvent Systems and Instrumentation in Countercurrent Chromatography

4.1 Introduction

In order to carry out CCC with ionic liquids, the instrument must be designed to cope with much higher backpressures than those that are encountered with many molecular solvents. In addition, the viscosity of ionic liquids in a CCC machine has received little attention in the literature. In this section, the instrument design, the solvent systems and their viscosities are described.

4.2 Instrument Design

The Quattro IL-Prep^{TM} ILLC instrument AECS-QuikPrep Ltd, London, UK contains two pairs of stainless steel tubing coils mounted on each of the two weight- and dynamically matched bobbins. The coils are held in place by aircraft-quality adhesive. Stainless steel is used for the coil tubing rather than the more conventional PTFE tubing [145, 146]. This change was implemented in order to allow the instrument to operate at up to 70 bar backpressure.

The coils (see Fig. 11) are connected to the pumps and detector using poly(1,1,2,2-tetrafluoroethylene) (PTFE) flying leads with an internal diameter (ID) of 0.8 mm (coils 1 and 2) and 0.5 mm (coils 3 and 4) and an external diameter (ED) of 1.6 mm (all coils). It was found that the 0.5-mm ID tubing had a greater

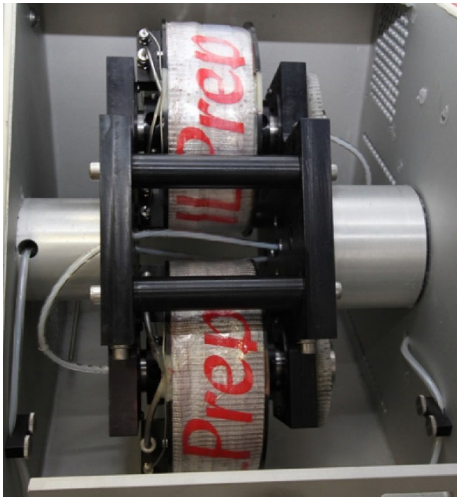

Fig. 11 The internal view of the four coils in the planetary centrifuge of the Quattro IL-Prep^{TM} ILLC instrument. *ILLC* Ionic liquid–liquid chromatography

service lifetime. The sample injection loops range in size from 0.5 to 10 cm^3 and are made from 0.8-mm ID stainless steel or 1.6-mm ID PTFE tubing. Further details and dimensions of the four coils are given in Table 3.

The J-type multilayer coil planet centrifuge (where the coils are rotated in planetary motion around a central axis) [145] has a revolution radius of 13 cm and produces a synchronous planetary motion of the coil holder. The β-value (the ratio of the planetary radius to the ratio of sun radius) of the pipes in the coil varies from 0.60 at the internal layer to 0.90 at the external layer [25]. The IL-Prep system is equipped with two HPLC pumps (0–40 cm^3 min^{-1}), a UV–Vis detector with four simultaneous channels (190–800 nm), a data station and a fraction collector. The rotation speed of the IL-Prep^{TM} instrument can be varied between 0 and 865 rpm, and the temperature of the coils can be controlled between 20 and 50 °C. The instrument, pumps and tubing can be operated at up to 70 bar pressure, and it has been tested by running for 48 h continuously at the maximum operating pressure, temperature and rotor speed [104].

The ILPrep^{TM} instrument can be operated in two modes. In dense phase as the stationary phase (DPS) mode, the mobile phase is pumped from the tail to the head of the coil; in light phase as the stationary phase (LPS) mode, the mobile phase is pumped from the head to the tail of the coil. The configuration is represented schematically in Fig. 12. The two immiscible phases are held in a large measuring cylinder, the two phases being pumped separately into the coils. When the solvent phases are not being collected, they are returned to the measuring cylinder via a return or recirculation pipe. This arrangement allows the contents of the coil to be calculated from the variation in the levels of the two phases in the measuring cylinder. Also, to assist in the calculation of the phase contents of the coil, the dead volume of the piping must be known (in the present case 4.0).

Table 3 Details of the J-type centrifuge coils installed within the IL-Prep ILLC instrument

Coil number	Bore ID (mm)	Length (L) (m)	Number of turns	Capacity (V_c/cm^3)	L/ID ratio	Flow velocity (mm s^{-1})[a]
1	1.0	13.35	26	12	13,350	12.73
2	2.1	36.02	76	133	17,152	2.887
3	1.0	39.89	78	34	39,890	12.73
4	3.7	23.83	52	236	6441	0.930

ID, internal diameter

[a] The flow velocity is defined as the speed of movement of a single phase of fluid along the length of the coil at an applied fluid flow rate of 1.0 cm^3 min^{-1}

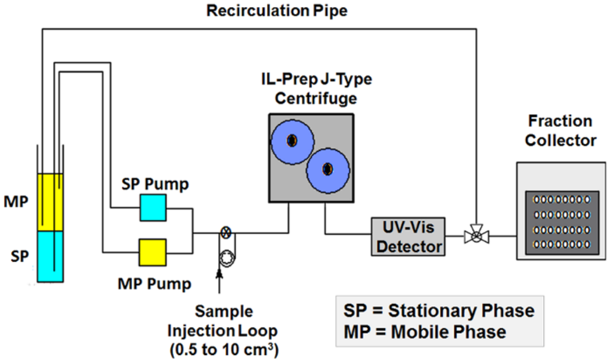

Fig. 12 The configuration of the IL-Prep™ instrument

4.3 Solvent Selection

There is a huge number of possible ionic liquid phases, and their selection must be made by considering their reactivity (or, perhaps, their lack of it), cost, viscosity, density, solvent behaviour and interfacial tension, among others. This requires both experience and a database of ionic liquid properties [147–149]. For the separations discussed here (Table 4), the biphasic combinations of ionic liquids and molecular solvents were chosen based on previous research into ionic liquid phase behaviour and solvent extraction studies (also see Section 3.4) [40, 42, 124, 125, 129, 141–143, 149]. One of the simple ways to find and select biphasic system consisting of ionic liquids and other solvents is demonstrated in Fig. 13. Here, a qualitative water and organic solvent miscibility guide for commonly used ionic liquid forming anions and cations is shown. In general, ionic liquids made from anions and cations on the left are hydrophilic and more soluble in polar solvents. Ionic liquids made from anions and cations on the right of the chart shown in Fig. 13 are generally hydrophobic and soluble in most organic solvents, except some alkanes; ionic liquids made from ions on the left of the chart are immiscible with most organic solvents less polar than butanol. Another way of looking at this (in the lower part of Fig. 13) is that hydrocarbons are immiscible with most ionic liquids, but solvents like butanol are only immiscible with

Table 4 Phase combinations used for ionic liquid–liquid chromatography separations

Stationary phase[a]	Mobile phase	Separations	Mode
$[C_{12}mim][NTf_2]$ (A)	Hexane	Alkene/oxygenated sesquiterpenes	DPS
$[C_{10}mim][OTf]$ (B)	Hexane	Alkane/aromatics	DPS
$[C_4mim]Cl$ (C)	3.0 M $K_2[HPO_4]$	Glucose/sucrose	LPS
$[P_{6\,6\,6\,14}]Cl$/ethyl ethanoate (D)	Water	Co(II), Ni(II), Cu(II) dichlorides	LPS
3.0 M $K_2[HPO_4]$ (E)	$[C_4mim]Cl$	Lentinan	DPS

DPS, Dense phase stationary (in biphasic solvent systems); LPS, light phase stationary (in biphasic solvent systems)

[a] Uppercase letters A-E in parenthesis are also used in Table 5, to refer to the solvent system composition. See Abbreviation List for details

ionic liquids on the far left of the chart [150]. The hydrophobicity, or hydrophilicity, of ionic liquids can also be calculated using COSMO-RS software [149].

It is a requirement that the combination of ionic liquids and molecular solvents used in ILLC forms a biphasic mixture and that there is a significant density difference between these two immiscible phases (preferably $>0.10\ \mathrm{g\ cm^{-3}}$). For example, $[C_{10}mim][OTf]$ cannot be used effectively in combination with water because the two phases (water and water saturated ionic liquid) have similar densities and do not separate from each other easily. However, $[C_6mim][OTf]$ and $[C_8mim][OTf]$ can be used in combination with water because the ionic liquids are significantly more dense than water. A second factor to consider in ILLC solvent selection is viscosity. An extensive list of ionic liquid viscosities can be found in the literature [41], but these data can only be used as a rough guide to determine which ionic liquids are suitable. As mentioned earlier in this chapter, the viscosity of the ionic phase in a biphasic mixture of a molecular liquid with an ionic liquid is dramatically reduced [105]. This reduction in viscosity of the ionic phase can be estimated using Eyring's absolute rate theory [151].

Ionic liquid selection involves finding or synthesising an ionic liquid that does not irreversibly react with the solutes being separated, but does have a high enough solubility for those solutes. Generally, an ionic liquid with coordinating anions, such as halides, short chain carboxylates or short chain sulfonates, are selected for polar or strongly hydrogen-bonding solutes. Ionic liquids with weakly coordinating anions, such as $[OTf]^-$ or $[NTf_2]^-$, are selected for solutes of low or no polarity. Next, an ionic liquid-immiscible solvent (usually water for polar solutes or a hydrocarbon for non-polar solutes), which also exhibits high solute solubility, is selected. The distribution ratios of the solutes between the two immiscible phases must then be measured (e.g. by electronic absorption or nuclear magnetic resonance spectroscopy). Finally, the ionic liquid is either redesigned, or a co-solvent is added to both phases, to adjust the distribution ratios so that they lie in the range of 0.25–4.0. It should be noted that addition of a co-solvent (or second molecular solvent) to an ionic liquid–molecular solvent biphasic mixture will significantly affect the distribution ratios of the solutes, as well as significantly reduce the

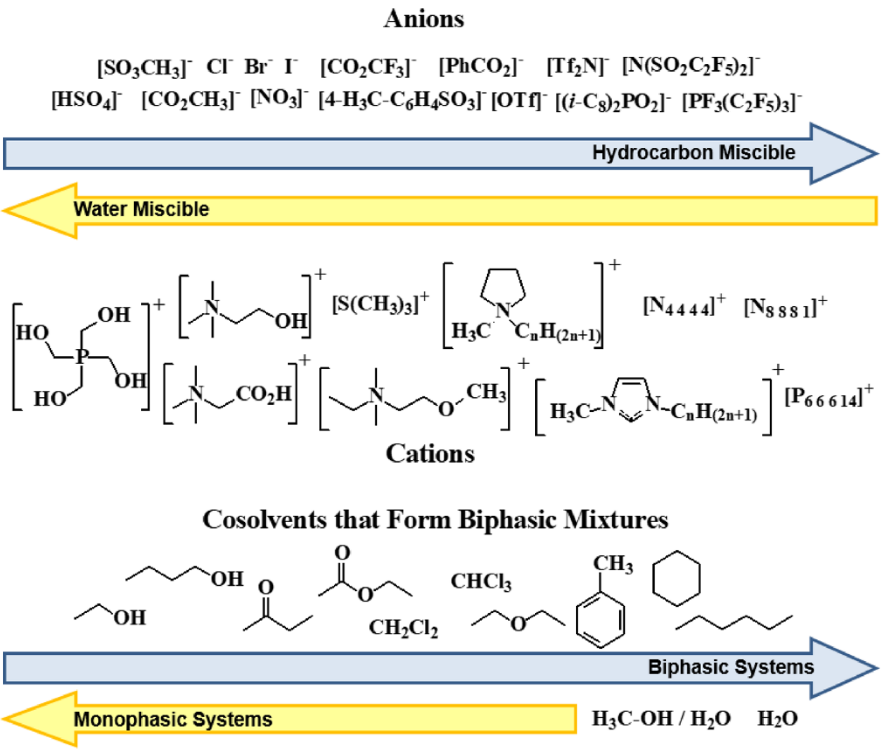

Fig. 13 Qualitative water and hydrocarbon miscibility of commonly used ionic liquid-forming anions and cations. Ionic liquids made from ions on the *left* (on both the *upper* and *lower rows*) are hydrophilic and more soluble in polar solvents, and ionic liquids made from ions on the *right* are more hydrophobic and hydrocarbon soluble. In order to form two-phase solvent systems for use in ionic liquid–liquid chromatography (ILLC), solvents in the *lower right* part of this figure are more likely to form biphasic mixtures

viscosity of the mixture [101]. This is a very effective way of fine-tuning the solute distribution ratios. Finally, a choice is made about which phase is to be used as the mobile phase and stationary phase. Generally, the mobile phase that is chosen is that from which it is easiest to remove the solute. Normally this means that the ionic liquid should be used as the stationary phase, as in Table 4 (Stationary phase label A–D). One exception to this is found in Table 4 (Stationary phase label E), where an ionic liquid was chosen as the mobile phase, since the solute (lentinan) can be precipitated from the ionic phase simply by adding ethanol.

Finally, some ionic liquid–molecular solvent combinations should be avoided due to the formation of unbreakable emulsions. Ionic liquids can in some cases be used to break (demulsify) emulsions [152], but surface active ionic liquids like $[C_{12}mim]Cl$ [153], especially when combined with halogenated solvents (CH_2Cl_2 or $CHCl_3$), can produce emulsions which do not separate on the timescales encountered in CCC.

4.4 Stationary Phase Retention Curves with Ionic Liquids

Obtaining a stationary phase retention curve is a prerequisite in all ILLC separations. This is used to find the optimal flow rate for a given separation and to determine the optimal rotation speed that is required. This is carried out in the apparatus illustrated in Fig. 12, with recirculation of the fluids. The stationary phase retention curves are a plot of the fraction of stationary phase that remains in a coil with increasing flow rates of the mobile phase. The amount of stationary phase remaining in the coil is calculated by measuring changes in the position of the mobile phase–stationary phase boundary in a graduated measuring cylinder (Fig. 12). The level of the interface between the two phases in the solvent reservoir is used to calculate the percentage stationary phase retention ($\% S_\mathrm{f}$) using Eq. (1) for the DPS mode and Eq. (2) for the LPS mode.

$$\% S_\mathrm{f} = 100 \times (1 - [V - V_0 - \mathrm{DV}]/V_\mathrm{c}) \tag{1}$$

for DPS

$$\% S_\mathrm{f} = 100 \times (1 - [V_0 - V + \mathrm{DV}]/V_\mathrm{c}) \tag{2}$$

for LPS, where $V =$ the observed volume (in cm^3) of the dense phase up to the interface between mobile and stationary phases in the measuring cylinder; V_0 = observed volume (in cm^3) of the dense phase up to the interface between the mobile and stationary phases in the measuring cylinder at the start of the experiment;V_c = volume of coil under test (in cm^3) (see Table 3 for details). DV is the dead volume, which is the volume of the pipework, connectors, UV–Vis detector cell, connectors and valves (experimentally measured to be 4.0 cm^3).

After setting the coil rotation rate (typically 300–865 rpm) and temperature (in the range 20–50 °C), the mobile phase is pumped in a stepwise manner (between 0.5 and 32 $\mathrm{cm}^3\ \mathrm{min}^{-1}$), into the rotating coil at increasing flow rates completely flushed from the coil, or the measured coil inlet pressure exceeds 70 bar. The graph of flow rate versus $\% S_\mathrm{f}$ is then plotted to give the stationary phase retention curve. This was carried out for the solvent systems in Tables 4 and 5.

For solvent system D (Tables 4, 5), the phase retention curves for all of the four coils (Table 5) were measured and calculated using Eq. (2), at 865 rpm and 35 °C. The flow rate versus stationary phase retention curves were determined and are shown in Fig. 14. In addition, the coil inlet pressure was measured at each flow rate with an analogue pressure gauge (0–140 bar) (shown in Fig. 15). With the solvent system (D), it can be seen that much of the backpressure comes from the flying leads and that the 0.5-mm-bore tubing generates much higher backpressures. Measurements show that the pressure drop over the lengths of coil 2 and coil 4 is <1 bar at a 32 $\mathrm{cm}^3\ \mathrm{min}^{-1}$ flow rate, so that the dashed lines in Fig. 15 show the pressure drop in the piping and flying leads of the IL-Prep$^\mathrm{TM}$ CCC system.

In Fig. 14, it can be seen that there are considerable differences between the behaviour of the two liquid phases in the four coils (for solvent system D). The rate of loss of the ionic liquid stationary phase is dependent on both the coil diameter and length. For example, coils 1 and 3 have the same ID, but have completely

Table 5 Solvent systems used in the generation of the stationary phase retention curves for the separations described in Table 4

Label	Stationary phase (mol%)	Mobile phase (mol%)	Solvent system	Ratio of solvent system components (v/v)
A	[C_{12}mim][NTf_2] (44%)/hexane (56%)	>99% hexane	[C_{12}mim][NTf_2]/ hexane	1 3
B	[C_{10}mim][OTf]/ hexane	>99% hexane	[C_{10}mim][OTf]/ hexane	1 3
C	[C_4mim]Cl (16%)/ H_2O (84%)	5.0 M $K_2[HPO_4]_{(aq)}$	[C_4mim]Cl/3.0 M $K_2[HPO_4]$	1 1
D	[$P_{6\ 6\ 6\ 14}$]Cl/ethyl ethanoate	92.5% water, 7.5% ethyl ethanoate	[$P_{6\ 6\ 6\ 14}$]Cl/ethyl ethanoate/water	1 1 4
E	5.0 M $K_2[HPO_4]_{(aq)}$	[C_4mim]Cl (16%)/ H_2O (84%)	[C_4mim]Cl/3.0 M $K_2[HPO_4]$	1 1

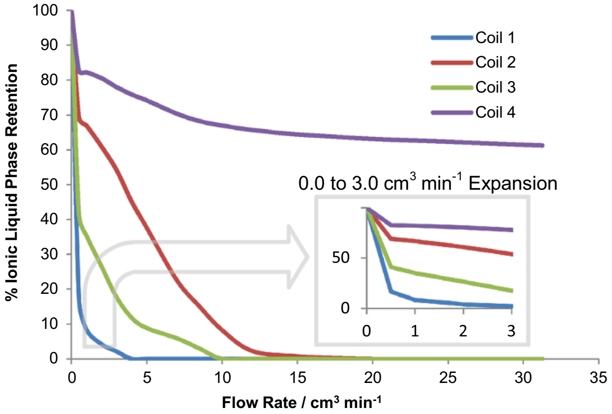

Fig. 14 The stationary phase retention curves within the four coils (see Table 3) for solvent system D (see Tables 4, 5), at 35 °C and 865 rpm

different phase retention curves. This implies that the stationary phase is not evenly distributed in the coil during operation and is concentrated at the head of the coil. This observation would have to be accounted for in any computer modelling of the ionic liquid solvent systems used in this study. For good separations, the instrument should be operated at rotation speeds and flow rates that maximise the value of S_f. Ideally, S_f values should be in the range of 60–95%. The best S_f values for D occur in the plateau region shown in the Fig. 14 inset. For coils 1 and 3, both of 1-mm bore (but different coil lengths), the best operating flow rates are at or below 0.5 $cm^3\ min^{-1}$. However, these S_f values of 12% for coil 1 and 38% for coil 3 are too low to give a reasonable separation. For coil 2 of 2.1-mm bore, the best operating region is at 0.5–2.0 $cm^3\ min^{-1}$ and for coil 4, 0.5–3.0 $cm^3\ min^{-1}$. For the

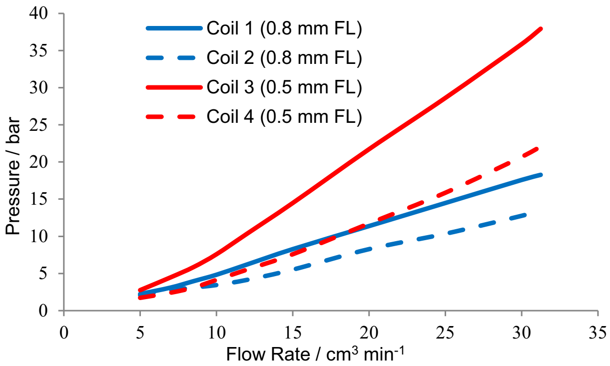

Fig. 15 The mobile phase operating pressures encountered during the experiment to determine the phase retention curves in Fig. 14, for the water/[$P_{6\ 6\ 6\ 14}$]Cl/ethyl ethanoate (4:1:1 v/v/v) solvent system with water as the mobile phase at 35 °C. Error = ±1.4 bar. *0.8 mm FL*, *0.5 mm FL* Inner diameter of the polytetrafluoroethylene flying leads, respectively

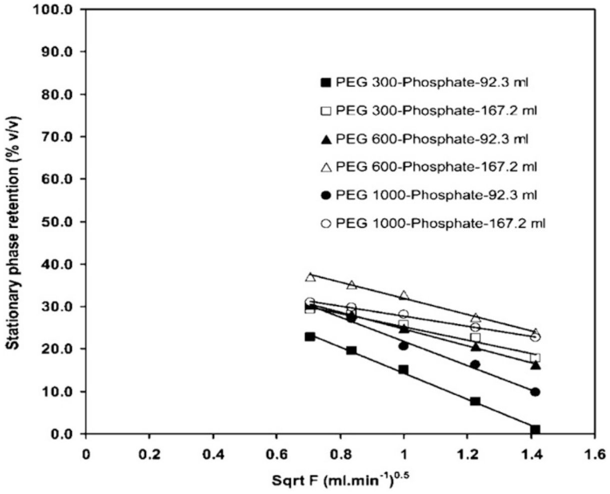

Fig. 16 The stationary phase retention for various polyethylene glycol (*PEG*) molecular weights plotted against the square root of the mobile phase flow rate using column volumes of 92.3 cm^3 (*closed symbols*) and 167.2 cm^3 (*open symbols*). Rotational speed: 600 rpm; mobile phase: $K_2[HPO_4]$ (18% w/w); stationary phase: PEG (18% w/w); direction: HEAD to TAIL. *Solid lines*: best fit linear regression [154]

solvent system in coil 4, the separations can be run at very high flow rates, since the value of S_f drops to 60% at 32 $cm^3\ min^{-1}$, which is a useable value.

For the water/ethanol/ethyl ethanoate/hexane solvent systems, a straight line in the graph of S_f versus $\sqrt{FR}$ occurs as the flow rate is increased, and therefore the relationship $S_f \propto \sqrt{FR}$ holds [146]. This relationship can also be seen in PEG–aqueous phosphate system shown in Fig. 16 [154]. The plot of the stationary phase retention versus the square root of flow rate for the water/[$P_{6\ 6\ 6\ 14}$]Cl/ethyl

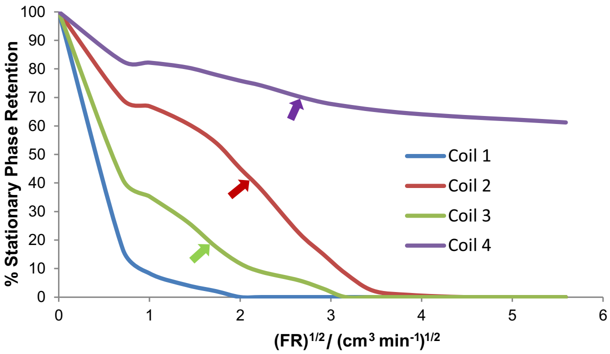

Fig. 17 The stationary phase retention within the four coils (Table 3) plotted against the square root of flow rate (FR)$^{1/2}$ for solvent system D, at 35 °C and 865 rpm. *Arrows* mark the points where the flow changes from laminar flow to emulsion flow of the two phases

ethanoate (4:1:1 v/v/v) solvent system (Table 4) is shown in Fig. 17. For this ionic liquid solvent system (Fig. 17), clearly the $S_f \propto \sqrt{\mathrm{FR}}$ relationship does not describe the stationary phase retention curve.

Inflection point is defined as a point at which a change in the direction of curvature occurs. For all coils in Fig. 17, there is a common inflection point at 0.75 cm^3 min^{-1}. Additionally, there are inflection points at 3 cm^3 min^{-1} (for coil 3), 5 cm^3 min^{-1} (for coil 2) and 7 cm^3 min^{-1} (for coil 4). Careful visual observation of the fluid exiting the coils at these flow rates reveals that there is a change from laminar flow to emulsion formation, which is most noticeable when the flow rate is increased [146].

The S_f of biphasic systems in the J-type centrifuge has been modelled by Wood et al. [25, 145, 155] and discussed by Berthod [156]. Generally high S_f values favour better separations. Unlike in conventional chromatography, in CCC any changes in the composition of one phase affects the composition and behaviour of the other phase [156]. In the metal(II) chloride separations that use water/[$P_{6\,6\,6\,14}$]Cl solvent systems, this can result in problems with the separation. For example, a solvent system in which the mobile phase is the least dense phase (normal phase CCC) will give good separations for small sample sizes (<0.5 g). However, for higher sample loadings of dense metal salts, the density of the mobile phase plus sample injected into the coil can exceed the density of the stationary phase (termed: phase inversion), resulting in the stationary phase being lost out of the end of the coil (termed: column bleed). To solve this problem, the separation is run in LPS mode with the mobile phase as the denser phase. The density of [$P_{6\,6\,6\,14}$]Cl is 0.882 g cm^{-3} [127], so any co-solvent used when combined with the ionic liquid must have a density of significantly less than the mobile phase density at the temperature of the separation (0.98 g cm^{-3} for water at 50 °C).

5 Ionic Liquid–Liquid Separations

A range of separations using ionic liquid-containing solvent systems, where the ionic liquid is a major component of one of the phases, has been carried out. These separations illustrate the versatility of the methodology, allowing many compounds to be separated by a single technique, where the main variable is the structure and composition of the solvent system rather than the apparatus. Provided that a suitable two-phase solvent system can be designed and implemented, the number of possible separations that can be achieved with this technique is enormous. Here we show, as an illustration of the technique's versatility, that ILLC can separate sugars, inorganic transition metal salts and low polarity organic molecules.

5.1 Separation of Organic Compounds

For the separation of organic compounds, there are two types of solvent systems which could be used: (1) ionic liquid/non-polar solvent or (2) ionic liquid/polar solvent (commonly water). We present here examples of the separations of sugars, aromatics from simulated petroleum feedstock and natural oils.

5.1.1 Separation of Saccharides

The separation of simple sugars has been studied by various chromatographic techniques [157], but these are not widely used on an industrial scale [158]. There are however many HPLC methodologies that can be used for the separation of glucose and fructose from sucrose and other saccharides on an analytical scale [159], with refractive index detection [160] or UV–Vis detection [161]. Preparative HPLC separations of sugars are also possible [162], such as with the use of a PL-Hi-Plex Ca 300 × 25 mm preparative HPLC column with water as the eluent [163], but these suffer from the problem of small sample sizes (injection volume 30 μl) [163]. Sugar separations using CCC has been achieved using aqueous biphasic solvent systems, such as aqueous salt/ethanol systems, or the ethanenitrile/aqueous 1.0 M sodium chloride (5:4) system [164], but the systems were only tested on 2-mg sample sizes.

The use of aqueous biphasic solvent systems based on chloride ionic liquids [109] has been tested in CCC by Berthod [117]. Here, it was possible to use the $[C_4mim]Cl$/aqueous $K_2[HPO_4]$ biphasic solvent systems in hydrostatic high-performance centrifugal partition chromatography (HPCPC) and hydrodynamic HPCCC instruments. However, with the J-type centrifuge with a volume of 53 cm^3, containing a 26-m Teflon® coil with an ID of 1.6 mm, operating at 500 or 900 rpm, only low stationary phase retention values were obtained [117]. These were typically <20%, and, in some cases, 0% at low flow rates [117]. The same biphasic system used in the IL-Prep machine (at 865 rpm and 30, 40 and 45 °C) gave very acceptable phase retention values of approximately 85% with a 2 cm^3 min^{-1} flow rate (Fig. 18). This is thought to be due to the use of a longer (36 m) and wider bore (ID 2.1 mm) coil than the one described by Berthod [117] (see coil 2 in Table 3). As

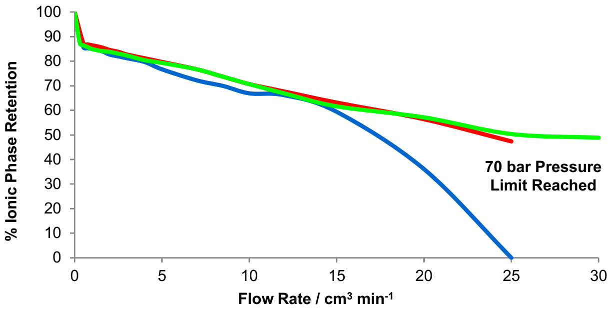

Fig. 18 The variation of percentage stationary phase retention with respect to flow rate for the [C_4mim]Cl/($K_2[HPO_4]$–H_2O; 3.0 M; 1:1) two-phase solvent system at 30 °C (*blue line*), 40 °C (*red line*) and 45 °C (*green line*), on coil 2 (see Table 3 for details)

can be seen, the variation of temperature has little effect on the phase retention at a flow rate of <15 cm^3 min^{-1}. However, higher temperatures allow higher stationary phase retentions at faster flow rates, without exceeding the maximum operating pressure of the stainless steel coils and flying leads. The maximum rated operating pressure (70 bar) was exceeded at 30 and 40 °C, with a flow rate of 25 cm^3 min^{-1}. At 45 °C, the pressure limit is reached at 30 cm^3 min^{-1} flow rate.

The DR_X of sucrose, fructose and glucose in the [C_4mim]Cl/(3.0 M aqueous $K_2[HPO_4]$; 1:1 v/v) two–phase solvent system was found to be 0.90, 0.22 and 0.26, respectively by ^{1}H nuclear magnetic resonance (NMR) analysis. From the DR_X values, the separation of glucose from fructose would not be possible because they are too close to anticipate a reasonable separation; however, the separation of glucose or fructose from sucrose would be achievable. Since all three sugars are optically active, polarimetry can be used to quantitatively measure the concentration of sugars in fractions collected in the ILLC separation. The separation of glucose (0.5 g) from sucrose (0.5 g) (red line) and fructose (0.5 g) from sucrose (0.5 g) (dark blue line) is shown in Fig. 19.

It can be clearly seen that complete separation of the two monosaccharides from the disaccharide (sucrose) was achieved working at a preparative scale (1.0 g). This separation is a proof-of-principle demonstration of the large increase of scale (from 2 to 1000 mg) that can be achieved with an ILLC system over previous CCC separations of sugars with aqueous biphasic solvent systems [164]. In practice, the separation of fructose or glucose from sucrose is achieved on an industrial scale using crystallisation techniques, and chromatographic techniques are not economical [165]. From a more application-orientated viewpoint, this same ILLC solvent system has been used successfully on high value saccharides, oligosaccharides and polysaccharides, the details of which are available elsewhere [42].

5.1.2 Aromatic/Alkane Separations

The extraction of aromatics from petroleum was modelled by using a simulant comprising of a solution of cumene (isopropylbenzene; 4 mol%) in hexane. A two-phase system was produced consisting of [C_{10}mim][OTf], mixed with hexane, with

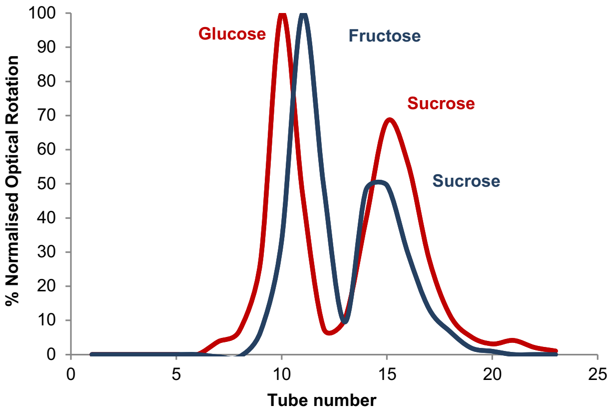

Fig. 19 The separation of glucose (*red*) and fructose (*blue*) (fractions 7–12) from sucrose (fractions 13–20) by ILLC using the [C_4mim]Cl/(K_2[HPO_4]–H_2O; 3.0 M; 1:1 v/v) two-phase solvent system at 45 °C, on coil 2. Percentage normalised optical rotation = 100 × measured optical rotation/specific rotation for each sugar × normalising factor

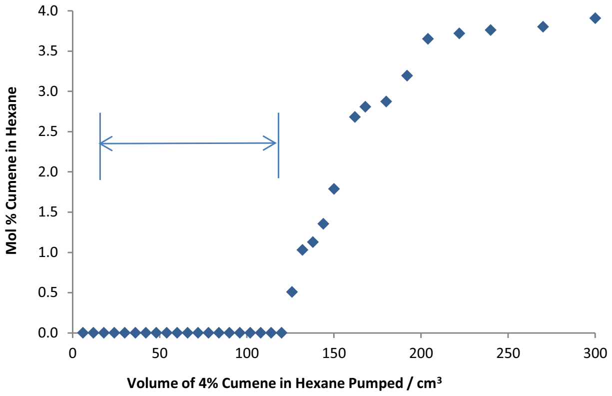

Fig. 20 Extraction of cumene from hexane on coil 4 using the ionic liquid [C_{10}mim][OTf]. The part of the graph from 0 to 11 cm^3 corresponds to hexane (initially contained within the coil) being pumped out of the coil, and the region of 11–110 cm^3 shows hexane which has been completely stripped of cumene

the ionic liquid phase used as the stationary phase and the hexane used as the mobile phase. Coil 4 was filled with the stationary phase, followed by the mobile phase (hexane) at 2 cm^3 min^{-1}, with the coils rotating at 865 rpm, resulting in stationary phase retention of 95%. The analyte was pumped into the coil, and aliquots (5 cm^3) were collected in the fraction collector. Offline analysis by ^1H NMR spectroscopy of the concentration of cumene in the collected fractions is shown in Fig. 20. As can be seen, the aromatics were completely captured by the stationary ionic phase, until the ionic liquid in the coil became saturated, and breakthrough of the cumene occurred at 110 cm^3. The stationary phase containing cumene was then back-flushed from the coil with fresh stationary phase, resulting in a transfer of cumene from hexane to the ionic phase. The cumene was then recovered by distillation from the ionic liquid, effecting a separation of cumene from hexane. This process has the potential to be automated using simulated moving bed (SMB) technology [166, 167] and provides a means for the complete separation of aromatics from alkanes.

5.1.3 Separation of Vetiver Oil

Vetiver oil is extracted from the roots of *Chrysopogon zizanioides* [168, 169] by steam distillation [170], with a worldwide production of about two hundred and fifty tons per year [171]. The oil is widely used in the fragrance industry and is comprised of over three hundred compounds [172]. Constituents of interest to the fragrance industry include polycyclic alkenes (such as α-cadinene and β-vetivenene, as in Fig. 21) and polycyclic alcohols, such as khusimol [173]. Although separation into each individual component is not practical, or even desired, a rough separation into two main classes of 15 carbon sesquiterpenes can be achieved using only one run of ILLC.

The separation was carried out using a solvent system based on the $[C_{12}mim][NTf_2]$/hexane [124]. The ionic liquid is insoluble in the hexane phase (less than 0.1 mol% and could not be detected by ^1H NMR spectroscopy), however hexane is soluble in the $[C_{12}mim][NTf_2]$ phase (56 mol%, or 21 vol% or 13 wt%, as determined by ^1H NMR spectroscopy). The stationary phase retention curves of the $[C_{12}mim][NTf_2]$/hexane solvent system (Table 4), using the ionic liquid phase as the stationary phase and hexane as the mobile phase (using the DPS operating mode as described in Table 4), were determined at a range of different rotation speeds, and are shown in Fig. 22. For the best separations, the instrument should be operated with high stationary phase retentions in the lightest green region or plateau region (where $S_f = 85$–95%) on the graph. The lower rotation speeds reduce wear on the instrument and reduce power consumption, while in this case giving rise to good phase retention values at speeds as low as 300 rpm and flow rates at or below a

Literature predicted alkenes in vetiver oil

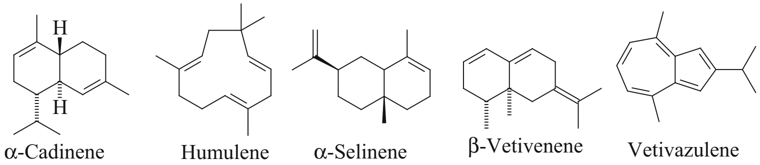

GCMS identified alkenes in vetiver oil

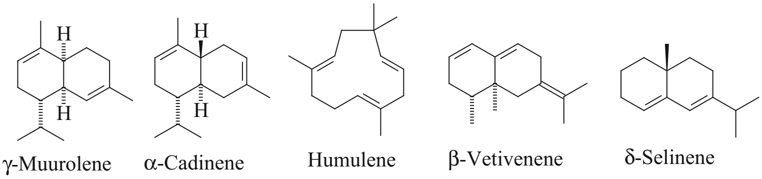

Fig. 21 Five literature examples of alkenes present in vetiver oil and five compounds found in tubes 6–29 in the ILLC separation of vetiver oil, identified by GC-MS software [173]

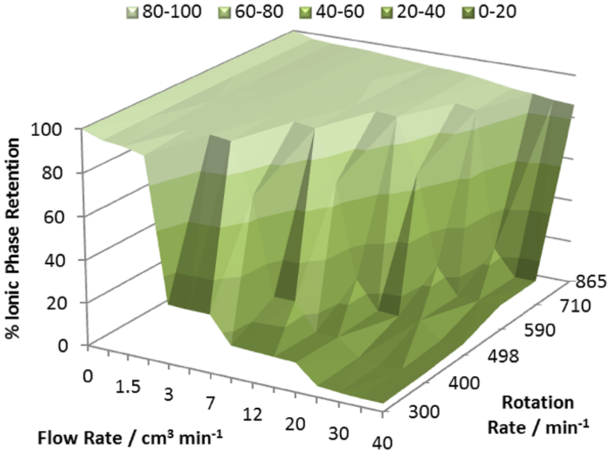

Fig. 22 The variation of % stationary phase retention with respect to coil rotation rate and flow rate for the hexane (mobile phase)/[C_{12}mim][NTf_2] (stationary phase) (3:1) biphasic solvent system at 30 °C on coil 4 (Table 5)

2 cm^3 min^{-1}. These are very high stationary phase retention values, and hence there exists the potential to carry out very fast separations at high flow rates.

It is noticeable that the stationary phase retention curves of this solvent system are more complex than those encountered by He and Zhao [146]. The relationship $\%S_f = 100 + k\sqrt{\text{FR}}$ (where $k = -2.20 \pm 0.13$, $R^2 = 0.98$) holds only for the plateau region of the graph, and it was found that the S_f value was independent of the rotation rate in rpm.

The vetiver oil (1.0 g) dissolved in mobile phase (4 cm^3) was injected at 2 cm^3 min^{-1} into Coil 2 ($S_f = 95\%$) and 106 fractions (5.0 cm^3) were collected. A representative set of fractions were collected and analysed by GC–MS, and four of the GC traces are shown in Fig. 23. The GC analysis of the fractions revealed that the vetiver oil sample was composed of sesquiterpenes, which were separated into two main classes [174, 175]. The fractions in the T6-T25 range contained sesquiterpene alkenes with the formula $C_{15}H_{24}$ or $C_{15}H_{26}$ [175]. Examples include α-muurolene, β-cadinene, humulene, β-vetivenene and δ-selinene (Fig. 21). From fraction T26 onwards, the compounds isolated were mostly oxygenated hydrocarbons such as ethers, epoxides and alcohols, eluting in order of increasing distribution ratio. The chemical formula of these oxygenated products were $C_{15}H_{24}O$ and $C_{15}H_{26}O$ by GC-MS analysis. This isocratic ILLC process can therefore be used to carry out a sesquiterpene alkene from oxygenated sesquiterpene separation.

5.2 Separation of Transition Metal Salts

5.2.1 Previous Research

Aqueous copper(II), nickel(II) and cobalt(II) chloride can be separated from each other using a diverse range of techniques. On the preparative scale, examples

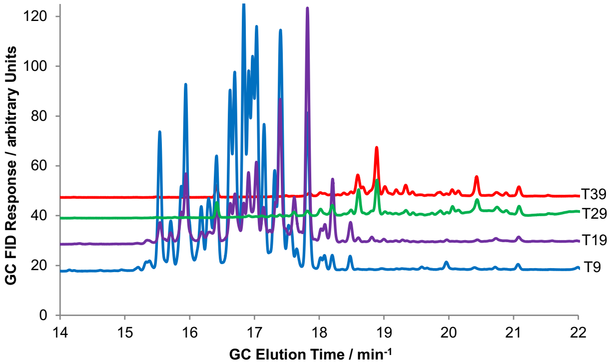

Fig. 23 The gas chromatography (GC) response for selected fractions (*T9*, *T19*, *T29* and *T39*, where *T* is tube number) in the separation of vetiver oil with a hexane/[C_{12}mim][NTf_2] biphasic solvent system using hexane as the mobile phase. Tube numbers 6 to 25 contain C_{15} hydrocarbon terpenes (alkenes) and tube numbers >26 contain predominately oxygenated C_{15} terpenes. *FID* Flame ionisation detector

include a complex nine-stage process [176] involving a combination of solvent extraction and electro-refining. Nickel(II) and cobalt(II) chloride have been separated by a five-stage continuous process using the ionic liquid [$P_{6\,6\,6\,14}$]Cl [177]. The chromatographic separation of these metal(II) salts has been carried out using a number of techniques, including anion-exchange chromatography [178], adsorption thin layer chromatography (TLC) of metal(II) chelates [179], TLC [180], HPLC of diaminostilbene complexes [181], chromatographic separation of amino acid chelates [182], micellar electrokinetic chromatography [183], a guar-based chelating ion exchange resin chromatography [184], and a dibenzyl sulfoxide solution supported on silica as a stationary phase [185].

The direct single-step preparative chromatographic separation of these metal(II) salts, with high sample loadings, without losing any metal(II) salts and without using metal(II) chelates or corrosive acids, would represent a significant improvement on these many processes. Hence, based on knowledge of the speciation of Ni(II), Co(II), and Cu(II) chloride ionic liquids and with the use of a hydrophobic chloride ionic liquid, a biphasic solvent system based on water and [$P_{6\,6\,6\,14}$]Cl (a hydrophobic ionic liquid) was tested and found to be suitable for ILLC separation.

5.2.2 *Transition Metal Behaviour in the Water/[$P_{6\,6\,6\,14}$]Cl/Ethyl Ethanoate Solvent System*

When nickel(II), cobalt(II) or copper(II) chloride are dissolved in water, they form the well known hydrated [$M(H_2O)_6$]Cl_2 salts (where M = Co, Ni or Cu) [186]. If this solution is mixed with a water-immiscible chloride salt such as the ionic liquid [$P_{6\,6\,6\,14}$]Cl, a biphasic solution is formed (shown in Fig. 24) [40]. In the chloride ionic liquid phase, the metals are presumed to exist as the tetrahedral [MCl_4]$^{2-}$ complexes (see Fig. 25) [187–189]. The three metals distribute themselves between both phases, with the nickel(II) and cobalt(II) salts both preferring to dissolve mostly in the aqueous phase, and the copper(II) salt preferring the ionic liquid

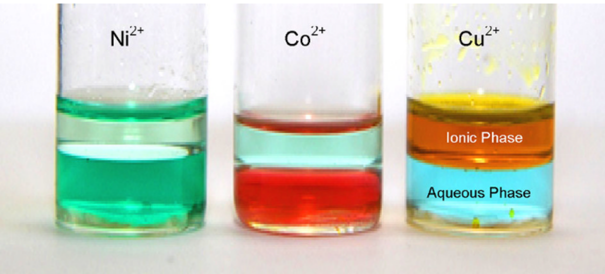

Fig. 24 Solutions of nickel(II) (Ni^{2+}) chloride ($NiCl_2$, *left*), cobalt(II) (Co^{2+}) chloride ($CoCl_2$, *centre*) and copper(II) (Cu^{2+}) chloride ($CuCl_2$, *right*) dissolved in a biphasic mixture of water/[$P_{6\ 6\ 6\ 14}$]Cl/ethyl ethanoate in the ratio of 4:1:1 v/v/v. The upper phase is the ionic liquid [$P_{6\ 6\ 6\ 14}$]Cl and ethyl ethanoate and the lower phase is water, saturated with ethyl ethanoate. In the aqueous phase, the metals exist as octahedral $[M(H_2O)_6]^{2+}$ [186] (Fig. 25), and in the chloride ionic liquid phase, the tetrahedral $[MCl_4]^{2-}$ complex is formed (Fig. 25)

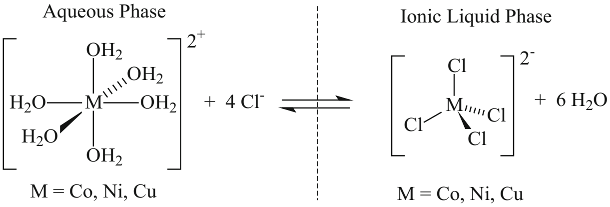

Fig. 25 The equilibria between metal(II) chloride complexes (Co, Ni, or Cu) in the aqueous phase and in the chloride ionic liquid phase

phase. The distribution ratios of the metals between the water and the [$P_{6\ 6\ 6\ 14}$]Cl/ethyl ethanoate phases can be estimated from the graph of the metal(II) chloride separation in Fig. 26, or can be derived by UV–Vis spectrophotometry of the metal(II) chlorides dissolved in each of the two phases. These DR_X are shown in Table 6. The values calculated from the peak maximum heights differ slightly from the values obtained from single metal(II) chloride salts obtained by UV–Vis spectroscopy.

The mobile aqueous phase is composed of water saturated with ethyl ethanoate (7.6 wt% at 30 °C and 7.2 wt% at 40 °C) [190]. The recovery of the metal halide salts from this phase involves simply evaporation of the mobile phase. The ionic liquid used in the stationary phase is [$P_{6\ 6\ 6\ 14}$]Cl, which is a viscous, hydrophobic ionic liquid. The viscosity of 98% pure [$P_{6\ 6\ 6\ 14}$]Cl (with 115 ppm water content) is 2161 cP at 298.15 K [191], which is too high to be pumped using standard HPLC pumps. Hence, the [$P_{6\ 6\ 6\ 14}$]Cl ionic liquid had to be diluted with a water immiscible co-solvent, such as ethyl ethanoate. Other co-solvents tested include dichloromethane, hexane, propanone, butan-1-ol, butanone and pentan-2-one, all of which were also found to be effective co-solvents, with pentan-2-one giving the best separations. Typically, the scale of the separations was 0.5–6.0 g (at approx. 0.6–7.0 M concentration dissolved in the mobile phase) on coil 2 and 1–10 g on coil 4 (see Table 3 for coil details).

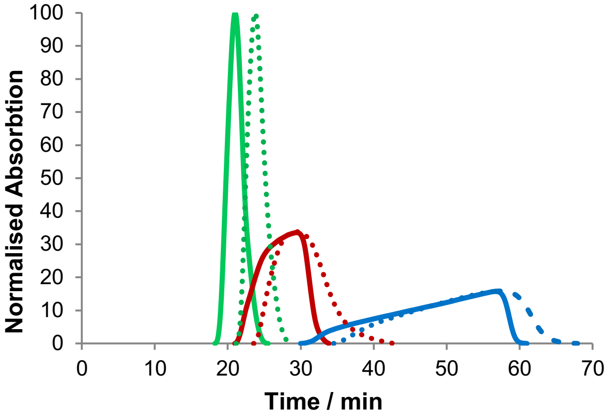

Fig. 26 The concentration of aqueous cobalt(II) (*red line*), nickel(II) (*green line*) and copper(II) (*blue line*) at 30 °C (*dotted lines*) and 40 °C (*solid lines*) on coil 2, showing the normalised absorption of the metal halide salts where aqueous $NiCl_2 = 100$ (equal areas under each curve). Error = ± 2% in UV absorption readings

Table 6 The distribution ratios calculated from the elution time of the metal(II) complexes described in Section 5.2.3 and from UV–Vis spectrophotometry

Metal complexes	Temperature (°C)	Peak maximum/min[a]	Distribution ratio from ILLC separation	Distribution ratio from UV–Vis spectrophotometry
Ni	30	23.5	0.31	0.2
Co	30	29.5	0.62	0.6
Cu	30	56.8	2.22	2.2
Ni	40	20.8	0.16	0.2
Co	40	29.8	0.66	0.6
Cu	40	55.3	2.07	2.1

[a] Solvent front elution time occurred at 18 min

5.2.3 Transition Metal Separation

To achieve an effective separation of the aqueous metal(II) chloride salts $[M(H_2O)_6]Cl_2$ (where M = Co, Ni or Cu), a biphasic solvent system (degassed) consisting of $[P_{6\,6\,6\,14}]Cl$ (250 cm^3), ethyl ethanoate (250 cm^3) and deionised water (1000 cm^3) was prepared. The ionic phase was found to contain the majority of the ethyl ethanoate, and forms the upper liquid layer. The aqueous phase of water (92.4–92.8 wt%) and ethyl ethanoate (7.2–7.6 wt%) was analysed by ^1H NMR and found not to contain the ionic liquid $[P_{6\,6\,6\,14}]Cl$ (the concentration of $[P_{6\,6\,6\,14}]Cl$ in the mobile water phase was not detectable and estimated to be < 0.5 mol% concentration by this technique) [144].

The separation of the copper(II), nickel(II) and cobalt(II) aqueous complexes dissolved in water was analysed by means of a UV–Vis detector situated before the fraction collector. A mixture of metal halides (approx. 2.9 M of MCl_2 in the aqueous mobile phase, where M = Ni, Co or Cu) was prepared from $NiCl_2$, $CoCl_2$ and $CuCl_2$ (a mixture of 0.50 g of each metal salt, dissolved in 5.0 cm^3 of mobile phase). The separation was performed on coil 2 at 30 and 40 °C, with a mobile phase flow rate of 2.0 $cm^3\ min^{-1}$. The raw data obtained from the UV–Vis detector were somewhat noisy and contained a number of spurious peaks due to tiny bubbles of stationary phase passing through the detector. The data were processed by computer subtraction of the baseline signal (at 590 nm, where the three metal salts do not absorb light) from the Ni(II) (390 nm), Co(II) (505 nm) and Cu(II) (790 nm) signals. This had the effect of eliminating baseline drift, removing the artifacts due to stationary phase bubbles passing through the detector cell and increasing the signal-to-noise ratio. Next, the data were smoothed with a moving average filter (taking the average over 42 s of data), the start of each metal peak was set to zero and a linear baseline adjustment was made to each peak to adjust the end of the peak to zero. The peak areas were normalised and equalised for each metal, compensating for the different molar absorption coefficients, to give the curves shown in Fig. 26. The separation of these three metal salts is visually demonstrated in Fig. 27, where the three separated metal salts are clearly distinguishable in the fraction collector.

At 30 °C, a partial separation was achieved with some of the cobalt(II) chloride ending up mixed with the copper(II) and nickel(II) chloride eluents. At 40 °C the separation performance improved (see Table 7; Fig. 26), and the separation time was reduced from 68 to 61 min. In Table 7, the area of overlap of the peaks and the percentage of pure unmixed metal chloride salt that can be obtained are shown. These figures have been obtained on a non-optimised system and are illustrative of the potential of this technique. The peak shape of the copper(II) complex in Fig. 26 is unusual and is showing anti-Langmuirian behaviour [192]. This is largely due to the presence of nickel(II) and cobalt(II) complexes affecting the phase equilibria of the copper(II) complexes, leading to the observed triangular peak shape.

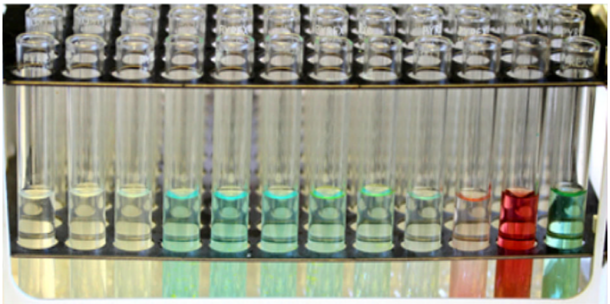

Fig. 27 The separation of aqueous $CoCl_2$ (*pink/red*), $NiCl_2$ (*dark green*) and $CuCl_2$ (*light blue*) by ILLC as viewed in the fraction collector, showing tubes 13 (*right*) through to 24 (*left*) in sequence

Table 7 Percentage area of overlap of nickel(II)/cobalt(II) peaks and cobalt(II)/copper(II) peaks at 30 and 40 °C and the percentage integration of pure nickel(II), cobalt(II), and copper(II) chlorides eluted (area of each peak that does not overlap)

Temperature (°C)	% Area overlap nickel(II)/cobalt(II)	% Area overlap cobalt(II)/copper(II)	% Pure nickel(II)	% Pure cobalt(II)	% Pure copper(II)
30	14.7	3.98	36	57	88
40	10.7	1.26	48	73	98

6 Conclusions

The use of ionic liquids in ILLC was originally thought to be too difficult to be of use in conventional CCC equipment. With the focussed design of the equipment by AECS-QuikPrep Ltd., this problem has now been solved. Currently there is very little literature precedent for the use of ionic liquids in CCC or LLC, and so much of this technology has had to be developed from first principles. This has required the designing of ionic liquids and solvent systems which give acceptable distribution ratios for the solutes being separated. The testing of these new solvent systems has been carried out in a specially designed ILLC instrument which can handle higher viscosity solvent systems than are usually found in CCC and LLC. Despite this, ILLC has been shown to be a very versatile technology which allows a diverse range of separations, including the direct separation of both organic and inorganic systems. The instrumentation for ILLC separations is closely related to conventional HPCCC/HSCCC equipment, but uses coils that are made from stainless steel (rather than PTFE), and the bottlenecks in the solvent flow pathways have been removed.

Ionic liquids can be designed to suit a particular separation by modifying their structure and therefore their properties. Factors such as viscosity, density, density difference, interfacial tension and relative solubility of solutes can all be adjusted. Thus, this technique allows the separation of practically any soluble mixture, provided a suitable two-phase solvent system can be designed or found. One way of regarding ILLC is as a method of using “designer solvents for designer separations”. Whilst still in its infancy, ILLC research should have significant impact on separations which are currently either too difficult or too expensive to

Table 8 The comparison of ionic liquid–liquid chromatography, high-performance liquid–liquid chromatography, high-performance liquid chromatography and gas chromatography systems

Characteristic	ILLC	HPLLC	HPLC	GC
Rapid separations	🟩	🟩	🟩	🟩
Small scale (<0.1 g)	🟩	🟩	🟩	🟩
Preparative scale (>1 g)	🟩	🟩	🟨	🟥
Large scale (>1 kg)	🟩	🟩	🟥	🟥
Low solubility analytes	🟩	🟨	🟥	🟥
Inorganic compounds	🟩	🟨	🟥	🟥
Corrosive compounds	🟩	🟨	🟥	🟥
Column lifetime	🟩	🟩	🟨	🟨

Colour codes: *red* poor, *yellow* intermediate, and *green* good perform at scale. Compounds thought to be too insoluble or too immiscible with biphasic solvent systems comprised of molecular solvents can now be separated by ILLC. One such example is the separation of lentinan [42], where the scale of separation was boosted by a factor of 100, from the tens of milligrams to the gram scale, on a similar sized apparatus, by replacement of a water/PEG biphasic solvent system with an ionic liquid/aqueous phosphate solvent system. With larger capacity ILLC instruments and through the use of CPC instrument designs, much larger scale separations could be achieved. In Table 8, the versatility and relative advantages of ILLC (in comparison with conventional HPCCC, HPLC and GC) methodologies are shown, and it is clear that ILLC offers major benefits.

Acknowledgements We would like to express our gratitude to the EPSRC (grant number EP/M026671/1) for funding the metal separation research, Invest NI for the Collaborative Grants for R&D: RD0210506 and RD1111867, and the QUILL Research Centre for funding this work. We would also like to thank Professor Paul Davey and Givaudan for useful discussions.

References

1. Cazes J (2009) Encyclopedia of chromatography, 3rd edn. Taylor & Francis, Boca Raton
2. Snyder LR, Kirkland JJ (1979) Introduction to modern liquid chromatography. Wiley, New York
3. Menet J, Menet M, Thiébaut D, Rosset R (1995) Modern countercurrent chromatography. ACS Symposium Series, no. 593). American Chemical Society, Washington DC
4. Oka F, Oka H, Ito Y (1991) J Chromatogr 538:99–108. doi:10.1016/s0021-9673(01)91626-7
5. Werner S, Haumann M, Wasserscheid P (2010) Annu Rev Chem Biomol Eng 1:203–230. doi:10.1146/ANNUREV-CHEMBIOENG-073009-100915
6. Garrard IJ (2005) J Liq Chromatogr Relat Technol 28:1923–1935. doi:10.1081/jlc-200063571
7. Friesen JB, Pauli GF (2005) J Liq Chromatogr Relat Technol 28:2777–2806. doi:10.1080/10826070500225234
8. Ito Y (1996) In: Ito Y, Conway WD (eds) High-speed countercurrent chromatography. Wiley, New York, pp 3–44
9. Sutherland I, Ignatova S, Hewitson P, Janaway L, Wood P, Edwards N, Harris G, Guzlek H, Keay D, Freebairn K, Johns D, Douillet N, Thickitt C, Vilminot E, Mathews B (2011) J Chromatogr A 1218:6114–6121. doi:10.1016/j.chroma.2011.01.016
10. Kostanyan AE (2015) J Chromatogr A 1406:156–164. doi:10.1016/j.chroma.2015.06.010
11. Rafson HJ (1998) Odor and VOC control handbook. McGraw-Hill, New York
12. Du QZ, Ke CQ, Ito Y (1998) J Liq Chromatogr Relat Technol 21:157–162. doi:10.1080/10826079808001944
13. Drueckhammer DG, Gao SQ, Liang XF, Liao JZ (2013) ACS Sustain Chem Eng 1:87–90. doi:10.1021/sc300044c
14. Welton T (2015) Proc R Soc A 471. doi:10.1098/rspa.2015.0502
15. Sutherland IA (2010) In: Cazes J (ed) Industrial applications of CCC, 3rd edn. Taylor & Francis, Boca Raton, pp 2116–2119
16. Berthod A, Carda-Broch S (2003) J Liq Chromatogr Relat Technol 26:1493–1508. doi:10.1081/jlc-120021262
17. Brennecke JF, Maginn EJ (2001) AIChE J 47:2384–2389. doi:10.1002/AIC.690471102
18. Web of Science^{TM} Core Collection (2017) Clarivate Analytics, Manchester

19. Freemantle M (2010) An introduction to ionic liquids. Royal Society of Chemistry, Cambridge
20. Armstrong DW, He L, Liu YS (1999) Anal Chem 71:3873–3876
21. Brown L, Earle MJ, Gîlea MA, Plechkova NV, Seddon KR (2017) Aust J Chem 70:923–932. doi:10.1071/CH17004
22. Ito Y (1986) CRC Crit Rev Anal Chem 17:65–143. doi:10.1080/10408348608542792
23. Guzlek H, Wood PL, Janaway L (2009) J Chromatogr A 1216:4181–4186. doi:10.1016/j.chroma.2009.02.091
24. Berthod A, Ruiz-Angel M, Carda-Broch S (2008) J Chromatogr A 1184:6–18. doi:10.1016/j.chroma.2007.11.109
25. Wood PL (2010) J Chromatogr A 1217:1283–1292. doi:10.1016/j.chroma.2009.12.038
26. Ito Y (1984) Adv Chromatogr 24:181–226
27. Sutherland IA, Brown L, Forbes S, Games G, Hawes D, Hostettmann K, McKerrell EH, Marston A, Wheatley D, Wood P (1998) J Liq Chromatogr Relat Technol 21:279–298. doi:10.1080/10826079808000491
28. Ignatova S, Hawes D, van den Heuvel R, Hewitson P, Sutherland IA (2010) J Chromatogr A 1217:34–39. doi:10.1016/j.chroma.2009.10.055
29. Sutherland IA, Heywoodwaddington D, Ito Y (1987) J Chromatogr 384:197–207. doi:10.1016/s0021-9673(01)94671-0
30. Berthod A, Hassoun M, Ruiz-Angel MJ (2005) Anal Bioanal Chem 383:327–340. doi:10.1007/s00216-005-0016-7
31. Chadwick LR, Fong HHS, Farnsworth NR, Pauli GF (2005) J Liq Chromatogr Relat Technol 28:1959–1969. doi:10.1081/jlc-200063634
32. Du QZ, Shu AM, Ito Y (1996) J Liq Chromatogr Relat Technol 19:1451–1457. doi:10.1080/10826079608007194
33. Qiu F, Friesen JB, McAlpine JB, Pauli GF (2012) J Chromatogr A 1242:26–34. doi:10.1016/j.chroma.2012.03.081
34. Gallistl C, Vetter W (2016) J Chromatogr A 1442:62–72. doi:10.1016/j.chroma.2016.03.015
35. Caldwell DJ, Armstrong TW, Barone NJ, Suder JA, Evans MJ (2000) AIHAJ 61:881–894. doi:10.1202/0002-8894(2000)061<0881:hsedca>2.0.co;2
36. Angell CA (2010) In: Gaune-Escard M, Seddon KR (eds) Molten Salts and Ionic Liquids: Never the Twain? Wiley, Hoboken, pp 1–24
37. Earle MJ, Esperanca J, Gîlea MA, Lopes JNC, Rebelo LPN, Magee JW, Seddon KR, Widegren JA (2006) Nature 439:831–834. doi:10.1038/NATURE04451
38. Plechkova NV, Seddon KR (2008) Chem Soc Rev 37:123–150. doi:10.1039/b006677j
39. Seddon KR (1999) In: Boghosian S, Dracopoulos V, Kontoyannis CG, Voyiatzis GA (eds) The International George Papatheodorou Symposium: Proceedings Institute of Chemical Engineering and High Temperature Chemical Processes, Patras, pp 131–135
40. Arce A, Earle MJ, Katdare SP, Rodriguez H, Seddon KR (2006) Chem Commun 2548–2550. doi:10.1039/b604595b
41. Wasserscheid P, Welton T (eds) (2008) In ionic liquids in synthesis, 2nd edn. Wiley, Weinheim
42. Earle MJ, Gilea MA (2013) Lentinan extraction process from mushrooms using ionic liquid. World patent WO2013140185A1
43. Anderson JL, Armstrong DW, Wei GT (2006) Anal Chem 78:2892–2902. doi:10.1021/AC069394O
44. Qin W, Li SFY (2002) Electrophoresis 23:4110–4116
45. Franco P, Blanc J, Oberleitner WR, Maier NM, Lindner W, Minguillon C (2002) Anal Chem 74:4175–4183. doi:10.1021/ac020209q
46. Ma Y, Ito Y (2014) Curr Chromatogr 1:69–80. doi:10.2174/2213240611309999000l
47. Wang SS, Han C, Wang SS, Bai LJ, Li SS, Luo JG, Kong LY (2016) J Chromatogr A 1471:155–163. doi:10.1016/j.chroma.2016.10.036
48. Stepnowski P, Muller A, Behrend P, Ranke J, Hoffmann J, Jastorff B (2003) J Chromatogr A 993:173–178
49. Zhang WZ, He LJ, Liu X, Jiang SX (2004) Chin J Chem 22:549–552
50. Sigma-Aldrich Co. LLC. Supelco Ionic Liquid GC column literature and applications. http://www.sigmaaldrich.com/analytical-chromatography/gas-chromatography/columns/ionic-liquid-literature.html. Accessed 15 Feb 2017
51. Liu JF, Jonsson JA, Jiang GB (2005) Trac Trends Anal Chem 24:20–27. doi:10.1016/j.trac.2004.09.005
52. Xiao XH, Liu SJ, Liu X, Jiang SX (2005) Chin J Anal Chem 33:569–574

53. Pandey S (2006) Anal Chim Acta 556:38–45. doi:10.1016/j.aca.2005.06.038
54. Li ZJ, Chang J, Shan HX, Pan JM (2007) Rev Anal Chem 26:109–153
55. Shamsi SA, Danielson ND (2007) J Sep Sci 30:1729–1750. doi:10.1002/jssc.200700136
56. Sun W, Gao RF, Jiao K (2007) Chin J Anal Chem 35:1813–1819
57. Buszewski B, Studzinska S (2008) Chromatographia 68:1–10. doi:10.1365/s10337-008-0662-y
58. Soukup-Hein RJ, Warnke MM, Armstrong DW (2009) In ionic liquids in analytical chemistry. Annu Rev 2:145–168
59. Sun P, Armstrong DW (2010) Anal Chim Acta 661:1–16. doi:10.1016/j.aca.2009.12.007
60. Zhang JJ, Shen XH, Chen QD (2011) Curr Org Chem 15:74–85. doi:10.2174/138527211793797765
61. Joshi MD, Anderson JL (2012) RSC Adv 2:5470–5484. doi:10.1039/c2ra20142a
62. Ho TD, Zhang C, Hantao LW, Anderson JL (2014) Anal Chem 86:262–285. doi:10.1021/ac4035554
63. Soares B, Passos H, Freire CSR, Coutinho JAP, Silvestre AJD, Freire MG (2016) Green Chem 18:4582–4604. doi:10.1039/c6gc01778a
64. Stalcup AM, Cabovska B (2004) J Liq Chromatogr Relat Technol 27:1443–1459. doi:10.1081/jlc-120030611
65. Stepnowski P (2006) Int J Mol Sci 7:497–509. doi:10.3390/i7110497
66. Lopez-Pastor M, Simonet BM, Lendl B, Valcarcel M (2008) Electrophoresis 29:94–107. doi:10.1002/elps.200700645
67. Xu YH, Wang EK (2009) J Chromatogr A 1216:4817–4823. doi:10.1016/j.chroma.2009.04.024
68. Huang Y, Yao S, Song H (2013) J Chromatogr Sci 51:739–752. doi:10.1093/chromsci/bmt076
69. Tang S, Liu SJ, Guo Y, Liu X, Jiang SX (2014) J Chromatogr A 1357:147–157. doi:10.1016/j.chroma.2014.04.037
70. Ding J, Armstrong DW (2005) Chirality 17:281–292. doi:10.1002/chir.20153
71. Bica K, Gaertner P (2008) Eur J Org Chem 3235–3250. doi:10.1002/ejoc.200701107
72. Sun HH, Gao Y, Zhai YA, Zhang Q, Liu FQ, Gao G (2008) Prog Chem 20:698–712
73. Payagala T, Armstrong DW (2012) Chirality 24:17–53. doi:10.1002/chir.21975
74. Kapnissi-Christodoulou CP, Stavrou IJ, Mavroudi MC (2014) J Chromatogr A 1363:2–10. doi:10.1016/j.chroma.2014.05.059
75. Poole CF, Karunasekara T, Ariyasena TC (2013) J Sep Sci 36:96–109. doi:10.1002/jssc.201200709
76. Han D, Tian M, Park DW, Choi DK, Row KH (2009) Korean J Chem Eng 26:1353–1358. doi:10.2478/s11814-009-0209-4
77. Yao C, Anderson JL (2009) J Chromatogr A 1216:1658–1712. doi:10.1016/j.chroma.2008.12.001
78. Poole CF, Poole SK (2011) J Sep Sci 34:888–900. doi:10.1002/jssc.201000724
79. Poole CF, Lenca N (2014) J Chromatogr A 1357:87–109. doi:10.1016/j.chroma.2014.03.029
80. Sun XJ, Xing J, Zhai YX, Li ZX (2014) Prog Chem 26:647–656. doi:10.7536/pc130847
81. Calabuig-Hernandez S, Garcia-Alvarez-Coque MC, Ruiz-Angel MJ (2016) J Chromatogr A 1465:98–106. doi:10.1016/j.chroma.2016.08.048
82. Hantao LW, Toledo BR, Augusto F (2016) Quim Nova 39:81–93. doi:10.5935/0100-4042.20150177
83. Polyakova Y, Koo YM, Row KH (2006) Biotechnol Bioprocess Eng 11:1–6. doi:10.1007/bf02931860
84. Wang Y, Tian ML, Bi WT, Row KH (2009) Int J Mol Sci 10:2591–2610. doi:10.3390/ijms10062591
85. Paszkiewicz M, Stepnowski P (2011) Curr Org Chem 15:1873–1887
86. Bi WT, Zhou J, Row KH (2012) Sep Sci Technol 47:360–369. doi:10.1080/01496395.2011.608402
87. Pino V, Afonso AM (2012) Anal Chim Acta 714:20–37. doi:10.1016/j.aca.2011.11.045
88. Garcia-Alvarez-Coque MC, Ruiz-Angel MJ, Berthod A, Carda-Broch S (2015) Anal Chim Acta 883:1–21. doi:10.1016/j.aca.2015.03.042
89. Poole CF (2004) J Chromatogr A 1037:49–82. doi:10.1016/j.chroma.2003.10.127
90. Marszall MP, Kaliszan R (2007) Crit Rev Anal Chem 37:127–140. doi:10.1080/10408340601107847
91. Padron MET, Afonso-Olivares C, Sosa-Ferrera Z, Santana-Rodriguez JJ (2014) Molecules 19:10320–10349. doi:10.3390/molecules190710320
92. Shi XZ, Qiao LZ, Xu GW (2015) J Chromatogr A 1420:1–15. doi:10.1016/j.chroma.2015.09.090
93. Zhang ML, Mallik AK, Takafuji M, Ihara H, Qiu HD (2015) Anal Chim Acta 887:1–16. doi:10.1016/j.aca.2015.04.022

94. Pino V, German-Hernandez M, Martin-Perez A, Anderson JL (2012) Sep Sci Technol 47:264–276. doi:10.1080/01496395.2011.620589
95. Roth M (2009) J Chromatogr A 1216:1861–1880. doi:10.1016/j.chroma.2008.10.032
96. Qiao LZ, Shi XZ, Xu GW (2016) Trac Trends Anal Chem 81:23–33. doi:10.1016/j.trac.2016.03.021
97. Earle MJ, Seddon KR (2013) Ionic liquid separations. Patent WO2013121219A1
98. Earle MJ, Seddon KR (2013) Ionic liquid separations. World patent WO2013121220A1
99. Berthod A, Maryutina T, Spivakov B, Shpigun O, Sutherland IA (2009) Pure Appl Chem 81:355–387. doi:10.1351/pac-rep-08-06-05
100. Friesen JB, Pauli GF (2007) J Chromatogr A 1151:51–59. doi:10.1016/J.CHROMA.2007.01.126
101. Berthod A, Carda-Broch S (2004) Anal Bioanal Chem 380:168–177. doi:10.1007/s00216-004-2717-8
102. Berthod A, Ruiz-Angel M-J, Carda-Broch S (2009) In: Koel M (ed) Ionic Liquids in Chemical Analysis. CRC Press, Boca Raton, pp 211–227
103. Earle MJ, Gordon CM, Plechkova NV, Seddon KR, Welton T (2007) Anal Chem 79:758–764. doi:10.1021/ac061481t
104. Earle MJ, Seddon KR, Self R, Brown L (2013) Ionic liquid separations. World patent WO2013121218A1
105. Seddon KR, Stark A, Torres MJ (2000) Pure Appl Chem 72:2275–2287. doi:10.1351/pac200072122275
106. Carda-Broch S, Berthod A, Armstrong DW (2003) Anal Bioanal Chem 375:191–199. doi:10.1007/s00216-002-1684-1
107. Swatloski RP, Holbrey JD, Rogers RD (2003) Green Chem 5:361–363. doi:10.1039/b304400a
108. Tariq M, Carvalho PJ, Coutinho JAP, Marrucho IM, Lopes JNC, Rebelo LPN (2011) Fluid Phase Equilib 301:22–32. doi:10.1016/j.fluid.2010.10.018
109. Gutowski KE, Broker GA, Willauer HD, Huddleston JG, Swatloski RP, Holbrey JD, Rogers RD (2003) J Am Chem Soc 125:6632–6633. doi:10.1021/JA0351802
110. Zeng Y, Liu G, Ma Y, Chen XY, Ito Y (2013) J Liq Chromatogr Relat Technol 36:504–512. doi:10.1080/10826076.2012.660725
111. Iqbal M, Tao YF, Xie SY, Zhu YF, Chen DM, Wang X, Huang LL, Peng DP, Sattar A, Shabbir MA, Hussain HI, Ahmed S, Yuan ZH (2016) Biol Proced Online 18:18. doi:10.1186/s12575-016-0048-8
112. Mekaoui N, Faure K, Berthod A (2012) Bioanalysis 4:833–844. doi:10.4155/bio.12.27
113. Jiang ZG, Du QZ, Sheng LY (2009) Chin J Anal Chem 37:412–416
114. Bridges NJ, Gutowski KE, Rogers RD (2007) Green Chem 9:177–183. doi:10.1039/b611628k
115. Freire MG, Claudio AFM, Araujo JMM, Coutinho JAP, Marrucho IM, Lopes JNC, Rebelo LPN (2012) Chem Soc Rev 41:4966–4995. doi:10.1039/c2cs35151j
116. Ward DP, Cardenas-Fernandez M, Hewitson P, Ignatova S, Lye GJ (2015) J Chromatogr A 1411:84–91. doi:10.1016/j.chroma.2015.08.006
117. Ruiz-Angel MJ, Pino V, Carda-Broch S, Berthod A (2007) J Chromatogr A 1151:65–73. doi:10.1016/j.chroma.2006.11.072
118. Liu Y, Garzon J, Friesen JB, Zhang Y, McAlpine JB, Lankin DC, Chen SN, Pauli GF (2016) Fitoterapia 112:30–37. doi:10.1016/j.fitote.2016.04.019
119. Fan C, Cao XL, Liu M, Wang W (2016) J Chromatogr A 1436:133–140. doi:10.1016/j.chroma.2016.01.069
120. Fan C, Li N, Cao XL (2015) J Sep Sci 38:2109–2116. doi:10.1002/jssc.201500172
121. Pereira JFB, Ventura SPM, Silva FAE, Shahriari S, Freire MG, Coutinho JAP (2013) Sep Purif Technol 113:83–89. doi:10.1016/j.seppur.2013.04.004
122. Xu LL, Li AF, Sun AL, Liu RM (2010) J Sep Sci 33:31–36. doi:10.1002/jssc.200900528
123. Mai NL, Ahn K, Koo YM (2014) Process Biochem 49:872–881. doi:10.1016/j.procbio.2014.01.016
124. Arce A, Earle MJ, Rodriguez H, Seddon KR (2007) J Phys Chem B 111:4732–4736. doi:10.1021/jp066377u
125. Arce A, Earle MJ, Rodriguez H, Seddon KR, Soto A (2009) Green Chem 11:365–372. doi:10.1039/b814189d
126. Andanson JM, Meng X, Traikia M, Husson P (2016) J Chem Thermodyn 94:169–176. doi:10.1016/j.jct.2015.11.008
127. Neves C, Carvalho PJ, Freire MG, Coutinho JAP (2011) J Chem Thermodyn 43:948–957. doi:10.1016/j.jct.2011.01.016
128. Berthod A, Hassoun M, Harris G (2005) J Liq Chromatogr Relat Technol 28:1851–1866. doi:10.1081/jlc/200063489

129. Arce A, Earle MJ, Rodriguez H, Seddon KR, Soto A (2008) Green Chem 10:1294–1300. doi:10.1039/b807222a
130. Dimitrijevic A, Zec N, Zdolsek N, Dozic S, Tot A, Gadzuric S, Vranes M, Trtic-Petrovic T (2016) J Ind Eng Chem 40:152–160. doi:10.1016/j.jiec.2016.06.017
131. Canales RI, Brennecke JF (2016) J Chem Eng Data 61:1685–1699. doi:10.1021/acs.jced.6b00077
132. Robles PA, Cisternas LA (2015) J Chem Thermodyn 90:1–7. doi:10.1016/j.jct.2015.06.013
133. Dominguez I, Gonzalez EJ, Dominguez A (2014) Fuel Process Technol 125:207–216. doi:10.1016/j.fuproc.2014.04.001
134. Albertson PA (1960) Partition of cell particles and macromolecules. Wiley, New York
135. Sun HL, He BF, Xu JX, Wu B, Ouyang PK (2011) Green Chem 13:1680–1685. doi:10.1039/c1gc15042a
136. Kurnia KA, Freire MG, Coutinho JAP (2014) J Phys Chem B 118:297–308. doi:10.1021/jp411933a
137. Zhou XY, Zhang J, Xu RP, Ma X, Zhang ZQ (2014) J Chromatogr A 1362:129–134. doi:10.1016/j.chroma.2014.08.034
138. Li YL, Huang R, Zhu Q, Yu YH, Hu J (2017) J Chem Eng Data 62:796–803. doi:10.1021/acs.jced.6b00844
139. Wang RP, Chang YN, Tan ZJ, Li FF (2016) J Mol Liq 222:836–844. doi:10.1016/j.molliq.2016.07.079
140. Chakraborty A, Sen K (2016) J Chromatogr A 1433:41–55. doi:10.1016/j.chroma.2016.01.016
141. Arce A, Earle MJ, Katdare SP, Rodriguez H, Seddon KR (2007) Fluid Phase Equilib 261:427–433. doi:10.1016/j.fluid.2007.06.017
142. Arce A, Earle MJ, Rodriguez H, Seddon KR (2007) Green Chem 9:70–74. doi:10.1039/b610207g
143. Arce A, Earle MJ, Katdare SP, Rodriguez H, Seddon KR (2008) Phys Chem Chem Phys 10:2538–2542. doi:10.1039/b803094b
144. Anderson K, Rodriguez H, Seddon KR (2009) Green Chem 11:780–784. doi:10.1039/b821925g
145. Wood PL, Hawes D, Janaway L, Sutherland IA (2003) J Liq Chromatogr Relat Technol 26:1373–1396. doi:10.1081/jlc-120021256
146. He CH, Zhao CX (2007) AIChE J 53:1460–1471. doi:10.1002/aic.11185
147. Zhang SJ, Sun N, He XZ, Lu XM, Zhang XP (2006) J Phys Chem Ref Data 35:1475–1517. doi:10.1063/1.2204959
148. Liu W, Cheng L, Zhang Y, Wang H, Yu M (2008) J Mol Liq 140:68–72
149. Zhou T, Chen L, Ye Y, Chen L, Qi Z, Freund H, Sundmacher K (2012) Ind Eng Chem Res 51:6256–6264. doi:10.1021/ie202719z
150. Klahn M, Stuber C, Seduraman A, Wu P (2010) J Phys Chem B 114:2856–2868. doi:10.1021/jp1000557
151. Atashrouz S, Zarghampour M, Abdolrahimi S, Pazuki G, Nasernejad B (2014) J Chem Eng Data 59:3691–3704. doi:10.1021/je500572t
152. Abullah MMS, Al-Lohedan HA, Attah AM (2016) J Mol Liq 219:54–62. doi:10.1016/j.molliq.2016.03.011
153. Hezave AZ, Dorostkar S, Ayatollahi S, Nabipour M, Hemmateenejad B (2013) Colloids Surf A Physicochem Eng Asp 421:63–71. doi:10.1016/j.colsurfa.2012.12.008
154. Al-Marzouqi I, Levy MS, Lye GJ (2005) J Liq Chromatogr Relat Technol 28:1311–1332. doi:10.1081/jlc-200054806
155. Sutherland IA, Du Q, Wood P (2001) J Liq Chromatogr Relat Technol 24:1669–1683. doi:10.1081/jlc-100104370
156. Berthod A (2009) In: Grinberg N, Grushka E (eds) Advances in Chromatography. CRC Press/Taylor & Francis, Boca Raton, 47:352
157. Verzele M, Simoens G, Vandamme F (1987) Chromatographia 23:292–300. doi:10.1007/BF02311783
158. Nitsch E (1974) Method of producing fructose and glucose from sucrose. World patent 3812010
159. Shaw PE, Wilson CW (1983) J Sci Food Agric 34:109–112. doi:10.1002/JSFA.2740340116
160. Filip M, Vlassa M, Coman V, Halmagyi A (2016) Food Chem 199:653–659. doi:10.1016/j.foodchem.2015.12.060
161. Schmid T, Baumann B, Himmelsbach M, Klampfl CW, Buchberger W (2016) Anal Bioanal Chem 408:1871–1878. doi:10.1007/s00216-015-9290-1
162. Gonzalez J, Remaud G, Jamin E, Naulet N, Martin GG (1999) J Agric Food Chem 47:2316–2321. doi:10.1021/JF981093V
163. Veronese T, Bouchu A, Perlot P (1999) Biotechnol Tech 13:43–48. doi:10.1023/a:1008857613103

164. Shinomiya K, Ito Y (2006) J Liq Chromatogr Relat Technol 29:733–750. doi:10.1080/10826070500509298
165. Doremus RH (1985) J Colloid Interface Sci 104:114–120. doi:10.1016/0021-9797(85)90015-3
166. Deckert P, Arlt W (1994) Chem Ing Tec 66:1334–1340. doi:10.1002/cite.330661004
167. Rodrigues RCR, Silva RJS, Mota JPB (2010) J Chromatogr A 1217:3382–3391. doi:10.1016/j.chroma.2010.03.009
168. Adams RP, Zhong M, Turuspekov Y, Dafforn MR, Veldkamp JF (1998) Mol Ecol 7:813–818. doi:10.1046/J.1365-294X.1998.00394.X
169. Guenther E (1950) In: Guenther E (ed) Individual essential oils of the plant families Gramineae, Lauraceae, Burseraceae, Myrtaceae, Umbelliferae and Geraniaceae. Van Nostrand Company, New York, pp 156–180
170. Guenther E (1948) In: Guenther E (ed) The essential oils. Van Nostrand Company, New York
171. Massardo DR, Senatore F, Alifano P, Del Giudice L, Pontieri P (2006) Biochem Syst Ecol 34:376–382. doi:10.1016/J.BSE.2005.10.016
172. Kim HJ, Chen F, Wang X, Chung HY, Jin ZY (2005) J Agric Food Chem 53:7691–7695. doi:10.1021/JF050833E
173. Fahlbusch KG, Hammerschmidt FJ, Panten J, Pickenhagen W, Schatkowski D, Bauer K, Garbe D, Surburg H (2003) Flavors and Fragrances: Ullmann's Encyclopedia of Industrial Chemistry, Wiley-VCH, Weinheim, Germany. doi:10.1002/14356007.a11_141
174. Chahal KK, Bhardwaj U, Kaushal S, Sandhu AK (2015) Indian J Nat Prod Resour 6:251–260
175. Mallavarapu GR, Syamasundar KV, Ramesh S, Rao BRR (2012) Nat Prod Commun 7:223–225
176. Zhu Z, Zhang W, Pranolo Y, Cheng CY (2012) Hydrometallurgy 127:1–7. doi:10.1016/j.hydromet.2012.07.001
177. Wellens S, Goovaerts R, Moeller C, Luyten J, Thijs B, Binnemans K (2013) Green Chem 15:3160–3164. doi:10.1039/c3gc41519h
178. Kauffman GB, Adams ML (1989) J Chem Educ 66:166–167
179. Bhave NS, Dhudey SR, Kharat RB (1978) Sep Sci Technol 13:193–199. doi:10.1080/01496397808057101
180. Mohammad A, Iraqi E, Sirwal YH (2003) Sep Sci Technol 38:2255–2278. doi:10.1081/ss-120021623
181. Khuhawar MY, Soomro AI (1992) J Chem Soc Pak 14:206–212
182. Toyota E, Itoh K, Sekizaki H, Tanizawa K (1996) Bioorg Chem 24:150–158. doi:10.1006/bioo.1996.0013
183. Mirza MA, Khuhawar MY, Arain R, Choudhary MA, Kandhro AJ, Jahangir TM (2013) Asian J Chem 25:3719–3724
184. Loonker S, Sethia JK (2009) Bul Chem Commun 41:19–22
185. Vlacil F, Khanh HD (1980) Fresenius Z Anal Chem 302:36–39. doi:10.1007/bf00469760
186. Barrera NM, McCarty JL, Dragojlovic V (2002) Chem Educ 7:142–145. doi:10.1007/s00897020559a
187. Winter A, Thiel K, Zabel A, Klamroth T, Poppl A, Kelling A, Schilde U, Taubert A, Strauch P (2014) New J Chem 38:1019–1030. doi:10.1039/c3nj01039b
188. Ruhlandt-Senge K, Müller U (1990) Z Naturforsch B 45:995–999
189. Piecha-Bisiorek A, Bienko A, Jakubas R, Boca R, Weselski M, Kinzhybalo V, Pietraszko A, Wojciechowska M, Medycki W, Kruk D (2016) J Phys Chem A 120:2014–2021. doi:10.1021/acs.jpca.5b11924
190. Altshuller AP, Everso HE (1953) J Am Chem Soc 75:1727
191. Cholico-Gonzalez D, Avila-Rodriguez M, Reyes-Aguilera JA, Cote G, Chagnes A (2012) J Mol Liq 169:27–32. doi:10.1016/j.molliq.2012.03.002
192. Williamson Y, Davis JM (2005) Electrophoresis 26:4026–4042. doi:10.1002/elps.200500245

Top Curr Chem (Z) (2017) 375:25
DOI 10.1007/s41061-017-0110-2

REVIEW

Proteins in Ionic Liquids: Current Status of Experiments and Simulations

Christian Schröder[1]

Received: 9 November 2016 / Accepted: 18 January 2017 / Published online: 7 February 2017

Abstract In the last two decades, while searching for interesting applications of ionic liquids as potent solvents, their solvation properties and their general impact on biomolecules, and in particular on proteins, gained interest. It turned out that ionic liquids are excellent solvents for protein refolding and crystallization. Biomolecules showed increased solubilities and stabilities, both operational and thermal, in ionic liquids, which also seem to prevent self-aggregation during solubilization. Biomolecules can be immobilized, e.g. in highly viscous ionic liquids, for particular biochemical processes and can be designed to some extent by the proper choice of the ionic liquid cations and anions, which can be characterized by the Hofmeister series.

Keywords Direct and reversed Hofmeister series · Ionic liquid · Crystallization · Solubility · Extraction · Separation · Detection · Stabilization · Denaturation

1 Introduction

In contrast to common solvents, each ionic liquid intrinsically consists of two species, cations and anions, which both interact with the solute, but often in a completely different way. This offers the possibility to tune particular interactions with the solute, e.g. hydrogen bonding to one of the species, usually the anions. However, protic ionic liquid cations are also capable of forming strong hydrogen

---

Chapter 5 was originally published as Schröder, C. Top Curr Chem (Z) (2017) 375: 25. DOI 10.1007/s41061-017-0110-2.

✉ Christian Schröder
christian.schroeder@univie.ac.at

[1] Faculty of Chemistry, Department of Computational Biological Chemistry, University of Vienna, Vienna, Austria

bonds [1, 2]. Cations or anions may possess long alkyl chains facilitating the penetration of a hydrophobic solute surface.

In addition to the competition to dissolve these solutes, cations and anions also interact quite strongly with each other via Coulomb forces due to their ionic nature. The exchange of the cationic and/or the anionic species or their modification results in drastic changes of the physico-chemical properties [3–5] such as the viscosity from 20 mPa s to several thousands of mPa s. Even while keeping the cationic or anionic species fixed and varying only the other, a large range of physico-chemical properties may still be accessible. However, most ionic liquids share low vapor pressures, low flammability, and significant thermal conductivity.

The interplay between ions gets even more complicated when mixing the ionic liquid with other liquids. By far, the most frequently used co-solvent is water due to its abundance, non-toxicity and biological relevance. However, depending on the nature of the composing ions, one or two phase systems with water are formed. Moreover, even one phase mixtures may be heterogeneous as ionic liquids are known to form micelles [6–9] or microemulsions [8–11]. The present review concentrates on the effects of the ionic liquid ions, whereas the consequences for water play only a minor role here. Excellent reviews focussing on water are Refs. [12–14].

2 From the Ionic Liquids Point of View

2.1 Polarity and Hydrophobicity

Chemical intuition tries to understand solvent effects and miscibility in terms of solvent polarity. According to Reichardt, polarity is defined as the overall solvation capability for molecules, including specific and non-specific interactions [15]. This rather general definition is the reason why single parameter polarity scales are often insufficient to map all interactions promoting or prohibiting solvation on a single value. Consequently, some solvation aspects are described in one solvation scale better than in the others [15, 16].

The non-specific electrostatic interactions in a liquid can be measured by dielectric spectroscopy [17]. The static (low frequency) value of the generalized dielectric constant $\Sigma_0(0)$ measures the polarization of the liquid, i.e. the total dipole moment per volume. From the amplitude of dielectric peaks it is possible to estimate the molecular dipole moment of the corresponding species. Molecules with higher dipole moments are believed to behave more polar. The high frequency limit of the dielectric constant $\Sigma_0(\omega \rightarrow \infty) = \epsilon(\infty)$ depends on the refractive index of the liquid and hence on the polarizability per volume. Altogether, polar liquids tend to have higher dielectric constants $\Sigma_0(0)$ than apolar liquids and the corresponding values for ionic liquids are comparable to ethanol or acetone [18, 19]. Dielectric constants of aqueous mixtures depends on the occupied volume of bulk water, pressure-retarded osmosis water, and the ionic liquid [20].

The imaginary part of the dielectric spectrum of liquids with charged molecules is dominated by the static conductivity $\sigma(0)$ and, therefore, always reported in publications concerning dielectric spectroscopy. Many ionic liquids have lower conductivities than expected from their diffusion coefficients. However, this is rather due to the collective interactions of all ionic liquid ions with the other ions than to the existence of neutral ion pairs. For example, non-neutral ion aggregates (see Fig. 1a) also reduce the number of charge carriers and consequently the conductivity. These aggregates with more than two ions are already possible at moderate concentrations for simple, atomic, and small inorganic ions [14]. For example, at 1 mol L^{-1}, 20–30% of the ions in an aqueous solution of K[SCN] form cluster with an average size of two or three anions [14]. As ions tend to be less homogeneously distributed in ionic liquid mixtures compared to these simple ions, the concentration threshold is even lower in ionic liquids.

As depicted in Fig. 1a, clusters involving several contacts of cations are quite common even for short alkyl chains [2, 14, 21]. The non-specific dispersion interaction (gray area) between the alkyl chains is in this case stronger than the Coulombic repulsion (denoted by the black arrow). Of course, strong Coulombic attractions exist between cations and anions (also denoted by the corresponding arrow). In aqueous mixtures, water interacts with the ions and hence decreases the Coulomb attraction between the ions. However, this weakening does not necessitate that water molecules become interstitial [22] but dielectric measurements revealed that solvent assisted ion pairs (see Fig. 1b) are much more common than direct contact ion pairs/aggregates [12, 17, 23, 24]. The "solvent assistance" was explained by Robinson and Harned as "localized hydrolysis" $\ominus \cdots H^{\delta+} \cdot OH^{\delta-} \cdots \oplus$ [12, 25].

Based on solvatochromic studies another single-value scale of the polarity are E_T^N-values by Reichardt and co-workers [15, 26], which also characterize ionic liquids as polar as lower alcohols [15, 26–28]. A complementary polarity scale is offered by the Kamlet–Taft parameters [29]: here, dipolarity parameter (π_{KT}) reflects the polarity of the solvent. It is measured by transition from ground to excited state of various dyes. As these states are stabilized by solvent dipoles and polarizabilities, the measured fluorescence shift should correlate with the solvent polarity. However, π_{KT} strongly depends on the nature of the dye and is, therefore,

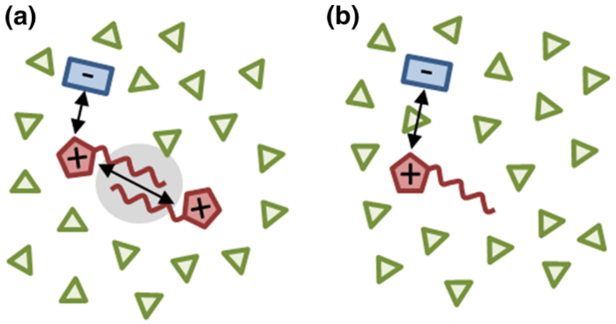

Fig. 1 Ionic liquids in aqueous mixtures (cations in *red*, anions in *blue,* and water molecules in *green*): **a** ion aggregates and **b** solvent shared ion pairs. The *arrows* indicate strong Coulomb interactions and the *gray area* shows strong dispersion forces

of reduced relevance. In addition to this non-specific interaction parameter, the Kamlet–Taft scale also characterizes local, specific interactions as the Kamlet–Taft parameter α_{KT} and β_{KT} reflect hydrogen bond donor and acceptor capabilities. The hydrogen bond acidity (α_{KT}) is mainly determined by the ionic liquid cations. Protic cations like ethylammonium have higher α_{KT}-values than aprotic cations like imidazoliums indicating better hydrogen bond donor capabilities. The hydrogen bond basicity (β_{KT}) reflects the hydrogen bond acceptor capabilities. In particular, acetate and chloride based compounds excel the other ionic liquids [29] and explain to some extent the important role for cellulose treatment [30, 31].

Hydrophobicity is a more narrow concept of polarity [32] as it characterizes the absence of favorable interaction of the solvent to water. It can be measured by the partition coefficient $\log P$ in octanol/water mixtures. High $\log P$ values indicate hydrophobic solvents. For example, hexane has a $\log P$ value of 3.5. However, 1-butyl-3-methylimidazolium acetate, nitrate and hexafluorophosphate have extremely low $\log P$ values of -2.8, -2.9 and -2.4 indicating they are much more polar than ethanol, which has $\log P = -0.24$. The $\log P$ value increases with increasing cationic alkyl chain length as expected [33].

Although hydrophobic solvents are suggested to be more favorable for enzymatic reactions [34], which was also reported by [35], protein stability may decrease with rising hydrophobicity [33, 36]. Russell and co-workers [37] could not correlate $\log P$ values with the enzyme activity and argued that the anion is responsible for the reactivity, which points to nucleophilicity or hydrogen bond basicity [32].

2.2 Anionic Hydrogen Bonding and Cationic Surfactant Effects

1-butyl-3-methylimidazolium chloride [C_4mim]Cl dissolves cellulose [38–40] since chloride wins the hydrogen bonding competition for cellulose OH-groups versus the intramolecular hydrogen bond network. In a molecular dynamics study of 1,3-dimethylimidazolium chloride [C_1mim]Cl, Youngs et al. also reported that hydrogen bonds of chloride to the hydroxy groups of the carbohydrate dominated the solvation interaction [41, 42]. Armstrong and co-workers showed that the high hydrogen bond basicity is a key factor to dissolve complex polar biomolecules [43, 44]. Since hydrogen bonding is the central topic of another chapter by Patricia Hunt in this book, we will restrict our discussion to aqueous mixtures of ionic liquids.

Hydrophilic ionic liquids usually consist of small anions, which can be easily implemented in the three-dimensional water network of hydrogen bonds. However, this effect of the ions is very local since femtosecond mid-IR pump-probe spectroscopy showed that only the structure of water in direct contact with the ion is influenced [45] and the effect on further solvation shells of the ion is negligible. We showed [22] that hydrophilic anions act as mediator between the more hydrophobic imidazoliums and water, which was confirmed by other authors [21, 46–49]. If the hydrogen bonded anion-water network is very strong, cations are expelled to some extent. Even at short alkyl chain lengths they may form clusters or structures similar to micelles as sketched in Fig. 2, which are held together by significant dispersion forces of the alkyl chains (gray area). Additionally, these aggregates also minimize

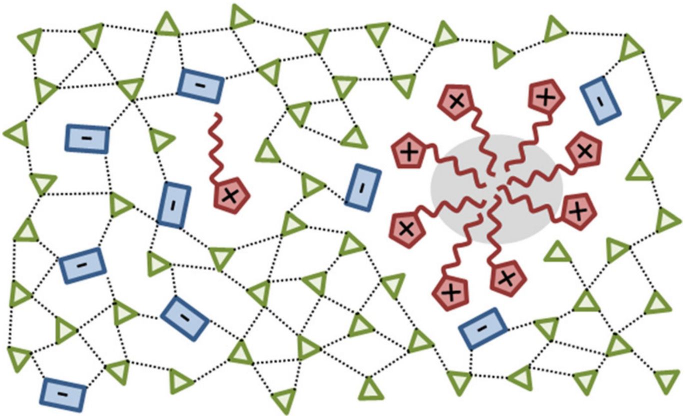

Fig. 2 The sketch of an aqueous mixture of aprotic ionic liquids shows anion-water networks and cationic micellar-like structures

the disturbance of the three dimensional water network because the multiple hydration of single ionic liquid cations would do much more damage to the network than the inclusion of one bigger aggregate. Such water network forces were reported by several groups [12]. The segregation into polar and apolar domains for pure ionic liquids [2, 50] and in aqueous mixtures [21] is accepted in the ionic liquid community. Consequently, the cations may accumulate at the apolar domains of proteins as well [51]. The longer the cationic alkyl chain gets, the stronger is the respective surfactant effect, which affects the stability and activity of the proteins [9, 33, 52].

2.3 Hofmeister Series

Concerning biomolecular solvation, the so-called Hofmeister series provides a new scale to the solvation properties of ions. In 1888 Franz Hofmeister ranked several inorganic ions for their effectiveness in egg white protein precipitation. Sharing the same cation, the protein solubility increased in aqueous solutions in the following manner [53, 54]:

$$SO_4^{2-} < HPO_4^{2-} < F^- < CH_3COO^- < Cl^- < Br^- < NO_3^- < I^- < ClO_4^- < SCN^-$$

However, this ranking is also used to predict protein stability in aqueous electrolyte solutions. Unfortunately, depending on the solvent conditions and the protein under investigation, the ranking is partially or even completely reversed as one may easily conduct from the plethora of rankings displayed in Ref. [55]. In order to bring some light into this confusion, we start with the underlying definitions and concepts of the Hofmeister series before jumping into its application in protein science (see Sect. 3).

A tentative Hofmeister series based on the information of Refs. [54–59] is depicted in Fig. 3 using the cation 1-butyl-3-methylimidazolium. At first sight, the Kamlet–Taft dipolarity parameter π_{KT} and hydrogen bond acidity or donor

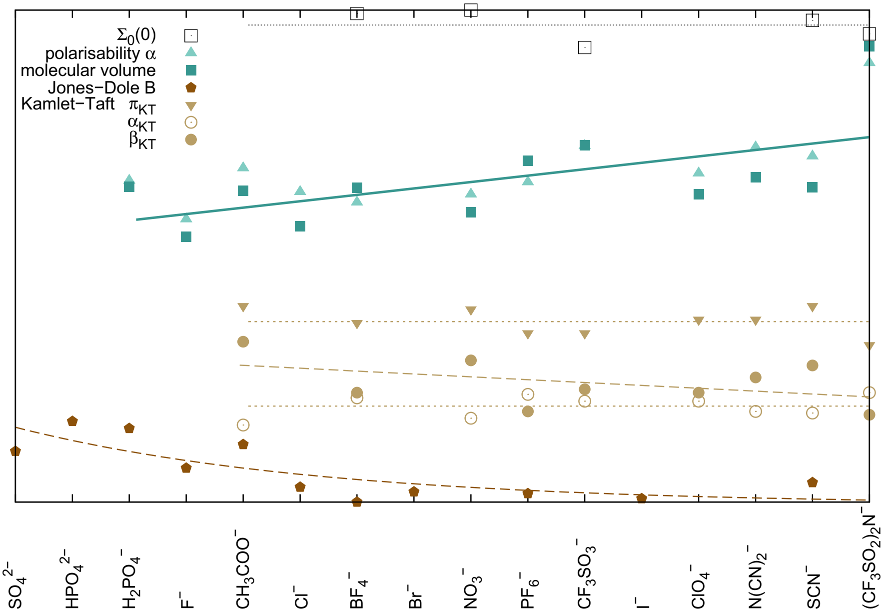

Fig. 3 Tentative Hofmeister series (kosmotropic anions on the *left* and chaotropic anions on the *right*) including typical ionic liquid anions and their dependence on various physico-chemical descriptors (normalized and constantly shifted values). *Dashed* and *solid lines* represent decreasing and increasing trend, respectively

capability α_{KT} show no trend in Fig. 3, which is not astonishing as the cation usually plays the major role for these descriptors in case of ionic liquids. The decreasing Kamlet–Taft hydrogen bond accepting capability β_{KT} is also expected as kosmotropes should be more interested in hydrogen bonding than chaotropes.

Interestingly, the static dielectric constant $\Sigma_0(0)$, as well as the Reichardt's polarity parameter E_T^N (data not shown) do not systematically change from kosmotropic to chaotropic anions. In contrast, the polarizability α increases emphasizing the increasing importance of dispersion forces. Since the polarizability correlates with the molecular volume V, the same trend is also observed for V.

2.3.1 Kosmotropic and Chaotropic Ions

Protein stability and solubility depends on its interface with the solvent. In addition to particular interactions of single cations and anions with distinct amino acids at the protein surface, the ionic impact on protein solubility is attributed to modifying the water structure and hence the protein hydration. Ions, which strongly interact with water, are called "kosmotropic" (Greek *kosmos* = order) or "structure-making". In contrast, if the interaction with water is weak, the ions act "chaotropic" (Greek *chaos* = disorder) or "structure-breaking" [60]. The basic characteristics of kosmotropes and chaotropes are summarized in Table 1. The concept of structure-making and breaking on larger dimensions was disproved by spectroscopy [45] and

Table 1 Characteristics of kosmotropes and chaotropes adapted from [57] and including results from Fig. 3

	Kosmotropes	Chaotropes
Size	Small	Large
Hydration	Strong	Weak
Hydrogen bonds	Many	Few
Dispersion	Weak	Strong
Polarizability	Low	High
Charge density	High	Low

thermodynamic considerations [61], which showed that the influence of a central ion on the surrounding water structure is restricted to the first hydration shell and the impact on further water shells is quite small. Nevertheless, even if the effect of the ion is limited to its direct environment, the degree of hydration or hydrogen bonding may have consequences for the solvent properties. Looking at Fig. 2 again, many typical ionic liquid anions like tetrafluoroborate, triflate, or acetate show kosmotropic behavior whereas imidazoliums act more and more chaotropic when prolonging the alkyl side chains.

2.3.2 Law of Matching Water Affinities

Collins introduced the law of matching water affinities [62–64], which basically states that kosmotropic cations form ion pairs with kosmotropic anions and chaotropic cations with chaotropic anions, whereas ion pairs of mixed type do not exist, as shown in Fig. 4. In this simple volcano plot, the difference of the hydration energy of the anions and cations is correlated with the solution enthalpy of the ionic liquid. Kosmotropic anions (blue boxes without a tail) should be better dissolved in water than chaotropic cations (red pentagons with tail). As a result, $\Delta\Delta H_{\mathrm{hyd}} = \Delta H^{\ominus}_{\mathrm{hyd}} - \Delta H^{\oplus}_{\mathrm{hyd}}$ is quite negative and the dissociated pair can be found at the left part of Fig. 4. The existing Coulombic interaction between these ions is not strong enough to keep the ion pair configuration in water as visible by $\Delta H_{\mathrm{solv}} < 0$. As a

Fig. 4 Law of matching water affinity by Collins adapted from Ref. [62] applied to the case of ionic liquids. ΔH_{solv} is the enthalpy of solution and $\Delta\Delta H_{\mathrm{hyd}}$ the difference of the hydration enthalpy of the anions and the cations. Kosmotropic and chaotropic ions are depicted with and without an alkyl chain, respectively. Ion pairs in aqueous solution are only expected above the *dotted line* since their dissociation in water is favorable at negative ΔH_{solv}

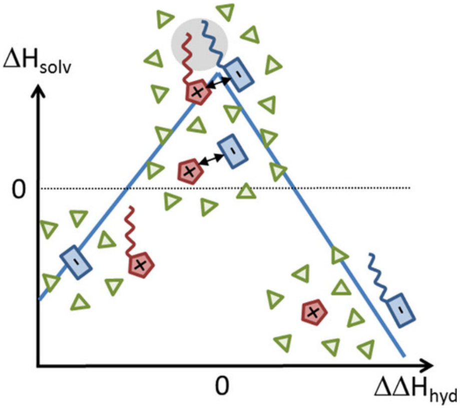

consequence, the anion will hydrogen bond to water, expelling the cations from the anion-water network. Kosmotropic cations and kosmotropic anions possess similar hydration enthalpies and $\Delta\Delta H_{\text{hyd}} \simeq 0$. Their strong Coulombic interaction may survive in water keeping the ions together [65]. However, the strongest interaction between cations and anions exists if both are chaotropic. Here at $\Delta\Delta H_{\text{hyd}} = 0$, the Coulombic interaction is accompanied by strong dispersion forces. The hydrophobic tails also make these ions less attractive for water which will not penetrate the ion pair. Combining a kosmotropic ion like Li^+ with a chaotropic anion like octylsulfate ($\Delta\Delta H_{\text{hyd}} > 0$) will also result in a weak ion pair dissociating in water. However, the situation described here concerns the bulk phase of the solvent. Chaotropic ions expelled from the hydrogen bond network may act as surfactants for the dissolved protein.

2.3.3 Determination of Kosmotropic/Chaotropic Character

For simple classical ions, the kosmotropic or chaotropic character in aqueous solution can be related to the relative viscosity

$$\frac{\eta}{\eta_0} = 1 + A\sqrt{c} + B \cdot c \tag{1}$$

describing the current viscosity η with a salt concentration of c with respect to the pure solvent viscosity η_0 [58, 62]. The Falkenhagen A-coefficients depend on the electrostatics of the system and are usually small [54], whereas the B coefficients are ion specific and called Jones–Dole coefficients. Because of their strong interaction, kosmotropic ions hinder the motion of water and, therefore, increase the viscosity η resulting in a positive B value. Chaotropic solutes should have negative B values. Table 2 shows some Jones–Dole B values of cations and anions and their kosmotropic/chaotropic assignment by Zhao [58]. Despite some minor issues concerning the anions, the assignment is quite questionable for ionic liquid cations. Many cations with long alkyl chain are claimed to be kosmotropic because of their positive B values. Although the high viscosities may be partially due to hydrophobic hydration [58] (and hence some interaction between the cation and water), much more importantly the viscosity rises because of adding a more viscous ionic liquid to the more fluid water. A significant source of the increased viscosity of ionic liquids are the dispersion forces in the apolar domains. Quite intuitively, prolonging the alkyl side chain should make the cation more hydrophobic and consequently less interactive with water but maybe more interactive with hydrophobic protein surfaces [53]. However, since many authors use the kosmotropic/chaotropic assignment based on B values, their cationic Hofmeister series shows a reversed effect [54, 55, 57]. We will stick to the simple characterization in Table 1 (as also suggested by Collins [62]) for further discussion here and concentrate on the effect of the anions in order to avoid confusion.

Table 2 Experimental Jones–Dole *B*-coefficients [58]

cation	B [L mol^{-1}]	anion	B [L mol^{-1}]
N^+_{1111}	0.123	SO_4^-	0.206
N^+_{2222}	0.385	HPO_4^{2-}	0.382
N^+_{3333}	0.916	$H_2PO_4^-$	0.340
N^+_{4444}	1.275	F^-	0.107
N^+_{5555}	1.149	CH_3COO^-	0.246
C_1py^+	0.144	Cl^-	-0.005
C_2py^+	0.228	Br^-	-0.33
C_4py^+	0.396	BF_4^-	-0.093
C_2mim^+	0.491	NO_3^-	-0.043
C_4mim^+	0.610	PF_6^-	-0.210
Al^{3+}	0.744	I^-	-0.073
Mg^{2+}	0.385	SCN^-	0.022
Li^+	0.146		
Na^+	0.085		
K^+	-0.009		

The degree of gray shading imply a stronger chaotropic character based on the considerations by Zhao. The values of the imidazoliums are calculated on the basis of an empirical equation instead of a measurement

2.3.4 Impact of Ion Concentration

Regardless of the definition of kosmotropy/chaotropy, the Hofmeister ranking characterizing the protein solubility faces another problem: in 1932, Green [66] reported that the solubility of proteins in the presence of added salts, S, and without salt, S_0, followed the ionic strength I in a bell-shaped manner

$$\log \frac{S}{S_0} = \frac{1}{2} \frac{z_1 \cdot z_2 \sqrt{I}}{1 + A\sqrt{I}} - K_s \cdot I \qquad (2)$$

with the ion valences z_1 and z_2 and a characteristic salt coefficient K_s. Although K_s seems to increase with the ion volume [53] and hence chaotropic ions are expected to decrease the protein solubility, an actual Hofmeister ranking of ions depends on the ion concentration as the maximum solubility in a particular electrolyte shifts for each investigated salt. Therefore, ions may switch their position in the Hofmeister series when changing the salt concentration.

3 Through the Eyes of the Protein

Despite all the issues concerning the “correct” ranking of the ions, the concept of a Hofmeister series is often used in the literature and has proven to be valuable to explain trends for the interaction with proteins [54, 55, 67, 68] in various fields of applications as sketched in Fig. 5 and discussed in the following sections. Wang and co-workers [70] pointed out that this particular research field is quite young, but is attracting enormous interest in chemical, food, and pharmaceutical industries. Although not taking into account all publications concerning the interactions of ionic liquids with proteins they concluded that the overwhelming number of publications (see Fig. 5) deal with protein stability in the various ionic liquid environments. Ionic liquids are able to promote or prevent denaturation (which may result in (un-)wanted fibrillation of the protein). It is also possible to activate enzymes with ionic liquids for particular reactions. Other scientific areas concern the solubility (which may be used for the crystallization) and the separation of proteins (from extraction to their detection). All these topics are discussed within the next sections with a special emphasis on protein peculiarities and their impact on the Hofmeister series.

3.1 Protein Solubility

The vast majority of protein solubility studies concerns aqueous solutions or water mixtures with various co-solvents. Although it is possible to dissolve amino acids [71, 72] and protein in pure ionic liquids [73, 74], aqueous mixtures are preferred because of higher solubilities and/or increased stabilities of the biomolecule, as well as reduced costs.

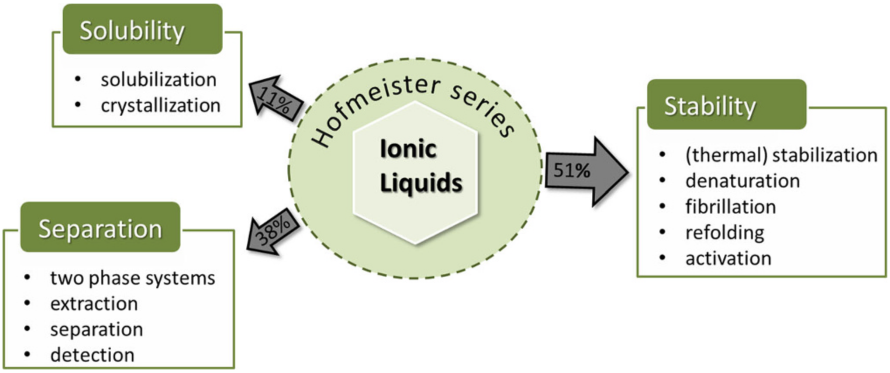

Fig. 5 Protein applications of ionic liquids and their percentage of publications in the last decade (adapted from Refs. [69, 70])

3.1.1 At the Protein Surface

Because of their different hydrophobic/hydrophilic/amphiphilic character, water and ionic liquid ions interact with the non-polar, polar, and charged surface areas of proteins in their own specific way resulting in an accumulation or depletion at these different regions as depicted in Fig. 6. Several simulations show that the concentration of cations exceeds that of anions at the protein surface irrespective of the protein charge [51, 75, 77–80]. This can be rationalized by the hydrogen-bonded network of the anions and water in the bulk phase (see Fig. 2 [51, 81]). Since the cations are not able to contribute to this network in the same manner, they are expelled and forced to the surface of the other hydrogen bond network violator, i.e. the protein.

Another protein solvation aspect is the strong amphiphilic character of most ionic liquid cations. Long alkyl chains attached to the "charge center" offer apolar regions with increased dispersion interactions (gray areas in Fig. 6), which are of significant importance [53, 82]. Here, hydrophobic solutes, like apolar amino acids, may find a favorable interaction partner. Klähn and co-workers reported that the alkyl chains prefer to point towards the non-polar protein surface in this case [83]. Water molecules arrange themselves in a quasi-crystalline structure (often termed "iceberg"). As a result, this hydrophobic solvation decreases the water entropy at the surface of the protein compared to bulk water [60]. However, "iceberg" models have been questioned by several groups (see [13] for details).

Since the cations are also a charged species, they compete with the anions for favorable solvation sites at the polar protein surface. The majority of cationic alkyl chains now point away from the protein surface [83]. Of course, the negatively charged amino acids attract more cations than anions, but they still are in competition with water molecules (green triangles in Fig. 6), which may form hydrogen bonds to the surface amino acids in contrast to the cations. The approach of cations to the positively charged protein surface is not excluded per se since cationic charge densities are low and is also enabled by the close-by anions at the protein surface.

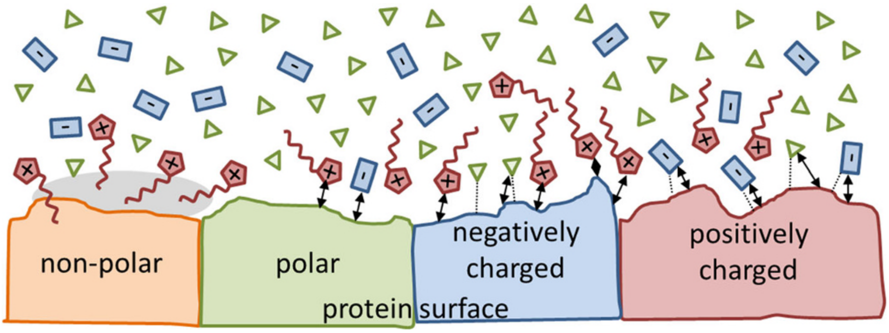

Fig. 6 Sketch of the interactions (*dotted lines* hydrogen bonding, *gray areas* dispersion, and *arrows* strong Coulomb interaction) of the solvent species with the protein surface at higher ion concentrations (adapted from [51, 75, 76])

The (hydrophilic) anions seem to prefer the positively charged surface as they try to establish hydrogen bonds to lysine, arginine, or histidine (if positively charged) [44] and show strong Coulomb interaction with these amino acids due to their high charge density. Overall, the Coulombic interaction of the anions with the protein is stronger compared to the cations resulting in a longer residence time of that molecule near the respective amino acids [75, 78]. The cations are quite mobile at the non-polar and polar protein surface and only show increased residence times in the proximity of glutamic and aspartic acid. This cationic mobility may be also a reason that active protein sites are visited more by cations than anions [75].

Both cations and hydrophilic anions usually interact stronger with the protein than water and hence remove water from the protein surface with increasing ionic liquid concentration [71, 75]. Here, the impact of the anion seems to be more important [71]. However, the water removal may have positive and/or negative consequences for the protein solubility [84]. Hydrophobic ionic liquids may form two phase systems with water resulting in less depletion of water molecules from the protein surface and hence an increased protein solubility [85, 86].

3.1.2 Following the Hofmeister Series

In addition to these surface effects, the Hofmeister series discussed in the last chapter concerns the impact of the ions on the bulk water structure that influences the water structure at the protein surface. A significant correlation between water-water hydrogen bonding and the experimental solubility data for hydrophobic solutes was found in computer simulations [87] as expected by the Hofmeister effect. Quite generally, the term "salting in" refers to the effect at moderate ion concentrations up to $1\,\mathrm{mol\,L^{-1}}$ that increasing ionic strength of a solution enhances the solubility of the proteins. Looking at the Hofmeister series, the protein solubility increases with the chaotropic character of the anions [82, 88] and results in an opposite "salting-out" effect for strong kosmotropic anions like phosphate and sulfate [53, 82]. MD simulations [89] showed that the reduction of hydrophobic interactions leads to salting-in and may be entropic and/or enthalpic whereas the salting-out induced by kosmotropes is purely an enthalpic effect. However, one has to keep in mind that "salting-in" and "salting-out" also depend on the nature of the protein [60, 90, 91] since they are not homogeneous in charge, hydrophilicity/hydrophobicity, as well as secondary and ternary structure [53]. Netz and co-workers pointed out that the Hofmeister prediction is (more or less) valid for negatively charged proteins whereas the reversed order may be more appropriate for neutral or positively charged proteins [90, 91]. This reversed Hofmeister series seems to be "the rule rather than the exception" for the small inorganic cations and anions [91].

3.1.3 Protein Crystallization

However, high protein solubilities are not always desirable since (more or less) controlled precipitation and protein crystallization in good quality are worthwhile for X-ray structure determinations [92]. Usually, at high ion concentrations, the protein solubility drops significantly and the protein precipitates. This process can be used for the separation of proteins to get purer crystals since the necessary salt concentration depends on the nature of the protein. In particular, due to their manifold and "tunability" ionic liquids attracted interest as co-solvents for protein precipitation and crystallization since 1999 when Garlitz and co-workers reported on lysozyme crystallization modified by ethylammonium nitrate [93]. Judge et al. reported that various proteins (lysozyme, catalase, myoglobin, trypsin, glucose isomerase, and xylanase) grow crystals of larger size with ionic liquids as co-solvent, which provide a better X-ray diffraction resolution [92]. However, the impact of ionic liquids on the crystallization process is more pronounced than for precipitation [92, 94]. Several authors report on less crystal polymorphism and improved tolerance to concomitant impurities during crystallization [94–99].

Peter Nockemann and co-workers noticed that increasing the concentration of the ionic liquid (regardless of the Hofmeister character) results in a reduction of crystal nucleation density and improved crystal quality [76]. Choline based ionic liquids showed less efficiency than imidazolium based ionic liquids and prolonging the cationic alkyl chain length in the imidazolium salts improved the efficiency. However, the concentration dependence observed by Green [66] and discussed in the Hofmeister Sect. 2.3.4 was also observed for ionic liquids [76]. Electrostatic forces play the major role at low ion concentrations and the specific impact of the ion correlates with their screening of the protein surface charges to reduce the repulsion between like-charged biomolecular regions and hence promotes protein aggregation. He also pointed out that the dehydration of the anions is important for the binding to the protein surface, i.e. the anion-water network in Fig. 2 has to be overcome making kosmotropic anions less effective. Cations may have the opposite effect since the binding to non-polar residues (cf. Fig. 6) counteracts the previously discussed effect and reduce the interfacial tension promoting protein-solubility. As a result, ions, which bind to the protein surface and screen the surface charges at low concentration promoting salting-out, induce salting-in at higher concentrations by remaining hydrated at the protein surface.

3.2 Separation of Proteins

The separation of target protein accounts for 50–80% of its total production costs [100, 101] and the tunability of ionic liquids has been exploited in this context [100–108]. Also, the recovery and purification of enzymes from bioreaction media gained importance because of a increasing demand for biotechnologically manufactured fine chemicals and biomolecules [105].

In principle, the pure ionic liquid or its mixture with water may be used to dissolve the proteins. However, in pure ionic liquids most proteins are dispersed, but not homogeneously dissolved [102, 107, 109, 110]. Furthermore, pure ionic liquids may denaturate the protein (which will be discussed in the next Sect. 3.3) as they need water to maintain their natural structure and function.

Aqueous mixtures of ionic liquids can also be decomposed in "hydrated ionic liquids" (high ion concentrations) and electrolyte like solutions (low ion concentrations), which have different solvation properties for a particular protein. Furthermore, these solutions may also change their solvation behavior as a function of temperature offering a nice route to extraction and separation by precipitation [107].

3.2.1 Two-Phase Systems

The largest area of ionic liquid application for extraction and separation of proteins are two-phase systems: Of course, hydrophobic ionic liquids form two phases with water. However, these hydrophobic ionic liquids are usually more expensive and viscous than hydrophilic ionic liquids and may denature proteins [106]. Rogers and co-workers [111] were the first to report on two-phase systems with hydrophilic ionic liquids at certain concentrations overcoming the limitations mentioned above. The aqueous phase usually contains K_2HPO_4. The kosmotropic anion interacts stronger with water than the interaction between water molecules. The water-hydrogen bond network is therefore enhanced resulting in a stronger expelling of the cations (see Fig. 2). Various salts including K_3PO_4, K_2CO_3, K_2SO_4 , and others also have been tested [112] but K_2HPO_4 combined a high solubility in water with an excellent ability to promote phase separation with the ionic liquid. These two-phase systems are distinguished by their protein selectivity, robustness, short processing time, low energy consumption and easy scale up opportunities [108, 113]. Cation [101] and anion [104] effects have been studied by the Coutinho group. As expected, long alkyl chains attached to imidazoliums promote phase separation and partitioning [100, 101]. Inserting double bonds, benzyl or hydroxyl groups leads to less efficiency. Kragl and co-workers [105] reported a strong correlation between the protein charge and the partition behavior and suggested that electrostatic interactions at the protein surface with the cations are the major driving force of protein partitioning in the two phases. The efficiency of the two phase system also follows the Hofmeister series for the anions [104, 106].

The extraction efficiency seems to increase with increasing temperature indicating an endothermic process [100]. The enthalpic $\Delta H^0_{\mathrm{ILphase}}$ and entropic change $\Delta S^0_{\mathrm{ILphase}}$ associated with the protein partitioning measured by the Gibbs energy $\Delta G^0_{\mathrm{ILphase}}$ is obtained from the partitioning coefficient K

$$\Delta G^0_{\mathrm{ILphase}} = -RT\ln K = \Delta H^0_{\mathrm{ILphase}} - T\Delta S^0_{\mathrm{ILphase}} \tag{3}$$

as a function of temperature. Both $\Delta H^0_{\mathrm{ILphase}}$ and $\Delta S^0_{\mathrm{ILphase}}$ are positive for the transition of the protein bovine serum albumin from the K_2HPO_4 to the ionic liquid rich phase. However, the overall $\Delta G^0_{\mathrm{ILphase}}$ is negative since $T\Delta S^0_{\mathrm{ILphase}}$ exceeds $\Delta H^0_{\mathrm{ILphase}}$. The importance of entropic effects indicate the major role of hydrophobic interactions [100, 108].

3.2.2 Protein Detection

However, ionic liquids are not only advantageous for extraction and separation, but also for the detection of particular proteins. Traditional capillary electrophoresis for protein separation results in broadened bands and low protein recovery. Dynamic coating of the capillary with imidazolium-based ionic liquids suppress protein adsorption and generates an anodic electroosmotic flow [114–116]. A recent review [117] summarizes the current status of capillary electrophoresis. Furthermore, the vacuum stability of ionic liquids and their solvation properties is also beneficial for ionic liquid matrices in matrix-assisted laser desorption/ionization mass spectrometry (MALDI) [118]. Particularly, ionic liquid matrices promote sample homogeneity, increase ion peak intensities, and lower detection limits compared to conventional solid matrices [119].

3.3 Protein Stability

Proteins are a particularly heterogeneous class of biological macromolecules. For their functioning, it is very important to maintain their secondary structure, i.e. α-helices, β-sheets, and coil regions. These structural elements are held together via a complex balance of hydrogen bonds, disulfide bridges, hydrophobic and ionic interactions. In most of these interactions solvent molecules participate or compete with the involved amino acids. Consequently, changing solvent conditions like viscosity, pH value, buffer conditions, addition of (ionic) co-solvents, and temperature has a severe impact on the secondary structure of the protein. The influence of solvent viscosity differs from the other solvent conditions since higher viscosities decelerate the overall dynamics of the solvent and the dissolved protein, mimicking higher protein stability within the observed time window [16, 77, 120]. However, the viscosity η is a central solvent property.

3.3.1 Gibbs Free Energy of Unfolding

The pH value of the solvent and the presence of ions are important for the Coulomb interactions of the solvent with the protein. The preferred protonation state of the amino acids within the protein changes significantly with the pH and the buffer conditions thereby changing the character of the local protein surface from polar to charged or back (changing also the protein preference for solvent molecules depicted in Fig. 6). As a function of ion concentration, these amino acids will have stronger or weaker interactions with the solvent contributing to stabilization enthalpy. The temperature, on the other hand, and the exchange of water, cations, and anions at the surface of the protein govern the entropic contributions.

In fact, native protein structure is only marginally stable as visible by the slightly positive Gibbs free energy of unfolding [68]

$$\Delta G_{\text{unfolding}} = \Delta H_{\text{unfolding}} - T \cdot \Delta S_{\text{unfolding}} \tag{4}$$

describing the transition from the native to an unfolded state. The low value of $\Delta G_{\text{unfolding}}$ is based on the mutual compensation of significant enthalphic

($\Delta H_{\mathrm{unfolding}}$) and entropic ($\Delta S_{\mathrm{unfolding}}$) contributions [68], which can be shifted by adding co-solvents like ionic liquids. For example, choline dihydrogen phosphate stabilizes cytochrome c [110, 121] and lysozyme [122] for months. Brogan and Hallett [73] reported on the freeze-drying properties of 1-butyl-1-methylpyrrolidinium salts. Overall, the protein storage lifetime ranges from a few days to more than a year depending on the nature of the protein and its environment [110, 123, 124].

Ionic liquids may shift the subtle balance of $\Delta H_{\mathrm{unfolding}}$ and $\Delta S_{\mathrm{unfolding}}$ in one or the other direction resulting in denaturing [56, 125–131] or refolding/stabilizing of the protein [33, 109, 123, 126, 132–135]. In principle, the native protein structure and the (partially) unfolded state of the protein are in a reversible equilibrium (Fig. 7, [124, 134, 136]). This unfolding/refolding equilibrium is disturbed by an irreversible protein aggregation followed by fibrillation which completely deactivates the protein. The protein aggregation can be hindered by ionic liquid as co-solvents [132, 137, 138] protecting the hydrophobic parts of the protein surface. The cations seem to cover these hydrophobic areas and suppress interprotein accumulation.

However, ionic liquids can also be applied to enhance the activity of the native protein. This area of applications is reviewed elsewhere [16, 32, 57, 113] in more detail and only briefly summarized here: they may chemically modify the protein or stabilize a (genetic) protein modification or immobilize the protein at a surface for chemical reactions [32]. Because of their tunable properties, particular ionic liquids are capable to selectively solubilize reactions and/or products, which offers in two-phase systems better product separation and improved recoverability of the catalyzing protein (as discussed in the Sect. 3.2). Ionic liquids also influence the enantioselectivity of reactions [55].

In contrast to classical polar organic solvents some polar ionic liquids seem to activate particular proteins [32, 113, 120, 139], whereas the activity of another enzymes is diminished [32, 37, 113, 140]. One has to bear in mind that reaction

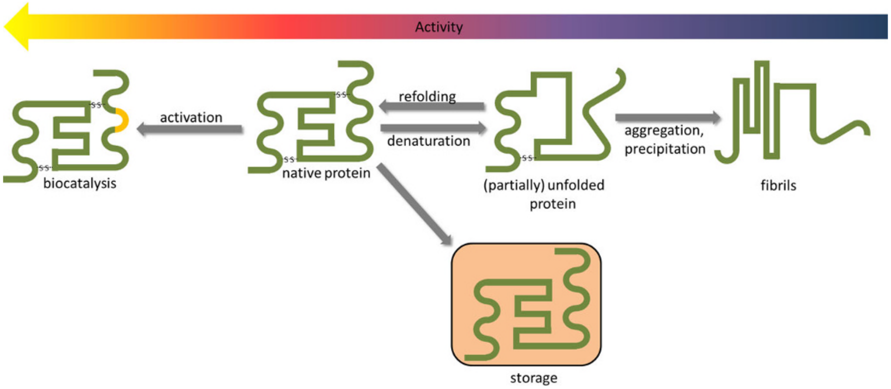

Fig. 7 The protein activity depends on secondary structure. Ionic liquids may be used to activate particular amino acids, to store proteins for longer time periods, to help refolding and to prevent aggregation

rates in different ionic liquids are usually compared at the same amount of water. Under such conditions, solvents with higher polarity would have less water associated with the protein probably reducing the reaction rate. On the other side, the increased water content in the bulk phase reduces the viscosity and thereby increases the protein mobility [141] and hence the activity. Depending on the importance of these factors for the protein, the reaction rate increases or drops.

3.3.2 Computer Simulations

There are several experimental techniques to study the protein conformation like UV-vis, fluorescence, IR, Raman, and NMR spectroscopy, circular dichroism, tensiometry, small-angle neutron scattering, differential scanning calorimetry, and microcalorimetry are listed in [69] and references therein. Since experiments monitor only the overall effect of the ionic liquids on these topics of protein activity, protein simulations are quite useful for the interpretation of the role of particular cations and anions. The current state of the art was recently reviewed by Shaw [142]. In principle, the protein stability can be followed in molecular dynamics computer simulations in various ways:

1. Monitoring the van der Waals and Coulomb interactions

$$U = \sum_i \sum_j 4\epsilon_{ij}\left(\left(\frac{\sigma_{ij}}{r_{ij}}\right)^{12} - \left(\frac{\sigma_{ij}}{r_{ij}}\right)^{6}\right) + \sum_i \sum_j \frac{q_i \cdot q_j}{4\pi\epsilon_0 r_{ij}} \tag{5}$$

   between the protein and the solvent or within the protein. If the atom i is part of a protein and the atom j belongs to a solvent molecule, the sum above represents the protein–solvent interactions [75]. In this case, major contributions of the van der Waals part commonly stem from the interaction of the amphiphilic ionic liquid cations with the protein, whereas very strong Coulombic interactions between the ionic liquid anion and positively charged amino acids can be found. Steinhauser and co-workers [77] computed the van der Waals and Coulomb interaction within the protein as a function of the mole fraction of water in the aqueous 1-ethyl-3-methylimidazolium triflate mixture. With increasing water content, the Coulomb interaction rises whereas the van der Waals interaction decreases, which was explained by a transition from dipolar screening to charge screening and its consequences on the solvation structure. Dipolar screening describes the reduction of Coulomb attraction and repulsion by interstitial water molecules, which is quite effective due to the high dielectric constant of water. The ionic liquid ions screen the protein surface charge since these interactions are usually stronger than the attraction or repulsion between neighboring amino acids. Interestingly, the most unfavorable U was found at a mole fraction $x_{\mathrm{H_2O}}$ of 0.93, which also coincides with the lowest conservation of secondary structure.
2. Programs like DSSP [143] assign secondary structure elements to each amino acid based on the current protein coordinates from the trajectory. This way, the extension or shrinking of α-helices and β-strands can be followed during

simulations and compared to the native protein structure. Over the complete trajectory averaged stability values were compared for several mole fractions in Ref. [77] also detecting the lowest protein stability at $x_{H_2O} = 0.93$, which indicates that the stability of ubiquitin and the zinc finger is not a monotonic function of the solvent viscosity.

3. The transient root-mean-square deviation RMSD(t) of a protein is defined as

$$\mathrm{RMSD}t) = \sqrt{\frac{\sum_i \left(\mathbf{r}_i^{\mathrm{ref}} - \mathbf{r}_i(t)\right)^2}{N}} \tag{6}$$

 using the current coordinates of the ith protein atom $\mathbf{r}_i(t)$ and those values of a reference state $\mathbf{r}_i^{\mathrm{ref}}$, which is usually the protein in its native configuration. If the RMSD(t) is monitored for longer time periods one should also consider the protein rotation before applying Eq. 6.

 Growing RMSD(t) indicate that the protein moves away from its native state. It is also possible to compute RMSD(t) for particular secondary structure elements of a protein. Thus, the stability of particular α-helices and β-sheets can be characterized. For example, the increase of RMSD(t) of α-helices in serine protease cutinase when adding [C$_4$mim][PF$_6$] or [C$_4$mim][NO$_3$] was interpreted by Soares et al. [81] as an attack of the ions on the secondary structure. Klähn and co-workers [79] also detected by RMSD less stable α-helices compared to β-sheets with the same ionic liquids but in the lipase *Candida antarctica B*.

4. The radius of gyration $R_g(t)$ is also an indicator: since unfolding goes along with an increase of the protein volume, the loss of secondary structure leads to an increase of the radius of gyration

$$R_g(t) = \sqrt{\frac{\sum_i m_i(\mathbf{r}_i(t) - \mathbf{r}_{\mathrm{CM}}t))^2}{M}} \tag{7}$$

 as the protein loses its compactness and increase the average distance of the protein atom i to the proteins center-of-mass $\mathbf{r}_{\mathrm{CM}}(t)$. The sum of each atomic mass m_i is the mass of the protein M. Klähn [79] observed that the radius of gyration, the RMSD and the stability of α-helices and β-sheets followed the same trend for the investigated ionic liquids.

5. The effect of (partial) unfolding is even more prominent in the solvent accessible surface since coil regions are much more accessible by the solvent molecules than α-helices and β-strands. In Ref. [79] changes of the solvent accessible surface area coincide with the stability criteria mentioned above. However, for the zinc finger in [77] the correlation between the surface accessible area and the protein stability is detectable but not very pronounced.

All these methods aim for the (more or less) collective effect of the solvent at a mesoscopic level. The next section deals with the impact of the ionic liquid ions at the molecular level.

3.3.3 The Impact of the Ionic Liquid Ions

Weingärtner et al. [136] ranked typical ionic liquid ions in a Hofmeister series for the *ribonuclease A* stability in the following order:

$$\mathrm{N}^+_{1111}||\mathrm{chol}^+ > \mathrm{N}^+_{2222} \simeq \mathrm{C_2mim}^+ \simeq \mathrm{gua}^+ > \mathrm{C_4C_1py}^+ > \mathrm{C_4mim}^+ \simeq \mathrm{N}^+_{3333} > \mathrm{C_6mim}^+ \simeq \mathrm{N}^+_{4444}$$

with chol^+ and gua^+ being choline and guadinium respectively and

$$\mathrm{SO_4^{2-}} > \mathrm{H_2PO_4^-} > \mathrm{CH_3COO^-} > \mathrm{Cl^-}||\mathrm{EtSO_4^-} > \mathrm{BF_4^-} > \mathrm{OTf^-} > \mathrm{SCN^-} \simeq \mathrm{N(CN)_2^-} \gg \mathrm{NTf_2^-}$$

Ions on the left side of || stabilize ribonuclease, whereas the others destabilize the protein. This finding corresponds to classical Hofmeister behavior that kosmotropic ions increase and chaotropic ions decrease the protein stability [82, 144]. However, other authors argued that proteins are more stable in hydrophobic ionic liquids [75, 79, 109, 124, 145] since they keep the protein water layer intact [79, 81, 120]. The supporters of the direct Hofmeister series displayed above argue that the protein solubility in hydrophobic ionic liquids is very low and the observed stabilization of protein refers to finely dispersed proteins in a heterogeneous solvent [136].

The central role of the anions was pointed out by several computational studies [77–79, 81]. Although the concentration of cations seems to be usually higher than that of the anions [51, 77–79], the mean residence time of the anion at the surface [77] is much longer due to the strong Coulomb and hydrogen bonding interaction sketched in Fig. 6. The affinity trends to particular functional groups were analyzed for classical inorganic anions in Ref. [91] and is tabulated in Table 3. Although typical ionic liquid ions were not investigated in [91] the trends should still hold. This may have positive and/or negative consequences for the unfolding/refolding equilibrium. Klähn et al. [79] pointed out that the interaction of cations and anions with a positively charged protein surface is enhanced during the unfolding process as sketched in Fig. 8a. They assume that the ionic liquid ions prefer to approach the protein surface pairwise due to their strong cation-anion network. The Coulomb repulsion of the cation with the protein surface is overcompensated by the attraction of the anion to the surface (left picture of Fig. 8a). As a consequence, the positively charged amino acid moves towards the anion starting the unfolding process depicted in the right figure of Fig. 8a). Although the repulsion to the cation gets stronger, the increased attraction to the anion promotes this step. However, as discussed for Fig. 2, neutral cation-anion clusters are not favorable, in particular for hydrophilic anions which prefer hydrogen bonding to water [22, 46]. Consequently, the “anion

Table 3 Ion specific affinities for surfaces with different functional groups [91]

Functional group	Anion binding affinity	Cation binding affinity
Hydrophobic $\mathrm{CH_3}$	Reversed Hofmeister	Direct Hofmeister
Polar $\mathrm{OH^-}$	Direct Hofmeister	Inconclusive
Polar COOH	Direct Hofmeister	Direct Hofmeister
Charged $\mathrm{COO^-}$	Direct Hofmeister	Reversed Hofmeister

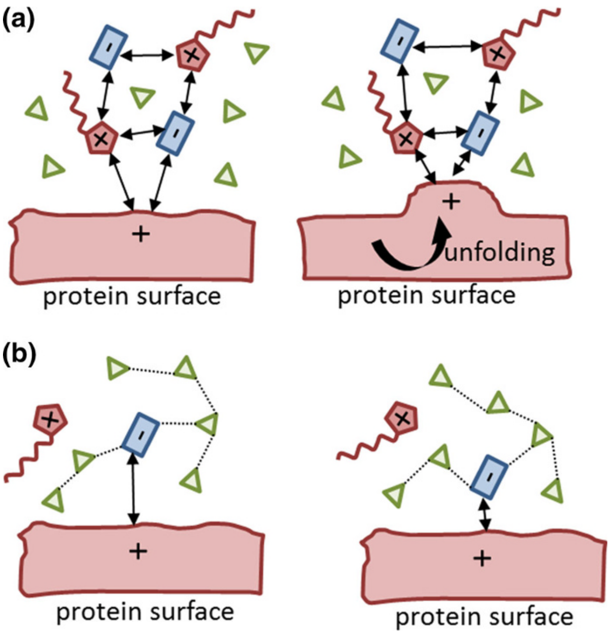

Fig. 8 **a** Unfolding mechanism proposed by Ref. [79], **b** alternative interpretation of the strong interaction of the anion with the protein surface

clusters" possess less mass than an ion pair. If the anion is attracted to the protein surface, it will move towards the surface (see Fig. 8b). On the other hand, the positively charged amino acid moves not very much towards the solvent phase in contrast to Fig. 8a.

Strong interaction between the anion and the positively charged amino acids may also lead to refolding as depicted in Fig. 9 and suggested by Summers and Flowers [132]. Because of the strong interaction of an anion with several positively charged amino acids, these amino acids are forced into a more compact structure facilitating the building of hydrogen bonds necessary for the secondary structure elements, i.e. α-helices and β-strands. The structure compressing in case of apolar amino acids can be promoted by the apolar regions of the amphiphilic cations. However, more computational studies investigating various ionic liquid ions and their interaction on particular amino acids including the consequences on the secondary structure are necessary to finalize the picture of the ionic liquid impact on the protein structure.

3.3.4 Thermodynamics of the Hofmeister Series

Ebbinghaus and co-workers reported that the protein stability is also a function of the ion concentration [68]: At low ion concentration ($c_{\mathrm{IL}} < 0.5\,\mathrm{mol\,L^{-1}}$) almost all aqueous ionic liquid mixtures denature proteins. At higher ionic liquid concentration above $1\,\mathrm{mol\,L^{-1}}$ ion-specific effect becomes dominant and the Hofmeister series more meaningful [68]. Therefore, the concentration behavior of stabilizing

Fig. 9 Adapted refolding mechanism of Ref. [132]. *Blue*, *red*, *green*, and *orange areas* reflect negatively charged, positively charged, polar and non-polar amino acid sequences. The *arrows* denote strong Coulomb interaction and the *gray shaded area* strong dispersion

and destabilizing ionic liquids is different as measured by the salt-induced shift of the protein melting temperature ΔT_m. At $c_{\mathrm{IL}} = 0\,\mathrm{mol\,L^{-1}}$ the shift starts at $\Delta T_m = 0\,\mathrm{K}$. Adding small amounts of the ionic liquid destabilize the protein resulting in negative ΔT_m-values for all ionic liquids. However, in stabilizing ionic liquids ΔT_m increases with increasing concentration reaching values of more than 20 K for choline dihydrogenphosphate at $c_{\mathrm{IL}} = 4\,\mathrm{mol\,L^{-1}}$ [68]. In destabilizing ionic liquids, ΔT_m always decreases with increasing ion concentration reaching values of $\Delta T_m = -25\mathrm{K}$ for $[\mathrm{C_2mim}][\mathrm{SCN}]$ at $c_{\mathrm{IL}} = 1.5\,\mathrm{mol\,L^{-1}}$. Interestingly, ΔT_m directly correlates with $\Delta\Delta G_{\mathrm{unfolding}}$ defined by

$$\Delta\Delta G_{\mathrm{unfolding}} = \Delta G^{\mathrm{IL}}_{\mathrm{unfolding}} - \Delta G^{\mathrm{buffer}}_{\mathrm{unfolding}} \tag{8}$$

$$= \Delta\Delta H_{\mathrm{unfolding}} - T \cdot \Delta\Delta S_{\mathrm{unfolding}} \tag{9}$$

Both contributions in Eq. 9 are very ion specific and follow the direct Hofmeister series or its reversed order as visible in Table 4. For example, $\Delta\Delta S_{\mathrm{unfolding}}$ follows the direct Hofmeister series for the cations whereas the reversed ranking is observed for $\Delta\Delta H_{\mathrm{unfolding}}$.

This has several consequences:

- based on the sign of $\Delta\Delta S_{\mathrm{unfolding}}$ the mechanism to stabilize the protein may be primarily enthalpic or entropic.
- because of the common enthalpy-entropy compensation at room temperature, varying the temperature changes the stabilizing/denaturing property of the ionic co-solvent. In other words, the Hofmeister series is temperature dependent.
- since the enthalpic and entropic contribution depend on the pH of the solution and protein charge, isoelectric point, and hydrophobicity, sometimes the overall impact of the ions neither follow the direct nor the reversed Hofmeister series.

However, stabilizing enthalpic contribution ($\Delta\Delta H_{\mathrm{unfolding}} > 0$) and the counteracting entropic contribution ($T \cdot \Delta\Delta S_{\mathrm{unfolding}} > 0$) tend to rise with increasing

Table 4 Trends of the generalized Hofmeister behavior [68, 91] at salt concentrations of 1 mol L^{-1}

Cations	
Protein surface ⊕	Reversed Hofmeister
Protein surface ⊖	Direct Hofmeister
ΔT_m	Reversed Hofmeister
$\Delta\Delta G_{\text{unfolding}}$	Reversed Hofmeister
$\Delta\Delta H_{\text{unfolding}}$	Reversed Hofmeister
$T \cdot \Delta\Delta S_{\text{unfolding}}$	Direct Hofmeister
Anions	
Protein surface ⊕	Reversed Hofmeister
Protein surface ⊖	Direct Hofmeister
ΔT_m	Direct Hofmeister
$\Delta\Delta G_{\text{unfolding}}$	Direct Hofmeister
$\Delta\Delta H_{\text{unfolding}}$	Inconclusive
$T \cdot \Delta\Delta S_{\text{unfolding}}$	Inconclusive

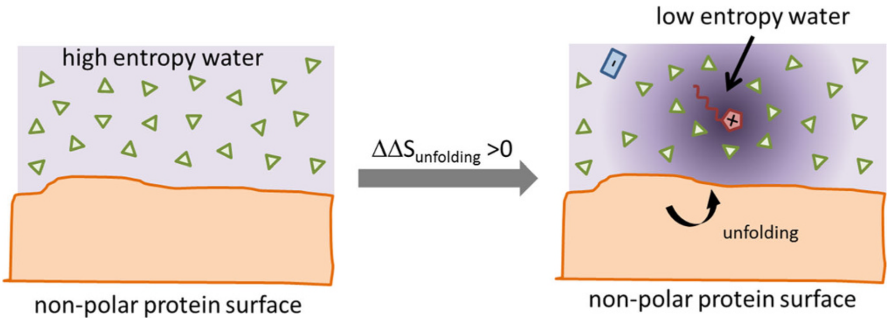

Fig. 10 Hydrophobic solvation of hydrophobic co-solutes reduces the water entropy and promotes unfolding since the penalty due to the solvation of the hydrophobic residues is less severe. This figure is adapted from [68]

hydrophobicity of the ionic liquid cation. If the water entropy is reduced by the hydrophobic co-solute, the entropy decrease due to unfolding and hence solvation of hydrophobic protein residues becomes less important and is, therefore, promoted by the hydrophobic co-solute as visible in Fig. 10.

4 Conclusion

Many appealing solvation properties of ionic liquids and their tunability by proper choice of the cation and anion combination have been investigated in various areas of biochemistry in the past two decades. The findings for the protein solubility, crystallization, separation, and stability are often mapped on the Hofmeister series or its reversed order.

Unfortunately, the involved interactions and effects compensate each other to a large extent. Consequently, the overall effect of a particular ionic liquid on a protein cannot be predicted and necessitates further investigation from experimenter and computational scientist. In particular, it would be useful to apply a reasonable set of the very same ionic liquids to several areas of protein research depicted in Fig. 5. So far, the comparison and the deeper understanding of the underlying mechanisms is hampered by the fact that majority of publications use very special ionic liquids or reaction conditions, which do not allow for generalizations.

Acknowledgement Open access funding provided by University of Vienna.

References

1. Fumino K, Wulf A, Ludwig R (2009) Angew Chemie Int Ed 48:3184
2. Hayes R, Warr GG, Atkin R (2015) Chem Rev 115:6357
3. Wilkes JS (2004) J Mol Catal A Chem 214:11
4. Zhang S, Sun N, He X, Lu X, Zhang X (2006) J Phys Chem Ref Data 35:1475
5. Greaves TL, Drummond CJ (2008) Chem Rev 108:206
6. Blesic M, Marques MH, Plechkova NV, Seddon KR, Rebelo LPN, Lopes A (2007) Green Chem 9:481
7. Jungnickel C, Łuczak J, Ranke J, Fernández JF, Müller A, Thöming J (2008) Coll Surf A 316:278
8. Zech O, Kunz W (2011) Soft Matter 7:5507
9. Greaves TL, Drummond CJ (2008) Chem Soc Rev 37:1709
10. Eastoe J, Gold S, Rogers SE, Paul A, Welton T, Heenan RK, Grillo I (2005) J Am Chem Soc 127:7302
11. Kusano T, Fujii K, Hasimoto K, Shibayama M (2014) Langmuir 30:11890
12. Marcus Y, Hefter G (2006) Chem Rev 106:4585
13. Laage D, Stirnemann G, Sterpone F, Rey R, Hynes JT (2011) Annu Rev Phys Chem 62:395
14. van der Vegt NFA, Haldrup K, Roke S, Zheng J, Lund M, Bakker HJ (2015) Chem Rev 116:7626
15. Reichardt C (2005) Green Chem 7:339
16. van Rantwijk F, Sheldon RA (2007) Chem Rev 107:2757
17. Buchner R, Hefter G (2009) Phys Chem Chem Phys 11:8984
18. Wakai C, Oleinikova A, Ott M, Weingärtner H (2005) J Phys Chem B 109:17028
19. Huang MM, Jiang Y, Sasisanker P, Driver GW, Weingärtner H (2011) J Chem Eng Data 56:1494
20. Schröder C, Sega M, Schmollngruber M, Gailberger E, Braun D, Steinhauser O (2014) J Chem Phys 140:204505
21. Bernardes CE, Minas da Piedade ME, Canongia JN (2011) Lopes. J Phys Chem B 115:2067
22. Schröder C, Rudas T, Neumayr G, Benkner S, Steinhauser O (2007) J Chem Phys 127:234503
23. Bešter-Rogač M, Hunger J, Stoppa A, Buchner R (2011) J Chem Eng Data 56:1261
24. Bešter-Rogač M, Stoppa A, Buchner R (2013) J Phys Chem B 118:1426
25. Robinson RA, Harned HS (1941) Chem Rev 28:454
26. Machado VG, Stock RI, Reichardt C (2014) Chem Rev 114:10429
27. Carmichael AJ, Seddon KR (2000) J Phys Org Chem 13:591
28. Aki SNVK, Brennecke JF, Samanta A (2001) Chem Commun 413
29. Ab Rani MA, Brant A, Crowhurst L, Dolan A, Lui M, Hassan NH, Hallett JP, Hunt PA, Niedermeyer H, Perez-Arlandis JM, Schrems M, Welton T, Wilding R (2011) Phys Chem Chem Phys 13:16831

30. Hermanutz F, Gähr F, Uerdingen E, Meister F, Kosan B (2008) Macromol Symp 262:23
31. Zhao B, Greiner L, Leitner W (2012) RSC Adv 2:2476
32. Zhao H (2010) J Chem Technol Biotechnol 85:891
33. Yamamoto E, Yamaguchi S, Nagamune T (2011) Appl Biochem Biotechnol 164:957
34. Laane C, Boeren S, Vos K, Veeger C (1987) Biotechnol Bioeng 30:81
35. Nara SJ, Harjani JR, Salunkhe MM (2002) Tetrahedron Lett 43:2979
36. Lange C, Patil G, Rudolph R (2005) Protein Sci 14:2693
37. Kaar JL, Jesionowski AM, Berberich JA, Moulton R, Russell AJ (2003) J Am Chem Soc 125:4125
38. Swatloski RP, Spear SK, Holbrey JD, Rogers RD (2002) J Am Chem Soc 124:4974
39. Remsing RC, Swatloski RP, Rogers RD, Moyna G (2006) Chem Commun 1271
40. Zhu S, Wu Y, Chen Q, Yu Z, Wang C, Jin S (2006) Green Chem 8:325
41. Youngs TGA, Hardacre C, Holbrey JD (2007) J Phys Chem B 111:13765
42. Youngs TGA, Holbrey JD, Deetlefs M, Nieuwenhuyzen M, Costa Gomes MF, Hardacre C (2006) Chem Phys Chem 7:2279
43. Armstrong DW, He L, Liu YS (1999) Anal Chem 71:3873
44. Anderson JL, Ding J, Welton T, Armstrong DW (2002) J Am Chem Soc 124:14247
45. Omta AW, Kropman MF, Woutersen S, Bakker HJ (2003) Science 301:347
46. Spickermann C, Thar J, Lehmann SBC, Zahn S, Hunger J, Buchner R, Hunt PA, Welton T, Kirchner B (2008) J Chem Phys 129:104505
47. Fazio B, Triolo A, Di Marco G (2008) J Raman Spectrosc 39:233
48. Takamuku T, Kyoshoin Y, Shimomura T, Kittaka S, Yamaguchi T, J Phys Chem B 113:10817
49. Zhang QG, Wang NN, Yu ZW (2010) J Phys Chem B 114:4747
50. Canongia Lopes JN, Pádua AAH (2006) J Phys Chem B 110:3330
51. Haberler M, Schröder C, Steinhauser O (2012) J Chem Theory Comput 8:3911
52. Tariq M, Freire MG, Saramago B, Coutinho JAP, Canongia JN, Lopes LPN (2012) Rebelo Chem Soc Rev 41:829
53. Salis A, Ninham BW (2014) Chem Soc Rev 43:7358
54. Zhao H (2016) J Chem Technol Biotechnol 91:25
55. Zhao H (2005) J Mol Catal B Enzym 37:16
56. Constantinescu D, Weingärtner H, Herrmann C (2007) Angew Chem Int Ed 46:8887
57. Yang Z (2009) J Biotechnol 144:12
58. Zhao H (2006) J Che Technol Biotechnol 81:877
59. Naushad M, Alothman ZA, Khan AB, Ali M (2012) Int J Biol Macromol 51:555
60. Zangi R (2010) J Phys Chem B 114:643
61. Batchelor JD, Oltenanu A, Tripathy A, Pielak GJ (2004) J Am Chem Soc 126:1958
62. Collins KD (1997) Biophys J 72:65
63. Collins KD (2004) Methods 34:300
64. Collins KD (2012) Biophys Chem 167:43
65. Gujt J, Bešter-Rogač M, Hribar-Lee B (2014) J Mol Liq 190:34
66. Green AA (1932) J Biol Chem 95:47
67. Collins KD, Washabaugh MW (1985) Q Rev Biophys 18:323
68. Senske M, Constantinescu-Aruxandei D, Havenith M, Herrmann C, Weingärtner H, Ebbinghaus S (2016) Phys Chem Chem Phys 18:29698
69. Patel R, Kumari M, Khan AB (2014) Appl Biochem Biotechnol 172:3701
70. Chen X, Liu J, Wang J (2010) Anal Meth 2:1222
71. Seduraman A, Wu P, Klähn M (2012) J Phys Chem B 116:296
72. Vasantha T, Kumar A, Attri P, Venkatesu P, Rama Devi RS (2014) Protein Peptide Lett 21:15
73. Brogan APS, Hallett JP (2016) J Am Chem Soc 138:4494
74. Strasburg S, Bermudez H, Hoagland D (2016) Biomacromolecules 17:2233
75. Klähn M, Lim GS, Seduraman A, Wu P (2011) Phys Chem Chem Phys 13:1649
76. Muldoon M, Lagunas-Castedo C, Nockemann P (2012) Cryst Eng Comm 14:4912
77. Haberler M, Schröder C, Steinhauser O (2011) Phys Chem Chem Phys 13:6955
78. Haberler M, Steinhauser O (2011) Phys Chem Chem Phys 13:17994
79. Klähn M, Lim GS, Wu P (2011) Phys Chem Chem Phys 13:18647
80. Lesch V, Heuer A, Tatsis VA, Holm C, Smiatek J (2015) Phys Chem Chem Phys 17:26049
81. Micaêlo NM, Soares CM (2008) J Phys Chem B 112:2566
82. Zhang Y, Cremer PS (2006) Curr Opin Chem Biol 10:658
83. Lim GS, Zidar J, Cheong DW, Jaenicke S, Klähn M (2014) J Phys Chem B 118:10444

84. Zaks A, Klibanov AM (1988) J Biol Chem 263:8017
85. Laszlo JA, Compton DL (2002) J Mol Catal B Enzym 18:109
86. Dang LP, Fang WZ, Li Y, Wang Q, Xiao HZ, Wang ZZ (2013) Appl Biochem Biotechnol 169:290
87. Thomas AS, Elcock AH (2007) J Am Chem Soc 129:14887
88. Gibb CLD, Gibb BC (2011) J Am Chem Soc 133:7344
89. Zangi R, Hagen M, Berne BJ (2007) J Am Chem Soc 129:4678
90. Schwierz N, Horinek D, Netz RR (2013) Langmuir 29:2602
91. Schwierz N, Horinek D, Sivan U, Netz RR (2016) Curr Opin Coll Interf Sci 23:10
92. Judge RA, Takahashi S, Longenecker KL, Fry EH, Abad-Zapatero C, Chiu ML (2009) Cryst Growth Des 9:3463
93. Garlitz JA, Summers CA, Flowers RA II, Borgstahl GEO (1999) Acta Crystallogr D 55:2037
94. Pusey ML, Paley MS, Turner MB, Rogers RD (2007) Cryst Growth Des 7:787
95. Chen X, Ji Y, Wang J (2010) Analyst 135:2241
96. Hekmat D, Hebel D, Joswig S, Schmidt M, Weuster-Botz D (2007) Biotechnol Lett 29:1703
97. Hekmat D, Hebel D, Weuster-Botz D (2008) Chem Eng Technol 31:911
98. Li X, Xu X, Dan Y, Feng J, Ge L, Zhang M (2008) Cryst Res Technol 43:1062
99. Kennedy DF, Drummond CJ, Peat TS, Newman J (2011) Cryst Growth Des 11:1777
100. Pei Y, Wang J, Wu K, Xuan X, Lu X (2009) Separ Purif Technol 64:288
101. Neves CMSS, Ventura SPM, Freire MG, Marrucho IM, Coutinho JAP (2009) J Phys Chem B 113:5194
102. Du Z, Yu YL, Wang JH (2007) Chem Eur J 13:2130
103. Xu Y, Li J, Wang E (2008) J Chromat A 1207:175
104. Ventura SPM, Neves CMSS, Freire MG, Marrucho IM, Oliverira J, Coutinho JAP (2009) J Phys Chem B 113:9304
105. Dreyer S, Salim P, Kragl U (2009) Biochem Eng J 46:176
106. Li Z, Pei Y, Wang H, Fan J, Wang J (2010) Trends Anal Chem 29:1336
107. Kohno Y, Saita S, Murata K, Nakamura N, Ohno H (2011) Polym Chem 2:862
108. Lin X, Wang Y, Zeng Q, Ding X, Chen J (2013) Analyst 138:6445
109. Fujita K, MacFarlane DR, Forsyth M (2005) Chem Commun 4804
110. Fujita K, Forsyth M, MacFarlane DR, Reid RW, Elliott GD (2006) Biotechnol Bioeng 94:1209
111. Gutowski KE, Broker GA, Willauer HD, Huddleston JG, Swatloski RP, Holbrey JD, Rogers RD (2003) J Am Chem Soc 125:6632
112. He C, Li S, Liu H, Li K, Liu F (2005) J Chromat A 1082:143
113. Sivapragasam M, Moniruzzaman M, Goto M (2016) Biotechnol J 11:1000
114. Jiang TF, Gu YL, Liang B, Li JB, Shi YP, Ou QY (2003) Anal Chim Acta 479:249
115. Li T, Li B, Dong S, Wang E (2007) Chem Eur J 13:8516
116. Corradini D, Nicoletti I, Bonn GK (2009) Electrophoresis 30:1869
117. Xu Y, Wang E (2009) Chromatogr A 1216:4817
118. Armstrong DW, Zhang LK, He L, Gross ML (2001) Anal Chem 73:3679
119. Zabet-Moghaddam M, Heinzle E, Lasaosa M, Tholey A (2006) Anal Bioanal Chem 384:215
120. Lozano P, de Diego T, Guegan JP, Vaultier M, Iborra JL (2001) Biotechnol Bioeng 75:563
121. Fujita K, MacFarlane DR, Foryth M, Yoshizawa-Fujita M, Murata K, Nakamura N, Ohno H (2007) Biomacromolecules 8:2080
122. Vrikkis RM, Fraser KJ, Fujita K, MacFarlane DR, Elliott GD (2009) J Biomech Eng 131:074514
123. de Diego T, Lozano P, Gmouh S, Vaultier M, Iborra JL (2005) Biomacromolecules 6:1457
124. Byrne N, Wang LM, Belires JP, Angell CA (2007) Chem Commun 2714
125. Byrne N, Angell CA (2008) J Mol Biol 378:707
126. Page TA, Kraut ND, Page PM, Baker GA, Bright FV (2009) J Phys Chem B 113:12825
127. Baker GA, Heller WT (2009) Chem Eng J 147:6
128. Heller WT, O'Neill HM, Zhang Q, Baker GA (2010) J Phys Chem B 114:13866
129. Constatinescu D, Herrmann C, Weingärtner H (2010) Phys Chem Chem Phys 12:1756
130. Figueiredo AM, Sardinha J, Moore GR, Cabrita EJ (2013) Phys Chem Chem Phys 15:19632
131. Li W, Wu P (2014) Soft Matter 10:6161
132. Summers CA, Flowers RA II (2000) Protein Sci 9:2001
133. Mann JP, McCluskey A, Atkin R (2009) Green Chem 9:785
134. Constatinescu D, Herrmann C, Weingärtner H (2009) Phys Chem Chem Phys 12:1756
135. Buchfink R, Tischer A, Patil G, Rudolph R, Lange C (2010) J Biotechnol 150:64
136. Weingärtner H, Cabrele C, Herrmann C (2012) Phys Chem Chem Phys 14:415

137. Kumar A, Venkatesu P (2012) RSC Adv 3:362
138. Kumar A, Venkatesu P (2014) RSC Adv 4:4487
139. Park S, Kazlauskas RJ (2001) J Org Chem 66:8395
140. Yang Z, Pan W (2005) Enzyme Microbial Technol 37:19
141. Pandey S, Fletcher KA, Baker SN, Baker GA (2004) Analyst 129:569
142. Dror RO, Dirks RM, Grossman JP, Xu H, Shaw DE (2012) Annu Rev Biophys 41:429
143. Kabsch W, Sander C (1983) Biopolymers 22:2577
144. Rodrigues JV, Prosinecki V, Marrucho I, Rebelo LPN, Gomes CM (2011) Phys Chem Chem Phys 13:13614
145. Hernández FJ, de los Ríos AP, Tomás-Alonso F, Gómez D, Víllora G (2009) Can J Chem Eng 87:910

Top Curr Chem (Z) (2017) 375:65
DOI 10.1007/s41061-017-0148-1

REVIEW

Metal Nanoparticles in Ionic Liquids

Susann Wegner[1] · **Christoph Janiak**[1]

Received: 16 January 2017 / Accepted: 9 May 2017 / Published online: 6 June 2017

Abstract During the last years ionic liquids (ILs) were increasingly used and investigated as reaction media, hydrogen sources, catalysts, templating agents and stabilizers for the synthesis of (monometallic and bimetallic) metal nanoparticles (M-NPs). Especially ILs with 1,3-dialkyl-imidazolium cations featured prominently in the formation and stabilization of M-NPs. This chapter summarizes studies which focused on the interdependencies of the IL with the metal nanoparticle and tried to elucidate, for example, influences of the IL-cation, -anion and alkyl chain length. Qualitatively, the size of M-NPs was found to increase with the size of the IL-anion. The influence of the size of imidazolium-cation is less clear. The M-NP size was both found to increase and to decrease with increasing chain lengths of the 1,3-dialkyl-imidazolium cation. It is evident from such reports on cation and anion effects of ILs that the interaction between an IL and a (growing) metal nanoparticle is far from understood. Factors like IL-viscosity, hydrogen-bonding capability and the relative ratio of polar and non-polar domains of ILs may also influence the stability of nanoparticles in ionic liquids and an improved understanding of the IL-nanoparticle interaction would be needed for a more rational design of nanomaterials in ILs. Furthermore, thiol-, ether-, carboxylic acid-, amino- and hydroxyl-functionalized ILs add to the complexity by acting also as coordinating capping ligands. In addition imidazolium cations are precursors to *N*-heterocyclic carbenes, NHCs which form from imidazolium-based ionic liquids by in situ deprotonation at the acidic C2-H ring position as intermediate species during the nanoparticle

---

Chapter 6 was originally published as Wegner, S. & Janiak, C. Top Curr Chem (Z) (2017) 375: 65. DOI 10.1007/ s41061-017-0148-1.

✉ Christoph Janiak
janiak@uni-duesseldorf.de

[1] Institut für Anorganische Chemie und Strukturchemie, Heinrich-Heine Universität Düsseldorf, Universitätsstr. 1, 40225 Düsseldorf, Germany

seeding and growth process or as surface coordinating ligand for the stabilization of the metal nanoparticle.

Keywords Ionic liquids · Metal nanoparticles · Cation and anion effects · Alkyl chain effects · Stabilization

1 Introduction

Already in the nineteenth century the first research efforts were seen on the synthesis of nanoparticles and the study of their properties [1–6]. Michael Faraday found in 1857 that nano-alloys can be synthesized by chemical reduction of noble-metal compounds and placed solutions of metal salt precursors with Au, Pt and Ag in a reducing atmosphere of "sulphured hydrogen" [7]. Over the last decades the evolvement of imaging methods like electron and scanning microscopies together with the application oriented interest in their properties has led to an exponential growth of metal nanoparticle (M-NP) research [8–10]. M-NPs have become significant for applications in medicine [11, 12], optics [13, 14], electronics [15], luminescence [16] and catalysis [17–19].

The synthesis of metal nanoparticles can be commonly carried out by chemical reduction [20–22], electrochemical reduction [23] and thermal decomposition [24] also induced by microwave heating [25–27]. Through the synthetic methodology, it is possible to vary the morphology, size and size distribution of M-NPs. Strong reducing agents such as sodium hydride seldom control the size and shape of M-NPs but mild reducing agents such as sodium citrate and ascorbic acid [28] which simultaneously act as coordinating capping ligands can control the size and shape of metal NPs. The size of metal nanoparticles could also be controlled by varying the concentration of metal salt precursors, reducing agents, pH, and temperature [28].

Depending on the application, e.g., in catalysis a small nanoparticle size of for example less than 5 nm may be desirable. At the same time, agglomeration of such small nanoparticles in the process of Ostwald-ripening needs to be avoided (Fig. 1).

To avoid agglomeration the nanoparticles have to be stabilized sterically or electrostatically (see also Sect. 4). For this, M-NPs are typically surrounded by coordinating (capping) ligands, by surfactants (electrostatic stabilization) or organic polymers (steric stabilization) (Fig. 2) [30]. Examples for common capping ligands are thiols, organic acids, alcohols or amines. Protic ligands like thiols and organic acids become deprotonated upon surface coordination and bind to the surface metal atoms as thiolates and carboxylates. In turn, the metal surface layer can be assumed to become cationic [31, 32]. The mean size of dodecanethiolate-stabilized Au nanoclusters can be finely adjusted by the Au:dodecanethiolate ratio and the temperature and rate at which the reduction is conducted to vary between diameters of 1.5 and 5.2 nm (~110–4800 Au atoms/core) [31]. Phosphine-stabilized gold nanoparticles can be easily prepared from $HAuCl_4$ trihydrate and sodium borohydride in the presence of triphenylphosphine in a water/toluene mixture where tetraoctylammonium bromide transferred the reactants into the organic phase. The biphasic synthesis can be carried out quickly under ambient conditions, permits

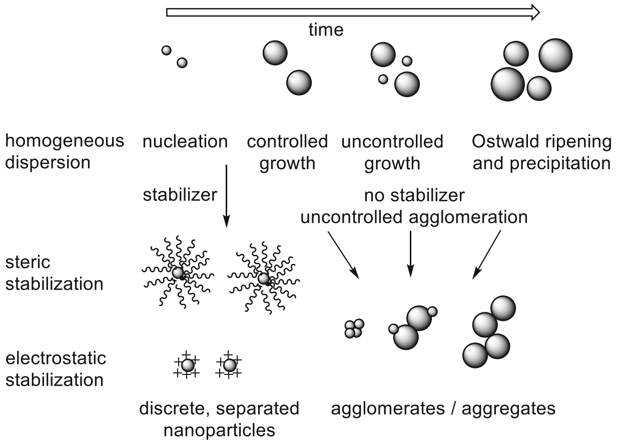

Fig. 1 Schematic presentation of (metal) nanoparticle growth and stabilization [29]

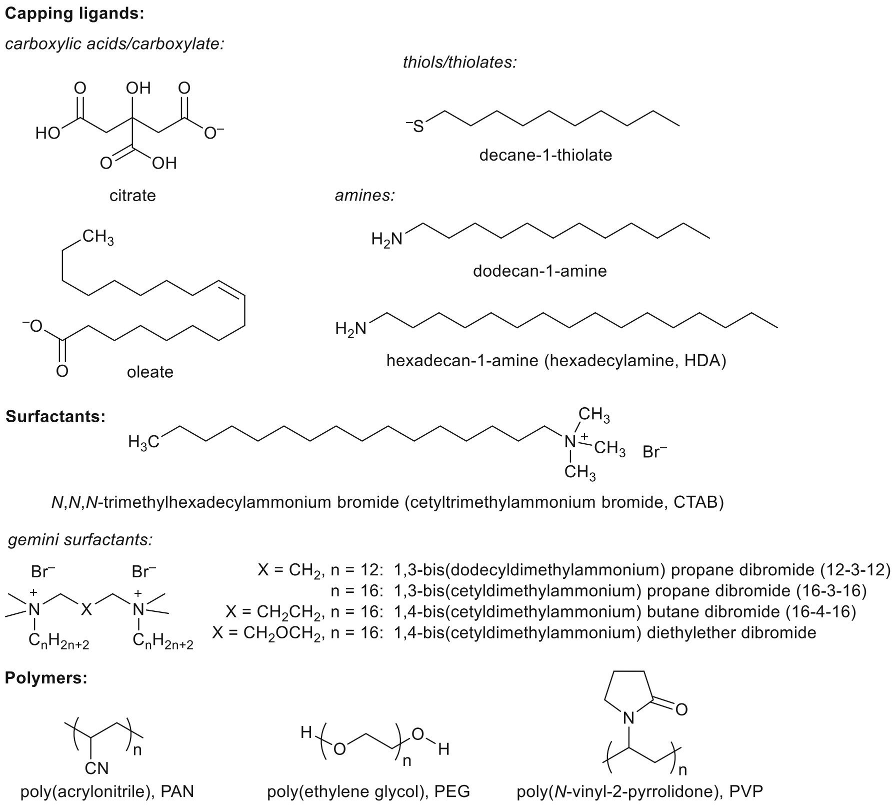

Fig. 2 Examples of typical classic stabilizers for metal nanoparticles

the use of a variety of phosphines as passivating ligands, and provides control over particle core size to produce 1.5-nm nanoparticles [33]. Phosphine-stabilized nanoparticles are precursors to other functionalized nanoparticle building blocks where nearly any functional group can be introduced into the ligand shell, and the metal core size can be tuned from 1.4 to 10 nm in diameter through ligand exchange reactions [34]. Further, non-agglomerated Ru- and Pt-NPs with a diameter of 2 ± 1 nm were prepared in ethylene glycol with acetate as coordination and stabilizing ligand [35], small Ru-NPs with a diameter of 2–3 nm were stabilized with alkylamines and alkylthiols [36].

Examples for surfactants used in the stabilization of metal nanoparticles are sodium dodecylsulfate (SDS) for Pd-NPs [37], gemini surfactants (cf. Figure 2) for Au-NPs, Ag-NPs, Au/Ag-alloy-NPs, Pd-NPs and Pt-NPs [38–42] or cetyltrimethylammonium bromide (CTAB) [42].

Examples for stabilizing polymers (cf. Figure 2) are poly(ethylene glycol), poly(acrylonitrile) and poly(vinylpyrrolidone). Poly(ethylene glycol) (PEG) can be used to control the formation and stability of Ag-NPs [43]. With poly(acrylonitrile) (PAN) it is possible to stabilize Pd-NPs with a nanoparticle diameter of 10–60 nm [44] and poly(vinylpyrrolidone) (PVP) can be used as stabilizer for Ag-NP in hybrid latex mini-emulsion at higher temperatures above 150 °C [45]. Gold and silver nanoparticles can be prepared from $HAuCl_4$ and $AgNO_3$, respectively, by using polysaccharides as reducing/stabilizing agents to obtain positively charged chitosan-stabilized gold nanoparticles and negatively charged heparin-stabilized silver nanoparticles inside the nanoscopic polysaccharide templates. The morphology and size distribution of prepared gold and silver nanoparticles varied with the concentration of both the polysaccharides and the precursor metal salts [46].

At the same time, the stabilization of M-NPs by the aforementioned coordinating capping ligands, surfactants or polymers results in a change of the surface properties and the surface accessibility of the nanoparticles particularly with regard to applications in catalysis [47].

2 Ionic Liquids

An alternative way for stabilizing metal nanoparticles can be the use of ionic liquids (ILs). By definition ionic liquids are molten organic or inorganic salts with a melting point below 100 °C [48–51], for practical purposes ILs are preferably already liquid at room temperature (RTILs). The low melting point of the ionic liquids is due to their low lattice energy, which in turn is a consequence of having weakly coordinating cations and anions. The weakly coordinating ion character derives from having large and mostly only single-charged ions so that the charge is delocalized over a large surface area. Consequently, the Coulomb attraction between ions with an effectively low surface charge density is weak. Examples of typical non-functionalized IL cations and anions are shown in Fig. 3. ILs have a very low vapor pressure which makes them easy to handle solvents [52], albeit problematic to recycle and purify by distillation. The thermal stability of typical ILs usually extends to 200 °C and even above [53–57]. Further, their physical properties

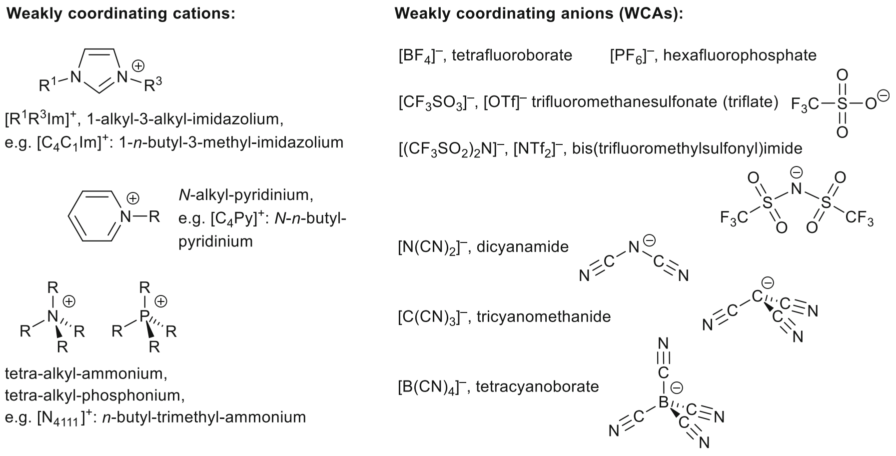

Fig. 3 Typical cations and anions of common non-functionalized ILs

like high polarity, high charge density and high dielectric constant [58] together with the formation of supramolecular mesoscopic networks [59] sets them apart from conventional organic solvents.

The well-established and probably most studied ILs contain an imidazolium cation (e.g. 1-ethyl-3-methylimidazolium $[C_2C_1Im]^+$ or 1-butyl-3-methylimidazolium $[C_4C_1Im]^+$) [60] and weakly-coordinating anions (WCAs) such as tetrafluoroborate $[BF_4]^-$, hexafluorophosphate $[PF_6]^-$ and trifluoromethylsulfonate (triflate) $[CF_3SO_3]^-$ ($[OTf]^-$) or bis(trifluoromethylsulfonyl)imide (triflimide) $[(CF_3SO_2)_2N]^-$ ($[NTf_2]^-$) [61, 62]. ILs with the 1-*n*-butyl-3-methylimidazolium $[C_4C_1Im]^+$ cation and the relatively weakly coordinating anions tetrafluoroborate, hexafluorophosphate and trifluoromethanesulfonate, are liquids over a large range of temperatures (down to −80 °C), possess high thermal and chemical stability, a large electrochemical window, high ion density, relatively low viscosity, and negligible vapor pressure [63].

Variation of the side chain R, R^1, R^3 (cf. Figure 3) of the cation or variation of the anion results in a change of the physicochemical properties of the IL like thermal behavior, viscosity and density. The viscosity increases with the length of the side chain of the imidazolium cation from $[C_2C_1Im][(CF_3SO_2)_2N]$ to $[C_8C_1Im][(CF_3SO_2)_2N]$ whereas the ionic conductivity decreases [64].

3 Metal Nanoparticles in Ionic Liquids

In the last years many different M-NPs (monometallic and bimetallic) in ILs were obtained. The activities in this field have already been summarized in reviews which provide an overview of available metal nanoparticles in ionic liquids with their precursor, size and size dispersion. “A short review on stable metal nanoparticles using ionic liquids, supported ionic liquids and poly(ionic liquids)” focused on supported IL-like phases and on different types of poly(ionic liquids) [P(ILs)] and polyelectrolytes as stabilizing agents for the synthesis of M-NPs. P(ILs) are an emerging class of cationic polymers with a poly(vinyl) backbone, e.g., from the polymerization of 1-vinyl-3-alkyl-imidazolium salts. P(ILs) possess properties of polymers as well as ILs with tunable properties through the anion and varying imidazolium alkyl chain length [8]. The main focus of the review "On the structural and surface properties of transition-metal nanoparticles in ionic liquids" [65] is on the different synthesis methods of transition-metal nanoparticles in ILs, the polar and non-polar regions in the M-NP/IL dispersion and steric and electronic protective layer formation against aggregation or agglomeration of the M-NPs. Further this review discusses the use of stable transition-metal NPs in ILs as green catalysts for several reactions and also as novel materials for chemical sensors. Particular attention is also paid to the stabilization models proposed to explain the stability and properties of the M-NP/IL dispersion [65]. The reviews entitled "naked metal nanoparticles from metal carbonyls in ionic liquids: Easy synthesis and stabilization" [47] and "synthesis and application of metal nanoparticle catalysts in ionic liquid media using metal carbonyl complexes as precursors" [66] *inter alia* summarize work on the synthesis of metal nanoparticles in ionic liquids from metal carbonyls. Commercially available binary metal carbonyls $M_x(CO)_y$ are unique precursors as they contain the metal atoms already in the zero-valent oxidation state needed for M-NPs. Thus, no reduction process is necessary and the only side-product CO is easily given off to the gas phase and removed from the reaction mixture. The microwave induced thermal decomposition of metal carbonyls in ILs provides an especially rapid and energy-saving procedure because of the ILs significant absorption efficiency for microwave energy. Examples for the direct use of M-NP/IL dispersions in hydrogenation catalysis of cyclohexene and benzene, Fischer–Tropsch reaction, and dehydration catalysis are also given in these reviews [47, 66]. The synthesis of metal nanoparticles from bulk metals, metal salts, metal complexes and metal carbonyls in ILs was reviewed in [30, 67, 68]. The synthesis of M-NPs in ILs can be carried out by chemical or electroreduction, thermolysis and photochemical methods including decomposition by microwave or sono-/ultrasound irradiation. Gas-phase syntheses can use sputtering, plasma/glow-discharge electrolysis and physical vapor deposition or electron beam and γ-irradiation. The in situ deposition of the M-NPs on supports, such as graphene-type materials was also addressed as was the use of M-NP/IL dispersions or on supports as catalysts for C–C coupling or hydrogenation catalysis [30, 67, 68]. The minireview "ionic liquids for the convenient synthesis of functional nanoparticles and other inorganic nanostructures" focusses on ionic liquids in the synthesis of crystalline nanoparticles at ambient temperatures and self-assembled, highly organized hybrid nanostructures [69].

The scope of this review here is the stabilization of metal nanoparticles in ionic liquids and the elucidation of the different factors which play a role in the stabilization and control the metal nanoparticle formation.

Briefly, metal nanoparticles of Rh, Pd, Pt, Ir, Fe, Ru, Co, Au, Ag, Cu and Ni were obtained from $RhCl_3 \cdot 3H_2O$, $PdCl_2$, $Pt_2(dba)_3$ (dba = dibenzylidene acetone), $[Ir(COD)Cl]_2$, $Fe_2(CO)_9$, Ru(COD)(COT), $Co_2(CO)_8$, $KAuCl_4$, $AgBF_4$, $Cu(NO_3)_2$ and $Ni(COD)_2$. Metal nanoparticles have been synthesized mostly in the ionic liquids $[C_4C_1Im][PF_6]$, $[C_4C_1Im][BF_4]$, $[C_4C_1Im][CF_3SO_3]$, $[C_{10}C_1Im][NTf_2]$, $[C_4C_1Im][NTf_2]$ by hydrogenation, chemical reduction and thermal decomposition. Sizes of M-NPs in ILs were found from 2.3 nm (Rh) [70], 4.2 ± 0.8 nm (Pd) [71], 2.8–3.3 nm (Pt) [116], 2–3 nm (Ir) [76], 5.2 nm (Fe) [72], 2.6 ± 0.4 nm (Ru) [73], 14 nm (Co) [164], 2.6-200 nm (Au) [74], 3–5 nm (Ag) [75], 3.5–9.5 nm (Cu) [76] and 5.1–5.9 nm for Ni [137]. Imidazolium ILs feature prominently in the formation and stabilization of M-NPs [77]. Imidazolium ILs are air, water and electrochemically stable with a wide liquidus range.

1-Alkyl-3-alkyl'-imidazolium ILs simultaneously act as reaction media, hydrogen sources, catalysts, templating agents and stabilizers for the synthesis of metal nanoparticles. It should be clear, however, that there are ILs which (i) have a strong influence on particle formation, (ii) which are good nucleation aids, but poor stabilizers, (iii) which are good nucleation aids and good stabilizers, and (iv) are none of this [78].

Examples of recent M-NP syntheses are given in Table 1. The examples show that metal nanoparticle synthesis occurs often by reduction of metal salts with added reducing agents such as H_2 or $NaBH_4$. Alternatively, the IL imidazolium cation with its protic C2-H or salt anions such as acetate, acetylacetonate, 1-(dimethylamino)propan-2-olate ($^{-}OCH(Me)CH_2NMe_2$) or amidinate ($MeC(N^iPr)_2^-$) act as internal or intramolecular reductants. The entries in Table 1 also show that microwave induced heating features prominently because of the very high absorption efficiency of ILs for microwave energy.

4 Stabilization of Metal Nanoparticles

Generally, the stabilization of M-NPs occurs through (I) electrostatic or (II) steric stabilization or (III) a combination of both electrostatic and steric stabilization [91]. The effect of stabilizing agents for nanoparticles is to build up a repulsive force between the particles [92], or at least to decrease any attractive van der Waals forces. Stabilizing agents surround NPs to prevent the agglomeration. The mechanism of stabilization has first been described in the Derjaguin–Landau–Verwey–Overbeek theory [93, 94].

4.1 Derjaguin-Landau-Verwey-Overbeek theory (DLVO theory)—Electrostatic Stabilization and Van Der Waals Interactions

The classic and most commonly used theory of a “mechanism of stabilization” was put forward by Derjaguin and Landau in 1940 as a quantitative theory [95] and later by Verwey and Overbeek in 1948 [96]. Both descriptions referred to colloidal materials. This basic theory combines repulsive Coulomb and attractive van der Waals (vdW) forces through the sum of an effective electrostatic term and a van der Waals term for the stabilization of these materials. Van der Waals forces originate from correlations between electron motions leading to non-spherical electron distributions in two adjacent particles or molecules. VdW forces are short-range, unidirectional and relatively weak compared to other intermolecular interactions.

Table 1 Recent mono and bimetallic NP synthesis in imidazolium ILs

Ionic liquid	Precursor	Conditions, reducing agent	NP with particle diameter	References
			Monometallic M-NPs	
$[C_4C_1Im][PF_6]$	$RhCl_3 \cdot 3H_2O$	H_2	Rh 3.5 nm	[79]
$[C_4C_1Im][BF_4]$	$CoCl_2 \cdot 6H_2O$	$NaBH_4$ Ultrasound	Co 30 ± 5 nm	[80]
	$Cu[OCH(Me)CH_2NMe_2]_2$ $Cu(OAc)_2 \cdot H_2O$	Microwave heating, intramolecular red. or IL	Cu 3.3 ± 0.9 m Cu_2O nanocubes 43 ± 15 nm	[81]
	Cu(I)-amidinate Zn(II)-amidinate $[Cu\{MeC(N^iPr)_2\}]_2$ $[Zn\{MeC(NiPr)_2\}]$	Microwave heating, intramolecular red. or IL	Cu 11 ± 6 nm Zn 3 ± 1 nm	[82]
	$Ir_4(CO)_{12}$	Microwave heating,	Ir 1.0 ± 0.4 m	[83]
		electron beam	2.7 ± 0.7 nm	
$[C_4C_1Im][NTf_2]$	$(NH_4)_6Mo_7O_{24} \cdot 4H_2O$	$NaBH_4$	Mo 10–50 nm	[84]
			Bimetallic M-NPs	
$[C_4C_1Im][BF_4]$	$Fe_2(CO)_9$ $Ru_3(CO)_{12}$	Thermal decomposition	FeRu 1.65 ± 0.3 nm	[85]
	Cu(I)-amidinate Zn(II)-amidinate $[Cu\{MeC(N^iPr)_2\}]_2$ $[Zn\{MeC(NiPr)_2\}]$	Microwave heating, intramolecular red. or IL	β-CuZn 51 ± 29 nm γ-Cu_3Zn 48 ± 12 nm	[82]
	$Ni(COD)_2$ $Ga(C_5Me_5)$	H_2	NiGa 14 ± 5 nm	[86]
	Triple-decker ruthenocene, Anionic ruthenocene	Microwave heating, intramolecular red. or IL	RuSn 4.3 ± 1.5 nm	[87]
$[C_4C_1Im][NTf_2]$	$Co(acac)_3$ $Pt(acac)_2$	Thermal decomposition, intramolecular red. or IL	CoPt-nanorods 8 nm	[88]
	[Ru(COD)(COT)] [CuMes]	H_2	RuCu 1.9–2.8 nm	[89]
$[C_4C_1Im][PF_6]$	$HAuCl_4$ K_2PdCl_4	$NaHB_4$ H_2	PdAu 5.3 ± 3.0 nm	[90]

Electrostatic and van der Waals interactions are present in nearly all colloidal and nanoparticular systems [97]. DLVO theory assumes flat surfaces of the particles and a homogeneous charge density, even upon approach of the particles. The concentration of the counter-ions, which cause the electric potential, is taken as constant. DLVO theory treats anions as ideal point charges. The influence of the solvent is considered only through its dielectric constant. DLVO theory is fundamental for colloids and predicts very well the stability of lyophobic colloids [98].

Ionic components as in surfactants or ionic liquids will generate an ionic double or Debye layer around the NPs (Fig. 3) resulting in electrostatic repulsion between equally surrounded NPs which will prevent the aggregation of the NPs in the dispersion. The effectiveness of such an electrostatic stabilization depends on parameters like pH, temperature, and concentration [92, 99]. Electrostatic repulsion is an important contribution for the stabilization of NPs using ionic compounds. The outer part of the ionic double layer may be formed by the bulky and less surface-coordinating alkyl ammonium, sulfonium, phosphonium, and imidazolium moieties which then add a steric stabilization (see below) [8].

For metal nanoparticles the anion of an original metal salt precursor has to be taken into account as electrostatic stabilizer. Small halide anions come closest to the “DLVO-type” point charge electrostatic stabilizers. DLVO theory predicts that the anion charges should be the primary source of stabilization for the unsaturated, electrophilic and possibly positively charged metal nanoparticles [100, 101]. The metal nanoparticles and their anion layer on the surface form then an overall negatively charged particle and are subject to Coulomb repulsion within the DLVO theory [47].

The stability of a colloid increases with the thickness of the Debye layer, which is the sum of the layers of counter-ions surrounding the particle. A thicker Debye layer stabilizes the particles by increasing the distance between them and reducing their van der Waals attraction. Also, the stability of colloids increases with the dielectric constant of the medium [102].

Limits of the DLVO theory are that it can only be applied to dilute systems ($<5 \times 10^{-2}$ mol/L) and cannot be applied to multiply charged ions or to sterically stabilized systems [103]. DLVO theory needs to be extended for effects such as hydrogen bonding, the hydrophobicity and steric interactions.

4.2 Steric Stabilization

Another important contribution in preventing aggregation of metal NPs is steric stabilization. Coordinating capping ligands like thiols, carboxylates, alcohols, long-alkyl-chain surfactants or polymers/oligomers act more or less through this type of stabilization [8].

When two nanoparticles enclosed by polymers or surrounded by long alkyl chains of ligands adsorbed on their surface approach each other, the polymer or alkyl chain layers will be compressed which results in a strong repulsion which is termed steric stabilization [104]. Steric repulsion derives from combination of entropic and osmotic contributions. The entropic part stems from a volume restriction effect that decreases the number of possible configurations in the compressed region. The osmotic effect is due to an increase in concentration of the adsorbed polymers or ligand in the region between the two nanoparticles surfaces as they approach closer. Steric interactions in colloidal dispersions in molecular solvents have been extensively studied [104–108].

4.3 Combination of Both Electrostatic and Steric Stabilization

Compounds which stabilize both through electrostatic and steric effects are, for example, surfactants with long alkyl chains, such as cetyltrimethylammonium bromide (CTAB) or its gemini derivatives (cf. Fig. 2) [38–42], polymers containing ionic charges such as carboxyl-terminated poly(ethylene glycol) [93] or ionic liquids (see below). From theoretical and experimental studies, it became evident that the effectiveness of electrostatic stabilization increases with increasing particle size, whereas the effectiveness of steric stabilization increases with decreasing particle size [109]. The combination of electrostatic and steric stabilization is also referred to as *electrosteric* stabilization.

5 Stabilization of Metal Nanoparticles in Ionic Liquids

5.1 Electrostatic and Steric = Electrosteric Stabilization

ILs offer an interesting potential for stabilizing materials in the synthetic process. Their low interface energy is favorable for stabilizing small particles. ILs consist of cations and anions, which can act as electrostatic stabilizing agents. The IL ions or ion clusters are attracted to the nanoparticle surface by electrostatic forces [110]. The nature of the immediate ion layer around metal nanoparticles in ILs is still a matter of debate. DLVO theory predicts that the anion charges should be the primary source of stabilization for the unsaturated, electrophilic and probably positively charged metal nanoparticles [100, 101]. The metal nanoparticles and their anion layer on the surface would then form an overall negatively charged particle and are subject to Coulomb repulsion within the DLVO theory [47]. On the other hand, there are statements that the ionic liquid cations are attracted to the surface of a negatively charged nanoparticle to form a positive ion layer, and then counter-anions form a second layer on the nanoparticle surface by electrostatic attraction [111–113].

Palladium nanoparticles, which were grown onto multiwalled carbon nanotubes modified with imidazolium groups were claimed to be stabilized by the electrostatic interaction occurring between the imidazolium cations and the nanoparticle surface due to a coordination involving the imidazolium cation [114]. Upon exchange of the imidazolium counter-anion from Br^- and $[SbF_6]^-$ to $[NTf_2]^-$ no change in the material structure was noticed, i.e. no separation of the nanoparticles from the multiwalled carbon nanotubes [114]. Also, results from an X-ray photoelectron spectroscopy (XPS) investigation of functionalized imidazolium ILs with gold or platinum nanoparticles were seen to support this cationic coordination mode. Three

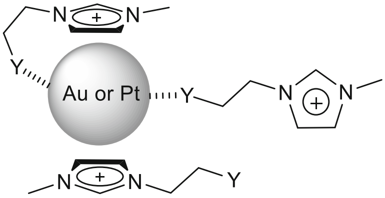

Fig. 4 Schematic proposed stabilization possibilities between metal nanoparticles and functionalized imidazolium cations [115]

possible interactions, involving either the functional group and/or the imidazolium ring were proposed (Fig. 4) [115].

On the other hand, an XPS and an extended X-ray fine structure spectroscopy study (EXAFS) of iridium or platinum nanoparticles in the imidazolium ILs $[C_4C_1Im][BF_4]$, $[C_4C_1Im][PF_6]$ and $[C_4C_1Im][OTf]$ showed interactions of the ionic liquid with the metal surface and the formation of an ionic liquid protective layer surrounding the metal particles [116, 117]. With small-angle X-ray scattering (SAXS) a variation in the protective layer length, from 2.8 to 4 nm, was evidenced depending on the type of anion. Moreover, the XPS analyses proved that the interaction between the metal surface and the IL occurs through F^-, when the anion is $[BF_4]^-$ of $[PF_6]^-$ or through O with the triflate, $[CF_3SO_3]^-$ anion [116, 117]. Consequently, one would assume that the ionic multilayer is composed of anions located immediately adjacent to the nanoparticle surface (Fig. 5) [166].

Density functional theory (DFT) binding energy (BE) calculations in a gas phase model favor interactions of Au_n clusters ($n = 1, 2, 3, 6, 19, 20$) between IL anions, such as $[BF_4]^-$, instead of imidazolium cations. This suggests an Au···F interaction and anionic Au_n stabilization in fluorous IL-anions [119]. Free imidazole bases (*e.g.* 1-methylimidazole) show similar binding energies. The Cl^- anions have the highest binding energy and can therefore be expected to bind to the NP if present in the solution. At the same time no significant binding of the $[C_4C_1Im]^+$ or $[HC_1Im]^+$ imidazolium cations was found. These findings support the model of preferred interaction between anions and Au-NPs, but also confirm the importance to consider a possible presence of Cl^- anions in the ionic liquid solution [74, 119].

The DFT study used the binding energy (BE) of different IL-ions, free bases and the Cl^- anion to gold clusters of various sizes as a relative measure for the interaction strength. The BE is defined as the difference of the relaxed energies of the gas phase anions and the Au_n clusters to the energy of their adduct (Eq. 1) [74, 119].

$$\begin{aligned} \mathrm{BE} &= E(\text{substrate, i.e., anion, free base or cation}) + E(\mathrm{M}_n \text{with M} = \text{ Au, Pd}) \\ &\quad - E(\text{substrate adduct to } \mathrm{M}_n). \end{aligned} \tag{1}$$

Figure 6 shows the Au_n–IL anion binding configurations and the variation of the BE with cluster size n. Figure 7 illustrates other substrate–Au_n binding configurations and the variation of the BE with cluster size n for $[BF_4]^-$ in comparison with other common substrate ligands. The BE of $[C_4C_1Im]^+$ is very weak and not included here [74, 119]. The BE of $[C_4C_1Im]^+$ is only 0.35 eV towards Au_6 or

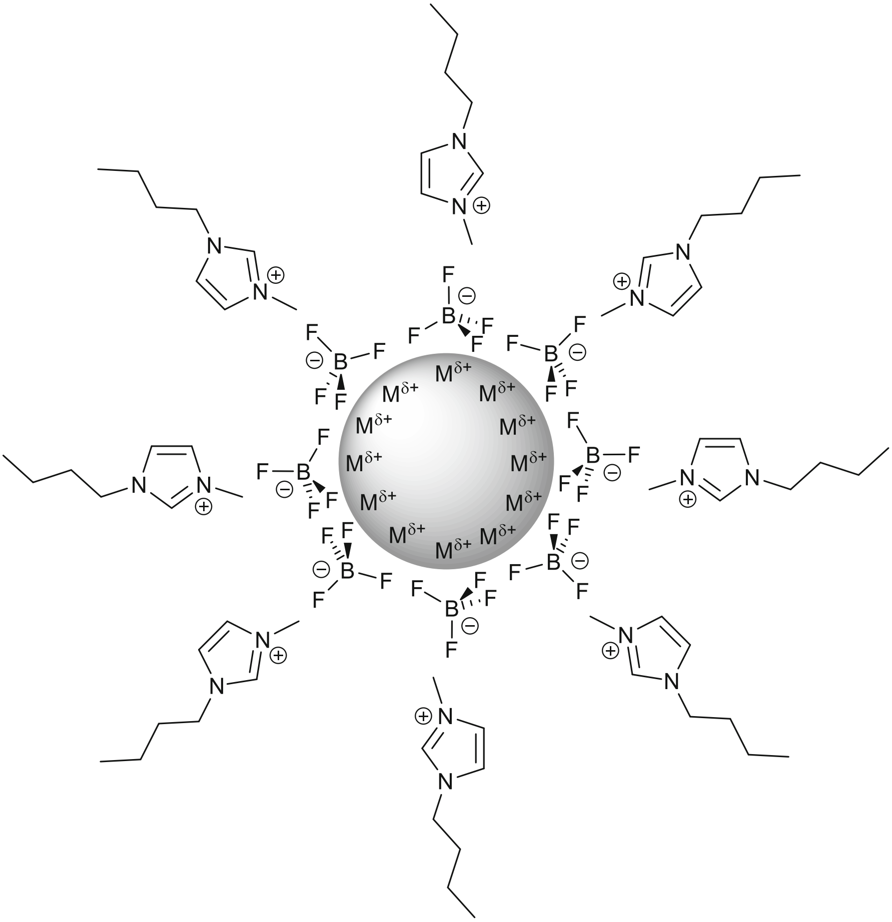

Fig. 5 Schematic depiction of proposed interactions between immediate IL anions, shown here for $[BF_4]^-$ anions and the metal nanoparticle surface with the IL-cations forming the second shell of the ionic double layer around a metal nanoparticle [118]

0.43 eV towards Au_{19} while the BE of $[BF_4]^-$ towards Au_6 and Au_{19} is 1.08 and 1.2 eV, respectively (1 eV = 23.06 kcal/mol). The BE comparison with chloride, citrate, PH_3 and H_2O illustrates the critical influence of the ionic charge and electron delocalization from the ligand to Au_n (Fig. 7). The softer the anion or ligand, that is, the more charge transfer or electron delocalization (according to Pearson's hard-soft concept and the nephelauxetic series) [120] to Au_n is possible, the better the stabilizing effect. H_2O as a hard and neutral ligand offers the least stabilization, hence, reduction of gold salts by $SnCl_2$ in water led immediately to the red purple solution (known as the Purple of Cassius). Remarkably, the relatively soft chloride anion shows the largest BE in agreement with the strong covalent binding of chloride ions to the Au(111) surface found in recent DFT simulations [121].

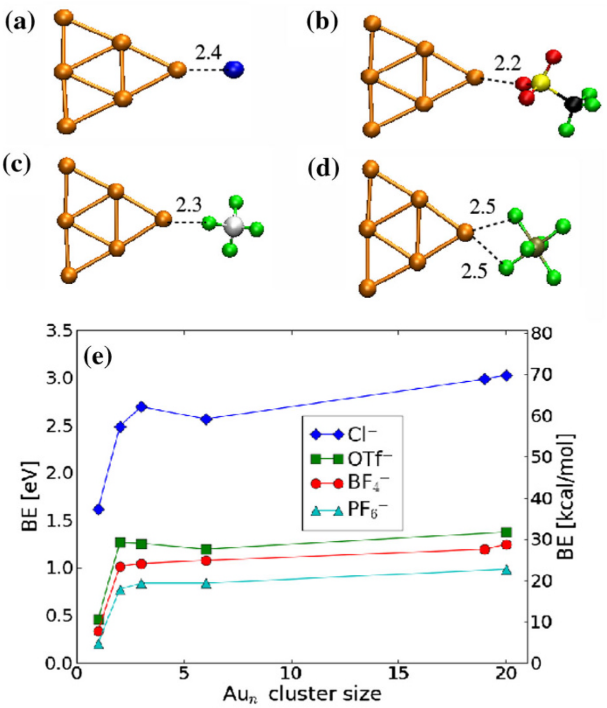

Fig. 6 Relaxed configurations of Au_6 bound to **a** Cl^-, **b** $[OTf]^-$, **c** $[BF_4]^-$ and **d** $[PF_6]^-$. The bond lengths are given in Å. **e** Binding energy. All the anions show a similar behavior in their BE: The BE to a single gold atom $n = 1$ is quite low and more than doubles for Au_2 ($n = 2$), therefrom is stays rather invariant with increasing the cluster size to $n = 20$, i.e., the BE is already saturated for Au_2. The chloride anion shows the largest BE of all anions and can be expected to bind to the clusters if it is present in the dispersion. Reprinted with permission from the author of Ref. [119]. Copyright Wiley–VCH 2009

A later combined DFT/vibrational spectroscopy approach found that palladium nanoparticles interact more strongly with the $[BF_4]^-$ anions than with the 1,3-dimethylimidazolium ($[C_1C_1Im]^+$) and 1-ethyl-3-methylimidazolium ($[C_2C_1Im]^+$) cations of the considered ILs. This suggested an important role of the anions in Pd-NP formation and stabilization in ILs. At the same time, the binding between isolated Pd atoms and the C atoms of the 1,3-dimethylimidazolium cation is stronger than Pd–$[BF_4]^-$ binding [122].

A similar DFT binding energy (BE) calculation with the 1-(2′-hydroxylethyl)-3-methylimidazolium cation $[HOC_2C_1Im]^+$ and a Pd_5 cluster pointed to the interaction of Pd_5 lying above the plane of the imidazolium ring and being in short contacts with C4 and C5 atoms of the imidazolium moiety and the oxygen atom of the hydroxyl group [123]. Yet, even with the added interaction of the functional hydroxyl group the binding energy is ca. 11 kcal/mol smaller than the BE of $[BF_4]^-$ anion to the Pd_5 cluster, suggesting a less important role of the cations with respect to stabilization of Pd-NPs relative to the role of the anions. This is in agreement with the above BE results, obtained earlier, for the Au_n clusters [119].

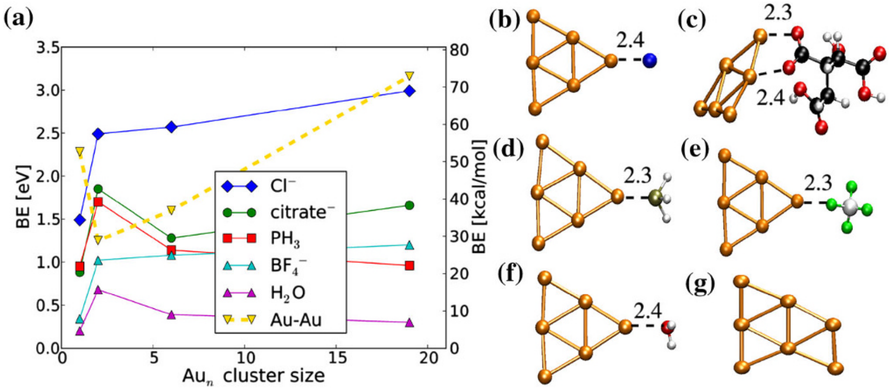

Fig. 7 **a** Binding energies (BE) and Au-atom addition energies depending on the cluster size. **b**–**f** Relaxed configurations of Au_6 bound to **b** Cl^-, **c** citrate$^-$ ($C_6H_7O_7^-$), **d** PH_3, **e** BF_4^- and (f) H_2O. **g** Relaxed configuration of Au_7. The bond lengths are in Å [74]. Reproduced from Ref. [74] with permission, copyright 2010 The Royal Society of Chemistry

The order of the calculated BEs was obtained for interaction energies between a Pd_5 cluster and the anions was $[CF_3CO_2]^-$ (~47 kcal/mol) > $[BF_4]^-$ (~41 kcal/mol) > $[OTf]^-$ (~34 kcal/mol) > $[PF_6]^-$ (~31 kcal/mol) ≅ $[NTf_2]^-$ (~31 kcal/mol) [124].

For further examples of cation and anion effects on the formation of metal nanoparticles in ILs, see also the separate section on “cation and anion effects” below.

The IL-cations with alkyl chains can further contribute to the steric stabilization of nanoparticles. If the ionic liquid cation contains a long alkyl side chain, e.g., from imidazolium- or pyrazolium-based cations, the cations on or near the nanoparticle surface can provide steric forces by stretching out their bulky side-chains, thus hindering the nanoparticles from approaching each other (cf. Figure 5) [125]. ILs can also be designed with functional coordinating groups primarily in the alkyl chains of the cations, which thereby act as coordinating capping ligands (see Sect. 6 with Fig. 12 below) [126].

As noted above for stabilizing ionic components the cations and anions of ionic liquids, possibly as charged ion clusters, will surround the nanoparticle surface to build an electric double-layer, thus providing an electrostatic force to keep the nanoparticles apart from each other [65]. The role of electrostatics in stabilizing the nanoparticles in ionic liquids has been well recognized [115, 127–133].

The interaction energies of ILs with different cations and anions to Ru-NPs were compared by titration calorimetry and by molecular simulation. Structural information from the molecular simulation suggests that the charged parts of both the IL cation and the anion are in contact with the surface of the nanoparticle, with only small charge separation at the interface. The results of this study suggest an IL-dependent balance between electrostatic, van der Waals, and H-bond forces for the stabilization of metal nanoparticles [128].

For nanoparticles in ionic liquids, steric stabilization can emerge from bulky groups in the IL cation (or anion) and/or from the addition of macromolecules, both of which hinder nanoparticles from contacting each other and from aggregation [125]. When only small amounts of polymer are added to the nanoparticle–ionic liquid dispersion, the nanoparticle surfaces are partially covered by polymers and polymer coils extend from one particle surface to another particle. Thereby, the polymers chains can function as bridges between nanoparticles. As an excess of polymer is added, the polymers can fully cover the nanoparticle surface to form an adsorbed polymer layer [134]. Then steric repulsion and stabilization arises from the adsorbed polymer layers of neighboring nanoparticles as noted above. Block copolymers have been utilized to stabilize nanoparticle dispersion [105]. PEO–PPO–PEO block copolymer Pluronic P123 ($EO_{20}PO_{70}EO_{20}$) formed a lamellar lyotropic liquid crystal structure in pyrrolidinium nitrate ([Pyrr][NO_3]) ionic liquid at the 58–82 wt% polymer concentration range. Gold nanoparticles were prepared by reducing $HAuCl_4$ in this lyotropic liquid crystal [135].

Various and also yet unknown factors influence the stability of nanoparticles in ionic liquids and lead to nanoparticle size [136–139] and/or morphology [140–145] changes during synthesis. Smaller diameter and narrower distributions of synthesized nickel metal and zinc oxide nanoparticles were prepared in ionic liquids with longer side chains [137, 141]. Larger size or varied morphologies of synthesized nanoparticles can be caused by conglomeration of unstable primary nanoparticles, which may result from smaller ionic liquid anions exhibiting stronger cation–anion Coulomb attraction [145], or less coordinating anions of ionic liquids [116, 144] or higher temperature decreasing the viscosity of the ionic liquid and increasing the diffusive velocities of the nanoparticles [146, 147]. An improved understanding of the stability of nanoparticle dispersions in ionic liquids is still needed to assist efforts directed toward the synthesis of nanoparticles with controlled size and morphology in ionic liquids [125].

5.2 Hydrogen Bonding Interactions

Imidazolium cations through their imidazolium-C–H groups can form hydrogen bonds to the fluorine or oxygen atoms of the IL anions [148–150] that induce structural directionality (IL effect). This is different from tetraalkylammonium ILs that, by contrast, display charge-ordered structures. The ILs act as stabilizing media, but importantly also display self-organization on the nanomolecular scale. The imidazolium ILs form extended hydrogen-bond networks at the liquid state and therefore are by definition ‘‘supramolecular’’ fluids. This structural organization of ILs can be used as ‘‘entropic drivers’’ (the so-called ‘‘IL effect’’) for the spontaneous, well-defined and extended ordering of nanoscale structures. The properties of especially the imidazolium-based ILs are based on their formation of aggregates rather than on their isolated cations and anions [151, 152]. The structures of 1,3-dialkylimidazolium salts form an extended network of cations and anions connected together by hydrogen bonds in the condensed phase, which is maintained to a great extent in the gas phase [152].

Thus, hydrogen bond interactions are present in imidazolium-based ionic liquid nanoparticle dispersions in addition to electrostatic, van der Waals and steric interactions [153, 154]. Metal nanoparticles can possess hydroxido and/or oxido ligands on their surface, which can also hydrogen bond with ionic liquids [155]. Such metal-surface bound oxygen species can be derived from crystal water of the metal salt precursor (cf. Table 1), from difficult to remove residual water in the IL or from gaseous dioxygen (as impurity even when working under inert gas). The IL-cation–anion hydrogen bond and NP–IL hydrogen bond compete with each other and contribute to nanoparticle stabilization in ionic liquids, as shown in Fig. 8 [156, 157].

The interaction energies of ILs with an additional alkyl group in the C-2 position of the imidazolium cation ($[C_4C_1C_1Im][NTf_2]$ with 1-butyl-2,3-dimethylimidazolium) and a *N*-butyl-*N*-methylpyrrolidinium cation ($[C_4C_1Pyrr][NTf_2]$) to Ru-NPs were compared to other $[C_nC_1Im]^+$-ILs by titration calorimetry and by molecular simulation. Ionic liquids with cations which are less likely to form hydrogen bonds such as $[C_4C_1C_1Im]^+$ or $[C_4C_1Pyrr]^+$ also interact less favorably with Ru-NPs [113].

Qualitative direct comparison (for the same IL-anion) of an IL with the $[C_4C_1Im]^+$-cation which has hydrogen-bonding possibility and a cation with no significant H-bond formation reveals the former to be better stabilizers for Au- or Cu-NPs whereas in the latter ILs fast particle growth and agglomeration was observed [156]. The stable time of the colloidal dispersion in $[C_4C_1Im][N(CN)_2]$ and trihexyltetradecylphosphonium dicyanamide $[P_{66614}][N(CN)_2]$ was 3 days versus 1 day. In $[C_4C_1Im][BF_4]$ or $[C_4C_1Im][NTf_2]$ Au-NPs were stable for 1 week while in *N*-butyl-*N*-methyl-pyrrolidinium, $[C_4C_1Pyr][NTf_2]$ or in *N*-butyl-pyridinium$[C_4Py][NTf_2]$ fast precipitation occurred due to fast particle growth and agglomeration [156].

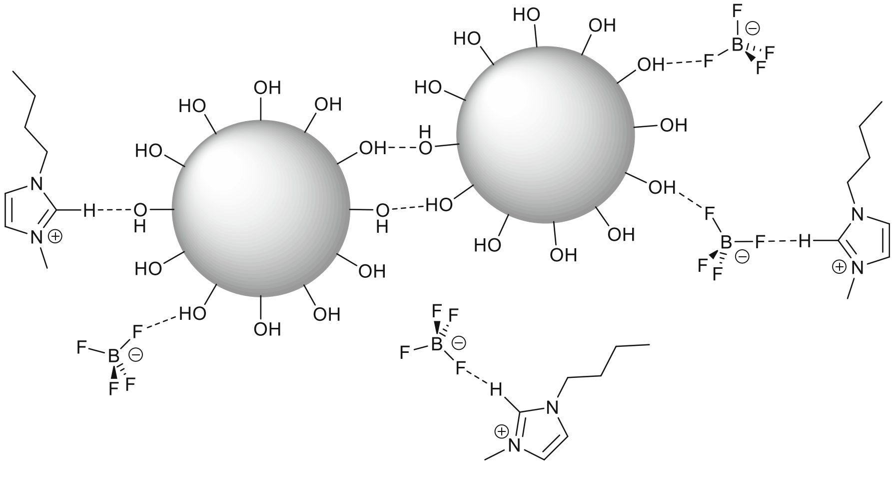

Fig. 8 Hydrogen bonds formed between the surface hydroxyl-groups of metal nanoparticles and ions of ionic liquids and between cations and anions of ionic liquids

5.3 Influence of Polar and Non-Polar Domains in ILs

The segregation of hydrophilic or hydrophobic regions, polar and non-polar domains in imidazolium-based ILs is an important physicochemical property which effects their solvation and interaction with dissolved species (Fig. 9) [158–160]. Expectedly polar substrates, like metal salts are preferentially dissolved in polar domains and non-polar compounds like organometallic precursors in non-polar IL regions [159, 161]. Consequently, the nature of the metal precursor—ionic or neutral for instance—is also a key determinant of the size and shape of the prepared metal NPs as the polarity and the volume of these IL nanoregions may modulate this. The nanoparticle growth process is probably controlled by the local concentration of the precursor and possibly limited to the size and shape of the IL polar or non-polar domains (Fig. 9) [65].

5.4 Cation and Anion Effects

Nanoparticle preparation in ILs is often accompanied by heating to over 100 °C or even 200 °C. Changing the anions or the cations can have a strong influence on the thermal behavior, density, viscosity (see below), or conductivity [160]. For example, the simple sum of the cationic and anionic self-diffusion coefficients ($D_{\mathrm{cation}} + D_{\mathrm{anion}}$) for selected room temperature ILs follows the (anion) order $[C_4C_1Im][NTf_2] > [C_4C_1Im][CF_3CO_2] > [C_4C_1Im][OTf] > [C_4C_1Im][BF_4] > [C_4C_1Im][(F_5C_2SO_2)_2N] > [C_4C_1Im][PF_6]$ at 30 °C. This order of the diffusion coefficients is as expected the reverse of the order of the viscosity (see below). The degree of ionic association can be estimated from the ratio of the molar conductivity obtained from the impedance measurement (Λ_{imp}) and the molar conductivity calculated from the ionic diffusivity (Λ_{NMR}). For the anions at the given $[C_4C_1Im]^+$ cation the degree of association increases according to $[PF_6]^- < [BF_4]^- < [(F_5C_2SO_2)_2N]^- < [NTf_2]^- < [OTf]^- < [CF_3CO_2]^-$. In the order from $[PF_6]^-$ to $[NTf_2]^-$ electronegative fluorine atom and electron-withdrawing perfluorosulfonyl groups contribute to the distribution of the anionic

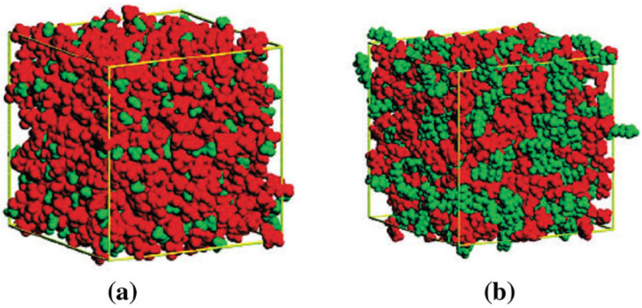

Fig. 9 Simulation study of two imidazolium-based hexafluorophosphate ILs (each *box* contains 700 ions) showing polar (*red*) and non-polar (*green*) domains for **a** 1-ethyl-3-methylimidazolium, $[C_2C_1Im]^+$ and **b** 1-methyl-3-*n*-octylimidazolium $[C_8C_1Im]^+$. Reprinted with permission from Ref. [162]. Copyright 2006 American Chemical Society

charge. Also, the surface coverage of the anion backbone by fluorine atoms may be a significant factor for only weak interactions with the $[C_4C_1Im]^+$ cation. Whereas, the relatively higher anionic charge localization in $[OTf]^-$ ($=[CF_3SO_3]^-$ and $[CF_3CO_2]^-$) leads to their stronger interaction with the $[C_4C_1Im]^+$ cation [160]. The interaction energies of ILs with $[C_4C_1Im]^+$ and the anions $[NTf_2]^-$ or $[PF_6]^-$ were compared by titration calorimetry and by molecular simulation to Ru-NPs. No significant differentiating effect of the two anions was observed. Structural information from the molecular simulation suggests that the charged parts of both the IL cation and the anion are in contact with the surface of the nanoparticle, with only small charge separation at the interface [128]. The relative order of anion stabilities for ILs with the $[C_1C_4Im]^+$ cation was observed as $[NTf_2]^- > [PF_6]^- > [BF_4]^- \gg Cl^-$ [163].

The size of M-NPs was found to increase with the molecular volume of the anion of the IL. Metal nanoparticles synthesized in $[C_4C_1Im]^+$ ILs increased in size with the size of the IL-anion from small $[BF_4]^-$ over $[OTf]^-$ to the large $[NTf_2]^-$ anion [20, 164, 165]. The IL-anion molecular volume was taken as the size of the IL-anion. The effect was shown for Rh- [164], Ag- [20] and W-NPs [165]. Figure 10 depicts the correlation between the nanoparticle size of W- and Rh-NPs and the molecular volume of the anion.

The influence of the anion to metal nanoparticles was also observed by several other research groups [116, 167–170]. 1-*n*-Butyl-methyl-imidazolium salts $[C_4C_1Im]^+$ with weakly coordinating perfluorinated counter anions ($[BF_4]^-$, $[PF_6]^-$ or $[NTf_2]^-$) were qualitatively found to be better stabilizers compared to ILs with anions of higher coordination strength (dicyanamide, $[N(CN)_2]^-$). In the former ILs Au- or Cu-NPs were stable colloidal dispersions, that is, without precipitation or aggregation for 1 week to several weeks. In $[C_4C_1Im][N(CN)_2]$ Au-NPs were stable for only 3 days due to fast particle growth and agglomeration [156].

The IL-anion had an effect on the dissolution and reaction rate when fabricating copper nanoparticles from Cu flakes (of 1–5 µm) in ILs [171]. When $[C_4C_1Im][BF_4]$, $[C_4C_1Im][PF_6]$ and $[C_2C_1Im][BF_4]$ were used, it took a relatively long

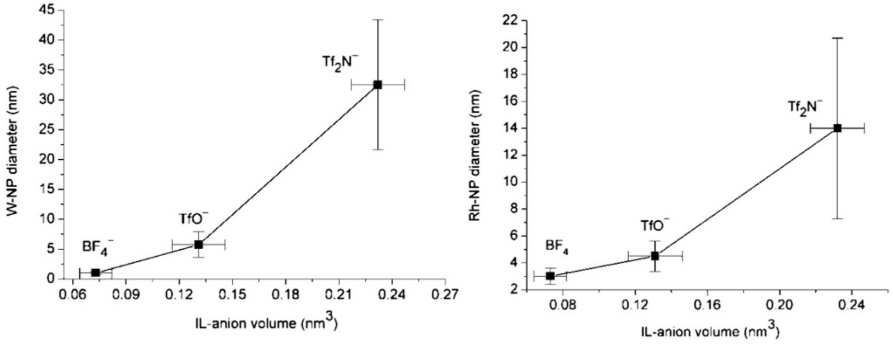

Fig. 10 Correlation between nanoparticle size of W- and Rh-NPs from TEM measurements and the IL anion molecular volume with standard deviation (1σ) as *error bars* [164, 165]. Left part is reproduced from Ref. [165] with permission, copyright 2008 The Royal Society of Chemistry; right part is adapted from Ref. [164] with permission, copyright 2009 Elsevier B.V.

time, of 24 h to obtain the copper nanoparticles while in $[C_4C_1Im][NO_3]$ dissociation of Cu flakes to Cu nanoparticles took place in about 5 min. It was suggested that the favorable interaction between free nitrate anion of $[C_4C_1Im][NO_3]$ and the Cu metal surface caused the flakes to dissociate in the ionic liquid, forming as much smaller nanoparticles than in the other ILs. From TEM the average diameter of the obtained Cu-NPs in $[C_4C_1Im][NO_3]$ was 10 nm [171] while the size range in $[C_4C_1Im][BF_4]$ was 50–100 nm [172] or 20–200 nm [124] and in $[C_4C_1Im][PF_6]$ and $[C_2C_1Im][BF_4]$ it was 80–100 nm [172]. Overall, these results suggested that the pristine micro-sized copper flakes were already clusters of primary nanoparticles, which were dis-agglomerated to nanoparticles by introduction in ILs to a different extent.

Decomposition of $Pd(OAc)_2$ in a series of hydroxyl-functionalized ionic liquids (ILs) with the 1-(2′-hydroxylethyl)-3-methylimidazolium cation $[HOC_2C_1Im]^+$ and the anions $[BF_4]^-$, $[PF_6]^-$, $[OTf]^-$ $[CF_3CO_2]^-$ ($[ATf]^-$) or $[NTf_2]^-$ gave Pd-NPs with slightly different medium diameters from 2.3 ± 0.4 nm in $[HOC_2C_1Im][ATf]$ or 2.4 ± 0.5 nm in $[HOC_2C_1Im][OTf]$ to 4.0 ± 0.6 nm in $[HOC_2C_1Im][BF_4]$ [124]. Noteworthy from comparison with the non-functionalized IL, $[C_4C_1Im][NTf_2]$ (medium diameter 6.2 ± 1.1 nm) significantly smaller nanoparticles were obtained. More importantly, the ease of formation of the Pd-NPs in the $[HOC_2C_1Im]^+$-based ILs followed the order $[NTf_2]^-$, $[PF_6]^- > [BF_4]^- > [OTf]^- > [ATf]^-$ based on the residual unreacted amount of $Pd(OAc)_2$ in the dispersion. This order does not relate to the stability towards aggregation. For this, it could only be noted that in $[HOC_2C_1Im][PF_6]$ a series of larger Pd-NPs over 8 nm (compared to the average 3.1 ± 0.7 nm) were also present and the Pd-NPs were least stable in this $[PF_6]^-$ IL. From the ratio of metallic Pd to PdO observed in the XPS the relative resistance of the Pd-NPs towards oxidation may be determined. The ability of the $[HOC_2C_1Im]^+$-ILs to prevent the Pd NPs from undergoing oxidation follows the trend $[NTf_2]^- > [PF_6]^- > [ATf]^- > [OTf]^- > [BF_4]^-$. For example, only 12.6% of PdO was present in the NPs isolated with the $[NTf_2]^-$-anion whereas nearly half the Pd amount was oxidized to PdO in the case of the $[BF_4]^-$-anion. Studies for $[PF_6]^-$ and $[NTf_2]^-$ showed that these are the least nucleophilic anions [173] and also the most hydrophobic ones in the series while $[BF_4]^-$ is the least hydrophobic/most hydrophilic one of the anions used in this comparison. Therefore, the oxidation-protecting effect may be accounted for by the fact that water and oxygen are repelled most by the $[PF_6]^-$ and $[NTf_2]^-$ anions [124].

Strong anion effects were seen on gold nanoparticle formation in ionic liquids of $[C_2C_1Im]^+$ with ethyl sulfate ($[EtSO_4]^-$), $[OTf]^-$ and methanesulfonate ($[CH_3SO_3]^-$) anions [78]. Face-centered cubic gold nanoparticles were grown by reduction of $HAuCl_4 \cdot 3H_2O$ with glycerol at temperatures between 120 and 180 °C. The $[CH_3SO_3]^-$ anion yielded nanoparticles with diameters between 5 and 7 nm, which increasingly aggregate at higher reaction temperatures but the primary particle size is not affected. Thus, the $[CH_3SO_3]^-$ anion or more accurate the anion-cation ($[C_2C_1Im]^+$) combination under the given reaction conditions is able to efficiently trap very small gold nanoparticles. High temperatures like 180 °C do not lead to a further growth of the particles, but rather to a controlled aggregation. From $[OTf]^-$ also small 5–7 nm particles formed, but only at low temperatures whereas above ca. 160 °C, large, ill-defined and aggregated particles were obtained. Apparently the $[OTf]^-$ anion is only partially able to stabilize small gold particles and above a certain reaction temperature the stabilization exerted by the IL is broken and led to larger aggregates. With the $[EtSO_4]^-$ anion polydisperse samples formed at all temperatures except 160 °C. In the temperature window around 160 °C individual, controlled ca. 15–20 nm particles were grown from $[C_2C_1\text{-}Im][EtSO_4]$ [78].

It is evident from many reports on cation and anion effects of ILs that the interaction between an IL and a (growing) nanocrystal is far from understood but that a detailed understanding of the IL–nanoparticle interaction, of the thermodynamics and kinetics, and of the initial nucleation process would be needed for a more rational design of nanomaterials in ILs [78].

5.5 Alkyl Chain Effects

The interaction energies of ILs with different alkyl chain lengths ($[C_nC_1Im][NTf_2]$ ($n = 2, 4, 6, 8, 10$)), an additional alkyl group in the C-2 position of the imidazolium cation ($[C_4C_1C_1Im][NTf_2]$ with 1-butyl-2,3-dimethylimidazolium) and a *N*-butyl-*N*-methylpyrrolidinium cation ($[C_4C_1Pyrro][NTf_2]$) to Ru-NPs were compared by titration calorimetry and by molecular simulation. The interaction energy of $[C_nC_1Im][NTf_2]$ ($n = 6, 8, 10$) with Ru-NPs is larger than that of $[C_4C_1Im][NTf_2]$ indicating that longer alkyl side chains enhance the interactions with Ru-NPs. Here $[C_2C_1Im][NTf_2]$ also has stronger interactions with the nanoparticles, but this deviation was explained by the cation not having a significant nonpolar moiety. Structural information from the molecular simulation suggests that the alkyl chains tend to point away from the surface but are still within interaction range [128].

Trends for the influence of the alkyl chain length were invoked by many other research groups [174–177] such that the alkyl chain length has an influence of the particle size of M-NPs [21, 174]. In the well-designed series of mono- and dicationic imidazolium ILs with different alkyl chain length and $[NTf_2]^-$ as anion (Fig. 11) Ni-NPs were synthesized by spontaneous decomposition of [bis(1,5-cyclooctadiene)nickel(0)], $Ni(COD)_2$. Well dispersed Ni-NPs with a small mean size and narrow size distribution could be obtained. The Ni-NP size increased with increasing chain lengths from 2.4 ± 0.8 nm in $[C_{12}C_1Im][NTf_2]$ over 2.9 ± 0.4 nm in $[C_{18}C_1Im][NTf_2]$, 4.0 ± 0.5 nm in $[C_{12}C_{12}Im][NTf_2]$ about equal to 4.4 ± 0.7 nm in $[C_{12}C_1C_{12}Im][NTf_2]$, 5.4 ± 1.6 nm in $[C_{12}Im\text{-}\mu\text{-}C_6\text{-}ImC_{12}][NTf_2]$, (200 nanoparticle were measured in the first four cases, 50 NPs in the last case). When an ethereal oxygen donor atom was introduced in the functional IL $[C_{12}Im\text{-}\mu\text{-}C_2OC_2\text{-}ImC_{12}][NTf_2]$ the particle size decreased to 3.4 ± 0.2 nm (based on 200 NPs). In addition, formation of regularly interspaced NP arrays was also observed in such long chain ILs [174].

For Au-NPs in imidazolium-based ILs the particles diameter increases from 0.75 to 3.5 nm diameter for $[C_2C_1Im]^+$, $[C_4C_1Im]^+$ and $[C_8C_1Im]^+$ cations and $[BF_4]^-$ as counter ion [178, 179]. Further, decomposition of $Ni(COD)_2$ in $[C_nC_1Im][NTf_2]$ ILs gave Ni-NPs with an average diameter from 2.4 to 5.4 nm [174] or 4.9 to

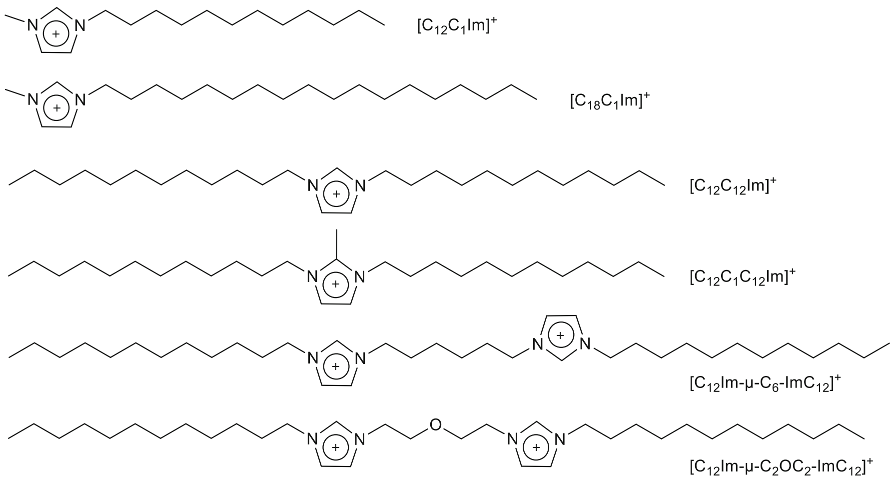

Fig. 11 Series of ionic liquid cations with increasing chain length and $[NTf_2]^-$ as the common anion used in the comparative synthesis of Ni-NPs from $Ni(COD)_2$ to elucidate the chain-length effect on the metal nanoparticle size [174]

5.9 nm [180] with conflicting trends such that the particle diameter increased or decreased with the cation size.

When interpreting such trends with seemingly small differences in nanoparticle size, the standard deviation σ of the size distribution must be considered, however. The, at first sight, slightly larger nanoparticle size may still well be within 1σ or certainly within 3σ of the average diameter of another size.

In another study, nickel nanoparticles were obtained by decomposition of $Ni(COD)_2$, again with different nanoparticle diameter, depending on the chain length of the imidazolium cation with $[NTf_2]^-$ as anion. The results were 5.9 ± 1.4 nm for $[C_4C_1Im]^+$, 5.6 ± 1.3 nm for $[C_8C_1Im]^+$, 4.9 ± 0.9 nm for $[C_{10}C_1Im]^+$, 5.1 ± 0.9 nm for $[C_{14}C_1Im]^+$ and 5.5 ± 1.1 nm for $[C_{16}C_1Im]^+$. While it may appear that an increase of the alkyl chain (from *n*-butyl to *n*-hexadecyl) induces the formation of nanoparticles with a smaller diameter and size-distribution, all distributions are strongly overlapped within their 1σ regions already. The differences in diameter and size distribution are relatively small and could be a TEM artefact (sample preparation and/or particle counting, for instance) as the authors admit themselves [180].

Table 2 illustrates that a change in imidazolium cation or rather in 1-*n*-alkyl chain length does not give a clear trend in the size of the Ni-NPs synthesized by nickel(II)-bis(amidinate) or $Ni(COD)_2$ precursor decomposition through microwave assisted heating. The size distributions overlap considerably already within the 1σ standard deviation. Only in the case of the $Ni(COD)_2$ precursor there is an indication of Ni-NP size increase from n-butyl over *n*-octyl to *n*-dodecyl which is reverse from the aforementioned trend [181].

In terms of stabilization, short alkyl-chain-methyl-imidazolium salts $[C_4C_1Im]^+$ with weakly coordinating perfluorinated counter anions ($[BF_4]^-$, $[PF_6]^-$ or $[NTf_2]^-$)

Table 2 Ni-NP diameter and distribution from different precursors and in different ILs

Ni-precursor[a], IL	TEM Ø (1σ) [nm][bc]
$[Ni(AMD)_2]$	
$[C_4C_1Im][BF_4]$	5 (±2)
$[C_{12}C_1MIm][BF_4]$	7 (±2)
$[C_4C_1Im][PF_6]$	7 (±4)
$[C_8C_1Im][PF_6]$	7 (±1)
$[C_{12}C_1Im][PF_6]$	9 (±3)
$[C_4C_1Im][NTf_2]$	10 (±2)
$[C_8C_1Im][NTf_2]$	10 (±3)
$[C_{12}C_1Im][NTf_2]$	10 (±4)
$Ni(COD)_2$	
$[C_4C_1Im][PF_6]$	8 (±3)
$[C_8C_1Im][PF_6]$	10 (±2)
$[C_{12}C_1Im][PF_6]$	15 (±2)

[a] 1.0 wt. % Ni-NP/IL dispersions obtained by microwave-assisted heating with 100 W for 10 min at 220 °C

[b] The size distribution was calculated from a manual diameter determination over a minimum of 50 isolated particles

[c] Average diameter and standard deviation

were qualitatively found to be better stabilizers compared to ILs with cations bearing long alkyl chains (trihexyltetradecylphosphonium $[P_{66614}]^+$, 1-octyl-3-methylimidazolium $[C_8C_1Im]^+$) and anions of higher coordination strength (dicyanamide, $[N(CN)_2]^-$) (see above). In $[C_4C_1Im]^+$ with $[BF_4]^-$, $[PF_6]^-$ or $[NTf_2]^-$ anions Au- or Cu-NPs were stable colloidal dispersions, that is, without precipitation or aggregation for 1 week to several weeks. In $[C_4C_1Im][N(CN)_2]$ Au-NPs were stable for 3 days. In comparison in $[C_8C_1Im][PF_6]$ or in $[P_{66614}][N(CN)_2]$ fast precipitation or stability for only 1 day, respectively, was observed due to fast particle growth and agglomeration [156].

5.6 Viscosity

Viscosity of the reaction medium can be expected to have a crucial influence on the growth and agglomeration of nanoparticles. Unfortunately, differences in viscosity cannot be treated separately from concomitant changes in alkyl chain length or anion. Thus, viscosity dependence for nanoparticle size and size distribution appears to be seldom addressed [64].

For example, for $[C_4C_1Im]^+$-ILs the viscosity at 30 °C follows the anion order $[PF_6]^- > [(F_5C_2SO_2)_2N]^- > [BF_4]^- > [OTf]^- > [CF_3CO_2]^- > [NTf_2]^-$, which is as expected opposite to the order of the diffusion coefficients (see above).

For the $[C_nC_1Im][BF_4]$ ($n = 2, 4, 6$) [182], $[C_nC_1Im][PF_6]$ ($n = 4$–9) and $[C_nC_1Im][NTf_2]$ ($n = 2$–10) series the viscosity increases with increasing the number n of carbon atoms in the linear alkyl chain in the imidazolium cation. However, the trends are quite different. An almost linear dependence of the viscosity as a function of the alkyl chain length group is observed for the $[NTf_2]^-$ ILs while the dependence for the $[PF_6]^-$ ILs is more like an exponential increase with a local maximum at $n = 7$. Also, the $[C_nC_1Im][PF_6]$ ionic liquids are much more viscous than their $[NTf_2]^-$ analogs [183].

6 Influence of Functional ILs to Metal Nanoparticles

Functionalized imidazolium ILs can be used to modify the surface of metal NPs [184, 185], in particular to provide stable dispersion of NPs in water [113, 186], which is important to many applications [187]. Thiol- [184, 188, 189], ether- [113], carboxylic acid- [115], amino- [190] and hydroxyl-functionalized imidazolium ILs are available (Fig. 12), for example, to prepare aqueous dispersions of noble metal NPs.

From comparison of the decomposition of $Pd(OAc)_2$ in a series of hydroxyl-functionalized ionic liquids (ILs) with the 1-(2′-hydroxylethyl)-3-methylimidazolium cation $[HOC_2C_1Im$ or $HOEMIm]^+$ and the anions $[BF_4]^-$, $[PF_6]^-$, $[OTf]^-$, $[CF_3CO_2]^-$ or $[NTf_2]^-$ and the non-functionalized IL, $[C_4C_1Im][NTf_2]$ it appeared that the hydroxyl group accelerated the formation of the NPs, and also helped to protect the NPs from oxidation once formed. Significantly smaller Pd-NPs were obtained in the [HOEMIm or $HOC_2C_1Im]^+$-ILs with average diameters from 2.3 ± 0.4 nm in the $[CF_3CO_2]^-$ salt to 4.0 ± 0.6 nm in the $[BF_4]^-$ analog while in non-functionalized $[C_4C_1Im][NTf_2]$ the average diameter was 6.2 ± 1.1 nm [124].

An X-ray photoelectron spectroscopic study of purified aminoethyl-methylimidazolium bromide, $[H_2NC_2C_1Im$ or AEMIm]Br-stabilized Au-NPs suggested that both the imidazolium ring and the functional amino group were involved in the interaction with the NP surface (cf. Figure 4) [115]. A shift in binding energies in the peaks of the carbon and nitrogen atoms in the imidazolium ring and amino N atom and a change in the width of the N1 s peak were observed. The XPS results were interpreted as either an electrostatic interaction between the imidazolium cation and the negatively charged metal surface, an interaction between the amino group and surface metal atom or the simultaneous coordination of the imidazolium cation and the functional group with the metal NPs. The electrostatic imidazolium-metal interaction would change the positive charge density of the imidazole ring. Amino group coordination to the metal NPs surface would induce a shift in N atom binding energies in the peak of the amino group and a change in the width of the N1 s peak [115].

Comparison between the closely related di-cationic ILs $[C_{12}Im\text{-}\mu\text{-}C_6\text{-}ImC_{12}][NTf_2]$, and $[C_{12}Im\text{-}\mu\text{-}C_2OC_2\text{-}ImC_{12}][NTf_2]$ (cf. Figure 11) revealed a significant decrease in Ni-NP size (obtained from spontaneous decomposition of $Ni(COD)_2$) from 5.4 ± 1.6 nm to 3.4 ± 0.2 nm when an ethereal oxygen donor atom was introduced. This indicates a better templating and stabilization effect due to coordination of the negatively polarized O-atom on the metal surface [174].

The synthesis of Co-NPs and Mn-NPs by microwave-heating induced decomposition of the metal carbonyls $Co_2(CO)_8$ and $Mn_2(CO)_{10}$, respectively, yields smaller and better separated particles in the functionalized IL 1-(3-carboxyethyl)-3-methyl-imidazolium tetrafluoroborate [CEMIm or $HO_2CC_2C_1Im][BF_4]$ (1.6 ± 0.3 and 4.3 ± 1.0 nm, respectively) than in the non-functionalized IL $[C_4C_1Im][BF_4]$. The particles are stable in the absence of capping ligands (surfactants) for more than 6 months although some variation in particle size could be observed by TEM (Fig. 13) [191].

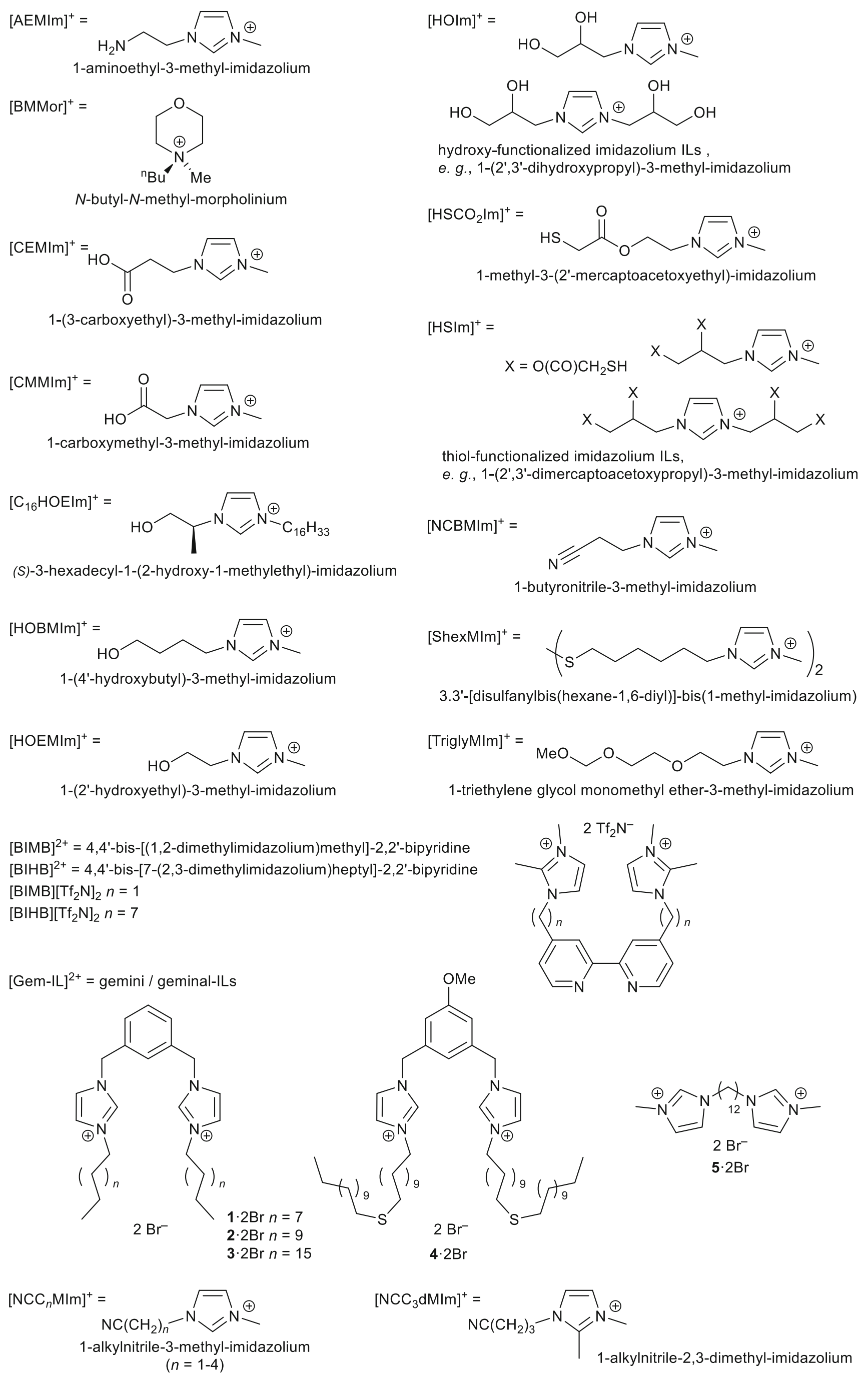

Fig. 12 Examples of functionalized imidazolium ILs. Graphical collection reprinted with permission from the author of Ref. [30]. Copyright Wiley-VCH 2013

A special type of functionalized ILs are gemini imidazolium amphiphiles (cf. Figure 12) [192]. Gemini-type ILs based on imidazolium salts are investigated as simultaneous nanoparticle stabilizers, surfactants and transfer agents into organic media. Au-NPs with imidazolium ligands of the gemini-ILs **1**·2Br to **4**·2Br (cf. Figure 12) that are stable in dispersion and where the IL plays a triple role: phase transfer of the gold precursor salt $H[AuCl_4]$ from an aqueous phase to toluene during the synthesis, stabilization of the gold colloid, and binding agent for an ibuprofenate guest. The bis-imidazolium IL ions around the gold nanoparticles do not exchange with thiolate ligands. When both species are present the gold surface prefers the IL cation and anion to thioether ligands. The long alkyl chains in **3**·2Br (cf. Figure 12) could incorporate ibuprofenate, a model for carboxylate-containing anionic drugs, and release it at a slower rate [192].

7 *N*-Heterocyclic Carbene Formation During Metal Nanoparticle Synthesis in Imidazolium ILs

During the last 20 years *N*-heterocyclic carbenes (NHCs) established themselves as a leading class of ligands in molecular organometallic chemistry [193]. NHCs are neutral electron-rich σ-donor ligands, which often form very strong metal ligand σ-bonds. These properties would also be very attractive for the stabilization and reactivity modulation of metal NPs [194–197]. NHCs have been proven to bind efficiently to the surfaces of Ru- [198–201], Ag- [202], Au- [202–205], Pd- [205, 206] and Pt-NPs [207]. Furthermore, there is evidence that NHCs could be intermediate species, by in situ deprotonation of the imidazolium cation at the acidic C2-H position when NPs are formed and stabilized in imidazolium-based ionic liquids for Au-NPs [208], Pd-NPs [208, 209], Rh-NPs [210], Ir-NPs [210, 211] and Ni-NPs [212].

NHC-stabilization of Au- and Pd-NPs was promoted by deprotonation of the bis(*N*,*N*'-*n*-hexyl)imidazolium cation $[C_6C_6Im]^+$ prior to reduction. This was achieved by treating the imidazolium salt $[C_6C_6Im]^+\ {}_n[MCl_4]^{n-}$ with sodium

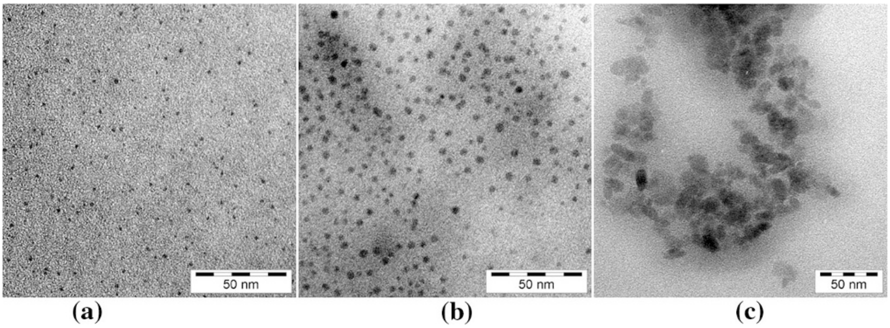

Fig. 13 TEM-images of Co-NPs in [CEMIm or $HO_2CC_2C_1Im$][BF_4] (cf. Figure 12) **a** 6 weeks after synthesis; **b** 6 months after synthesis; **c** Co-NPs from $Co_2(CO)_8$ in [BMIm][BF_4]. Reprinted with permission. Copyright the Royal Society of Chemistry, 2011 [191]

hydride in 1: 1 dichloromethane–toluene, before adding sodium borohydride to reduce the tetrachloridoaurate(III) ($n = 1$) and dibromidodichloridopalladate(II) ($n = 2$) metal precursor. The ^{1}H NMR spectrum of the Au-NPs revealed the disappearance of the acidic imidazolium C2 proton resonance, while broadening and splitting was observed for the other peaks, which is typical of NP-coordinated ligands. ^{13}C NMR also failed to locate a peak for C2, which is probably due to anisotropy resulting from the NHC to Au-NP surface coordination. Conversely, the C2 ^{1}H peak was observed for the Pd-NPs produced without prior imidazolium deprotonation. TEM analysis gave slightly larger sizes of 2.7 ± 0.9 nm for the NHC-capped Pd-NPs than for the imidazolium halide surfactant stabilized Pd-NPs with 1.8 ± 0.4 nm [208].

The Pd-NHC complex (C_4C_1Im-NHC)Pd(PPh_3)X (X = Br, Cl) formed from [Pd(Ar)Br(PPh_3)$_2$] and [$PdCl_2(PPh_3)_2$] in [C_4C_1Im][BF_4] when aqueous Na_2CO_3 was added for imidazolium deprotonation [209].

NHC complexes of rhodium and iridium were obtained in neat [C_4C_1Im][NTf_2] from metal complexes with basic anionic ligands, [M(COD)(PPh_3)X], X = OEt, $MeCO_2$, which reacted with the imidazolium cation under deprotonation giving the M-NHC moiety and the free protonated base HOEt, $MeCO_2H$ [210].

The synthesis of Ir nanoparticles by reduction of [(COD)Ir(CH_3CN)$_2$]BF_4 with H_2 or D_2 in the presence of Proton Sponge (PS^{TM}) in acetone with set but variable amounts of [C_4C_1Im][NTf_2] gave evidence for the formation of at least transiently surface-ligand-coordinated NHCs. When using D_2 deuterium incorporation was apparent from ^{2}H NMR spectroscopy at the imidazolium C2-H, C4-H, C5-H, and butyl –(CH_2CH_2)C8–H(CH_3) positions of the [C_4C_1Im]$^+$ cation. Conversely, ^{1}H NMR spectra showed a decreased intensity of the 2-, 4-, 5-, and 8-H hydrogens in the [C_4C_1Im]$^+$ cation. Without the presence of Ir-NPs no D incorporation into the imidazolium cation occured. A sequence of N-heterocyclic carbene formation by oxidative addition of the imidazolium cation, followed by H/D scrambling atop the nanoparticle surface, then reductive elimination of a imidazolium-C-D bond is suggested [211].

During the auto-decomposition of Ni(COD)$_2$ in imidazolium ILs the formation of bis(imidazolylidene)nickel complexes [(NHC)$_2$NiH]$^+$ was detected by mass spectrometry [212].

8 Conclusion

In the last years many different M-NPs (monometallic and bimetallic) in ILs were obtained. Especially ILs with imidazolium cations feature prominently in the formation and stabilization of M-NPs. Such imidazolium ILs simultaneously act as reaction media, hydrogen sources, catalysts, templating agents and stabilizers for the synthesis of metal nanoparticles.

Various and also yet unknown factors influence the stability of nanoparticles in ionic liquids and lead to nanoparticle size and/or morphology changes during synthesis. An improved understanding of the stability of nanoparticle dispersions in ionic liquids is still needed to assist efforts directed toward the synthesis of nanoparticles with controlled size and morphology in ionic liquids.

An influence of the anion to metal nanoparticles was also observed by several other research groups. Qualitatively, the size of M-NPs was found to increase with the molecular volume of the anion of the IL. Also, an influence of the imidazolium alkyl-chain length on the particle size of M-NPs is often invoked, yet the unclear direction. It is both found that the NP size increased with increasing chain lengths whereas in other studies an increase of the alkyl chain gave nanoparticles with a smaller diameter and size-distribution.

It is evident from many reports on cation and anion effects of ILs that the interaction between an IL and a (growing) nanocrystal is far from understood but that a detailed understanding of the IL–nanoparticle interaction would be needed for a more rational design of nanomaterials in ILs.

Furthermore, thiol-, ether-, carboxylic acid-, amino- and hydroxyl-functionalized ILs can be used to coordinate to the surface of metal NPs akin to the action of coordinating capping ligands. Also, for imidazolium-based ionic liquids there is evidence that *N*-heterocyclic carbenes, NHCs could be formed by in situ deprotonation of the imidazolium cation at the acidic C2-H position, at least as intermediate species, during the nanoparticle seeding and growth process.

References

1. Sankar M, Dimitratos N, Miedziak PJ, Wells PP, Kiely CJ, Hutchings GJ (2012) Chem Soc Rev 41:8099–8139
2. Turkevich J, Stevenson PC, Hillier J (1951) Discuss Faraday Soc 11:55–75
3. Brust M, Walker M, Bethell D, Schriffrin DJ, Whyman RJ (1994) J Chem Soc Chem Commun 801–802
4. Bönnemann H, Braun G, Brijoux W, Brinkmann R, Schulze Tilling A, Seevogel K, Siepen K (1996) J Organomet Chem 520:143–162
5. Aiken JD III, Finke RG (1999) J Mol Catal A 145:1–44
6. Schmid G (2001) Nanoscale materials in chemistry In: Klabunde KJ (ed) Wiley-Interscience, New York, p 15
7. Faraday M (1857) Philos Trans R Soc. London 147:145–181
8. Manojkumar K, Sivaramakrishna A, Vijayakrishna K (2016) J Nanopart Res 18:103–125
9. Lu AH, Salabas EL, Schüth F (2007) Angew Chem Int Ed 46:1222–1244
10. Feldheim DL, Foss CA (2001) Metal nanoparticles: synthesis, characterization and applications. Taylor and Francis, London
11. Bruchez M, Moronne M, Gin P, Weiss S, Alivisatos AP (1998) Science 281:2013–2016
12. Saha K, Agasti SS, Kim C, Li X, Rotello VM (2012) Chem Rev 112:2739–2779
13. Li JH, Zhang JZ (2009) Coord Chem Rev 253:3015–3041
14. Barnes WL, Dereux A, Ebbesen TW (2003) Nature 424:824–830
15. Poizot P, Laruelle S, Grugeon S, Dupont L, Tarascon JM (2000) Nature 407:496–499
16. Armelao L, Quici S, Barigelletti F, Accorsi G, Bottaro G, Cavazzini M, Tondello E (2010) Coord Chem Rev 254:487–505
17. Navalon S, Dhakshinamoorthy A, Alvaro M, Garcia H (2016) Coord Chem Rev 312:99–148
18. Walker JM, Zaleski JM (2016) Nanoscale 8:1535–1544
19. Zhao P, Feng X, Huang D, Yang G, Astruc D (2015) Coord Chem Rev 287:114–136
20. Redel E, Thomann R, Janiak C (2008) Inorg Chem 47:14–16

21. Migowski P, Zanchet D, Machado G, Gelesky MA, Teixeira SR, Dupont J (2010) Phys Chem Chem Phys 12:6826–6833
22. Pachon LD, Rothenberg G (2008) Appl Organomet Chem 22:288–299
23. Lee W, Scholz R, Nielsch K, Gösele U (2005) Angew Chem 117:6204–6208
24. Davar F, Loghman-Estarki MR, Salavati-Niasari M, Mazaheri M (2016) J Clust Sci 27:593–603
25. Wang H, Xu JZ, Zhu JJ, Chen HY (2002) J Cryst Growth 244:88–94
26. Chen WX, Lee JY, Liu Z (2002) Chem Commun 2588-2589
27. Sreeju N, Rufus A, Philip D (2016) J Mol Liq 221:1008–1021
28. Qin Y, Ji X, Jing J, Liu H, Wu H, Yang W (2010) Colloids Surf A 372:172–176
29. Goesmann H, Feldmann C (2010) Angew Chem Int Ed 49:1362–1395
30. Janiak C (2013) Z Naturforschung B 68:1059–1089. doi:10.5560/ZNB.2013-3140
31. Hostetler MJ, Wingate JE, Zhong C-J, Harris JE, Vachet RW, Clark MR, Londono JD, Green SJ, Stokes JJ, Wignall GD, Glish GL, Porter MD, Evans ND, Murray RW (1998) Langmuir 14:17–30
32. Templeton AC, Wuelfing WP, Murray RW (2000) Acc Chem Res 33:27–36
33. Weare WW, Reed SM, Warner MG, Hutchison JE (2000) J Am Chem Soc 122:12890–12891
34. Schmid G, Pfeil R, Boese R, Bandermann F, Meyer S, Calis GHM, van der Velden JWA (1981) Chem Ber 114:3634–3642
35. Yang J, Deivaraj TC, Too H-P, Lee JY (2004) Langmuir 20:4241–4245
36. Pan C, Pelzer K, Philippot K, Chaudret B, Dassenoy F, Lecante P, Casanove MJ (2001) J Am Chem Soc 123:7584–7593
37. Lee CL, Wan CC, Wang YY (2001) Adv Funct Mater 11:344–347
38. Tiwari AK, Gangopadhyay S, Chang CH, Pande S, Saha SK (2015) J Colloid Interface Sci 445:76–83
39. Esumi K, Hara J, Aihara N, Usui K, Torigoe K (1998) J Colloid Interface Sci 208:578–581
40. Xu J, Hu J, Peng C, Liu H, Hu Y (2006) J Colloid Interface Sci 298:689–693
41. Bakshi MS, Sharma P, Banipal TS (2007) Mater Lett 61:5004–5009
42. Song C, Wu D, Zhang F, Liu P, Lu Q, Feng X (2012) Chem Commun 48:2119–2121
43. Kumar KS, Vasuki R, Priya R (2016) J Pharm Techn 8:12130–12143
44. Demir MM, Gulgun MA, Menceloglu YZ, Erman B, Abramchuk SS, Makhaeva EE, Khokhlov AR, Matveeva VG, Sulman MG (2004) Macromolecules 37:1787–1792
45. Crespy D, Landfester K (2009) Polymer 50:1616–1620
46. Huang H, Yang X (2004) Carbohydr Res 339:2627–2631
47. Vollmer C, Janiak C (2011) Coord Chem Rev 255:2039–2057
48. Wender H, Migowski P, Feil AF, Teixeira SR, Dupont J (2013) Coord Chem Rev 257:2468–2483
49. Welton T (2004) Coord Chem Rev 248:2459–2477
50. Welton T (1999) Chem Rev 99:2071–2083
51. Hallett JP, Welton TT (2011) Chem Rev 111:3508–3576
52. Morris RE (2009) Chem Commun 2990–2998
53. Voronchikhina LI, Zhuralev OE, Verolainen NV, Krotova NI (2016) Russ J Gen Chem 86:1314–1318
54. Villanueva M, Coronas A, Garcia J, Salgado J (2013) Ind Eng Chem Res 52:15718–15727
55. Kosmulski M, Gustafsson J, Rosenholm JB (2004) Thermochim Acta 412:47–53
56. Ngo HL, LeCompte K, Hargens L, McEwen AB (2000) Thermochim Acta 357–358:97–102
57. Chen G, Kang S, Ma Q, Chen W, Tang Y (2014) Magn Reson Chem 52:673–679
58. Craig SL (2009) Angew Chem Int Ed 48:2645–2647
59. Daniel MC, Astruc D (2004) Chem Rev 104:246–293
60. Parvulescu VI, Hardacre C (2007) Chem Rev 107:2615–2665
61. Steinrück HP, Wasserscheid P (2015) Catal Lett 145:380–397
62. Freudenmann D, Wolf S, Wolff M (2011) Feldmann C. Angew Chem 123:11244–11255
63. Dupont J, de Souza RF, Suarez PAZ (2002) Chem Rev 102:3667–3691
64. Tokuda H, Hayamizu K, Ishii K (2005) Susan MdABH, Watanabe M. J Phys Chem B 109:6103–6110
65. Dupont J, Scholten JD (2010) Chem Soc Rev 39:1780–1804
66. Marcos Esteban R, Janiak C (2017) In Nanocatalysis in Ionic Liquids In: Prechtl M (ed) chapter 8. Wiley-VCH, Weinheim, p 147–169
67. Janiak C (2014) in Catalysis in ionic liquids: from catalyst synthesis to application In: Hardacre C, Parvulescu V, chapter 11. RSC Publishing, Cambridge, p 537–577
68. Janiak C (2015) Topics Organomet Chem 51:17–53. doi:10.1007/3418_2013_70

69. Antonietti M, Kuang D, Smarsly B, Zhou Y (2004) Angew Chem Int Ed 43:4988–4992
70. Fonseca GS, Umpierre AP, Fichtner PFP, Teixeira SR, Dupont J (2003) Chem Eur J 9:3263–3269
71. Huang J, Jiang T, Han B, Gao H, Chang Y, Zhao G, Wu W (2003) Chem Commun 1654-1655
72. Krämer J, Redel E, Thomann R, Janiak C (2008) Organometallics 27:1976–1978
73. Silveira ET, Umpierre AP, Rossi LM, Machado G, Morais J, Soares GV, Baumvol IJR, Teixeira SR, Fichtner PFP, Dupont J (2004) Chem Eur J 10:3734–3740
74. Redel E, Walter M, Thomann R, Hussein L, Krüger M, Janiak C (2010) Chem Commun 46:1159–1161
75. Stellaci F, Bauer CA, Meyer-Friedrichsen T, Wenseleers W, Alain V, Kuebler SM, Pond SJK, Zhang Y, Marder SR, Perry JW (2002) Adv Mater 14:194–198
76. Mohan B, Woo H, Jang S, Lee S, Park S, Park KH (2013) Solid State Sci 22:16–20
77. Zhang B, Yuan Y, Philippot K, Yan N (2015) Catal Sci Technol 5:1683–1692
78. Khare V, Li Z, Mantion A, Ayi AA, Sonkaria S, Voelkl A, Thünemann AF, Taubert A (2010) J Mater Chem 20:1332–1339
79. Jiang HY, Zheng HH (2015) Appl Cat A 499:118–123
80. Dewan M, De A (2015) Mozumdar. Inorg Chem Commun 53:92–96
81. Esteban RM, Meyer H, Kim J, Gemel C, Fischer RA, Janiak C (2016) Eur J Inorg Chem 2106-2113
82. Schütte K, Meyer H, Gemel C, Barthel J, Fischer RA, Janiak C (2014) Nanoscale 6:3116–3126
83. Esteban RM, Schütte K, Brandt P, Marquardt D, Meyer H, Beckert F, Mülhaupt R, Kölling H, Janiak C (2015) Nano-Struct Nano-Objects 2:11–18
84. Ayi AA, Anyama CA, Khare V (2015) J Mat, vol. 2015, Article ID 372716, http://dx.doi.org/10.1155/2015/372716
85. Andanson JM, Marx S, Baiker A (2012) Catal Sci Technol 2:1403–1409
86. Schütte K, Doddi A, Kroll C, Meyer H, Wiktor C, Gemel C, van Tendeloo G, Fischer RA, Janiak C (2014) Nanoscale 6:5532–5544
87. Wegner S, Saito M, Barthel J, Janiak C (2016) J Organomet Chem 821:192–196
88. Wang Y, Yang H (2005) J Am Chem Soc 127:5316–5317
89. Arquillière PP, Helgadottir IS, Santini CC, Haumesser P-H, Aouine M, Massin L, Rousset J-L (2013) Top Catal 56:1192–1198
90. Dash P, Dehm NA, Scott RWJ (2008) J Mol Catal A 286:114–119
91. Stankus DP, Lohse SE, Hutchison JE, Nason JA (2010) Environ Sci Technol 45:3238–3244
92. Astruc D (2008) Nanoparticles and catalysis. Wiley Online Library, Weinheim
93. Jiang J, Oberdörster G, Biswas P (2009) J Nanopart Res 11:77–89
94. Kim T, Lee K, Gong M-s, Joo S-W (2005) Langmuir 21:9524–9528
95. Derjaguin B, Landau L (1940) Acta Phys Chem USSR 14:1–30
96. Verwey EJW, Overbeek JThG (1948) Theory of the stability of lyophobic colloids. Elsevier, Amsterdam
97. Li Q, Jonas U, Zhao XS, Kappl M (2008) Asia-Pac J Chem Eng 3:255–268. doi:10.1002/apj.144
98. Ninham BW (1999) Adv Col Interf Sci 83:1–17
99. Raveendran P, Fu J, Wallen SL (2003) J Am Chem Soc 125:13940–13941
100. Verwey EJW, Overbeek JTG (1999) Theory of the stability of lyophobic colloids. Dover Publications Mineola, New York
101. Finke RG (2002) Metal nanoparticle: synthesis, characterization and applications. Marcel Dekker, New York
102. Ott LS, Finke RG (2006) Inorg Chem 45:8283–8393
103. Boström M, Williams DRW, Ninham BW (2001) Phys Rev Lett 87:168103–168107
104. Liang Y, Hilal N, Langston P, Starov V (2007) Adv Col Interf Sci 134–135:151–166
105. Sarkar B, Venugopal V, Tsianou M, Alexandridis P (2013) Col Surf 422:155–164
106. Napper DH (1977) J Col Interf Sci 58:390–407
107. Lin Y, Smith TW, Alexandridis P (2002) J Col Interf Sci 255:1–9
108. Luckham PF (1991) Adv Col Interf Sci 34:191–215
109. Morrison ID, Ross S (2002) Colloidal dispersions: suspensions, emulsions, and foams. Wiley-Interscience, New York
110. Zhao M, Li N, Zheng L, Li G, Yu L (2008) J Dispers Sci Technol 29:1103–1105
111. Obliosca JM, Arellano IHJ, Huang MH, Arco SD (2010) Mater Lett 64:1109–1112
112. Rubim JC, Trindade FA, Gelesky MA, Aroca RF, Dupont J (2008) J Phys Chem C 112:19670–19675

113. Schrekker HS, Gelesky MA, Stracke MP, Schrekker CML, Machado G, Teixeira SR, Rubim JC, Dupont J (2007) J Col Interf Sci 316:189–195
114. Chun YS, Shin JY, Song CE, Lee SG (2008) Chem Commun 942–944
115. Zhang H, Cui H (2009) Langmuir 25:2604–2612
116. Scheeren CW, Machado G, Teixeira SR, Morais J, Domingos JB, Dupont J (2006) J Phys Chem B 110:13011–13020
117. Fonseca GS, Machado G, Teixeira SR, Fecher GH, Morais J, Alves MCM, Dupont J (2006) J Col Interf Sci 301:193–204
118. Kang SW, Char K, Kang YS (2008) Chem Mater 20:1308–1311
119. Redel E, Walter M, Thomann R, Vollmer C, Hussein L, Scherer H, Krüger M, Janiak C (2009) Chem Eur J 15:10047–10059
120. Pearson RG (1997) Chemical hardness. Application from molecules to solids. Wiley-VCH, Weinheim
121. Baker TA, Friend CM, Kaxiras E (2008) J Am Chem Soc 130:3720–3721
122. Katsyuba SA, Zvereva EE, Yan N, Yuan X, Kou Y, Dyson PJ (2012) ChemPhysChem 13:1781–1790
123. Kim J, Kang SW, Mun SH, Kang YS (2009) Ind Eng Chem Res 48:7437–7441
124. Yuan X, Yan N, Katsyuba SA, Zvereva EE, Kou Y, Dyson PJ (2012) Phys Chem Chem Phys 14:6026–6033
125. He Z, Alexandridis P (2015) Phys Chem Chem Phys 17:18238–18261
126. Kang X, Sun X, Han B (2016) Adv Mater 28:1011–1030
127. Vanecht E, Binnemans K, Patskovsky S, Meunier M, Seo JW, Stappers L, Fransaer J (2012) Phys Chem Chem Phys 14:5662–5671
128. Podgorsek A, Pensado A, Santini C, Gomes M, Padua A (2013) J Phys Chem C 117:3537–3547
129. Frolov AI, Kirchner K, Kirchner T, Fedorov MV (2012) Faraday Discuss 154:235–247
130. Cheng P, Liu C, Yang Y, Huang S (2015) Chem Phys 452:1–8
131. Pensado AS, Padua AAH (2011) Angew Chem 123:8842–8846
132. Knapp R, Wyrzgol SA, Reichelt M, Hammer T, Morgner H, Müller TE, Lercher JA (2010) J Phys Chem C 114:13722–13729
133. Bernardi F, Scholten JD, Fecher GH, Dupont J, Morais J (2009) Chem Phys Lett 479:113–116
134. Rosen MJ, Kunjappu JT (2012) Surfactants and Interfacial Phenomena. Wiley, Weinheim
135. Li Q, Li A (2012) Asian J Chem 24:847–850
136. Wender H, de Oliveira LF, Migowski P, Feil AF, Lissner E, Prechtl MHG, Teixeira SR, Dupont J (2010) J Phys Chem C 114:11764–11768
137. Torimoto T, Okazaki KI, Kiyama T, Hirahara K, Tanaka N, Kuwabata S (2006) Appl Phys Lett 89:243117
138. Hatakeyama Y, Okamoto M, Torimoto T, Kuwabata S, Nishikawa K (2009) J Phys Chem C 113:3917–3922
139. Kessler MT, Hentschel MK, Heinrichs C, Roitsch S, Prechtl MHG (2014) RSC Adv 4:14149–14156
140. Scariot M, Silva DO, Scholten JD, Machado G, Teixeira SR, Novak MA, Ebeling G, Dupont J (2008) Angew Chem Int Ed 47:9075–9078
141. Wang L, Chang L, Zhao B, Yuan Z, Shao G, Zheng W (2008) Inorg Chem 47:1443–1452
142. Li X, Liu Y, Guo W, Chen J, He W, Peng F (2014) Electrochim Acta 135:550–557
143. Lorbeer C, Cybinska J, Mudring AV (2014) J Mater Chem C 2:1862–1868
144. Patil AB, Bhanage BM (2014) Phys Chem Chem Phys 16:3027–3035
145. Liu CH, Mao BH, Gao J, Zhang S, Gao X, Liu Z, Lee ST, Sun XH, Wang SD (2012) Carbon 50:3008–3014
146. Hatakeyama Y, Takahashi S, Nishikawa K (2010) J Phys Chem C 114:11098–11102
147. Kameyama T, Ohno Y, Kurimoto T, Okazaki KI, Uematsu T, Kuwabata S, Torimoto T (2010) Phys Chem Chem Phys 12:1804–1811
148. Tsuzuki S, Tokuda H, Hayamizu K, Watanabe M (2005) J Phys Chem B 109:16474–16481
149. Hardacre C, Holbrey JD, McMath SEJ, Bowron DT, Soper AK (2003) J Chem Phys 118:273–278
150. Dupont J, Suarez PAZ (2006) Phys Chem Chem Phys 8:2441–2452
151. Gozzo FC, Santos LS, Augusti R, Consorti CS, Dupont J, Eberlin MN (2004) Chem Eur J 10:6187–6193
152. Neto BAD, Santos LS, Nachtigall FM, Eberlin MN, Dupont J (2006) Angew Chem 118:7409–7412
153. Dupont J (2011) Acc Chem Res 44:1223–1231
154. Dong K, Zhang SJ (2012) Chem Eur J 18:2748–2761

155. Chang HC, Hung TC, Chang SC, Jiang JC, Lin SH (2011) J Phys Chem C 115:11962–11967
156. Richter K, Birkner A, Mudring AV (2011) Phys Chem Chem Phys 13:7105–7110
157. Wittmar A, Ulbricht M (2012) Ind Eng Chem Res 51:8425–8433
158. Dupont J (2004) J Braz Chem Soc 15:341–350
159. Schröder U, Wadhawan JD, Compton RG, Marken F, Suarez PAZ, Consorti CS, de Souza RF, Dupont J (2000) New J Chem 24:1009–1015
160. Tokuda H, Hayamizu K, Ishii K, Hasan Susan MdAB, Watanabe M (2004) J Phys Chem B 108:16593–16600
161. Anderson JL, Armstrong DW (2003) Anal Chem 75:4851–4858
162. Lopes JNA, Padua AAH (2006) J Phys Chem B 110:3330–3335
163. Reddy RG (2006) J Phase Equilib Diffus 27:210–211
164. Redel E, Krämer J, Thomann R, Janiak C (2009) J Organomet Chem 694:1069–1075
165. Redel E, Thomann R, Janiak C (2008) Chem Commun 15:1789–1791
166. Neouze MA (2010) J Mater Chem 20:9593–9607
167. Peng H, Lin L, Ding G (2015) Energy 89:410–420
168. Navolotskaya DV, Toh HS, Batchelor-McAuley C, Compton RG (2015) ChemistryOpen 4:595–599
169. Wang XM, Zhou DD, Zou QQ, Xia YY (2012) J Mater Chem 22:15418–15426
170. Keul HA, Ryu HJ, Möller M, Bockstaller MR (2011) Phys Chem Chem Phys 13:13572–13578
171. Hong GH, Kang SW (2013) Ind Eng Chem Res 52:794–797
172. Han KI, Kang SW, Kim J, Kang YS (2011) J Membr Sci 374:43–48
173. Lancaster NL, Welton T (2004) J Org Chem 69:5986–5992
174. Yang M, Campbell PS, Santini CC, Mudring AV (2014) Nanoscale 6:3367–3375
175. Gutel T, Santini CC, Philippot K, Padua A, Pelzer K, Chaudret B, Chauvin Y, Basset JM (2009) J Mater Chem 19:3624–3631
176. Banerjee A, Theron R, Scott RWJ (2012) ChemSusChem 5:109–116
177. Jacquemin J, Husson P, Majer V, Costa Gomes MF (2007) J Solut Chem 36:967–979
178. Hatakeyama Y, Okamoto M, Torimoto T, Kuwabata S, Nishikawa K (2009) J Phys Chem C 113:3917–3922
179. Hatakeyama Y, Onishi K, Nishikawa K (2011) RSC Adv 1:1815–1821
180. Migowski P, Machado G, Texeira SR, Alves MCM, Morais J, Traverse A, Dupont J (2007) Phys Chem Chem Phys 9:4814–4821
181. Wegner S, Rutz C, Schütte K, Barthel J, Bushmelev A, Schmidt A, Dilchert K, Fischer RA, Janiak C (2017) Chem Eur J 23:6330–6340 (http://dx.doi.org/10.1002/chem.201605251)
182. Wittmar A, Gajda M, Gautam D, Dörfler U, Winterer M, Ulbricht M (2013) J Nanopart Res 15:1–12
183. Dzyuba S, Bartsch RA (2002) ChemPhysChem 2:161–166
184. Itoh H, Naka K, Chujo Y (2004) J Am Chem Soc 126:3026–3027
185. Chen H, Dong S (2007) Langmuir 23:12503–12507
186. Wei GT, Yang Z, Lee CY, Yang HY, Wang CRC (2004) J Am Chem Soc 126:5036–5037
187. Lewis LN (1993) Chem Rev 93:2693–2730
188. Kim KS, Demberelnyamba D, Lee H (2004) Langmuir 20:556–560
189. Gao S, Zhang H, Wang X, Mai W, Peng C, Ge L (2005) Nanotechnology 16:1234–1237
190. Marcilla R, Mecerreyes D, Odriozola I, Pomposo JA, Rodriguez J (2007) NANO Br Rep Rev 2:169–173
191. Marquardt D, Xie Z, Taubert A, Thomann R, Janiak C (2011) Dalton Trans 40:8290–8293
192. Casal-Dujat L, Rodrigues M, Yagüe A, Calpena AC, Amabilino DB, Gonzalez-Linares J, Borras M, Perez-Garcia L (2012) Langmuir 28:2368–2381
193. Diez-Gonzalez S, Marion N, Nolan SP (2009) Chem Rev 109:3612–3676
194. Richter C, Schaepe K, Glorius F, Ravoo BJ (2014) Chem Commun 50:3204–3207
195. Magna L, Chauvin Y, Niccolai GP, Basset JM (2003) Organometallics 22:4418–4425
196. Lecocq V, Olivier-Bourbigou H (2007) Oil Gas Sci Technol 62:761–773
197. Holloczki O, Gerhard D, Massone K, Szarvas L, Nemeth B, Veszpremi T, Nyulaszi L (2010) New J Chem 34:3004–3009
198. Martinez-Prieto LM, Ferry A, Lara P, Richter C, Philippot K, Glorius F, Chaudret B (2015) Chem Eur J 21:17495–17502
199. Martinez-Prieto LM, Urbaneja CC, Palma P, Campora J, Philippot K, Chaudret B (2015) Chem Commun 51:4647–4650
200. Lara P, Rivada-Wheelaghan O, Conejero S, Poteau R, Philippot K, Chaudret B (2011) Angew Chem Int Ed 50:12286–12290

201. Gonzalez-Galvez D, Lara P, Rivada-Wheelaghan O, Conejero S, Chaudret B, Philippot K, van Leeuwen PWNM (2013) Catal Sci Technol 3:99–105
202. Ling X, Schaeffer N, Roland S, Pileni M (2013) Langmuir 29:12647–12656
203. Roland S, Ling X, Pileni MP (2016) Langmuir 32:7683–7696
204. Vignolle J, Tilley TD (2009) Chem Commun 7230–7232
205. Hurst EC, Wilson K, Fairlamb IJS, Chechik V (2009) New J Chem 33:1837–1840
206. Rühling A, Schaepe K, Rakers L, Vonhören B, Tegeder P, Ravoo BJ, Glorius F (2016) Angew Chem Int Ed 55:5856–5860
207. Baquero EA, Tricard S, Flores JC, de Jesus E, Chaudret B (2014) Angew Chem Int Ed 53:1–6
208. Serpell CJ, Cookson J, Thompson AL, Brown CM, Beer PD (2013) Dalton Trans 42:1385–1393
209. Mathews CJ, Smith PJ, Welton T, White AJP, Williams DJ (2001) Organometallics 20:3848
210. Hintermair U, Gutel T, Slawin AMZ, Cole-Hamilton DJ, Santini CC, Chauvin Y (2008) J Organomet Chem 693:2407–2414
211. Ott LS, Cline ML, Deetlefs M, Seddon KR, Finke RG (2005) J Am Chem Soc 127:5758–5759
212. Prechtl MHG, Campbell PS, Scholten JD, Fraser GB, Machado G, Santini CC, Dupont J, Chauvin Y (2010) Nanoscale 2:2601–2606

Top Curr Chem (Z) (2017) 375:78
DOI 10.1007/s41061-017-0166-z

REVIEW

Lewis Acidic Ionic Liquids

Lucy C. Brown[1] · **James M. Hogg**[1] ·
Małgorzata Swadźba-Kwaśny[1]

Received: 24 May 2017 / Accepted: 10 August 2017 / Published online: 21 August 2017

Abstract Until very recently, the term Lewis acidic ionic liquids (ILs) was nearly synonymous with halometallate ILs, with a strong focus on chloroaluminate(III) systems. The first part of this review covers the historical context in which these were developed, speciation of a range of halometallate ionic liquids, attempts to quantify their Lewis acidity, and selected recent applications: in industrial alkylation processes, in supported systems (SILPs/SCILLs) and in inorganic synthesis. In the last decade, interesting alternatives to halometallate ILs have emerged, which can be divided into two sub-sections: (1) liquid coordination complexes (LCCs), still based on halometallate species, but less expensive and more diverse than halometallate ionic liquids, and (2) ILs with main-group Lewis acidic cations. The two following sections cover these new liquid Lewis acids, also highlighting speciation studies, Lewis acidity measurements, and applications.

Keywords Lewis acidity · Halometallate ionic liquids · Liquid coordination complexes · Solvate ionic liquids · Borenium cations

1 Introduction

The development and applications of Lewis acids hold an important place in chemical research. In industrial processes, heterogeneous Lewis acids are dominant, from simple metal halides to metal oxides with Lewis acidic sites (alumina,

---

Chapter 7 was originally published as Brown, L. C., Hogg, J. M. & Swadźba-Kwaśny, M. Top Curr Chem (Z) (2017) 375: 78. DOI 10.1007/s41061-017-0166-z.

✉ Małgorzata Swadźba-Kwaśny
m.swadzba-kwasny@qub.ac.uk

[1] School of Chemistry and Chemical Engineering, The Queen's University of Belfast, David Keir Building, Stranmillis Road, Belfast BT9 5AG, UK

zirconia, titania) [1, 2]. Lewis acids, such as BF_3 or $AlCl_3$, are also combined with Brønsted acids to yield Brønsted superacidic catalysts. In organic synthesis, a wide variety of Lewis acids are used, both in stoichiometric and catalytic quantities, with acidic metal centers varying from alkali metals (Li, Na), through to group 13 elements (Al^{III}, Ga^{III}, In^{III}), to Zn^{II}, Sn^{II} and Sn^{IV}, Hf^{IV} and lanthanides [3]. In addition to simple halides, metal triflates and bistriflamides are also used, as well as organometallic Lewis acids, with an increasing focus on water-stable Lewis acids [4]. Elaborate chiral ligands are used for asymmetric reactions [5]. In main-group chemistry, frustrated Lewis pairs, which are combinations of Lewis acids and bases prevented from forming an adduct by steric hindrance [6], have recently opened up the field of metal-free catalysis and small molecule activation [7]. In this context, the archetypical Lewis acid is $B(C_6F_5)_3$, though a plethora of charge-neutral and cationic Lewis acids, based predominantly on boron, but also on phosphorus, silicon and main-group metals, have been synthesized [8–10].

Against this backdrop, the chemistry of Lewis acidic ionic liquids appears structurally monotonous, with a strong focus on halometallate Lewis acidic anions—in particular chloroaluminate(III) ILs. These were the first group of ionic liquids to capture the attention of chemists across disciplines, and remained the center of research efforts until ca. 2000 [11, 12]. Afterwards, the spotlight has shifted to 'air- and water-stable' systems [13], but research on Lewis acidic halometallate ILs has been under continuous development, which was reviewed in 2014 by Estager et al. [14]. Recent years have been marked by: (1) the maturing of chloroaluminate(III) ILs in catalysis, expressed in engineering advances and the announcement of several full-scale industrial processes, (2) the development of new ionic liquid-like systems, based on metal chloride eutectics (liquid coordination complexes), and (3) the naissance of ILs with Lewis acidic cations, with hopefully a lot of inspiring chemistry still to come. All three families of Lewis acidic ionic liquids will be discussed, including the historical context, speciation studies, quantification of acidity, and examples of applications. Abbreviations used throughout the text are listed in Table 1.

2 Chlorometallate Ionic Liquids

2.1 Historical Context

The study of modern ionic liquids originated from high-temperature inorganic molten salts (studied as heat transfer fluids and electrolytes), which lead to lower melting organic salts, especially chloroaluminate(III) ILs (Fig. 1, left), based on $[AlCl_4]^-$ and $[Al_2Cl_7]^-$ anions [15]. In parallel, mechanistic studies on $AlCl_3$-promoted Friedel–Crafts chemistry revealed $[AlCl_4]^-$ and $[Al_2Cl_7]^-$ anions to balance the charge of the intermediate, a protonated toluenium cation [12, 16]. This naturally led to studies of Friedel–Crafts chemistry in the $[C_2mim]Cl–AlCl_3$ system [17], which may be considered the starting point of Lewis acid catalysis in chlorometallate ILs, with over 400 citations to date.

Table 1 Abbreviations used in this work (where n = alkyl chain length)

Notation	Full name
$[C_n mim]^+$	1-Alkyl-3-methylimidazolium cation
$[P_{nnnn}]^+$	Tetraalkylphosphonium cation
$[N_{nnnn}]^+$	Tetraalkylammonium cation
MX_m	Metal halide
$[OTf]^-$	Triflate anion
$[NTf_2]^-$	*Bis*(trifluoromethanesulfonyl)imide anion, $[N(SO_2CF_3)_2]^-$
$[BETI]^-$	*Bis*(trifluoroethanesulfonyl)imide anion, $[N(SO_2C_2F_5)_2]^-$
G*n*	Glycol ether (glyme), with $n + 1$ oxygens in its structure
RON	Research octane number
SILP	Supported ionic liquid phase
SCILL	Solid catalyst with ionic liquid layer
TEPO	Triethylphosphine oxide

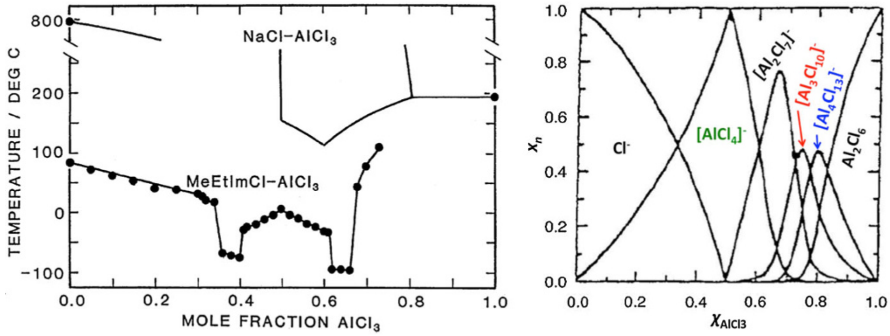

Fig. 1 *Left* Comparison of phase diagrams of NaCl–$AlCl_3$ and 1-ethyl-3-methylimidazolium chloride-$AlCl_3$ [15]. *Right* Concentration of anionic species in the $[C_2mim]Cl–AlCl_3$ system, at 200 °C, calculated from a thermodynamic model. (From [14], adapted from [18])

Boon's work was preceded—by over a decade—by Parshall, who in 1972 used organic molten salts, $[N_{2222}][SnCl_3]$ and $[N_{2222}][GeCl_3]$, as solvents for $PtCl_2$ [19]. They also acted as Lewis acidic co-catalysts in hydrogenation and other Pt-catalyzed reactions, through the formation of Pt active species, such as $[Pt(SnCl_3)_5]^{3-}$. It was a visionary paper, but initially went almost unnoticed, and was only sparsely cited until its re-discovery in the community around 2000. This possibly asserted the dominance of chloroaluminate(III) ILs as the archetypical Lewis acidic ionic liquids.

2.2 Speciation

Halometallate ILs are synthesized by the reaction of a metal halide with an organic halide salt, at various molar ratios (Eq. 1) [14]. The composition of the ionic liquid is typically reported as the molar ratio of metal halide, $\chi_{\mathrm{MX}m}$ (see Eq. 2 and Fig. 1).

$$[\mathrm{cation}]X + nMX_m \rightarrow [\mathrm{cation}][M_nX_{n\times m+1}] \tag{1}$$

$$\chi_{\mathrm{MX}m} = n(\mathrm{MX}_m)/\Sigma(n) \tag{2}$$

The range of $\chi_{\mathrm{MX}m}$ values that yield homogenous ILs varies, depending on the metal and the halide. Within this range, different halometallate anions may be formed, depending on the composition. More often than not, several anions in a dynamic equilibrium with each other are present.

2.2.1 Chloroaluminate(III) Ionic Liquids

Complex anionic speciation of halometallate ionic liquids is reflected in the exemplary phase diagram for chloroaluminate(III) ILs (Fig. 1). It is the speciation that dictates their physical properties and chemical behavior, including Lewis acidity. Organic cations are considered to affect physical properties of halometallate ILs, such as viscosity, density, or melting points, but typically have little influence on the anionic speciation, and thus on Lewis acidity [14]. Anionic speciation in chloroaluminate(III) systems was confirmed using multiple direct techniques, such as ^{27}Al NMR spectroscopy [20], Raman spectroscopy [21], and supporting techniques, such as phase diagrams [22]. In-depth discussion of these techniques is beyond the scope of this work, but extensive primary literature exists, as well as older reviews [11, 23] and a recent review by our group [14].

Concentration of anionic chlorometallate(III) species as a function of composition, calculated from a thermodynamic model for $[\mathrm{C_2mim}]\mathrm{Cl}$–$\mathrm{AlCl_3}$ (Fig. 1, right), is concurrent with phase diagram for the same system (Fig. 1, left). For the $\chi_{\mathrm{AlCl3}} = 0.50$ composition (equimolar), there is only one anion present, $[\mathrm{AlCl_4}]^-$; the peritectic point in the phase diagram (Fig. 1, left) indicates the formation of a compound, $[\mathrm{C_2mim}][\mathrm{AlCl_4}]$. For all other compositions, multiple equilibrated species are present. With excess of $[\mathrm{C_2mim}]\mathrm{Cl}$ ($\chi_{\mathrm{AlCl3}} < 0.50$), free chloride is in equilibrium with $[\mathrm{AlCl_4}]^-$. For an excess of $\mathrm{AlCl_3}$, up to $\chi_{\mathrm{AlCl3}} = 0.67$ (2:1 ratio), dinuclear $[\mathrm{Al_2Cl_7}]^-$ and monomeric $[\mathrm{AlCl_4}]^-$ are equilibrated. In both cases, this is reflected in the formation of very low-melting, eutectic compositions. Finally, for large excess of $\mathrm{AlCl_3}$ ($\chi_{\mathrm{AlCl3}} > 0.67$), oligomeric anions were postulated (Fig. 1, right), but these exist in equilibrium with solid aluminium(III) chloride. Therefore, homogenous ionic liquids are only formed for compositions $\chi_{\mathrm{AlCl3}} \leq 0.67$, and the slightest excess of $\mathrm{AlCl_3}$ added above this ratio results in cloudiness of otherwise clear liquid. The main anionic equilibrium in chloroaluminate(III) ILs is shown in Eq. 3.

$$2[AlCl_4]^- \rightleftarrows [Al_2Cl_7]^- + Cl^- \tag{3}$$

There is a crucial link between speciation and Lewis acidity. The four chloride ligands around the aluminium center in $[AlCl_4]^-$ effectively prevent other ligands from coordinating to form five- and six-coordinate complexes, and thus render the anion neutral. In the vast majority of Lewis acid-catalyzed reactions, ILs with this anion have no activity. Halide anions are Lewis basic [24, 25], therefore the $\chi_{AlCl3} < 0.50$ compositions are Lewis basic. The dimeric $[Al_2Cl_7]^-$ anion is Lewis acidic [26, 27], however, it is worth noting that also here the chloride species pose enough steric hindrance to prevent the formation of higher coordination. However, it is a 'latent' Lewis acid [28] due to an easily broken chloride bridge, which reacts with a base following Scheme 1.

There are many applications of chloroaluminate(III) ILs, such as electrode positions, which are not directly related to their Lewis acidity. The primary use of chloroaluminates(III) as Lewis acids is in catalysis; they are used directly as Lewis acidic catalysis (for example Diels–Alder reactions), or they react with residual water/protic additives to generate a Brønsted superacid (carbocationic reactions, e.g., isomerization) [11, 14]. Chloroaluminates(III) have also been used as solvents and Lewis acidic co-catalysts in reactions catalyzed by transition metal complexes [29]. A more recent addition to Lewis acidic applications of chloroaluminate(III) ILs is the area of inorganic synthesis, where they were used in multiple roles of solvent, reactant, and base scavenger [30].

Although they are the most common family of halometallate ionic liquids, the speciation of chloroaluminate(III) ILs can never be considered as the 'benchmark'; numerous studies have explicitly shown that anionic speciation is unique for each metal, and must be investigated for every system anew, before we can understand its chemistry [14].

For known chlorometallate ILs, dominant species as a function of composition are listed in Table 2 [14]. The common denominator is that at low (basic) metal chloride loadings, the anionic species are a mixture of free chloride and saturated chlorometallate anions. As metal chloride loading increases, at a certain χ_{MXm} value there is no free chloride anions, as they are bound to the metal, forming coordinatively saturated (neutral) halometallate complex—typically this is associated with the compound formation point in a phase diagram. Upon further increasing of metal chloride content, there are three scenarios possible: (1) oligomeric ('latent' Lewis acidic) chlorometallate anions are formed, (2)

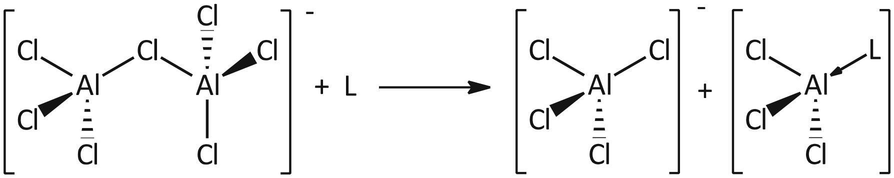

Scheme 1 Reaction of the Lewis acidic anion $[Al_2Cl_7]^-$, with a base L

Table 2 Anionic speciation of known chlorometallate ILs, in the liquid state, as a function of composition. Adapted and updated from [14]

χ_{MXx}							Analysis methods
	0.25	0.33	0.50	0.60	0.67	0.75	
Ti(IV)		$[TiCl_6]^{2-}$			$[Ti_2Cl_9]^-$		IR, Raman [31]
Zr(IV)	Cl^-; $[ZrCl_6]^{2-}$*	$[ZrCl_6]^{2-}$*	$[Zr_2Cl_{10}]^{2-}$*		$[Zr_2Cl_9]^-$*		DSC [32], crystallography
Hf(IV)	Cl^-; $[HfCl_6]^{2-}$*	$[HfCl_6]^{2-}$*	$[Hf_2Cl_{10}]^{2-}$*		$[Hf_2Cl_9]^-$*		DSC [32]
Nb(V)	Cl^-; $[NbCl_6]^-$		$[NbCl_6]^-$	$[NbCl_6]^-$; Nb_2Cl_{10}			Raman [33]
Ln(III)**	$[LnCl_6]^{3-}$						EXAFS, crystallography [34]
Mn(II)		$[MnCl_4]^{2-}$	$[MnCl_3]^-$*				Raman, IR [35], EXAFS [36]
Fe(II)		$[FeCl_4]^{2-}$		$[FeCl_4]^{2-}$; $FeCl_2\downarrow$			Raman, XPS [37, 38]
Fe(III)	Cl^-; $[FeCl_4]^-$		$[FeCl_4]^-$	$[FeCl_4]^-$; $[Fe_2Cl_7]^-$	$[FeCl_4]^-$; $[Fe_2Cl_7]^-$; $FeCl_3\downarrow$		Raman, IR, XPS [37–39]
Co(II)	Cl^-; $[CoCl_4]^{2-}$	$[CoCl_4]^{2-}$	$[CoCl_2(CoCl_4)_2]^{4-}$; $[Co(CoCl_4)_3]^{4-}$*	$[CoCl_2(CoCl_4)_2]^{4-}$; $[Co(CoCl_4)_3]^{4-}$; $CoCl_2\downarrow$*			UV–Vis [40]
Ni(II)	Cl^-; $[NiCl_4]^{2-}$	$[NiCl_4]^{2-}$	$[NiCl_4]^{2-}$; $NiCl_2\downarrow$				Crystallography [36], EXAFS [41, 42]
Cu(I)	Cl^-; $[CuCl_{(2+n)}]^{(1-n)-}$		$[CuCl_2]^-$		$[Cu_2Cl_3]^-$		IR, Raman [43], viscometry [44]
Cu(II)		$[CuCl_4]^{2-}$	$[Cu_2Cl_6]^{2-}$*				UV–VIS, EXAFS [45, 46]
Au(III)	Cl^-; $[AuCl_4]^-$		$[AuCl_4]^-$	$[AuCl_4]^-$; $AuCl_3\downarrow$			Raman, ab initio [47]
Zn(II)	Cl^-; $[ZnCl_4]^{2-}$	$[ZnCl_4]^{2-}$	$[Zn_2Cl_6]^{2-}$	$[Zn_2Cl_6]^{2-}$; $[Zn_3Cl_8]^{2-}$	$[Zn_3Cl_8]^{2-}$	$[Zn_4Cl_{10}]^{2-}$	Raman, crystal structure, EXAFS [48]
Cd(II)		$[CdCl_4]^{2-}$*	$[Cd_2Cl_6]^{2-}$*				Crystal structure [49]
Hg(II)	Cl^-; $[HgCl_4]^{2-}$	$[HgCl_4]^{2-}$	$[Hg_2Cl_6]^{2-}$	$[Hg_3Cl_8]^-$	$[Hg_2Cl_5]^-$		Crystal structure [50], ^{199}Hg NMR, Raman [51], EXAFS [52]
Al(III)	Cl^-; $[AlCl_4]^-$		$[AlCl_4]^-$	$[AlCl_4]^-$; $[Al_2Cl_7]^-$	$[Al_2Cl_7]^-$	$[Al_xCl_y]^-$; $AlCl_3\downarrow$	Raman [21], ^{27}Al NMR [20]

Table 2 continued

χ_{MXx}							Analysis methods
	0.25	0.33	0.50	0.60	0.67	0.75	
Ga(III)	Cl^-; $[GaCl_4]^-$		$[GaCl_4]^-$	$[GaCl_4]^-$; $[Ga_2Cl_7]^-$	$[Ga_2Cl_7]^-$	$[Ga_3Cl_{10}]^-$	Raman [53], ^{71}Ga NMR, EXAFS [53–55]
In(III)	$[InCl_6]^{3-}$	$[InCl_5]^{2-}$	$[InCl_4]^-$	$[InCl_4]^-$; $InCl_3\downarrow$			Raman, ^{115}In NMR, XPS [55–57]
Sn(II)	Cl^-; $[SnCl_3]^-$		$[SnCl_3]^-$	$[SnCl_3]^-$; $[Sn_2Cl_5]^-$	$[SnCl_3]^-$; $[Sn_2Cl_5]^-$; $SnCl_2\downarrow$		Raman, XPS [58]
Pb(II)	Cl^-; $[PbCl_4]^{2-}$	$[PbCl_4]^{2-}$	$[PbCl_4]^{2-}$; $[PbCl_3]$-; $PbCl_2\downarrow$				Raman, ^{207}Pb NMR [59]

Dominant anions in given compositions are listed, along with major techniques used to confirm the speciation

* Speciation assumed based on stoichiometry, solid-state studies or indirect techniques, such as DSC

** Ln = La, Ce, Pr, Nd, Sm, Eu, Gd, Tb, Dy, Ho, Er, Tm, Yb, Lu monomeric, coordinatively unsaturated (Lewis acidic) chlorometallate species exist, and (3) excess metal chloride precipitates.

It is crucial to note that, for asserting correct assignment of species present in each composition, a range of techniques should be used, preferably applied directly to neat ionic liquid: multinuclear NMR spectroscopy, IR, and Raman spectroscopies, XPS. In addition to these, phase diagrams are indispensable.

2.2.2 Chlorogallate(III) Ionic Liquids

Gallium follows aluminium in Group 13 of the periodic table, and indeed follows a very similar speciation pattern. However, whereas $AlCl_3$ precipitates from $\chi_{AlCl3} > 0.67$ compositions, chlorogallate(III) ILs remain homogenous at least up to $\chi_{GaCl3} = 0.75$, and even beyond this composition, forming very reactive and strongly Lewis acidic anions, such as $[Ga_3Cl_{10}]^-$ [53–55]. Despite high catalytic activity, far fewer catalytic applications are described when compared to chloroaluminates(III); most likely due to the higher price of $GaCl_3$ vs. $AlCl_3$. Nevertheless, they have been used in acetalization of aldehydes [60], oligomerization of 1-decene [61], alkylation of isobutane with butane [53], and Bayer–Villiger oxidation with H_2O_2 [62]. In general, enhanced moisture stability compared to chloroaluminates(III) was noted, which led to some advantages, such as: good recyclability in refinery alkylation [53], decreased isomerization in oligomerization of 1-decene [61], and the relative stability of the active intermediate, $[GaCl_3OH]^-$, in Bayer–Villiger oxidation [62].

2.2.3 Chloroindate(III) Ionic Liquids

Also belonging to Group 13, chloroindate(III) anions are not capable of formation of oligomeric species, but $InCl_3$ precipitates readily at $\chi_{InCl3} > 0.50$. However, in contrast to smaller icosagens, indium(III) can accommodate up to six chlorides, forming a compound at $\chi_{InCl3} = 0.25$, with $[InCl_6]^{3-}$ (Eq. 4) [55–57]. At $\chi_{InCl3} = 0.33$, some quantities of $[InCl_5]^{2-}$ may be forming, although this is not explicitly proven, and the equilibrium in Eq. 4, may be very strongly shifted to the right.

$$[\text{cation}]\text{Cl} + 3\text{InCl}_3 \rightarrow [\text{cation}]_3[\text{InCl}_6] \quad (4)$$

$$4\text{Cl}^- + 2\text{InCl}_3 \rightarrow 2[\text{InCl}_5]^{2-} \rightleftarrows [\text{InCl}_6]^{3-} + [\text{InCl}_4]^- \quad (5)$$

Finally, like other icosagenes, chloroindate(III) ILs at $\chi_{InCl3} = 0.50$ form $[InCl_4]^-$. However, this composition is not neutral—$[InCl_4]^-$ is coordinatively unsaturated, and reacts with a base as a mild Lewis acid (Eq. 6).

$$[\text{InCl}_4]^- + 2\text{L} \rightarrow [\text{InCl}_4\text{L}_2]^- \quad (6)$$

Chloroindate(III) ionic liquids are hydrolytically stable [63] and mildly Lewis acidic [27], which contrasts with systems based on lighter icosagenes, and opens up new application routes, such as: transesterification (biodiesel synthesis) [64], alkylation of phenols or catechols with alcohols [63], as well as for the protection of alcohols, followed by their conversion to acetates and trimethylsilyl ethers [65]. Noteworthy, in some instances compositions with excess of $InCl_3$ are used ($\chi_{InCl3} > 0.50$), even though they form a suspension/paste, rather than the ionic liquid [66].

2.2.4 Chloroferrate(III) Ionic Liquids

Ionic liquids based on iron(III) chloride form neutral $[FeCl_4]^-$ at $\chi_{FeCl3} = 0.50$, and both $[FeCl_4]^-$ and the Lewis acidic $[Fe_2Cl_7]^-$ can be detected at $\chi_{FeCl3} = 0.60$ [37, 38]. However, analogy with chloroaluminate(III) systems proves to be deceitful, as $FeCl_3$ has been reported to precipitate at $\chi_{FeCl3} > 0.60$ compositions [67]. Consequently, attaining homogenous ILs at $\chi_{FeCl3} = 0.67$ is impossible.

Catalytic applications of chloroferrates(III) were reviewed in 2011 by Bica and co-workers [68]. Their mild Lewis acidity is combined with interesting physical properties: thermomorphic behavior with water (thermally induced demixing) [39, 69] and paramagnetic behavior [70, 71], which were both suggested as routes for facile separation and recycling. Notably, despite their rather hydrophobic nature, chloroferrates(III) hydrolyze slowly in the presence of moisture [69].

2.2.5 Chlorozincate(III) Ionic Liquids

These ionic liquids are typically more viscous and higher melting than other halometallates, as chlorozincate(II) form doubly negatively charged anions [25, 33, 48, 72, 73]. A neutral compound is formed at $\chi_{ZnCl2} = 0.33$, with the $[ZnCl_4]^{2-}$ anion (Eq. 7), and all $\chi_{ZnCl2} > 0.33$ compositions are Lewis acidic. Several oligomeric chlorozincate(II) anions exist: $[Zn_2Cl_6]^{2-}$, $[Zn_3Cl_8]^{2-}$ and $[Zn_4Cl_{10}]^{2-}$ have all been postulated. Reaction of a base with an oligomeric chlorozincate anion, which is a 'latent' Lewis acid, can be envisaged as shown in Eq. 8.

$$[\text{cation}]\text{Cl} + 2\text{ZnCl}_2 \rightarrow [\text{cation}]_2[\text{ZnCl}_4] \tag{7}$$

$$[\text{Zn}_2\text{Cl}_6]^{2-} + 2\text{L} \rightarrow [\text{ZnCl}_4]^{2-} + [\text{ZnCl}_2\text{L}_2] \tag{8}$$

It is important to note that, based on early mass spectrometry studies, some authors postulated that chlorozincate(II) ILs adopt speciation analogous to that of chloroaluminate(III) ILs, i.e., to form $[ZnCl_3]^-$ and $[Zn_2Cl_5]^-$ anions. This assumption is still very prevalent in the literature, however, there are a number of arguments against it:

- tricoordinate zinc complexes are very few and only found in extremely sterically hindered environments; otherwise, tetracoordinate geometry is strongly preferred;
- not a single crystal structure exists with $[ZnCl_3]^-$ or $[Zn_2Cl_5]^-$ anions, in contrast to plethora of structures with tetracoordinate chlorozincate(II) anions;

- physical properties of chlorozincate ILs (high viscosity) are consistent with doubly charged anions;
- all spectroscopic techniques applied directly to the liquid phase (XPS, EXAFS, Raman spectroscopy) support the existence of zinc(II) in tetracoordinate environment;
- MS is a gas-phase technique, which may give erroneous results for the speciation of liquid with dense network of Coulombic and hydrogen bonding interactions.

In terms of catalysis, chlorozincate(II) ILs are appreciated for their low cost and stability against moisture, which leads to robust and recyclable catalysts [74, 75]. They find uses where stronger acids would either hydrolyze, or destroy the reactants, such as *O*-acylation of cellulose [76]. In an interesting recent application, chlorozincate(II) ionic liquids diluted with $[C_4mim][BF_4]$ were used as a liquid support and co-catalyst in chemoselective reduction of heteroarenes, promoted by Rh nanoparticles [77].

2.2.6 Chlorostannate(II) Ionic Liquids

Anionic speciation of chlorostannate(II) ILs is worth contrasting with chlorozincates(II); chlorostannates(II) do form tricoordinate $[SnCl_3]^-$ and $[Sn_2Cl_5]^-$ anions (Eqs. 9, 10), with a free electron pair occupying the fourth coordination position around the tin(II) atom in pseudo-tetrahedral trigonal pyramidal geometry (Fig. 2)

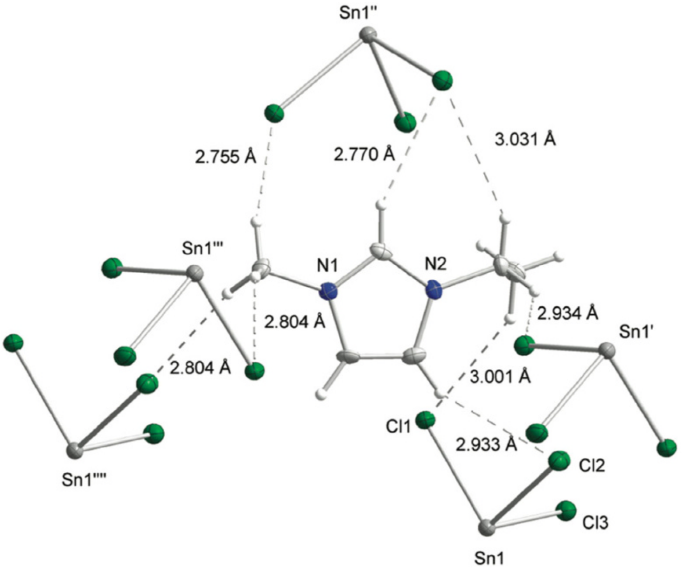

Fig. 2 Crystal structure of $[C_2mim][SnCl_3]$, showing the hydrogen-bonding interactions of the 1-ethyl-3-methylimidazolium cation and the $[SnCl_3]^-$ anion [58]

[58]. In addition, although known in crystalline state, chlorostannate(II) ILs do not form $[SnCl_4]^{2-}$ in the liquid state.

$$[\text{cation}]\text{Cl} + \text{SnCl}_2 \rightarrow [\text{cation}][\text{SnCl}_3] \tag{9}$$

$$[\text{cation}]\text{Cl} + 2\text{SnCl}_2 \rightarrow [\text{cation}][\text{Sn}_2\text{Cl}_5] \tag{10}$$

Chlorostannate(II) anions are amphoteric, which is expressed in moderately high donor and acceptor properties of chlorostannate(II) ionic liquids [24]. In 1972, Parshall used chlorostannate(II) ILs (then called fused salts) as solvents for $PdCl_2$, and Lewis basic co-catalysts for hydrogenation, isomerization, hydroformylation and carboalkoxyaltion of olefins [19]. The mechanism of a similar process, Pt^{II}-promoted hydroformylation in chlorostannate ILs, was studied over thirty years later by van Eldik and co-workers, who explicitly shown the $[SnCl_3]^-$ coordinating to the platinum center in the active form of the catalyst [78]. On the other side of the spectrum, Abbott and co-workers used chlorostannate(II) ILs as Lewis acidic catalysts for Diels–Alder reaction, in which they were less active than chlorozincate(II) analogues [75]. Zhang and co-workers used them for the preparation of highly isotactic and optically pure L-lactide, remarking on their low price, good moisture stability and tunability of the acidity by altering the χ_{SnCl2} value [79]. However, it must be noted that chlorostannate(II) anions are not entirely stable towards atmospheric oxygen, and upon prolonged exposure oxidize to $[SnCl_6]^{2-}$, especially in the presence of free chlorides [19, 58].

2.3 Acidity Measurements

The strength of interaction of a Lewis acid–base pair depends on the size, shape and relative energies of the LUMO of the acid and the HOMO of the base, in addition to steric effects from both components [80]. Consequently, the strength of a Lewis acid depends on the base it is interacting with. This is in contrast to Brønsted acids, which are always quantified with respect to the same species: the proton. As such, there is no absolute, direct method of quantifying the strength of a Lewis acid. Rather, there is a number of established Lewis acidity scales, whereby a basic probe molecule or ion is used, and the strength interaction between the probe and the acid is quantified by: (1) computational calculations [81, 82], (2) a physical measurement [83–85], or (3) by reaction rate of a model reaction catalyzed by the studied acid [86, 87]. Discussed below are selected methods used for quantifying Lewis acidity in ionic liquids.

2.3.1 Gutmann Acceptor Number: NMR Spectroscopic Method

The Gutmann AN approach, initially developed to study donor/acceptor properties of solvents and then expanded to liquid acids [84, 88], has been the first method used to quantify Lewis acidity of ILs [26, 89]. In the Gutmann Acceptor Number (AN) method, triethylphosphine oxide (TEPO) is used as the ^{31}P NMR spectroscopic probe. Advantages of TEPO include good sensitivity of the ^{31}P nucleus (naturally 100% abundant, spin 1/2, highly sensitive to its environment), relative stability towards strong acids, low steric hindrance and good solubility in a wide variety of solvents [90]. Coordination of the phosphine oxide to a Lewis acid induces change in the ^{31}P NMR chemical shift. The scale was arbitrarily defined based upon the ^{31}P NMR chemical shift of the probe molecule in hexane (AN = 0) and $SbCl_5$ in 1,2-dichloroethane (AN = 100) [91]. To eliminate the influence of concentration, ^{31}P NMR spectra of TEPO at several small concentrations are recorded, and the chemical shift is extrapolated to infinite dilution (δ_{inf}), which is then normalized with respect to infinite dilution of TEPO in hexane ($\Delta\delta_{\mathrm{inf}}$). AN values are calculated from Eq. 11.

$$\mathrm{AN} = 2.348 \times \Delta\delta_{\mathrm{inf}} \tag{11}$$

Beckett et al. proposed a modified method, in which a constant mass of TEPO is dissolved in a constant volume of sample, without extrapolating to infinite dilution [85]. The Gutmann–Beckett method gained popularity for the study of molecular Lewis acids; however, it was observed that for complex equilibria found in Lewis acidic ILs, even small changes in concentration affect the chemical shift, therefore extrapolating to infinite dilution is recommended for the highest reproducibility [27]. Although TEPO decomposition was never reported for ILs, some extremely strong Lewis acids have been known to decompose it [92].

The scale is very versatile, it was used to study not only strong Lewis acids, but to distinguish between subtle differences in acceptor properties of ILs cations [24, 93].

Gutmann AN was firstly used by Osteryoung and co-workers, to quantify the acidity of chloroaluminate(III) ILs [26]. AN = 98.2 was recorded for a Lewis basic system ($\chi_{\mathrm{AlCl3}} = 0.45$) and AN = 103.2 was reported for the most Lewis acidic one ($\chi_{\mathrm{AlCl3}} = 0.67$). For different cations the discrepancy between two systems at the same composition ($\chi_{\mathrm{AlCl3}} = 0.55$) was marginal, AN = 98.2 and 98.6 recorded for $[C_4py]^+$ and $[C_2mim]^+$, respectively. Compared to hexane (AN = 0) and water (AN = 54.8), all compositions appeared to be strong acids, which is clearly false. It was demonstrated that, due to high oxophilicity of aluminium, ligand displacement took place (Eq. 12).

$$[\mathrm{AlCl_4}]^- + \mathrm{TEPO} \rightarrow [\mathrm{AlCl_3(TEPO)}] + \mathrm{Cl}^- \tag{12}$$

In their subsequent work, Osteryoung and co-workers were able to fit equations to ^{31}P NMR chemical shifts recorded for TEPO in chloroaluminate(III) ILs (for $\chi_{\mathrm{AlCl3}} \leq 0.50$), and relate them to the concentration of $[AlCl_4]^-$ and $[Al_2Cl_7]^-$ [94]. This was possible for neat chloroaluminate ionic liquids, and for those where acidity was buffered with alkali metal salts (Eq. 13).

$$[\mathrm{Al_2Cl_7}]^- + \mathrm{MCl}_{(s)} \rightarrow 2[\mathrm{AlCl_4}]^- + \mathrm{M}^+ (\mathrm{M} = \mathrm{Li},\ \mathrm{Na},\ \mathrm{K}) \tag{13}$$

In studying systems other than chloroaluminate(III), we found a very good agreement between AN values and speciation proposed for the given metallate [27, 58, 72]. To summarize these research efforts, AN values for five [C$_8$mim]Cl–

MCl_x systems (M = Al^{III}, Ga^{III}, In^{III}, Zn^{II} and Sn^{II}) are plotted, as a function of composition, in two graphs constituting Fig. 3. The $[C_8mim]Cl–AlCl_3$ system, in agreement with the literature, gave consistently high values across the compositional range. In $[C_8mim]Cl–GaCl_3$, AN = ca. 22 were recorded for basic compositions ($\chi_{GaCl3} < 0.50$), with an increase to ca. 95 for acidic ones ($\chi_{GaCl3} < 0.50$), and a further increase to AN = ca. 107 for $\chi_{GaCl3} = 0.67$. These values can be assigned to consecutively dominant anions: $[GaCl_4]^-$, $[Ga_2Cl_7]^-$ and $[Ga_3Cl_{10}]^-$ (Table 2). Chloroindate(III) systems were reported to be mild Lewis acids, containing only monomeric anions: $[InCl_6]^{3-}$, $[InCl_5]^{2-}$ and $[InCl_4]^-$ (Eq. 5)—indeed, AN values increase stepwise to plateau at AN = ca. 57 for $\chi_{InCl3} \geq 0.50$ (Fig. 3). Chlorostannates(II) were reported to contain $[SnCl_3]^-$, equilibrated with $[Sn_2Cl_5]^-$ at $\chi_{SnCl2} > 0.50$ (Eqs. 9, 10), which is in agreement with one sharp change in Lewis acidity, from AN = ca. 18 at $\chi_{SnCl2} < 0.50$ to AN = ca. 76 for $\chi_{SnCl2} > 0.50$ (Fig. 3) [58]. In contrast, the $[C_8mim]Cl-ZnCl_2$ system was reported to contain multiple equilibrated anions, with Lewis acidic dimer, $[Zn_2Cl_6]^{2-}$, occurring for $\chi_{ZnCl2} > 0.33$—again, in agreement with the measured AN values (Fig. 3) [72]. For a handy reference, all measured AN values are listed in Table 3.

From the comparison in Fig. 3, it transpires that chlorometallate ILs cover a wide range of Lewis acidities, from very mild to Lewis superacids (AN > 100), giving great promise for tunability in catalytic applications. At the same time, as already discussed, different probe molecules may give different orders of acidity [95], especially when acids with different nucleophilic centers are compared [96–98].

Aside from studying per se Lewis acidic ionic liquids, the AN approach was used to study donor/acceptor properties of non-halometallate ILs as solvents, in the spirit of Gutmann's original work [24, 93, 99]. Although this is outside the scope of this review, it is worthy of note that AN values for such ionic liquids have been quantified using other spectroscopic techniques, such as Raman spectroscopy [100, 101], which could be of great use for studying halometallate ILs with paramagnetic nuclei.

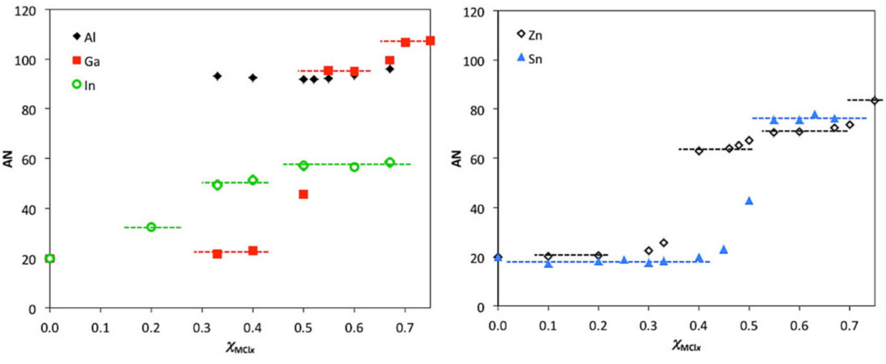

Fig. 3 AN values for five $[C_8mim]Cl-MCl_x$ systems (M = Al, Ga, In, Zn and Sn^{II}), plotted as a function of composition. Data adapted from [27, 58, 72]

Table 3 AN values for five [C_8mim]Cl-MCl_x systems (M = Al, Ga, In, Zn and Sn^{II}), as a function of composition [27, 58, 72]

χ_{MClx}	AN values for [C_8mim]Cl-MCl_x, where M =				
	Al	Ga	In	Zn	Sn^{II}
0.00	19.86	19.86	19.86	19.86	19.86
0.10				20.14	17.29
0.20			32.53	20.50	18.19
0.25					18.97
0.30				22.51	17.59
0.33	93.19	21.65	49.25	25.63	18.10
0.40	92.35	23.22	51.22	63.09	19.83
0.45					23.01
0.46				64.01	
0.48				65.24	
0.50	91.81	45.85	57.11	67.26	42.89
0.52	91.85				
0.55	92.19	95.30		70.55	75.45
0.60	93.30	95.09	56.53	70.86	75.66
0.63					77.91
0.67	95.95	99.54	58.36	72.49	76.14
0.70		106.71		73.57	
0.75		107.47		83.50	
1.00	85.60	75.90	74.30	66.00	75.20

Owing to their negligible vapor pressure, ILs give the unique opportunity of studying liquid matter via X-ray photoelectron spectroscopy (XPS), which is a high-vacuum technique. Licence and co-workers studied a range of chlorometallate systems as a function of their composition, and derived solvent properties from XPS spectra [25]. For chlorozincate(II) systems, a correlation between Zn $2p_{3/2}$ binding energies and AN values was observed, which opens up another strategy of quantifying Lewis acidity in ILs.

2.3.2 Adapted Solid-State Methods: FT-IR Spectroscopy

Lewis acidity in solid acids is commonly quantified employing vibrational spectroscopy and *N*-donor probes (pyridine, acetonitrile), typically used in near-stoichiometric quantities with respect to acidic sites. It is a very simple and time-efficient measurement, in which also paramagnetic ILs may be studied in contrast to NMR methods. A further advantage over the AN approach is the ability to distinguish between pyridine coordinating to Brønsted and Lewis acids, with vibrations for py-H and py-L.A. seen at ca. 1550 and 1450 cm^{-1} respectively [102]. Acetonitrile is sensitive only to Lewis acids, but not to Brønsted acids. A disadvantage, in the context of halometallate ionic liquids, is the need for high quantity of the probe (typically used at 0.33 mol ratio with respect to the metal center), which may disrupt equilibria in the liquid, as well as low sensitivity and resolution, compared to NMR spectroscopic probes.

In their seminal work, Kou et al. used both pyridine and acetonitrile as FT-IR spectroscopic probes to study Lewis acidity of a range of chlorometallate ILs [103]. The $[C_4mim]Cl–MCl_x$ series was studied, with Lewis acidity ranked as: $Cu^I < Fe^{III} < Zn < Al$, based on pyridine characteristic band vibration in acidic composition (Table 4). Studying the $[C_4mim]Cl-MCl_3$ system in several compositions, a py-L.A. band at 1448 cm^{-1} was assigned to $[AlCl_4]^-$, and 1454 cm^{-1} to $[Al_2Cl_7]^-$. AcCN-L.A. band was detected for $\chi_{AlCl3} \geq 0.55$. A study on chlorozincate(II) ILs, within a broad compositional range ($\chi_{ZnCl2} = 0.25 - 0.75$), revealed acidic band appearing for all $\chi_{ZnCl2} \geq 0.33$ compositions (Table 4), in agreement with Eq. 8 (but in contradiction to the speciation proposed in the same paper) [104]. Numerous papers followed afterwards, studying chlorometallates with different cations and varying combinations of metal chlorides and χ_{MClx} values [105, 106]. Typically, a good agreement between the catalytic activity and py-L.A. vibrational frequency is reported, but—depending on the cation and the paper—the reports deviate ±2 cm^{-1} from exemplary data in Table 4, which indeed gives a very low resolution. In general, the authors using this approach are less concerned with physical and inorganic chemistry of the studied systems, but more focused on the catalytic performance of the studied ionic liquids.

Isobutene alkylation with 2-butene (refinery alkylation), catalyzed by chloroaluminate(III) ILs, is known to be enhanced by amount of CuCl and water (or protic additives). Several publications report on the use of pyridine as the IR probe to gain insight into Brønsted/Lewis acidity of this complex system [108–110]. In particular, Liu and co-workers combined ^{27}Al NMR and IR spectroscopies to firstly identify Brønsted and Lewis acidic species in the system (Fig. 4) [109], and recently—to quantify them using pyridine titration method [110]. This distinction between Brønsted and Lewis species appears to be the key advantage of the IR spectroscopic approach.

Table 4 Py-L.A. vibrations chlorometallate ionic liquids, as a function of composition [103, 104, 107]

χ_{MClx}	Py-L.A. stretching frequencies (cm^{-1}) for chlorometallate ILs, where *M* =					
	Al	Cu^I	Fe	Zn	Sn^{II}	Sn^{II}
0.00	1438			1439		
0.33	1438, 1448			1439(sh), 1450		
0.40	1438, 1448					
0.50	1438, 1448			1439(sh), 1450		
0.55	1448					
0.60	1449, 1454(sh)					
0.67	1450(sh), 1454	1444	1446	1450	1449	1449
0.75				1450, 1454(sh)		

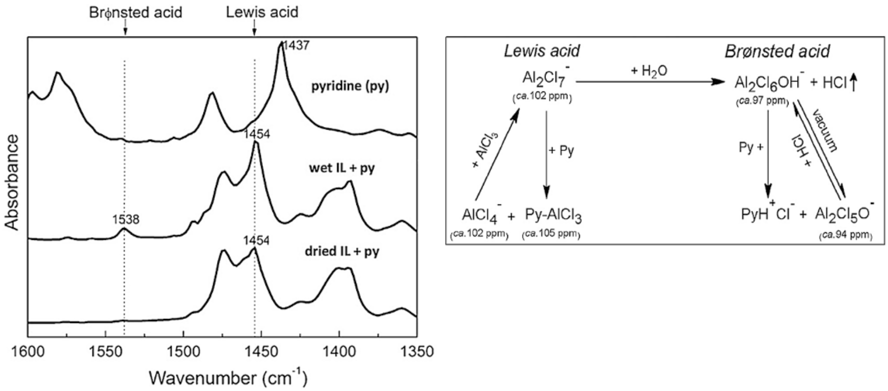

Fig. 4 *Left* FT-IR spectra of neat pyridine compared to 10% pyridine in wet $[HN_{222}]Cl\text{-}AlCl_3$ ($\chi_{AlCl3} = 0.64$), and 10% pyridine in high-vacuum dried $[HN_{222}]Cl\text{-}AlCl_3$ ($\chi_{AlCl3} = 0.64$). *Right* Acidic species in the catalytic system, with assigned ^{27}Al NMR chemical shifts. Adapted from [109]

2.3.3 Activity in Catalytic Process

In his seminal work, Olah and co-workers used Fridel–Crafts chemistry to measure the strength of Lewis acids [86]. Beckett et al. used epoxide polymerization rate, which correlated well with AN values measured by Gutmann–Beckett method for boron Lewis acids [111]. Hilt and Nödling used Diels–Alder reaction rates to rank Lewis acidity of silyl triflates, which correlated with the $\Delta\delta(^2H)$ values of deuterated quinolizidine-Lewis Acid adducts [112]. Finally, Kobayashi et al. studied both reaction rate and selectivity of the addition of a silyl enolate to an aldehyde and an aldimine, to form a complex classification of metal halides [87].

In ionic liquids, there were a number of publications where several Lewis acids were tested in a reaction, and ranked according to their strength [113]. Nevertheless, none of the above-cited standard reactions were adopted as the standard method. In the recent years, Diels–Alder has been gaining increasing popularity as the benchmark reaction of choice [75, 114–117].

2.4 Selected Applications

Chlorometallate ionic liquids are used in a plethora of applications, not all of them directly related to their Lewis acidity (viz. electrochemistry). Here, three selected examples of applications of chlorometallate ILs as Lewis acids are presented: recent industrial applications, the development of supported ILs, and inorganic synthesis with Lewis acidic ionic liquids.

2.4.1 Refinery Alkylation with Chloroaluminate(III) Ionic Liquids

The review on industrial applications of ionic liquids by Seddon and Plechkova listed explicitly two industrial applications of Lewis acidic ILs: Difasol by IFP and Ionikylation by PetroChina—both using chloroaluminate(III) systems [118]. The interest of other major oil companies in this chemistry (BP, Exxon Mobil, Chevron) was inferred from a rich patent portfolio, owned by each company.

Currently, refinery alkylation catalyzed with chloroaluminate(III) ILs appears to be the center of attention of the many petrochemical companies. Firstly, in 2006 PetroChina reported retrofitting a 65 kt/y H_2SO_4 alkylation unit for use with a mixed chlorometallate (Al^{III}/Cu^{I}) ionic liquid in the Ionikylation process [119]. In 2013, a 100 kt/y plant was announced to operate successfully, a very similar catalytic system [composite ionic liquid alkylation (CILA)], with involvement from PetroChina, Shell, Deyang and National Science Foundation of China [120, 121]. In 2016 Chevron Phillips, who have been developing their ISOALKYL ionic liquid alkylation technology over the past 20 years, committed to converting a 4500 barrel per day HF alkylation unit with to the ISOALKYL technology, and has licensed the process through Honeywell UOP [122]. Plans to retrofit the alkylation unit (Fig. 5) in Utah, USA were to commence in 2017, pending planning permission [123]. This new technology set to reduce catalyst consumption and tackle the safety concerns associated with HF, in particular with its transport in bulk [124], as regeneration of the CIL catalyst can be performed on site. The ionic liquid process also has the advantage of being able to utilize more varied feedstocks than the liquid acid alkylation process and typically gives less conjunct polymers than liquid acid alkylations [125].

These industrial implementations of chloroaluminate(III) ILs in refinery alkylation have been underpinned by decades of research, some of them already highlighted in the discussion on quantifying acidity via FT-IR spectroscopy (Sect. 2.3.2). Refinery alkylates for use in high octane fuels had been produced on an industrial scale using either H_2SO_4 or HF as the acid catalyst [124], with aluminium(III) chloride described as too acidic and thus inducing side reactions, such as cracking [126]. However, Chauvin and co-workers reported the successful use of chloroaluminate ILs as catalysts for isobutane–butene alkylations, which was then expanded upon by Jess et al. [108, 127–129]. Tuneable acidity of the ionic liquid was found to play a crucial role: high χ_{AlCl3} values led to cracking (like neat $AlCl_3$), whilst low acidity caused polyalkylations [130]. In addition to acidity control, it is very likely that charge stabilization of the transition-state charged intermediates, which occurs in ILs but not with $AlCl_3$, contributes strongly to curtailing side reactions [131].

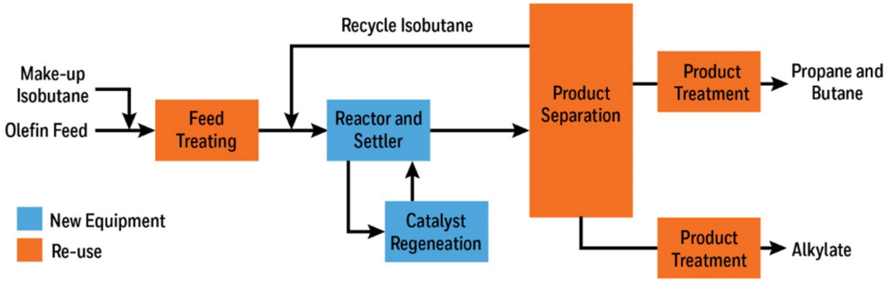

Fig. 5 IONALKYLATION plant scheme showing retrofit strategy [125]

Protic additives increased selectivity to the desired product up to a certain loading, but caused polyalkylation when that loading was exceeded (viz. speciation insight in Sect. 2.3.2) [128]. Addition of aromatic compounds also increased selectivity to the desired product, decreasing simultaneously light and heavy ends, which was attributed to an interaction between the Lewis acid and the π system of the aromatic ring [132]. Finally, studying metal halide additives, Liu and co-workers reported CuCl to increase the selectivity RON of the product [120, 133, 134]. Initially, it was attributed to the presence of a heterometallic chlorometallate anion, $[AlCl_4CuCl]^-$, which was suggested to be the origin of the peak at ca. 97 ppm in the ^{27}Al NMR spectrum, and was observed in FAB-MS. However, other authors argued that the peak at ca. 97 ppm originates from a hydrolysis product, $[Al_2Cl_6OH]^-$, which was confirmed by the drying of the sample under high vacuum, upon which the signal disappeared [109]. The same group proposed that Cu^I substitutes the proton in the $[HN_{222}]^+$ cation, generating HCl (Scheme 2). This also found spectroscopic confirmation in increased intensity of the py-H band in the FT-IR spectrum of CuCl-containing ionic liquid (viz. Sect. 2.3.2) [108].

Alkylation catalyzed with Lewis acidic ILs is currently of great interest, both commercially and scientifically, and more exciting new developments on both fronts can be expected.

2.4.2 SILP and SCILL

Homogenous and heterogenous catalysis both have their advantages and disadvantages, the former benefiting from good phase contact, no mass transfer limitation and control over catalytic species, and the latter from easy catalyst separation and low cost (with their disadvantages being the reverse) [135]. The strategy of depositing a thin layer of an ionic liquid on a solid support has been used to harvest benefits of both heterogenous and homogenous catalysis, with two core approaches being: supported ionic liquid phase (SILP) and more recently proposed solid catalyst with an ionic liquid layer (SCILL). The older SILP concept was shortly reviewed in 2006 [136], with broader reviews on both SILP and SCILL published in 2014 [137] and 2015 [138].

Both concepts utilize a typically highly porous support (silica, activated carbon, carbon nanotubes), which is coated with a small quantity of an ionic liquid, forming a thin layer. The IL may be either covalently tethered to the support material, usually by way of the cation, or simply adsorbed onto the surface. Covalently bound

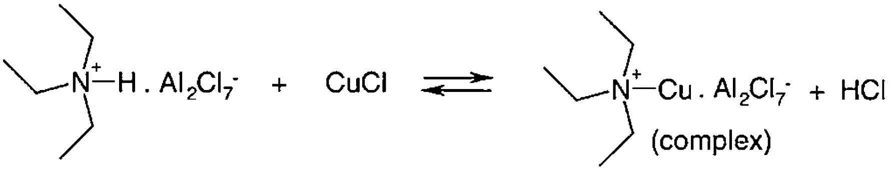

Scheme 2 Proposed mechanism for the generation of a Brønsted acid from protic chloroaluminate (III) ionic liquid and copper (I) chloride [108]

systems were reviewed in detail in 2016 [139]. In SILPs, the ionic liquid is either catalytically active, or has a catalyst dissolved in it in the form of coordination complex (Fig. 6, left). In SCILL, in contrast, the solid support is either catalytically active or has a solid catalyst deposited on the surface (viz. Pd/C), with the IL acting as a co-catalyst, stabilizing reactive species and/or altering the availability of reactants at catalytic sites (Fig. 6, right).

Initially, SILP systems did not utilize Lewis acidic ILs; notably, they are not even mentioned in the 2006 review on SILPs [136]. Wasserscheid and Haumann pioneered $[C_2mim][Al_2Cl_7]$-containing SILPs as catalysts for the alkylation of cumene [140, 141]. The time required to reach 80% conversion was six times shorter with SILP, compared to the liquid–liquid biphasic reaction using the same ionic liquid. The catalyst could be recycled four times without the loss of activity. An increasing number of publications on chloroaluminate(III) SCILLs followed, predominantly testing known chemistry in the new engineering setting, and often reporting beneficial/synergistic effect of the support [138].

Chlorostannate(IV) ILs tethered to a silica support were used in Barbier–Prins condensation of paraformaldehyde and isobutene [142]. The SILP catalyst afforded the desired product (3-methy-3-buten-1-ol) with lower yield but higher selectivity compared to $SnCl_4$, and in contrast to $SnCl_4$—no leaching of tin was observed when SILP was used. Chlorostannate(II) and chlorozincate(II) ILs, supported on alumina, were used for gas sweetening (desulfurization) in the continuous mode [143]. Chrobok and co-workers used chloroaluminate(III) and chlorogallate(III) ILs, covalently tethered onto multimodal porous silica, in solventless Diels–Alder reaction [116]. Catalytic performance of Lewis acidic chloroaluminate(III) and chlorogallate(III) systems were equally good, but the chlorogallate(III) system was selected for the recycling studies due to higher moisture stability.

SCILL systems were introduced in 2012 by Wasserscheid and co-workers. The first example was the $[C_4mim]Cl–AlCl_3$ ($\chi_{AlCl3} = 0.67$) ionic liquid on Pt/silica for the isomerization of *n*-octane in a slurry-phase reaction, under H_2 pressure [144]. High selectivity was observed due to Pt centers catalyzing hydrogenation of undesired olefinic by-products, whereas enhanced reaction rate was attributed to increased Brønsted acidity in this unique $Pt/H_2/[C_4mim]Cl–AlCl_3$ ($\chi_{AlCl3} = 0.67$)

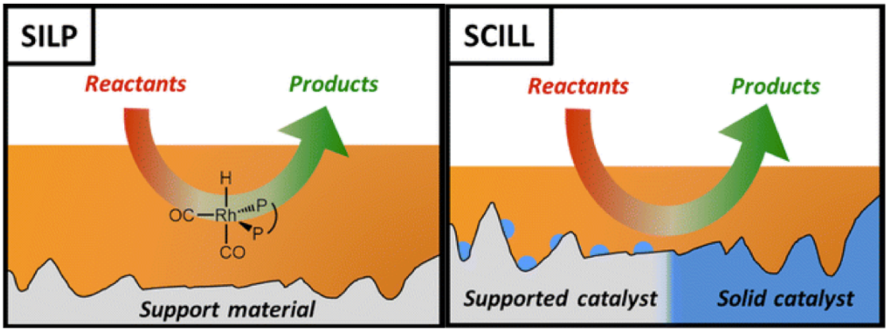

Fig. 6 Pictorial representation of SILP and SCILL concepts. Modified from [138]

system. Very recently, SCILLs with Lewis acidic ionic liquids were used for arene hydrogenation, and also in this case activity enhancement was observed [145], in analogy to earlier-reported homogenous study [131].

The study on SILP/SCILL materials with Lewis acidic systems is still in its infancy, and from the several papers published—it appears to be an interesting direction, opening up opportunities for ambitious fundamental studies on the nature of these complex catalytic systems.

2.4.3 Inorganic Synthesis

Ionic liquids in inorganic synthesis are typically used in a dual role of solvents and templating agents, often at relatively high temperatures (negligible boiling point results in low autogenic pressures). Developed initially by Morris and co-workers, this synthetic procedure is called ionothermal synthesis, in analogy to solvothermal synthesis in molecular solvents [146, 147]. Lewis acidic ILs, in particular haloaluminates, have been extensively used in ionothermal synthesis, the research direction led by Ruck and co-workers. In a recent review, the role of Lewis acidic systems in the synthesis of polycations of heavy main-group elements, such as Te, Bi, Sb–Se and Bi–Te, is extensively discussed [30]. Ionic liquids with Lewis acidic anions of a general formula $[M_2X_7]^-$ act as solvents and scavengers for bases. Scavenging halides increases the solubility of certain precursors, e.g., enables dissociation of BiX_3 to $[BiX_2]^+$ and X^-, whereas scavenging water provides (to an extent) a self-drying reaction environment.

Altering the halide (Cl or Br) and the χ_{AlX3} value of haloaluminate(III) ILs, as well as the reaction temperature, was used to fine-tune the structure of the final product, as exemplified in Fig. 7 [30].

From the viewpoint of this review, particularly interesting is the manipulation of the composition (χ_{AlCl3}) at different stages of synthesis. As shown in Fig. 7, typically a large excess of AlX_3 is used during the reaction, above the formation of homogenous ionic liquid at room temperature (Fig. 1). This affords very weakly coordinating $[Al_2X_7]^-$ anions, which are beneficial during the synthesis, but hinder the subsequent crystallization. This was addressed by Groh et al. by the addition of NaCl after the reaction, which shifts the equilibrium in Eq. 3 towards tetrahedral $[AlX_4]^-$, thus leading to crystallization [148]. The role of chloroaluminate(III) anions was studied computationally by Kirchner and co-workers [149]. A molecular precursor, Te_4Br_2, was studied in $[C_2mim]Cl$ and $[C_2mim]Cl\text{-}AlCl_3$, ($\chi_{AlCl3} = 0.57$). Only in the latter system did dissociation of the precursor occur, proceeding through bromide abstraction by the Lewis acidic aluminium(III) center, yielding a cationic $[Te_4Br]^+$ species, and the $[AlCl_3Br]^-$ anion.

This area of inorganic chemistry is very prolific, and under constant development. The research started from accessing simple bismuth [150] and tellurium [151] polycations, developed into the synthesis of cluster compounds, such as $Sn^{II}[Sn^{II}Cl][W_3Cl_{13}]$ [152], to recently reported clusters with metal inclusions, such as $[Pt@Bi_{10}][AlBr_4]_2[Al_2Br_7]_2$ (Fig. 8) or $[Pd@Bi_{10}][AlBr_4]$ [153]. It is apparent that a plethora of synthetic opportunities await here, possibly using non-haloaluminate(III) ILs to open up another dimension of study.

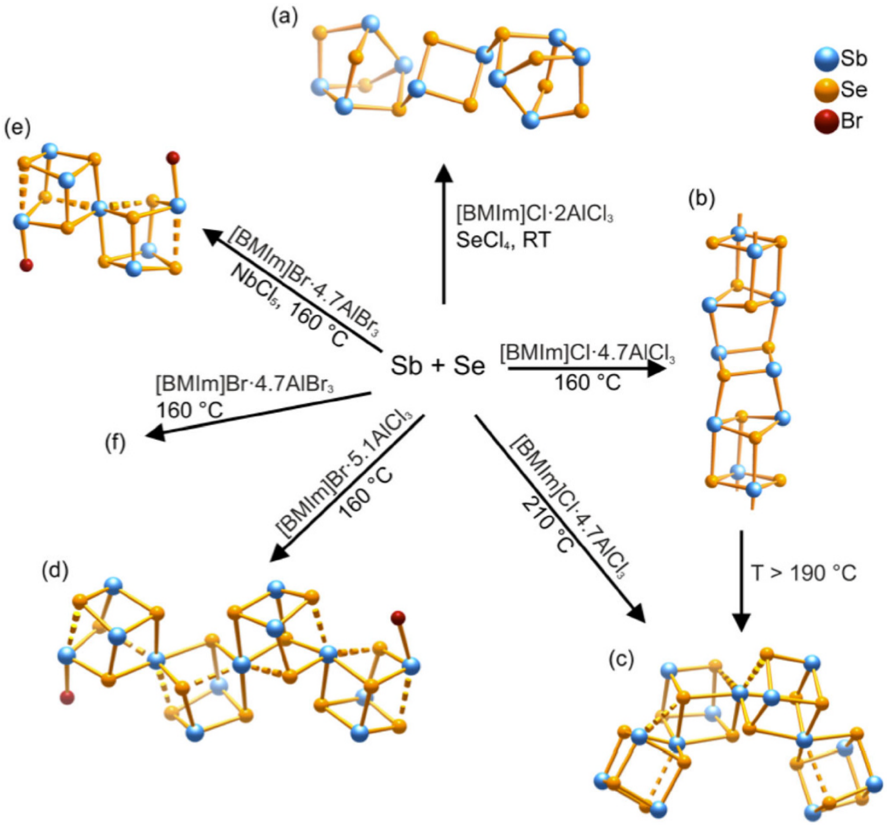

Fig. 7 Structural diversity of antimony-selenium heteropolycations accessible in haloaluminate(III) ILs under various reaction conditions [30]

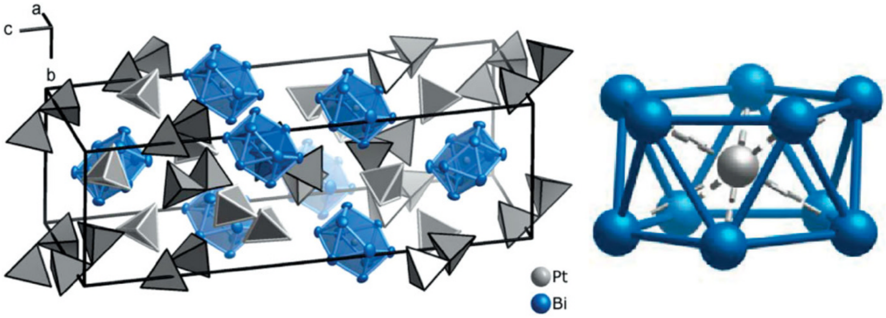

Fig. 8 *Left* The crystal structure of $[Pt@Bi_{10}][AlBr_4]_2[Al_2Br_7]_2$, where *blue polyhedra* are the $[Pt@Bi_{10}]^{4+}$ cations, and *grey tetrahedra* are bromoaluminate anions: $[AlBr_4]^-$ with *white outlines*, $[Al_2Br_7]^-$ with *black outlines*; *right* the structure of the *arachno* polycation, $[Pt@Bi_{10}]^{4+}$. The *ellipsoids* are at 90% probability level [153]

3 Liquid Coordination Complexes (LCCs)

3.1 Historical Context

Combinations of a metal halide, in most cases is aluminium(III) chloride, and an aprotic organic donor, such as THF, acetonitrile or dimethylformamide, are used as Lewis acidic reagents in organic chemistry. The Lewis basic donor is used to modify the Lewis acidity/reactivity of the metal halide [154–156]. Typically, reactions are performed in solutions, and ratios of metal halide to donor vary in a wide range. Speciation and physical properties of neat reagents are never the focus of such studies, but in isolated cases they have been mentioned to be liquids rather than solids.

In coordination chemistry, adducts of aluminium halides with organic donor molecules have been demonstrated to crystallize as either neutral molecular complexes, such as $[AlCl_3(THF)]$ and $[AlCl_3(THF)_2]$, or ionic species, e.g., $[Al_2Cl_2(THF)_4][AlCl_4]$—with symmetric or asymmetric splitting of the 'Al_2Cl_6' unit taking place depending on the concentration and reaction conditions [157, 158].

Experience with halometallate ILs allowed for observation of these low melting metal–ligand combinations in a new light, and rather than seeing an 'oil' that failed to crystallize, an opportunity to develop a new generation of Lewis acidic liquids was spotted. Herein, such materials are referred to as liquid coordination complexes (LCCs). Much like halometallate ILs evolved from molten salts, LCCs were developed as a less expensive and easier to synthesize alternative to chlorometallate ionic liquid [159, 160].

3.2 Speciation

In 2007, Abbott and co-workers reported that urea formed ambient-temperature eutectics with $SnCl_2$ and $FeCl_3$ [159]. $ZnCl_2$ was reported to form eutectics with urea (at eutectic point $\chi_{ZnCl2} = 0.22$, or 78% urea—see Fig. 9), acetamide ($\chi_{ZnCl2} = 0.20$), ethylene glycol ($\chi_{ZnCl2} = 0.20$) and hexanediol ($\chi_{ZnCl2} = 0.25$). The Lewis acidity of these liquids has never been studied, but it is unlikely for them to be of significant Lewis acidity, considering the excess of basic urea (ca. 4:1).

Subsequently, eutectic mixtures of $AlCl_3$ and urea, acetamide or *N*,*N*-dimethylurea were reported ($0.50 \leq \chi_{AlCl3} \leq 0.60$) [161]. Swadźba-Kwaśny and co-workers described a range of L-MCl_3 combinations, where M = Al or Ga, and L = acetamide (AcA), urea (Ur), thiourea (SUr), trioctylphosphine (P_{888}) or trioctylphosphine oxide ($P_{888}O$), with varying metal chloride proportions ($0.50 \leq \chi_{AlCl3} \leq 0.60$ and $0.50 \leq \chi_{GaCl3} \leq 0.75$) [160]. Liu and co-workers studied combinations of $AlCl_3$ with acetamide, *N*-methylacetamide and *N*,*N*-dimethylacetamide ($0.51 \leq \chi_{AlCl3} \leq 0.60$) [162]. Finally, Dai and co-workers reported on mixtures of $AlCl_3$ and 4-propylpyridne ($0.52 \leq \chi_{AlCl3} \leq 0.60$) [163] and dipropylsulphide (up to $\chi_{AlCl3} = 0.51$) [164].

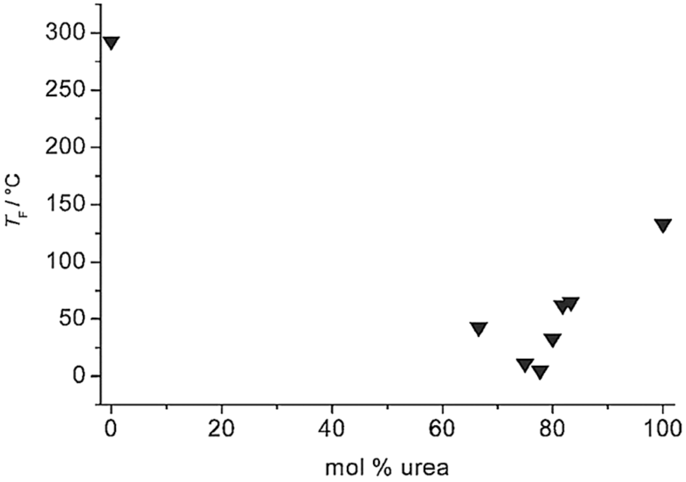

Fig. 9 Phase diagram urea–$ZnCl_2$ system as a function of composition [159]

Speciation studies on $AlCl_3$ and $GaCl_3$ combined with above-listed *O*-, *P*- and *S*-donors, based on ^{27}Al NMR and Raman spectroscopy, revealed equilibrated neutral, cationic and anionic complexes of aluminium (Fig. 10) [160].

Naturally, speciation of LCCs as a function of χ_{MCl3} was different from that determined for chloroaluminate(III) and chlorogallate(III) ILs (Table 2). For $\chi_{MCl3} = 0.50$, all mixtures contained only monomeric complexes: $[MCl_2L_2]^+$, $[MCl_3L]$ and $[MCl_4]^-$ (Eq. 14), whereas at $\chi_{MCl3} = 0.60$, there were dimeric, Lewis acidic species prevalent: $[M_2Cl_6L]$ and $[M_2Cl_7]^-$, in addition to mononuclear cation, $[MCl_2L_2]^+$ (Eq. 15).

$$2L + 2MCl_3 \rightarrow 2[MCl_3L] \rightleftarrows [MCl_2L_2][MCl_4] \tag{14}$$

$$2L + 3MCl_3 \rightarrow [MCl_3L] + [M_2Cl_6L] \rightleftarrows [MCl_2L_2][M_2Cl_7] \tag{15}$$

For higher metal chloride loadings ($\chi_{MCl3} > 0.60$), $AlCl_3$ was found to precipitate, whereas $GaCl_3$-LCCs remained liquid until $\chi_{MCl3} = 0.75$, suggesting the formation of oligomeric, highly Lewis acidic complexes (Eq. 16) [160]. This is in agreement with findings for chlorometallate ILs, where only mono- and dinuclear chloroaluminate(III) anions are stable, but chlorogallate(III) anions have the ability to form higher oligomers (viz. Table 2).

$$2L + 4MCl_3 \rightarrow 2[Ga_2Cl_6L] \rightleftarrows [GaCl_2L_2][Ga_3Cl_{10}] \tag{16}$$

Further refinement upon this speciation was proposed by Liu and co-workers, who studied the amide-$AlCl_3$ combinations [162]. All three ligands: AcA, NMA and DMA have the potential to act as *O*-donors and *N*-donors. It has been demonstrated that acetamide coordinated exclusively through the oxygen atom, with a small contribution from Al–N coordination mode in NMA, and a larger Al–N contribution in DMA. LCCs containing methylated acetamides had a higher proportion of

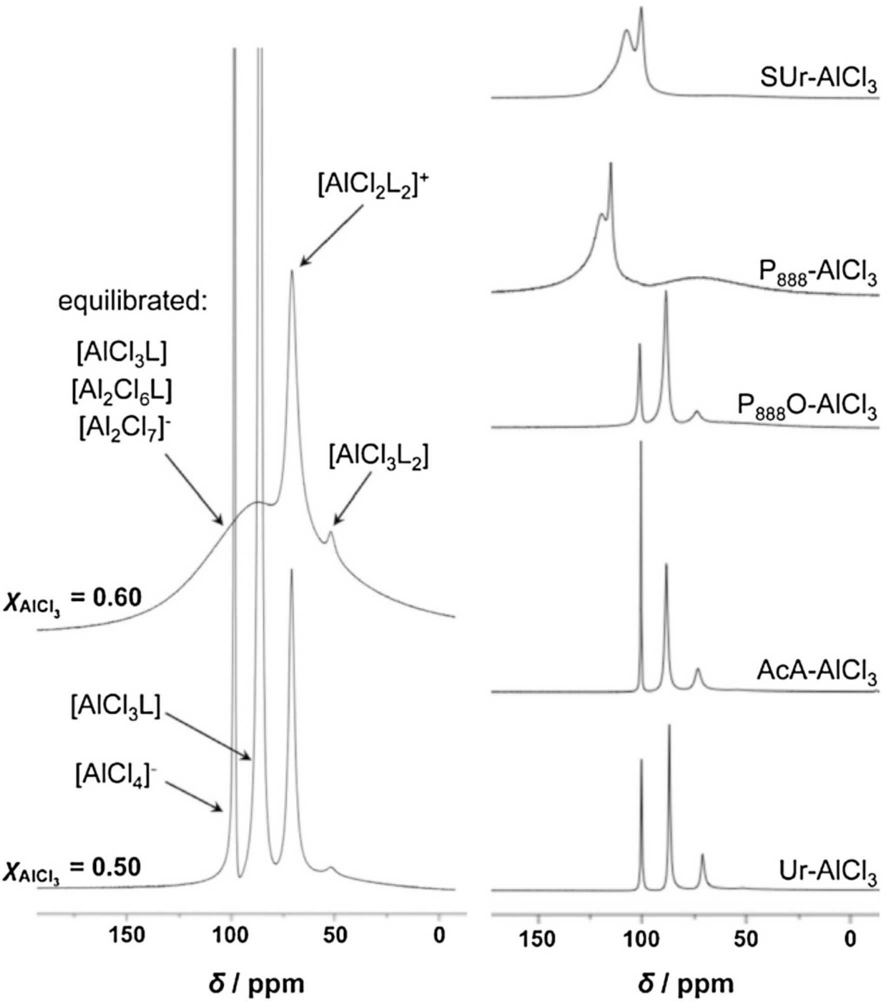

Fig. 10 ^{27}Al NMR spectra of AcA-AlCl$_3$ $\chi_{AlCl3} = 0.50$ and 0.60 (*left*), and L-AlCl$_3$ $\chi_{AlCl3} = 0.50$ (*right*) [160]

$[AlCl_4]^-$ than acetamide in the same composition, which the authors interpreted as the formation of $[AlCl_2(\eta^2\text{-}L)]^+$ in the former case, shifting equilibrium in Eq. 16 to the right.

Mixtures of 4-propylpyridne and AlCl$_3$, liquid at $0.52 \leq \chi_{AlCl3} \leq 0.60$, were investigated using a combination of multiple techniques: ^{27}Al NMR and FT-IR spectroscopy, mass spectrometry, TGA, DSC and viscometry, followed by comprehensive electrochemical study [163]. ^{27}Al NMR spectra were compared to these of an archetypical chloroaluminate(III) IL, [C$_2$mim]Cl-AlCl$_3$ (Fig. 11).

The existence of an ionic compound, $[AlCl_2(\text{4-proylpyridine})_2][AlCl_4]$, at $\chi_{AlCl3} = 0.50$, is postulated based on ^{27}Al NMR spectroscopy and mass spectrometry. For $\chi_{AlCl3} = 0.52$, no $[Al_2Cl_7]^-$ was observed in mass spectra—in accordance

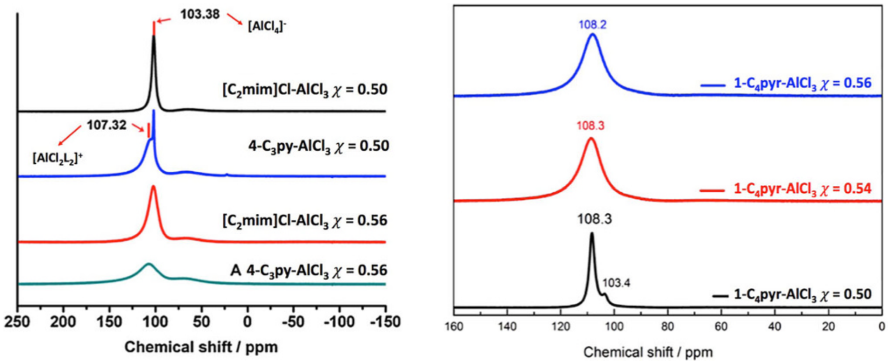

Fig. 11 Comparison of ^{27}Al NMR spectra. *Left* ionic liquid, $[C_2mim]Cl\text{-}AlCl_3$, and an LCC, $4\text{-}C_3py\text{-}AlCl_3$, at two molar ratios of aluminium(III) chloride: $\chi_{AlCl3} = 0.50$ and 0.56. *Right* $1\text{-}C_4py\text{-}AlCl_3$, at three molar ratios of aluminium(III) chloride: $\chi_{AlCl3} = 0.50$, 0.54 and 0.56. *Left* Adapted from [163]. *Right* Adapted from [165]

to earlier reports of Abbott and co-workers [161]. This might be disputed due to problems with using mass spectrometry for speciation of chlorometallate ILs in general [14, 72]. However, the conclusion is supported by Endres and co-workers, who studied a similar system, 1-butylpyrolidine and $AlCl_3$ (liquid for $0.47 \leq \chi_{AlCl3} \leq 0.55$), using more reliable in this context vibrational spectroscopy, and also have seen no evidence for the Lewis acidic $[Al_2Cl_7]^-$ anion [165].

Based on very interesting changes in conductivity found from their electrochemical studies, Dai and co-workers suggest the presence of equilibria found in Eqs. 17 and 18 [163].

$$2AlCl_3 \rightleftarrows [AlCl_2]^+ + [AlCl_4]^- \tag{17}$$

$$[AlCl_2]^+ + \left[AlCl_2(4 - C_3py)_2\right]^+ \rightleftarrows 2[AlCl_2(4 - C_3py)]^+ \tag{18}$$

Should such species exist, this liquid should be extremely Lewis acidic due to the presence of a dicoordinate cation, $[AlCl_2]^+$. However, such cation has never been reported in the literature, and there is no direct, spectroscopic evidence for its existence presented in the paper. Chemical shifts in ^{27}Al NMR spectroscopy depend strongly on coordination number and geometry around the studied nuclei. In general, tetracoordinate complexes of Al(III) give signals around 100 ppm, pentacoordinate around 50 pm and hexacoordinate around 0 ppm [166]. ^{27}Al NMR spectra of the $4\text{-}C_3py\text{-}AlCl_3$ system feature two signals at 103 and 107 ppm, assigned to tetracoordinate $[AlCl_4]^-$ and $[AlCl_2(4\text{-}C_3py)_2]^+$, respectively. The same range of chemical shifts is recorded by Endres and co-workers [165]. There was no indication of an extremely deshielded ^{27}Al NMR signal that would suggest the presence of the previously unreported $[AlCl_2]^+$.

3.3 Acidity Measurements

There is relatively little information published with regards to quantified Lewis acidity of LCCs. Coleman et al. reported AN = 103 for DMA-$GaCl_3$, $\chi_{GaCl3} = 0.60$, and AN = 96–103 (several signals for the probe were recorded) for DMA-$AlCl_3$, $\chi_{AlCl3} = 0.60$. These are slightly higher than acceptor numbers recorded for the corresponding chlorometallate ILs (AN = 93–95) [27]. Yet unpublished data recorded by our group indicate that, in many cases, multiple signals are recorded for TEPO dissolved in LCCs, therefore it requires a careful consideration how these could be presented in a meaningful manner.

3.4 Applications

In analogy to halometallate ionic liquids, there are two major strands emerging in the newly developing LCC research: electrochemistry (led by Abbott, Dai, Endres) and Lewis acidic catalysis (Swadźba-Kwaśny, Liu). The focus of this review is on the latter strand of work.

The first catalytic studies using LCCs were on carbocationic reactions. Abbott reported the acetylation of ferrocene with acetic anhydride, promoted by Ur–$AlCl_3$ and AcA–$AlCl_3$ (both $\chi_{AlCl3} = 0.60$), which led to a mixture of mono- and diacetylated products [161]. Interestingly, both systems gave significantly different results, with markedly higher conversion to diacetlyated product for AcA–$AlCl_3$ (both $\chi_{AlCl3} = 0.60$), which indicates higher Lewis acidity of the later.

Swadźba-Kwaśny and co-workers used a range of LCCs based on $AlCl_3$ and $GaCl_3$ for the oligomerization of 1-decene to polyalphaolefins (PAOs) [167]. Low-viscosity polyalphaolefins (PAO_4 and PAO_6 lubricant base oil grades) were obtained, with all quantified physical parameters aligned with the industrial requirements for the commercial products. Changing metal and ligand, distribution of oligomers could be tuned within a wide range (Fig. 12). Particularly significant was the stark contrast between distribution of oligomers achieved with acetamide (AcA), and structurally very similar dimethylacetamide (DMA), which highlights the influence of speciation of LCCs on their catalytic performance (viz. research of Liu and co-workers, discussed in Sect. 3.2) [162].

L-$GaCl_3$ LCCs were used to catalyze Friedel–Crafts alkylation of benzene with 1-decene [168]. Although higher reaction rates were achieved with L = Ur or DMA, lipophilic ligands (L = P_{888} or $P_{888}O$) enabled easy phase separation from the product. Working at lower conversions (ca. 50%) gave very high selectivities to the desired 2-phenyldecane (up to 50%).

Liu and co-workers used amide-$AlCl_3$ systems to catalyze refinery alkylation of isobutene with 2-butene to high-octane fuels [169]. Compared to chloroaluminate(III) ILs, LCCs gave less polyalkylates and better selectivity, at the same composition ($\chi_{AlCl3} = 0.60$). In analogy to the PetroChina process, the addition of CuCl increased RON, up to a maximum value of RON 98.40.

Finally, an LCC, Ur-$AlCl_3$ $\chi_{AlCl3} = 0.60$, and a chloroaluminate(III) ionic liquid, [C_4mim]Cl-$AlCl_3$ $\chi_{AlCl3} = 0.67$, were supported on Pd/C to form SCILL, and used as co-catalysts for the hydrogenation of toluene [145]. Both catalysts saw an

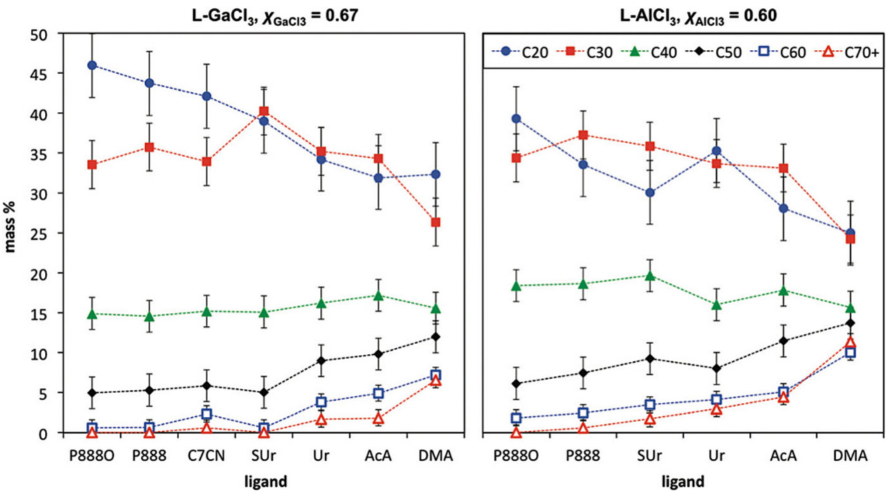

Fig. 12 Distributions of 1-decene oligomers, produced in L-MCl$_3$-catalyzed oligomerizations (120 °C, 1.707 mmol of LCC), where M = Al or Ga, and L = P888O, P888, C7CN (octanenitrile), SUr, Ur, AcA or DMA [167]

increased rate of hydrogenation compared to the uncoated catalyst. Interestingly, at lower temperatures (<60 °C) the IL was a more effective co-catalyst, whereas at elevated temperatures (>60 °C) the LCCs co-catalyst performed better. This was attributed to significant changes in speciation of LCC as a function of temperature, already demonstrated by variable temperature ^{27}Al NMR spectroscopy [160, 162].

4 Ionic Liquids with Lewis Acidic Cations

Lewis acidic species are characterized by the local electron density deficiency. Lewis acidity is therefore enhanced by the positive change on the Lewis acidic center. This has been exploited in main-group chemistry, with increasing interest in borocation, phosphorus cations, and other positively charged species as strong Lewis acids. It is therefore ironic that, in the field of ILs (which lends itself to manipulation of ionic species), the overwhelming majority of Lewis acids are Lewis acidic at the anion! Only very recently, a handful of ILs bearing Lewis acidic cations were reported, but the field is already expected to grow rapidly. Structurally, these newly reported examples can be divided into two categories: solvate ionic liquids and borenium ionic liquids.

4.1 Solvate Ionic Liquids

4.1.1 Historical Context

It has been demonstrated that certain complexes of lithium have very low melting points; for example, whereas [Li(G1)][NTf$_2$] and [Li(G2)][NTf$_2$] are solids,

$[Li(G3)][NTf_2]$ is liquid at room temperature [170]. In 2010, Watanabe and co-workers reported liquid complexes of glymes (G*n*) and lithium salts, designed in analogy to crown ether complexes of alkali metals, to be ionic liquids [171]. Equimolar mixtures of $Li[NTf_2]$ and triglyme, G3, or tetraglyme, G4 (Fig. 13), formed liquid materials of high thermal stability, high conductivity (0.6–1.6 mS cm^{-1} at 30 °C) and low viscosity (68.0–156.0 mPa s) [171].

Following Angell's categorization of ionic liquids, [12] these were classified as solvate ILs, because the cation was solvated by a neutral glyme [173]. In subsequent years, the studies were expanded, predominantly by Watanabe and co-workers, to include Group 1 and 2 metal salts [174], with various non-coordinating anions, primarily $[NTf_2]^-$, $[OTf]^-$ and $[BETI]^-$ [175], and a range of glymes [176]—all with the outlook to produce electrolytes for metal-ion batteries. Kitada et al. studied the electrochemistry of concentrated solutions of $AlCl_3$ in glymes, which were shown to contain $[AlGn]^{3+}$ cations and $[AlCl_4]^-$ anions [177, 178]. Just recently, the Lewis acidity of solvate ILs was investigated, with only lithium cations covered to date [114, 179].

4.1.2 Speciation

Like other families of Lewis acidic liquids discussed in this work, solvate ILs are characterized by complex dynamic equilibria. The main one is the competition between the cation–anion interaction and the ligand–cation interaction (Eq. 19) [175].

$$M[A] + Gn \rightleftarrows [M(Gn)][A] \tag{19}$$

If the equilibrium is shifted to the left, the liquid behaves like a solution of a salt in molecular solvent; upon shifting to the right, it has properties of ionic liquid. In IL, the glyme is coordinated in a multi-dentate mode to the metal center, and therefore: (1) has negligible or significantly lowered vapor pressure [173], (2) is not corrosive to polysulfide electrodes, in contrast to free glyme [180]. Basic anions are more likely to closely associate with the alkali metal center, thus causing the release of free glyme, whereas $[NTf_2]^-$, $[ONf]^-$ and $[PF_6]^-$ generate ILs [181]. In addition, a good cavity size match is important: Li^+ matches with G3 or G4, Na^+ with G4 and G5 and K^+ with G5 [174, 181, 182]. Ligands with lower hapticity, such as THF or G2 do form $[Li(THF)_4]^+$ or $[Li(G2)_2]^+$, but overall Li^+-ligand binding energy is obviously weaker, thus concentrated electrolyte solutions are formed [176].

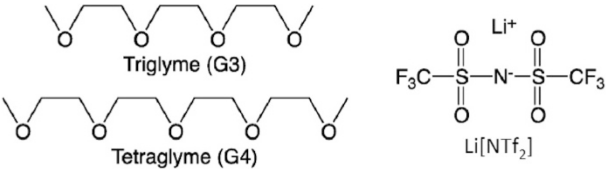

Fig. 13 The structure of components of two solvate ionic liquids: $[Li(G3)][NTf_2]$ and $[Li(G4)][NTf_2]$ [172]

Details of coordination depend on metal–glyme–anion combination. For example, molecular dynamics simulations of equimolar mixtures of G3 or G4 with Li[NTf$_2$] revealed that the first shell of lithium in [Li(G3)][NTf$_2$] contained 4 oxygen atoms from G3 and 1 oxygen from the sulfonyl group of the anion, whereas the first shell of lithium in [Li(G4)][NTf$_2$] contained 4.5 oxygens from G4, and 0.5 oxygen from [NTf$_2$]$^-$ (Fig. 14) [172].

4.1.3 Acidity Measurements

In contrast to earlier-discussed ILs, Lewis acidity of solvate ILs has been probed by Kamlet–Taft parameters. The Kamlet–Taft method uses solvachromatic dyes to determine three independent parameters of a liquid polarity: hydrogen bond donor ability (α), hydrogen bond acceptor ability (β), and dipolarity/polarizability (π^*)—the last one interpreted as the sum of all interactive forces between molecules which do not result in a chemical change [183]. Kamlet–Taft measurements arise from changes to spectroscopic shifts (UV/Vis) from a solvochromatic probe molecule dissolved in the solvent. The approach, well-established for molecular liquids for

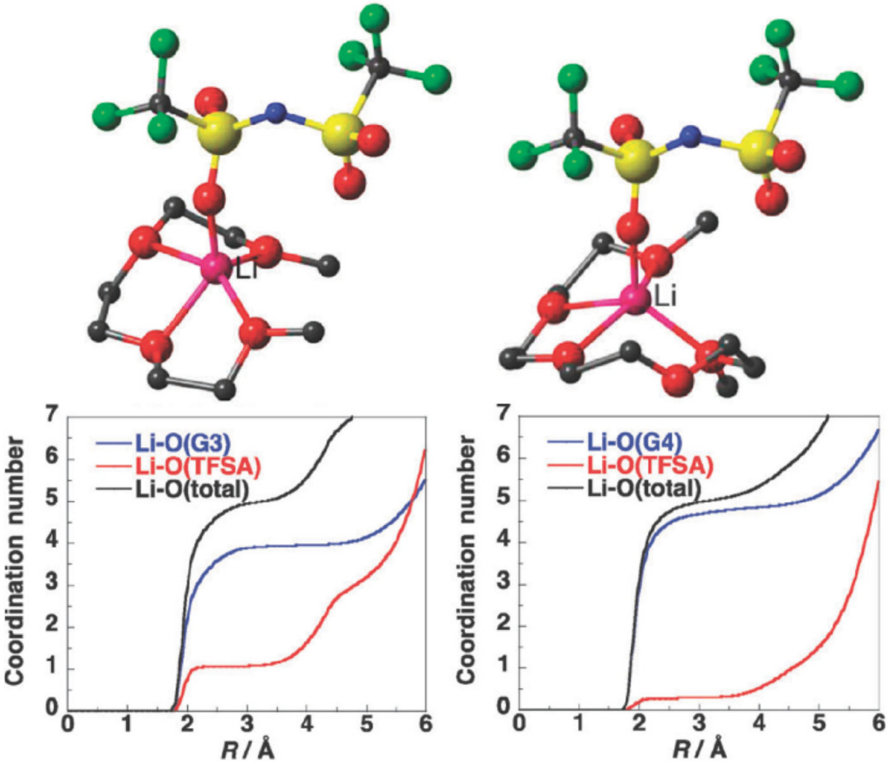

Fig. 14 Optimized structures and coordination numbers of [Li(G3)][NTf$_2$] (*left*) and [Li(G4)][NTf$_2$] (*right*). Structures: Li *purple*, O *red*, C *silver*, N *blue*, S *yellow*, F *light blue* (H atoms omitted for clarity) [172, 173]

which it accurately describes solvent polarizability parameters, has been popularly used also in ionic liquids. Holzweber, Linert and co-workers challenged the validity of the Kamlet-Taft in ILs, arguing that cations and anions affect each other donor/acceptor abilities, and thus interaction with the dyes, possibly rendering the numbers meaningless [99]. However, with the aid of computational chemistry it is viable to elucidate the contribution of each ionic liquid component on the α, β and π^* values [179]. *N.B.*, strongly Lewis acidic ILs, e.g., chloroaluminate(III) systems, can promote decomposition of the dye, preventing meaningful UV–Vis measurements [184].

Kamlet–Taft parameters are not typically employed to report on Lewis acidity; rather, the α parameter is associated with hydrogen bond donor strength/Brønsted acidity. However, Henderson and co-workers demonstrated that, in the absence of acidic protons, α can be interpreted as the measure of Lewis acidity [179]. Moreover, in their original paper, Kamlet and Taft introduced a variety of equations for comparison of their data to allow conversion between the π^*, β and α parameters and the Gutmann acceptor number (see Sect. 2.3.1), allowing for specific data comparisons [183].

The values of α, β and π^* parameters, measured by Henderson and co-workers for [Li(G3)][NTf$_2$], [Li(G4)][NTf$_2$] and the glymes, are listed along polarity and AN values (Table 5) [179]. The α parameters for solvate ILs were much higher than the value recorded for [C$_4$mim][NTf$_2$], 1.3 vs. 0.6. In the absence of strong hydrogen bond donors, this high value was attributed to Lewis acidity of the lithium center, which was supported by a computational model. It was suggested that the interaction of the probe (a model base) with Li^+ occurs by replacing the weakly coordinated anion (viz. Fig. 14) in the axial position.

Almost in parallel, Warr and co-workers published an extensive study on Kamlet–Taft parameters for a wide range of solvate ILs [187]. Corroborating with Henderson and co-workers, they note striking increase in α values for solvate ILs, compared to pure glymes. Moreover, higher α values are obtained for ‘good ionic liquids’ with weakly coordinating anions, than for ‘poor ILs’ with more basic anions (Fig. 15)—this corroborates with Henderson’s postulate that the base

Table 5 Polarity (E_N^T), Kamlet–Taft parameters (α, β and π^*) and acceptor numbers (AN) for solvate ILs: [Li(G3)][NTf$_2$] and [Li(G4)][NTf$_2$], compared to neat glymes, G3 and G4, and a benchmark IL, [C$_4$mim][NTf$_2$]. Adapted from [114, 179, 185, 186]

Solvent	E_T^N	α	β	π^*	AN
[Li(G3)][NTf$_2$]	1.03	1.32	0.41	0.94	26.5
[Li(G4)][NTf$_2$]	1.03	1.35	0.37	0.90	26.5
G3	0.30	0.01	0.96	0.65	0.23
G4	0.28	0.05	0.96	0.67	0.23
[C$_4$mim][NTf$_2$]	0.59	0.59	0.29	0.96	11.9
[C$_4$mim][NTf$_2$]	0.55	0.61	0.24	0.98	3.10

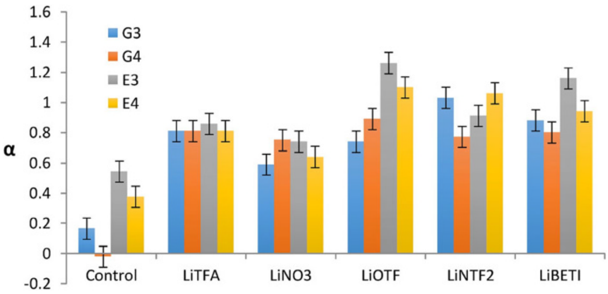

Fig. 15 The α values of equimolar mixtures of Li[A] salts and glymes (G*n*) or glycols (E*n*). The control values are pure G*n* or E*n* [187]

replaces/competes with the anion in coordinating to the lithium center, and possibly points towards future direction in design of Lewis acidic ILs with alkali metal cations.

Henderson and co-workers measured also acceptor numbers for [Li(G3)][NTf_2] and [Li(G4)][NTf_2] [114, 179]. AN values were estimated at AN = 26.5 for both systems, compared to AN = ca. 0.2 for the glymes, and AN = 11.9 and 3.10 (two signals recorded) for a benchmark ionic liquid, [C_4mim][NTf_2] [114]. Comparing these data (Table 5), it is clear that Lewis acidity of the solvate ILs is higher than the benchmark ionic liquid. However, comparison with the literature data is more difficult, as the authors used an alternative methodology: AN values were recorded not for neat ILs, but for solutions in d_6-benzene, and a large molar ratio of TEPO to IL (1:3) was employed. For comparison, Schmeisser et al. reported AN values for several [$C_n$mim][NTf_2] ionic liquids, tested neat, and they were within the range of AN = 25.0–27.4 [24]. AN values measured for chlorometallate ILs are also higher, reaching up to AN = 105 for strongly Lewis acidic compositions (Fig. 3). Possibly, studied neat, AN values for solvate ILs would have been higher.

4.1.4 Applications

To date, a single application as a Lewis acidic catalyst was reported by Henderson and co-workers, with [Li(G3)][NTf_2] and [Li(G4)][NTf_2] used as solvents and catalysts for Diels–Alder [4 + 2] and for [2 + 2] cycloadditions. They performed better, and were safer and easier to use, than the benchmark 5 M ether solution of lithium perchlorate (Fig. 16) [114]. This result is in agreement with the studied on Lewis acidity of solvate ILs: lower hapticity ligands, such as diethyl ether, make ‘poor ILs’ [176], therefore have lower α values, which corresponds to a lower Lewis acidity [187].

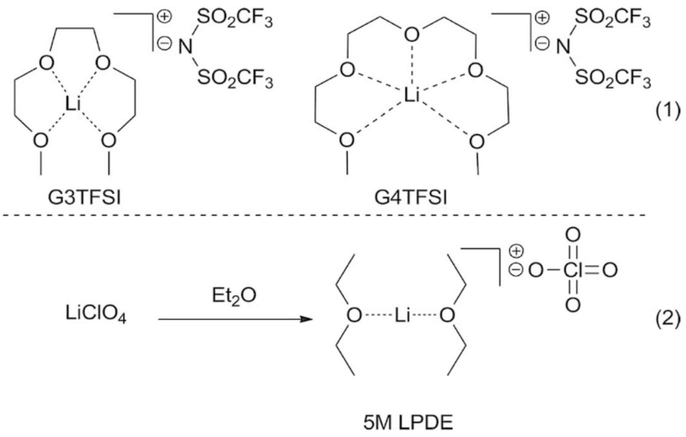

Fig. 16 Comparison of the structure of solvate ILs, $[Li(G3)][NTf_2]$ and $[Li(G4)][NTf_2]$, and a simplified structure of 5 M LPDE [114]

4.2 Borenium ILs (Group 13 Lewis Acids)

4.2.1 Historical Context

Tricoordinate, molecular boron compounds (boranes, boron halides) are commonly used Lewis acids, their acidity derived from the empty *p*-orbital situated on boron. Lewis acidity depends on substituents; for example, in boron halides it increases in the order $BF_3 < BCl_3 < BBr_3 < BI_3$, which is related to decreasing π-back donation from halide to *p*-orbital on the boron, as atomic size of the halide increases [3]. Another strategy to increase electrophilicity relies on introducing a positive charge on the boron center. Tricoordinate borenium cations are stronger Lewis acids compared to structurally similar boranes, having both a net positive charge and a formally vacant *p*-orbital [28].

Synthetic strategies leading to borocations include using aromatic donors to disperse and stabilize charge, and introducing weakly coordination anions, such as $[Al_2Cl_7]^-$ or $[NTf_2]^-$ (viz. examples in Schemes 3 and 4)—which lends itself to be translated to IL realm. However, despite increasing interest in these strong Lewis acids in main-group and organic community [28, 188, 189], their uses in ILs are both very recent and very rare [115, 190].

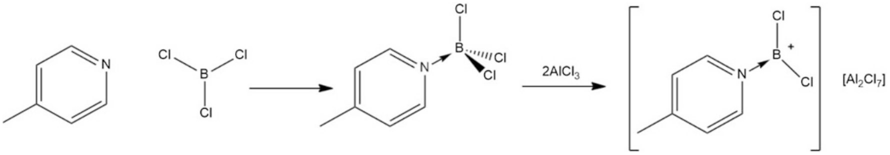

Scheme 3 Synthesis of a borenium ionic liquid via chloride abstraction [191]

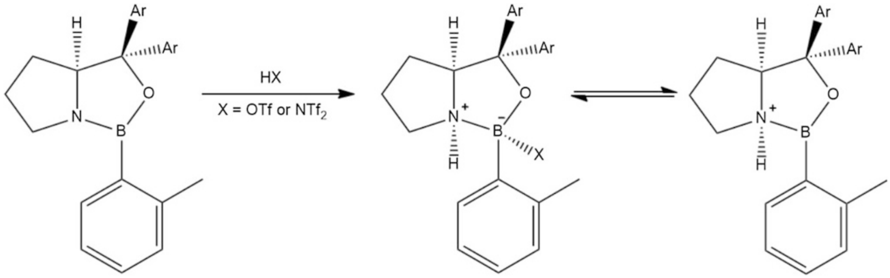

Scheme 4 Synthesis of a borenium salt via protonation with a strong Brønsted acid [192]

4.2.2 Speciation

In 2015, Swadźba-Kwaśny and co-workers reported on a range of Lewis acidic ILs synthesized from tetracoordinate boron adducts, [BCl_3L], and one or two moles of MCl_3 (M = Al or Ga) [190]. Synthetic procedure was analogous to that of Ryschkevitsch and Wiggins (Scheme 3) [191], albeit the second step (metal chloride addition) was carried out solventless. Ligands (L) included pyridine (py), 3-picoline (3pic), 4-picoline (4pic), 1-methylimidazol (mim), trioctylphosphine (P_{888}) and trioctylphosphine oxide ($P_{888}O$).

Upon the addition of MCl_3 (M = Al, Ga), the ^{11}B NMR signal shifted from 5 to 10 ppm (characteristic of four-coordinate boron) to 30–50 ppm, which suggested the formation of a tricoordinate species. In addition to the main broad signal, a sharp peak/shoulder, appearing consistently at 45 ± 1 ppm suggested the presence of molecular BCl_3, due to ligand transfer to the metal center (Eq. 20). The percentage of ligand transfer was relatively small, with the exception of $P_{888}O$ systems, especially combined with $AlCl_3$. In this case, where virtually all ligand was transferred to the metal center—thus making an LCC, $P_{888}O–MCl_3$, with dissolved BCl_3, rather than a borenium IL.

$$[BCl_2L][MCl_4] \rightleftarrows BCl_3 + [MCl_3L] \rightleftarrows BCl_3 + 0.5[MCl_2L_2][MCl_4] \qquad (20)$$

In summary, ILs of nominal general formulas [BCl_2L][MCl_4] and [BCl_2L][M_2Cl_7] were formed for L = phosphine or aromatic amine, and M = Al or Ga. All these contained some equilibrated BCl_3 (Eq. 20), therefore notation L-BCl_3-$n$$MCl_3$ was adopted, to avoid oversimplification.

4.2.3 Acidity Measurements

In ^{11}B NMR spectra of borenium ILs, signals from cations with $[MCl_4]^-$ counterions were more shielded than those from cations with $[M_2Cl_7]^-$ counterions (Fig. 17, left) [190]. This indicates stronger cation–anion interaction for mononuclear $[MCl_4]^-$, compared to dinuclear $[M_2Cl_7]^-$, and is in agreement with observations for halometallate ILs [14, 58], and with studies on borenium cations in solutions [28].

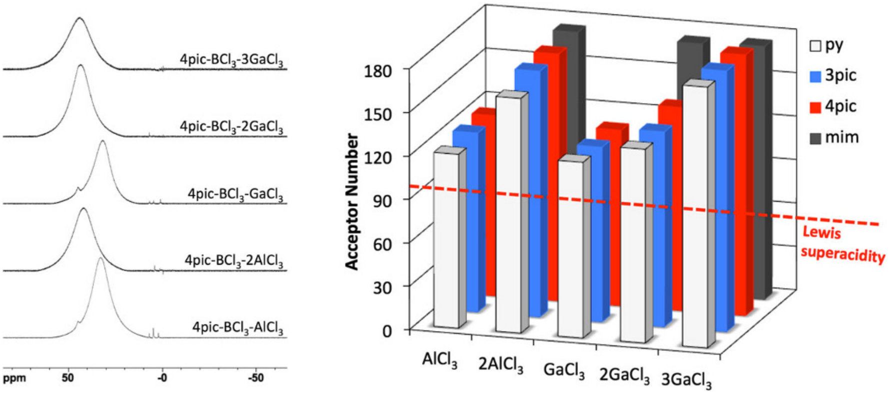

Fig. 17 *Left* ^{11}B NMR spectra (128.37 MHz, 27 °C, neat liquid with d$_6$-DMSO lock) of borenium ILs (composition given on each spectrum); *right* AN values measured for borenium ILs of a general formula L-BCl$_3$-nMCl$_3$, for four different ligands (L), two metals (M) and n = 1–3. Adapted from [190]

AN values were measured for all ILs of a general formula L-BCl$_3$-nMCl$_3$, where L = *N*-donor. All ILs were found to be Lewis superacids (AN >100), with some systems reaching AN >180—the highest values reported in the literature [190]. ILs with $[MCl_4]^-$ anions had lower acidities than these with oligomeric anions, in particular $[Al_2Cl_7]$- and $[Ga_3Cl_{10}]^-$ (Fig. 17, right), indicating that non-coordinating oligonuclear anions result in the existence of 'naked', very acidic borenium cations. Finally, it was shown that AN values recorded for neat IL were higher than those recorded for a solution of this liquid in a molecular solvent.

4.2.4 Applications

A single application of borenium ILs has been reported to date: as Lewis acidic catalysts in Diels–Alder cycloaddition [115]. Their catalytic performance was correlated with AN values through a sigmoidal curve (Fig. 18), i.e., there was a cut-

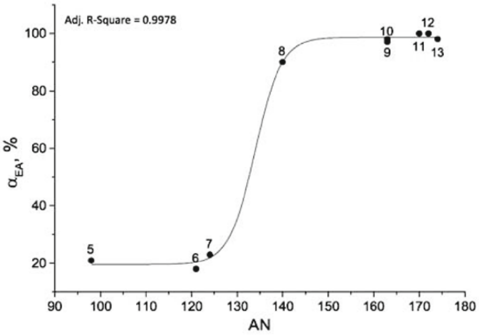

No	Catalyst	AN	α_{EA}, %
5	$[BCl_2(P_{888})][Al_2Cl_7]$	98	21
6	$[BCl_2(4pic)][GaCl_4]$	121	18
7	$[BCl_2(4pic)][AlCl_4]$	124	23
8	$[BCl_2(4pic)][Ga_2Cl_7]$	140	90
9	$[BCl_2(dma)][Al_2Cl_7]$	163	98
10	$[BCl_2(dma)][Ga_2Cl_7]$	163	97
11	$[BCl_2(4pic)][Al_2Cl_7]$	170	100
12	$[BCl_2(mim)][Ga_2Cl_7]$	172	100
13	$[BCl_2(mim)][Al_2Cl_7]$	174	98

Fig. 18 *Left* Conversions in Diels–Alder cycloaddition of cyclopentadiene to ethyl acrylate, catalyzed by 0.10 mol% of borenium ILs *vs*. AN values of the catalysts; *right* tabulated data listing the formula of each IL catalyst, their corresponding ANs and conversions in Diels–Alder reaction. Adapted from [115]

off point for which a sudden increase in conversion was noted, which is characteristic of Lewis acid-catalyzed reactions [85]. Using ILs with the higher ANs, full conversions were achieved within 5 min at 0.1 mol% of catalyst loading, which surpassed all Lewis acidic ILs previously studied in this reaction (viz. Sect. 2.3.3) [75, 114–117].

Considering the immense catalytic potential of such strong acids, new developments in this area are to be expected, particularly in generating ILs with non-coordinating, non-halometallate anions, thereby eliminating the equilibrium presented in Eq. 20.

5 Conclusions

All Lewis acidic ILs discussed in this chapter are characterized by complex speciation, which relates directly to their Lewis acidity and catalytic potential. Therefore, speciation studies—preferably using several in situ techniques—are indispensable to understanding and optimizing the catalytic system. Furthermore, quantifying the Lewis acidity of ILs is a very challenging task. Like in all Lewis acids, the measurement is probe-dependent, therefore order of strength on Lewis acidity scale may alter, depending on the probe used and the methodology adopted.

After being overshadowed by ‘air- and water-stable ILs’, we are witnessing the renaissance of interest in Lewis acidic halometallate ILs, from industrial processes to exciting inorganic synthesis. Liquid coordination complexes (LCCs), which to an extent evolved from halometallate ILs, are of increasing interest. They are expected to gain significantly more attention in the future, due to their higher tunability and lower price.

Finally, the first examples of ILs based on cationic main-group Lewis acids were developed in recent years. This is an entirely new direction of research into Lewis acidic ILs, and the one that potentially can bring the most innovation in the upcoming decade—but also the most synthetic challenges.

References

1. Corma A, Garcia H (2003) Chem Rev 103:4307–4365
2. Busca G (2007) Chem Rev 107:5366–5410
3. Yamamoto H (2000) Lewis acids in organic synthesis. Wiley, New York
4. Qiu R, Chen Y, Yin S-F, Xu X, Au C-T (2012) RSC Adv 2:10774–10793
5. Yamamoto H (2008) Proc Jpn Acad Ser B Phys Biol Sci 84:134–146
6. Stephan DW, Erker G (2015) Angew Chem Int Ed Engl 54:6400–6441
7. Power PP (2010) Nature 463:171–177
8. Bayne JM, Stephan DW (2016) Chem Soc Rev 45:765–774
9. Weicker SA, Stephan DW (2015) Chem Eur J 21:13027–13034

10. Peréz M, Caputo CB, Dobrovetsky R, Stephan DW (2014) PNAS 111:10917–10921
11. Welton T (1999) Chem Rev 99:2071–2084
12. Austen Angell C, Ansari Y, Zhao Z (2012) Faraday Discuss 154:9–27
13. Wilkes JS, Zaworotko MJ (1992) J Chem Soc Chem Comm 965–967
14. Estager J, Holbrey JD, Swadźba-Kwaśny M (2014) Chem Soc Rev 43:847–886
15. Wilkes JS (2002) Green Chem 4:73–80
16. Brown HC, Pearsall HW (1952) J Am Chem Soc 74:191–195
17. Boon JA, Levisky JA, Pflug JL, Wilkes JS (1986) J Org Chem 51:480–483
18. Øye HA, Jagtoyen M, Oksefjell T, Wilkes JS (1991) Mat Sci Forum 73:183–190
19. Parshall GW (1972) J Am Chem Soc 94:8716–8719
20. Takahashi S, Saboungi M-L, Klingler RJ, Chen MJ, Rathke JW (1993) J Chem Soc Faraday Trans 89:3591–3595
21. Gale RJ, Gilbert B, Osteryoung RA (1978) Inorg Chem 17:2728–2729
22. Fannin AA Jr, Floreani DA, King LA, Landers JS, Piersma BJ, Stech DJ, Vaughn RL, Wilkes JS, Williams John L (1984) J Phys Chem 88:2614–2621
23. Hussey C (1983) Room temperature molten salt systems. Adv Molten Salt Chem 5:185–229
24. Schmeisser M, Illner P, Puchta R, Zahl A, van Eldik R (2012) Chem Eur J 18:10969–10982
25. Taylor AW, Men S, Clarke CJ, Licence P (2013) RSC Adv 3:9436–9445
26. Zawodzinski TA Jr, Osteryoung RA (1989) Inorg Chem 28:1710–1715
27. Estager J, Oliferenko AA, Seddon KR, Swadźba-Kwaśny M (2010) Dalton Trans 39:11375–11382
28. Ingleson MJ (2015) Top Organomet Chem 49:39–71
29. Olivier-Bourbigou H, Magna L, Morvan D (2010) Appl Catal A Gen 373:1–56
30. Groh M, Wolff A, Grasser M, Ruck M (2016) Int J Mol Sci 17:1452
31. Gao L, Wang L, Qi T, Chu J, Qu J (2009) J Electrochem Soc 156:P49–P55
32. Mains GJ, Nantsis EA, Carper WR (2001) J Phys Chem A 105:4371–4378
33. Alves MB, Soares VCD, Suarez PAZ, Rubim JC (2008) J Raman Spectrosc 39:1388–1395
34. Alvarez-Vicente J, Dandil S, Banerjee D, Gunaratne HQN, Gray S, Felton S, Srinivasan G, Kaczmarek AM, Van Deun R, Nockemann P (2016) J Phys Chem B 120:5301–5311
35. Pitula S, Mudring AV (2010) Chem Eur J 16:3355–3365
36. Neve F, Francescangeli O, Crispini A (2002) Inorg Chim Acta 338:51–58
37. Sitze MS, Schreiter ER, Patterson EV, Freeman RG (2001) Inorg Chem 40:2298–2304
38. Taylor AW, Qiu F, Villar-Garcia IJ, Licence P (2009) Chem Commun (Camb) 5817–5819
39. Pei Y, Cao Y, Huang Y, Song X, Wang H, Zhao Y, Wang J (2016) Sci China Chem 59:587–593
40. Nockemann P, Nockemann P, Pellens M, Pellens M, Van Hecke K, Van Hecke K, Van Meervelt L, Van Meervelt L, Wouters J, Wouters J, Thijs B, Thijs B, Vanecht E, Vanecht E, Parac-Vogt TN, Parac-Vogt TN, Mehdi H, Mehdi H, Schaltin S, Schaltin S, Fransaer J, Fransaer J, Zahn S, Zahn S, Kirchner B, Kirchner B, Binnemans K, Binnemans K (2010) Chem Eur J16:1849–1858
41. Carmichael AJ, Hardacre C, Holbrey JD, Nieuwenhuyzen M, Seddon KR (1999) Anal Chem 71:4572–4574
42. Zhong C, Sasaki T, Tada M, Iwasawa Y (2006) J Catal 242:357–364
43. Axtell DD, Good BW, Porterfield WW, Yoke JT (1973) J Am Chem Soc 95:4555–4559
44. Bolkan SA, Yoke JT (1986) J Chem Eng Data 31:194–197
45. Li G, Camaioni DM, Amonette JE, Zhang ZC, Johnson TJ, Fulton JL (2010) J Phys Chem B 114:12614–12622
46. De Vreese P, Brooks NR, Van Hecke K, Van Meervelt L, Matthijs E, Binnemans K, Van Deun R (2012) Inorg Chem 51:4972–4981
47. Schreiter ER, Stevens JE, Ortwerth MF, Freeman RG (1999) Inorg Chem 38:3935–3937
48. Abbott AP, Barron JC, Frisch G, Gurman S, Ryder KS, Fernando Silva A (2011) Phys Chem Chem Phys 13:10224–10231
49. Tang S, Mudring AV (2009) Eur J Inorg Chem 2009:1145–1148
50. Mallick B, Metlen A, Nieuwenhuyzen M, Rogers RD, Mudring A-V (2012) Inorg Chem 51:193–200
51. Metlen A, Mallick B, Murphy RW, Mudring A-V, Rogers RD (2013) Inorg Chem 52:13997–14009
52. Boada R, Cibin G, Coleman F, Diaz-Moreno S, Gianolio D, Hardacre C, Hayama S, Holbrey JD, Ramli R, Seddon KR, Srinivasan G, Swadźba-Kwaśny M (2016) Dalton Trans 45:18946–18953
53. Xing X, Zhao G, Cui J (2012) Sci China Chem 55:1542–1547
54. Wicelinski SP, Gale RJ, Williams SD, Mamantov G (1989) Spectrochim Acta Part A 45:759–762

55. Hardacre C, Murphy RW, Seddon KR, Srinivasan G, Swadźba-Kwaśny M (2010) Aust J Chem 63:845–848
56. Yang J, Yang J, Tian P, Tian P, He L, He L, Xu W, Xu W (2003) Fluid Phase Equilib 204:295–302
57. Apperley DC, Hardacre C, Licence P, Murphy RW, Plechkova NV, Seddon KR, Srinivasan G, Swadźba-Kwaśny M, Villar-Garcia IJ (2010) Dalton Trans 39:8679–8687
58. Currie M, Estager J, Licence P, Men S, Nockemann P, Seddon KR, Swadźba-Kwaśny M, Terrade C (2013) Inorg Chem 52:1710–1721
59. Coleman F, Feng G, Murphy RW, Nockemann P, Seddon KR, Swadźba-Kwaśny M (2013) Dalton Trans 42:5025–5035
60. Kim YJ, Varma RS (2005) Tetrahedron Lett 46:7447–7449
61. Atkins MP, Seddon KR, Swadźba-Kwaśny M (2011) Pure Appl Chem 83:1391–1406
62. Markiton M, Chrobok A, Matuszek K, Seddon KR, Swadźba-Kwaśny M (2016) RSC Adv 6:30460–30467
63. Gunaratne HQN, Lotz TJ, Seddon KR (2010) New J Chem 34:1821–1824
64. Da Silveira Neto BA, Alves M, Lapis A, Nachtigall F, Eberlin MN, Dupont J, Suarez PAZ (2007) J Catal 249:154–161
65. Mohammadpoor-Baltork I, Moghadam M, Tangestaninejad S, Mirkhani V, Khosropour AR, Mirjafari A (2011) C R Chim 14:568–579
66. Earle M, Hakala U, Hardacre C, Karkkainen J, McAuley B, Rooney D, Seddon K, Thompson J, Wahala K (2005) Chem Commun 903–905
67. Li J-G, Hu Y-F, Peng X-M, Zhang X-M (2016) J Chem Thermodyn 97:277–281
68. Bica K, Bica K, Leder S, Leder S, Gaerther P, Gaerther P (2011) Curr Org Synth 8:824–839
69. Xie Z-L, Taubert A (2011) ChemPhysChem 12:364–368
70. Miao C-X, Wang J-Q, Yu B, Cheng W-G, Sun J, Chanfreau S, He L-N, Zhang S-J (2011) Chem Commun (Camb) 47:2697–2699
71. Li M, De Rooy SL, Bwambok DK, El-Zahab B, Ditusa JF, Warner IM (2009) Chem Commun Camb 45:6922–6924
72. Estager J, Nockemann P, Seddon KR, Swadźba-Kwaśny M, Tyrrell S (2011) Inorg Chem 50:5258–5271
73. Hartley JM, Ip C-M, Forrest GCH, Singh K, Gurman SJ, Ryder KS, Abbott AP, Frisch G (2014) Inorg Chem 53:6280–6288
74. Abbott AP, Capper G, Davies DL, Munro HL, Rasheed RK, Tambyrajah V (2001) Chem Commun (Camb) 2010–2011
75. Abbott AP, Capper G, Davies DL, Rasheed RK, Tambyrajah V (2002) Green Chem 4:24–26
76. Abbott AP, Bell TJ, Handa S, Stoddart B (2005) Green Chem 7:705
77. Karakulina A, Gopakumar A, Akçok İ, Roulier BL, LaGrange T, Katsyuba SA, Das S, Dyson PJ (2015) Angew Chem 128:300–304
78. Illner P, Zahl A, Puchta R, van Eikema Hommes N, Wasserscheid P, van Eldik R (2005) J Org Chem 690:3567–3576
79. Jiang B, Tantai X, Zhang L, Hao L, Sun Y, Deng L (2015) RSC Adv 5:50747–50755
80. Laurence C, Gal J-F (2009) Lewis basicity and affinity scales: data and measurement. Wiley, New York
81. Mendez M, Cedillo A (2013) Comput Theor Chem 1011:44–56
82. Christe KO, Dixon DA, McLemore D, Wilson WW (2000) J Fluor Chem 101:151–153
83. Childs RF, Mulholland DL (1982) Can J Chem 60:801–808
84. Gutmann V (1976) Electrochim Acta 21:661–670
85. Beckett MA, Strickland GC, Holland JR, Sukumar Varma K (2003) Polymer 37:4629–4631
86. Olah GA, Kobayashi S, Tashiro M (1972) J Am Chem Soc 94:7448–7461
87. Kobayashi S, Busujima T, Nagayama S (2000) Chemistry 6:3491–3494
88. Gutmann V (1979) The extension of the donor-acceptor concept. Pure Appl Chem 51:2197–2210
89. Quarmby IC, Osteryoung RA (1994) J Am Chem Soc 116:2649–2650
90. Gutmann V (1971) Pure Appl Chem 27:73–88
91. Mayer U, Gutmann V, Gerger W (1975) Mon Chem 106:1235–1257
92. Holthausen MH, Mehta M, Stephan DW (2014) Angew Chem Int Ed 53:6538–6541
93. Schmeisser M, van Eldik R (2014) Dalton Trans 43:15675–15692
94. Mantz RA, Trulove PC, Carlin RT, Theim TL, Osteryoung RA (1997) Inorg Chem 36:1227–1232
95. Britovsek GJP, Ugolotti J, White AJP (2005) Organometallics 24:1685–1691
96. Clark ER, Ingleson MJ (2013) Organometallics 32:6712–6717

97. Clark ER, Del Grosso A, Ingleson MJ (2013) Chem Eur J 19:2462–2466
98. Böhrer H, Trapp N, Himmel D, Schleep M, Krossing I (2015) Dalton Trans 44:7489–7499
99. Holzweber M, Lungwitz R, Doerfler D, Spange S, Koel M, Hutter H, Linert W (2012) Chem Eur J19:288–293
100. Kimura Y, Fukuda M, Fujisawa T, Terazima M (2005) Chem Lett 34:338–339
101. Fujisawa T, Fukuda M, Terazima M, Kimura Y (2006) J Phys Chem A 110:6164–6172
102. Morterra C, Cerrato G, Bolis V, Di Ciero S, Signoretto M (1997) J Chem Soc Faraday Trans 93:1179–1184
103. Yang Y-L, Kou Y (2004) Chem Commun (Camb) 226–227
104. Lecocq V, Graille A, Santini CC, Baudouin A, Chauvin Y, Basset J-M, Arzel L, Bouchu D, Fenet B (2005) N J Chem 29:700
105. Deshmukh KM, Qureshi ZS, Dhake KP, Bhanage BM (2010) Cat Commun 12:207–211
106. Yang Y, He W, Jia C, Ma Y, Zhang X, Feng B (2012) J Mol Catal A Chem 357:39–43
107. Wang XH, Tao GH, Wu XM, Kou Y (2005) Acta Phys Chim Sin 21:528–533
108. Le Thuy Bui T, Korth W, Jess A (2012) Cat Commun 25:118–124
109. Cui J, de With J, Klusener PAA, Su X, Meng X, Zhang R, Liu Z, Xu C, Liu H (2014) J Catal 320:26–32
110. Zhang X, Zhang R, Liu H, Meng X, Xu C, Liu Z, Klusener PAA (2016) Ind Eng Chem Res 55:11878–11886
111. Beckett MA, Bland CC, Sukumar Varma K (2008) Polyhedron 27:2226–2230
112. Hilt G, Nödling A (2011) Eur J Org Chem 2011:7071–7075
113. Amarasekara AS (2016) Chem Rev 116:6133–6183
114. Eyckens DJ, Champion ME, Fox BL, Yoganantharajah P, Gibert Y, Welton T, Henderson LC (2016) Eur J Org Chem 2016:913–917
115. Matuszek K, Coffie S, Chrobok A, Swadźba-Kwaśny M (2017) Catal Sci Technol 7:1045–1049
116. Matuszek K, Chrobok A, Latos P, Markiton M, Szymańska K, Jarzębski A, Swadźba-Kwaśny M (2016) Catal Sci Technol 6:8129–8137
117. Chiappe C, Malvaldi M, Pomelli CS (2010) Green Chem 12:1330–1339
118. Plechkova NV, Seddon KR (2008) Chem Soc Rev 37:123–150
119. Liu ZC, Zhang R, Xu CM, Xia RG (2006) OGJ 104:52–56
120. Ma H, Zhang R, Meng X, Liu Z, Liu H, Xu C, Chen R, Klusener PAA, de With J (2014) Energy Fuels 28:5389–5395
121. Xu C (2014) New refinery alkylation processes: composite using ionic liquids alkylation (CILA). Gordon research conference “Green Chemistry”, Hong Kong
122. Simley J (2016) Honeywell UOP https://www.uop.com/?press_release=honeywell-uop-introduces-ionic-liquids. Accessed 30 Mar 2017
123. Brelsford R (2016) OGJ 114:26–27
124. Albright LF (2002) Ind Eng Chem Res 41:5627–5631
125. Gasoline (2016) Honeywell UOP. https://www.uop.com/processing-solutions/refining/gasoline/#alkylation. Accessed 24 May 2017
126. Wang A, Zhao G, Liu F, Ullah L, Zhang S, Zheng A (2016) Ind Eng Chem Res 55:8271–8280
127. Schilder L, Maaß S, Jess A (2013) Ind Eng Chem Res 52:1877–1885
128. Bui TLT, Korth W, Aschauer S, Jess A (2009) Green Chem 11:1961–1967
129. Aschauer SJ, Jess A (2012) Ind Eng Chem Res 51:16288–16298
130. Yoo K, Namboodiri VV, Varma RS, Smirniotis PG (2004) J Catal 222:511–519
131. Deshmukh RR, Lee JW, Shin US, Lee JY, Song CE (2008) Angew Chem Int Ed 47:8615–8617
132. Zhang J, Huang C, Chen B, Ren P, Pu M (2007) J Catal 249:261–268
133. Liu Z, Meng X, Zhang R, Xu C, Dong H, Hu Y (2014) AIChE J 60:2244–2253
134. Huang C, Liu Z, Xu C, Chen B, Liu Y (2004) Appl Catal A Gen 277:41–43
135. Hagen J (2006) Industrial catalysis: a practical approach. Wiley, New York
136. Riisager A, Fehrmann R, Haumann M (2006) Eur J Inorg Chem 2006:695–706
137. Fehrmann R, Riisager A, Haumann M (2014) Supported ionic liquids: fundamentals and applications. Wiley, New York
138. Steinrück H-P, Wasserscheid P (2015) Catal Lett 145:380–397
139. Giacalone F, Gruttadauria M (2016) ChemCatChem 8:664–684
140. Joni J, Haumann M, Wasserscheid P (2009) Adv Synth Cat 351:423–431
141. Joni J, Haumann M, Wasserscheid P (2010) Appl Catal A Gen 372:8–15
142. Zhao X-L, Liu L, Chen Y-J, Wang D (2006) Tetrahedron 62:7113–7120

143. Kohler F, Roth D, Wasserscheid P, Haumann M (2010) Green Chem 12:979–984
144. Meyer C, Hager V, Schwieger W, Wasserscheid P (2012) J Catal 292:157–165
145. Lijewski M, Hogg JM, Swadzba-Kwasny M, Wasserscheid P, Haumann M (2017) RSC Adv 7:27558–27563
146. Cooper ER, Andrews CD, Wheatley PS, Webb PB, Morris RE (2004) Nature 430:1012–1016
147. Parnham ER, Parnham ER, Morris RE, Morris RE (2006) Chem Mater 18:4882–4887
148. Groh MF, Mueller U, Ahmed E, Rothenberger A, Ruck M (2013) Z Naturforsch B 68:1108–1122
149. Elfgen R, Hollóczki O, Ray P, Groh MF, Ruck M, Kirchner B (2016) Z Anorg Allg Chem 643:41–52
150. Ahmed E, Köhler D, Ruck M (2009) Z Anorg Allg Chem 635:297–300
151. Ahmed E, Ahrens E, Heise M, Ruck M (2010) Z Anorg Allg Chem 636:2602–2606
152. Ahmed E, Groh M, Ruck M (2010) Eur J Inorg Chem 2010:5294–5297
153. Groh MF, Wolff A, Wahl B, Rasche B, Gebauer P, Ruck M (2016) Z Anorg Allg Chem 643:69–80
154. Yous S, Poupaert JH, Lesieur I, Depreux P, Lesieur D (1994) J Org Chem 59:1574–1576
155. Guenadil F, Aichaoui H (2002) Phosphorus. Sulfur Silicon Relat Elem 177:2633–2638
156. Fringuelli F, Girotti R, Pizzo F, Vaccaro L (2006) Org Lett 8:2487–2489
157. Means NC, Means NC, Means CM, Means CM, Bott SG, Bott SG, Atwood JL, Atwood JL (2001) Inorg Chem 26:1466–1468
158. Cowley AH, Cushner MC, Davis RE, Riley PE (1981) Inorg Chem 20:1179–1181
159. Abbott AP, Barron JC, Ryder KS, Wilson D (2007) Chemistry 13:6495–6501
160. Coleman F, Srinivasan G, Swadźba-Kwaśny M (2013) Angew Chem Int Ed Engl 52:12582–12586
161. Abood HMA, Abbott AP, Ballantyne AD, Ryder KS (2011) Chem Commun (Camb) 47:3523–3525
162. Hu P, Zhang R, Meng X, Liu H, Xu C, Liu Z (2016) Inorg Chem 55:2374–2380
163. Yoshii K, Jiang X, Sun XG, Tsuda T, Mehio N, Dai S (2015) Electrochim Acta 160:82–88
164. Fang Y, Jiang X, Sun X-G, Dai S (2015) Chem Commun (Camb) 51:13286–13289
165. Pulletikurthi G, Bödecker B, Borodin A, Weidenfeller B, Endres F (2015) Prog Nat Sci Mat Int 25:603–611
166. Atwood DA (1998) Coord Chem Rev 176:407–430
167. Hogg J, Coleman FM, Ugalde AF, Atkins MP, Swadzba-Kwasny M (2015) Green Chem 17:1831–1841
168. Matuszek K, Chrobok A, Hogg JM, Coleman F, Swadźba-Kwaśny M (2015) Green Chem 17:4255–4262
169. Hu P, Wang Y, Meng X, Zhang R, Liu H, Xu C, Liu Z (2017) Fuel 189:203–209
170. Henderson WA, McKenna F, Khan MA, Brooks NR, Young VG, Frech R (2005) Chem Mater 17:2284–2289
171. Tamura T, Yoshida K, Hachida T, Tsuchiya M, Nakamura M, Kazue Y, Tachikawa N, Dokko K, Watanabe M (2010) Chem Lett 39:753–755
172. Tsuzuki S, Shinoda W, Matsugami M, Umebayashi Y, Ueno K, Mandai T, Seki S, Dokko K, Watanabe M (2015) Phys Chem Chem Phys 17:126–129
173. Mandai T, Yoshida K, Ueno K, Dokko K, Watanabe M (2014) Phys Chem Chem Phys 16:8761–8772
174. Mandai T, Yoshida K, Tsuzuki S, Nozawa R, Masu H, Ueno K, Dokko K, Watanabe M (2015) J Phys Chem B 119:1523–1534
175. Shimizu K, Freitas AA, Atkin R, Warr GG, FitzGerald PA, Doi H, Saito S, Ueno K, Umebayashi Y, Watanabe M, Canongia Lopes JN (2015) Phys Chem Chem Phys 17:22321–22335
176. Zhang C, Yamazaki A, Murai J, Park J-W, Mandai T, Ueno K, Dokko K, Watanabe M (2014) J Phys Chem C 118:17362–17373
177. Kitada A, Nakamura K, Fukami K, Murase K (2014) Electrochem 82:946–948
178. Kitada A, Nakamura K, Fukami K, Murase K (2016) Electrochim Acta 211:561–567
179. Eyckens DJ, Demir B, Walsh TR, Welton T, Henderson LC (2016) Phys Chem Chem Phys 18:13153–13157
180. Dokko K, Tachikawa N, Yamauchi K, Tsuchiya M, Yamazaki A, Takashima E, Park JW, Ueno K, Seki S, Serizawa N, Watanabe M (2013) J Electrochem Soc 160:A1304–A1310
181. Mandai T, Tsuzuki S, Ueno K, Dokko K, Watanabe M (2015) Phys Chem Chem Phys 17:2838–2849
182. Mandai T, Nozawa R, Tsuzuki S, Yoshida K, Ueno K, Dokko K, Watanabe M (2013) J Phys Chem B 117:15072–15085
183. Kamlet MJ, Abboud J, Abraham MH, Taft RW (1983) J Org Chem 48:2877–2887

184. Lungwitz R, Spange S (2008) N J Chem 32:392–394
185. Reichardt C (2008) Green Chem 7:339–351
186. Crowhurst L, Falcone R, Lancaster NL, Llopsis-Mestre V, Welton T (2006) J Org Chem 71:8847–8853
187. Dolan DA, Sherman DA, Atkin R, Warr GG (2016) ChemPhysChem 17:3096–3101
188. De Vries TS, Prokofjevs A, Vedejs E (2012) Chem Rev 112:4246–4282
189. Piers WE, Bourke SC, Conroy KD (2005) Angew Chem Int Ed Engl 44:5016–5036
190. Coffie S, Hogg JM, Cailler L, Ferrer-Ugalde A, Murphy RW, Holbrey JD, Coleman F, Swadźba-Kwaśny M (2015) Angew Chem Int Ed Engl 54:14970–14973
191. Ryschkewitsch GE, Wiggins JW (1970) J Am Chem Soc 92:1790–1791
192. Corey EJ, Shibata T, Lee TW (2002) J Am Chem Soc 124:3808–3809

Top Curr Chem (Z) (2017) 375:59
DOI 10.1007/s41061-017-0142-7

REVIEW

Quantum Chemical Modeling of Hydrogen Bonding in Ionic Liquids

Patricia A. Hunt[1]

Received: 2 January 2017 / Accepted: 16 April 2017 / Published online: 18 May 2017

Abstract Hydrogen bonding (H-bonding) is an important and very general phenomenon. H-bonding is part of the basis of life in DNA, key in controlling the properties of water and ice, and critical to modern applications such as crystal engineering, catalysis applications, pharmaceutical and agrochemical development. H-bonding also plays a significant role for many ionic liquids (IL), determining the secondary structuring and affecting key physical parameters. ILs exhibit a particularly diverse and wide range of traditional as well as non-standard forms of H-bonding, in particular the doubly ionic H-bond is important. Understanding the fundamental nature of the H-bonds that form within ILs is critical, and one way of accessing this information, that cannot be recovered by any other computational method, is through quantum chemical electronic structure calculations. However, an appropriate method and basis set must be employed, and a robust procedure for determining key structures is essential. Modern generalised solvation models have recently been extended to ILs, bringing both advantages and disadvantages. QC can provide a range of information on geometry, IR and Raman spectra, NMR spectra and at a more fundamental level through analysis of the electronic structure.

Keywords Hydrogen bonding · Ionic liquids · DFT

Chapter 8 was originally published as Hunt, P. A. Top Curr Chem (Z) (2017) 375: 59. DOI 10.1007/s41061-017-0142-7.

✉ Patricia A. Hunt
p.hunt@imperial.ac.uk

[1] Imperial College of Science, Technology and Medicine, London, UK

1 Introduction

Hydrogen bonding (H-bonding) is an important and very general phenomenon. H-bonding is part of the basis of life in DNA, key to the environment in controlling the properties of water and ice, and critical to modern applications such as crystal engineering, catalysis applications, pharmaceutical and agrochemical development. H-bonding also plays a significant role for many ionic liquids (IL) in determining the secondary structuring and in affecting key physical parameters. ILs are being explored for an astonishingly wide range of applications; highlights include making industrial processes more sustainable, nanomaterial synthesis, solubilising metal oxides, extracting metals from ore, clean metal electrodeposition, electrolytes for batteries, biocatalysis, biomass processing, pharmaceutical and agrochemical active formulation and delivery, energetic materials, engineering fluids (lubricants, heat transfer agents) and fuels. Understanding the fundamental nature of the H-bonds that form within ILs is very important, and one way of accessing this information is through quantum chemical electronic structure (QC) calculations.

The first part of this review briefly introduces ILs and the basic concept of a H-bond. The unusual nature and wide variety of H-bonds found within ILs is emphasised and a new class of H-bond, the doubly ionic H-bond, found predominantly in ILs is introduced. QC calculations are a key route to understanding the H-bonds that form within ILs, and the importance of QC calculations in providing a benchmark for a “pure” H-bond free of external influences is discussed.

In interpreting the results and in evaluating the quality of a QC study some knowledge of the relative accuracy and utility of different QC methods is required, even for those just reading the literature and not themselves carrying out calculations. Unfortunately the literature is littered with reports of poor quality QC calculations that are substandard in terms of the methods or procedures used. The second part of this review provides an assessment of the quality of different QC approaches, suggestions are made for the minimum appropriate level of QC calculation, and for the best general methodologies to employ when studying H-bonding in ILs. QC calculations are not the only computational methods used to study ILs; classical and ab initio molecular dynamics (MD) are also employed (more so than QC methods). It is important to be aware of the differences, and to have knowledge of the strengths and weaknesses of these other computational methods relative to QC techniques. Information from QC calculations, such as partial charges, is often used as input for MD methods; therefore, an appreciation of the limitations of both QC and MD in regard to the generation and use of partial charges is highly relevant.

To the uninitiated, establishing the correct method and basis sets, and the correct procedures to employ can be daunting. How QC calculations are carried out, the procedures used to establish key structures and an understanding of the interactions between ions is not straightforward. The correct approach for a robust study is outlined and how to identify poor procedures will be discussed. The properties that can be obtained from QC calculations and methods for interrogating the electronic structure are identified. Most QC calculations to date have been carried out on isolated ions, ion pairs and very rarely on ion pair dimers or larger clusters. However, the recent development of parameters for ILs has made the use of polarizable continuum models (PCM) possible. A broad stroke description of PCM is provided, followed by a discussion of the parameters required to model ILs using PCM. The review closes with a discussion of potential issues around using a PCM methodology.

2 H-bonds and ILs

Ionic liquids (ILs) are liquids formed from structurally and chemically diverse ions. IL ions tend to be less symmetrical, larger and more diffuse than the ions found in traditional solid salts. H-bonding plays a key role in determining the chemical and physical properties of a significant number of ILs [1]. The range and versatility of ILs is in part due to the diverse range of H-bonding interactions that can occur within different ILs (Fig. 1). This extends from IL that barely exhibit H-bonding (and resemble more closely molten salts) to ILs that are formed by the transfer of a proton and exist in equilibrium with their neutral conjoiners (protic ILs).

H-bonding plays a crucial role in many of the ILs being developed for practical applications. H-bonding is key in the ability of ILs to dissolve materials that are

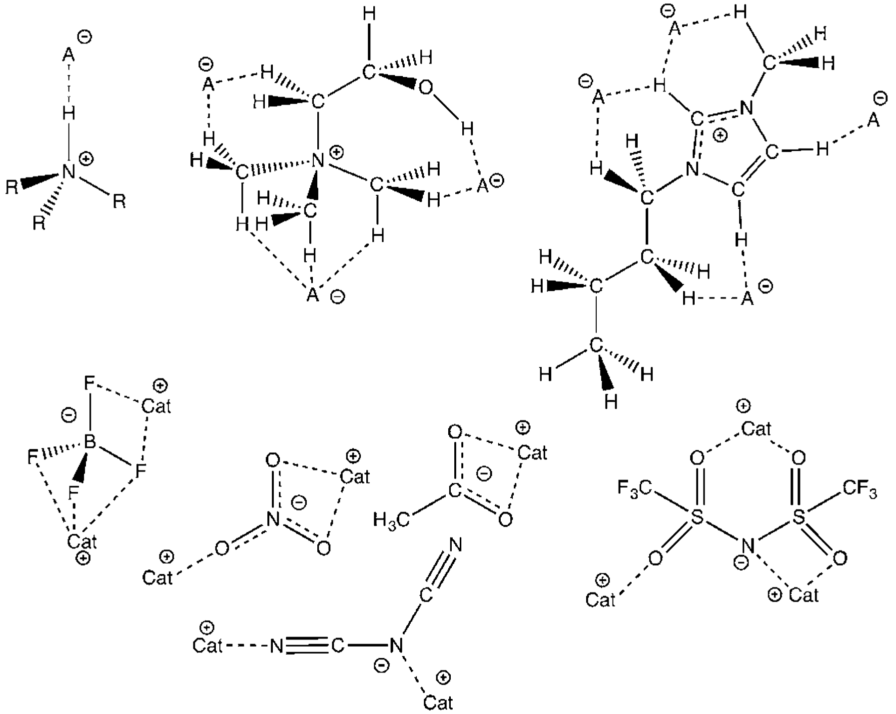

Fig. 1 Selected H-bonding interactions

insoluble in any other medium and for the ability of ILs to act as extraction and separation media [2–4]. For example, ILs are being used in analytical chemistry [5], in pharmaceutical applications [5, 6], in the pretreatment and dissolution of biomass components [7] and in solubilising metal oxides [8, 9]. Many reactions can be influenced by the presence of a H-bond to stabilise a key transition state. This includes biological processes, e.g. enzymic catalysis and protein stabilisation [10–12], or materials applications, e.g. proton transfer in fuel cell technologies [13, 14]. The H-bonding ability of an IL is crucial for any process that includes liquids or materials that can undertake H-bonding and in particular for any H-bonding solutes, e.g. industrial chemical reactions, solvating spectroscopic probe dyes, solvating agrochemical or pharmaceutical actives, ILs acting as electrolytes, or when the IL has small amounts of impurities or absorbed water.

H-bonding is important for supramolecular aggregation, self-assembly of biological molecules, microscopic ordering, the generation of nanoscale domains, formation of micelles and for the development of structured liquid crystal phases in crystal engineering [15–22]. Changing the H-bonding can also disrupt many of these interactions. The viscosity of an IL is heavily dependent on the H-bonding within the IL [23–25], and many potential applications in materials and engineering such as heat transfer liquids, lubricants, fuels and electrolytes depend crucially on the fluidity of the IL. In all of these applications the ability of the IL to undertake H-bonding is crucial; H-bonding plays an important but very complex role. As a result of the range of cations and anions possible, ILs can display a large range of H-bonding capability, and thus the character of the H-bonding is very system dependent [1].

Traditionally H-bonds have been defined as forming between a H-bond donor functionality (such as O–H) and a H-bond acceptor, typically with a lone pair of electrons (such as N). The H-bond forms between the small positive partial charge on the H atom and partial negative charge on the electron donor, $\mathrm{O}^{\delta-}{-}\mathrm{H}^{\delta}\cdots\mathrm{N}^{\delta-}$. Early understanding of the H-bond focused on a single, primarily linear interaction and was considered to be essentially ionic. This view of H-bonding has now been left in the past and the identification of many new types of H-bond has led to a continuous development and blurring of the characteristics ascribed to the H-bond [26–29]. Establishing a universally accepted general definition for the H-bond is particularly challenging as opinions can differ widely. Nevertheless, general principles can be established, and IUPAC has supplied a definition with an accompanying technical report [30, 31].

It is essential to initiate any discussion on H-bonding with a description of the parameters to be employed in identifying the H-bond. We will employ the definition that a H-bonding interaction $\mathrm{X{-}H}\cdots\mathrm{Y}$ occurs if X–H acts as a proton donor to Y, where H is explicitly involved in the interaction. Nevertheless, H-bonding is not an on–off phenomenon but is a graduated scale which makes quantifying and clearly demarking H-bonding difficult. The low strength of (most) H-bonds in ILs makes them dynamic, able to form and break at room temperature. The characteristics and features of H-bonding in ILs cover an extremely wide and diverse range, and are not well understood [1, 32].

The commonly recognised *ionic H-bond* is one between a neutral molecule and a charged ion. However, the H-bond in an IL is between two ions, and this *doubly ionic H-bond* has not been recognised in the H-bonding community for the unique (type) but very common (in ILs) case it really constitutes. The characteristics of H-bonds within ILs represent a new area of development for H-bonding which currently requires further exploration [1]. The established guidelines for H-bonding have been developed primarily on the basis of traditional H-bonds, without reference to the possibility of a large range of multiple and strong doubly ionic H-bonds as found in ILs. An understanding of the doubly ionic H-bond requires reassessment of these boundaries. Many specialised definitions, based on particular properties, have been developed for the more traditional H-bond. For example, geometric distances and angles, IR spectroscopy, NMR, association energy and topological analysis of the electron density [33]. Extreme care should be taken before simply applying these definitions outside of the assigned region of applicability (traditional H-bonds) and to the doubly ionic H-bonds found in ILs [26]. Moreover, the H-bonding in ILs is not static but fluctuates and has dynamic character; this aspect of H-bonding in ILs is only just being probed.

When IL cations contain H atoms and IL anions contain atoms with lone pairs, there is the potential to form H-bonds. In typical aprotic ILs (e.g. in 1-alkyl-2-methylimidazolium-based cations $[C_nC_1im]^+$) the primary H-bond donor is a (non-traditional) C–H unit. Formation of the H-bond is facilitated by the positive charge on the cation. Protic ILs are formed by proton transfer from a Brønsted acid to a Brønsted base. In protic ILs the cation becomes the primary H-bond donor, and the H atom is covalently bound to the heavy atom carrying the formal charge, typically N or P. If complete proton transfer is not effected, the precursor to the “anion” is a neutral acid which can also form H-bonds with fully formed anions. In addition, anions carrying a H atom can undergo H-bonding to form anion–anion H-bonds [34]. Moreover, there is also potential for alkyl groups (in the cation or anion) to be functionalized. Typical functionalities can include groups that can form strong H-bonds such as alcohols, amines and carboxylic acids. Cations with H-bond acceptor functional groups can also H-bond together; however, in this case the substituents are often shielded from the cation charge and behave more like traditional H-bonds. There has also been recent debate on smaller systems where the H atom in question is much closer to the charged centres, where “anti-electrostatic” H-bonds are suggested to form between two like charged ions [35–37]. Deep eutectic solvents (DES) are also relevant; these are formed from IL ions but also contain a neutral H-bond donor and/or H-bond acceptor molecule (e.g. urea) in varying molar ratios. Thus, in ILs, most H-bond acceptors are halogen, oxygen or nitrogen atoms and most H-bond donors are –NH, –CH or –OH groups.

Networks of H-bonds form within ILs; unlike in liquids such as water, these are not one donor–one acceptor-type H-bonds but rather exhibit bifurcated (or trifurcated) and chelating H-bonds (Fig. 2). With multiple donor and acceptor sites available H-bond networking is extensive, and it can also be highly disordered, with many “vacant” H-bonding sites. Mixtures of two or more ILs, or mixtures of ILs with traditional solvents (such as methanol) can also introduce a more diverse range of H-bonding interactions. This is particularly true of DES [38]. The characteristics

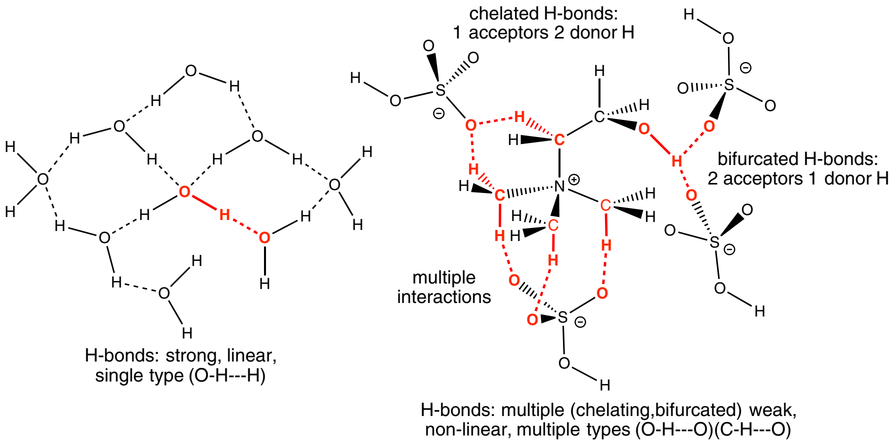

Fig. 2 Types H-bonding interaction

of mixtures can be heavily influenced by the H-bonding interactions that take place. For example water is a ubiquitous contaminant of ILs and is capable of forming H-bonds with the IL ions; the physical properties of the resultant liquid change with the proportion of water present. Thus, the H-bonding within ILs exhibits a large range of distinctive features.

This review focuses on the QC study of H-bonding within ILs. The experimental characterization of H-bonding in ILs is a significant task and not covered here. Typically fully liquid (or even solid state) systems are studied and an “average” of all the different types and forms of H-bond is probed; studies often include a range of techniques, e.g. neutron scattering, NMR, IR, Raman, optical Kerr effect spectroscopy, or UV–vis [2, 39–43]. However, in some cases, such as in gas-phase or cryogenic ion studies, individual H-bonds can be explored [44, 45].

3 Quantum Chemical Computational Modeling of H-bonds Within ILs

Ab initio QC calculations offer one way to investigate H-bonding within ILs. The computational study of traditional H-bonds through ab initio gas-phase methods is well developed and provides structural, electronic, vibrational and NMR properties. Gas-phase, or more accurately isolated molecule, calculations on ion pairs or small clusters generate very accurate association energies, electron density maps and molecular orbitals (MOs). Further analysis can be carried out on the orbital make-up (NBO [46, 47]) on the electron density (AIM [48], NCIPlot [49]) and on the electrostatic potential. With the advent of the SMD descriptors for ILs [50], the effects of a generalised solvent environment on the H-bond can also be explored. The energy associated with internal molecular rearrangements such as relative cation–anion positioning and torsional rotation in alkyl chains can also be obtained. Other computational methods such as classical MD and ab initio MD provide complementary information and have been extensively applied to ILs providing important contributions [51–55]. The focus here will be on the use of QC methods for investigating ILs and in particular H-bonding within ILs.

QC calculations provide a benchmark for a “pure” H-bond free of external influences (such as crystal packing or solvation effects). QC methods also offer a uniform mechanism for comparing H-bonds and can be used as a reference for evaluating the impact of local environmental effects (such as solvation). The fundamental isolated gas-phase doubly ionic H-bond is of substantial interest and should not be overlooked in the desire to mimic the liquid environment. Modern experimental techniques are capable of studying cold (mass) composition-selected clusters and analysing the H-bonding through IR and Raman spectra [45, 56]. The relevance of isolated ion pairs or small clusters is also evident when the mass spectra of selected clusters are analysed [57], or when small isolated clusters or ion pairs (dilute IL) are examined within a low dielectric solvent medium [43, 58–60]. An understanding of the “pure” tightly associated ion pair of an IL can offer a starting point and significant insight into the more dynamic, multiple and looser interactions within the bulk liquid state an IL. In this context, QC ion pair studies can be considered to provide a lower bound for bond lengths because the isolated ion pairs will be contracted due to a maximised Coulombic attraction. Simple ion pair studies can also offer insight into the effects at the liquid–gas interface where H-bonding is not saturated.

4 Quantum Chemical Methods

In interpreting the results and in evaluating the quality of a QC study some knowledge of the relative accuracy and utility of different QC methods is required. In carrying out simple calculations to evaluate a system, to the uninitiated, establishing the correct method and basis sets to employ can be problematic. Moreover, results can be sensitive to the computational method and basis set, making it important to use a method for which the errors are reasonable and well known. This section includes a brief discussion of QC methods and their limitations, providing some assessment of the quality of different approaches. A suggestion is made for the best general methodologies to employ when carrying out QC calculations on ILs. A recent detailed and higher-level review of the various quantum chemical approaches to studying ILs (in general) has recently been published [61].

To obtain the best energies (those converging towards an ideal “real” value), higher-level methods should be employed; these methods require very good and thus extended basis sets. Small molecules can be treated with very high levels of theory (CISD, CASSCF/MP2, CPMCSCF). However, there is a substantial increase in computational resource as the method/basis set improves and large polarizable ions, such as those found in ILs, are not easily accessible. Nevertheless, it is well established that the geometry “converges” more rapidly than the energy and little advantage will be obtained in going beyond B3LYP/6-311+G(d,p) unless there are strong dispersion or correlation effects in which case a dispersion-corrected functional or MP2-level calculation will be suitable. An often used compromise is to compute (optimise) the geometry at a lower level such as B3LYP-D3BJ/6-311+G(d,p) and then carry out a (single point) energy calculation at this geometry but now employing a higher-level method such as CCSD(T)/aug-cc-pVTZ.

Dispersion is an important consideration for ILs; ILs contain highly polarisable species and negative ions which can undergo closed shell interactions. Alkyl–alkyl associations, weak H-bonding, π-stacking, and anion–π interactions are all important. Thus for ILs, B3LYP-D3BJ (or an alternative dispersion-corrected functional) is the minimum good level that should be employed. Standard (hybrid) density functional theory (DFT) methods can under bind stable minima up to ≈ 30 kJ/mol ($\approx 5\%$ of the interaction energy) [62]. Dispersion effects can be significant, changing the relative geometry and orientation of the constituent ions within an IL; thus to obtain accurate results geometries must be computed with a dispersion-corrected method, and this is particularly important for the top conformers of imidazolium-based ILs [63, 64]. It is no surprise that when comparing across a range of typical IL anions, the dispersion contributions increase for more diffuse molecular anions; corrections are in the range of 15–25 kJ/mol [65]. Early studies on simple ion pairs were unable to evaluate the effects of π-stacking; however, a recent study on $[C_1C_4im]_2Cl_2$ ion pair dimers has established the importance of including dispersion corrections to correctly recover π-interactions and the relative energy ordering between π-stacked and non-π-stacked structures [63]. More concerning is a result from the same study which showed that different dispersion corrections can shift relative energies in opposing directions [63]. In addition, as the size of the alkyl groups on the ions increases, or as the number of ion pairs considered increases, dispersion contributions will increase. Recent studies employing dispersion-corrected functionals indicate that there may be some overenhancement of dispersion effects [66, 67]. The best approach therefore is to test a small number of different functionals and dispersion corrections and to be aware of the errors involved.

One need not be particularly attached to the B3LYP functional or the dispersion corrections of Grimme; there are a variety of exchange potential-incorporating functionals of similar accuracy, revPBE-D3, M06-2X or ωB97X-D [68, 69]. These dispersion-corrected functionals not only differ in the form of the DFT functional (PBE, M06, B97, B3LYP) but also in the methodology of the dispersion correction. D, D2, D3 and the more recent implementation D3BJ provide increasingly complex and more accurate ad hoc corrections based on the known functional form for classical dispersion [69–71]. The M06 suite of functionals are highly parametrised using a wide range of data including specifically noncovalent interactions such as H-bonding, charge-transfer complexes, dipole interaction complexes, weak interaction complexes and π–π stacking. The ωB97X-D functionals are range-separated functionals where the self-interaction error (which is largest at long range) is corrected by including more exact HF exchange at long range; ω is the range parameter controlling the switchover point [72, 73]. Thus, in a robust study all of these functionals will be tested on a limited set of structures; if the results are all very similar, one functional can then be selected to carry out all subsequent calculations with reasonable confidence.

Typically Pople basis sets [such as 6-311+G(d,p)] are less robust than Dunning-Huzinaga basis sets (such as aug-cc-pVTZ), but cost substantially less in time and resource. Generally employing a basis set beyond aug-cc-pVTZ is prohibitively expensive. Where there are polarizable anions a flexible basis set is needed; this is achieved by increasing the number and reducing the contraction of basis functions, and is indicated by the 311 in Pople and VTZ in Dunning-Huzinaga basis sets. For diffuse anions and aromatic cations diffuse functions are required; this is indicated by the "+" in Pople or the "aug" in Dunning-Huzinaga basis sets, these recover the movement of the loosely bound electron, well away from the atomic core. However, diffuse functions can make optimisation difficult, moreover diffuse functions can introduce spurious errors into population analysis. Where there is H-bonding diffuse and polarization functions are required in the basis set. Polarisation functions are indicated by the (d,p) in Pople and the "p" in Dunning-Huzinaga basis sets; these allow the sAO electron of H and the lone pairs of the H-bond acceptor to polarize towards each other, thus forming the H-bond. Basis sets must be balanced; having a very good basis set on one atom and a poor basis set on other atoms introduces errors which should be avoided. In general, for main group elements in the first and second row of the periodic table there is little advantage, and some disadvantage, in adding f-functions (e.g. in having (2df,p) in Pople notation) as the basis set becomes unbalanced. Those who specialise in H-bonding (as opposed to ILs) typically employ methods such as MP2/aug-cc-pVDZ and e.g. M06-2X/6-31+G(d,p) for larger systems where MP2 methods are too expensive [74]. As a baseline the minimum level for computationally studying normal H-bonding is B3LYP/6-31+G(d,p), where both the polarization and diffuse functions are important [75].

Population analysis methods tend to work best with medium-level basis sets; population analysis undertaken with highly extended basis sets or basis sets with more than one diffuse function per atom should be checked carefully. Too many diffuse functions cause small overlapping contributions that create instabilities and impact badly on the partition of the electron density. Large basis sets are required to obtain accurate energies; however, they can perform poorly when employed for population analysis. The self-interaction error of DFT methods generates overdelocalisation; in ILs this appears as a delocalisation of the MOs of the cation onto the anion, effectively transferring charge from the anion to the cation. The self-interaction error can be alleviated by including some HF exchange. Hybrid density functionals with a larger (>30%) HF exchange have been recommended [62].

Very recently a substantial study, focused specifically on non-covalent interactions, was carried out over a number of geometry and energy-based data sets. Non-equilibrium geometries, system size and computational time were explicitly evaluated. The functionals B3LYP-D3, M06-2X and ωB97X-D all performed well [68]. Detailed evaluations of methods and basis sets have been undertaken for a range of ILs and have shown the expected trend of accuracy for ion pair association energies; DFT methods not including HF exchange or dispersion perform poorly ($\approx$15–30 kJ/mol), hybrid-DFT methods that include some HF exchange are better ($\approx$15–20 kJ/mol) and methods that include HF exchange and dispersion corrections reach qualitative accuracy ($\approx$5–10 kJ/mol). These data have been evaluated for frozen geometries optimised at the B3LYP/6-31+G(d) or MP2/6-31+G(d,p) level

[76, 77]. A more definitive analysis would optimise each structure at the level to be tested.

For ILs, which have large ions and where dispersion plays an important role, B3LYP-D3 (or an alternative dispersion-corrected functional such as M06-2X or ωB97X-D) is the minimum good level that should be employed. On balance considering the performance (accuracy and time) for pure ionic liquids, H-bonding, and the ability to accurately model interactions with neutral solutes, or mixtures with molecular solvents, M06-2X may be, by a slight margin, the better choice. Because calculations must include aromatic π-density, anions and H-bonding a large basis set, which includes polarisation (to model electron movement particularly for the H atoms) and diffuse functions (to model anions correctly and to recover longer range H-bonding interactions properly) the minimum basis set is 6-311+G(d,p). At the quantitative level geometries should be optimised at the MP2/aug-cc-pVTZ level, but this can be very expensive. To carry out calculations at higher levels is extremely expensive; however, a single point energy at the CCSD(T)/aug-cc-pVTZ level is desirable. More usually computational limitations may require that CCSD(T)/aug-cc-pVDZ be employed and then there is a balance between the MP2/aug-cc-pVTZ calculation with the low method but better basis set and the CCSD(T)/aug-cc-pVDZ calculation with the better method but lower basis set.

To accurately assess the energy of a normal H-bond, it has been thought that basis set superposition error (BSSE) corrections must be applied; however, more recently the use of BSSE corrections has been questioned [78]. In general, for a high level of accuracy zero point energy (ZPE) corrections should be applied. For IL ion pairs BSSE and ZPE often lead to sizable absolute corrections, and this is particularly true when employing the MP2 method with a double-zeta basis set. When comparing different IL conformers the difference in BSSE and ZPE between the conformers is much less [63].

For ab initio methods computational resources are a major limiting factor [79]. These methods are expensive particularly when applied to larger clusters; however, there are schemes which can simplify the computational cost. Recently a number of techniques have been applied to recover the local environmental effects within the context of ab initio methods [80–82]. However, these methods are relatively new and, while they offer promising advances, they are not well tested.

5 Comparison with Other Computational Methods

Ab initio MD computes the wavefunction but within a periodically repeating boundary that mimics the liquid environment. Thus, ab initio MD includes some wavefunction and density information and some dynamics information and is a particularly powerful tool in this respect. The electron density can polarise and bond making and breaking can be studied; these are particularly important in terms of the dynamic nature of H-bonding. Ab initio MD can also provide highly relevant information on the two-dimensional space of H-bond distances (anion-H vs cation-H) [83].

From a QC perspective the disadvantage of ab initio MD is that the electronic structure cannot be computed to a high level (and typically is evaluated without HF exchange). While periodic codes have started to include HF exchange, these calculations are extremely expensive, and many codes simply do not have MP2 methods implemented. Many earlier simulation studies on ILs, state-of-the-art at the time, use non-hybrid functionals and do not include a dispersion correction, particularly ab initio MD studies. As a result of the expense ab initio MD studies are generally limited to a small number of ion pairs and the simulation "box" is necessarily small. This means there can be "image" effects as a molecule in one box is able to interact with its image in the next box. Simulations of this size cannot adequately recover nanoscale structuring, and they cannot be run for long enough to ensure phase space has been completely sampled, a particular issue for ILs which are very viscous. This also means that the initial state (derived from a classical MD simulation) may have a larger than expected impact on the ab initio simulation. The combined (electronic + periodic) nature of ab initio MD offers significant advantages, but also generates disadvantages. Thus, the best approach is to be aware of the limitations and errors inherent in each method and, where possible, combine information from a range of techniques.

The evolution of more accurate approaches which include hybrid functionals and dispersion corrections does not render earlier studies obsolete, rather the inherent small errors must be recognised when interpreting data. Earlier studies provide a valuable reference point, because we can now evaluate the effects of dispersion and/or HF exchange on the structures and dynamics within ILs. For strong H-bonds the ionic or covalent components will dominate the dispersion and exchange, and traditional ab initio methods (and even classical MD) will describe the H-bonding well; however, when H-bonds are weak or when accurate energies are required calculations must employ MP2 or the latest dispersion-corrected DFT methods, with a functional that includes a significant proportion of exchange.

Our purpose is not to discuss classical methods in any detail; however, an appreciation of the limitations and additional information classical simulation can provide is useful to place QC methods in context. Classical MD simulations recover bulk properties and macroscopic quantities such as diffusion coefficients, conductivity, viscosity and melting point. The animated trajectories obtained from MD also provide a visual interpretation of the motions occurring within the liquid, and these can be surprisingly informative. The distribution of different structures within the liquid environment is recovered. Classical MD methods capture long-range structuring within the liquids and model the nano-structured domains that exist within ILs. Classical MD also allows us to examine a key aspect of H-bonding—the dynamics. The mechanism, rate of bond breaking and reforming and the lifetime of a H-bond all contribute to our understanding of H-bonding within ILs.

The disadvantage of classical MD methods is that the potential needs to be carefully constructed to recover key chemistry, and this is particularly difficult in the case of H-bonding [54]. The problems with generating a good H-bonding water potential have shown that creating a good all round classical potential is extremely difficult [84–86]. MD simulations are only as good as the potential employed and thus can return artificial data [87]. The focus in creating MD potentials to study ILs has typically been to generate good structural averages and macroscopic properties, and not to accurately capture the H-bonding.

The first problem is that many classical MD simulations are based on a “static” electronic distribution of fixed atomic charges. While the H-bonding in IL is dominated by the ionic component, for an accurate description covalent and polarization contributions need to be recovered. Static point charges cannot represent local polarization or electron transfer within a liquid. For example, asymmetric H-bonding in clusters of $[N_{2111}][NO_3]$ observed at the QC level has not been reproduced in MD simulations, and this was ascribed to the highly symmetric force field employed for the NO_3^- anion which could not adequately reproduce the polarization occurring when only two of the O atoms within NO_3^- formed a H-bond. Thus, the use of symmetric force fields can be expected to overstructure an IL [88]. This is a severe and critical limiting factor when studying H-bonding.

Potential functions and charges are fit to reproduce macroscopic thermodynamic parameters and not local interactions, and this means that atomic charges can vary substantially between models [89]. As ILs are composed of ions, the precise charge on an ion is important. This may not be such a problem at “long range” where the electrostatic potential is accurately represented; however, at H-bonding distances, the impact of local charges is significant particularly when the H-bonding is predominantly ionic. The local “charge” on an atom shifts dynamically, and the ability of an “average” charge to recover key features will depend on the full range of charge oscillations and on their frequency. Small rapid oscillations are likely well recovered by an average quantity; however, slower large oscillations are much less likely to be well represented by an average charge. It has been shown that the partial charges employed for an IL potential can strongly influence the H-bonding within the resulting simulation [87].

There has been recent debate within the community regarding the extent to which charge transfer should be accommodated within the potential [90]. Charge transfer occurs via the overlap of orbitals (which decay exponentially), and this is a close-range phenomenon and relative to the liquid environment is overestimated by gas-phase QC calculations. Moreover in a liquid environment as the H-bonding changes, the amount of charge transfer will change also. Thus, it is inappropriate to use the charge transfer predicted by the tightly bound gas-phase ion pairs for liquid-phase simulations. A slightly reduced charge on of all the ions can potentially recover some of the average effects [90]. The development of polarisable force fields able to recover the “sloshing” of charge within an ion is highly desirable, particularly if H-bonding is to be well described. It is clear that the MD representation of H-bonding in ILs needs to be improved; however, the mechanism by which this can best be achieved is less clear [90, 91].

Each computational method has strengths and weaknesses and it is the combined information from these methods which has the greatest power to offer understanding and insight. Even within each methodology there is a trade-off between complexity of the method and computation expense, e.g. the complexity of the potential vs duration of the trajectory in MD methods or the amount of exchange and correlation included in ab initio methods. Ab initio and MD methods are most informative when they are applied to exactly the same IL, and the information obtained from each can be overlapped to check each against the other; used in combination both methodologies can extend our understanding.

6 Procedures for Carrying Out Calculations

The appropriate method and basis set to select when studying ILs have been discussed. How the relevant ion pair structures (for in-depth analysis) are arrived at is important. In traditional QC studies one finds the lowest energy structure and ignores higher energy conformers. This is not an appropriate procedure when there are a range of different structures with very similar energies; all the low energy structures should be interrogated. IL cation–anion pairs almost always exhibit a range of low energy structures. In each case the ion pair conformers exhibit very different H-bonding motifs. It is unfortunate that many studies compute and analyse only a single conformer.

Putting together the lowest energy structures computed for the individual isolated cation and anion (separately) will not necessarily lead to the lowest energy ion pair [92]. This has been shown to be the case for clusters as small as the $[C_1C_1im]Cl$ ion pair dimers [63]. Simply placing the anion close to the C^2–H group of the imidazolium cation and optimising a single structure will not necessarily lead to the lowest energy structure, or provide any indication that there are a significant number of other potential structures with similar energies. A good study will need to sample a full range of both low and high energy structures to obtain a balanced picture of the H-bonding and conformers available. In terms of ILs it is known that the anion can occupy different positions and orientations around the cation. For example, the energy difference between the front (C^2–H-based interaction) and top conformers (anion above the ring) of the imidazolium ILs can be less than 5 kJ/mol [92]. Rotation of the alkyl chain can also lead to multiple minima, some of which will be stabilized more by the presence of the anion than others [92–94]. For example, the *all-trans* alkyl chain of $[C_4C_1im]^+$ is not the most stable in the ion pair $[C_4C_1im]Cl$ or within a larger cluster [92]. Thus, the energy associated with internal molecular rearrangements such as torsional rotation in alkyl chains should be ascertained. The position of the alkyl chains effects which H atoms are accessible and most favourable for H-bonding.

Because 5–10 kJ/mol is the “ballpark” level of accuracy for DFT methods, it is essential that all structures within 10 kJ/mol of the lowest energy conformer are considered. Such structures are more properly thought of as being essentially degenerate. Moreover, the energy ordering of structures can change depending on the particular method employed [92]. In a liquid environment a range of low energy conformers will be sampled, and thus it is important to consider more than the lowest energy structure when attempting to model a liquid IL. Slightly higher energy conformers could be stabilized by other surrounding molecules in the liquid phase thus making an apparently higher energy structure in reality a favoured conformer within the liquid phase. If the study is to offer insight into a liquid environment, it is very important to consider a range of local conformers. Recently it has been established that high energy IL ion pairs (35–60 kJ/mol) can be stabilized in systems as small as ion pair dimers [63]. This makes it even more important to sample a good range of structures when considering only the ion pairs.

It is well established in the study of ion or molecular solvation that each solvent molecule added to a solvation shell increases the number of possible structural isomers; moreover, the isomers can be close in energy, separated by small thermally accessible barriers [28]. Sampling of clusters can be minimized when there is a strong energy sink, one cluster size or conformer that is significantly more stable than others. However, for ILs, this will almost certainly not be the case; there will be a large range of low energy structures with substantial geometric and H-bonding differences. ILs in this context are reminiscent of strongly H-bonding liquids, amorphous solids or glassy systems. The very large number of possible conformers means that qualitative sampling, ideally of relevant conformers, is generally imposed. The caveat that must always be applied is that the most stable or the most relevant cluster may have been missed. Hence, it is important to explain in detail the robust processes for structural sampling.

The study of ion pairs probes detailed intermolecular interactions and for the study of IL provides information that is best used in association with additional data on longer-range properties (experimental or computational). Clusters can be built up starting from ion pair dimers (two cations, two anions) to ion pair trimers and so on. Cluster calculations at the ab initio level allow for some of the longer-range effects and larger system interactions to be recovered. The more molecules that are present, the larger the calculation and in many cases the method and basis set must be reduced to make the calculations tractable. Thus as one aspect of the computation is improved, another must be downgraded.

Properties such as charge polarization and vibrational modes are highly dependent on the specific arrangement of ions, and examining a single conformer or cluster motif cannot give a balanced picture. Thus, it is very important that a suitable range of low energy cluster conformers are sampled. A minimum number of different clusters to sample would be in the range of 20–30 structures. How large should a cluster be? The size of cluster is more likely to be determined by the maximum computational resources available. There is some evidence that clusters of eight ion pairs may be sufficient to recover key features of the electronic character of the liquid environment [80, 95]. However, along with larger clusters, and increased numbers of cluster conformers comes an overload of information which can be difficult to process and pull into a cohesive model or description.

7 Properties and Bonding Analysis

Calculations can be used to obtain structural, energetic, spectroscopic and bonding information. Structural information such as bond distances and angles comes from optimised geometries. These will be free of the strong crystal packing effects due to the ionic nature of the solids. The vibrational analysis provides information on intensity enhancement and the H-bonding red shift [23, 92]. Vibrations can be animated and the individual atomic motions viewed. Vibrational data can be linked to experimental spectra (IR and Raman). However, for ion pairs and small clusters spectroscopic matrix isolation studies offer the best experimental technique for direct comparison with computed vibrations [45, 56, 96]. The computation of NMR spectra is also possible [81, 97, 98]. Accurate calculations on electronic excitations are more difficult, but can be linked to experimental UV–vis spectra [99].

Ab initio calculations provide the means for obtaining significant fundamental insight into H-bonds through analysis of the local electrostatic potentials (ESPs), electronic wavefunction and density [89]. The local ESP at particular atoms can be computed, as can the ESP at a given iso-surface defined around the outside of the molecule [99]. Population analysis methods deliver partial charges and dipole moments. Molecular orbitals can be depicted and interpreted [100]. Changes in the electron density $\rho(r)$ on forming a H-bond, as well as the gradient and Laplacian of $\rho(r)$ can be examined to characterize the formed H-bond [1]. Information on bonding and delocalisation, is readily obtained.

Each method provides a new dimension for examining the H-bond, and we obtain a rich resource of information that can be combined to obtain a fuller picture. Such methods can also be more or less sensitive to the computational method and basis set used to derive the geometry, electron density or energy, and so it is important to ascertain an estimate of the variation and/or error introduced by the method and basis set [101]. Thus, the best ab-initio studies will not just examine the relevant H-bond distances but will also consider other H-bonding characteristics such as IR-vibrations, electron density distributions and orbital descriptors.

Two methods in particular stand out in the study of H-bonds—the quantum theory of atoms in molecules (AIM) method of Bader [48] and the natural bond orbital (NBO) analysis of Weinhold [46, 102]. The proper interpretation of NBO results has recently been under debate [37, 47, 103, 104]. Different population analysis methods are based on different computed properties, e.g. AIM (density), ELF [kinetic energy density and $\rho(r)$ gradient], NBO (wavefunction) and CHelpG (ESP) are popular choices [27]. Partial charge methods recover different information (and give different results for the same IL systems) [89, 101]. Thus, although the outputs of these methods are all called "charges" they reflect different properties, particularly in the case of density versus ESP-based methods. Comparing different structures via the same methodology is appropriate. A quantitative comparison between different methods to identify a "true" method will not be sensible; however, a qualitative comparison does provide better overall understanding. Establishing correlations between the charges from one of these methods and another property is very useful; in this case a "best method" for one particular correlation may be established. However, this does not mean that the method is the best for evaluating another property or chemical descriptor. Each of these methods provides a new dimension for examining the H-bond, and a rich resource of information is obtained that can be combined to form a better overall picture of H-bonding.

8 Generalised Solvation

Ab initio calculations can employ a generalised solvation model (particularly polarizable continuum models, PCM) to recover average solvation effects [105, 106]. These models surround a molecule with a solvent cavity placing

Fig. 3 Representation of generalised solvation model

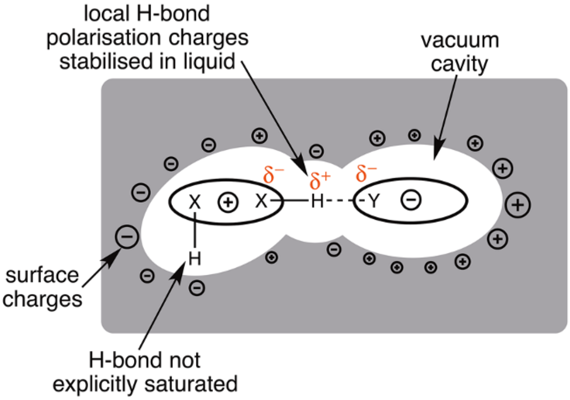

charges (or a continuous charge density) on the surface of the cavity to mimic the charge stabilisation of the solvent environment; the charges are modulated by the dielectric of the proposed solvent (Fig. 3). Inside the cavity the molecule still experiences a vacuum dielectric. Qualitatively, the molecule is not surrounded by solvent molecules, but the effect of the solvent environment is represented through an accumulation of opposing charge gathered on the cavity boundary. PCM methods have been traditionally developed for application to neutral organic solvents, but now extend to conducting solvents [107].

PCM models have proven extremely effective particularly for organic chemistry. However, there are known weaknesses and problems, even for organic molecules [108]. The definition of the cavity is crucial and commonly based on scaled atomic radii, which can vary with implementation [109]. Issues arise due to the use of neutral atom radii for charged ions, a rapid change of the dielectric at the cavity boundary and "escaped" charge from the exponential decay of the charge density beyond the cavity boundary (a particular issue for anions). The radii of ions have been found to be sensitive to the dielectric applied, making cations larger and anions smaller [110]. There are additional complications in applying such methods to ions, either as a solute or solvent, because of the stronger interactions. An error is introduced when the continuum model is applied too close to the ions, e.g. it has been shown that screening of (small monoatomic) ions in aqueous solution is only correct beyond 7 Å [111]. One could expect this distance to be much larger for ILs. Cavity shape can also have a strong impact, particularly where there are diverse conformers.

A key input into PCM solvation models is the dielectric constant. The polarity of an IL is difficult to pin down; on the one hand ILs are made up of oppositely charged ions and can be expected to be extremely polar. On the other hand each ion is immediately surrounded by ions of the opposite charge which shield the central ion; moreover, these surrounding ions are well distributed, reducing polarization of the central ion in any one specific direction. Ions further away are also well shielded, reducing long-range Coulombic forces. Although formed from ions, ILs are typically thought to have a static permittivity (dielectric constant) close to that of alcohols (IL $\varepsilon < 30$, ethanol $\varepsilon = 25$) and much less than that of water ($\varepsilon = 78$) [2].

The interpretation of measurements of the static dielectric is not straightforward, and spectroscopic probe methods typically characterise ILs as having a higher dielectric than data extrapolated from dielectric relaxation spectra [112–114]. Values obtained from experimental dielectric relaxation spectra place the static dielectric permittivities of common ILs close to $\varepsilon \approx$ 12–17 [115].

The (conductor-like) COSMO-RS method has been employed successfully with ILs for some time and has recently been reviewed [116]. A number of early studies have also employed a traditional solvent such as ethanol or methanol to mimic the dielectric environment of an IL [42, 117]. The SMD method of Truhlar is based on PCM and has recently been extended to ILs solvents [50]. The SMD method computes a solute–solvent interaction but also includes terms due to cavitation, dispersion, repulsion and structure effects. The SMD method therefore requires additional data as well as the static or zero-frequency dielectric constant (ε), data include; the dynamic or optical dielectric constant [which is defined in this context as the square of the index of refraction (n^2)], the H-bond acidity (α), the H-bond basicity (β), the surface tension (γ), the fraction of non-H-atoms that are aromatic carbon atoms (φ) and the fraction of non-H-atoms that are electronegative halogen atoms (ψ). φ and ψ are easily determined as they depend only on the chemical formula of the IL. Kamlet-Taft measurements of α and β are also available for a large number of ILs [112]. However, where values are not available these can be readily estimated by computational methods [99]. The surface tension and refractive index for many ILs can be found on the IUPAC ionic liquids database project (IL Thermo) or from a literature search. Truhlar et al. have suggested the use of generic values as a compromise when specific data are not available [50]. A generalised solvation model specific to ILs offers the opportunity to distinguish explicit from generalised solvation effects, and an opportunity to examine (at an ab initio level) the effect of solvating one IL ion pair as solute within different ILs.

IL ions are expected to be less strongly associated in a polar dielectric medium where the surrounding charge stabilises the ions. There may be a stronger “external” impact on the $X \cdots Y$ association coordinate, and thus the doubly ionic H-bond. In this case, H-bond distances may not be a good measure of H-bond strength. For example, both neutral and ionic H-bonds have shown the same increase in bond distance with increasing polarity of a solvent medium (the solvent medium was expected to impact the ionic H-bond more strongly than the neutral H-bond) [74]. How doubly ionic H-bonds respond to a similar change in environment has not yet been fully explored [117]. In the gas phase an ion pair is closely associated and there is significant electron transfer reducing the charge on the individual ions; the neutral state is more highly favoured. In a more polar environment an ion pair will be less closely associated, electron transfer will be reduced and the individual ions will be stabilised in a more highly charged state. The change in stabilisation/destabilisation on going from a “neutral” to a “polarized” state will effect the H-bonding proton position, and all of the X–H, $X \cdots Y$ and X–Y distances. The impact of the environment will be particularly important for (protic) systems with a low barrier to proton transfer [117, 118].

Generalised solvent-based methods cannot account for specific solute–solvent interactions, such as H-bonding. To recover these a supermolecular or cluster-based approach has often been followed for more traditional solute–solvent systems. For solutes that undertake normal H-bonding a combination of explicit solvent molecules and a surrounding continuum solvent description provides improvements over both explicitly solvated gas-phase clusters and isolated solute continuum solvation [75]. The solute and first solvation shell of solvent molecules are placed within the cavity. Placing a small cluster in a cavity has the associated issues of which cluster geometry to employ and problems associated with the definition of the solvent cavity. As the cavity surface is defined from the overlap of the atomic radii, what happens if there are “holes” where the spheres of different ions do not completely overlap within the confines of the cluster? This is a particular problem if reaction paths are explored within a PCM model.

Different cluster geometries may result in significantly different shapes and sizes of cluster cavity. How many solvent molecules should be included? Where the first solvation shell is well defined these methods can work well; however, many ions do not have strongly bound solvation shells and the number of ions in the first solvation shall can vary. Thus, the number and geometry of the solvent molecules around the solute become key parameters, as does the number of clusters sampled (e.g. from a MD trajectory). Cluster models have been tested for more traditional solute–solvent systems [119], and applied to small ions in solvents such as methanol [120]. However, in most cases the solvent molecules have been small, such as water or methanol. IL ions are large and full solvation will require a large number of these ions.

Because ILs consist of two components, the question then arises as to the treatment of the ions: should they be placed in a cavity individually, as a combined ion pair or as a small neutral or charged cluster? Ion pairs placed within a cavity will experience a strongly anisotropic polarisation due to the single explicit counter ion vs the remaining implicit counter ions. Within an explicit liquid environment each ion will be surrounded by other associating ions providing a more isotropic distribution of charge. While H-bonding solute molecules can be “saturated” by solvent molecules, as with other extended H-bond networking solvents, when more IL ions are added, increasing numbers of unsaturated H-bonds are introduced. Because IL ions undertake a large number and type of H-bonds this could be an issue with cluster/continuum solvation models applied to ILs. Weak H-bonding ILs may not be as strongly affected as protic ILs. A balance needs to be reached between the additional accuracy of including specific explicit H-bonds and the errors associated with an uneven description of the H-bonding and polarisation.

If placed within a cavity as an ion pair, explicit H-bonding is retained for one H-bond, but a generalised environment is presented for the other H-bonds; this unequal treatment of the H-bonding may lead to artefacts. However, without the explicit presence of at least one H-bond there is no charge transfer, and the ions (and the surrounding cavity surface) are “over charged”. Nevertheless, in the gas phase charge transfer is overemphasised as neutralisation of the total charge is favoured. Explicit solvation of the component ions in [C_1C_1im][$MeSO_4$] has been shown to result in a reduced total ionic charge when compared to the gas phase [121]. As the amount of charge transferred within ILs is small 0.1–0.2 e, these effects might be considered as relatively minor.

9 Conclusions

We have seen that H-bonding plays a critical role in ILs, and that ILs exhibit a particularly diverse and wide range of traditional and non-standard forms of H-bonding, in particular the doubly ionic H-bond is important. QC calculations offer one way to investigate H-bonding within ILs, providing information on geometry, IR and Raman spectra and through analysis of the electronic structure. ILs are not easy systems to study using QC techniques; however, information and insight can be obtained that cannot be recovered by any other computational method. An appropriate method of calculation combined with a robust procedure for determining key structures is required. Moreover, an appreciation of the limitations and advantages of QC techniques is important, even for those just reading the literature and not carrying out calculations. It is a combination of data and information, from a range of computational and experimental methods, which has the greatest power to offer understanding and insight.

References

1. Hunt PA, Ashworth CR, Matthews RP (2015) Chem Soc Rev 44(5):1257
2. Hallett JP, Welton T (2011) Chem Rev 111(5):3508
3. Zhang Q, Vigier KDO, Royer S, Jerome F (2012) Chem Soc Rev 41(21):7108
4. Werner S, Haumann M, Wasserscheid P (2010) Annu Rev Chem Biomol Eng 1(1):203
5. Ho TD, Zhang C, Hantao LW, Anderson JL (2014) Anal Chem 86(1):262
6. Marrucho IM, Branco LC, Rebelo LPN (2014) Annu Rev Chem Biomol Eng 5(1):527
7. Wang H, Gurau G, Rogers RD (2012) Chem Soc Rev 41(4):1519
8. Abbott AP, Capper G, Davies DL, McKenzie KJ, Obi SU (2006) J Chem Eng Data 51(4):1280
9. Nockemann P, Thijs B, Parac-Vogt TN, Van Hecke K, Van Meervelt L, Tinant B, Hartenbach I, Schleid T, Ngan VT, Nguyen MT, Binnemans K (2008) Inorg Chem 47(21):9987
10. Gorke J, Srienc F, Kazlauskas R (2010) Biotechnol Bioprocess 15(1):40
11. Zhao H (2016) J Chem Technol Biotechnol 91(1):25
12. Fujita K, MacFarlane DR, Forsyth M (2005) Chem Commun 99(38):4804
13. Díaz M, Ortiz A, Ortiz IJ (2014) Membr Sci 469:379
14. Rana UA, Forsyth M, MacFarlane DR, Pringle JM (2012) Electrochim Acta 84:213
15. Desiraju GR (1996) Acc Chem Res 29(9):441
16. Roesky HW, Andruh M (2003) Coord Chem Rev 236(1–2):91
17. Broer DJ, Bastiaansen CMW, Debije MG, Schenning APHJ (2012) Angew Chem Int Ed Engl 51(29):7102
18. Paleos CM, Tsiourvas D (2010) Liq Cryst 28(8):1127
19. Wang D, Su Y, Jin C, Zhu B, Pang Y, Zhu L, Liu J, Tu C, Yan D, Zhu X (2011) Biomacromol 12(4):1370
20. Kim B-S, Park SW, Hammond PT (2008) ACS Nano 2(2):386
21. Saunders LK, Nowell H, Raithby PR, Wilson CC (2016) CrystEngComm 18(31):5916
22. Janczak J (2015) Cryst Growth Des 15(10):5097
23. Hunt PA (2007) J Phys Chem B 111(18):4844
24. Otani A, Zhang Y, Matsuki T, Kamio E, Matsuyama H, Maginn EJ (2016) Ind Eng Chem Res 55(10):2821

25. Gutowski KE, Maginn EJ (2008) J Am Chem Soc 130(44):14690
26. Steiner T (2002) Angew Chem Int Ed Engl 41(1):48
27. Grabowski S (2006) Hydrogen bonding—new insights. Springer, Berlin
28. Meot-Ner Mautner M (2012) Chem Rev 112(10):RP22
29. Grabowski SJ (2011) Chem Rev 111(4):2597
30. Arunan E, Desiraju GR, Klein RA, Sadlej J, Scheiner S, Alkorta I, Clary DC, Crabtree RH, Dannenberg JJ, Hobza P, Kjaergaard HG, Legon AC, Mennucci B, Nesbitt DJ (2011) Pure Appl Chem 83(8):1619
31. Arunan E, Desiraju GR, Klein RA, Sadlej J, Scheiner S, Alkorta I, Clary DC, Crabtree RH, Dannenberg JJ, Hobza P, Kjaergaard HG, Legon AC, Mennucci B, Nesbitt DJ (2011) Pure Appl Chem 83(8):1637
32. Dong K, Zhang S, Wang J (2016) Chem Commun 52(41):6744
33. Jeffrey GA (1997) An introduction to hydrogen bonding. Oxford University Press, Oxford
34. Ribeiro MCC (2012) J Phys Chem B 116(24):7281
35. Weinhold F, Klein RA (2014) Angew Chem Int Ed Engl 53(42):11214
36. Weinhold F, Klein RA (2014) Angew Chem Int Ed Engl 53(48):12992
37. Frenking G, Caramori GF (2015) Angew Chem Int Ed Engl 54(9):2596
38. Ashworth CR, Matthews RP, Welton T, Hunt PA (2016) Phys Chem Chem Phys 18(27):18145
39. Paschoal VH, Faria LFO, Ribeiro MCC (2017) Chem Rev. doi:10.1021/acs.chemrev.6b00461
40. Fumino K, Peppel T, Geppert-Rybczyńska M, Zaitsau DH, Lehmann JK, Verevkin SP, Köckerling M, Ludwig R (2011) Phys Chem Chem Phys 13(31):14064
41. Bowron DT, D'Agostino C, Gladden LF, Hardacre C, Holbrey JD, Lagunas MC, McGregor J, Mantle MD, Mullan CL, Youngs TGA (2010) J Phys Chem B 114(23):7760
42. Dhumal NR, Noack K, Kiefer J, Kim HJ (2014) J Phys Chem A 118(13):2547
43. Matthews RP, Villar-Garcia IJ, Weber CC, Griffith J, Cameron F, Hallett JP, Hunt PA, Welton T (2016) Phys Chem Chem Phys 18(12):8608
44. Cooper R, Zolot AM, Boatz JA, Sporleder DP, Stearns JA (2013) J Phys Chem A 117(47):12419
45. Fournier JA, Wolke CT, Johnson CJ, McCoy AB, Johnson MA (2015) J Chem Phys 142(6):064306
46. Glendening ED, Landis CR, Weinhold F (2013) J Comput Chem 34(16):1429
47. Weinhold F, Landis CR, Glendening ED (2016) Int Rev Phys Chem 35(3):399
48. Bader R (1985) Acc Chem Res 18(1):9
49. Contreras-Garcia J, Johnson ER, Keinan S, Chaudret R, Piquemal J-P, Beratan DN, Yang W (2011) J Chem Theory Comput 7(3):625
50. Bernales VS, Marenich AV, Contreras R, Cramer CJ, Truhlar DG (2012) J Phys Chem B 116(30):9122
51. Thar J, Brehm M, Seitsonen AP, Kirchner B (2009) J Phys Chem B 113(46):15129
52. Cremer T, Kolbeck C, Lovelock KRJ, Paape N, Wölfel R, Schulz PS, Wasserscheid P, Weber H, Thar J, Kirchner B, Maier F, Steinrück H-P (2010) Chem Eur J 16(30):9018
53. Bhargava BL, Balasubramanian S (2006) Chem Phys Let 417(4–6):486
54. Maginn EJ (2009) J Phys Condens Matter 21(37):373101
55. Watanabe H, Doi H, Saito S, Matsugami M, Fujii K, Kanzaki R, Kameda Y, Umebayashi Y (2016) J Mol Liq 217:35
56. Johnson CJ, Fournier JA, Wolke CT, Johnson MA (2013) J Chem Phys 139(22):224305
57. Gozzo FC, Santos LS, Augusti R, Consorti CS, Dupont J, Eberlin MN (2004) Chem Eur J 10(23):6187
58. Dupont J (2004) J Braz Chem Soc 15(3):341
59. Consorti CS, Suarez PAZ, de Souza RF, Burrow RA, Farrar DH, Lough AJ, Loh W, da Silva LHM, Dupont J (2005) J Phys Chem B 109(10):4341
60. Bonhote P, Dias AP, Papageorgiou N, Kalyanasundaram K, Gratzel M (1996) Inorg Chem 35(5):1168
61. Izgorodina EI, Seeger ZL, Scarborough DLA, Tan SYS (2017) Chem Rev. doi:10.1021/acs.chemrev.6b00528
62. Grimme S, Hujo W, Kirchner B (2012) Phys Chem Chem Phys 14(14):4875
63. Matthews RP, Welton T, Hunt PA (2014) Phys Chem Chem Phys 16(7):3238
64. Zahn S, Kirchner B (2008) J Phys Chem A 112(36):8430
65. Izgorodina EI, Golze D, Maganti R, Armel V, Taige M, Schubert TJS, MacFarlane DR (2014) Phys Chem Chem Phys 16(16):7209
66. Savarese M, Brémond É, Adamo C (2016) Theor Chem Acc 135(4):99

67. Castro L, Kirillov E, Miserque O, Welle A, Haspeslagh L, Carpentier J-F, Maron L (2014) ACS Catal 5(1):416
68. Li A, Muddana HS, Gilson MK (2014) J Chem Theory Comput 10(4):1563
69. Grimme S, Antony J, Ehrlich S, Krieg H (2010) J Chem Phys 132(15):154104
70. Grimme S (2006) J Comput Chem 27(15):1787
71. Grimme S, Ehrlich S, Goerigk L (2011) J Comput Chem 32(7):1456
72. Chai J-D, Head-Gordon M (2008) Phys Chem Chem Phys 10(44):6615
73. Chai J-D, Head-Gordon MJ (2008) Chem Phys 128(8):084106
74. Adhikari U, Scheiner S (2013) J Phys Chem A 117(40):10551
75. Rozas I (2007) Phys Chem Chem Phys 9(22):2782
76. Izgorodina EI, Bernard UL, MacFarlane DR (2009) J Phys Chem A 113(25):7064
77. Zahn S, MacFarlane DR, Izgorodina EI (2013) Phys Chem Chem Phys 15(32):13664
78. Mentel ŁM, Baerends EJ (2013) J Chem Theory Comput 10(1):252
79. Carlin CM, Gordon MS (2016) J Phys Chem A 120(30):6059
80. Izgorodina EI, Rigby J, MacFarlane DR (2012) Chem Commun 48(10):1493
81. Bagno A, D'Amico F, Saielli G (2007) ChemPhysChem 8(6):873
82. Bagno A, D'Amico FA, Saielli G (2006) J Phys Chem B 110(46):23004
83. Hollóczki O, Firaha DS, Friedrich J, Brehm M, Cybik R, Wild M, Stark A, Kirchner B (2013) J Phys Chem B 117(19):5898
84. van der Spoel D, van Maaren PJ, Berendsen H (1998) J Chem Phys 108(24):10220
85. Patra M, Karttunen M (2004) J Comput Chem 25(5):678
86. Warren GL, Patel S (2008) J Phys Chem B 112(37):11679
87. Kohagen M, Brehm M, Thar J, Zhao W, Mueller-Plathe F, Kirchner B (2011) J Phys Chem B 115(4):693
88. Bodo E, Mangialardo S, Ramondo F, Ceccacci F, Postorino P (2012) J Phys Chem B 116(47):13878
89. Hunt PA, Kirchner B, Welton T (2006) Chem Eur J 12(26):6762
90. Dommert F, Wendler K, Berger R, Delle Site L, Holm C (2012) ChemPhysChem 13(7):1625
91. de Cavalcante AO, Ribeiro MCC, Skaf MS (2014) J Chem Phys 140(14):144108
92. Hunt PA, Gould IR (2006) J Phys Chem A 110(6):2269
93. Tsuzuki S, Arai AA, Nishikawa K (2008) J Phys Chem B 112(26):7739
94. Umebayashi Y, Hamano H, Tsuzuki S, Canongia Lopes JN, Padua AAH, Kameda Y, Kohara S, Yamaguchi T, Fujii K, Ishiguro S-I (2010) J Phys Chem B 114(36):11715
95. Wendler K, Zahn S, Dommert F, Berger R, Holm C, Kirchner B, Delle Site L (2011) J Chem Theory Comput 7(10):3040
96. Horikawa M, Akai N, Kawai A, Shibuya K (2014) J Phys Chem A 118(18):3280
97. Balevicius V, Gdaniec Z, Dziaugys L, Kuliesius F, Marsalka A (2011) Acta Chim Slov 58(3):458
98. Chen S, Vijayaraghavan R, MacFarlane DR, Izgorodina EI (2013) J Phys Chem B 117(11):3186
99. Niedermeyer H, Ashworth C, Brandt A, Welton T, Hunt PA (2013) Phys Chem Chem Phys 15(27):11566
100. Matthews RP, Ashworth C, Welton T, Hunt PA (2014) J Phys Condens Matter 26(28):284112
101. Rigby J, Izgorodina EI (2013) Phys Chem Chem Phys 15(5):1632
102. Weinhold F, Landis CR (2005) Valency and bonding. Cambridge University Press, Cambridge
103. Weinhold F (2012) J Comput Chem 33(30):2440
104. Stone AJ (2017) J Phys Chem A 121(7):1531
105. Tomasi J, Mennucci B, Cammi R (2005) Chem Rev 105(8):2999
106. Karampinos DC, Georgiadis JG (2007) Nanosc Microsc Therm 11(3–4):363
107. Marenich AV, Cramer CJ, Truhlar DG (2009) J Phys Chem B 113(18):6378
108. Guthrie JPP, Povar I (2009) Can J Chem 87(8):1154
109. Marenich AV, Cramer CJ, Truhlar DG (2008) J Chem Theory Comput 4(6):877
110. Couto PC, Chipman DM (2010) J Phys Chem A 114(48):12788
111. Darden T, Pearlman D, Pedersen LG (1998) J Chem Phys 109(24):10921
112. Ab Rani MA, Brant A, Crowhurst L, Dolan A, Lui M, Hassan NH, Hallett JP, Hunt PA, Niedermeyer H, Perez-Arlandis JM, Schrems M, Welton T, Wilding R (2011) Phys Chem Chem Phys 13(37):16831
113. Lui MY, Crowhurst L, Hallett JP, Hunt PA, Niedermeyer H, Welton T (2011) Chem Sci 2(8):1491
114. Sangoro JR, Kremer F (2011) Acc Chem Res 45(4):525
115. Huang M-M, Jiang Y, Sasisanker P, Driver GW, Weingartner H (2011) J Chem Eng Data 56(4):1494

116. Klamt A (2011) Wiley Interdiscip Rev Comput Mol Sci 1(5):699
117. Clough MT, Geyer K, Hunt PA, Mertes J, Welton T (2013) Phys Chem Chem Phys 15(47):20480
118. Pacios LF, Gomez PC, Galvez O (2006) J Comput Chem 27(14):1650
119. da Silva EF, Svendsen HF, Merz KM (2009) J Phys Chem A 113(22):6404
120. Pliego JR Jr, Miguel ELM (2013) J Phys Chem B 117(17):5129
121. Beichel W, Trapp N, Hauf C, Kohler O, Eickerling G, Scherer W, Krossing I (2014) Angew Chem Int Ed Engl 53(12):3143

Top Curr Chem (Z) (2017) 375:58
DOI 10.1007/s41061-017-0147-2

REVIEW

Mesoscopic organization in ionic liquids

Olga Russina[1] · **Fabrizio Lo Celso**[2] · **Natalia Plechkova**[3] ·
Charl J. Jafta[4] · **Giovanni Battista Appetecchi**[5] ·
Alessandro Triolo[6]

Received: 16 January 2017 / Accepted: 8 May 2017 / Published online: 17 May 2017

Abstract We discuss some published results and provide new observations concerning the high level of structural complexity that lies behind the nanoscale correlations in ionic liquids (ILs) and their mixtures with molecular liquids. It turns out that this organization is a consequence of the hierarchical construction on both spatial (from ångström to several nanometer) and temporal (from fraction of picosecond to hundreds of nanosecond) scales, which requires joint use of experimental and computational tools.

Keywords Ionic liquid · X-ray and neutron scattering · Molecular dynamics simulation · Mesoscopic and microscopic structure

---

Chapter 9 was originally published as Russina, O., Celso, F. L., Plechkova, N., Jafta, C. J., Appetecchi, G. B. & Triolo, A. Top Curr Chem (Z) (2017) 375: 58. DOI 10.1007/s41061-017-0147-2.

✉ Alessandro Triolo
triolo@ism.cnr.it

[1] Dipartimento di Chimica, Università di Roma Sapienza, Rome, Italy

[2] Dipartimento di Fisica e Chimica, Università di Palermo, Palermo, Italy

[3] QUILL, The Queen's University of Belfast, Stranmillis Road, Belfast, Northern Ireland, UK

[4] Helmholtz-Zentrum Berlin für Materialien und Energie GmbH, Hahn-Meitner-Platz 1, Berlin, Germany

[5] Department SSPT-PROMAS-MATPRO, ENEA, 00123 Rome, Italy

[6] Laboratorio Liquidi Ionici, Istituto Struttura della Materia, Consiglio Nazionale delle Ricerche, Rome, Italy

1 Introduction

Ionic liquids (ILs) are a class of compounds composed solely of ionic species with melting point below 100 °C. Interest in these materials arises from their appealing chemical and physical properties as well as the possibility of identifying applications where they can act as environmentally responsible replacements for polluting compounds. Their applications include fields such as synthesis [1–3], catalysis [4, 5], separation [6], electrochemistry [7–9], and materials science [10, 11]. It is now well accepted that many of their peculiar and specific properties stem from the complex organization that characterizes their structure at mesoscopic level.

Mesoscopic order in ILs has been the focus of a large number of studies [12–64], reflecting the impact that this feature plays in the understanding and potential optimization of bulk properties of ILs and their mixtures. A wide variety of physical parameters and chemical factors have been found to affect the morphology of ILs at mesoscopic scales. While complete understanding of the mesoscopic organization in ILs and their mixtures is a necessary step to achieve thorough control over these designer solvents, several aspects of their morphology are yet to be fully understood. Since the experimental proof of the existence of mesoscopic order in bulk ILs, which was provided 10 years ago [12], several of its aspects have been explored, and the efficient and intelligent combination of experimental and computational techniques [24] now provides a powerful tool for further investigation of this exciting issue.

We aim herein to re-present selected published results and describe new observations related to the high level of structural complexity that lies behind the nanoscale correlations in ILs and their mixtures with molecular liquids. Due to the intricate interplay between coulombic and dispersive interactions in these systems, they are characterized by mutual organization of different moieties (e.g., side alkyl tails, charged polar heads, hydrogen-bonding interacting sites, etc.), which leads to a highly hierarchical construction on both spatial (from ångström to several nanometer) and temporal (from fraction of picosecond to hundreds of nanosecond) scales.

2 Effect of cation symmetry

Among the chemical manipulations that can be envisaged to affect the chemical and physical properties of imidazolium salts, one of the interesting ones is preparation of symmetrically substituted imidazolium salts, i.e., imidazolium salts bearing two identical alkyl chains at 1 and 3 position of the ring. Such salts have been widely explored over recent years using both experimental and computational tools [65–72]. Structural studies have highlighted the fact that, similarly to asymmetric 1-alkyl-3-methylimidazolium salts, symmetric dialkyl salts are also characterized by a distinct degree of polar–apolar alternation that manifests itself in X-ray diffraction patterns as a low-Q peak whose position depends on the chain length.

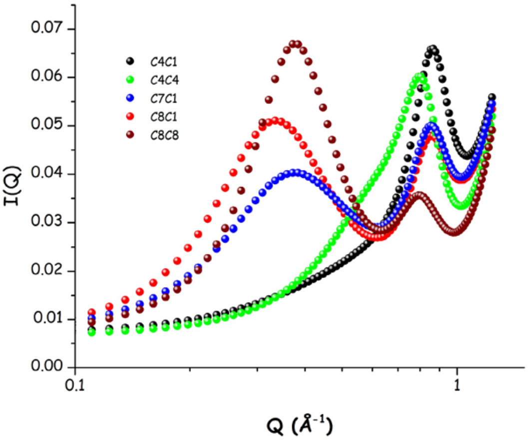

Fig. 1 Small- and wide-angle X-ray scattering patterns for a series of ILs with asymmetric and symmetric cations at ambient temperature (see text for details)

Exploration of diffraction features by probing samples with different degrees of symmetry and chain lengths is useful to rationalize the nature of the structural organization in these systems and to understand better the role of symmetry in determining their mesoscopic structure. Inspection of the small- and wide-angle X-ray scattering (SWAXS) patterns shown in Fig. 1 for a range of ILs is useful to demonstrate the information available from such datasets. In particular, this figure shows datasets for $[NTf_2]^-$-based ILs, where $[NTf_2]^-$ refers to the bis(trifluoromethylsulfonyl)amide anion, with the following cations: $[C_4C_1im]$ (black symbols), $[C_4C_4im]$ (green symbols), $[C_7C_1im]$ (blue symbols), $[C_8C_1im]$ (red symbols), and $[C_8C_8im]$ (wine symbols); all samples were measured at ambient temperature, where they are liquid. The generic formula $[C_xC_yim]$ corresponds to an imidazolium cation bearing two chains at 1 and 3 position with x and y carbon atoms, respectively. Inspection of Fig. 1 shows some general trends: (a) symmetric cations (e.g., $[C_4C_4im]$ and $[C_8C_8im]$) are characterized by higher amplitude of their low-Q peak than their asymmetric equivalents ($[C_4C_1im]$ and $[C_8C_1im]$, respectively); (b) on the other hand, comparison between $[C_8C_8im]$ and $[C_8C_1im]$ indicates that the low-Q peak falls at lower Q values for asymmetric than symmetric cations. This is presumably related to the constrained conformation that is found in the symmetric cations due to the segregated alkyl tails (see, e.g., Fig. 4 in Bernardes et al. [72]), which shortens the extent of the apolar domains with respect to the case of asymmetric cations. This difference implies that the characteristic size of polar–apolar alternation, D, will be larger in the case of asymmetric cations for given value of the longest side chain (e.g., $D_{[C8C1im]} = 18.6\ \text{Å} > D_{[C8C8im]} = 16.7\ \text{Å}$); (c) while densities measured in salts that bear the same total number of methylene/methyl group are approximately the same (e.g., $[C_4C_4im]$ and $[C_7C_1im]$, see references [67, 68], which bear a total of eight between methylene and methyl groups), indicating that there are no major structural reorganization effects at macroscopic level, the mesoscopic organization of this kind of ILs differs substantially. It is evident that the mesoscopic characteristic sizes are distinctly different for $[C_4C_4im][NTf_2]$ and $[C_7C_1im][NTf_2]$, which show a low-Q peak centered at 0.58 and 0.37 Å^{-1}, respectively (corresponding to size of 10.8 and 17.0 Å, respectively). It is the longest chain that determines the characteristic size of the polar–apolar alternation, and as mentioned above in point (b), there are nonnegligible differences in this size between symmetric and asymmetric cations for given longest side chain.

3 Effect of pressure

Pressure has rarely been exploited as a tool to affect the mesoscopic order in ILs, although high-pressure (HP) studies have been used to determine the phase diagram and conformational equilibrium in ILs and their mixtures [73]. This physical parameter can play an efficient role in accessing thermodynamic phases as well as conformational states that are otherwise difficult to reach at ambient pressure; For example, this parameter has been used to access crystallization of ILs that do not show this transition at ambient-pressure conditions (APC) (e.g., in the case of [C_4-mim][BF_4]) or to detect crystalline phases that are difficult to find at APC. Only recently has the role of HP in determining the mesoscopic organization in ILs been assessed. The first paper in this respect was the experimental study by Yoshimura et al., who used the small-angle X-ray scattering (SAXS) technique to observe the peculiar disappearance of the low-Q peak for [C_8mim][BF_4] [74]. This is an interesting result: Crystallization or entrance into a glassy region upon HP application had been successfully probed. However, the fact that liquid samples are affected by HP in a way that reduces their degree of mesoscopic order was rather unexpected, and as such is presently being studied using various complementary techniques. Driven by the experimental SAXS data from Yoshimura, we simulated the same IL at different thermodynamic conditions (constant $T = 320$ K and different pressures in the range between ambient and 10 katm) [58]. Our study covered the pressure range where the major changes were detected experimentally and successfully reproduced these features; namely, we observed that application of HP led to progressive and smooth disappearance of the low-Q peak. The characteristic alternation of polar and apolar domains, for which the low-Q peak is a hallmark, was disrupted by application of HP. Figure 2 shows the simulated SAXS patterns at two extreme pressure states (ambient pressure and 10 katm) for [C_8mim][BF_4]. The same figure shows SAXS patterns for

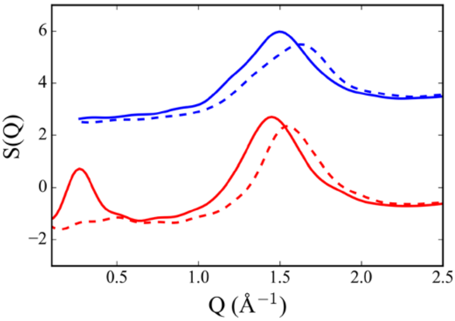

Fig. 2 Calculated small-angle X-ray diffraction patterns for [C_8mim][BF_4] (*red lines*) and [C_2mim][BF_4] (*blue lines*) at 1 atm and 10 katm (*dashed* and *continuous lines*, respectively) at 320 K

$[C_2mim][BF_4]$ in the same states, simulated using a method similar to that developed for $[C_8mim][BF_4]$ [58]. In the latter case, as the side ethyl chain is short, no low-Q peak is found even at ambient pressure, in agreement with experimental results [75, 55]. Investigating the morphology of $[C_2mim][BF_4]$ as a function of pressure changes can be a reliable way to monitor the effect of pressure on coulombic interactions in ILs, to distinguish them from the role of pressure in affecting structural features correlated to dispersive interactions. Molecular dynamics (MD) simulations on the effects of high pressure on the structural organization of aprotic (e.g., dialkylimidazolium) ILs are rare, and only a few studies have focused on the mesoscopic organization in these systems to date. Having validated our MD simulations by confirming the disappearing of the low-Q peak for $[C_8mim][BF_4]$ upon increasing pressure and its absence for $[C_2mim][BF_4]$, we now compare typical pair distribution functions (pdfs). In particular, Fig. 3 shows a comparison of correlations between charged moieties, namely cation–cation, anion–anion, and cation–anion, where "cation" corresponds to the geometrical center of the imidazolium ring and "anion" corresponds to the boron position. Analogously to the observation made for the case of $[C_8mim][BF_4]$, $[C_2mim][BF_4]$ is not characterized by major changes in interionic correlations upon application of HP conditions. Only anion–anion correlations show some effect with increasing pressure, but these occur over a scale of a few ångströms and presumably are not related to the mesoscopic change leading to the disappearance of the low-Q peak in the case of $[C_8mim][BF_4]$. On the other hand, the change in pressure has drastic effects on the distance probability distribution (dpd) for the ring nitrogen and terminal methyl group (hereinafter denoted as C_T) in $[C_8mim][BF_4]$. The same dpd does not show appreciable changes in the case of $[C_2mim][BF_4]$ (Fig. 4). While the dpd remains essentially unaffected by pressure in the latter case, we already reported the fact that, in the former case, substantial folding of the octyl chain is observed, leading to shortening of the end-to-end distance for this chain with increasing pressure. Similarly to results reported by Kashyap et al. for pyrrolidinium ILs [76], in the case of $[C_8mim][BF_4]$, a characteristic change in the $N-C_T$ distance is found [58]. The effect of pressure on $[C_8mim][BF_4]$ drives the long, flexible side chain to curl, in a characteristic scorpion-like fashion [77], in an attempt to minimize the molar volume of the cation. The present results indicate that, when the side chain is short, the response to increased pressure is minimal and no major structural readaptation is observed at mesoscopic level.

4 Effect of ether chains

The role of amphiphilicity in determining the polar–apolar alternation in the mesoscale of bulk ILs has been assessed in recent years through a series of experimental and computational studies. Being composed of a charged polar part (e.g., the imidazolium ring) and a distinctly apolar moiety such as the alkyl tail, whose length can be easily varied, which are covalently bound, ILs are characterized by an inherent amphiphilicity that is combined with their liquid state at ambient conditions. This leads to a typical organization where polar and apolar moieties tend to occupy volumes avoiding each other. The strong coulombic forces

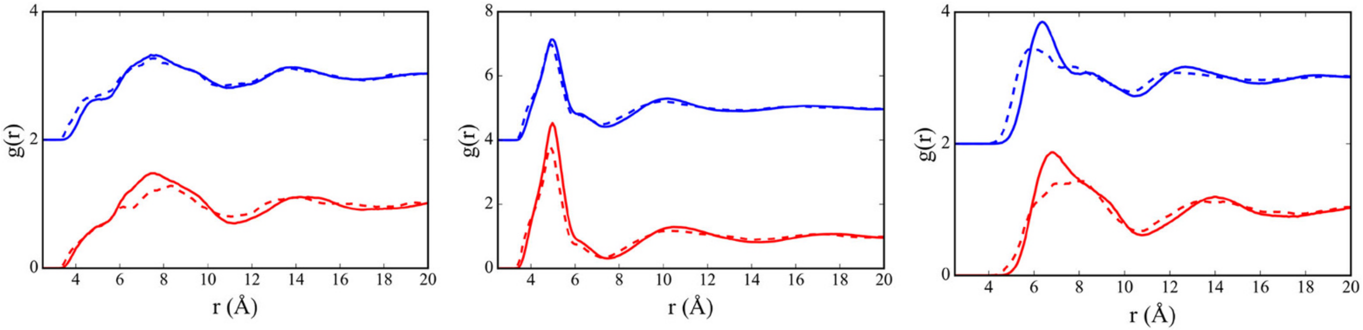

Fig. 3 Selected pair distribution functions for [C_8mim][BF_4] (*red lines*) and [C_2mim][BF_4] (*blue lines*) at 1 atm and 10 katm (*dashed* and *continuous lines*, respectively) at 320 K: *left* ring–ring; *center* ring–anion, *right* anion–anion correlations

Fig. 4 Distance distribution functions for [C_8mim][BF_4] (*red lines*) and [C_2mim][BF_4] (*blue lines*) at 1 atm and 10 katm (*dashed* and *continuous lines*, respectively) at 320 K for the nitrogen–terminal methyl group (C_T) vector

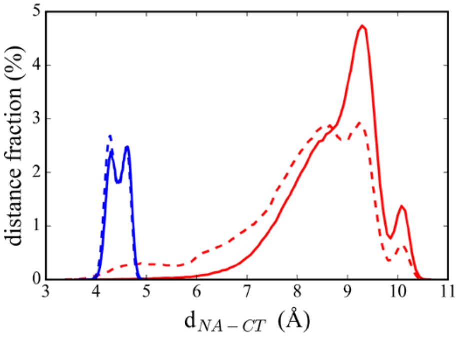

will lead to a well-defined three-dimensional charged network, where the apolar moieties will tend to segregate into nanoscale domains. Such organization introduces a characteristic spatial length that appears in diffraction experiments in the small-angle part of the pattern. Aiming to confirm this structural model driven by polar–apolar alternation, we studied a series of samples where methylene units were replaced by an oxygen atom, leading to ether-like side chains. Such side chains are characterized by a distribution of local charges that is distinctly different from that observed in simple alkyl tails. The oxygen moieties can potentially interact with cation heads, thus removing the fully apolar character of alkyl side chains. Such interaction will then remove the driving force for mutually excluding segregation of tails with respect to polar heads and, as a consequence, to the disappearance of the low-Q peak. Figure 5 shows SAXS data for a series of imidazolium ILs with either alkyl or ether chain [78]. In this set of samples, it is clear that, while the [C_6mim][NTf_2] IL shows the typical low-Q peak centered at ca. 4 nm^{-1}, indicating spatial heterogeneity with size on the order of 15 Å, the IL bearing the ether side chain is featureless in the same Q range. Simple replacement of a methylene unit by an oxygen atom should not deliver such major changes in the X-ray diffraction pattern, as the two moieties (CH_2 and O) are isoelectronic. On the other hand, this example, as well as those for related systems [30, 38, 77, 79], shows that replacement of the apolar side chain with a polar, e.g., ether, moiety induces a drastic change in the mesoscopic organization of the IL, as the typical polar–apolar

Fig. 5 Small- and wide-angle X-ray scattering data for 1-hexyl-3-methyl-imidazolium bistriflamide ([C_6mim][NTf_2], *continuous red line*) and 1-methoxyethoxymethyl-3-methylimidazolium bistriflamide ([$C_1OC_2OC_1$mim][NTf_2], *dashed black line*) at ambient conditions Adapted from Russina et al. [78] with permission from *The Royal Society of Chemistry*

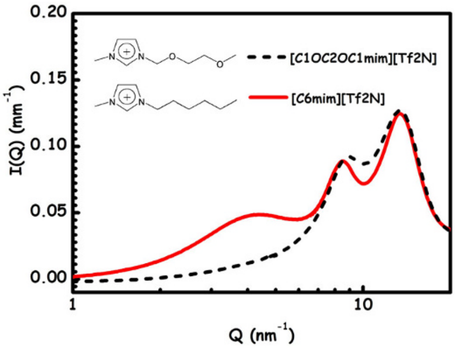

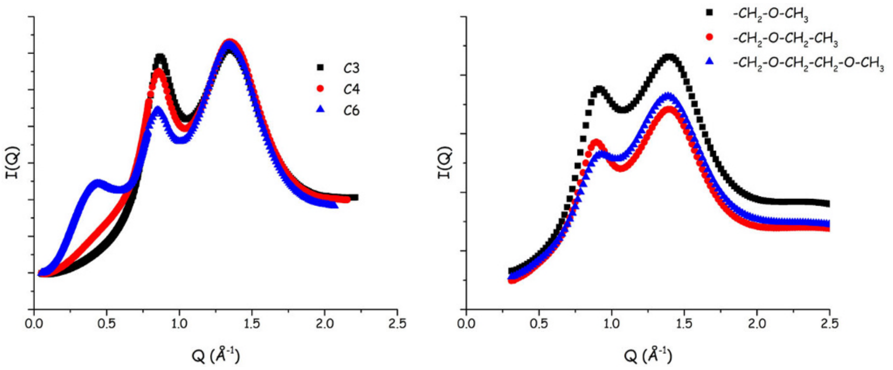

Fig. 6 Small- and wide-angle X-ray scattering data for: *left* 1-alkyl-3-methyl-imidazolium bistriflamide (alkyl = propyl, butyl, and hexyl) and *right* isoelectronic salts (with the same chain lengths) bearing one or two oxygen atoms replacing methylene units, at ambient conditions

mutual segregation no longer takes place and instead a more homogeneous structural organization is found. Figure 6 shows a further series of examples including the dataset from Fig. 5, supporting this experimental evidence. In particular, a comparison is shown between SWAXS data from 1-alkyl-3-methylimidazolium ($[NTf_2]$, where alkyl = propyl, butyl, and hexyl) and the equivalent salts bearing one (or two) oxygen atom(s) replacing one (or two) methylene unit(s) (see figure caption for description). The scenario depicted in the previously mentioned works is supported, in agreement with the computational findings of Shimizu et al. [77]. Again, while with increasing alkyl chain length, distinct development of a low-Q peak occurs, indicating the development of polar–apolar differentiation, when the tail is polar, the enhanced interactions with other polar moieties in the system (e.g., with the imidazolium ring, through either intra- or intermolecular interactions) will remove the distinction between anion/cation head and tail, leading to a much more mesoscopically homogeneous system.

5 Effect of fluorination

Recently, some of us introduced the concept of triphilicity to account for the structural properties of complex ILs bearing, together with the conventional side alkyl tail, also a fluorinated side chain [80]. Previously, related observations were reported for the case of protic ILs bearing fluorinated tails with melting point above room conditions by Greaves et al. [81]. The simultaneous coexistence of two different kinds of incompatible and apolar moieties (e.g., alkyl and perfluoroalkyl) can be expected to lead to a further level of structural complexity in the mesoscopic organization of ILs in bulk state. This kind of ILs have been explored in the past by means of MD [82–86], and the effect of fluorinated tails on the specific density, diffusive and structural behavior assessed. In our recent paper, we explored a series of aprotic ILs bearing a short side alkyl tail (typically an ethyl or methyl group) in the cation and a longer (butyl) perfluorinated side chain in the anion [80]. These ILs, based on the {(trifluoromethyl)sulfonyl} {(nonafluorobutyl)sulfonyl} amide anion (hereinafter denoted as [IM_{14}]) [87], are presently attracting great attention: due to their strongly asymmetric geometry, they show a very wide liquid-state range, with low tendency to crystallize. Moreover, the existence of medium-length fluorinated tails can lead to formation of fluorous domains, where fluorinated compounds might easily dissolve in a nanostructured environment that might allow development of separation and/or reactive processes with high potential impact. While the compounds investigated in references [81] and [85] are protic and as such characterized by an extended and quite rigid hydrogen-bonding (HB) network that most likely adds a further driving force for mutual exclusion of fluorinated and alkyl tails, the ILs reported by Russina et al. [80] tend to behave as "good ILs," as indicated by the Walden plot (of experimental data for log molar conductivity versus log inverse viscosity) for this class of compounds [80]. In this case then, there is no additional driving force for the orientation and mutual exclusion of alkyl and perfluoroalkyl chains, apart from the nature of their mutual interactions. It is noteworthy then that, even in this situation, the appearance of a low-Q peak indicates the existence of polar–(fluorous)apolar alternation in these systems. As shown by Russina et al. [80], this low-Q peak shows up only when the temperature is decreased below ca. 220 K. Figure 7 shows the temperature dependence of the SWAXS patterns for dimethylpyrrolidinium [IM_{14}] ([pyr_{11}][IM_{14}]), showing that, similarly to other related compounds (e.g., [C_2mim][IM_{14}] and [NEt_4][IM_{14}], see Russina et al. [80]), at high temperature, the SAXS data do not show any indication of polar–fluorous domain alternation (which would appear as a low-Q peak); however, on decreasing the temperature, a peak shows up at ca. 0.45 Å^{-1}, a position where ILs bearing butyl chains (e.g., [C_4mim][NTf_2], see Russina et al. [49]) are characterized by the presence of a distinct broad shoulder indicating segregation of the alkyl tails. A detailed explanation for this behavior is not yet available, and we are presently working to try to rationalize this puzzling phenomenology. Apart from the above-mentioned differences between the samples studied by Shen et al. [81] and Hettige et al. [85] and the present compounds based on the [IM_{14}] anion, the analysis conducted by Hettige et al. in [85] is very helpful for understanding the

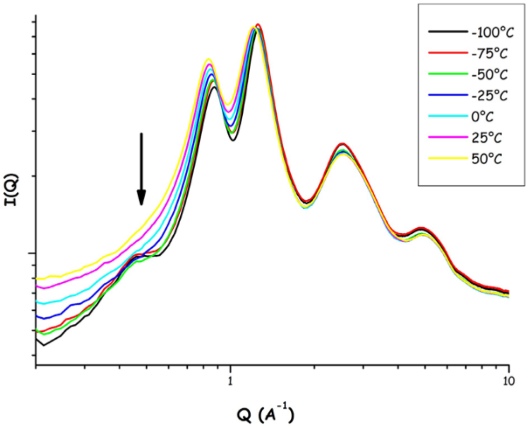

Fig. 7 Small- and wide-angle X-ray scattering data for dimethylpyrrolidinium [IM_{14}] ([pyr_{11}][IM_{14}]), as function of temperature between 50 and −100 °C. The *vertical arrow* indicates the position of the emerging low-Q peak with decreasing temperature Adapted from Russina et al. [80] with permission from *The Royal Society of Chemistry*

Fig. 8 Small- and wide-angle X-ray scattering data for 1-alkyl,3-methylimidazolium [IM_{14}], with alkyl = ethyl, butyl, and octyl, respectively ([C_2mim][IM_{14}], [C_4mim][IM_{14}], and [C_8mim][IM_{14}], respectively), at 20 °C

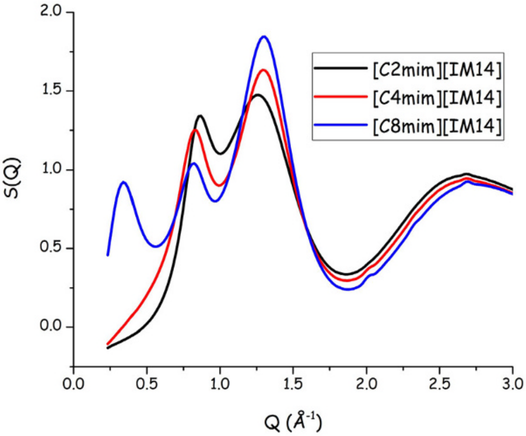

nature of the structural correlations occurring at mesoscopic scales in this kind of fluorinated ILs. In the present case, where essentially no alkyl chain is present in the sample (as only two methyl groups are connected to the pyrrolidinium ring), one does not expect to observe diffraction features related to segregation of alkyl tails. Accordingly, the only kind of segregated domain that can be considered to be responsible for the appearance of the peak at 0.45 Å^{-1} is that related to fluorinated tails. Work is now in progress to rationalize the observation that such self-assembly is observed only at low temperature. On the other hand, it will be of interest to explore the nature of the SAXS patterns when considering fluorinated ILs bearing an alkyl chain long enough to deliver a low-Q peak related to segregation of the alkyl tails that are mutually excluded from the anion's fluorinated ones. We have already started such investigation, and Fig. 8 shows SWAXS data collected for a series of [$C_n$mim][IM_{14}] samples with varying side alkyl chain on the imidazolium ring (specifically $n = 2, 4, 8$) at 20 °C. The presence of the low-Q peak is clearly observed in the case of the octyl-based IL, lying however in the Q range ($\sim$0.35 Å^{-1}) where other ILs with 1-octyl,3-methylimidazolium cation (e.g., [C_8mim][NTf2], see Russina et al. [49]) show their peak. This peak is therefore the hallmark of the alkyl chain segregation, and no indication of mutual exclusion of alkyl and fluorinated domains can be obtained from this room-temperature dataset.Very recently a report from some of us shed some new light into this puzzling phenomenology and we invite the interested reader to refer therein [88].

6 Binary mixtures of ethylammonium nitrate and alcohols: amphiphile meets amphiphile

Above, we reported recent results obtained on the description and exploration of neat ILs. One field that is attracting growing attention is that of binary mixtures including an IL and molecular liquid. These mixtures are interesting as they allow modulation of the properties of the resultant mixture without the need to discover new compounds. Driven by several analogies between protic ionic liquids (PILs), such as ethylammonium nitrate (EAN), and linear alcohols, we undertook an exploration of mixtures of these compounds. PILs are generated by proton exchange between a Brønsted acid and base. As a consequence, hydrogen bonding (HB) plays an important role in determining several properties of this class of compounds, due to the presence of an extended HB network in the bulk structure [89]. Furthermore, PILs show the characteristic polar–apolar structural differentiation, for which the low-Q peak in X-ray/neutron diffraction patterns is a hallmark [35, 38, 90, 91]. These features nicely resemble analogous properties of linear alcohols, whose amphiphilicity induces segregation between the HB moieties into domains embedded in an apolar matrix, leading to the appearance of a low-Q peak with features very similar to those observed for ILs [12, 13]. Accordingly, driven by the common observation that polar compound(s) would preferentially dissolve in the IL's polar domain and, correspondingly, apolar compounds would homogeneously distribute into the IL's apolar domain [20, 92], we undertook structural exploration of mixtures of EAN with linear alcohols, expecting a simple structural repartition of alcohol in such a way that the alkyl tails would be embedded in EAN's apolar pools and the alcohol's hydroxyl group would simply interact with the charged moieties through HB interactions. Such a structural scenario would then imply a rather homogeneous organization of guest and host compounds, without the occurrence of specific effects such as phase separation. On the other hand, existing evidence indicates that such mixtures might not behave as simply as this picture might suggest: EAN–octanol mixtures are well known to show a liquid–liquid equilibrium with upper consolute point at 315.2 K [93, 94]. Longer alcohols are immiscible with EAN at ambient conditions. Analogously, indications of complex structural reorganization phenomena in mixtures of linear alcohols and other, aprotic ILs are also known (see, e.g., [94–98]). The first structural study highlighting the existence of nanoscale heterogeneities in EAN–alcohol mixtures dates to 2011, when Greaves et al. reported SWAXS data from a series of PILs with selected linear alcohols (from ethanol to butanol) [99]. In 2014, some of us reported the first exploration of joint X-ray and neutron diffraction patterns from EAN–methanol mixtures, where the existence of an excess low-Q scattering feature could be clearly

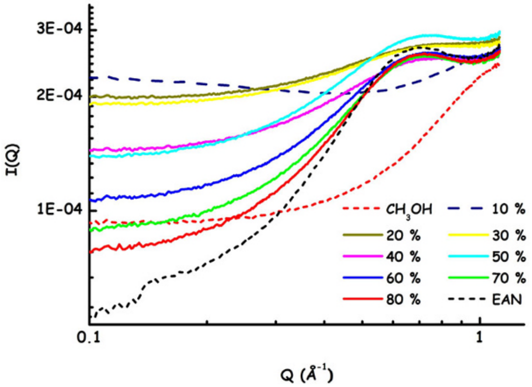

Fig. 9 Small-angle X-ray scattering data for EAN–methanol mixtures as function of the EAN molar fraction at ambient conditions Adapted with permission from Russina et al. [100] copyright (2014) *American Chemical Society*

appreciated [100]. Such excess scattering in the SAXS patterns occurred at lower Q values than those characteristic for the low-Q peak in either EAN or methanol and could be detected only in a restricted concentration window. Figure 9 shows selected SAXS data for EAN–methanol mixtures at ambient conditions as a function of the EAN molar fraction. It appears that, upon adding methanol to neat EAN (dark short dashed line), a progressive increase in the low-Q limit is observed, reaching a maximum at ca. 10 % EAN. Such a feature indicates the development of density fluctuations on the spatial scale of several ångströms in mixtures that appear otherwise macroscopically homogeneous. Joint modeling of energy-dispersive X-ray diffraction (EDXD) and neutron diffraction (ND) patterns using the empirical potential structural refinement (EPSR) approach led to an atomistic-level description of the morphology of these systems, and we could conclude that methanol-rich mixtures are characterized by the presence of ionic species clusters that are not efficiently solvated by the excess methanol [100].

The existence of complex morphology in EAN–alcohols (as well as other PILs–alcohol) mixtures was confirmed by a series of subsequent experimental studies using small-angle X-ray scattering techniques. Jiang et al. reported SAXS data from EAN mixed with ethanol, butanol, and hexanol [101], highlighting the existence of a large low-Q excess resembling the observations made for EAN–methanol. In that paper, the authors accounted for these features by assuming the occurrence of self-assembly phenomena involving the alcohols, which led to the formation of micelles and/or microemulsion-like aggregates. However, this model was not substantiated by a quantitative fit in the original paper. Recently, some of us reported related SAXS data from binary mixtures of EAN and *n*-pentanol as a function of concentration and temperature [102]. While the concentration dependence of the SAXS patterns resembles the behavior reported previously for related EAN–alcohol mixtures, the temperature dependence of the SAXS patterns of these mixtures was not described earlier. A related study by Bonetti and coworkers described the temperature dependence of the small-angle neutron scattering (SANS) pattern from EAN–deuterated octanol in the vicinity of the critical point for this mixture [103]. Presumably, for contrast reasons, the SAXS dataset reported by Schroer et al. [102] shows more clearly the large increase of the low-Q excess scattering with

Fig. 10 Small-angle X-ray scattering data for EAN–*n*-pentanol mixture ($X_{\mathrm{EAN}} = 0.5$) as function of temperature between 313 and 193 K Adapted with permission from Schroer et al. [102] copyright (2016) *American Chemical Society*

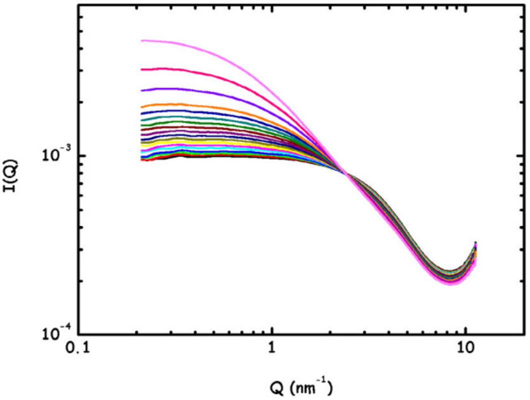

decreasing temperature, approaching the supposed-to-be liquid–liquid equilibrium (LLE) point (Fig. 10). Unfortunately, the EAN–pentanol mixture at the chosen concentration demixes into two phases before providing clear evidence of the existence of a LLE. However, the observed trend could be well described in terms of an Ornstein–Zernike contribution related to density fluctuations whose size drastically increases with decreasing temperature. Recent neutron scattering results presented by Murphy and coworkers on propylammonium nitrate (PAN)–octanol mixtures tend to identify weakly structured aggregates of alcohol in the IL [104]. In that work, the role of the polar–apolar segregated nanostructure in PAN is highlighted as enabling self-assembly of octanol. We observe that, while this model might account for experimental observations for the mentioned system, it does not seem to be able to provide a description for the EAN–methanol situation, for which low-Q excess scattering is observed in a concentration window where no nanostructuring associated with EAN's polar–apolar alternation can be detected (see Fig. 9, where no indication of a low-Q peak can be found at EAN molar fraction of 0.1, where the low-Q excess is maximum). Accordingly, we believe that a more articulated structural model needs to be developed to account for the highly structured morphology in EAN–alcohol mixtures.

In an attempt to further explore this phenomenology, we recently collected a detailed SANS dataset on a related system, namely an EAN–*n*-butanol mixture at EAN molar fraction of 0.5 [102, 105]. Taking advantage of selective deuteration, we obtained SANS datasets for EAN–butanol mixtures with the following deuterations: (a) d8–d10, (b) h8–d10, (c) d3–d10, and (d) d8–d10. The corresponding SANS datasets are plotted in Fig. 11 (note that dataset a for d8–d10 is multiplied by a factor of three), together with SAXS data collected on an unsubstituted mixture (this dataset is multiplied by a factor of 10 for the sake of clarity). Apart from the d8–d10 sample, which showed no coherent scattering, all the other datasets are characterized by distinct low-Q scattering. Figure 11 shows a joint fit of the whole datasets, leading to the continuous lines that represent an Ornstein–Zernike (O–Z) term: $I(Q) = I_0/(1 + Q^2\xi^2)$, where the parameter ξ, representing the characteristic size of

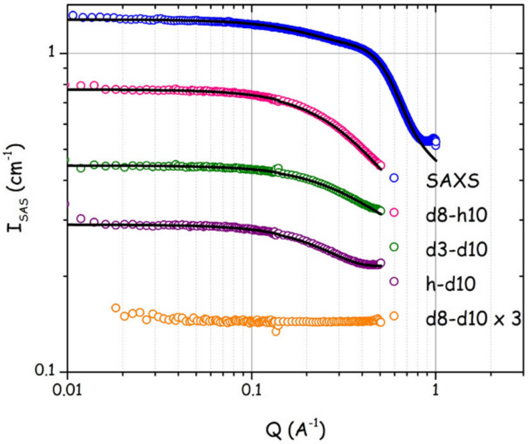

Fig. 11 Small-angle neutron and X-ray scattering data for EAN–*n*-butanol mixture ($X_{EAN} = 0.5$). SANS data are for samples with the same nominal composition but different isotopical substitution (see text for details). SAXS data were collected from a sample with natural isotopic composition and are shifted vertically for the sake of clarity Adapted with permission from Russina et al. [105] copyright (2017) *American Chemical Society*

density fluctuations responsible for the low-Q scattering, was kept constant for the four datasets. The fit also included a variable background to account for incoherent scattering in the mixtures with different deuterium/hydrogen ratios and a variable parameter I_0 to account for the different contrast of the structural heterogeneities with respect to the matrix. In the case of the SAXS dataset, a Gaussian term was also included to account for the diffraction feature centered at ca. 0.5 $\mathring{A}^{-1}$, which is the hallmark of the polar–apolar alternation in this mixture. As can be appreciated, the joint fit is of excellent quality and describes the four different scattering datasets in terms of a unique characteristic size of $\xi = 4$ Å for the density fluctuations. This finding provides further confirmation of the nature of the structural heterogeneities that are responsible for the low-Q excess scattering, especially if one considers that previous studies on EAN–*n*-pentanol showed that, when decreasing the temperature, the O–Z behavior can account for the structural evolution over a wide temperature range.

7 Conclusions

The mesoscopic organization in ionic liquids is far from being spatially homogeneous. While this has already been confirmed using both experimental and computational tools, several aspects of the highly hierarchical nanoscale construction in these systems remain to be explored and assessed. One can envisage that powerful tools such as small (as well as ultra small)-angle X-ray and neutron scattering techniques will turn out to be fundamental to access those structural features extending above the nanometer scale. On the other hand, these efforts are fully justified by the enhanced potential of such a class of compounds whose morphology offers so many variations. While understanding of neat ILs is approaching a satisfactory level and it can be said that state-of-the-art simulations can efficiently reproduce experimental datasets, we identify binary (or more) systems based on ILs as a new frontier where unexpected phenomenology can be discovered leading to unpredictable applications of these materials [105].

Acknowledgements Access to Large Scale Facilities (ESRF, HZB) through different programs is acknowledged. In particular, the role of instrument local contacts [E. Di Cola (ESRF) and S. Prevost (ESRF)] is gratefully acknowledged. N.P. thanks the industrial advisory board of QUILL for their support. A.T. acknowledges Prof. P. J. Dyson for kindly making available to us the samples containing ether chains. We also acknowledge useful discussions with Prof. J. A. P. Coutinho and E. L. Quitevis (symmetric cations) and Prof. W. Schroer and B. Rathke (PIL–alcohols).

References

1. Welton T (1999) Chem Rev 99:2071
2. Hallett JP, Welton T (2011) Chem Rev 111:3508
3. Chiappe C, Pieraccini D (2005) J Phys Org Chem 18:275
4. Pârvulescu VI, Hardacre C (2007) Chem Rev 107:2615
5. Welton T (2004) Coord Chem Rev 248:2459
6. Han X, Armstrong DW (2007) Acc Chem Res 40:1079
7. Armand M, Endres F, MacFarlane DR, Ohno H, Scrosati B (2009) Nat Mater 8:621

8. MacFarlane DR, Forsyth M, Howlett PC, Kar M, Passerini S, Pringle JM, Ohno H, Watanabe M, Yan F, Zheng W, Zhang S, Zhang J (2016) Nat Rev Mater 1:15005
9. Gebresilassie Eshetu G, Armand M, Scrosati B, Passerini S (2014) Angew Chem Int Ed 53:13342
10. Antonietti M, Kuang DB, Smarsly B, Yong Z (2004) Angew Chem Int Ed 43:4988
11. Taubert A, Li Z (2007) Dalton Trans 723
12. Triolo A, Russina O, Bleif H-J, Di Cola E (2007) J Phys Chem B 111:4641
13. Triolo A, Russina O, Fazio B, Triolo R, Di Cola E (2008) Chem Phys Lett 457:362
14. Urahata SM, Ribeiro MCC (2004) J Chem Phys 120:1855
15. Wang Y, Voth GA (2006) J Phys Chem B 110:18601
16. Jiang W, Wang Y, Voth GA (2007) J Phys Chem B 111:4812
17. Wang Y, Jiang WEI, Yan T, Voth GA (2007) Acc Chem Res 40:1193
18. Canongia Lopes JN, Pádua AAH (2006) J Phys Chem B 110:3330
19. Canongia Lopes JN, Costa Gomes MF, Pádua AAH (2006) J Phys Chem B 110:16816
20. Pádua AAH, Costa Gomes MF, Canongia Lopes JN (2007) Acc Chem Res 40:1087
21. Annapureddy HVR, Kashyap HK, De Biase PM, Margulis CJ (2010) J Phys Chem B 114:16838
22. Kashyap HK, Hettige JJ, Annapureddy HVR, Margulis CJ (2012) Chem Commun (Camb) 48:5103
23. Kashyap HK, Santos CS, Daly RP, Hettige JJ, Murthy NS, Shirota H, Castner EW, Margulis CJ (2013) J Phys Chem B 117:1130
24. Araque JC, Hettige JJ, Margulis CJ (2015) J Phys Chem B 119:12727
25. Amith WD, Hettige JJ, Castner EW, Margulis CJ (2016) J Phys Chem Lett 7:3785
26. Wishart JF, Castner EW (2007) J Phys Chem B 111:4639
27. Castner EW, Wishart JF (2010) J Chem Phys 132:120901
28. Santos CS, Murthy NS, Baker GA, Castner EW (2011) J Chem Phys 134:1211011
29. Castner EW, Margulis CJ, Maroncelli M, Wishart JF, Jr EWC (2011) Annu Rev Phys Chem 62:85
30. Triolo A, Russina O, Caminiti R, Shirota H, Lee HY, Santos CS, Murthy NS, Castner EW (2012) Chem Commun (Camb) 48:4959
31. Wu B, Shirota H, Lall-Ramnarine S, Castner EW (2016) J Chem Phys 145:114501
32. Umebayashi Y, Chung W-L, Mitsugi T, Fukuda S, Takeuchi M, Fujii K, Takamuku T, Kanzaki R, Ishiguro SI (2008) J Comput Chem Jpn 7:125
33. Yamaguchi T, Mikawa K, Koda S, Fujii K, Endo H, Shibayama M, Hamano H, Umebayashi Y (2012) J Chem Phys 137:104511
34. Fujii K, Kanzaki R, Takamuku T, Kameda Y, Kohara S, Kanakubo M, Shibayama M, Ishiguro S, Umebayashi Y (2011) J Chem Phys 135:244502
35. Song X, Hamano H, Minofar B, Kanzaki R, Fujii K, Kameda Y, Kohara S, Watanabe M, Ishiguro S-I, Umebayashi Y (2012) J Phys Chem B 116:2801
36. Atkin R, Warr GG (2008) J Phys Chem B 112:4164
37. Atkin R, Bobillier SMC, Warr GG (2010) J Phys Chem B 114:1350
38. Hayes R, Imberti S, Warr GG, Atkin R (2011) Phys Chem Chem Phys 13:3237
39. Hayes R, Imberti S, Warr GG, Atkin R (2013) Angew Chem 125:4721
40. Hayes R, Bernard SA, Imberti S, Warr GG, Atkin R (2014) J Phys Chem C 118:21215
41. Murphy T, Atkin R, Warr GG (2015) Curr Opin Colloid Interface Sci 20:282
42. Hayes R, Warr GG, Atkin R (2015) Chem Rev 115:6357
43. Aoun B, Goldbach A, González MA, Kohara S, Price DL, Saboungi M-L (2011) J Chem Phys 134:104509
44. Li S, Feng G, Bañuelos JL, Rother G, Fulvio PF, Dai S, Cummings PT (2013) J Phys Chem C 117:18251
45. Martinelli A, Marechal M, Östlund Å, Cambedouzou J (2013) Phys Chem Chem Phys 15:5510
46. Nayeri M, Nygård K, Karlsson M, Maréchal M, Burghammer M, Reynolds M, Martinelli A (2015) Phys Chem Chem Phys 17:9841
47. Triolo A, Russina O, Fazio B, Triolo R, Di Cola E (2008) Chem Phys Lett 457:362
48. Gontrani L, Russina O, Lo Celso F, Caminiti R, Annat G, Triolo A (2009) J Phys Chem B 113:9235
49. Russina O, Triolo A, Gontrani L, Caminiti R, Xiao D, Hines LG Jr, Bartsch RA, Quitevis EL, Pleckhova N, Seddon KR (2009) J Phys Condens Matter 21:424121
50. Triolo A, Russina O, Fazio B, Appetecchi GB, Carewska M, Passerini S (2009) J Chem Phys 130:164521
51. Russina O, Gontrani L, Fazio B, Lombardo D, Triolo A, Caminiti R (2010) Chem Phys Lett 493:259

52. Bodo E, Gontrani L, Caminiti R, Plechkova NV, Seddon KR, Triolo A (2010) J Phys Chem B 114:16398
53. Macchiagodena M, Gontrani L, Ramondo F, Triolo A, Caminiti R (2011) J Chem Phys 134:114521
54. Russina O, Triolo A (2012) Faraday Discuss 154:97
55. Russina O, Triolo A, Gontrani L, Caminiti R (2012) J Phys Chem Lett 3:27
56. Méndez-Morales T, Carrete J, Cabeza Ó, Russina O, Triolo A, Gallego LJ, Varela LM (2014) J Phys Chem B 118:761
57. Russina O, Caminiti R, Méndez-Morales T, Carrete J, Cabeza O, Gallego LJ, Varela LM, Triolo A (2015) J Mol Liq 205:16
58. Russina O, Lo Celso F, Triolo A (2015) Phys Chem Chem Phys 17:29496
59. Greaves TL, Drummond CJ (2013) Chem Soc Rev 42:1096
60. Greaves TL, Ha K, Muir BW, Howard SC, Weerawardena A, Kirby N, Drummond CJ (2015) Phys Chem Chem Phys 17:2357
61. Greaves TL, Kennedy DF, Weerawardena A, Tse NMK, Kirby N, Drummond CJ (2011) J Phys Chem B 115:2055
62. Greaves TL, Kennedy DFDF, Kirby N, Drummond CJ (2011) Phys Chem Chem Phys 13:13501
63. Greaves TL, Drummond CJ (2015) Chem Rev 115:11379
64. Hardacre C, Holbrey JD, Mullan CL, Youngs TGA, Bowron DT (2010) J Chem Phys 133:74510
65. Dzyuba SV, Bartsch RA (2001) Chem Commun 1466
66. Xiao D, Hines LG, Li S, Bartsch RA, Quitevis EL, Russina O, Triolo A, Hines LG Jr (2009) J Phys Chem B 113:6426
67. Zheng W, Mohammed A, Hines LG, Xiao D, Martinez OJ, Bartsch RA, Simon SL, Russina O, Triolo A, Quitevis EL (2011) J Phys Chem B 115:6572
68. Rocha MAA, Neves CMSS, Freire MG, Russina O, Triolo A, Coutinho JAPP, Santos LMNBF (2013) J Phys Chem B 117:10889
69. Raju SG, Balasubramanian S (2010) J Phys Chem B 114:6455
70. Rocha MAA, Coutinho JAP, Santos LMNBF (2013) J Chem Phys 139:104502
71. Rocha MAA, Coutinho JAP, Santos LMNBF (2014) J Chem Phys 141:134502
72. Bernardes CES, Shimizu K, Lobo Ferreira AIMC, Santos LMNBF, Canongia Lopes JN (2014) J Phys Chem B 118:6885
73. Russina O, Fazio B, Schmidt C, Triolo A (2011) Phys Chem Chem Phys 13:12067
74. Yoshimura Y, Shigemi M, Takaku M, Yamamura M, Takekiyo T, Abe H, Hamaya N, Wakabayashi D, Nishida K, Funamori N, Sato T, Kikegawa T (2015) J Phys Chem B 119:8146
75. Kanzaki R, Mitsugi T, Fukuda S, Fujii K, Takeuchi M, Soejima Y, Takamuku T, Yamaguchi T, Umebayashi Y, Ishiguro S (2009) J Mol Liq 147:77
76. Sharma S, Gupta A, Kashyap HK (2016) J Phys Chem B 120:3206
77. Shimizu K, Bernardes CES, Triolo A, Canongia Lopes JN (2013) Phys Chem Chem Phys 15:16256
78. Russina O, Triolo A (2012) Faraday Discuss 154:97
79. Kashyap HK, Santos CS, Daly RP, Hettige JJ, Murthy NS, Shirota H, Castner EW, Margulis CJ (2013) J Phys Chem B 117:1130
80. Russina O, Lo Celso F, Di Michiel M, Passerini S, Appetecchi GB, Castiglione F, Mele A, Caminiti R, Triolo A (2013) Faraday Discuss 167:499
81. Shen Y, Kennedy DF, Greaves TL, Weerawardena A, Mulder RJ, Kirby N, Song G, Drummond CJ (2012) Phys Chem Chem Phys 14:7981
82. Almantariotis D, Gefflaut T, Pádua AAH, Coxam J-Y, Costa Gomes MF (2010) J Phys Chem B 114:3608
83. Smith GD, Borodin O, Magda JJ, Boyd RH, Wang Y, Bara JE, Miller S, Gin DL, Noble RD (2010) Phys Chem Chem Phys 12:7064
84. Hollóczki O, Macchiagodena M, Weber H, Thomas M, Brehm M, Stark A, Russina O, Triolo A, Kirchner B (2015) ChemPhysChem 16:3325
85. Hettige JJ, Araque JC, Margulis CJ (2014) J Phys Chem B 118:12706
86. Weber H, Hollóczki O, Pensado AS, Kirchner B (2013) J Chem Phys 139:84502
87. Appetecchi GB, Montanino M, Carewska M, Moreno M, Alessandrini F, Passerini S (2011) Electrochim Acta 58:1300
88. Lo Celso F et al (2017) Phys Chem Chem Phys. doi10.1039/c7cp01971h
89. Fumino K, Wulf A, Ludwig R (2009) Angew Chem Int Ed Engl 48:3184
90. Gontrani L, Bodo E, Triolo A, Leonelli F, D'Angelo P, Migliorati V, Caminiti R (2012) J Phys Chem B 116:13024

91. Greaves TL, Kennedy DF, Mudie ST, Drummond CJ (2010) J Phys Chem B 114:10022
92. Canongia Lopes JN, Costa Gomes MF, Pádua AAH (2006) J Phys Chem B 110:16816
93. Weingaertner H, Merkel T, Kashammer S, Schroer W, Wiegand S (1993) Berichte Der Bunsen-Gesellschaft Phys Chem Chem Phys 97:970
94. Schröer W, Wiegand S, Weingaertner H (1993) Ber Bunsenges Phys Chem 97:975
95. Vale VR, Rathke B, Will S, Schröer W (2011) J Chem Eng Data 56:4829
96. Vale VR, Will S, Schröer W, Rathke B (2012) ChemPhysChem 13:1860
97. Takamuku T, Honda Y, Fujii K, Kittaka S (2008) Anal Sci 24:1285
98. Shimomura T, Fujii K, Takamuku T (2010) Phys Chem Chem Phys 12:12316
99. Greaves TL, Kennedy DF, Kirby N, Drummond CJ (2011) Phys Chem Chem Phys 13:13501
100. Russina O, Sferrazza A, Caminiti R, Triolo A (2014) J Phys Chem Lett 5:1738
101. Jiang HJ, Fitzgerald PA, Dolan A, Atkin R, Warr GG (2014) J Phys Chem B 118:9983
102. Schroer W, Triolo A, Russina O (2016) J Phys Chem B 120:2638
103. Bonetti M, Calmettes P (1998) Int J Thermophys 19:1555
104. Murphy T, Hayes R, Imberti S, Warr GG, Atkin R (2016) Phys Chem Chem Phys 18:12797
105. Russina O, Lo Celso F, Plechkova NV, Triolo A (2017) J Phys Chem Lett 8:1197

Top Curr Chem (Z) (2017) 375:52
DOI 10.1007/s41061-017-0140-9

REVIEW

Hydrogen Sulfide and Ionic Liquids: Absorption, Separation, and Oxidation

Cinzia Chiappe[1] · **Christian Silvio Pomelli**[1]

Received: 8 November 2016 / Accepted: 11 April 2017 / Published online: 26 April 2017

Abstract Economical and environmental concerns are the main motivations for development of energy-efficient processes and new eco-friendly materials for the capture of greenhouse gases. Currently, H_2S capture is dominated by physical and/or chemical absorption technologies, which are, however, energy intensive and often problematic from an environmental point of view due to emission of volatile solvent components. Ionic liquids have been proposed as a promising alternative to conventional solvents because of their low volatility and other interesting properties. The aim of the present review paper is to provide a detailed overview of the achievements and difficulties that have been encountered in finding suitable ionic liquids for H_2S capture. The effect of ionic liquid anions, cations, and functional groups on the H_2S absorption, separation, and oxidation are highlighted. Recent developments on yet scarcely available molecular simulations and on the development of robust predictive methods are also discussed.

Keywords Hydrogen sulfide capture · Oxidation · Ionic liquids · Acidic gases

1 Introduction

Since the Industrial Revolution, the effects of human processes such as fossil-fuel burning, urban expansion, deforestation and the use of chemicals, have determined the onset of several environment concerns going from air–water–soil pollution, resource depletion, and the loss of biodiversity. Unfortunately, prior to the 1960s

---

Chapter 10 was originally published as Chiappe, C. & Pomelli, C. S. Top Curr Chem (Z) (2017) 375: 52. DOI 10.1007/s41061-017-0140-9.

✉ Cinzia Chiappe
cinzia.chiappe@unipi.it

[1] Dipartimento di Farmacia, via Bonanno 33, 56126 Pisa, Italy

and 1970s, these problems have attracted relatively little attention from the public, media, and governments. However, during the last two decades, not only the environment consciousness is inbuilt, at least in a part of the world population, but also the interest is slowly shifted from local to wider, national and global issues. Beginning from 1970, the planet is undergoing rapid changes: the world's population has almost doubled, and the rates of energy consumption and resource depletion have increased alarmingly, becoming progressively clearer that many of the Earth's resources are not limitless. Utilization or combustion of fossil fuels for electricity, heat, and transportation has determined a parallel increase in acid gases emission: these activities represent indeed today the largest source of CO_2, SO_2, and H_2S, although in the case of H_2S also natural sources (e.g., volcanoes, natural gas wells, sulfur springs) and other industrial activities (e.g., pulp and paper mills, tanning industry, large pig farms, Portland cement kilns, municipal waste landfills, coke ovens, asphalt production and storage, and geothermal power plants) contribute [1].

In the past, oil or gas wells containing significant amounts of acid impurities were considered unprofitable. However, with the depleting number of potential reservoirs and with increasing oil and gas demands, nowadays, also these sites have been included in the valuable sources of energy, and wet scrubbing processes employing liquid absorbents represent the most widely applied method of reducing the emission of acidic gases from a controllable source [2].

In the last few years, industrial and academic research has been focalized mainly on the development of new CO_2 removal technologies, this compound being the principal contaminant found in natural gas and the major contributor for the global greenhouse gas emissions [3]. However, hydrogen sulfide is an undesirable compound being highly toxic and corrosive for transmission pipelines and process equipment and the improvement of selective removal processes is equally desirable.

Traditionally, two types of liquid solvents are used for this purpose: solvents able to capture acidic gases by physical sorption (e.g., 1-methyl-2-pyrrolidone, sulfolane, propylene carbonate, dimethylsulfoxide, polyethylene glycol dimethyl ethers, etc.), and solvents able to trap gases by chemical sorption (e.g., ethanolamine, *N*-methyldiethanolamine, *tert*-butylaminoethoxyethanol, etc.). Physical solvents can be applied advantageously when partial pressure of the acid-gas components in the feed gas is high (typically, $>50\psi$). Their loading capacity increases indeed proportionally with the acid gas partial pressure, in agreement with Henry's law and under specific conditions (high partial pressure and low temperature) they can be competitive with chemical solvents: in principle, their loading capacity is not limited by the stoichiometry. Furthermore, physical solvents can be easily regenerated through pressure and temperature swing: in some processes the interaction between absorbed gas and the absorbent is so weak (i.e., Fluor solvent process) that no heating is required and the solvent is regenerated by vacuum flashing or by stripping with inert gas. However, physical solvents tend to absorb heavier hydrocarbons and this is a disadvantage if the acid gas is fed to a Claus plant for sulfur recovery.

In contrast, solvents able to trap gases by chemical sorption (in particular, the above-mentioned amines), exhibit high load for sour gases, especially in the low-pressure range. The involved chemical reactions are reversible and, even in this case, it is possible to regenerate the solvent by changing temperature and pressure. However, the desorption process is highly energy intensive and the volatilization of organic amines can occur with dangerous effects for the environment. Moreover, amines are generally used in water: transfer of water into the gas stream during the desorption stage and degradation of alkanolamines in this environment to corrosive by products represent further disadvantages, which make these processes economically expensive [4].

In conclusion, physical solvents are generally useful in bulk-removal processes which are, however, followed by a final clean-up using a chemical solvent since only these latter are able to achieve the H_2S limit specified for sales gas. It is noteworthy that for gas containing low amounts of H_2S it is sometimes considered more economically appealing the use of scavenger solvents or solid agents. In such processes, the compound reacts chemically through an irreversible reaction with the H_2S and is consumed in the sweetening process, requiring the sweetening agent to be periodically replaced [5].

Related to the sulfur recovery, the Claus process is presently the most widely used method. However, for the process to work efficiently, the acidic gases entering the process must have a high H_2S/CO_2: i.e., H_2S concentration should be not less than 55%. Therefore, when the acid gas trapped by the above-mentioned gas treating systems is poor in H_2S, it is advantageous to "enrich" the mixture by contacting it with a second solvent, having the important role of absorbing essentially all H_2S from the acidic gases mixture. The enriching process can often raise the H_2S concentration by a factor of five or more, however, the selectivity of industrially amine-based solvents used for this purpose is not high enough when H_2S concentration in the acid gas mixture is too low. Consequently, it is very challenging to find alternative processes both for H_2S capture and sulfur recovery.

The substitution of conventional physical solvents or alkanolamine solutions with ionic liquids, ILs, for the acid gases capture from flue and post combustion gases, as well as in the challenging gas separation and purification processes, represent research areas of increasing interest [6]. Investigated, starting from the end of last century, mainly as green solvents due to some of their unique properties (such as negligible vapor pressure, ease of separation from molecular organic solvents and water, high solvent power and chemical compatibility with many components) [7], ILs have shown more recently their potentiality for application in challenging research areas of chemistry and chemical engineering [8–12]. Similar to inorganic salts, ILs are composed exclusively of a cation (generally, an organic cation such as imidazolium, pyridinium, and ammonium) and a polyatomic anion (such as hexafluorophosphate, tetrafluoroborate, bis(trifluoromethyl)sulfonylimide and dicyanamide). However, unlike conventional salts, their melting points are normally below 100 °C. Moreover, through an accurate selection of cation and anion, it is possible to modify all the physico-chemical properties: it is noteworthy that each IL, even a simple one such as dialkylimidazolium chloride or bromide, is generally a complex three-dimensional dynamic structure with polar and apolar regions containing several sites able to specifically interact with guest molecules [13].

ILs have been largely investigated for capture and separation of acidic gases and reliable experimental data on gas solubilization together with correlation/model have been reported especially for CO_2: several comprehensive reviews have already been published on this topic [14–19], including also a recent critical review having the important aim of dispelling some mythos about CO_2 solubility in ILs [20]. The present paper is instead focused on capture and separation of H_2S, mainly centering on the research related to H_2S absorption, separation, and oxidation. Data about physical, chemical, and oxidative absorption are analyzed and discussed at the light of the proposed mechanisms and computational studies are also included.

1.1 Capture and Separation by Physical and/or Chemical Absorption

In the last 10 years, several studies have been carried out to evaluate the ability of common or functionalized ILs to capture H_2S by physical absorption, considering also its mixtures with other acidic gases. In Fig. 1 are reported the structures of the investigated ILs and in Table 1 are collected some H_2S solubilities values. Since these measurements have been carried out using different techniques (microbalances, static high-pressure equipment, NMR) under non-identical conditions (temperature and pressure), we decided to report for each IL the values at the limit temperatures (the lowest and highest at which measurements were carried out) and, for each temperature, the values at the limit pressures (lowest and highest). Furthermore, since gas solubility is often expressed in literature in several different ways, making the comparison sometimes difficult, gas solubilities have been reported as molar fraction and weight%. We retain indeed that the molar fraction can give information about the absorption mechanism at molecular level but the weight% can be useful to compare the efficiency of different ILs, as well as to compare ILs and molecular solvents, considering the high molecular weights characterizing many ILs.

The Henry's law constants at zero pressure, K_H, are given in Table 2, where the Gibbs free energy of solvation, enthalpy, and entropy of solvation, are also reported. It is noteworthy that $\Delta_{sol}H$ and $\Delta_{sol}S$ values are negative for all absorbents at any temperature, showing, however, a non-homogeneous behavior with temperature increase.

Starting from the pioneering work of Jou and Mather [21–24], reporting the solubility of H_2S in [bmim][PF_6] at temperatures ranging from 298.15 to 403.15 K and pressures up to 9.6 MPa, this IL, despite its viscosity and moderate stability in the presence of humidity, has been employed in different investigations and its H_2S capture ability has been compared with that of other ILs. Jalili et al. have indeed reported [25, 26] the solubility of H_2S in [C_4mim][PF_6], [C_4mim][BF_4], and [C_4mim][Tf_2N], at temperatures ranging from 303.15 to 343.15 K and pressures up to 1 MPa and, subsequently, in [C_6mim][PF_6], [C_6mim][BF_4], and [C_6mim][Tf_2N] [27] including also, more recently, [C_8mim][Tf_2N] [28]. By the comparison of the experimental data arising from these studies (Henry law constants and Gibbs free energy, Table 2), the authors claim that H_2S solubility in [$C_n$mim][Tf_2N] ILs increases as the number of carbon atoms in the alkyl substituent of methylimidazolium cation, n, increases, attributing this effect to the increased free volume:

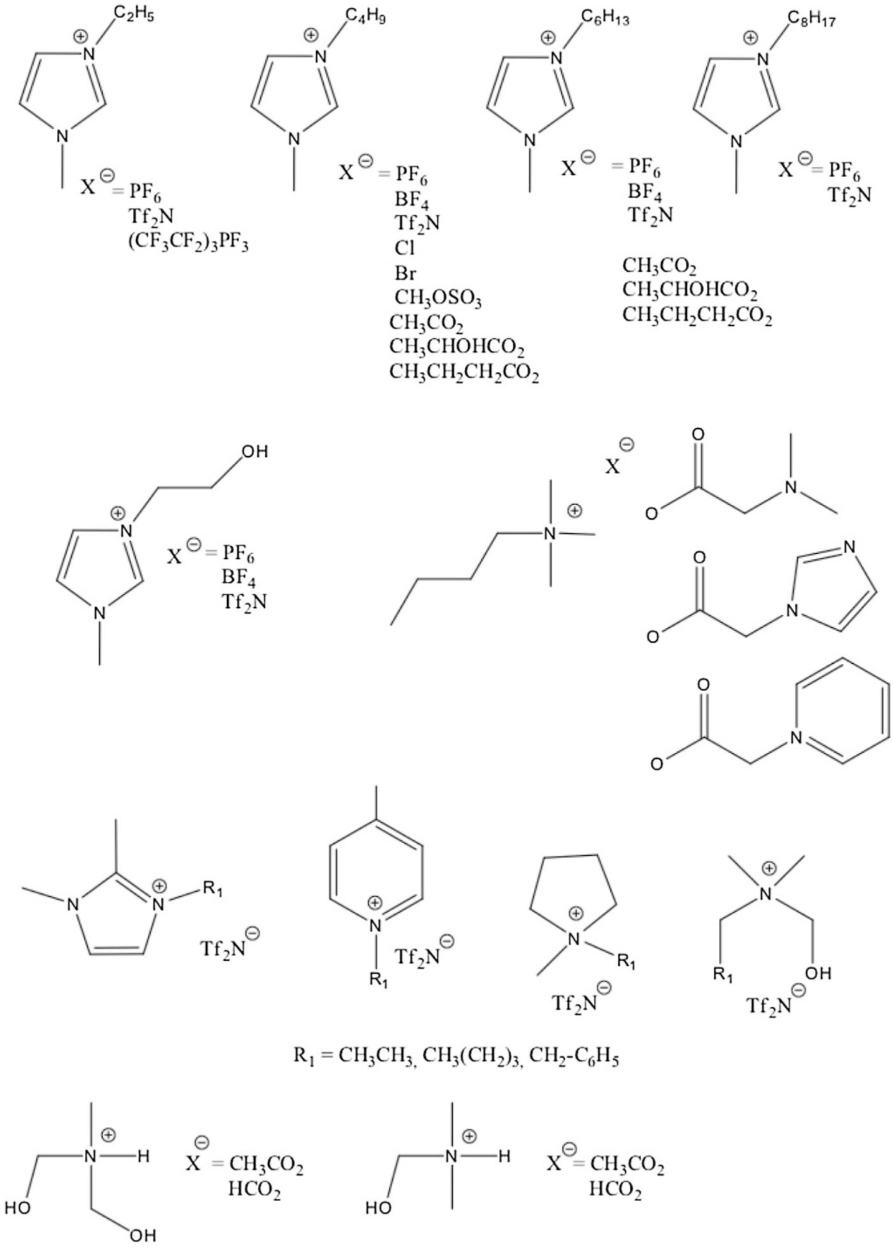

Fig. 1 Investigated ILs for H_2S capture

molar density decreases indeed on going from [C_2mim][Tf_2N] to [C_8mim][Tf_2N]. Therefore, with the aim to further decrease IL molar density, the solubility of CO_2 and H_2S has been evaluated [29] also in a less common IL, 1-ethyl-3-methylimidazolium tris(pentafluoroethyl)trifluorophosphate ([C_2mim][eFAP]), showing that

Table 1 ILs H_2S absorption ability

Cation	Anion	*T*/K	*P*/bar	H_2S molar fraction	H_2S weight%	Method
C_4mim	BF_4	303.15	0.61	0.039	0.018	ISM[17a]
		303.15	7.36	0.354	0.224	
		343.15	1.12	0.030	0.014	
		343.15	8.13	0.227	0.124	
C_4mim	PF_6	298.15	0.69	0.046	0.57	WM[16a]
		298.15	21.2	0.875	45.64	
		313.15	1.15	0.056	0.71	
		313.15	28.9	0.853	14.84	
		403.15	1.32	0.016	0.19	
		403.15	96.3	0.643	8.82	ISM[17a]
		303.15	1.65	0.075	0.96	
		303.15	8.26	0.405	4.48	
		333.15	1.37	0.044	0.55	
		333.15	10.11	0.285	4.56	
C_4mim	Tf_2N	303.15	0.944	0.07	0.04	ISM[17a]
		303.15	8.26	0.51	7.80	
		343.15	1.46	0.051	0.43	
		343.15	9.16	0.299	3.35	
C_2mim	PF_6	333.15	1.45	0.038	0.52	ISM[16c
		333.15	15.8	0.359	4.23	
		363.15	1.72	0.032	0.44	
		363.15	19.33	0.306	5.54	
C_2mim	Tf_2N	303.15	0.944	0.07	0.04	ISM[16c]
		303.15	8.26	0.51	0.32	
		343.15	1.46	0.051	0.47	
		343.15	9.16	0.299	3.58	
C_6mim	BF_4	303.15	1.11	0.072	1.03	ISM[16b]
		303.15	8.73	0.499	6.64	
		343.15	1.87	0.06	0.06	
		343.15	10.7	0.345	6.60	
C_6mim	PF_6	303.15	1.38	0.067	0.78	ISM[16b]
		303.15	9.17	0.441	7.93	
		343.15	2.2	0.05	0.04	
		343.15	9.57	0.247	3.46	
C_6mim	Tf_2N	303.15	0.685	0.0539	0.43	ISM [19]
		303.15	15.43	0.7012	15.16	
		353.15	1.07	0.0368	2.55	
		353.15	20.17	0.4922	6.88	
C_8mim	PF_6	303.15	0.845	0.0672	8.06	ISM[16d]
		303.15	15.75	0.6972	18.74	
		353.15	1.239	0.0463	0.48	
		353.15	19.226	0.4672	8.07	

Table 1 continued

Cation	Anion	*T*/K	*P*/bar	H_2S molar fraction	H_2S weight%	Method
C_8mim	Tf_2N	303.15	0.935	0.0807	0.66	ISM[19]
		303.15	15.087	0.7355	17.48	
		353.15	1.343	0.063	0.51	
		353.15	16.869	0.5181	7.57	
C_2OHmim	BF_4	303.15	1.36	0.039	0.64	ISM[34]
		303.15	10.27	0.247	4.97	
		353.15	1.65	0.02	0.02	
		353.15	10.47	0.126	2.24	
C_2OHmim	PF_6	303.15	1.336	0.047	0.65	ISM[35]
		303.15	15.08	0.462	10.25	
		353.15	1.828	0.0347	0.48	
		353.15	16.83	0.261	4.49	
C_2OHmim	Tf_2N	303.15	1.562	0.0798	0.72	ISM[35]
		303.15	15.45	0.572	10.06	
		353.15	2.192	0.0575	0.51	
		353.15	16.34	0.347	4.26	
C_4mim	Cl	298.15	14	0.86	54.52	NMR[28]
		358.15	14	0.87	56.63	
C_4mim	BF_4	298.15	14	0.79	36.19	
C_4mim	TfO	298.15	14	0.78	29.53	
C_4mim	PF_6	298.15	14	0.72	25.49	
C_4mim	Tf_2N	298.15	14	0.77	21.39	
C_2mim	Tf_2N	298.15	14	0.81	27.08	
$M_{1,2}E_3$im	Tf_2N	298.15	14	0.82	27.67	
C_4M’py	Tf_2N	298.15	14	0.85	30.99	
phCH_2Py	Tf_2N	298.15	14	0.84	28.45	
C4mim	Tf_2N	298.15	14	0.77	21.39	
C4py	Tf_2N	298.15	14	0.89	39.86	
BzMPyrr	Tf_2N	298.15	14	0.9	40.21	
BDmim	Tf_2N	298.15	14	0.79	22.83	
$N_{112,EtOH}$	Tf_2N	298.15	14	0.74	19.60	
$N_{114,EtOH}$	Tf_2N	298.15	14	0.73	17.78	
C_2mim	CH_3COO	293.15	0.014	0.111	2.44	EQ[31]
		293.15	3.208	0.510	17.25	
		333.15	0.49	0.103	2.25	
		333.15	3.229	0.376	10.77	
C_2mim	CH_3CH_2COO	293.15	0.011	0.160	3.40	
		293.15	3.167	0.587	20.82	
		333.15	0.109	0.131	2.71	
		333.15	3.239	0.383	10.30	

Table 1 continued

Cation	Anion	*T*/K	*P*/bar	H_2S molar fraction	H_2S weight%	Method
C_2mim	L-lactate	293.15	0.078	0.120	2.27	
		293.15	3.205	0.489	14.01	
		333.15	0.131	0.313	7.20	
		333.15	3.216	0.325	7.58	
C_4mim	CH_3COO	293.15	0.001	0.0739	1.35	
		293.15	3.219	0.578	19.06	
		333.15	0.008	0.0676	1.23	
		333.15	3.415	0.442	11.99	
C_6mim	CH_3COO	293.15	0.003	0.122	2.05	
		293.15	3.236	0.609	19.01	
		333.15	0.006	0.089	1.45	
		333.15	3.267	0.476	12.04	
C_2mim	$(C_2F_5)_3PF_3$	303.15	0.604	0.0385	0.25	ISM[20]
		303.15	13.957	0.592	8.22	
		353.15	0.781	0.0219	0.14	
		353.15	19.415	0.427	4.40	
C_4mim	Br	299.1	1	0.030	0.48	WM[29]
$(CH_2OH)_2CH_3NH$ (MDEAH)	CH_3COO	303.2	0.097	0.030	0.69	EQ[37]
		303.2	1.179	0.1618	4.17	
		333.2	0.129	0.0095	0.22	
		333.2	1.182	0.0969	2.36	
$(CH_2OH)_2CH_3NH$ (MEDAH)	HCO_2	303.2	0.101	0.0103	0.26	
		303.2	1.1	0.0807	2.14	
		333.2	0.141	0.0061	0.15	
		333.2	1.129	0.0427	1.10	
$(CH_3)_2(CH2OH)NH$ (DMEAH)	CH_3COO	303.2	0.045	0.0158	0.40	
		303.2	1.108	0.2085	6.24	
		333.2	0.08	0.0106	0.27	
		333.2	1.052	0.0773	2.07	
$(CH_3)_2(CH2OH)NH$ (DMEAH)	HCO_2	303.2	0.062	0.0116	0.33	
		303.2	1.03	0.1189	3.66	
		333.2	0.089	0.0065	0.18	
		333.2	1.042	0.052	1.52	

ISM isochoric saturation method, *WM* weight method, *NMR* medium-pressure NMR spectroscopy, *EQ* equilibrium method

[C_2mim][eFAP] has an increased affinity for CO_2 and H_2S, at least when compared to other unfunctionalized [C_2mim]-based ILs. However, this effect is moderate and less relevant that in the case of CO_2. Consequently, although at fixed temperature and pressure the amount of dissolved H_2S is more than twice the amount of CO_2, the selectivity in this IL decreases with respect to other ILs. Furthermore, considering the high molecular weight of this IL, when H_2S solubility is expressed in terms of

Table 2 Thermodynamic properties of H_2S in ionic liquids

Cation	Anion	T/K	K_H/ MPa	ΔG/ KJ mol^{-1}	ΔH/ KJ mol^{-1}	ΔS/ (KJ mol^{-1} K^{-1})	Method
C_4MIM	PF$_6$	303.15	1.86	7.37	−14.5	−72.2	ISM[17b]
		343.15	3.38	10.0	−12.0	−64.2	
		298.15	1.43	6.59	−16.3	−76.9	ISM[16a]
		403.15	8.01	–	–	–	
	BF$_4$	303.15	1.55	6.91	−12.9	−65.5	ISM[17b]
		343.15	3.34	10.0	−13.2	−67.6	
	Tf$_2$N	303.15	6.51	6.51	−13.0	−64.3	
		343.15	9.31	9.31	−16.6	−75.6	
C_2MIM	EtSO$_4$	303.15	6.07	4.54	−12.0	−54.5	WM[16a]
		353.15	13.3	7.59	−16.2	−67.3	
C_2MIM	PF$_6$	333.15	3.74	10.0	−11.9	−65.9	ISM[16c]
		363.15	5.29	12.0	−11.2	−63.9	
	Tf$_2$N	303.15	1.48	6.79	−15.0	−71.8	
		353.15	3.16	10.1	−11.7	−62.0	
HOC$_2$MIM	BF$_4$	303.15	3.13	8.68	−22.9	−104	ISM[34]
		353.15	7.95	12.9	−10.6	−66.4	
	PF$_6$	303.15	0.754	5.10	−12.5	−58.0	ISM[35]
		353.15	1.40	7.73	−8.92	−47.2	
	Tf$_2$N	303.15	0.771	5.15	−15.2	−67.3	
		353.15	1.50	7.95	−13.1	−59.6	
	TfO	303.15	0.533	4.22	−11.7	−52.6	
		353.15	1.17	7.23	−16.7	−67.6	
C_6MIM	BF$_4$	303.15	1.25	6.37	−15.1	−70.9	ISM[16d]
		343.15	2.57	9.26	−15.9	−73.4	
	PF$_6$	303.15	1.79	7.27	−15.0	−73.4	
		343.15	3.97	10.5	−19.7	−87.9	
	Tf$_2$N	303.15	1.74	7.20	−16.4	−77.8	
		343.15	4.06	10.6	−20.6	−90.7	
C_6MIM	Tf$_2$N	303.15	1.25	6.35	–15.5	–71.9	ISM[19]
		353.15	2.86	9.84	–14.1	–67.7	
C_8MIM	Tf$_2$N	303.15	0.99	5.47	–13.3	–63.1	
		353.15	1.95	8.18	–11.4	–57.1	
	PF$_6$	303.15	1.22	6.44	−13.55	−65.97	ISM[16d]
		353.15	2.55	9.55	−10.97	−58.10	
C_2MIM	Ac	293.15	0.092	–	–	–	EQ[31]
		333.15	0.259	–	–	–	
	Pro	293.15	0.067	–	–	–	
		333.15	0.249	–	–	–	
	Lac	293.15	0.111	–	–	–	
		333.15	0.350	–	–	–	

Table 2 continued

Cation	Anion	T/K	K_H/ MPa	ΔG/ KJ mol^{-1}	ΔH/ KJ mol^{-1}	ΔS/ (KJ mol^{-1} K^{-1})	Method
C_4MIM	Ac	293.15	0.070	–	–	–	
		333.15	0.188	–	–	–	
HMIM	Ac	293.15	0.072	–	–	–	
		333.15	0.170	–	–	–	
C_2MIM	FAP	303.15	0.850	5.372	−14.8	−66.5	ISM[20]
		353.15	1.952	8.695	–	–	
MDEAH	Ac	303.2	0.55	4.3	−25.9	−100	EQ[37]
		333.2	1.39	7.3	–	−100	
	For	303.2	1.15	6.2	−19.7	−85	
		333.2	2.32	8.7	–	−85	
DMEAH	Ac	303.2	0.35	3.2	−29.7	−108	
		333.2	1.02	6.4	–	−108	
	For	303.2	0.59	4.5	−24.1	−94	
		333.2	1.39	7.3	–	−94	

W%, the efficiency results moderate, large amount of this IL are indeed necessary to capture H_2S.

[C_4mim][PF_6] [30] and, subsequently, [C_4mim][$MeSO_4$] [31] have also been employed by Shiflett et al. to investigate the separation of H_2S/CO_2. Using thermodynamic models based on equations of state (EOS, previously applied for refrigerant/lubricant oil mixtures [32] and to examine the solubility of acidic gases in ILs [33–35]), the authors evidence a significant increase in the CO_2/H_2S selectivity (from 3.7 to 13.5) on going from [C_4mim][PF_6] to [C_4mim][$MeSO_4$], which was generically attributed to the strong chemical absorption of H_2S in the latter medium. Nonetheless, the same authors state that [C_4mim][$MeSO_4$] might still not be the best choice for the gaseous separation and/or capturing of CO_2 and H_2S. Although bis(trifluoromethyl)sulfonylimide and, more extensively fluorinated anions, are probably the negatively charged species that can guarantee the lower anion-cation interaction [36], and therefore the higher free volume, the structural features of H_2S (its acidity and hydrogen bond donor ability) should favor dissolution also in ILs having more coordinating anions, even though these ILs have surely lower free volumes. Actually, when the solubility of H_2S was evaluated [37] in a series of [C_4mim]-based ILs with different anions (Cl^-, BF_4^-, PF_6^-, TfO^- and Tf_2N^-) and in a series of [Tf_2N]-based ILs with different cations, i.e., *N*-alkyl-*N*-methylimidazolium, 2-methyl-*N*-methyl-*N*-alkylimidazolium, *N*-alkylpyridinium, *N*-butyl-*N*-methylpyrrolidinium and *N*-alkyl-*N,N*-dimethyl-*N*-(2-hydroxyethyl)ammonium at 298.15 K and 1.4 MPa using medium-pressure NMR spectroscopy, it was evidenced that not only the observed H_2S solubilities were significantly higher than those reported for many other gases in ILs, but values suggested the occurrence of specific interactions between H_2S and some of the examined ILs. In particular, an extremely high solubility was observed in $[C_4mim]Cl$, where the small and highly coordinating anion is able to give strong hydrogen bond interactions, as discussed in detail below (computational section).

Probably, the recently shown [38] ability of $[C_4mim]Br$ to separate through a selective absorption H_2S–CO_2, and to solubilize H_2S better than commercial available MDEA-based solvents, can be attributed to the hydrogen bond donor ability of the bromide anion. Analogously, bromide anion plays an important role also when the caprolactam-tetrabutyl ammonium bromide mixtures have been used to solubilize H_2S at temperature ranging from 303.2 to 363.2 K and atmospheric pressure [39]. The solubility of H_2S in these media (caprolactame-tetrabutylammonium bromide, 1:1 mol ratio) was around 5.40% at 303.2 K and ambient pressure but decreased sharply as temperature increase and increases with the increasing mole ratio of caprolactam. It is moreover noteworthy that although in this case the absorption and desorption of H_2S has been reported as a practically reversible process using air, hydrogen sulfide can be oxidized in situ to elemental S: this latter reaction could facilitate the hydrogen sulfide recover.

On the other hand, the effect of ILs based on more basic hydrogen bond acceptor anions has been recently reported [40] by Huang, investigating the solubility of H_2S in five 1-alkyl-3-methylimidazolium carboxylates ionic liquids (1-ethyl-3-methylimidazolium acetate ($[C_2mim][AcO]$), 1-ethyl-3-methylimidazolium propionate ($[C_2mim][PrO]$), 1-ethyl-3-methylimidazolium lactate ($[C_2mim][Lac]$), 1-butyl-3-methylimidazolium acetate ($[C_4mim][AcO]$), and 1-hexyl-3-methylimidazolium acetate ($[C_6mim][AcO]$) at temperatures from 293.15 to 333.15 K and pressures up to 350 kPa. It is noteworthy that all these ILs, despite the strong anion–cation interactions, have significantly larger absorption capacities for H_2S than most of the common ILs. Moreover, as expected, solubility of H_2S increases with the increasing pressure and decreases with the increasing temperature. However, the absorption isotherms of H_2S in all the five carboxylate-based ILs show typically non-ideal profiles: solubility rises dramatically with pressure in the low-pressure region and increases gradually and almost linearly in the high-pressure region. This behavior has been attributed to the ability of carboxylate-based ILs to give not only physical absorption but also to chemically trap H_2S. The carboxylate-based ILs are good hydrogen bond acceptor solvents (they are characterized by high Kamlet–Taft β values) [41] and their basic anions can interact with H_2S, that has acidic and active protons, through acid–base interactions as well as through the formation of hydrogen bonds. Related to the ability of carboxylate anions to give acid–base interactions, it is noteworthy that recently the inherent relationship between the selective absorption performance and ILs alkalinity has been investigated using a series of substituted benzoate-based ILs [42]. These salts present indeed the peculiarity that the alkalinity can be easily tuned through grafting appropriate substituents (electron-donating or electron-withdrawing) to the benzene ring. A good correlation between acidic gases solubility (not only H_2S, but also SO_2 and CO_2 were investigated) and IL alkalinity was found showing the importance of this parameter and providing a more rational support for the future design of ILs with not only high absorption capacity but also high selectivity.

Although the hydrogen bond acceptor ability is generally a property strongly related to the IL anion, it is also possible to insert on cation-specific functional groups that can directly interact with the dissolved species. In the specific field of functionalized ILs, in 2010 Jalili et al. reported [43] the solubilities and diffusion coefficients of H_2S and CO_2 in 1-(2-hydroxyethyl)-3-methylimidazolium tetrafluoroborate, [HOC_2mim][BF_4], at temperatures ranging from 303.15 to 353.15 K and pressures up to 1.1 MPa. Even if also in this medium the solubility and diffusion coefficient of H_2S are greater than those of CO_2, indicating that this solvent could be used for separation of these two gases from each other, solubility of both gases is here lower than in conventional unfunctionalized ILs, [C_4mim][BF_4], and [C_6mim][BF_4]. Moreover, absorptions in [HOC_2mim][BF_4] follow both for CO_2 and H_2S the Henry's law and, therefore, this IL has been classified as a physical sorption trapping solvent. The reduced solubility of both gases in this medium with respect to unfunctionalized ILs is probably due to the ability of the hydroxyl group attached on the alkyl chain in cation to increase the cation–cation and cation–anion interactions, so increasing density and decreasing void volume, without significantly affecting the ability of the medium to interact chemically with acidic gases. In agreement with the expected correlation between density and solubility, when the dissolution of H_2S and CO_2 was investigated [44] in a series of 1-(2-hydroxyethyl)-3-methylimidazolium-based ILs containing different anions (PF_6^-, TfO^-, Tf_2N^-), it was evidenced that absorption increases as the number of trifluoromethyl groups in the anion increases. The solubility behavior of both gases follows the order [HOC_2mim][Tf_2N] $>$ [HOC_2mim][OTf] $>$ [HOC_2mim][PF_6] $\gg$ [HOC_2mim][BF_4]. The Henry constants, reported in Table 2, show that with the exception of [HOC_2mim][BF_4] all hydroxyl functionalized ILs are slightly more efficient trapping media for H_2S than the corresponding [bmim]-based ILs and the solvation enthalpy and entropy values, characterizing the process in these functionalized ILs, are not significantly different from those found in [bmim]-based ILs, the sole exception being represented by [HOC_2mim][BF_4]. Thus, this IL appears the sole having so strong cation–cation and cation–anion interactions to reduce the ability of the hydroxyl group attached on the cation to interact with the absorbed gas.

On the other hand, when more recently an interesting series of dual Lewis base functionalized ILs, based on onium cations and characterized by anions in which carboxyl and tertiary amine groups are tethered, has been investigated [45], it has been shown that these ILs can reversibly absorb relatively relevant amounts of H_2S (0.39–0.84 mol per mole of IL) at low pressure and temperature, 1 bar and 60 °C. Furthermore, since the CO_2 absorption in this class of ILs is quite limited relative to H_2S, an ideal absorption selectivity for H_2S/CO_2 (13–26 at 1 bar and 29-70 at 0.1 bar, 60 °C) was calculated. Based on spectroscopy studies and DFT calculations, the cooperative interaction of carboxyl—H_2S—amine has been proposed as the driving force to the high H_2S absorption capacity and H_2S/CO_2 selectivity. In these ILs, chemical absorption appears to dominate at low pressures whereas physical absorption probably prevails in the high-pressure range: consequently, selectivity depends strongly on the pressure and varies negatively with the increase of this parameter.

Considering that protic ILs (PILs) represent today probably the less expensive class of ILs, which can be easily prepared from highly available chemicals through simple neutralization reactions, it is not surprising that the ability of protic ILs to capture acidic gases, and eventually favor their separation, has been evaluated in these media despite the fact that PILs are generally characterized by strong anion–cation interactions and an acidic substrate should be absorbed in an acidic medium. Thus, the solubilities of H_2S and CO_2 in four protic onium PILs also having strong hydrogen bond acceptor anions (methyldiethanolammonium acetate, methyldiethanolammonium formate, dimethylethanolammonium acetate, and dimethylethanolammonium formate) were determined at 303.2–333.2 K and 0–1.2 bar [46]. The Henry's law constants of H_2S in the four PILs at 303.2 K varies from 3.5 to 11.5 bar, with the lowest value for [DMEAH][AcO] and the largest for [MDEAH][HCO_2], whereas the same constants for CO_2 are of a magnitude larger than that of H_2S (49–117 bar), implying that these PILs also exhibit much larger absorption capacity for H_2S than for CO_2. It is, however, noteworthy that the solubility of CO_2 in the acetate-based PILs is much lower than that in aprotic ILs with the same anion. As discussed in the paper, this behavior can be attributed to the different structures of protic ILs and aprotic ILs. In protic ILs, the protonated nitrogen in ammonium cation is weakly acidic but able to give relatively strong Brønsted acid–base (or hydrogen bonding) interactions with the basic acetate anion, thus reducing free voids and the affinity with CO_2. Solvation free entropy values found for these ILs are indeed large and negative (Table 2). On the other hand, in aprotic ILs, such interactions do not exist (or are weaker) and the acetate anion can attract CO_2 freely through Lewis acid–base interaction. Analogously, Brønsted acid–base interactions between protonated nitrogen and acetate anion can also reduce the dissolution of H_2S in protic ILs in comparison with aprotic ILs with the same anion. For instance, the solubility of H_2S in [C_2mim][AcO] is significantly higher than in these ILs. However, unlike CO_2 molecule, H_2S molecule has active protons, which can interact with the electron-donating groups of protic ILs (e.g., hydroxyl and carboxylate groups): therefore, H_2S is more favorably absorbed by protic ILs than CO_2. Similar results and analogous considerations have been reported even in a recent paper in which the absorption of H_2S and CO_2 has been investigated in alkanolamine-protic ionic liquids binary mixtures based on 2-hydroxyethyl-ammonium (MEA) or tri-ethanolammonium cations and residues of 2-hydroxy-5-sulfobenzoic acid or pyridine-3-carboxylic acid at various temperatures and partial gases pressures [47].

Since the three-dimensional structure of ILs and the cation–anions interactions are determined by the nature of both ionic components, to develop absorbents with high absorption capacity towards H_2S and large selectivity for H_2S/CO_2, Huang et al. have recently proposed [48] a new class of hydrophobic protic ILs containing a free tertiary amine group as functional site for the absorption of H_2S (Fig. 2).

These ILs have been easily synthesized through a simple neutralization-metathesis methodology by utilizing diamine compounds and bis(trifluoromethylsulfonyl)imide as the building block for cation and anion, respectively. Also in this case, despite the relatively high cost and molecular weight, the bis(trifluoromethylsulfonyl)imide anion has been selected being the negatively charged species able to

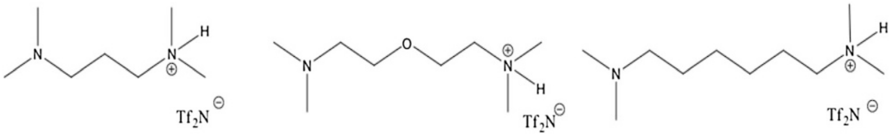

Fig. 2 Hydrophobic protic ILs

guarantee a weak cation–anion interaction and a relatively low viscosity. Interesting, when the amine group is sufficiently distant from the positive center, the solubility of H_2S reached 0.546 mol mol^{-1} (1 bar) and the selectivity of H_2S/CO_2 reached 37.2 (H_2S solubility at 1 bar vs. CO_2 solubility at 1 bar) at 298.2 K. The high solubility of H_2S in these ILs has been therefore attributed to the strong acid–base interaction between H_2S and tertiary amine group: the sequence of H_2S solubility reflects indeed the alkalinity of the free tertiary amine group tethered on the three hydrophobic protic ILs (see computational studies section). It is interestingly also to observe that the behavior of CO_2 absorption in these hydrophobic PILs is very similar. The solubility of CO_2 increases almost linearly with pressure, displaying an apparently physical absorption. Since there are no active protons in the CO_2 molecule, the tertiary amine group allows only very weak Lewis acid–base interaction with CO_2 and coordination of CO_2 with tertiary amine is thermodynamically unfavorable in comparison with that of H_2S with the same functional group. It is also noteworthy that, whereas the presence of water has little effect on the solubility of H_2S, it affects significantly (around 15 times, depending on IL structure) the solubility of CO_2, determining a significant decrease in selectivity, from 37.2 to 2.3 with the addition of water. This effect can be attributed to the formation of H_2CO_3 in the presence of water, which, much better than CO_2, interact with the tertiary amine group.

Recently, also mixtures of functionalized ILs and co-solvents, tetraethyl ammonium salts having amino acids as counteranion and ethylene glycol, have been used to capture dilute H_2S (0.005 MPa) [49]. Remarkably, it has been shown that these mixtures can absorb a large amount of H_2S from mixed gas depending on ethylene glycol content, temperature, H_2S mole fraction and type of IL (low pK_b of the amino group on amino acid increases the absorption ability). At 40 °C, the solubility of H_2S in the mixture can reach up to 2.36 mol H_2S per kilogram mixture (Fig. 3).

Based on the proposed mechanism, ethylene glycol not only decreases the viscosity of the capture mixture but also enhances the absorption capacity cooperating with the amino acid amino group to H_2S binding.

Finally, it is to mention the development of pyridinium and ammonium ILs bearing a Michael acceptor to scavenge H_2S gas and various thiols, in most cases, without the aid of any added bases (Fig. 4) [50].

These ILs, which exploit the thiol-ene chemistry to capture thiols and H_2S and immobilize them into a non-volatile ionic matrix, could find application in personal care products being able to trap not only H_2S but also other highly malodorous substances. Furthermore, considering that the Michael addition is a reversible

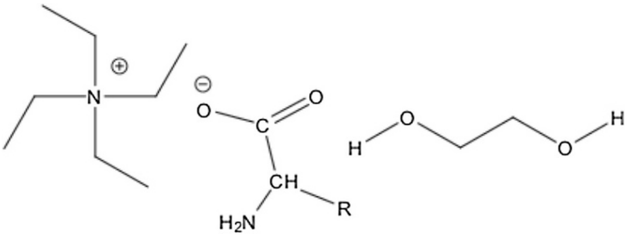

Fig. 3 Functionalized ILs and ethylglycol mixtures

process, this class of ILs has the potentiality, as stressed by the authors, to find application in the oil and gas industries. The IL cost might be in this case a critical point.

1.2 Absorption and Oxidation

As evidenced in the introduction, despite its limits, the Claus process represents today the most widely used method for sulfur recovery from highly concentrated streams and, recently, it has been shown that the ionic liquid-mediated Claus reaction might represent a significantly advanced development [51]. The reaction of H_2S with SO_2 proceeds indeed very fast and quasi-completely in the IL phase (seven

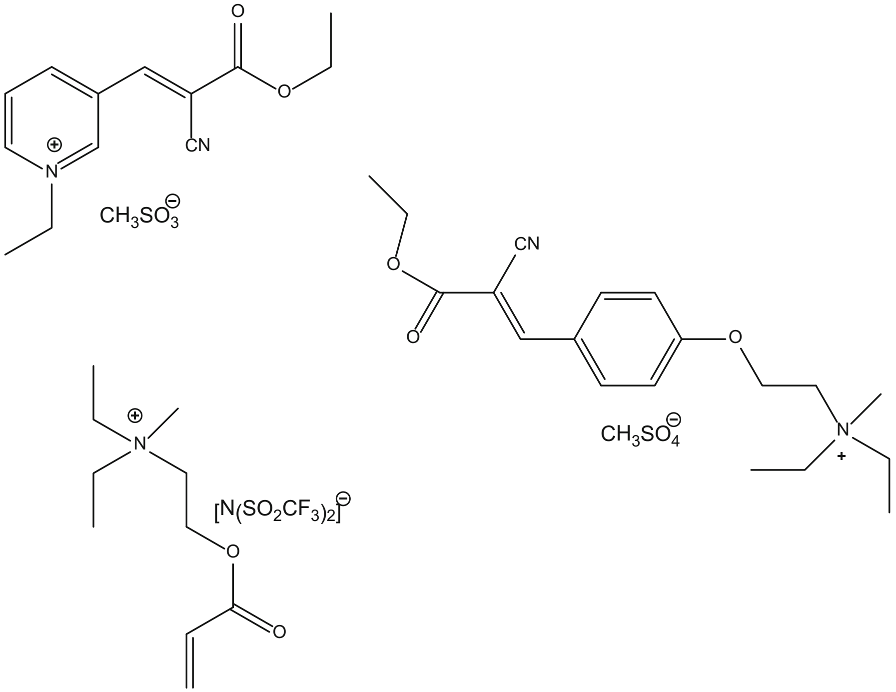

Fig. 4 Pyridinium and ammonium ILs bearing a Michael acceptor

imidazolium-based ILs have been investigated) to give a highly pure rhombic sulfur. This latter aspect might not be irrelevant.

$$2H_2S + SO_2 \leftrightarrow 3/8S_8 + 2H_2O$$

In [hmim]Cl, the process (performed through a pre-saturation of IL with SO_2 in a sealed reaction chamber followed by the subsequent addition of a stoichiometric amount of H_2S) is almost complete within 3 min reaching at 40 °C a final conversion ratio of H_2S of 96.4%, according to the residual gas pressure. This value is significantly higher than that found in diglycol monomethylether (81%), an organic solvent used for comparison. Related to the effect of IL structure on process efficiency, it is interesting to note that although the absorption capacity of SO_2 and H_2S in [emim][Ac] is even larger than that in [hmim]Cl, the alkalinity of the acetate-based IL is probably too strong, and the final conversion results significantly lower (84.6%). The authors suggest that $SO_3{}^{2-}$ is probably formed in the presence of water during the reaction of H_2S with SO_2 in [emim][Ac] and the formation of this anion prevents the further oxidation of H_2S: the oxidizability of $SO_3{}^{2-}$ is indeed much weaker than that of $HSO_3{}^{-}$.

On the other hand, the thermodynamic limitations of the Claus equilibrium reaction have led over time, independently of ILs, to the development of alternative processes to deal with the Claus tail gas, based on the oxidation of remaining traces (1 vol%) of H_2S by oxygen to meet ever stricter legislation requirements. Actually, since the direct oxidation of H_2S by oxygen at ambient temperatures is slow and side reactions tend to form undesirable sulfur oxo-acid salts as by-products, the process is generally carried out using an intermediate redox couple, definable as “catalyst”, whose reduced form, produced in the H_2S oxidation, is regenerated with air. Several redox couples (V^{5+}/V^{4+}; Fe^{3+}/Fe^{2+}; Co^{3+}/Co^{2+} and As^{5+}/As^{3+}) have been proposed and applied to this purpose, however, due to high oxidation rates of H_2S by Fe^{3+} and the toxicity and environmental concerns related to many of the other possible couples, the iron system is generally considered the most suitable catalyst for the liquid redox sulfur recovery process.

Therefore, liquid-phase oxidation processes using an iron(III) chelate catalytic solution represent today an alternative to the use of basic solutions and organic solvents for H_2S removal. This approach, which presents remarkable advantages such as converting H_2S directly to elemental sulfur at alkali pH and high H_2S removal efficiencies, has as main drawbacks (1) the rapid iron(III) chelate degradation, (2) the formation of sulfur oxo-acid salts as by-products, and (3) the fact that there are economic advantages only for 850–1050 kg/h of sulfur production due to low concentrations of the ferric complex in solution [52–55].

In order to improve the process efficiency, recently, 1-butyl-3-methylimidazolium tetrachloroferrate ([bmim][$FeCl_4$]) has been tested as alternative medium for the oxidation of H_2S [56]. This magnetic IL, characterized by a low viscosity and surface tension (appropriate properties for gas separation) also present good gas solubility [57] and catalytic activity [58]. In particular, He et al. in the first paper about this topic investigating the effects of temperature, oxygen flow rate and inlet

H_2S concentration on the catalytic oxidation of H_2S by [bmim][$FeCl_4$], suggest that the main desulfurization mechanism is the following:

$$\mathrm{Fe(III)\text{ - }IL + 1/2H_2S = H[Fe(II)\text{ - }IL] + 1/2S} \downarrow \tag{1}$$

$$\mathrm{H[Fe(II)\text{ - }IL] + 1/2O_2 = Fe(III)\text{ - }IL + 1/2H_2O} \tag{2}$$

where atmospheric oxygen plays an important role to re-oxidize Fe(II) to Fe(III), a process this latter surely affected by the low solubility of oxygen in ILs.

Nonetheless, Wang et al. more recently have demonstrated that [bmim][$FeCl_4$] could be reused four times without any loss of H_2S oxidative-absorption capability [59]. In this paper, the authors also evidenced that the catalytic oxidation of H_2S by acidic [bmim][$FeCl_4$] has high H_2S removal efficiency (over 99%), good regeneration due to the formation of Fe–Cl complex, no side reaction which cannot take place in an acid environment, and no degradation without water. Finally, considering a loss of 0.5% of IL during S separation and the current cost of [bmim]Cl (22000 \$/t quoted by Shanghai Cheng Jie Chemical Co. Ltd.), the authors conclude that the catalytic oxidation of H_2S by [bmim][$FeCl_4$] is the process that can generate profit.

Although the use of iron-based ILs can overcome the shortcomings of the aqueous iron-based catalysis without production of inorganic salt by-products and wastewater, unfortunately, [bmim][$FeCl_4$] capture still presents many unsolved problems [60]. Therefore, with the aim of investigating in which measure acidity and Fe(III) concentration affect the oxidation process, the same authors report the effects of the [bmim]Cl/$FeCl_4$ molar ratio showing that acidity and Fe(III) concentration have important effects on oxidation of H_2S to S8 and reduction of [bmim][$FeCl_4$] to [bmim][$FeCl_3$], which is then transformed into [bmim]Fe(II)Cl_4H as soon as it reacts with HCl. Furthermore, in the presence of water, the mass concentration of chloride was identified as the governing factor controlling HCl emissions during the oxidation of H_2S.

More recently, Yu et al. suggest that the addition of Fe(II), introduced in the system as [bmim][$FeCl_3$], and *N,N*-dimethylformamide can improve the hydrogen sulfide removal efficiency of [bmim][$FeCl_4$], contemporaneously giving a system that can be regenerated using the controlled-potential electrolysis method [61]. The addition of Fe(II) in Fe(III)-IL is indeed beneficial for both hydrogen sulfide removal and for the subsequent electrochemical regeneration of the desulfurizer. Whereas the desulfurization efficiency of Fe(III)-IL rapidly decreases, and after 70 min H_2S is no longer effectively removed, the desulfurization efficiency of Fe(III/II)-IL is still greater than 90% at 270 min: probably, Fe(II) reacts with the absorbed H_2S to form Fe(II)-HS^-, a species having a higher oxidation rate than HS^-. On the other hand, although the addition of DMF in Fe(III/II)-IL does not change the structure of the ionic mixture, it clearly decreases its acidity (favoring the absorption of the acidic H_2S), increases the electrolytic current and, considering that the oxidization of H_2S in iron-based ILs is accompanied by the cleavage of the Fe–Cl bond, decreases the stability of the Fe–Cl bond in Fe(III/II)-IL.

Finally, it is to mention that also Brønsted acidic iron-based ILs have been used for desulfurization. The sulfur capacities of H_2S have been indeed investigated [62] also in different mole ratios of Et_3NHCl and $FeCl_3$ (from 1.4:1 to 1.8:1) in the temperature range of 298.15 to 323.15 K, showing that the sulfur capacity of H_2S in 1.5:1 Et_3NHCl-$FeCl_3$ IL is higher than that of all the other mole ratios. Viscosity and oxidation capacity have been identified as the two main properties of the medium determining the process efficiency: these two properties are oppositely correlated with the molar ratios of Et_3NHCl and $FeCl_3$. The first one, i.e., the dynamic viscosity, increases sharply with the decrease of mole ratio of Et_3NHCl and $FeCl_3$, whereas the oxidation capacity increases with the decrease of mole ratio of Et_3NHCl and $FeCl_3$, due to the increasing content of $FeCl_3$. The 1.5:1 Et_3NHCl–$FeCl_3$ molar ratio therefore represents the medium composition assuring the best assembly between medium viscosity, H_2S mass transfer, and oxidation capacity. The dependence of sulfur capacity of H_2S in this IL with temperature is also affected by viscosity: it increases indeed sharply at low temperatures (288.15–303.15 K), decreases significantly at moderate temperatures (303.15–313.15 K), and decreases slowly at high temperatures (313.15–323.15 K). Since the interaction force between the anions and the cations decreases with increasing temperature, on increasing temperature the viscosity of the IL decreases, but contemporaneously also the solubility of H_2S in the ionic environment decreases. Therefore, at the low temperatures (288.15–303.15 K), the viscosity of IL is the key influence factor on the sulfur capacity and sulfur capacity sharply increases. At moderate temperatures, the solubility of H_2S becomes the key influence parameter on the sulfur capacity and sulfur capacity significantly decreases.

In conclusion, despite the recent activity in this field and the undouble ability of iron(III)-based ILs to capture and oxidize H_2S, much more work is necessary to improve the process of increasing efficiency and reducing drawbacks.

1.3 Computational Studies

1.3.1 Ab Initio Calculations

Although not yet extensively investigated, most of the theoretical studies on H_2S in ILs combine computational and experimental parts and sometimes report comparison with other acidic gases, like CO_2 or SO_2. From the computational point of view, the interactions of H_2S with ILs have been studied at different levels of theory, corresponding to model systems of significantly different size. The minimal system is indeed represented by a “super molecule” that includes one or more H_2S molecules and one or more IL ion pairs. These small systems have allowed accurate studies at the ab initio level showing that the interactions of the IL components (cations and anions) with H_2S are similar to those reported for H_2O: H_2S can indeed act as hydrogen bond donor through the two acidic hydrogens or as hydrogen bond acceptor through the lone pairs of the sulfur atom and, therefore, IL cations or anions generally are able to give strong hydrogen bonds with H_2S [63]. Some hydrogen bonding patterns, reported in the papers discussed below, are reproduced in Fig. 5.

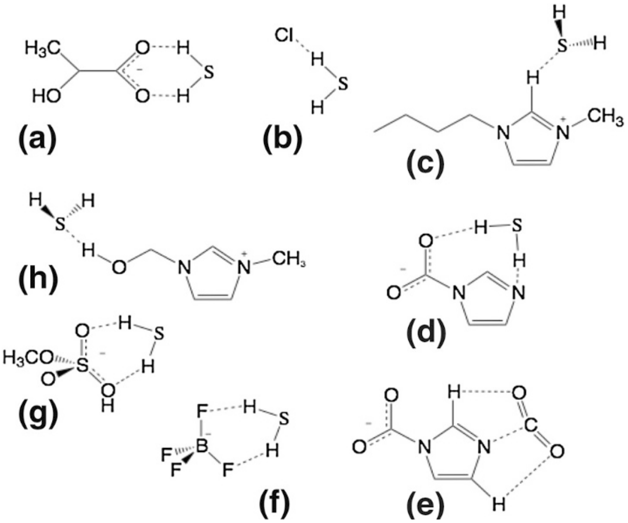

Fig. 5 Some examples of H_2S-ion interactions. **a** Lactate anion [65]. **b** Chloride anion [37]. **c** BMIM cation [37, 61]. **d**, **e** 1-Carboxy imidazole interacting, respectively, with H_2S and CO_2 [45] (**e**). **f** Tetrafluoroborate anion [37]. **g** Methylsulfate anion [61]. **h** 1-Hydroxymethyl-3-methylimidazolium cation [65]

The first theoretical study, performed at DFT and MP2 level with valence triple-split basis sets, was related to an experimental investigation on H_2S solubility using medium-pressure NMR. Published in 2007, it studied the 1:1 complexes of H_2S with several IL anions (Cl^-, BF_4^-, PF_6^-, TfO^-, Tf_2N^-), with some ion pairs ([bmim] Cl, [bmim] [BF_4], [bmim] [PF_6]) and larger complexes constituted by several H_2S molecules (up to 12) with Cl^- and BF_4^- [37]. The energy of interaction of H_2S with the investigated anions lies in the range of hydrogen bond complexes (28–65 kJ/mol). Furthermore, an upper limit of the coordination number of H_2S corresponding at eight for chloride and four for $[BF_4]^-$ was established. Tentative calculations with a larger number of H_2S molecules led to the expulsion of some H_2S molecules to the second coordination shell. A good correlation was moreover found between the calculated H–S stretching frequencies of these complexes and the experimental absorption bands in the FT-IR spectra. It is noteworthy that in the case of the two oxygenated anions (TfO^- and Tf_2N^-), H_2S is able to coordinate itself to two oxygen atoms, leading to a chelating complex.

A pure computational study, performed at the DFT level with a valence triple-split basis set and analyzed with the AIM topological theory, comparing the interaction of H_2S with two other acidic gases (CO_2 and SO_2), has been more recently performed by Costa et al. [64]. In this case, a large set of anions (including halogenides, sulfates, alkylsulfates, and acetate) and of cations (including tetralkyl ammonium, tetralkylphosphonium, and imidazolium) was taken into account. Although the focus of the paper is on CO_2 (many of the results related to H_2S are reports in S.I.), this is probably the most exhaustive ab initio study on this topic. The order of the interaction energies is $SO_2 > H_2S > CO_2$ for all investigated anions and cations. Furthermore, $[(CH_3)_4P]^+$, F^-, AcO^- and SO_4^{2-} exhibit the largest interaction energies with all gases. Probably, this result is not surprising, considering that these are the smallest single-charged ions and the sole double-charged anion considered, however, the reported geometries clearly show distance compatible with hydrogen bonds (established also through topological analysis), confirming that this kind of interaction is the preferred by H_2S in the ionic environment.

Finally, to conclude this short overview on ab initio calculations, we discuss specifically two papers focused on H_2S. The first one by Hu et al. reports [45] a combined computational/experimental study (this latter already discussed in the previous section) where specifically task-oriented ILs are first designed and then synthesized to optimize a selective and efficient capture of H_2S. These ILs, which are characterized by tertiary amines and carboxylate functional groups on the anion, allow the formation of a chelate involving H_2S and both the functional groups, whereas CO_2 interacts only with the amine group and the nearby acidic hydrogens (Fig. 5d, e).

The other paper by Li et al. reports [65] a multi-scale study where ab initio calculations are combined with molecular dynamics simulations. In particular, it initially investigates several 1:1 H_2S: ion pairs complexes, some analogous to those reported [37] by Pomelli et al. Furthermore, the same systems are studied with CH_4 in order to investigate the H_2S/CH_4 selectivity, whereas the Henry law constants are estimated using COSMO-RS calculations. Stepping up on the scale of the computational systems, molecular dynamics simulations have been used to calculate pair distribution functions and diffusion coefficients of both gases in more complex systems where ILs are supported on MOFs. As expected, H_2S presents a narrow and high peak related to a strong bonded first shell of solvation around both positive and negative ions, while the corresponding curve for CH_4 is broad and low. All these results show for all investigated ILs a high H_2S/CH_4 selectivity attributable to the strong and specific interaction between H_2S and the ionic solvent.

1.3.2 Dynamic Simulation

The number of papers reporting molecular dynamics simulations on H_2S and ILs is at the moment extremely limited. After the publication of Li [65], described in the previous section, Gallo et al. studied [66] the solvation thermodynamic of H_2S in conventional [bmim]-based ILs characterized by different spherical top anions: chloride, BF_4^- and PF_6^-. Results are compared with the experimental values reported for the same ILs in ref. 37, showing a good agreement. Moreover, in agreement with results obtained from ab initio studies, the radial distribution functions show that H_2S interact preferentially with the IL anion: the hydrogen atoms in H_2S are oriented toward the anions, while the sulfur atom is surrounded by the cations. A simple visual inspection of the radial distribution functions shows that the anion-hydrogen distance (anion-HS) increases with the anion size whereas the narrowness decreases. Other important interactions that emerge from these simulations are those between the H_2S sulfur atom (i.e., the hydrogen bond acceptor site in H_2S) and the protons at the imidazolium ring carbon in α position to the nitrogen atoms. It is also noteworthy that the calculated thermodynamic parameters evidence that the process is enthalpy driven: the contribution of the solvation enthalpy to the free energy of solvation is two times higher than the entropy contribution.

Finally, solvation of H_2S and of other two gases (CH_4 and CO_2) in a less common IL, hexamethylguanidinium lactate, has been investigated by Aparicio and Atilhan [67]. The pure IL presents strong electrostatic interactions, coherently with its viscosity and low self-diffusion coefficients, but the simultaneous absorption of the two acidic gases change this scenario. Although the pure IL structure does not contain cavities able to accommodate the investigated gases, gas dissolution determines a modification of the spatial distribution of anions and cations. This leads to a weakening of the IL structure so decreasing viscosity and increasing ions mobility. Interaction between H_2S and IL component appears therefore more important than the presence of free volume in the dissolution process: H_2S can modify the IL three-dimensional structure. Different is the situation of methane that, when present, arranges independently in the small apolar domains while CO_2 and H_2S still form 1:1 cybotactic clusters.

1.3.3 Predictive Models

Considering the strong applicative component of this kind of research and the fact that experimental measurements are not always easy to perform, since they are time consuming, expensive, and require the manipulation of a highly toxic compound, it is not surprising that the larger set of computational studies is related to developing predictive models to estimate H_2S solubility in ILs. The parametric cubic equation of state (CPA), based on empiric models for intermolecular interactions, is generally used for this purpose and some of these models have been applied successfully to ILs: a dedicated review has recently been published [68]. In particular, the statistical associating fluid theory (SAFT) is a well-known equation of state based on the combination of chained interaction centers. The parameters related to the interaction centers correspond roughly to a coarse-grained molecular dynamics potential: e.g., the five atoms of the imidazolium ring are generally considered a single center. This approach permits taking into account some molecular features, like shape or polarity, or ability to donate/receive hydrogen bond, without the necessity to consider explicitly the molecules at the atomistic level. A similar approach also characterizes the perturbed hard sphere chain theory (PHSC), where the molecular shape is modeled as a chained hard sphere and additional terms of the potentials are added with a perturbation scheme. Now, several variants of both and/or similar methods, based on analogous approaches, are known.

Recently, several studies applying this type of model to predict the solubility of H_2S in ILs have been published showing a good agreement between predicted and experimental values. The pure fluid-phase diagrams of acidic gases, including H_2S, were reproduced in excellent agreement with available experimental data, including the critical region. A key to the success of the modeling approach is the careful consideration of the appropriate cross-associating interactions among the different molecules. Therefore, prerequisite to apply these models becomes to have a set of parameters able to describe IL. Since, at the state of art, these are limited to few mainstream ILs, these studies are generally related to dialkylimidazolium ILs having as counteranion common ions: BF_4^-, Tf_2N^-, PF_6^-, AcO^- and $CH_3SO_4^-$ [69–73]. Unfortunately, this monotony, despite the nearly endless number of potential ILs, is quite common and characterizes a large part of the IL literature.

Another important class of predictive studies is based on machine learning. In this case, the molecular level is completely disregarded. From the point of view of these mathematical models, which range from neural networks to fuzzy logic, genetic algorithm, etc., the experimental data on H_2S solubility are practically a coherent collection of data ignoring completely the chemical nature of the capturing medium: thus, no specifically designed parameters are necessary. Consequently, related papers generally report results about large collections of ILs and, sometimes, explore the domain outside dialkylimidazolium region [74–79], including also tetraalkylammonium/phosphonium salts [72] and functionalized ILs [73]. These approaches appear, at the moment, to be able to estimate accurately the solubility of H_2S and of other acid gases in different media, including ILs.

2 Conclusions

In conclusion, experimental data reported in the literature demonstrate that ILs can be used for H_2S capture and in gas absorption–separation processes. Hydrogen sulfide is a self-associating molecule with dipolar and quadrupole moments. Structurally speaking, H_2S is similar to water, with an angle between the hydrogen and the sulfur atoms of 92.1° and a couple of electron pairs on the sulfur atom. However, sulfur is not as electronegative as oxygen and hence hydrogen sulfide is less polar than water, although more acidic and, comparatively, weaker intermolecular forces exist in H_2S. These features determine the nature and strength of interactions between H_2S and ILs and therefore the solubility of this gas in the ionic environment. Although on the basis of free volume considerations, it has been more times stressed that H_2S solubility in ILs is strictly related to the presence of spaces able to accommodate the gas, solubility indeed increases on weakening of the anion–cation interaction and increasing the free volume, as evidenced also by theoretical calculations, it is probably mainly determined by the occurrence of specific solute–IL interactions and, more importantly, these interactions can be able to modify IL structure.

Furthermore, the acidic nature of this gas favors its dissolution in basic ILs, containing appropriate functional groups on cation and/or anion (NH_2, NH), or simply, having sufficiently strong hydrogen bond acceptor anions (Cl^- and Br^-) or basic anions (AcO^-, etc.).

Although presently only a limited number of computational studies at the atomistic level (ab initio and molecular dynamics) on H_2S absorption in ILs have been reported, they are sufficient to identify the nature of these interactions, which are practically the same of water and ILs. Radial distribution functions from molecular dynamics and supermolecule structures obtained from ab initio calculations suggest indeed similar interactions involving preferentially the hydrogen atoms in H_2S and the IL anion. Thus, it is not surprising that hydrophilic ILs are able to capture H_2S and [bmim]Cl that is, at the state of art, the IL showing the highest absorption ability (in this IL the ratio H_2S molecules/IL ion pairs reaches 6:1) is practically deliquescent. The interactions between IL anion and H_2S are, however, stronger than those involving H_2O, therefore H_2S interact also with large anions such PF_6^-. Nonetheless, the small anions remain probably the best strategy to maximize the strength of these interactions and increase H_2S solubility.

Interesting also is the ability of protic ILs having suitable anions to dissolve H_2S. Although the loading capacity of the investigated ILs is generally lower than that of analogous non-acidic ILs, the different interaction ability of H_2S and CO_2 make these media suitable systems for H_2S/CO_2 separation. The eventual role of water in this latter case cannot be neglected.

Surely, the limited number of functionalized ILs (including also protic ILs) investigated and the positive results obtained despite the random strategy that appears to be at the basis of these studies (experiments have been carried out by different research groups on ILs having often low if any structural correlation) suggest the existence of large margins for the further optimization of absorbents. Low-cost and high-absorption-capacity salts, competing to the commercially available ILs, could be developed. These considerations can be also extended to sulfur recovery processes by oxidation: practically, only $FeCl_4^-$ bases ILs and the Claus process have been marginally investigated. Ab initio calculations, dynamic simulations, and predictive models, probably due to the intrinsic features of H_2S that makes some interactions largely dominant, could be a valid and rational support for the discovery of more efficient and sustainable ionic absorbents.

References

1. http://www.npi.gov.au/resource/hydrogen-sulfide. Accessed Apr 2017
2. Kohl AL, Nielsen RB (1997) Gas Purification, 5th edn. Gulf Publishing Company, Houston
3. Karadas F, Atilhan M, Aparicio S (2010) Energy Fuels 24:5817
4. Galán Sánchez LM, Meindersma GW, de Haan AB (2007) Trans I Chem E Part A Chem Eng Res Des 85:31
5. Amosa MK, Mohammed IA, Yaro SA (2010) NAFTA 61:85
6. Bates ED, Mayton RD, Ntai I, Davis JH (2002) J Am Chem Soc 124:926
7. Chiappe C, Pieraccini D (2005) J Phys Org Chem 18:275
8. Cevasco G, Chiappe C (2014) Green Chem 16:2375
9. Wasserscheid P, Welton T (2008) Ionic liquids in synthesis, 2nd edn. Wiley-VCH, Weinheim
10. Hallett JP, Welton T (2011) Chem Rev 111:3508
11. Ohno H (2011) Electrochemical aspects of ionic liquids, 2nd edn. Wiley, Hoboken
12. Plechkova NV, Seddon KR (2008) Chem Soc Rev 37:123
13. Hayes R, Warr GG, Atkin R (2015) Chem Rev 115:6357
14. Babamohammadi S, Shamiri A, Aroua AK (2015) Rev Chem Eng 31:383
15. MacFarlane DR, Tachikawa N, Forsyth M, Pringle JM, Howlett PC, Elliott GD, Davis JH, Watanabe M, Simon P, Angell CA (2014) Energy Environ Sci 7:232
16. Wang C, Luo X, Zhu X, Cui G, Jiang D, Deng D, Li H, Dai S (2013) RSC Adv 3:15518
17. Zhang L, Chen J, Lv JX, Wang SF, Cui Y (2013) Asian J Chem 25(5):2355–2358
18. Zhang X, Zhang X, Dong H, Zhao Z, Zhang S, Huang Y (2012) Energy Environ Sci 5:6668
19. Brennecke JF, Gurkan BE (2010) J Phys Chem Lett 1:3459

20. Carvalho PJ, Kurnia KA, Coutinho JAP (2016) Phys Chem Chem Phys 18:14757
21. Jou FY, Mather AE (2007) Int J Thermophys 28:490
22. Rahmati-Rostami M, Ghotbi C, Hosseini-Jenab M, Ahmadi AN, Jalili AH (2009) J Chem Thermodyn 41:1052
23. Sakhaeinia H, Jalili AH, Taghikhani V, Safekordi AA (2010) J Chem Eng Data 55:5839
24. Safavi M, Ghotbi C, Taghikhani V, Jalili AH, Mehdizadeh A (2013) J Chem Thermodyn 65:220
25. Jalili AH, Rahmati-Rostami M, Ghotbi C, Hosseini-Jenab M, Ahmadi AN (2009) J Chem Eng Data 54:1844
26. Jalili AH, Mehdizadeh A, Shokouhi MT (2010) J Chem Thermodyn 42:1298
27. Rahmati-Rostami M, Ghotbi C, Hosseini-Jenab M, Ahmadi AN, Jalili AH (2009) J Chem Thermodyn 41:1052
28. Jalili AH, Safavi M, Ghotbi C, Mehdizadeh A, Hosseini-Jenab M, Taghikhani V (2012) J Phys Chem B 116:2758
29. Jalili AH, Shokouhi M, Maurer G, Hosseini-Jenab M (2013) J Chem Thermodyn 67:55
30. Shiflett MB, Yokozeki A (2010) Fluid Phase Equilib 294:105
31. Shiflett MB, Niehaus AMS, Yokozeki A (2010) J Chem Eng Data 55:4785
32. Yokozeki A (2001) Int J Thermophys 22:1057
33. Shiflett MB, Yokozeki A (2007) J Phys Chem B 111:2070
34. Shiflett MB, Kasprzak DJ, Junk CP, Yokozeki A (2008) J Chem Thermodyn 40:25
35. Yokozeki A, Shiflett MB, Junk CP, Grieco LM, Foo T (2008) J Phys Chem B 112:16654
36. Bini R, Bortolini O, Chiappe C, Pieraccini D, Siciliano T (2007) J Phys Chem B 111:598
37. Pomelli CS, Chiappe C, Vidis A, Laurenczy G, Dyson PJ (2007) J Phys Chem B 111:13014
38. Handy H, Santoro A, Widodo A, Palgunadi J, Soerawidjaja TH, Indarto A (2014) Sep Sci Technol 49:2079
39. Guo B, Duan E, Zhong Y, Gao L, Zhang X, Zhao D (2011) Energy Fuels 25:159
40. Huang K, Cai D-N, Chen Y-L, Wu Y-T, Hu XB, Zhang ZB (2013) AIChE J 59:2227
41. Chiappe C, Pomelli CS, Rajamani S (2011) J Phys Chem B 115:9653
42. Huang K, Wu YT, Hu XB (2016) Chem Eng J 297:265
43. Shokouhi M, Adibi M, Jalili AH, Jenab MH, Mehdizadeh A (2010) J Chem Eng Data 55:1663
44. Sakhaeinia H, Taghikhani V, Jalili AH, Mehdizadeh A, Safekordi AA (2010) Fluid Phase Equilib 298:303
45. Huang K, Cai DN, Chen YL, Wu YT, Hu XB, Zhang ZB (2014) ChemPlusChem 79:241
46. Huang K, Zhang XM, Xu Y, Wu YT, Hu XB, Xu Y (2014) AIChE J 60:4232
47. Akhmetshina AI, Petukhov AN, Vorotyntsev AV, Nyuchev AV, Vorotyntsev IV (2017) ACS Sustainable Chem Eng. doi:10.1021/acssuschemeng.7b00092
48. Huang K, Zhang XM, Hu XB, Wu YT (2016) AIChE J 62:4480
49. Wang B, Zhang K, Ren S, Hou Y, Wu W (2016) RSC Adv 6:101462
50. Nimal Gunaratne HQ, Nockemann P, Seddon KR (2014) Green Chem 16:2411
51. Huang K, Feng X, Zhang X-M, Wu Y-T, Hu X-B (2016) Green Chem 18:1859
52. McManus D, Martell AE (1997) J Mol Catal A Chem 117:289
53. Karimi A, Tavassoli A, Nassernejad B (2010) Chem Eng Res Des 88:748
54. Wang R (2003) Sep Purif Technol 31:111
55. Eng SJ, Motekaitis RJ, Martell AE (2000) Inorg Chim Acta 299:9
56. He Y, Yu J, Chen LJ (2010) Chem Ind Eng (China) 61:963
57. Albo J, Santos E, Neves LA, Simeonov SP, Afonso CAM, Crespo JG, Irabien A (2012) Sep Purif Technol 97:26
58. Bica K, Gaertner P (2006) Org Lett 8:733
59. Wang J, Zhu L (2012) Nat Gas Chem Ind 37:29
60. Wang J, Zhang W (2014) Energy Fuels 28:5930
61. Guo Z, Zhang T, Liu T, Du J, Jia B, Gao S, Yu J (2015) Environ Sci Technol 49:5697
62. Li M, Guan J, Han J, Liang W, Wang KK, Duan E, Guo B (2015) J Mol Liquids 209:58
63. Chiappe C, Pomelli CS (2013) Phys Chem Chem Phys 15:412
64. Damas GB, Dias ABA, Costa L (2014) J Phys Chem B 118:9046
65. Chen J-J, Li W-W, Yu H-Q, Li X-L (2013) AIChE J 59:3824
66. Sanchez-Badillo J, Gallo M, Alvarado S, Glossman-Mitnik D (2015) J Phys Chem B 119:10727
67. Aparicio S, Atildan M (2010) Energy Fuels 24:4989
68. Maia FM, Tsivintzelis I, Rodriguez O, Macedo EA, Kontogeorgis GM (2012) Fluid Phase Equil 332:128

69. Ji X, Held C, Sadowski G (2014) Fluid Phase Equil 363:59
70. Shahriari R, Delganhi MR, Behzadi B (2012) Fluid Phase Equil 313:60
71. Llovell F, Marcos RM, MacDowell N, Vega LF (2012) J Phys Chem B 116:7709
72. Haghtalab A, Kheiri A (2015) J Chem Term 89:41
73. Llovell F, Oliveira MB, Coutinho JAP, Vega LF (2015) Catal Today 255:87
74. Ahmadi MA, Pouladi B, Javvi Y, Alfkhani S, Soleimani R (2015) J Supercrit Fluids 97:81
75. Amedi HR, Baghban A, Ahmadi MA (2016) J Mol Liq 216:411
76. Shafiei A, Ahmadi MA, Zaheri SH, Baghban A, Amirfakhrian A, Soleimani R (2014) J Supercrit Fluids 95:525
77. Sedghamiz MA, Rasoolzadeh A, Rahimpour MR (2015) J CO2 Util 9:39
78. Hanzehie ME, Fattahi M, Najibi H, Van der Bruggen B, Mazinani S (2015) J Nat Gas Sci Eng 24:106
79. Ahmadi MA, Haghbakhsh R, Soleimani R (2014) J Supercrit Fluids 92:60